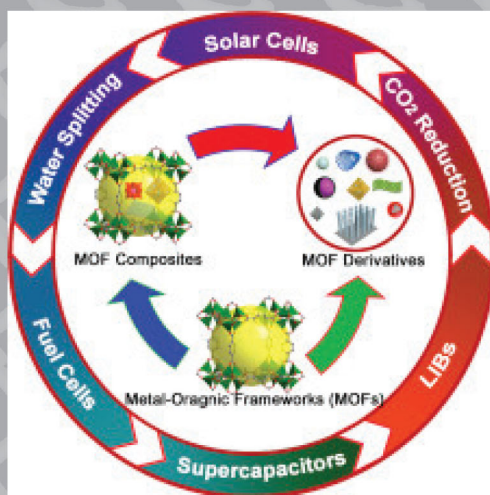


Metal-Organic Framework Composites

Volume II



Edited by
Anish Khan, Francis Verpoort,
Mohammed Muzibur Rahman, Ilyas MD Isa,
Abdullah M. Asiri, Malik Abdul Rub

M|R|F

Metal-Organic Framework Composites

Volume II

Edited by

**Anish Khan^{1,2}, Francis Verpoort^{3,4,5}, Mohammed Muzibur Rahman^{1,2},
Illyas MD Isa⁶, Abdullah M. Asiri^{1,2}, Malik Abdul Rub^{1,2}**

¹Chemistry Department, Faculty of Science, King Abdulaziz University, P.O. Box 80203,
Jeddah, 21589, Saudi Arabia

²Center of Excellence for Advanced Materials Research, King Abdulaziz University, Jeddah,
21589, Saudi Arabia

³Laboratory of Organometallics, Catalysis and Ordered Materials, State Key Laboratory of
Advanced Technology for Materials Synthesis and Processing, Wuhan University of
Technology, Wuhan 430070, PR China

⁴National Research Tomsk Polytechnic University, Lenin Avenue 30, 634050 Tomsk, Russian
Federation

⁵Ghent University, Global Campus, Songdo, Ywonsu-Gu, Incheon, Republic of Korea

⁶Department of Chemistry, Faculty of Science and Mathematics, Universiti Pendidikan Sultan
Idris, 35900 Tanjung Malim, Perak, Malaysia

Copyright © 2019 by the authors

Published by **Materials Research Forum LLC**
Millersville, PA 17551, USA

All rights reserved. No part of the contents of this book may be reproduced or transmitted in any form or by any means without the written permission of the publisher.

Published as part of the book series
Materials Research Foundations
Volume 58 (2019)
ISSN 2471-8890 (Print)
ISSN 2471-8904 (Online)

Print ISBN 978-1-64490-042-0
eBook ISBN 978-1-64490-043-7

This book contains information obtained from authentic and highly regarded sources. Reasonable efforts have been made to publish reliable data and information, but the author and publisher cannot assume responsibility for the validity of all materials or the consequences of their use. The authors and publishers have attempted to trace the copyright holders of all material reproduced in this publication and apologize to copyright holders if permission to publish in this form has not been obtained. If any copyright material has not been acknowledged please write and let us know so we may rectify this in any future reprints.

Distributed worldwide by

Materials Research Forum LLC
105 Springdale Lane
Millersville, PA 17551
USA
<http://www.mrforum.com>

Manufactured in the United States of America
10 9 8 7 6 5 4 3 2 1

Table of Contents

Preface

Multiscale Study of Hydrogen Storage in Metal-Organic Frameworks Seyfeddine Rahali, Mahamadou Seydou, Youghourta Belhocine, Bahoueddine Tangour	1
--	---

Metal Organic Frameworks Based Materials for Renewable Energy Applications

Haydar Göksu, Nursefa Zengin, Fatih Şen	19
---	----

Metal Organic Frameworks Composites for Lithium Battery Applications Rashid Iqbal, Pothu Ramykrishna, Rajender Boddula, Anish Khan.....	32
---	----

Metal-Organic-Framework-Quantum Dots (QD@MOF) Composites M. Ramesh, M. Muthukrishnan, Anish Khan, Mohammed Azam	49
---	----

Designing Metal-Organic-Framework for Clean Energy Applications Shivy Mangal, S. Shanmuga Priya, K.Sudhakar	85
---	----

Nanoporous Metal-Organic-Framework Sameer Ahmad, Afzal Ansari, Weqar Ahmad Siddiqi, M. Khursheed Akram	107
--	-----

Metal-Organic-Framework-Based Materials for Energy Applications Ashwini P. Alegaonkar, Vidya K. Kalyankar, Prashant S. Alegaonkar	140
---	-----

Metal-Organic-Framework Composites as Proficient Cathodes for Supercapacitor Applications Wei Ni, Lingying Shi	177
--	-----

Metal-Organic Frameworks and their Therapeutic Applications Fulya Gülbağça, Anish Khan, Fatih Şen.....	239
--	-----

Significance of Metal Organic Frameworks Consisting of Porous Materials R. Kumar, A. Arul Marcel Moshi, S.R. Sundara Bharathi, S. Sivaganesan, C. Dhanasekaran, P. Sentharamaikkannan, S.S. Saravanakumar, Anish Khan.....	290
---	-----

Metal Organic Frameworks (MOF's) for Biosensing and Bioimaging Applications Fulya Gülbağça, Kubilay Arıkan, Kemal Cellat, Anish Khan, Fatih Şen	308
---	-----

Nanoscale Metal Organic Framework for Phototherapy of Cancer Fulya Gülbağça, Fatima Elmusa, Kemal Cellat, Anish Khan, Fatih Şenl	361
--	-----

<i>Keyword Index</i>	276
----------------------------	-----

<i>About the Editors</i>	277
--------------------------------	-----

Dedication

*Editors are honoured to dedicate
this book to*

Mr.Rafiq

(Father of Dr. Anish Khan)

Preface

This book assembles the information and knowledge on MOFs materials and emphasizes the concept of the latest technology in the field of manufacturing and design. The book is beneficial to lecturers, students, researchers and industrialist who are working in the field of material science especially MOFs composites as a valuable reference book for teaching, learning, and research on energy applications. The book is the second volume on MFOs and focuses on the usage of composites in energy. It elaborates the design and manufacturing process of Metal Organic Frameworks (MOFs) materials in all aspect. The latest trends in application of Metal Organic Frameworks (MOFs) composites are described to the reader. The replacement of conventional composite materials with Metal Organic Frameworks (MOFs) composites in the area of manufacturing and design to achieve sustainable practice is highlighted with real applications.

Chapter 1 describes a multiscale study of hydrogen storage in metal–organic frameworks. Because of their high surface areas, crystallinity, and tunable properties, metal–organic frameworks have attracted intense interest as next-generation materials for gas capture and storage, especially the molecular hydrogen storage. Hydrogen storage remains one of the main challenges in the implementation of a hydrogen-based energy economy. In chapter 2, metal organic frameworks based materials for renewable environmental energy applications are discussed. Herein chapter 3, explain an overview about challenges and recent advances in electrochemical properties of MOF-derived carbon, pristine MOF and their composites with conductive materials to enhance the Li-ion batteries performance. Finally, by focusing on development of MOF materials, we proposed the future of Li-ion batteries for high energy density.

Chapter 4 summarizes the production mechanisms such as crystallization, interfacial diffusion, micro-fluidic processing, and vapour deposition methods of QD@MOF composites in detail. The application of QD@MOF in gas separation, nano-filtration, ionic sieving, stimuli responsiveness, and catalysis are reviewed, and the separation mechanisms are also discussed in detail. Moreover, the opportunities and challenges for further development of QD@MOF are pointed out.

Chapter 5 deals with various clean energy application of MOFs and their design considerations. Chapter 6 describes nanoporous metal-organic frameworks (MOFs) with three-dimensional porous lattices of inorganic-organic linkers. The fabrication of different MOFs by synthetic modifications method and description of most promising role in different fields such as gas separation, catalysis, gas storage, water treatment, and other different applications. In chapter 7, the authors have discussed the MOF's of

$\text{Ni}_3(\text{HITP})_2$ and $\text{Co}_3\text{O}_4\text{C}$ nanowire as sustainable renewable energy resources essentially applied as electro-catalysts in EDLC and OER mechanism toward energy storage application. This chapter includes a brief survey of MOF, particularly the study of $\text{Ni}_3(\text{HITP})_2$ and $\text{Co}_3\text{O}_4\text{C}$ nanowire MOF. The chapter includes the synthesis and characterization of $\text{Ni}_3(\text{HITP})_2$ and $\text{Co}_3\text{O}_4\text{C}$ nanowire MOF. They are studied as alternative sources for renewable energy. In chapter 8, the authors timely and comprehensively reviewed the impressive advancements achieved in recent years on MOFs and their composites for promising electrochemical capacitors (including supercapacitors, asymmetric supercapacitors and hybrid supercapacitors). The challenges and opportunities are also proposed for new breakthroughs in further development of MOF-based supercapacitors for ultimate practical applications.

Chapter 9, highlights various MOF types, their properties, and applications in various biomedical disciplines, with a particular focus on drug delivery and theranostics. Chapter 10 describes the significance of metal organic frameworks consisting of porous materials. In chapter 11 describes the used of MOFs in many applications and discusses the high-efficiency for biological detection and imaging. Chapter 12 summarizes the growing and evolving areas of nMOFs as nanoparticle photosensitizers for photodynamic therapy (PDT) and photothermal therapy (PTT).

Lastly we thanks for the excellent contributions of all authors all around the globe and their best effort to complete this project and making it unique. The MRF team's support and continues help is appreciable to complete this project.

Anish Khan

Francis Verpoort

Mohammed Muzibur Rahman

Illyas MD Isa

Abdullah M. Asiri

Malik Abdul Rub

Chapter 1

Multiscale Study of Hydrogen Storage in Metal-Organic Frameworks

Seyfeddine Rahali^{a,b,*}, Mahamadou Seydou^{c,*}, Youghourta Belhocine^d and
Bahoueddine Tangour^b

^a Department of Chemistry, College of Science & Arts at Al-Rass, Qassim University, P.O. 53,
Saudi Arabia

^b Université de Tunis El Manar, Unité de Recherche en Modélisation des Sciences
Fondamentales et Didactiques, Campus Universitaire Farhat-Hached Tunis, B.P. N 94,
Rommana, 1068, Tunisia

^c Université Paris Diderot, Sorbonne Paris Cité, ITODYS, UMR 7086 CNRS, 15 Rue J.-A. de
Baif, 75205, Paris Cedex 13, France

^d Department of Petrochemical and Process Engineering, Faculty of Technology, University of
20 August 1955 Skikda, El Hadaiek Road, 21000, Skikda, Algeria

*mahamadou.seydou@univ-paris-diderot.fr and saif.rahali@gmail.com

Abstract

Because of their high surface areas, crystallinity, and tunable properties, metal–organic frameworks have attracted intense interest as next-generation materials for gas capture and storage, especially the molecular hydrogen storage. Hydrogen storage remains one of the main challenges in the implementation of a hydrogen-based energy economy.

Contents

1. Introduction.....	2
2. DFT study of site characteristics in MOFs for hydrogen adsorption.....	4
3. Grand Canonical Monte Carlo (GCMC) for gravimetric and volumetric uptakes.....	8
Conclusion.....	13
Reference.....	13

1. Introduction

Its energy content is high, almost three times higher than that of gasoline, and its use in a fuel cell is a “zero emission” method which results in the formation of water without the emission of compounds polluting the environment or disrupting the climate [1]. However, many technical problems remain to be solved for hydrogen to become a carrier of energy in the future. Indeed, the storage of hydrogen, especially in embedded systems such as cars, poses a serious problem because hydrogen is very light and very sparse, therefore it requires particularly large volumes for storage. To solve the problem of hydrogen storage, different techniques are explored: storage under high pressure: compression of hydrogen, cryogenic storage in liquid form, absorption storage: Metal hydrides (Figure 1). These three techniques pose security, congestion and energy cost problems [2-8].

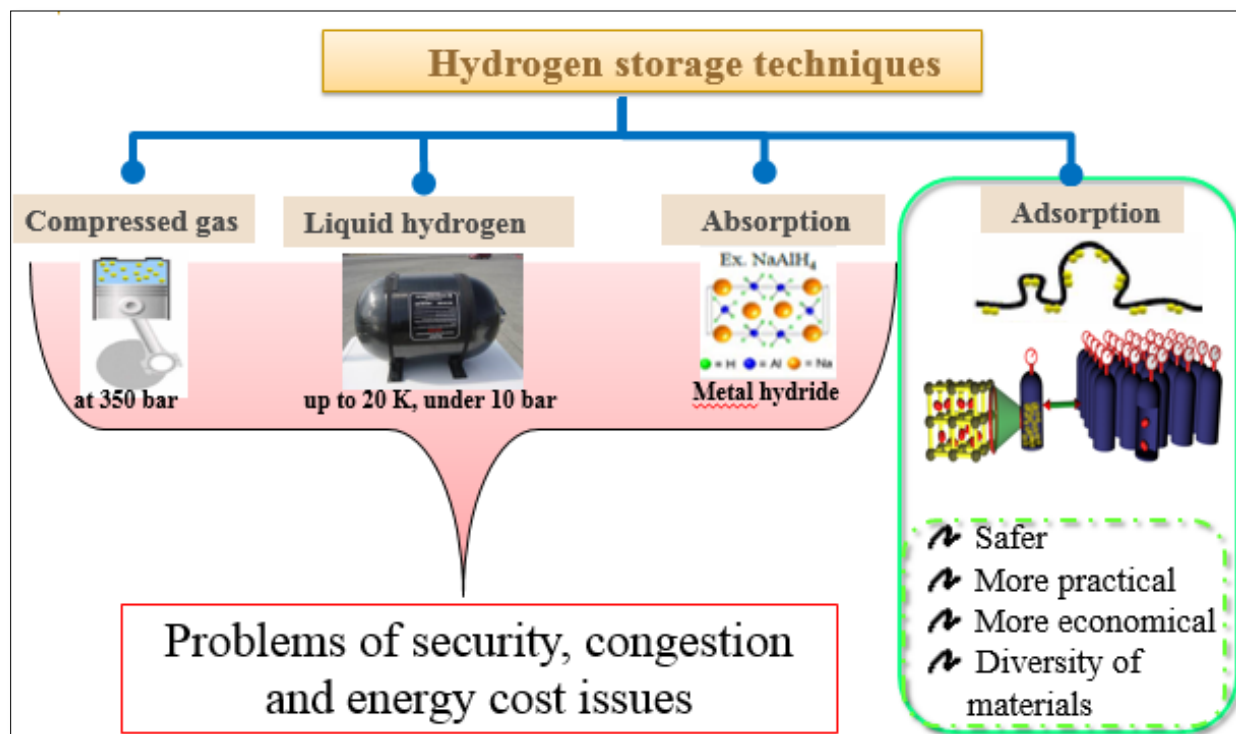


Figure 1: Presentation of hydrogen storage methods

To solve this problem, alternative methods of storing hydrogen by physical adsorption on porous or laminar substrates have been proposed. In these materials, the hydrogen remains adsorbed as a molecular species without any chemical reaction taking place. The advantages are manifold, the adsorption on a substrate implies the evacuation of the amounts of heat is much lower than during the formation of metal hydrides, on the one

hand and on the other hand, the adsorption/desorption cycles of hydrogen are much faster than those involved in chemical reactions producing metal hydrides.

Different classes of materials have been developed for this purpose, metal hydrides, carbon nanomaterials [9-13] and the nanoporous materials exhibiting a wide variety of interesting features such as metal-organic frameworks (MOFs) and zeolites [14-19].

Ideally, these materials would adsorb large amounts of hydrogen gas reproducibly at room temperature and moderate pressure. The primary purpose of the research in this emerging field is to fulfill the applications requirements and to meet the U.S. Department of energy (DOE) hydrogen storage target capacity of 5.5 wt% in 2017, at temperatures in the range of -233 and 333 K, and pressures up to 100 bar [20]. This value was adopted taking into account the needs of a vehicle to travel a distance of 500 km autonomously.

Table 1: DOE targets for hydrogen storage systems

Storage Parameter	Units	2017
Gravimetric capacity of system	kg H ₂ /kg _{system} or wt%	0,055 or 5,5
Volumetric capacity of system	kg H ₂ /L _{system}	0,040
Delivery temperature min / max	°C	-40/85
Maximum storage pressure	bar	100

For characterization MOFs as materials of hydrogen storage, there are two methods of measuring hydrogen adsorption: gravimetric and volumetric uptakes. To obtain the total amount of hydrogen in MOFs, both the amount absorbed hydrogen on its surface and the amount of hydrogen remaining in its pores should be considered. In addition to these two methods, there is another preliminary method that can give an idea of the hydrogen adsorption on the surface of MOFs. This method consists of studying the adsorption phenomenon by determining the different adsorption sites and the mechanism by determining the interaction energy.

To study these methods, there are several experimental and theoretical techniques. We focus only on the theoretical study in our discussion. We develop the application of the theoretical calculation methods, namely the Functional Density (DFT) method and the Grand Canonic Monte Carlo (GCMC) numerical simulations in order to identify the adsorption sites, to rationalize the adsorption properties by highlighting the nature of the interactions between the hydrogen molecules and MOFs and to estimate the gravimetric and volumetric capacity.

2. DFT study of site characteristics in MOFs for hydrogen adsorption

Identifying the gas adsorption sites in MOFs and their interactions with the hydrogen molecules are critically important to tune the adsorption sites to achieve maximum adsorption performance [21]. Determining whether adsorption sites lie on the metal oxide clusters or organic linkers, the number of adsorption sites and precise location of these sites are all important to gain molecular-level information for design and development of new MOFs specifically for gas storage applications. Theoretical calculations help provide information on the identification of preferred adsorption sites by comparing the adsorption energies of the adsorbates at adsorption sites. In general, the molecular interactions between hydrogen and the MOF atoms result from intermolecular contributions of van der Waals type [22]. Bhatia and Myers predicted an ideal binding energy of -15 kJ/mol to maximize the amount of adsorbed hydrogen [23].

Tim Mueller and Gerbrand Ceder performed the first study on hydrogen adsorption mechanism in MOF-5 using *ab initio* calculations. They found that adsorption energy at the level of the organometallic center Zn_4O that is stronger than that at the ligand BDC [34].

After, Srepusharawoot et al. have reported the adsorption energy of hydrogen with MOF-5 by employing density functional theory (DFT) [25]. They have also compared the calculated results with the previous studies. It was found that the adsorption energies calculated with LDA functionals (-8.74 and -16.34 kJ/mol) were higher than values obtained with GGA (PW91 1.8 and 4.1 kJ/mol). Lee and his colleagues have calculated the same using cluster model by employing PBE (1.5 and 2.8 kJ/mol) functional [26]. Kuc et al. have carried out MP2 calculations on the same using cluster models [27]. The calculated adsorption energy was found to vary from -1.26 to -5.1 kJ/mol for different adsorption sites in the cluster. They have shown that the results obtained from isolated clusters are qualitatively similar to values obtained from periodic calculations.

In the literature exists several studies of this type for deferent MOFs. Indeed, based on a purely energy evaluation, the best performance was obtained for the Ni-MOF-74 material with the highest initial adsorption energy of -13.5 kJ/mol [28]. Other MOFs such as IRMOF-1, which comes from the MOF-5 family, have interaction energies with hydrogen between -0.8 and -6.7 kJ/mol. Also, Yang and Zhong reported a computational study to understand hydrogen adsorption mechanism of MOF-505 [29]. They used DFT calculations and GCMC simulations and showed that metal (Cu)-oxygen clusters are preferential adsorption sites for H_2 and the strongest adsorption was found in the directions of coordinately unsaturated open metal sites. In another computational study, Forrest, et al reported the mechanism of hydrogen adsorption in PCN-61 [30]. Data

showed that the adsorption energy values in PCN-61 range from - 6.0 kJ/mol to - 6.5 kJ/mol, which are characteristic of hydrogen physisorption onto the metals. These simulations also revealed that there are three distinct favorable sites in PCN-61: cuboctahedron, the corner of the truncated tetrahedron, and the corner of the truncated octahedron.

In this context, we have studied in more detail the mechanism of hydrogen storage by adsorption on Pb-MOF and MOF-519. We started by studying the H₂ adsorption on Pb-MOF. This MOF of formula [Pb₂ (TETA)]·6H₂O was synthesized by Xian-Dong Zhu et al. using hydrothermal reaction of lead (II) with a macrocyclic ligand that is flexible and 1,4,8,11-tetraazacyclotetradecane-1,4,8,11-tetraacetic acid denoted H₄TETA (Figure 2). It has one type of hollow volume 2139.90 Å³ [31]. One of Pb-MOF important properties is its high flexibility, which means its ability to increase its volume.

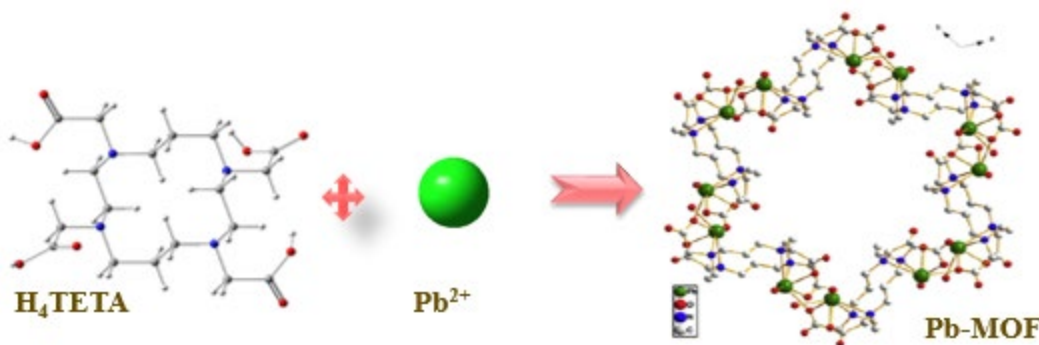


Figure 2: Representation of Pb-MOF geometry

Calculations were performed using the method of Density Functional Theory (DFT) in periodic conditions provided by means of the “VASP 5.2.11” (Vienna Ab Initio Simulation Package) code [32,33]. Electron-ion interactions were described by the “PAW” method (projector augmented wave) [34,35]. Convergence of the expansion of the plane wave was obtained with a cut-off of 500 eV. The generalized gradient approximation (GGA) was used with the Perdew-Burke- Ernzerhof (PBE) functional [36,37]. We based our study on the calculation of the adsorption energy to determine all the adsorption sites and the nature of interaction.

Our results revealed that the adsorption energy varies between -13.48 and -10.57 kJ/mol and hydrogen molecules are bound by a physisorption process [38]. For all different adsorption sites, one can see that the adsorption of H₂ on Pb-O is greater than that on the organic ligand. Therefore, the most stable adsorption sites for the MOF are the II, III and III sites, which are located adjacent to the metal oxide. They have Debye-type interaction energies which are very similar and have the same orientation of H₂ (Figure 3). This

outcome is similar to that found by Muller and Ceder for MOF-5 which has an adsorption energy at the level of the organometallic center Zn_4O that is stronger than that at the BDC ligand.

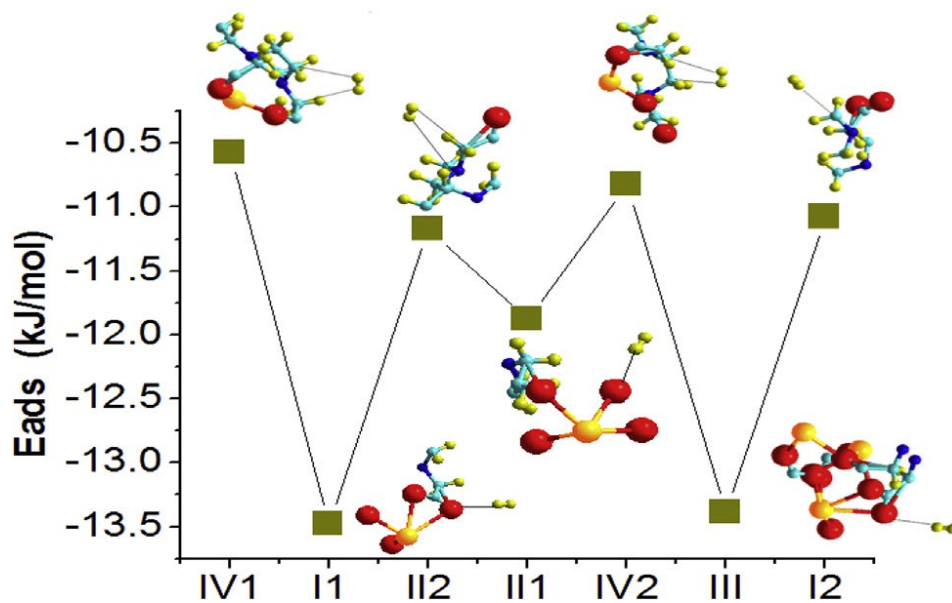


Figure 3: Adsorption energies of H_2 on different sites of Pb- MOF. The structures of cleaved fragments showing interactions with hydrogen molecules are inserted.

For all the sites considered, the interaction energies found are between -10.266 kJ/mol and -13.479 kJ/mol. These values are higher than those found for IRMOF-1 (-0.8 to -6.7 kJ/mol), PCN-61 (-6 and -6.5 kJ/mol) and for other MOFs (-4.8 to -12.9 kJ/mol). They are very close to that of Ni-MOF-74 (-13.5 kJ/mol) which has the highest hydrogen adsorption energy of all MOFs. They are also greater than the H_2 interaction energies with other types of nanostructured materials, such as carbon nanotubes (-4.6 kJ/mol for adsorption and -0.25 kJ/mol for confinement [39,40]). However, this Pb-MOF does not reach the optimal energy for H_2 adsorption (-15.1 kJ/mol) for its use as an energy source.

To improve the gas storage capacity, Yaghi et al. have recently synthesized new Aluminum-based MOFs, termed MOF-519 [41]. This new class of material retains a permanent porosity and exhibits high capacity of methane storage at ambient temperature and 77 K. The architecture of MOF-519 consists essentially of octametallic inorganic secondary build units (SBU) and 4,4',4''benzene-1,3,5-tryil-tribenzoate (BTB) as an organic linker (Figure 4).

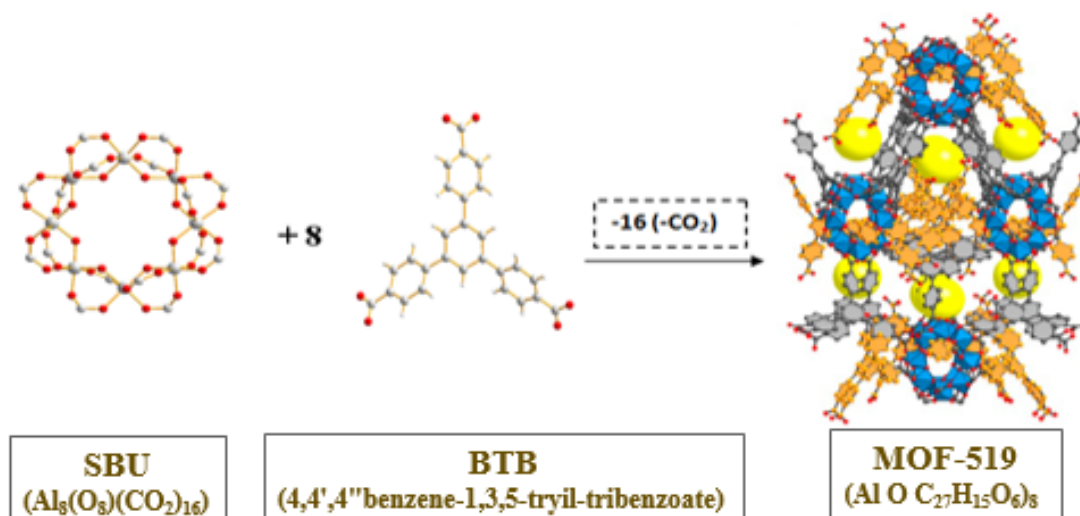


Figure 4: Representation of MOF-519 geometry.

We have used the density functional theory to study the hydrogen storage capacity of MOF-519. To adequately describe the effects of dispersion, all the computations reported in this paper are performed using Grimme's DFT-D3 method. We find that hydrogen molecule adsorption on the accessible surface inside the cavity occurs by physisorption at two sites, C₁ and C₂, with adsorption energies of -12.2 and -1.2 kJ/mol, respectively (Figure 5). Physisorption is slightly exothermic due to weak van der Waals interactions between hydrogen molecules and the surface dipole of the SBU [42].

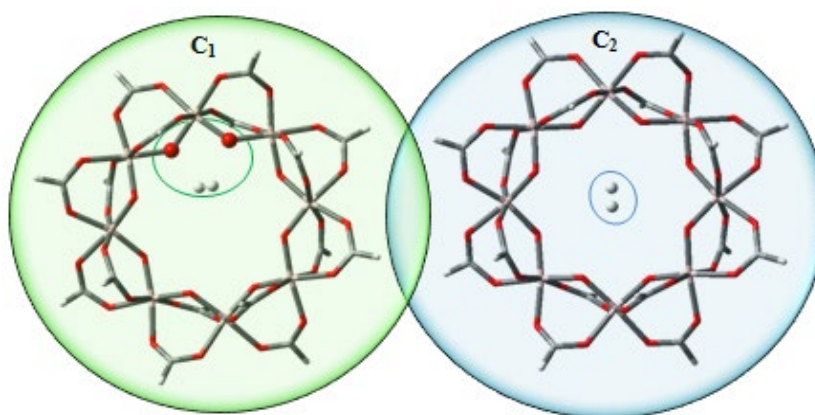


Figure 5: Optimized geometries of adsorbed hydrogen molecules inside SBU unit: Al, pink; O, red; C, grey; H, white sphere.

To completely describe MOF-519, we investigated the interaction between the hydrogen molecule and the BTB ligand. In order to determine the stable H₂ adsorption sites, hydrogen molecules were optimized in the vicinity of groups I and II. Optimization

calculations were performed with starting distances of three. The -COOH group was not considered since it was already studied with the unit SBU.

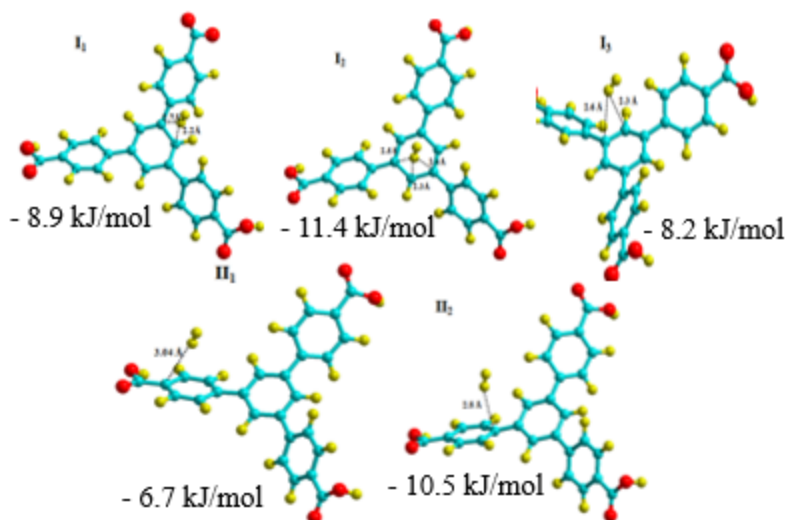


Figure 6: *Optimized structures and adsorption energies for hydrogen adsorption on BTB.*

The first region (I) has three adsorption sites, whereas the second region (II) has two favorable adsorption sites with energies between -6.7 kJ/mol and -11.37 kJ/mol. For phenyl group I the three most stable adsorptions sites are denoted I1, I2 and I3. For these sites, there is van der Waals physisorption with interatomic distances of 2.2 Å for I1 and 2.3 Å for I2 and I3 with adsorption energies of -8.9 kJ/mol, -11.4 kJ/mol and 8.2 kJ/mol, respectively. For the two adsorption sites of the second phenyl group (II1 and II2), the adsorption energies are -6.7 kJ/mol and -10.5 kJ/mol and interatomic distances are 3.04 and 2.8 Å. The geometric parameters of BTB are unchanged, with C-C bond lengths of 1.40 Å, and the bond length of the adsorbed H₂ is almost unchanged at 0.75 Å.

Overall, MOF-519 showed an interactions with H₂ comparable to that of Pb-MOF and Ni-MOF-74 and more important than the other MOFs that are studied for storage hydrogen.

3. Grand Canonical Monte Carlo (GCMC) for gravimetric and volumetric uptakes

Most theoretical studies in the literature use Grand Canonical Monte Carlo GCMC to evaluate the ability of MOFs to store hydrogen under specific thermodynamic conditions. Its main advantage is that it provides quantitative results that can be directly compared with the experimental values. For example, this method makes it possible to calculate the

gravimetric and volumetric capacity of the hydrogen stored in a structure defined at the molecular level. This approach makes it possible to calculate the isotherms and isobars of H₂ adsorption at different pressures up to 100 bar for a temperature range from 77 to 360 K [43,44]. We have summarized in Table 2 the gravimetric and volumetric uptakes of several MOFs to store hydrogen at room temperature and at 77 K.

Table 2: Gravimetric and volumetric capacities of some MOFs for hydrogen storage at room temperature and temperature 77 K.

MOFs	Gravimetric uptakes (wt%)	Volumetric uptakes (g/L)	T _{ads} (K)
MOF-5 [45,46]	5.10 (35 bar)	37.2 (35 bar)	77
	0.6 (100 bar)	-	298
MIL-101 [47]	6.1 (60 bar)	30.5 (35 bar)	77
	0.3 (70 bar)	1.84 (80 bar)	298
MOF-74 (Mg) [48]	2.26 (35 bar)	24.8 (35 bar)	77
	6.4 (70 bar)	27.8 (56 bar)	77
PCN-610 [49]	1.82 (1 bar)	-	298
	3.60 (35 bar)	37.3 (35 bar)	77
HKUST-1 [50,51]	1.12 (100 bar)	3.08 (65 bar)	298
	3.3 (30 bar)	35.6 (30 bar)	77
ZIF-8 [52]	0.13 (30 bar)	1.40 (30 bar)	298
	7.50 (35 bar)	21.2 (50 bar)	77
MOF-210 [53,54]	2.9 (95 bar)	-	298
	6.80 (35 bar)	36.9 (35 bar)	77
MOF-177 [55]	1.50 (100 bar)	9.5 (100 bar)	298
	2.3 (26 bar)	27 (26 bar)	77
MOF-74 [56]	8.10 (35 bar)	16.4 (50 bar)	77
	0.28 (90 bar)	-	298
MOF-200 [57]	6.24 (35 bar)	35 (33 bar)	77
	0.66 (90 bar)	3.74 (90 bar)	298
PCN-61 [58]	6.65 (35 bar)	29.6 (45 bar)	77
	0.78 (99 bar)	3.5 (90 bar)	298
PCN-66 [59]	7.32 (35 bar)	28 (50 bar)	77
	1.01 (35 bar)	4.10 (90 bar)	298
PCN-68 [60]	1.3 (35 bar)	28 (35 bar)	77
	0.22 (100 bar)	4.3 (100 bar)	298
Pb-MOF [38]	9.7 (35 bar)	59.2 (35 bar)	77
	3.3 (100 bar)	18.3 (100 bar)	298
MOF-519 [42]			

We applied GCMC simulations for Pb-MOF and MOF-519 using a code based on the DL_POLY2 molecular dynamics package [61] that has been previously applied to study gas adsorption in MOFs [62,63]. The atomic positions of the SBU unit were fixed in the simulations. Nonbonding interactions were calculated using Lennard-Jones (LJ) potentials and electrostatic interactions calculated with partial atomic charges. The LJ parameters for the fragment of the MOF were assigned from the universal force field (UFF) [64] and partial atomic charges were assigned by a charge equilibration method that was fitted to reproduce the quantum mechanical electrostatic potentials in nanoporous materials.

Firstly, we started by simulating the hydrogen adsorption isotherm at two different temperatures ($T = 77\text{K}$ and $T = 298\text{K}$) by varying the pressure from 0.1 to 100 bar. We impose this restriction because it allows us to compare our results with those already published in the literature. The gravimetric and volumetric capacities of Pb-MOF and MOF-519 are shown in the figure 7-a and 7-c.

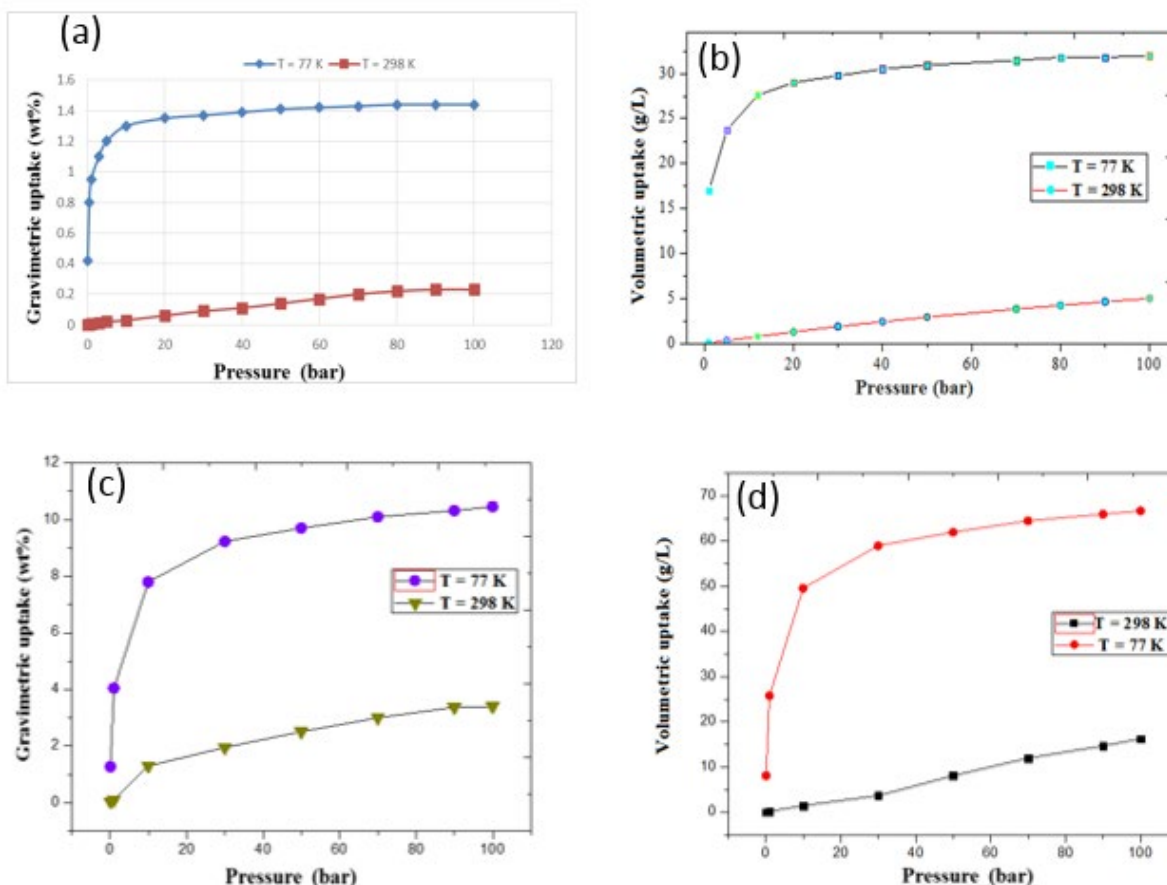


Figure 7: Simulated hydrogen adsorption isotherms for MOF-519 at 298 K and 77 K and at different pressures up to 100 bar.

It is clear that the gravimetric and volumetric capacity increase with the pressure. Under the cryogenic conditions of hydrogen storage (77 K), the gravimetric capacity of Pb-MOF does not exceed 1.5 wt%. It varies between 0.4 and 1.5 wt% for the pressures 0.1 and 100 bar. This is very small compared to the results found for other nano-porous materials (Figure 8). Whereas, MOF-519 has a high specific gravity of hydrogen adsorption which exceeds 10 wt% at 77 K and 100 bar. At the pressure $P = 35$ bar, the capacity of MOF-519 is 9.4 wt%. These values are larger than those given by other MOFs such as MOF-177 (6.8 wt%), MOF-210 (7.5 wt%) and MOF-200 (8.10 wt%) which are the most efficient in this field of application with the same conditions of temperature and pressure.

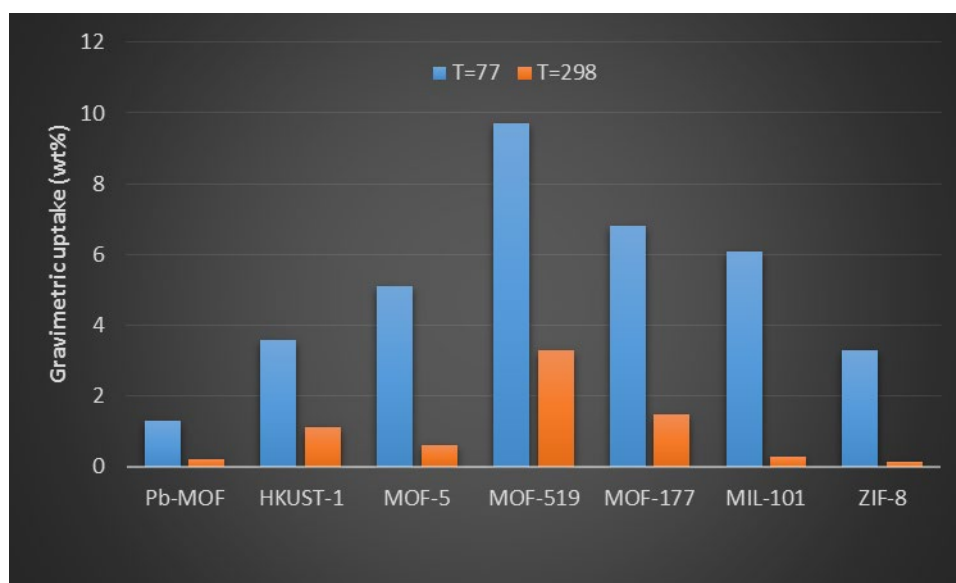


Figure 8: Comparison of the gravimetric capacities of different MOFs at 77 K and 298 K.

At room temperature, we note that the mass capacity of Pb-MOF varies between 0.02 and 0.23 wt% (Figure 7). This is similar to that given by ZIF-8 (0.13 wt%) and MIL-101 (0.3 wt%). But it is very weak compared to the mass capacities shown by other MOFs such as MOF-177 (1.5 wt% at 100 bar) and HKUST-1 (1.12 wt% at 100 bar). Thus, the mass capacity of MOF-519 can reach the value of 3.8 wt% which is the most important of all materials used for storing hydrogen.

The low gravimetric capacity of Pb-MOF can be explained by the importance of lead atom mass which constitutes this MOF. So it is necessary to determine volumetric storage capacity and compare it to that of other materials.

The results of the simulation of the volumetric capacity of Pb-MOF and MOF-519 to adsorb the molecular dihydrogen are illustrated in Figure 7-b and 7-d. We performed the simulations under the same conditions of the temperatures and pressures as the isotherms of the gravimetric capacity. It is clear that the Pb-MOF has a large volumetric capacity at the temperature 77 K which varies between 16 g/L at the pressure 0.1 bar and 32 g/L at the pressure 100 bar. This performance is similar to those given by other MOFs as shown in Figure 9. Also, MOF-519 has the best volumetric capacities compared to other materials tested for the hydrogen storage domain. Indeed, the volumetric capacity of this MOF exceeds the values 65 g/L and 16 g/L at the temperature 77 K and 298 K, respectively (Figure 9). These values are the most important compared to those of all the materials used for the storage of molecular hydrogen.

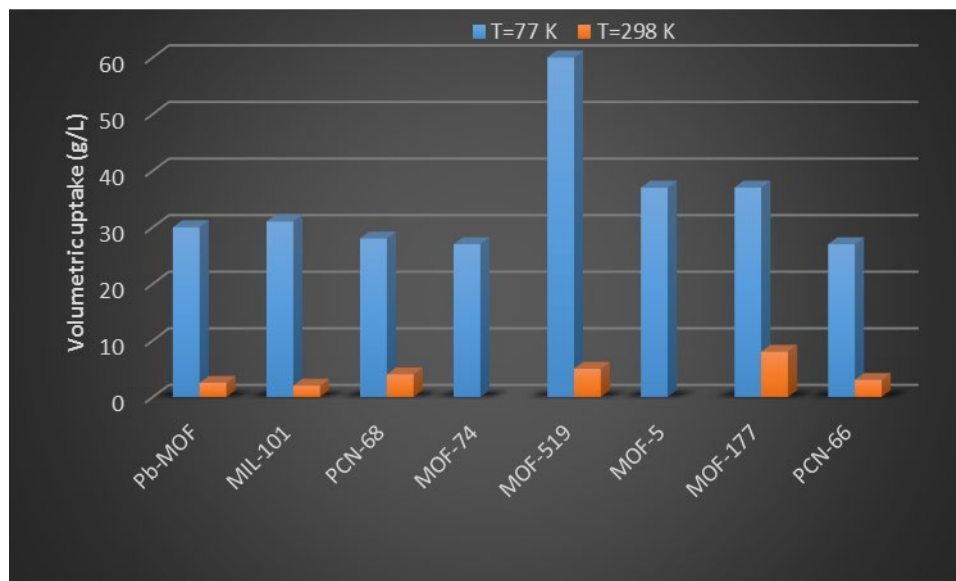


Figure 9: Comparison of the volumetric capacities of different metal organic frameworks at 77 K and 298 K.

To compare the adsorption performance of Pb-MOF and MOF-519 with the target DOE values, it proved to be interesting to perform simulations under the conditions recommended by the DOE. We determined the H₂ adsorption isobar at the pressure 100 bar by varying the temperature from 233 K up to 360 K. The results are shown in Figure 10.

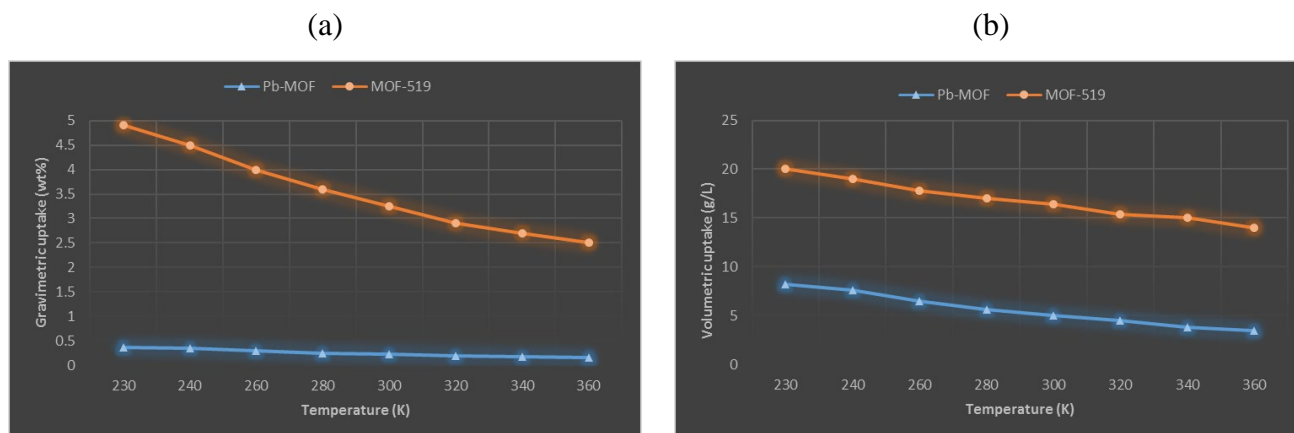


Figure 10: The H_2 adsorption isobars simulated for Pb-MOF and MOF-519 at $P = 100$ bar and at temperatures ranging from 230 K up to 360 K: (a) is the gravimetric capacity and (b) is the volumetric capacity.

Conclusion

It is remarkable that the adsorption capacity decreases with increasing temperature. The gravimetric capacity of Pb-MOF varies between 0.37 wt% and 0.15 wt% (Figure 10-a). Thus, its volumetric capacity reached the value of 8.2 g/L (Figure 14-b). This is negligible compared to the US Department of Energy's target value (5.5 wt% and 40 g/L) for the reversible storage of hydrogen. It is also noted that the MOF-519 has a high gravimetric capacity (4.9 wt% at $T = 233$ K) which is very close to the US Department of Energy's target value DOE. On the other hand, its volumetric capacity (20.3 g/L at $T = 233$ K) remains lower than the target value.

Reference

- [1] Satyapal S, Petrovic J, Read C, Thomas G, Ordaz G, Catal Today 2007;120:246-56. <https://doi.org/10.1016/j.cattod.2006.09.022>
- [2] S.M. Aceves, G.D. Berry, J. Martinez-Frias, F. Espinosa-Loza. Int. J. Hydro. Energy 2006;31:2274-2283. <https://doi.org/10.1016/j.ijhydene.2006.02.019>
- [3] B. Sakintuna, F. Lamari-Darkrim, M. Hirscher. Int. J. Hydrogen Energy 2007;32:1121-1140. <https://doi.org/10.1016/j.ijhydene.2006.11.022>
- [4] Z.X Guo, C. Shang, K.F Aguey-Zinsou. J. Eur. Cer. Soc. 2008;28:1467-1473. <https://doi.org/10.1016/j.jeurceramsoc.2007.12.019>

- [5] A. Zaluska, L. Zaluski, J.O Ström-Olsen. *J. Alloy. Compd.* 1999;288:217-225.
[https://doi.org/10.1016/S0925-8388\(99\)00073-0](https://doi.org/10.1016/S0925-8388(99)00073-0)
- [6] A. Zaluska, L. Zaluski, J.O Ström-Olsen. *J. Alloy. Compd.* 2000;298:125-134.
[https://doi.org/10.1016/S0925-8388\(99\)00666-0](https://doi.org/10.1016/S0925-8388(99)00666-0)
- [7] P. Chen, Z. Xiong, J. Luo, J. Lin, K.L Tan. *Nature* 2002;420:302-304.
<https://doi.org/10.1038/nature01210>
- [8] A. Züttel, P. Wenger, S. Rentsch, P. Sudan, P. Pauron, C. Emmegder. *J. Power Sources* 2003;118:1-7. [https://doi.org/10.1016/S0378-7753\(03\)00054-5](https://doi.org/10.1016/S0378-7753(03)00054-5)
- [9] Liu Z, Xue Q, Ling C, Yan Z, Zheng J. Hydrogen storage and release by bending carbon nanotubes. *Compu Mater Sci* 2013;68:121-6.
<https://doi.org/10.1016/j.commatsci.2012.09.025>
- [10] Chattaraj PK, Bandaru S, Mondal S. Hydrogen storage in clathrate hydrates. *J Phys Chem A* 2011;115:187-93. <https://doi.org/10.1021/jp109515a>
- [11] Surya VJ, Iyakutti K, Mizuseki H, Kawazoe Y. Modification of graphene as active hydrogen storage medium by strain engineering. *Comput Mater Sci* 2012;65:144-8.
<https://doi.org/10.1016/j.commatsci.2012.07.016>
- [12] Gtari WF, Tangour B. A theoretical study of the dihydrogen molecule confined inside carbon nanotube. *Int J Quantum Chem* 2013;113:2397-404.
<https://doi.org/10.1002/qua.24474>
- [13] Collins DJ, Zhou HC. Hydrogen storage in metal-organic frameworks. *J Mater Chem* 2007;17:3154-60. <https://doi.org/10.1039/b702858j>
- [14] Li JR, Kuppler RJ, Zhou HC. Selective gas adsorption and separation in metal-organic frameworks. *Chem Soc Rev* 2008;38:1477-504.
<https://doi.org/10.1039/b802426j>
- [15] Murry LJ, Dinca M, Long JR. Hydrogen storage in metal organic frameworks. *Chem Soc Rev* 2009;38:1294-314. <https://doi.org/10.1039/b802256a>
- [16] Hu YH, Zhang L. Hydrogen storage in Metal-Organic frameworks. *Adv Mater* 2010;22:117-30. <https://doi.org/10.1002/adma.200902096>
- [17] Calleja G, Botas JA, Sánchez MS, Orcajo MG. Hydrogen adsorption over Zeolite-like MOF materials modified by ion exchange. *Int J Hydrogen Energy* 2010;35:9916-23. <https://doi.org/10.1016/j.ijhydene.2010.02.114>
- [18] Satyapal, S.; Petrovic, J.; Thomas, G. *Sci. Am.* 2007, 81–87.

- [19] Srepusharawoot P, Swatsitang E, Amornkitbamrung V, Pinsook U, Ahuja R. Hydrogen adsorption of Li functionalized covalent organic framework-366: An ab initio study. *Int J Hydrogen Energy* 2013;38:1-5.
<https://doi.org/10.1016/j.ijhydene.2013.08.102>
- [20] DOE. Hydrogen and fuel cells program. 2013.
http://www.hydrogen.energy.gov/annual_progress13_storage.html.
<https://doi.org/10.2172/1219580>
- [21] N.L. Rosi, J. Eckert, M. Eddaoudi, D.T. Vodak, J. Kim, et al. *Science* 2003;300:1127-1129. <https://doi.org/10.1126/science.1083440>
- [22] K.A. Forrest, T. Pham, K. McLaughlin, J.L. Belof, A.C. Stern, M.J. Zaworotko, B. Space. *J. Phys. Chem. C* 2012;116:15538-15549. <https://doi.org/10.1021/jp306084t>
- [23] Bhatia, S. K.; Myers, A. L. *Langmuir* 2006, 22, 1688-1700.
<https://doi.org/10.1021/la0523816>
- [24] Mueller T, Ceder G. A Density Functional Theory Study of Hydrogen Adsorption in MOF-5. *J Phys Chem B* 2005; 109:17974-83. <https://doi.org/10.1021/jp051202q>
- [25] Srepusharawoot P, Araujo CM, Blomqvist A, Scheicher RH, Ahuja R. A comparative investigation of H₂ adsorption strength in Cd- and Zn-based metal organic framework-5. *J Chem Phys* 2008;129:164104-5.
<https://doi.org/10.1063/1.2997377>
- [26] Lee TB, Kim D, Jung DH, Choi SB, Yoon JH, Kim J, et al. Understanding the mechanism of hydrogen adsorption into metal organic frameworks. *Catal Today* 2007;120:330-5. <https://doi.org/10.1016/j.cattod.2006.09.030>
- [27] Kuc A, Heine T, Seifert G, Duarte HA. On the nature of the interaction between H₂ and metal-organic frameworks. *Theor Chem Account* 2008;120:543-50.
<https://doi.org/10.1007/s00214-008-0439-2>
- [28] Vitillo JG, Regli L, Chavan S, Ricchiardi G, Spoto G, Dietzel PDC, et al. Role of exposed metal sites in hydrogen storage in MOFs. *J Am Chem Soc* 2008;130:8386-96.
<https://doi.org/10.1021/ja8007159>
- [29] Uzun A, Keskin S. Site characteristics in metal organic frameworks for gas adsorption. *Int J Hydrogen Energy* 2014;39:56-79.
<https://doi.org/10.1016/j.progsurf.2013.11.001>
- [30] Forrest KA, Tony P, Ke ML, Belof JL, Stern AC, Zaworotko MJ. Simulation of the Mechanism of Gas Sorption in a Metal–Organic Framework with Open Metal Sites:

- Molecular Hydrogen in PCN-61. *J Phys Chem C* 2012;116:15538–49.
<https://doi.org/10.1021/jp306084t>
- [31] X.D. Zhu, T.X. Tao, W.X. Zhou, F.H. Wang, R.M. Liu, et al. *Inorg. Chem. Commun.* 2014;40:116-119. <https://doi.org/10.1016/j.inoche.2013.11.042>
- [32] Kresse G, Hafner J. Ab initio molecular dynamics for liquid metals. *Phys Rev B* 1993;47:558-61. <https://doi.org/10.1103/PhysRevB.47.558>
- [33] Kresse G, Hafner J. Ab initio molecular-dynamics simulation of the liquid-metal-amorphous-semiconductor transition in germanium. *Phys Rev B* 1994;49:14251-69. <https://doi.org/10.1103/PhysRevB.49.14251>
- [34] Blochl PE. Projector augmented-wave method. *Phys Rev B* 1994;50:17953-79. <https://doi.org/10.1103/PhysRevB.50.17953>
- [35] Kresse G, Joubert D. From ultrasoft pseudopotentials to the projector augmented-wave method. *Phys Rev B* 1999;59:1758-75. <https://doi.org/10.1103/PhysRevB.59.1758>
- [36] Hammer B, Hansen LB, Norskov JK. Improved adsorption energetics within density-functional theory using revised Perdew-Burke-Ernzerhof functionals. *Phys Rev B* 1999;59:7413-21. <https://doi.org/10.1103/PhysRevB.59.7413>
- [37] Perdew JP, Burke K, Ernzerhof M. Generalized gradient approximation made simple. *Phys Rev Lett* 1997;78:1396. <https://doi.org/10.1103/PhysRevLett.78.1396>
- [38] S. Rahali, M. Seydou, Y. Belhocine, F. Maurel, B. Tangour, *Int. J. Hydrogen Energy* 2016;41:2711-2719 <https://doi.org/10.1016/j.ijhydene.2015.12.153>
- [39] Schimmel HG, Kearley GJ, Nijkamp MG, Visserl CT, De Jong KP, Mulder FM. Hydrogen adsorption in carbon nanostructures: comparison of nanotubes, fibers, and coals. *Chem Eur J* 2003;9:4764-70. <https://doi.org/10.1002/chem.200304845>
- [40] Gtari WF, Tangour B. A theoretical study of the dihydrogen molecule confined inside carbon nanotubes. *Int J Quantum Chem* 2013;113:2397-404. <https://doi.org/10.1002/qua.24474>
- [41] Gándara F, Furukawa H, Lee S, Yaghi OM. High Methane Storage Capacity in Aluminum Metal–Organic Frameworks. *J Am Chem Soc* 2014;136:5271–4. <https://doi.org/10.1021/ja501606h>
- [42] S.Rahali, Y.Belhocine, M. Seydou F.Maurel, B. Tangour, *Int. J. Hydrogen Energy* 2017

- [43] L. Sarkisov, T. Düren, R.Q. Snurr. *Mol. Phys.* 2004;102:211-221.
<https://doi.org/10.1080/00268970310001654854>
- [44] G. Garberoglio, A.I. Skoulidas, J.K. Johnson. *J. Phys. Chem. B* 2005;109:13094-13103. <https://doi.org/10.1021/jp050948l>
- [45] A.G. Wong-Foy, A.J. Matzger, O.M. Yaghi. *J. Am. Chem. Soc.* 2006;128:3494-3495. <https://doi.org/10.1021/ja058213h>
- [46] S.S. Han, W.A. Goddard. *J. Am. Chem. Soc.* 2007;129:8422-8423.
<https://doi.org/10.1021/ja072599+>
- [47] M. Latroche, S. Surblé, C. Serre, C.M. Draznieks, P. Lewellyn, et al. *Angew Chem.* 2006;45:8227-8231. <https://doi.org/10.1002/anie.200600105>
- [48] H. Wu, W. Zhou, T. Yildirim. *J. Am. Chem. Soc.* 2009;131:4995-5000.
<https://doi.org/10.1021/ja900258t>
- [49] O.K. Farha, A.O. Yazadyn, I. Eryazici, C.D. Malliakas, B.G. Hauser, et al. *Nat. Chem.* 2010; 2:944-948. <https://doi.org/10.1038/nchem.834>
- [50] J.L.C. Rowsell, O.M. Yaghi. *J. Am. Chem. Soc.* 2006;128:1304-1315.
<https://doi.org/10.1021/ja056639q>
- [51] Y.W. Li, R.T. Yang. *AIChE J.* 2008;54:269-279. <https://doi.org/10.1002/aic.11362>
- [52] W. Zhou, H. Wu, M. R. Hartman, T. Yildirim, *J. Phys. Chem. C* 2007; 111:16131-16137. <https://doi.org/10.1021/jp074889i>
- [53] H. Furukawa, N. Ko, Y.B. Go, N. Aratani, S.B. Choi, E. Choi, et al. *Science* 2010;329:424-428. <https://doi.org/10.1126/science.1192160>
- [54] M. Cortés, L.J. Han, S. Soo, G. Wa, A. William. *J. Phys. Chem.* 2012;6:1621-1631.
- [55] Y.W. Li, R.T. Yang. *Langmuir* 2007;23:12937-12944.
<https://doi.org/10.1021/la702466d>
- [56] A.G. Wong-Foy, A.J. Matzger, O.M. Yaghi, *J. Am. Chem. Soc.* 2006;128:3494-3495. <https://doi.org/10.1021/ja058213h>
- [57] H. Furukawa, N. Ko, Y.B. Go, N. Aratani, S.B. Choi, E. Choi. *Science* 2010;329:424-428. <https://doi.org/10.1126/science.1192160>
- [58] D. Yuan, D. Zhao, D. Sun, H.C. Zhou. *Angew Chem. Int. Ed.* 2010;49:5357-5361.
- [59] M.P. Suh, H.J. Park, T.K. Prasad, D.W. Lim. *Chem. Rev.* 2012;112:782-835.
<https://doi.org/10.1021/cr200274s>

- [60] Z. Guo, H. Wu, G. Srinivas, Y. Zhou, S. Xiang, et al. Chen B Angew Chem. Int. Ed. 2011;50:3178-3181. <https://doi.org/10.1002/anie.201007583>
- [61] Smith W, Forester TR. DL_POLY_2.0: a general-purposeparallel molecular dynamics simulation package. J Mol Graph 1996;14:136-41. [https://doi.org/10.1016/S0263-7855\(96\)00043-4](https://doi.org/10.1016/S0263-7855(96)00043-4)
- [62] Vaidhyanathan R, Iremonger SS, Shimizu GKH, Boyd PG, Alavi S, Woo TK. Direct observation and quantification of CO₂ binding within an amine functionalized nanoporous solid. Science 2010;330:650-3. <https://doi.org/10.1126/science.1194237>
- [63] Vaidhyanathan R, Iremonger SS, Shimizu GKH, Boyd PG, Alavi S, Woo TK. Competition and cooperativity in carbon dioxide sorption by amine functionalized metal-organic frameworks. Angew Chem Int Ed Engl 2012;51:1826-9. <https://doi.org/10.1002/anie.201105109>
- [64] Rappe AK, Casewit CJ, Colwell KS, Goddard WA, Skiff WM. UFF a full periodic table force field for molecular mechanics and molecular dynamics simulations. J Am Chem Soc 1992;114:10024-35. <https://doi.org/10.1021/ja00051a040>

Chapter 2

Metal Organic Frameworks Based Materials for Renewable Energy Applications

Haydar Göksu^{1*}, Nursefa Zengin¹, Fatih Şen^{2*}

¹ Kaynasli Vocational College, Duzce University, 81900 Duzce, Turkey

² Sen Research Group, Department of Biochemistry, Dumlupınar University, 43100 Kütahya, Turkey

haydargoksu@duzce.edu.tr, fatih.sen@dpu.edu.tr

Abstract

Crystalline metal-organic frames (MOFs) fall into the category of high potential porous materials that can be used in gas storage, adsorption / separation, adsorption as adsorbent, catalysis, magnetism, sensor design and drug delivery. MOFs are typically formed by self-assembly, where secondary building units (SBUs) are connected with organic ligands to form complex networks. Organic ligands or metallic SBUs may be modified to be critical for their functionality and utility for specific applications in order to control the porosity of MOFs. MOFs are used in renewable energy and environmental applications, application of hydrogen energy, hydrogen storage, storage and conversion of CO₂, biogas production, thermal energy storage, rechargeable batteries and supercapacitors and in dye sensitized solar cells.

Keywords

Metal Organic Frameworks, Renewable Energy, Storage, Hydrogen, Biogas

Contents

1. Introduction.....	20
2. Need for renewal energy	21
3. Metal organic frameworks.....	22
4. MOFs for environmental applications and renewable energy	23
5. Metallic organic framework based materials for hydrogen energy applications	23

6. Hydrogen Storage by MOFs	24
7. Storage of gases and separation process by MOFs	24
8. Metal organic frameworks based materials for conversion and storage of CO₂.....	25
9. Use of MOFs for biogas.....	25
10. Storage of thermal energy using MOF materials	26
11. Metal organic frameworks based materials for oxygen catalysis	26
12. MOF based materials for rechargeable batteries and supercapacitors.....	26
13. Metal organic framework based materials in the use of dye sensitized solar cells	27
Conclusion.....	28
References	28

1. Introduction

Renewable (alternate) sources, which are free in nature and which constitute the inexhaustible energies once used, have the potential to play an important role in the solution of today's energy bottleneck and other environmental problems. Nowadays, a trend is shifting from the conventional energy systems of fossil origin to renewable energy systems. The fact that fossil reserves are limited in nature and inevitably will be exhausted makes the search for alternative sources mandatory. On the other hand, the increase in the negative conditions created by the use of fossil resources on the environment has revealed the necessity of dangerous and harmful effects for people. In recent years, global warming has reached the line phases and climate change has been the basis of natural disasters.

In the scenario created by the International Energy Agency for the year 2020, it is foreseen that the energy source CO₂ emissions will increase by 6%. In order to prevent this, additional investments in energy efficiency and low carbon technology should be made up to approximately \$430 billion by 2020 [1]. The globalizing world needs alternative energies to sustain its development under these harsh conditions. The energy demand of the growing human population is shown as a source of renewable energy as a

source that can respond to the security of the ecological balance and to ensure supply security.

Today, alternative energy sources in the commercial sector are hydraulic, wind, thermal, solar, hydrogen and biogas energy. Apart from these, it is possible to produce energy technically and there are also marine energy types with low economic dimensions. Alternative energy sources are in high demand because of climate change, energy security and pollution concerns. At this point, it is obvious that the consumption of fuels cause CO₂ gas release, especially in a way that disrupts the natural balance of the atmosphere, which is unsustainable neither economically nor environmentally.

In this respect, renewable and green energy sources stand out in this study: Hydro energy, Biogas, Solar energy, Thermal energy and Bio alcohols. The question of whether there will be a solution to the problems encountered in reaching and storing these energy sources will be discussed by asking if use of Metallic Organic Frameworks (MOFs) is appropriate or preferable.

2. Need for renewal energy

Our climate is changing as a result of our greenhouse gas emissions. Increased heat waves and droughts, heavy rains are perturbative signs. The world's climate is highly complex and there are significant uncertainties in predicting future risks. Furthermore, the presence of large traps holding greenhouse gases in the depths of the ocean and the reversal of the heat generated by this will take quite a long time [2]. Even if the greenhouse gas emissions are zeroed, we need to wait for centuries to stabilize the Earth's temperature. It is not right to lose more time to minimize greenhouse gas emissions. No further evidence is needed to take a quick step.

Even though fossil fuels have been seen as an important energy source for years, it is imperative that the emission be reset. While increasing amounts of nuclear and renewable energy are being converted into electricity in industrial applications, home applications such as lighting, cleaning and air conditioning reduce the carbon footprint in buildings. Additionally, developments about buildings reduce the carbon footprint. In this way, renewable energies can be stored even if they are not long lasting. Nowadays, it is necessary to talk about renewable energy sources which are obtained by using agricultural wastes instead of natural gas and oil industry. In particular, in the event of a reduction in costs, new catalyst systems will be developed for the use of certain waste solvents, as well as CO₂ and water, both as fuel and in chemical transformations. Furthermore, metal-organic frames are used to capture carbon from energy production, cement, aluminum, steel and plastic production and ultimately from the atmosphere [3].

3. Metal organic frameworks

Metal organic frames (MOF) are porous materials formed from metal containing organic binders and nodes. Because of their structural and functional adaptability as well as their ever-expanding scope of application, MOFs have become one of the most impressive material classes for scientists and engineers. It has been comprehensively studied not only for basic interests like catalytic intermediate capture and energy transfer, but also for practical applications such as storage and separation of gas, biomedical applications, heterogeneous catalysis, proton transmission and chemical detection [4].

When metal organic frames are used for specific applications, frame integrity has to be guaranteed to protect the functionality and features of their purposes. Actually, water or moisture is generally found in industrial applications like catalysis often need stability against coordinating anions. The imbalance of many metal organic frames in difficult conditions has significantly limited their both application and commercialization. Hence, the chemical stability of metal-organic frames has been increasing in the recent years. Researchers are trying to point the stability of metal organic frames in different conditions to understand ways of decomposition and to create more stable frame structures [5].

MOFs are structures in which organic ligands and metal oxides combine with covalent bonds. In this way, permanent porosity is supported and stable expanded structures are obtained. Both organic and inorganic components of MOFs can vary in their shape, size, composition, geometry and branching to produce a versatile porous crystalline solids class [6]. For this reason, the pore shape and size is designed to produce almost ultra-porous ($7,000 \text{ m}^2 \text{ g}^{-1}$ inner BET surface area) and MOF with pore sizes up to 98 \AA [7]. Metal oxide units and their rigidity and strong bond have led to a large number of MOFs with high architectural, thermal and chemical stability [8]. These properties have allowed covalent functionality, whereby internal cavity gaps are modified by performing reactions in organic binders and open metal regions. These modifications include the coordination of organic reactions, the coordination of ligands to open metal regions and the metallization of organic binders. The precision of producing and modifying MOFs, coupled with the preservation of high crystallinity after modification, motivated their work to refer to several examples in many applications, such as gas adsorption, selective separation, catalysis and imaging [9]. The term MOF was introduced in 1995 and the number added is roughly chronological exploration. Other terms are used in the nomenclature of MOFs, usually by the abbreviation of the location of discovery (eg HKUST, Hong Kong Science and Technology University) or by using a number of features (eg, PCN, porous coordination network) and then a number [10].

4. MOFs for environmental applications and renewable energy

Global energy consumption has increased exponentially in recent years and is expected to increase by 56% by 2040. In particular, the total energy consumption in 2010 was 524 quadrillion British thermal units (Btu). It is expected that this value will rise to 630 quadrillion Btu in the 2020s and in the 2040s it will be 820 quadrillion Btu [11]. Today, the ratio of fossil fuels to consumable global energy sources is about 80%, this causes vital energy crisis. This situation also causes global warming. These topics call on scientists to take advantage of environmentally friendly energy sources, including wind power, hydro energy and solar energy [12]. In order to benefit from these renewable energy sources, it is inevitable to balance energy efficient storage and storage systems. In addition, researchers are trying to achieve promising renewable energy through reducing global carbon emissions and capturing and converting carbon dioxide.

The actualisation of these enhanced applications is largely based on the use of developed exploited materials [13]. By utilizing very high porosity, controllable pore size, crystal structure and well-arranged structures, MOFs were applied in gas uptake. Moreover, the composite materials obtained by combining the metal organic frames with different materials have superior properties due to the synergistic effect between functional structures [14]. Also, the nanostructured MOFs are extensively studied as a precursor in the preparation of various nanomaterials with various porous structures from carbonaceous materials to metal based ones. We provide a comprehensive overview of metal organic frameworks based materials focusing on the use of hydrogen (H_2) adsorptions-evolutions, storage-conversion of CO_2 , rechargeable batteries, super capacitors and solar cells, oxygen catalyst.

5. Metallic organic framework based materials for hydrogen energy applications

Hydrogen gas is an alternative source available from internal sources and can be used as fuel in zero emission energy producers. However, because of the high pressure requirements in hydrogen storage, there are concerns for the automotive sector. Methods have been developed as a solution to this problem. One of them is to make storage in porous structures. Many porous structures store hydrogen by the interaction of weak Van Der Waals bonds. A stronger mechanism is also provided with metal nanoparticles. At this point, the use of porous MOFs is important because hydrogen storage is an alternative fuel for next generation vehicles [15].

6. Hydrogen Storage by MOFs

The description of metal organic frameworks refers the ability of adsorption-storage of gas. Former President of the United States G.W. Bush published an initiative program of hydrogen energy, that largely supported the storage of hydrogen exploration by metal organic frameworks based materials. This soon opened the door to a new investigation. The metal organic frameworks' hydrogen storage capability in 2003, then so many of metal organic frameworks were created and developed or stored in hydrogen [16]. Very high pore volume and surface area and also low density, metal organic frameworks offer excellent capacity gravimetric H_2 towards the store. Despite the continuous improvement of technology in the structural optimization and design of metal organic structures, the target is still hard to achieve. One possible cause is the adsorption force in the hydrogen tank, which has been weakened at elevated operating temperatures, based on Van Der Waals' weak working interactions. This difficulty has been tried to be overcome by scientists adding several adsorption sites to MOFs matrices, as observed with high isometric heat, to increase the interaction between hydrogen molecules and MOFs [17].

7. Storage of gases and separation process by MOFs

MOFs are a new material used in the separation and storage of some gases. High gas storage capability, robustness, high renewability and crystallinity etc. have more superior features than other solid adsorbents. They are easily adjustable thanks to different combinations of organic ligands and metal salts. MOFs are materials used to control pore sizes, to place different functional groups into these pores and to give unique structural flexibility. MOFs can be successfully applied to carbon dioxide/methane (CO_2-CH_4) separation for biogas elevation. The structural and stable porosity properties of MOFs create an environment that strengthens the adsorption of gases and brings new technological developments together. Successfully implemented MOFs as adsorbent should expand the biogas application use as an eco-friendly and sustainable fuel. In addition to its effect on biogas formation, impurities (NH_3 , H_2S and H_2O) will need to be considered in terms of energy requirements and long-term stability for the regeneration of adsorptive materials [18].

As hydrogen, methane is also taken into account as a green energy gas. Compared to oil, due to the high hydrogen-carbon ratio, it can provide much more energy and has much lower carbon emissions. The locations of the methane adsorption sites have been recently described with a series of isomorphous porous MOFs with neutron powder diffraction studies of CD_4 adsorption in MOF-5 [19] and different unsaturated metal centers (UMCs) [20]. The information obtained from these works is very key for future designs of metal organic frameworks which have capacities of storage of high methane. However,

in order to further explain the structure-performance correlations, the pore size, ligand functionality, etc. on the methane uptake in metal organic frameworks can be determined.

8. Metal organic frameworks based materials for conversion and storage of CO₂

Concerns of global warming drew the attention of the unprecedented public to the problem of CO₂ emissions. Carbon dioxide, which is usually caused by the combustion of fossil fuels, is accumulating at high degree. In order to compensate for the levels of CO₂, it is obligatory to develop applicable CO₂ capture and retention technologies. Based on the latest technologies, amine-based web brushing systems are dominant and costly [21]. The adsorption of CO₂ using highly porous solids arouses an increasing attraction for CO₂ capture applications [22]. Metallic organic frameworks are interesting due to their high surface area [23].

Separation of CO₂ from flue gases is a key issue and has attracted worldwide interest. The tail-shaped surface and the adjustable frame make MOFS candidate for capturing and separating CO₂. In order to achieve a successful capture and storage of carbon dioxide by MOFs, various pore modifications have been studied in order to increase the affinity between them. These have proven to be effective in the unsaturated metal regions - alkylamine groups' implantation [24].

Reduction of anthropogenic carbon emissions will be an important challenge in the 21st century due to the global warming problem caused by atmospheric CO₂ accumulation (such as ocean acidification). Numerous efforts have been made for CO₂ capture, storage and development of materials for conversion from process flows and flue gases. MOF based materials benefiting from the structural features have made great progress for the above mentioned applications and attracted great attention. Although CO₂ storage is not one of renewable energy sources, it will reduce the need for energy in the long term by decreasing the negative impact of global warming.

9. Use of MOFs for biogas

The developments about renewable and green energy sources namely bio alcohols has attracted attention recently because of emerging scarcity of fossil resources and the accompanying critical environmental concerns [25]. Adsorptive separation by using porous materials is thought as one of the most cost effective and environment friendly ways of recovering bio alcohols from fermentation broth produced from biomass. The use of hydrophobic MOFs for adsorptive separation of alcohol/water mixture is a probable solution for his issue as they have a less strong affinity to water compared to other porous materials such as activated carbons, zeolites and polymeric resins which

have as well been tested for this application [26]. Adjustable internal surface properties and tunable pore size, and hydrophobicity are key criteria for such materials' adsorption performances [27].

10. Storage of thermal energy using MOF materials

The storage of thermal energy reveals an important technological aspect to use renewable energy. It also offers a large potential for low-cost CO₂ emissions. Common thermal energy storage ways are sensitive heat storage and latent heat storage. Sensitive heat storage systems are based on heat exchange. Its process is between oxide ceramics, concrete and energy storage materials such as molten salts, water and oil. It is important to ensure that thermal energy is stored at high efficiency by reducing the volume of the tank [28].

Metal organic frameworks materials brings higher adsorption capacity compared to zeolite and silica gel which are conventional absorbents are used in storage of energy. There is limited information on the performance of metal-organic framework materials in energy storage applications and their performance compared to conventional adsorbents called silica gel and zeolite. MOFs that can be used instead of these traditional materials are among the materials with high expectations [28].

11. Metal organic frameworks based materials for oxygen catalysis

Oxygen development and reduction reaction are the basis of devices used for many energy transformations. These include fuel cells and water splitting. Batteries are also in that category. Effectiveness of energy conversion reactions mentioned is significantly limited. The limitation comes by the calm reaction kinetics of oxygen-containing structures. These species demand effective catalysts to deal with the energy barrier. Recently, electrolyzers for the reactions mentioned are based on precious metals. In addition, high cost and limited availability have caused considerable damage. Damages are to large-scale commercial applications. Metal organic frameworks based materials were also investigated for water cleavage and oxygen-containing reactions in fuel cells [29].

12. MOF based materials for rechargeable batteries and supercapacitors

In recent years, it is observed that there is an increasing growth in portable electronic devices. As a source of energy used for electronic devices mentioned, rechargeable batteries are progressing rapidly. Materials derived from metal organic frameworks are becoming electrodes for new generation. Because they are useful for producing

rechargeable batteries. These batteries should be with long cycle life and high capacity [29].

For performing energy storage there is a need for speed. Supercapacitors with high power densities are becoming important part of these researches. At this point superior speed performance is also needed in that process. According to mechanisms for energy storage, super capacitors should be taken into account in a broad view. They can be divided into three categories. These are namely; 1) electrochemical double layer capacitors based on carbon electrodes. They might also be derivatives. Those store charges by adsorption. The adsorption takes place on the surface of electrode material. 2) reversible on the surface Pulsocapacitors based on MnO_2 , RuO_2 and metal carbides/nitrides, which store the charge using physic reaction; 3) integrated super capacitors (HSCs) comprising a battery type and a capacitive electrode, in an electrochemical cell get both high density as well as high energy power. Because of the coexistence of metallic and organic parts of metal organic frameworks, metal organic framework based materials generally have high porosity and high surface areas for supercapacitors, especially electrochemical double layer capacitors and sufficient electroactive areas for HSCs. Electrochemical double layer capacitors based on carbon materials have several values. These can be exemplified as fast charge and low weight. Discharge rates are important parameters for bipolar operational flexibility. Thanks to their rich chemistries, metal organic frameworks have been selected as promotive precursors for acquiring derivatives with compounds optimized for nanoparticles (NPCs) or EDLCs [29].

13. Metal organic framework based materials in the use of dye sensitized solar cells

Solar batteries are potential candidates of photoelectric conversion devices. The devices are recently under intensive inspection. By utilizing low cost-high efficiency semiconductor based paint-sensitive solar cells (DSSCs) have become a promotive applicant. There is a belief for bringing a breakthrough. This thoughts and hopes are motivating facts for solving the global energy crisis and efficiency of energy conversion. The semiconductor function of metal organic frameworks is well studied by theoretical calculations. Other developments and researchs also approve adaptation of MOFs can be managed by metal nodes. Modifying ligands and adjusting coordination modes between inorganic and organic molecules are also been considered as part of this process. When light harvesting capabilities and large surface areas are considered, the metal organic framework based materials would be examined as photoanodes. They can also be examined as excipients for electrode sensitivity in paint-sensitive solar cells [29, 31]

Conclusion

Renewable green energy and environmental improvement is one of the main issues humanity is trying to deal with. Development of advanced materials is critical in this process. Late researches have proven, metal organic frameworks materials work as next generation materials. Due to their unique properties and extremely impressive performances we are able to insist on that. Mostly, creation of metal organic frameworks based materials are relatively simple. They are also scalable. As a result, many metal organic frameworks-based material systems have been appropriately created to date. This developments comes with comets, morphologies, structures, features and functions. In this study, it is provided that a general overview of metal organic frameworks based materials that can be summarized in the field of green energy and environmental applications: 1) To be able to collect sunlight and storing gas (H_2 and CO_2) solid metal organic frameworks with adjustable components and uniform pore size distributions were used. 2) Metal organic frameworks integrated with inorganic materials have been researched. They are also used in photocatalytic energy conversion. For solar cells MOFs are also useful. Each component in Metal organic frameworks based composites has important functionality that can overcome the disadvantages of a single equivalent. This process also create synergistic effects for improved performance. 3) Areas like rechargeable batteries, electrocatalysis and super capacitors metal organic frameworks are so fascinating. Because metal organic frameworks based materials have perfect conductivity. Moreover its components namely electroactive species are developed well and useful for this kind of storage.

References

- [1] International Energy Agency (IEA), How The Energy Sector Can Deliver On A Climate Agreement InCopenhagen, October, 2009, p.17
- [2] Roemmich, D., Church, J., Gilson, J., Monselesan, D., Sutton, P., Wijffels, S., Unabated planetary warming and its ocean structure since 2006, Nat. Clim. Change, 2015, 5, 240–245. <https://doi.org/10.1038/nclimate2513>
- [3] Boot-Handford, M. E. et al. Carbon capture and storage update, Energy Environ. Sci., 2014, 7, 130–189. <https://doi.org/10.1039/C3EE42350F>
- [4] Sumida, K., Rogow, D. L., Mason, J. A., McDonald, T. M., Bloch, E. D., Herm, Z. R., Bae, T. H., Long, J. R., Carbon dioxide capture in metal-organic frameworks, Chem. Rev., 2012, 112, 724-781. <https://doi.org/10.1021/cr2003272>

- [5] Bai, Y., Dou, Y., Xie, L.-H., Rutledge, W., Li, J.-R., Zhou, H.-C., Zr-based metal-organic frameworks: design, synthesis, structure, and applications, *Chem. Soc. Rev.*, 2016, 45, 2327-2367. <https://doi.org/10.1039/C5CS00837A>
- [6] Yaghi, O. M., O’Keeffe, M., Ockwig, N. W., Chae, H. K., Eddaoudi, M., Kim, J., Reticular synthesis and the design of new materials, *Nature*, 2003, 423, 705–714. <https://doi.org/10.1038/nature01650>
- [7] Deng, H. et al. Large-pore apertures in a series of metal–organic frameworks, *Science*, 2012, 336, 1018–1023. <https://doi.org/10.1126/science.1220131>
- [8] Eddaoudi, M., Moler, D. B., Li, H., Chen, B., Reineke, T. M., O’Keeffe, M., Yaghi, O. M., Modular chemistry: secondary building units as a basis for the design of highly porous and robust metal–organic carboxylate frameworks, *Acc. Chem. Res.*, 2001, 34, 319–330. <https://doi.org/10.1021/ar000034b>
- [9] Furukawa, H., Cordova, K. E., O’Keeffe, M., Yaghi, O. M., The chemistry and applications of metal–organic frameworks, *Science*, 2013, 341, 1230444. <https://doi.org/10.1126/science.1230444>
- [10] Schoedel, A., Ji, Z., Yaghi, O. M., The role of metal–organic frameworks in a carbon-neutral energy cycle. *Nature Energy*, 2016, 1(4), 16034. <https://doi.org/10.1038/nenergy.2016.34>
- [11] Banerjee, A., Halvorsen, K.E., Eastmond-Spencer, A., and Sweitz, S.R. Sustainable development for whom and how? Exploring the gaps between popular discourses and ground reality using the Mexican *Jatropha* biodiesel case, *Environ. Manage*, 2017, 59, 912–923. <https://doi.org/10.1007/s00267-017-0848-x>
- [12] Kim, S.W., Seo, D.H., Ma, X., Ceder, G., and Kang, K., Electrode materials for rechargeable sodium-ion batteries: potential alternatives to current lithium-ion batteries, *Adv. Energy Mater.*, 2012, 2, 710–721. <https://doi.org/10.1002/aenm.201200026>
- [13] Yu, L., Wu, H.B., and Lou, X.W., Selftemplated formation of hollow structures for electrochemical energy applications, *Acc. Chem. Res.*, 2017, 50, 293–301. <https://doi.org/10.1021/acs.accounts.6b00480>
- [14] Zhu, Q.-L., and Xu, Q., Metal-organic framework composites, *Chem. Soc. Rev.*, 2014, 43, 5468–5512. <https://doi.org/10.1039/C3CS60472A>
- [15] Falcaro, P., Ricco, R., Yazdi, A., Imaz, I., Furukawa, S., Maspoch, D., Ameloot, R., Evans, J. D., Doonan, C. J., Application of metal and metal oxide nanoparticles at

- MOFs, *Coor. Chem. Rew.*, 2016, 307, 237-254.
<https://doi.org/10.1016/j.ccr.2015.08.002>
- [16] Rosi, N.L., Eckert, J., Eddaoudi, M., Vodak, D.T., Kim, J., O'keeffe, M., Yaghi, O.M., Hydrogen storage in microporous metal-organic frameworks, *Science*, 2003, 300, 1127–1129. <https://doi.org/10.1126/science.1083440>
- [17] Wang, L., Yang, R.T., New sorbents for hydrogen storage by hydrogen spillover-a review, *Energy Environ. Sci.*, 2008, 1, 268–279. <https://doi.org/10.1039/b807957a>
- [18] Chaemchuen, S., Kabir, N. A., Zhou, K., Verpoort, F., Metal–organic frameworks for upgrading biogas via CO₂ adsorption to biogas green energy, *Chemical Society Reviews*, 2013, 42(24), 9304-9332. <https://doi.org/10.1039/c3cs60244c>
- [19] Wu, H., Zhou, W., Yildirim, T., Methane Sorption in Nanoporous Metal–Organic Frameworks and First-Order Phase Transition of Confined Methane, *J. Phys. Chem. C*, 2009, 113, 3029–3035. <https://doi.org/10.1021/jp8103276>
- [20] Wu, H., Zhou, W., Yildirim, T., High-Capacity Methane Storage in Metal–Organic Frameworks M2(dhtp): The Important Role of Open Metal Sites, *J. Am. Chem. Soc.*, 2009, 131, 4995–5000. <https://doi.org/10.1021/ja900258t>
- [21] Johnson, J., Carbon sequestration, clean-coal research mark government response to climate-change threat, *Chem. Eng. News*, 2004, 82, 36–42.
<https://doi.org/10.1021/cen-v082n051.p036>
- [22] Yong, Z., Mata, V., Rodrigues, A. E., Adsorption of carbon dioxide at high temperature a review, *Sep. Purif. Technol.*, 2002, 26, 195–205.
[https://doi.org/10.1016/S1383-5866\(01\)00165-4](https://doi.org/10.1016/S1383-5866(01)00165-4)
- [23] Férey, G., Hybrid porous solids: past, present, future, *Chem. Soc. Rev.*, 2008, 37, 191–214. <https://doi.org/10.1039/B618320B>
- [24] Zhang, Z., Yao, Z.-Z., Xiang, S., Chen, B., Perspective of microporous metalorganic frameworks for CO₂ capture and separation, *Energy Environ. Sci.*, 2014, 7, 2868–2899. <https://doi.org/10.1039/C4EE00143E>
- [25] Turner, J.A., A realizable renewable energy future, *Science*, 1999, 285, 687–689.
<https://doi.org/10.1126/science.285.5428.687>
- [26] Zhang, K., Lively, R.P., Dose, M.E., Li, L., Koros, W.J., Ruthven, D.M., McCool, B.A., Chance, R.R., Diffusion of water and ethanol in silicalite crystals synthesized in fluoride media., *Microporous Mesoporous Mater.*, 2013, 170, 259–265.
<https://doi.org/10.1016/j.micromeso.2012.12.015>

- [27] Antwi-Baah, R., Liu, H., Recent Hydrophobic Metal-Organic Frameworks and Their Applications, *Materials*, 2018, 11, 2250. <https://doi.org/10.3390/ma11112250>
- [28] Elsayed, A., Elsayed, E., Raya, A. D., Mahmoud, S., Elshaer, A., Kaialy, W., Thermal energy storage using metal–organic framework materials, *Applied energy*, 2017, 186, 509-519. <https://doi.org/10.1016/j.apenergy.2016.03.113>
- [29] Zhang, H., Nai, J., Yu, L., & Lou, X. W. D., Metal-organic-framework-based materials as platforms for renewable energy and environmental applications, *Joule*, 2017, 1(1), 77-107. <https://doi.org/10.1016/j.joule.2017.08.008>
- [30] Zhang, P., Guan, B.Y., Yu, L., Lou, X.W., Formation of double-shelled zinccobalt sulfide dodecahedral cages from bimetallic zeolitic imidazolate frameworks for hybrid supercapacitors, *Angew. Chem. Int. Ed.*, 2017, 56, 7141–7145. <https://doi.org/10.1002/anie.201702649>
- [31] Law, M., Greene, L.E., Johnson, J.C., Saykally, R., Yang, P., Nanowire dyesensitized solar cells. *Nat. Mater.*, 2005, 4, 455–459. <https://doi.org/10.1038/nmat1387>

Chapter 3

Metal Organic Frameworks Composites for Lithium Battery Applications

Rashid Iqbal^{1,2}, Pothu Ramyakrishna³, Rajender Boddula^{1*}, Anish Khan^{4,5}

¹ CAS Key Laboratory of Nanosystem and Hierarchical Fabrication, CAS Center for Excellence in Nanoscience, National Center for Nanoscience and Technology, Beijing 100190, China.

² University of Chinese Academy of Sciences, Beijing 100039, China.

³ College of Chemistry and Chemical Engineering, Hunan University, Changsha 410082, China

⁴ Chemistry Dep., Faculty of Science, King Abdulaziz University, Jeddah, 21589, Saudi Arabia

⁵ Centre of Excellence for Advanced Materials Research, King Abdulaziz University, Jeddah, 21589, Saudi Arabia

research.raaj@gmail.com

Abstract

Metal–organic frameworks (MOFs) have grabbed a lot of attention of scientist in the last two decades with more than 20,000 reported MOFs, due to tunable pore size, reticular design chemistry and higher surface area as compared to conventional amorphous materials. Moreover, these materials are applicable in energy storage, energy conversion, catalysis and separation. MOFs possesses capability to perform in the research area of Li-ion and Li-S batteries. Herein, an overview about challenges and recent advances electrochemical properties of MOF-derived carbon, pristine MOF and their composited with conductive materials to enhance Li-ion batteries performance. Finally, by focusing on development of MOF materials, we proposed the future of Li-ion batteries for high energy density.

Keywords

Metal–Organic Frameworks, Lithium-Ion Batteries, Lithium-Sulphur Batteries

Contents

1.	Introduction.....	33
2.	Applications of MOFs in lithium-ion batteries	33

3. Applications of MOFs in Lithium Sulphur batteries.....	38
4. Summary and outlook.....	42
References	43

1. Introduction

The pursuit for the synthesis of futuristic porous materials for green energy production has been a challenge around the worldwide research teams to develop eco-friendly energy devices. The porous materials like MOF give opportunity to design a reticular structure, which can be modified and tuned according to the requirement of applications. First introduced by Yaghi and co-workers in 1995 [1, 2]. These materials possess very high crystallinity and porosity are synthesized by metallic monomer (secondary building units (SBUs)) and organic units. The solvothermal reaction between the SBUs and the functional groups of the organic linkers above 22,000 variety of MOFs have been synthesized [3]. Furthermore, in order to investigate their broad range of application in gas storage and the application of MOFs in electrochemical systems is presently an developing field for the last decade. MOFs are the promising candidate for energy storage material as intrinsically contains the highest specific surface areas reported to date for microporous nanomaterials (up to $6200 \text{ m}^2 \text{ g}^{-1}$) [4] with huge internal pore volumes, well-aligned pore sizes.

In this chapter, comprehensive studies of new advances and developments for MOFs and their derivatives based Li-ion batteries. Numerous reports have been published previously regarding the synthesis of MOFs for green energy storage applications, fuel cells, lithium-ion batteries (LIBs), supercapacitors SCs [5-13]. Here, a thorough and comprehensive chapter specifically on LIBs. Firstly, illuminate recent advancement in negative electrode (cathode material) and positive electrode (anodic material), solid electrolytes for LIBs and then emphasis on the research of Li-S [14] both kinds of batteries innovations in research are receiving broad interest for their high energy densities. This chapter will enlighten and summarize the ground-breaking studies and endorse further expansion for MOF-based and MOF-derived Li-ion batteries.

2. Applications of MOFs in lithium-ion batteries

LIBs grasp a profitable achievement for the energy supply of smart electronic devices as these devices have potential to supply high energy density. Nevertheless, there is still a large gap to be filled as energy demands are exponentially increasing for large EES systems. In order to solve this problem, conventional material based LIBs need innovative design and discovering novel chemistry for Li storage and synthesis of new

materials is required [15]. Most importantly, LIBs have been studied extensively in details as far as its assembly is concerned, like anode, cathode and electrolyte. Moreover, still there are new kinds of futuristic materials available with outstanding properties like MOFs. This kind of material is easy to design and modified according to the required functional groups. These functional groups will act as redox active sites during the electrochemical reaction in LIBs [15-17]. Furthermore, MOFs have been used as composite electrode material with carbon material to increase its conductivity [15, 18-20]. MOFs so far reported are presented in order to evaluate their performance (Table 1)

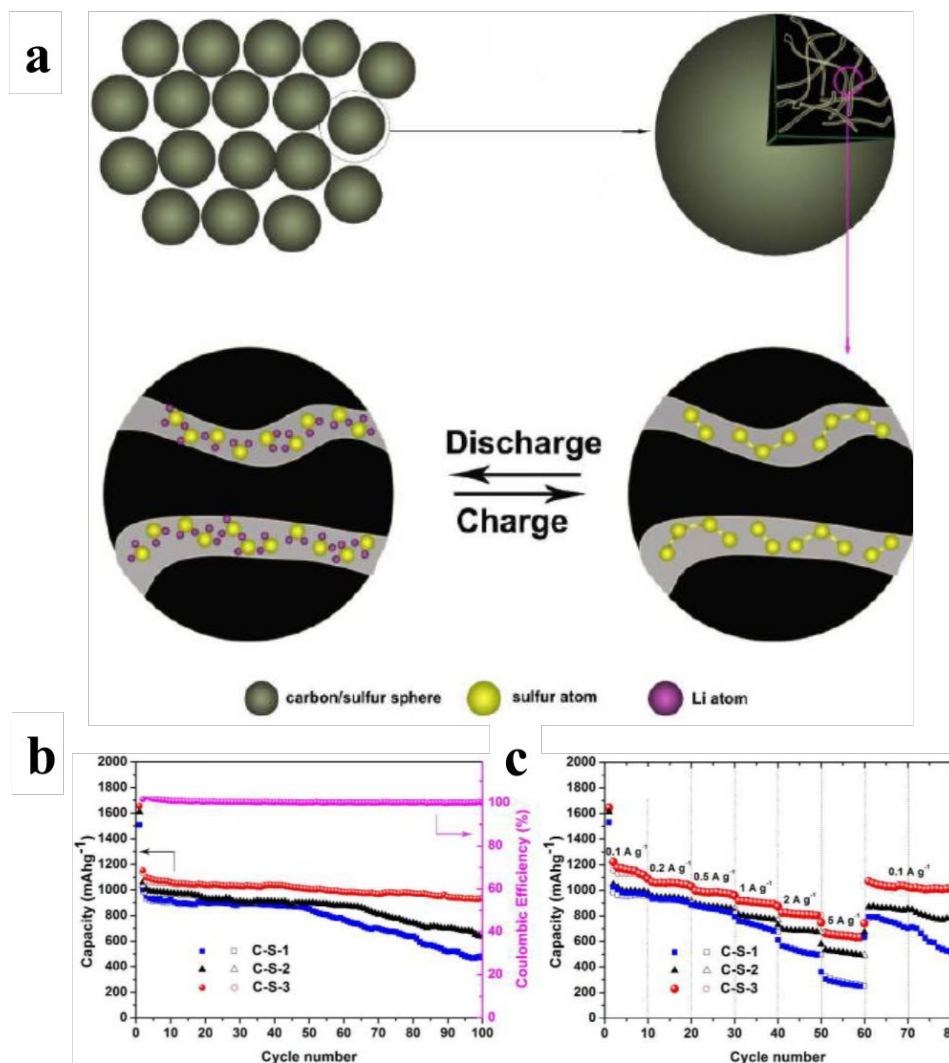


Figure 1. (a) Discharge and charge mechanism of C-S-3 hybrid cathode. (b) Cycling performance of C-S hybrids at 335 mA g⁻¹ (pink circles show the Coulombic efficiency of C-S-3 hybrid sample). (c) Rate capability performance of C-S hybrids. [Reprinted with permission from Ref. 43. Copyright 2015 ACS Applied Materials & Interfaces.]

Graphite have been used extensively as anode material for traditional LIBs, which shows a poor capacity of 372 mAh g^{-1} and low-slung rate capability. New anode material has been developed in order to meet the energy requirement in terms of huge energy and power densities. Among most emerging anodic materials are silicon and metal oxides, which are going on for research and development, yet a big gap to be commercialized [21, 22]. Furthermore, they have intrinsic well defined pore structure, which aids Li-ion to be stored and reversibly insertion and extraction of ions called insertion type electrodes [23]. In conventional materials, metal centers are required to store material with carbaneous template. Remarkably, MOFs act as ideal material with metal oxide and organic ligands to develop a unique porous structure, which is a unique way to prepare this kind of well define composited hybrid material. These captivating properties of this kind of material have numerous advantages over conventional anode materials [8].

MOF-177 was initially used directly as a rechargeable intercalation anode electrode material for LIBs [24]. Previously, two MOFs had been used to insert Li was not successful, results in alteration of the Zn-based MOF or Ni-based microporous phosphate into a Li_2O matrix and Zn-based nanocomposite or Ni nanoparticles, respectively [24, 25]. Férey and Tarascon was the pioneer researcher to use MOF as anode material and realized that an improved constancy could be attained by robust metal and oxygen bonds, fewer electrons by means of 3d transition metals with 3d orbitals except Ni or Zn, i.e. metals with higher oxidation number. Furthermore, in order to ease the electron storage in the framework, a varied valence state of the metallic material would be a better choice to attain stabile and sustainable electron delocalization. According to preceding studies [26], the authors examined the material $\text{Fe}^{\text{III}}(\text{OH})_{0.8}\text{F}_{0.2}(\text{bdc})\cdot\text{H}_2\text{O}$. In order to increase the conductivity of MOF, it is composited with 15 wt.% carbon for electrode preparation of a Li-ion battery, although Li-metal is used as cathode [27]. The extreme lithium uptake of $x = 0.6$ could be achieved during discharge), where x is represented as $\text{Li}_x\text{Fe}(\text{OH})_{0.8}\text{F}_{0.2}(\text{bdc})\cdot\text{H}_2\text{O}$. Moreover, as the quantity of x -values is higher, the discharge results in irreversible behavior, causes battery to outperform. A capacity of 75 mA h g^{-1} is achieved at $x = 0.6$. This capacity is practically lower because of the limited movement of lithium-ion and presence of density of the material. In this case, up to 50 cycles lithium insertion was filly reversible at 0.6 value.

Lately, the density functional theory (DFT) was used to investigate the detailed Li-insertion mechanism in the same material as shown in Fig. 2 [28, 29]. Insertion of Li-ion were identified at four different sites (Fig. 1). Between site A and B, (A is predicted to be slightly more favorable), when Li undergoes discharge between $0 < x < 0.25$. while for $0.25 < x < 0.5$, (i) 2 sites A occupied, (ii) 2 sites B occupied or (iii) 1 site occupied by each A and B, for the second Li insertion into the cell (4 Fe atoms) was of similar energy.

Site B lies near to the carboxylic group of the bdc linkers while, the site A lies adjacent to the hydroxyl bridging ligand of the inorganic chains.

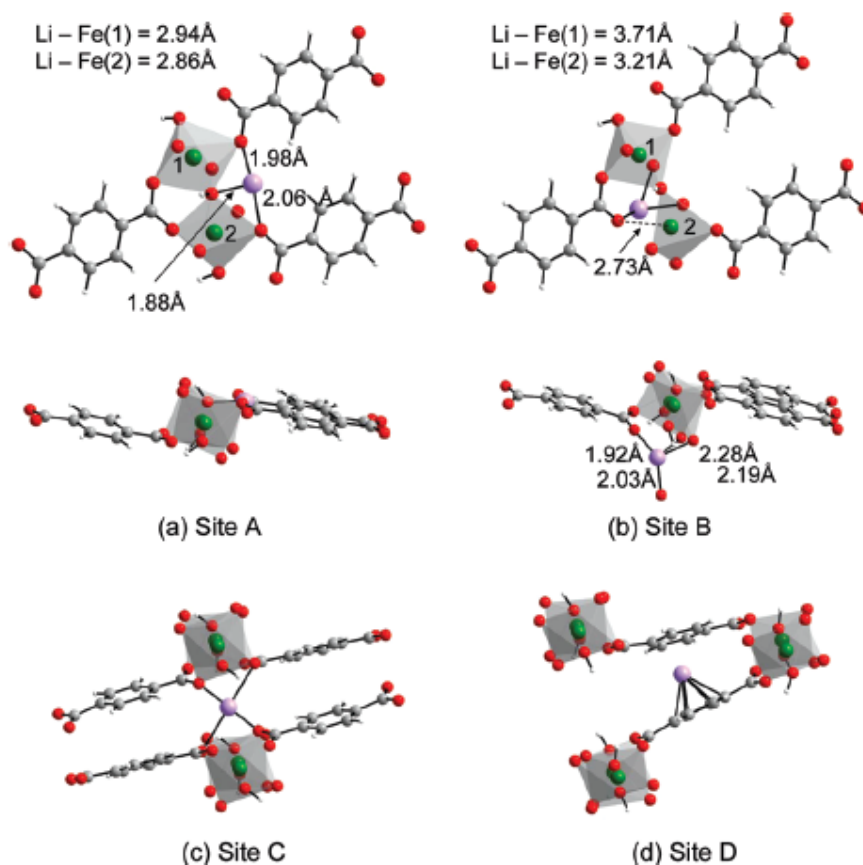


Figure 2. Results of the full structural relaxations performed at $x\text{Li}/\text{Fe}=0.25$ for the MIL53(Fe)-F0 system using the PW91 functional and $U_{\text{eff}} = 5$ eV for lithium sites (a) A, (b) B, (c) C, and (d) D. [Reprinted with permission from Ref. 29. Copyright 2010 J. Phys. Chem. C, ACS.]

Recently, another Fe-MIL-88B MOF reported having large specific capacity due to the conjugated functional carbonyl units in the materials [30]. In this study, they reported a half-battery and full-battery, this material sustained a capacity of 744.4 and 86.8 mA h g⁻¹ above 400 and 100 cycles, correspondingly. This MOF have polyhedral nanorod structural morphology, which holds the metal organic skeleton together during the course of the battery operation, hence, promotes that nanostructured MOFs are greatly appropriate choice for stable lithiation/delithiation procedures as compare to other structures. MOFs electrode materials have several advantages, their extraordinary conductivity and large surface area and small diffusion pathway are available for ion

movement and electron conduction, and consequently gives stable cycle performance at a high rate.

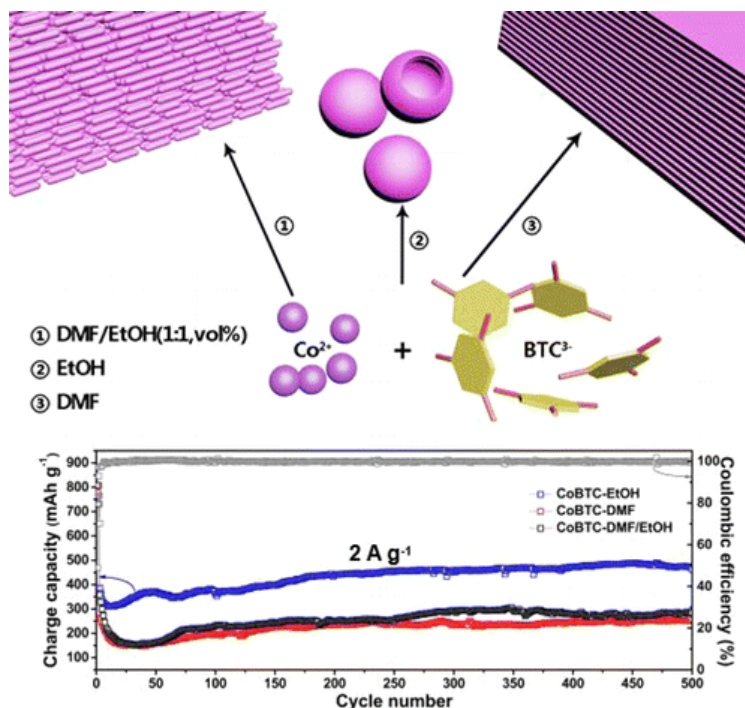


Figure 3. Schematic illustration of the preparation process of CoBTC CPs through a straightforward hydrothermal method, in which EtOH, DMF, and EtOH/DMF (1:1, vol%) are selected to form three CoBTC CPs with various morphologies and dimensions. [Reprinted with permission from Ref. 35. Copyright 2016 ACS Applied Materials & Interfaces.]

Co-MOFs as anode material has been used extensively [31-33]. For instance, Hu and his team synthesized a Co-BDC MOF as an electrode material through a single step synthesis technique [32]. Electrochemical performance presented that this MOF displayed large capacities at 200 mA g^{-1} , which is 1090 mA h g^{-1} . Lately, in another study S-Co-MOF also synthesized through solvothermal reaction between terephthalic acid and cobaltous nitrate [34]. Two kinds of edge-sharing found in CoO_6 octahedral, the structure of S-Co-MOF undergoes the deformation of the CoO_6 octahedral site during the test, displaying high cycling stability. Conversely, the lithium-ion battery performance was not satisfactory enough. Furthermore, the hydrothermal method is used by Song et al. [35] to fabricate one-dimensional cobalt coordination framework nanowires. The lithium-ion transmission process is shown in Fig. 1c. CoCOP provided a performance at 20 mA g^{-1} , which is 1100 mA h g^{-1} . Recently, Co-BTC bonded polymers synthesized by easier method of hydrothermal process Li's group [36], three different kinds of solvents system were used to synthesized MOF with various morphologies as shown in Fig. 3. The results

display that the cycling performances of the three CoBTC CPs have no major difference in performance at 100 mA g^{-1} . On the other hand, when the current densities increased to 2 A g^{-1} the difference is very obvious. The optimized CoBTC-EtOH product retained nearly 100% coulombic efficiency, while maintaining a capacity of 473 mA h g^{-1} at 2 A g^{-1} after 500 cycles. The convenient method can extend to various energy storage devices.

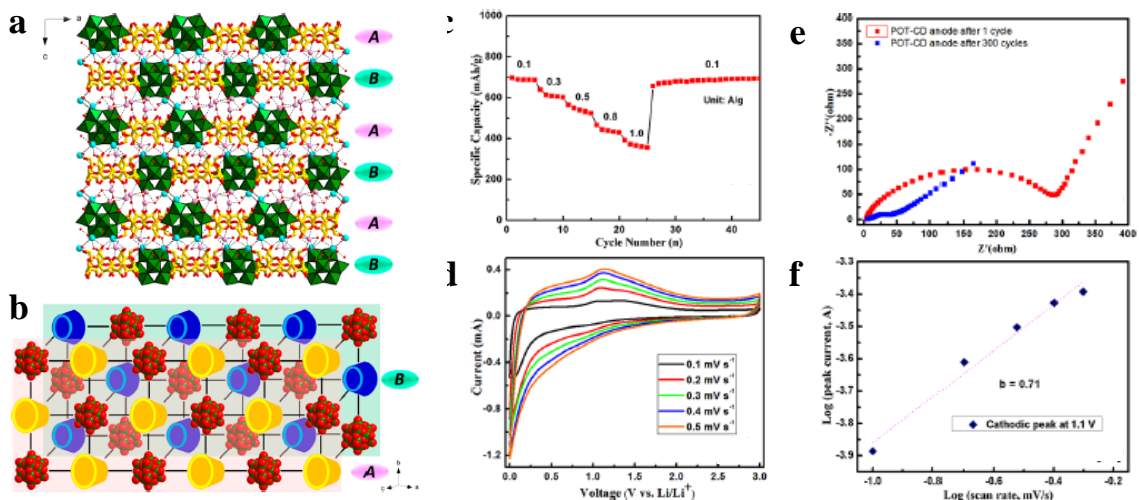


Figure 4. (a) Combined polyhedral/ball-and-stick representation of POT-CD. Color code: WO_6 , green octahedra; PO_4 , pink tetrahedra; K, turquoise; Na, magenta; O, red; C, yellow. (b) A schematic representation of the double-layer repeating unit. [Reprinted with permission from Ref. 11. Copyright 2019 Journal of the American Chemical Society.]

3. Applications of MOFs in lithium sulphur batteries.

For futuristic next-generation batteries, sulphur is the furthestmost promising material as cathode material. As it is environmentally friendly and available in copious amount on earth. Besides, it has a excellent theoretical capacity of 1676 mA h g^{-1} with energy density of 2500 W h kg^{-1} [37]. Conversion of sulphur to form Li_2S is a really important reaction, huge capacity is generated during this step. Conversely, these batteries have disadvantage of having large scale volume expansion up to 80% during above reaction. Furthermore, Li_2S and sulphur act as insulator, in order to solve this problem, conductive additives have to be mixed together with active material. In addition, migration of the redox intermediate polysulfides (Li_2S_x) between the cathode and anode, which are highly soluble in the electrolyte and also known as shuttle effect, subsequently lead to dramatic loss in capacity and obstructing the practical application of LiS batteries. Consequently, this is the major problem to store the dissolved polysulphide species, in order to avoid self-discharging of LiS batteries. Tarascon et al. studied the revolutionary work concentrating

on the application of MOFs as limited matrix for sulfur loading [38]. MIL-100(Cr) contains huge pore volume of $1 \text{ cm}^3 \text{ g}^{-1}$, which is thermally stable at higher temperature, hence, it can easy load sulphur during the melt diffusion process. Mainly two factors are responsible for the improved performance in this particular MOF: (1) the small aperture of the pore, reduced the diffusion of polysulphides within electrodes in electrolyte; (2) polarization of the pore walls surface can easily capture polysulphides, hence reduces the movement of Li_2S_x species.

Remarkably, ZIF-8 is one of the ideal MOF materials that owns cage like unique pores with apertures size of 3.4°A , attained high discharge capacities (at 0.1 C gives 1055 mA h g^{-1} and at 1 C gives 710 mA h g^{-1}) whereas, $1 \text{ C} = 1675 \text{ mA g}^{-1}$, additionally, performed very exceptionally up to 300 cycles with 0.08% decay per cycle. Two properties are very required to achieve longer stability and capacity in LiS batteries. In other words, in order to capture the polysulfide anions, small apertures as well as functional groups in the framework. Practically, MOF(ZIF-8) particle size of the templated material effect the performance in LiS batteries [39]. In this study, different particle size of ZIF-8 matrix was synthesized between $<20 \text{ nm}$ to $>1 \mu\text{m}$ as the particle size reduce more sulphur loading is possible in this MOF, however, 200 nm particle size have highest cyclic stability. Many reports have been found that claim the benefit of small apertures in MOFs [40], ordered porous structures [41] as shown in (Fig. 5), exposed metal sites [42] or Lewis acidic active sites for the S storage [39]. Above and beyond usage pristine MOFs to store soluble polysulphide, carbon materials derived from MOF by heat treatment have also been beneficial for sulfur storage. In another study [43], the electrochemical performance of carbon materials with various well defined pore shape derived from (ZIF-8, RT-MOF-5, Zn fumarate and solvo-MOF-5) four zinc-containing MOFs. The decreased boiling point of zinc allows it to be willingly removed as metallic vapor during heat treatment to make further increase pores quantity in the material. Results suggested that S-loaded is higher because of custom-made porous carbons with large quantity of micropores contribute to the superior cycle stability, whereas the carbons material with high mesoporous quantity deliver enhanced initial discharge capacity. Likewise, another carbon material derived from MOF-5 as matrix is explained [22]; the mixture of the material exhibited a discharge capacity of 730 mA h g^{-1} at a current rate of 0.5 C after 50 cycles. Another research reported [44], 27 wt% of Sulphur loaded ZIF-8 derived carbon as cathode after 100 cycles attained a reversible capacity of $936.5 \text{ mA h g}^{-1}$ as shown in Fig. 1. After heating the sulfur composite and ZIF-8 heat treated carbon at 300°C delivers high performance by further heating at 155°C for 6 h, thus removed the excess S_8 molecule on the superficial space and inner walls of the pores.

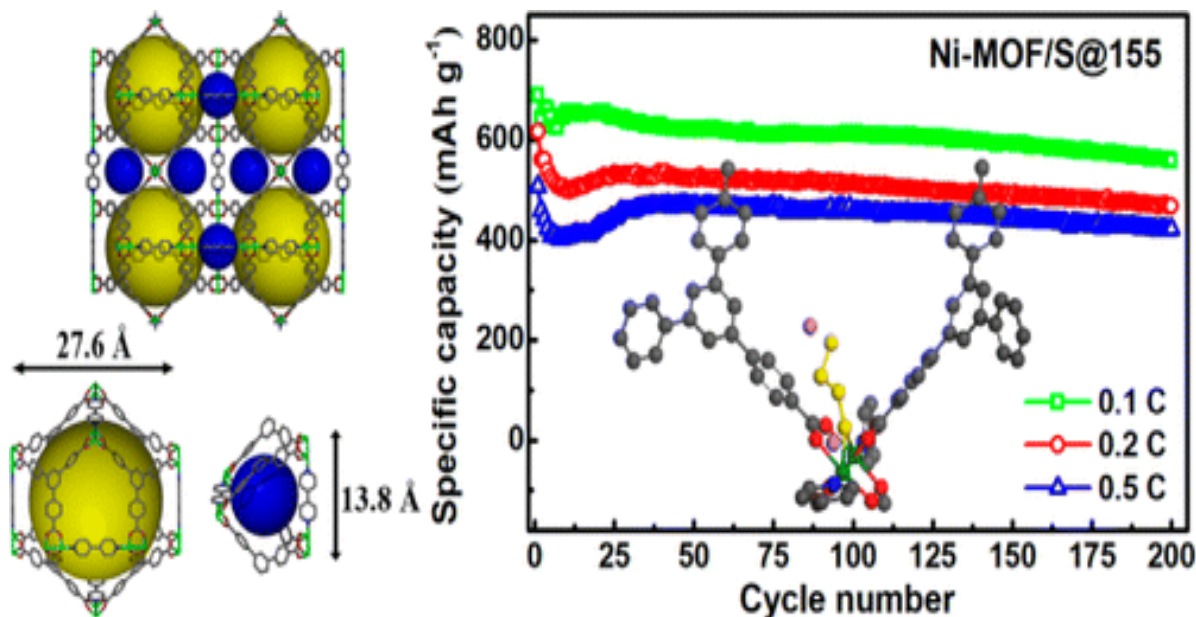


Figure 5. (a) Crystal structure of Ni-MOF containing two different types of pores represented by dark yellow sphere and blue sphere: mesopore (yellow sphere indicates pore volume; gray, C; red: O; green, Ni; blue, N); micropore (blue sphere indicates the pore volume) (b) Cycling performance of Ni-MOF/S composite at 0.1 and 0.2 C rates at a voltage range of 1.5–3.0 V. [Reprinted with permission from Ref. 40. Copyright 2014 Nano Letters.]

Iron-based MOFs also have been used to heat treatment and converted to carbons, thus also vigorously to serve as matrixes for Sulphur storage [45]. Commercially available iron-containing MOF (Basolite F300) prepared carbons with well-defined structured porosity. Graphitic shells formed after heating the highly dispersed Fe based MOFs. This material gives improved conductivity and after 40 cycles generated capacities of up to 550 mA h g⁻¹. Zou's group [40] published a study on synthesis of two Al metal contained organic gel (new class of MOFs) with various drying methods by treating them with; MOAs, CO₂ treated, S_{BET}= 3770 m²g⁻¹), (MOXs, air dried, S_{BET}= 1820 m²g⁻¹; and then heat treated to produce porous carbon materials (MOX-C, MOA-C). MOA-C/S with 50 wt% of Sulphur produced by a two-step heating technique showed greater capacity and improved cycling stability as compare with MOX-C/S with 30.3 wt% of sulphur content, which is obtained from the ordered pore framework of MOA-C. The capacity of MOA-C/S can give 1240 mA h g⁻¹ in the cycle no. 2, with capacity fading in the forth and further cycles. As discuss earlier, MOFs are not highly conductive materials, this problem is solved by compositing MOFs with carbon black, graphene, CNTs or conducting polymers [46-40]. In some Recent studies [51], ZIF-8 derived carbon composited thin

Table 1. Battery performance of MOF based materials.

MOFs	Sample	CC/DC	RC/rat	C	Vs/Li/	Ref
MOF-based anode materials						
MOF-177	MOF-177	110/425	-/50	2	0.1-1.6	[51]
Zn ₃ (HCOO) ₆	Zn ₃ (HCOO) ₆	693/134	560/60	60	0.005-	[52]
Mn-LCP	Mn(tfbdc)(4,4o-	610/180	390/50	50	0.1-3	[53]
Co ₂ (OH) ₂ BDC	Co ₂ (OH) ₂ BDC	1385/10	650/50	10	0.02-3	[30]
Li/Ni-NTC	Li/Ni-NTC	601/108	480/-	80	0.01-3	[54]
Co ₃ [Co(CN) ₆] ₂	Co ₃ [Co(CN) ₆] ₂	294.2/5	299.1/2	40	0.01-	[55]
Zn(IM) _{1.5} (abIM) _{0.5}	Zn(IM) _{1.5} (abIM) _{0.5}	-/-	190/10	20	0.01-3	[56]
[Cu ₂ (C ₈ H ₄ O ₄) ₄] _n	[Cu ₂ (C ₈ H ₄ O ₄) ₄] _n	194/149	161/48	50	0.01-	[57]
MONFs	Asp-Cu nanofibers	334/125	233/50	20	0.01-3	[58]
Ni-Me4bpz	Ni-Me4bpz	-/320	120/50	10	0.01-3	[59]
MOF-based and MOF-derived sulfur hosts						
ZIF-8	S/ZIF-8	-/-	1055/0.	10	1.8-2.8	[60]
MIL-53	S/MIL-53	-/-	1215/0.	10	1.8-2.8	[60]
NH ₂ -MIL-53	S/NH ₂ -MIL-53	-/-	1125/0.	10	1.8-2.8	[60]
HKUST-1	HKUST-1	-/-	526/0.1	10	1.8-2.8	[60]
ZIF-8	S@ZIF-8	-/-	968/0.5	25	1.8-2.8	
MIL-100	MIL-100(Cr)/S@155	-/-	1000/0.	60	1-3	[37]
Ni-MOF	Ni-MOF/S	-/-	689/0.1	20	1.5-3	[40]
HKUST-1	HKUST-1>S	-/1498	500/0.0	17	1-3	[41]
ZIF-8	S@ZIF-8	-/-	510/0.1	20	1-3	[39]
ZIF-8	GS-S/CZIF8-D	-/1171	561/16	12	1-3	[50]
Basolite F300	MDC-800-S	-/1100	550/0.2	40	1.8-2.6	[44]
MOF-based cathode materials						
MIL-53	MIL-53(Fe)	77/80	71/0.02	50	1.5-3.5	
MIL-53	MIL-53(Fe) Quinone	177.5/9	73/0.1	8	1.5-3.5	[62]
MIL-68	MIL-68(Fe)	31/40	32/0.02	12	1.5-3.5	
MIL-136	MIL-136(Ni)	-/-	10/10	50	2-4	[64]
MOPOF	K _{2.5} (VO) ₂ (HPO ₄) ₂ (C ₂ O ₄)	81/62	70/40	60	2.5-4.6	[65]
MOPOF	Li ₂ [(VO) ₂ (HPO ₄) _{1.5} (PO ₄)	78/55	80/12.5	25	2.5-4.5	[66]
MIL-101	MIL-101-Fe	65	-/-	30	2-3.5	
Cu(2,7-AQDC)	Cu(2,7-AQDC)	147	105/1		1.7-4	[68]
MOF-74(Ni)	-NiS	-/-	300/60	10	0.5-3	[69]
MIL-47	VIV(O)(BDC)	-/-	82/10	50	1.5-4	
MIL-132	K ₂ (TTF-TC)H ₂		50/10		2.3-	
RbxMnIIy[FeIII(CN) ₆]·nH ₂ O		60/50			2.0-4.3	[72]
MnIII[MnIII(CN) ₆]		197/30			2-4.2	
K _{2.5} [(VO) ₂ (HPO ₄) _{1.5} (PO ₄) _{0.5} (C ₂ O ₄)]		65/40			2.5-4.6	
[Mn(H ₂ O)][Mn(HCOO) _{2/3} (H ₂ O) _{2/3}] _{3/4}		30/10			3-4.3	[74]

layered graphene sheets, which performed as conducting bridges between the material. Therefore, obtained material shows retention of about 48% capacity after 120 cycles with an average columbic efficiency of $\sim 90\%$ and initial discharge capacity of 1171 mA h g^{-1} . similarly, Chen et al. design a composited cathode material comprised of graphene-wrapped MOF-101(Cr)/S and after 134 cycles, it supplied a reversible capacity of 809 mA h g^{-1} [47]. Zhang's group synthesized a series of composited of graphene oxide, reduced graphene oxide or multi-walled carbon nanotubes with pristine MOF or MOF derived carbon composites for LiS batteries [46, 48-50]. See table 1 for comparison of Li-S batteries performance comparison [37-41, 44, 50, 60], Li-ion batteries performance comparison for anode [51-59] and cathode [6-74] material.

4. Summary and outlook

In summary, MOFs as an anode material are an efficient method to fabricate nanoparticles composted material with different carbon materials. The doping of various metals in MOFs improved the conductivity of the material significantly and enhanced crystallinity of carbon in the as-prepared composites concurrently. The cooperative result is very significant in the Li-ion batteries performance. MOF composites can give an excellent reversible capacity as electrode materials.

Cathode materials for LIBs in this chapter clearly unveils the change in nanomaterials from bulk to nanoscale can expressively improve battery life cycle for energy storage. The nanomaterials advancement for high-performance Li-ion batteries could be benefited from the discrete properties, such as short diffusion paths, large quantities and high surface areas of active sites, as well as freedom for volume change during charging–discharging cycles. Among numerous methods to prepare nanomaterials, reticular chemistry design that include sol–gel reaction systems are easier, well-designed and frequently use organic molecules.

MOFs and MOFs based porous carbon have ability to loaded large amount of Sulphur and reduce the possibility of shuttle effect. The benefits of MOFs are summarized as follows: (1) high Sulphur mass loading in the well-defined pores, hence more efficient use of active material; (2) variable pore size and aperture windows of pore can capture formation of polysulfides products and so, avoid the damage of active framework; (3) due to the ease of polarity on the inner surface of MOFs, which can be beneficial in order to capture the charged polysulfides thus, reinforcing the control aptitude of redox species; (4) strong templates like MOFs can bare volume expansion during the redox reactions; (5) upon carbonizing of MOFs can gives abundant amount of micro and mesoporous material could be useful to capture polysulfides and on the other hand, the mesopores and

macropores promotes passage pathways and act as storage of electrolyte; (6) After heat treatment the conductivity of MOFs could greatly improve the electron transport.

References

- [1] O. Yaghi, H. Li, *Journal of the American Chemical Society*, 117 (1995) 10401-10402.
<https://doi.org/10.1021/ja00146a033>
- [2] O.M. Yaghi, G. Li, H. Li, *Nature*, 378 (1995) 703. <https://doi.org/10.1038/378703a0>
- [3] P.G. Yot, Z. Boudene, J. Macia, D. Granier, L. Vanduyfhuys, T. Verstraelen, V. Van Speybroeck, T. Devic, C. Serre, G. Férey, N. Stock, G. Maurin, *Chemical Communications*, 50 (2014) 9462-9464. <https://doi.org/10.1039/C4CC03853C>
- [4] G. Férey, *Chemical Society Reviews*, 37 (2008) 191-214.
<https://doi.org/10.1039/B618320B>
- [5] J.-K. Sun, Q. Xu, *Energy & Environmental Science*, 7 (2014) 2071-2100.
<https://doi.org/10.1039/c4ee00517a>
- [6] S.-L. Li, Q. Xu, *Energy & Environmental Science*, 6 (2013) 1656-1683.
<https://doi.org/10.1039/c3ee40507a>
- [7] W. Xia, A. Mahmood, R. Zou, Q. Xu, *Energy & Environmental Science*, 8 (2015) 1837-1866. <https://doi.org/10.1039/C5EE00762C>
- [8] S.J. Yang, S. Nam, T. Kim, J.H. Im, H. Jung, J.H. Kang, S. Wi, B. Park, C.R. Park, *Journal of the American Chemical Society*, 135 (2013) 7394-7397.
<https://doi.org/10.1021/ja311550t>
- [9] A.J. Clough, J.W. Yoo, M.H. Mecklenburg, S.C. Marinescu, *Journal of the American Chemical Society*, 137 (2014) 118-121. <https://doi.org/10.1021/ja5116937>
- [10] Z.-L. Wang, X.-F. Hao, Z. Jiang, X.-P. Sun, D. Xu, J. Wang, H.-X. Zhong, F.-L. Meng, X.-B. Zhang, *Journal of the American Chemical Society*, 137 (2015) 15070-15073. <https://doi.org/10.1021/jacs.5b09021>
- [11] P. Yang, W. Zhao, A. Shkurenko, Y. Belmabkhout, M. Eddaoudi, X. Dong, H.N. Alshareef, N.M. Khashab, *Journal of the American Chemical Society*, (2019).
- [12] P. Xiao, F. Bu, R. Zhao, M.F. Aly Aboud, I. Shakir, Y. Xu, *ACS nano*, 12 (2018) 3947-3953. <https://doi.org/10.1021/acsnano.8b01488>
- [13] M.-T. Li, X.-Y. Yang, J.-S. Li, N. Sheng, G.-D. Liu, J.-Q. Sha, Y.-Q. Lan, *Inorganic chemistry*, 57 (2018) 3865-3872. <https://doi.org/10.1021/acs.inorgchem.7b03228>

- [14] D. Wu, Z. Guo, X. Yin, Q. Pang, B. Tu, L. Zhang, Y.G. Wang, Q. Li, *Advanced Materials*, 26 (2014) 3258-3262. <https://doi.org/10.1002/adma.201305492>
- [15] X. Li, S. Zheng, L. Jin, Y. Li, P. Geng, H. Xue, H. Pang, Q. Xu, *Advanced Energy Materials*, (2018) 1800716. <https://doi.org/10.1002/aenm.201800716>
- [16] J.-Q. Sha, X.-Y. Yang, Y. Chen, P.-P. Zhu, Y.-F. Song, J. Jiang, *ACS applied materials & interfaces*, 10 (2018) 16660-16665. <https://doi.org/10.1021/acsami.8b04009>
- [17] W. Cheng, F.-C. Shen, Y.-s. Xue, X. Luo, M. Fang, Y.-Q. Lan, Y. Xu, *ACS Applied Energy Materials*, 1 (2018) 4931-4938. <https://doi.org/10.1021/acsaem.8b00938>
- [18] A. Morozan, F. Jaouen, *Energy & environmental science*, 5 (2012) 9269-9290. <https://doi.org/10.1039/c2ee22989g>
- [19] A. Petronico, T.P. Money Penny, B.G. Nicolau, J.S. Moore, R.G. Nuzzo, A.A. Gewirth, *Journal of the American Chemical Society*, (2018).
- [20] B.-J. Chae, Y.E. Jung, C.Y. Lee, T. Yim, *ACS Sustainable Chemistry & Engineering*, (2018).
- [21] Z.L. Wang, *Journal of physics: condensed matter*, 16 (2004) R829. <https://doi.org/10.1088/0953-8984/16/25/R01>
- [22] L. Wang, Y. Han, X. Feng, J. Zhou, P. Qi, B. Wang, *Coordination Chemistry Reviews*, 307 (2016) 361-381. <https://doi.org/10.1016/j.ccr.2015.09.002>
- [23] S.S. Park, Y. Tulchinsky, M. Dincă, *Journal of the American Chemical Society*, 139 (2017) 13260-13263. <https://doi.org/10.1021/jacs.7b06197>
- [24] X. Li, F. Cheng, S. Zhang, J. Chen, *Journal of power sources*, 160 (2006) 542-547. <https://doi.org/10.1016/j.jpowsour.2006.01.015>
- [25] P. Tran-Van, K. Barthelet, M. Morcrette, M. Herlem, J. Tarascon, A. Cheetham, G. Férey, *Journal of New Materials for Electrochemical Systems*, 6 (2003) 29-32.
- [26] K. Barthelet, J. Marrot, D. Riou, G. Férey, *Angewandte Chemie International Edition*, 41 (2002) 281-284. [https://doi.org/10.1002/1521-3773\(20020118\)41:2<281::AID-ANIE281>3.0.CO;2-Y](https://doi.org/10.1002/1521-3773(20020118)41:2<281::AID-ANIE281>3.0.CO;2-Y)
- [27] G. Férey, F. Millange, M. Morcrette, C. Serre, M.L. Doublet, J.M. Grenèche, J.M. Tarascon, *Angewandte Chemie International Edition*, 46 (2007) 3259-3263. <https://doi.org/10.1002/anie.200605163>
- [28] C. Combelles, M.B. Yahia, L. Pedesseau, M.-L. Doublet, *Journal of Power Sources*, 196 (2011) 3426-3432. <https://doi.org/10.1016/j.jpowsour.2010.08.065>

- [29] C. Combelles, M.B. Yahia, L. Pedesseau, M.-L. Doublet, *The Journal of Physical Chemistry C*, 114 (2010) 9518-9527. <https://doi.org/10.1021/jp1016455>
- [30] L. Gou, L.-M. Hao, Y.X. Shi, S.-L. Ma, X.-Y. Fan, L. Xu, D.-L. Li, K. Wang, *Journal of Solid State Chemistry*, 210 (2014) 121-124. <https://doi.org/10.1016/j.jssc.2013.11.014>
- [31] X. Hu, H. Hu, C. Li, T. Li, X. Lou, Q. Chen, B. Hu, *Journal of Solid State Chemistry*, 242 (2016) 71-76. <https://doi.org/10.1016/j.jssc.2016.07.021>
- [32] P. Sengodu, C. Bongu, M. Perumal, M. Paramasivam, *Journal of Alloys and Compounds*, 714 (2017) 603-609. <https://doi.org/10.1016/j.jallcom.2017.04.241>
- [33] C. Li, X. Hu, X. Lou, L. Zhang, Y. Wang, J.-P. Amoureux, M. Shen, Q. Chen, B. Hu, *Journal of Materials Chemistry A*, 4 (2016) 16245-16251. <https://doi.org/10.1039/C6TA06413B>
- [34] H. Song, L. Shen, J. Wang, C. Wang, *Journal of Materials Chemistry A*, 4 (2016) 15411-15419. <https://doi.org/10.1039/C6TA05925B>
- [35] C. Li, X. Lou, M. Shen, X. Hu, Z. Guo, Y. Wang, B. Hu, Q. Chen, *ACS Applied Materials & Interfaces*, 8 (2016) 15352-15360. <https://doi.org/10.1021/acsami.6b03648>
- [36] A. Manthiram, S.-H. Chung, C. Zu, *Advanced Materials*, 27 (2015) 1980-2006. <https://doi.org/10.1002/adma.201405115>
- [37] R. Demir-Cakan, M. Morcrette, F. Nouar, C. Davoisne, T. Devic, D. Gonbeau, R. Dominko, C. Serre, G. Férey, J.-M. Tarascon, *Journal of the American Chemical Society*, 133 (2011) 16154-16160. <https://doi.org/10.1021/ja2062659>
- [38] J. Zhou, X. Yu, X. Fan, X. Wang, H. Li, Y. Zhang, W. Li, J. Zheng, B. Wang, X. Li, *Journal of Materials Chemistry A*, 3 (2015) 8272-8275. <https://doi.org/10.1039/C5TA00524H>
- [39] Z. Wang, Z. Dou, Y. Cui, Y. Yang, Z. Wang, G. Qian, *Microporous and Mesoporous Materials*, 185 (2014) 92-96. <https://doi.org/10.1016/j.micromeso.2013.11.011>
- [40] J. Zheng, J. Tian, D. Wu, M. Gu, W. Xu, C. Wang, F. Gao, M.H. Engelhard, J.-G. Zhang, J. Liu, J. Xiao, *Nano Letters*, 14 (2014) 2345-2352. <https://doi.org/10.1021/nl404721h>
- [41] Z. Wang, X. Li, Y. Cui, Y. Yang, H. Pan, Z. Wang, C. Wu, B. Chen, G. Qian, *Crystal Growth & Design*, 13 (2013) 5116-5120. <https://doi.org/10.1021/cg401304x>

- [42] K. Xi, S. Cao, X. Peng, C. Ducati, R. Vasant Kumar, A.K. Cheetham, *Chemical Communications*, 49 (2013) 2192-2194. <https://doi.org/10.1039/c3cc38009b>
- [43] Z. Li, L. Yin, *ACS Applied Materials & Interfaces*, 7 (2015) 4029-4038. <https://doi.org/10.1021/am507660y>
- [44] M. Klose, K. Pinkert, M. Zier, M. Uhlemann, F. Wolke, T. Jaumann, P. Jehnichen, D. Wadewitz, S. Oswald, J. Eckert, L. Giebeler, *Carbon*, 79 (2014) 302-309. <https://doi.org/10.1016/j.carbon.2014.07.071>
- [45] W. Bao, Z. Zhang, Y. Qu, C. Zhou, X. Wang, J. Li, *Journal of Alloys and Compounds*, 582 (2014) 334-340. <https://doi.org/10.1016/j.jallcom.2013.08.056>
- [46] Z. Zhao, S. Wang, R. Liang, Z. Li, Z. Shi, G. Chen, *Journal of Materials Chemistry A*, 2 (2014) 13509-13512. <https://doi.org/10.1039/C4TA01241K>
- [47] Y. Yue, B. Guo, Z.-A. Qiao, P.F. Fulvio, J. Chen, A.J. Binder, C. Tian, S. Dai, *Microporous and Mesoporous Materials*, 198 (2014) 139-143. <https://doi.org/10.1016/j.micromeso.2014.07.026>
- [48] W. Bao, Z. Zhang, W. Chen, C. Zhou, Y. Lai, J. Li, *Electrochimica Acta*, 127 (2014) 342-348. <https://doi.org/10.1016/j.electacta.2014.02.043>
- [49] W. Bao, Z. Zhang, C. Zhou, Y. Lai, J. Li, *Journal of Power Sources*, 248 (2014) 570-576. <https://doi.org/10.1016/j.jpowsour.2013.09.132>
- [50] R. Chen, T. Zhao, T. Tian, S. Cao, P.R. Coxon, K. Xi, D. Fairen-Jimenez, R.V. Kumar, A.K. Cheetham, *APL Materials*, 2 (2014) 124109. <https://doi.org/10.1063/1.4901751>
- [51] X. Li, F. Cheng, S. Zhang, J. Chen, *Journal of Power Sources*, 160 (2006) 542-547. <https://doi.org/10.1016/j.jpowsour.2006.01.015>
- [52] K. Saravanan, M. Nagarathinam, P. Balaya, J.J. Vittal, *Journal of Materials Chemistry*, 20 (2010) 8329-8335. <https://doi.org/10.1039/c0jm01671c>
- [53] Q. Liu, L. Yu, Y. Wang, Y. Ji, J. Horvat, M.-L. Cheng, X. Jia, G. Wang, *Inorganic Chemistry*, 52 (2013) 2817-2822. <https://doi.org/10.1021/ic301579g>
- [54] X. Han, F. Yi, T. Sun, J. Sun, *Electrochemistry Communications*, 25 (2012) 136-139. <https://doi.org/10.1016/j.elecom.2012.09.014>
- [55] P. Nie, L. Shen, H. Luo, B. Ding, G. Xu, J. Wang, X. Zhang, *Journal of Materials Chemistry A*, 2 (2014) 5852-5857. <https://doi.org/10.1039/C4TA00062E>
- [56] Y. Lin, Q. Zhang, C. Zhao, H. Li, C. Kong, C. Shen, L. Chen, *Chemical Communications*, 51 (2015) 697-699. <https://doi.org/10.1039/C4CC07149B>

- [57] R. Senthil Kumar, C. Nithya, S. Gopukumar, M. Anbu Kulandainathan, *Energy Technology*, 2 (2014) 921-927. <https://doi.org/10.1002/ente.201402076>
- [58] C. Zhao, C. Shen, W. Han, *RSC Advances*, 5 (2015) 20386-20389. <https://doi.org/10.1039/C4RA16416D>
- [59] T. An, Y. Wang, J. Tang, Y. Wang, L. Zhang, G. Zheng, *Journal of Colloid and Interface Science*, 445 (2015) 320-325. <https://doi.org/10.1016/j.jcis.2015.01.012>
- [60] J. Zhou, R. Li, X. Fan, Y. Chen, R. Han, W. Li, J. Zheng, B. Wang, X. Li, *Energy & Environmental Science*, 7 (2014) 2715-2724. <https://doi.org/10.1039/C4EE01382D>
- [61] G. Férey, F. Millange, M. Morcrette, C. Serre, M.-L. Doublet, J.-M. Grenèche, J.-M. Tarascon, *Angewandte Chemie International Edition*, 46 (2007) 3259-3263. <https://doi.org/10.1002/anie.200605163>
- [62] G. de Combarieu, M. Morcrette, F. Millange, N. Guillou, J. Cabana, C.P. Grey, I. Margiolaki, G. Férey, J.M. Tarascon, *Chemistry of Materials*, 21 (2009) 1602-1611. <https://doi.org/10.1021/cm8032324>
- [63] A. Fateeva, P. Horcajada, T. Devic, C. Serre, J. Marrot, J.-M. Grenèche, M. Morcrette, J.-M. Tarascon, G. Maurin, G. Férey, *European Journal of Inorganic Chemistry*, 2010 (2010) 3789-3794. <https://doi.org/10.1002/ejic.201000486>
- [64] T.L.A. Nguyen, T. Devic, P. Mialane, E. Rivière, A. Sonnauer, N. Stock, R. Demir-Cakan, M. Morcrette, C. Livage, J. Marrot, J.-M. Tarascon, G. Férey, *Inorganic Chemistry*, 49 (2010) 10710-10717. <https://doi.org/10.1021/ic101906u>
- [65] M. Nagarathinam, K. Saravanan, E.J.H. Phua, M.V. Reddy, B.V.R. Chowdari, J.J. Vittal, *Angewandte Chemie International Edition*, 51 (2012) 5866-5870. <https://doi.org/10.1002/anie.201200210>
- [66] A. Shahul Hameed, M. Nagarathinam, M. Schreyer, M.V. Reddy, B.V.R. Chowdari, J.J. Vittal, *Journal of Materials Chemistry A*, 1 (2013) 5721-5726. <https://doi.org/10.1039/c3ta10464h>
- [67] J. Shin, M. Kim, J. Cirera, S. Chen, G.J. Halder, T.A. Yersak, F. Paesani, S.M. Cohen, Y.S. Meng, *Journal of Materials Chemistry A*, 3 (2015) 4738-4744. <https://doi.org/10.1039/C4TA06694D>
- [68] Z. Zhang, H. Yoshikawa, K. Awaga, *Journal of the American Chemical Society*, 136 (2014) 16112-16115. <https://doi.org/10.1021/ja508197w>
- [69] Z. Wang, X. Li, Y. Yang, Y. Cui, H. Pan, Z. Wang, B. Chen, G. Qian, *Journal of Materials Chemistry A*, 2 (2014) 7912-7916. <https://doi.org/10.1039/c4ta00367e>

- [70] W. Kaveevivitchai, A.J. Jacobson, *Journal of Power Sources*, 278 (2015) 265-273.
<https://doi.org/10.1016/j.jpowsour.2014.12.094>
- [71] T.L.A. Nguyen, R. Demir-Cakan, T. Devic, M. Morcrette, T. Ahnfeldt, P. Auban-Senzier, N. Stock, A.-M. Goncalves, Y. Filinchuk, J.-M. Tarascon, G. Férey, *Inorganic Chemistry*, 49 (2010) 7135-7143. <https://doi.org/10.1021/ic100950n>
- [72] M. Okubo, D. Asakura, Y. Mizuno, J.D. Kim, T. Mizokawa, T. Kudo, I. Honma, *The Journal of Physical Chemistry Letters*, 1 (2010) 2063-2071.
<https://doi.org/10.1021/jz100708b>
- [73] D. Asakura, M. Okubo, Y. Mizuno, T. Kudo, H. Zhou, K. Ikeda, T. Mizokawa, A. Okazawa, N. Kojima, *The Journal of Physical Chemistry C*, 116 (2012) 8364-8369.
<https://doi.org/10.1021/jp2118949>
- [74] M. Okubo, K. Kagesawa, Y. Mizuno, D. Asakura, E. Hosono, T. Kudo, H. Zhou, K. Fujii, H. Uekusa, S.-i. Nishimura, A. Yamada, A. Okazawa, N. Kojima, *Inorganic Chemistry*, 52 (2013) 3772-3779. <https://doi.org/10.1021/ic302364d>

Chapter 4

Metal-Organic-Framework-Quantum Dots (QD@MOF) Composites

M. Ramesh^{1*}, M. Muthukrishnan¹, Anish Khan^{2,3}, Mohammed Azam⁴

¹Department of Mechanical Engineering, KIT-Kalaignarkarunanidhi Institute of Technology,
Coimbatore-641402, Tamil Nadu, India

²Chemistry Department, Faculty of Science, King Abdulaziz University, Jeddah-21589, Saudi
Arabia

³Center of Excellence for Advanced Materials Research, King Abdulaziz University, Jeddah
21589, Saudi Arabia

⁴Department of Chemistry, College of Science, King Saud University, P. O. Box 2455, Riyadh
11451, Saudi Arabia

*mramesh97@gmail.com

Abstract

The developments in the field of metal-organic frameworks-quantum dot (QD@MOF) composites have improved recently, especially in terms of production, better performance, and wide area of industrial applications. The combination of the high surface areas, micro-porosity and tunable compositions of MOFs with QDs, allows the preparation of composite materials with enhanced properties for several applications such as photo-catalysis, energy storage, gas-storage and sensing. This chapter summarizes the production mechanisms such as crystallization, interfacial diffusion, micro-fluidic processing, and vapour deposition methods of QD@MOF composites in detail. The application of QD@MOF in gas separation, nano-filtration, ionic sieving, stimuli responsiveness, and catalysis are reviewed, and the separation mechanisms are also discussed in detail. Moreover, the opportunities and challenges for further development of QD@MOF are pointed out.

Keywords: Metal-Organic Frameworks, Quantum Dot Composites, Production Methodologies, Modification Strategies, Applications

Contents

1. Introduction.....	51
----------------------	----

1.1	Metal-organic frameworks	51
1.2	Quantum dots	51
1.3	Gold QDs (AuQDs)	53
2.	QD polymeric materials	55
2.1	Integration of QDs	55
2.2	Methods of encapsulating QD to polymer matrices	55
2.3	Incorporation into premade polymers.....	55
2.4	Suspension polymerization	57
2.5	Encapsulation via emulsion polymerization.....	57
2.6	Encapsulation via miniemulsion polymerization	57
3.	QD hybrid materials	58
3.1	Strategies to generate QD hybrid materials.....	58
3.2	Exchanging ligand between polymer and QDs	59
3.3	Polymer grafting to QDs.....	60
3.4	Polymer grafting from QDs	60
3.5	Polymer capping into QDs	61
3.6	QDs growth within polymer	61
3.7	Challenges in biocompatible polymer/QDs.....	61
4.	Applications of QD composites	62
4.1	Bio-imaging	62
4.2	Photo-thermal therapies	62
4.3	Opto-electric applications	63
4.3.1	QD LEDs	63
4.3.2	Polymer QD liquid crystal displays.....	63
4.3.3	QD polymer photo-voltaic devices.....	64
5.	Metallic NCs	64
5.1	Classification of metallic NCs	65
5.2	Production of metallic NCs	65
5.2.1	Metallic NCs synthesis methods.....	66
5.3	Applications of metallic nano-particles	67
5.3.1	Silver NCs.....	67

5.3.2 Pbs QDs	68
Conclusion.....	68
References	69

1. Introduction

1.1 Metal-organic frameworks

MOFs, sometimes referred to as porous coordination polymers, are a class of crystalline micro-porous materials formed from transition metal ions and poly-topic organic linkers which assemble into topologically diverse open network type structures [1-3]. These materials have been widely employed in numerous applications including gas storage, heterogeneous catalysis, molecular separation, sensing and for therapeutics and diagnostics in bio-medicine [4-9]. When compared to inorganic porous materials, MOFs offer an enormous variety of chemical composition allowing both their structure and functionality to be fine-tuned through judicious choice of building blocks. Further, their hybrid composition endows the frameworks with a degree of flexibility where typically linker-based motions can result in dynamic responsive behaviors [10, 11]. While the discovery of MOFs continues apace and detailed studies relating to their often unique behaviors and physical properties, recent research efforts are becoming increasingly focused on the growth and processing of MOFs into application specific configurations, including thin films, supported membranes and capsules [12-19]. MOF-based composites are also under increasing investigation, where the combination of MOFs with other components including ceramics, bio-polymers, nano-particles and proteins are leading to the development of new functional materials with enhanced properties [20].

1.2 Quantum dots

QDs are otherwise called as nano-crystals (NCs) because of their quantum size, i.e. in the range of 2-10 nanometers. They are made of nano-particles of conducting materials that have the ability to glow in various spectrum of colors when illuminated by light [21]. The size of the NCs determines the color of glow. A QD possess a discrete quantized energy spectrum of conduction band electrons, valence band holes, etc. The principle behind the NCs and glow is that when a QD is illuminated by light, some of the electrons in QD atoms tried to break from the atoms after receiving enough energy. The freed electrons have the ability to move through nano-particles by creating conductance band thus conducting electricity. These electrons emit light when they dropped back into valence band i.e. outer orbit of the atom. The energy difference between the conductance band

and valence band determines the color of the emission. When this higher blue color is emitted for the smaller nano-particle and for lower energy difference, the glow of QD will move towards the red spectrum for the large nano-particle. Due to high surface to volume ratio, QD displays intermediate properties of bulk semiconductors and discrete molecules [22-24]. The relationship between nano-particle size and the wavelength of the glow spectrum can be easily predicted by having control over the size of the NC [25]. It replicates the wave function for bulk semiconductors by applying a particle in a spherical model and derived the relation between the band gap and size of the NCs [26, 27]. Thus, QDs can be manufactured to emit any desired color of light by changing the size of the dots [28, 29].

QDs have received significant attention in the last two decades due to their unique tunable and size-dependent properties, making them of interest for but not limited to biological, analytical, medical and engineering applications [30-33]. These materials are comprised of thousands of atoms composed largely of elements from groups such as CdSe, ZnSe, ZnO, etc., and due to their small size being comparable to the wavelength of the electron, quantum confinement effects are often observed [34]. QDs have several advantages, including wide absorption bands, narrow and symmetrical emission bands, low photo-bleaching, long lifetimes and high quantum yields [35]. To date, many procedures to prepare these QD structures, including one-pot core-shell synthesis or growing the shell around the pre-synthesized core in a two-step methodology, have been reported [36, 37]. The dispersibility and stability of QDs in the desired media can be readily modulated by altering the nature of the surface ligands. Different organic ligands have been used to passivate QDs during synthesis, including phosphines, carboxylic acids, amines and thiols [38-41]. Ligand exchange, derivatization or encapsulation strategies can also be employed for further surface functionalization [42]. While ligand exchange often leads to a loss of QD fluorescence due to the creation of trapped states during the exchange process, it is a suitable alternative when the desired functional group cannot be incorporated onto the QD surface directly during synthesis. Derivatization of surface groups by facile organic transformations can endow the QDs with the appropriate functionality and reduce the amount of undesired ligands on the QD surface; however, a high QD stability under the organic reaction conditions is required. On the other hand, encapsulation of QDs in several media could enhance the physical properties and biocompatibility of the material. It has been shown that encapsulation of QDs in phospholipid micelles for example, endows the resulting composite with biocompatibility in addition to enhancing colloidal stability, which can be subsequently employed for in-vivo and in-vitro studies [43].

Coating QDs with an inorganic silica shell to yield QD@SiO₂ systems, it is demonstrated these hybrids to be bio-compatible, have low-toxicity and high water-dispersibility [44]. Organogelators also offer stability and good spatial distribution for metallic and non-metallic nano-particles. Thus, QD-organogel systems have also been reported, in which a symbiotic effect was observed: on one hand the critical concentration needed to form a stable organogel is reduced in the presence of the QD, and on the other the fluorescence quantum yield of the QD is enhanced when embedded in the organogel. In general, the QD comprises of core and shell structure. Multiple coatings around the core using different materials results in multiple shell structure and provides way for various applications. The important QD in this category are cadmium selenide (CdSe) and cadmium telluride (CdTe) which is widely used in electronics, photonics, photovoltaics and biomedicine. CdSe QD has its wide use in the optical industry preferably in quantum dot LED displays. Cadmium telluride QDs have found its application in thin film solar cells and bio-medicine labeling [45-49].

1.3 Gold QDs (AuQDs)

Gold nano-particles in quantum size (<2nm) behaves differently from noble gold metal and has high potential bio-medical, sensors and cosmetic field [50-52]. The advantages of AuQDs are high control over shape and size of AuQDs, high absorption bands in the visible spectrum, stability, bio-compatibility and high affinity towards various molecules. Between adjacent nano-particles, Au NCs exhibits Plasmon-plasmon optical interactions that changes its characteristic red color to bluish purple colour [53]. Fig. 1 shows the transmission electron micrographs of colloidal gold in various forms from nano-spheres, nano-rods and nano-prisms. Fig. 1(a) shows the Au nano-spheres developed using citrate reduction method and Fig. 1(d) represents the photographs of AuAg nano-particles colloidal dispersions with increasing Au nano-particles. Fig. 1(e) represents Au nano-rods of increasing aspect ratio developed by seeded growth (Fig. 1b). Ag nano-prisms with increasing lateral size (Fig. 1f) are developed (Fig. 1c).

Gold nano-shells are spherical NCs comprises dielectric silica or gold sulphide as core and thin layer of gold as shell. The Au-Plasmon resonance can be altered by varying the dimensions of the core and shell. Thus, Au nano-shells can be effectively used for near infra- red bio-sensing where the wavelength of the Au nano-shells are varied from visible spectrum to infrared and at near infrared region (between 700-1100nm), the tissues of living organisms are relatively transparent. Fig. 2 depicts that for the constant core radius, the wavelength of the core-shell can be stretched to longer wavelength with thinner shell. Also, the optically illuminated gold nano-shell effectively transfers heat to the surrounding environment at their resonant wavelength. This property can be used for

drug release at the target area in the living system [56]. Similarly, gold colloids are widely used in bio applications like hybridization assays, immunoblotting and flow cytometry owing to its excellent electron beam contrast and optical properties.

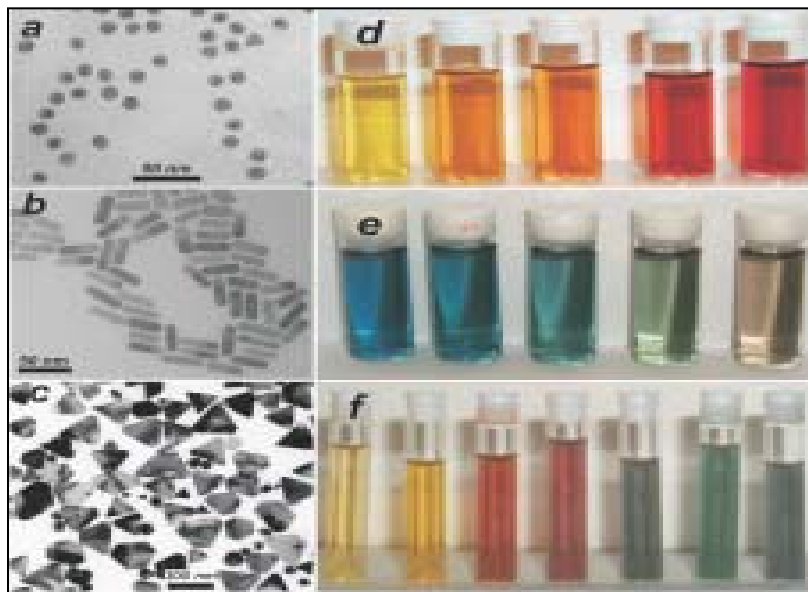


Fig. 1 Au nano-spheres and nano-rods [54].

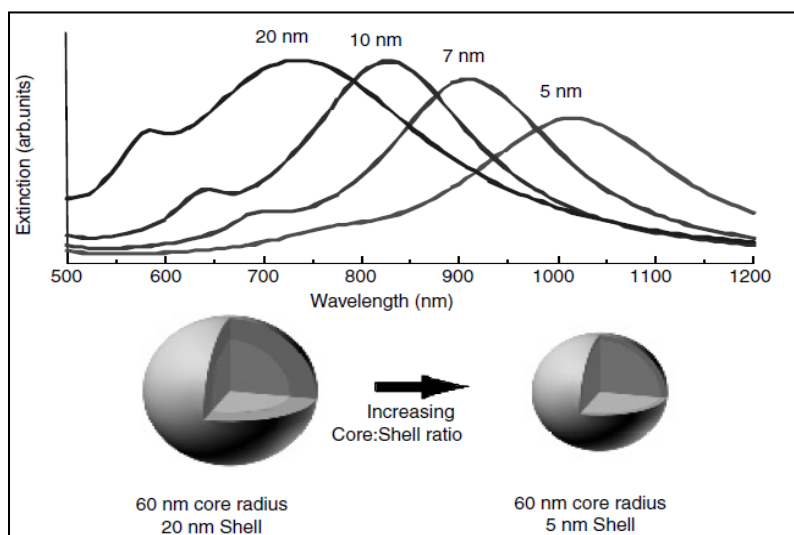


Fig. 2 Relation between Au core shell ratio and wavelength [55]

2. QD polymeric materials

2.1 Integration of QDs

Polymers are less dense than ceramic and metals due to low coordination number and have light-weight atoms of hydrogen and carbon. They possess excellent properties such as light-weight, corrosion resistance and are low-cost. They are transparent, flexible, easily processed and thus finds wider applications in automobile, defense, aerospace and electronics [57, 58]. The chemical properties of the polymers have the ability to assemble into ordered structures and their thermal behavior provides potential research interest for compatibilizing NCs. Thus various research efforts have been attempted in the integration of manipulating properties of polymer to that of the QD [59, 60]. NCs are susceptible to environment and mechanical damage during manipulation [61-63]. For the nano-structural applications like development of thin films, agglomeration and photoluminescence quenching should be avoided by protecting the individual properties of NCs. Thus, protecting the QD core by thin shell of organic material enhances the optical properties and bio-compatibility of NCs. Thus, various research attempts have been made to immobilize the QD core by embedding in the soft matter matrix of polymers. But, direct blending of polymers to NCs have issues of nano-particle segregation which reduces the distinct leading properties of NCs. Thus, encapsulation of QDs to polymers is one of the challenging research areas in organic-inorganic hybrid materials. Also due to their incompatibility with organic solvents and polymer matrices; it is generally difficult to induce high dispersion of QDs in the polymer matrix. Therefore, maintaining the inter-particle distance between the QDs which determines quantum yield of the resulting material is highly difficult [64-67].

2.2 Methods of encapsulating QD to polymer matrices

In order to encapsulate QDs to polymer matrices, four methods are generally used, as shown in Fig. 3. They are i) incorporation into premade polymers i.e. simple blending of QDs and polymers, ii) suspension polymerization i.e. the synthesis of QDs within polymers, iii) emulsion polymerization which involves the chain end attachment of polymers to QD surfaces and iv) mini emulsion polymerization that enables the growth of polymers directly from QD surfaces.

2.3 Incorporation into premade polymers

The general method used for incorporation into premade polymers is by loading of the QDs into polymer microgels avoiding surface damage to the QD core without affecting the quantity of QD into the polymer matrices. The microgel size can be controlled with

respect to the environment, pH, temperature and other parameters [69-71]. Kuang et al. [72] has reported works on tuning of pH levels for encapsulation of CdTe QDs into microgel. With the decrease in the pH levels, the microgel particles were swollen to trap QDs. On the other hand, the increase in pH level results in the shrinkage of microgel confining the QDs inside the microgel matrix. With further increase in the pH levels, QDs are released from the confinement (Fig. 4).

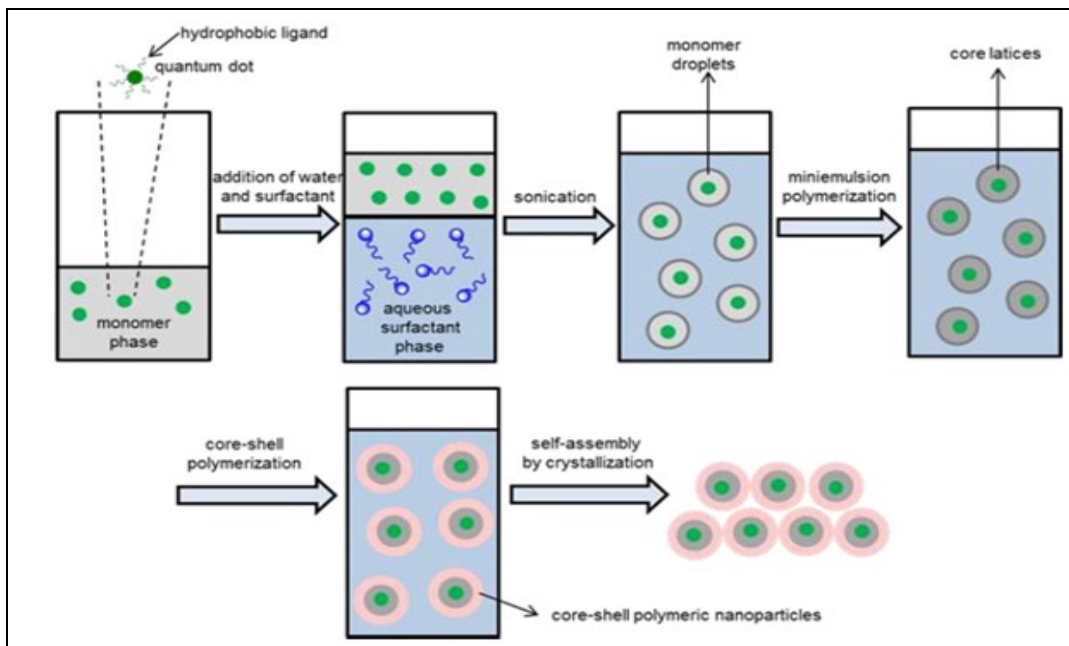


Fig. 3 Schematic illustration of QD to the core shell polymer nano-particles [68].

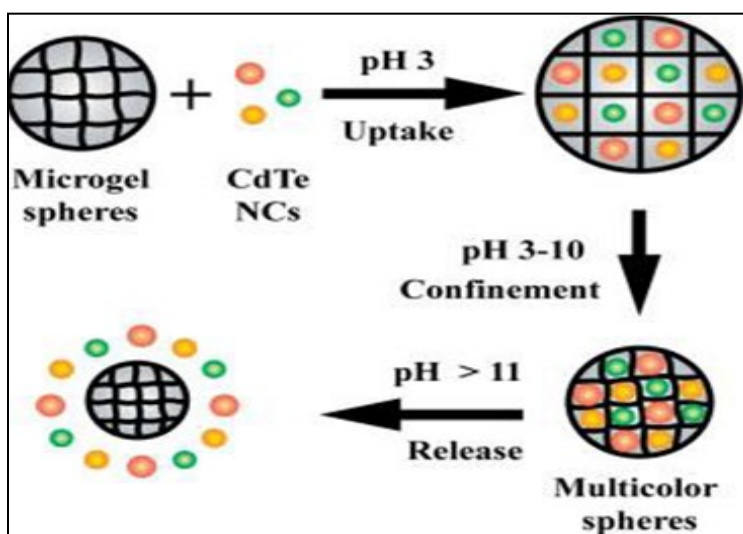


Fig. 4 Incorporation into premade polymers by swelling method by loading of CdTe NCs in PNIPVP spheres and their controlled release by pH [71].

2.4 Suspension polymerization

Suspension polymerization is one of the standard methods for encapsulating polymer QD hybrids. O'Brian et al. [73] synthesized polymerizable QD of hexadecylamine CdSe by ligand exchange. In suspension polymerization method, the NCs were made to disperse in styrene-divinyl benzene (DVB) monomer mixture using AIBN as initiator and polyvinyl alcohol was used as stabilizer. The homogeneity of the distribution of NCs can be measured by measuring the fluorescence at various points of the mixture. Bradley et al. [69] disperse QDs using suspension polymerization in a mixture of styrene and DVB. In this method, polyvinyl alcohol and benzoyl peroxide (BPO) is used as stabilizer and initiator respectively. Sheng et al. [74] develops QD-embedded polystyrene microspheres by dispersing CdSe/ZnCdS/ZnS QD in a continuous medium of ethanol using AIBN and poly (vinylpyrrolidone)(PVP) as initiator and stabilizer respectively.

2.5 Encapsulation via emulsion polymerization

Emulsion polymerisation is another method used to integrate QDs to colloidal polymer materials. Yang and Zhan [75] disperse the TOPO coated CdSe QD in toluene. At room temperature, the dispersion is added drop-wise to surfactant solution in water. To this prepared dispersion, monomer mixtures of styrene, DVB and methacrylic acid along with the AIBN initiator were added drop wise in an ice bath. Then, polymerization was carried out for 20 h after increasing the temperature to 70°C. Thus, emulsion polymerisation is a lengthy process where it requires attention in the surface preparation of the QDs to accommodate encapsulation of QDs into the polymers.

2.6 Encapsulation via miniemulsion polymerization

Miniemulsion polymerization method is used to generate hydrophobic dispersion of polymer particle that are compatible to integrate QDs. The miniemulsion polymerization system comprises monomer system, initiator type, surfactant and surface modification of QDs which determines the thermal equilibrium of the polymer NC system [76]. Fleischhaker and Zentel [77] developed core shell polymer-QD system which consists of PS/PMMA nano-particle encapsulated into fluorescent CdS/ZnS-coated CdSe QDs using miniemulsion polymerization method. For surface compatibility of the core with the polymer nano-particles, was made sodium dodecyl sulphate (SDS) and hexadecane (HD) is used as emulsifier and as co-stabilizer respectively. Lansalot et al. [78] have attempted core shell QDs by integrating polystyrene nano-particles to trioctylphosphine oxide (TOPO) coated CdSe/ZnS by both emulsion and mini emulsion polymerization methods. The results on observations indicated that conventional emulsion polymerization method was not successful in the integration of TOPO-coated QDs inside PS nano-particles.

3. QD hybrid materials

QDs show tremendous potential among biologists and chemists due to its three distinct advantageous i) the tunability of the QDs wavelength for band-edge absorption and fluorescence emission according to the size, ii) ability to detect photoluminescence spectra of QDs in a wide wavelength region iii) QDs are extremely photostable and have long luminescent life [79, 80]. Major viability of the QDs NC particles is restricted due to their toxicity. Many of the NC materials like cadmium, arsenic, tellurium, etc., are toxic and carcinogen agents and cannot be injected directly into the body. With the advancement of technologies, new QD materials were developed to address the environmental and toxicity. Thus non-toxic and bio-compatible NC particles that are cadmium free have found wider applications in bio-medical, medical imaging, bio-analytics and bio-labeling.

Another limitation of QDs which restrict its bio-compatibility apart from metallic toxicity is the non-dissolubility and photo luminescence instability i.e., decrease in the fluorescence quantum yields of QDs in the aqueous solution or any other biological medium. But by encapsulating the QDs into the polymer nano-particles, hybrid core-shell materials are developed that provide robust colloidal and photo luminescence stability in different biological mediums. Thus polymers coated QDs that are biocompatible have become potential candidates for wider bio-medical applications [81, 82] with their optical and electronic properties remain intact. Also, by introduction of functional groups for QDs, they can be manipulated for various end-use applications as shown in Fig. 5.

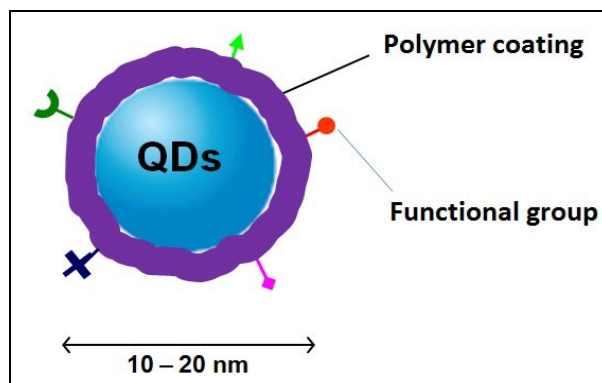


Fig. 5 Schematic depiction of polymer/QD hybrids [83].

3.1 Strategies to generate QD hybrid materials

Fig. 6 provides the five major strategies where QD surface are modified by polymers to generate biocompatible polymer/QD hybrid materials that are grouped as i) exchanging

ligand between polymer and QDs; ii) polymer grafting to QDs; iii) polymer grafting from QDs; iv) polymer capping onto QDs; v) growing QDs within polymer template.

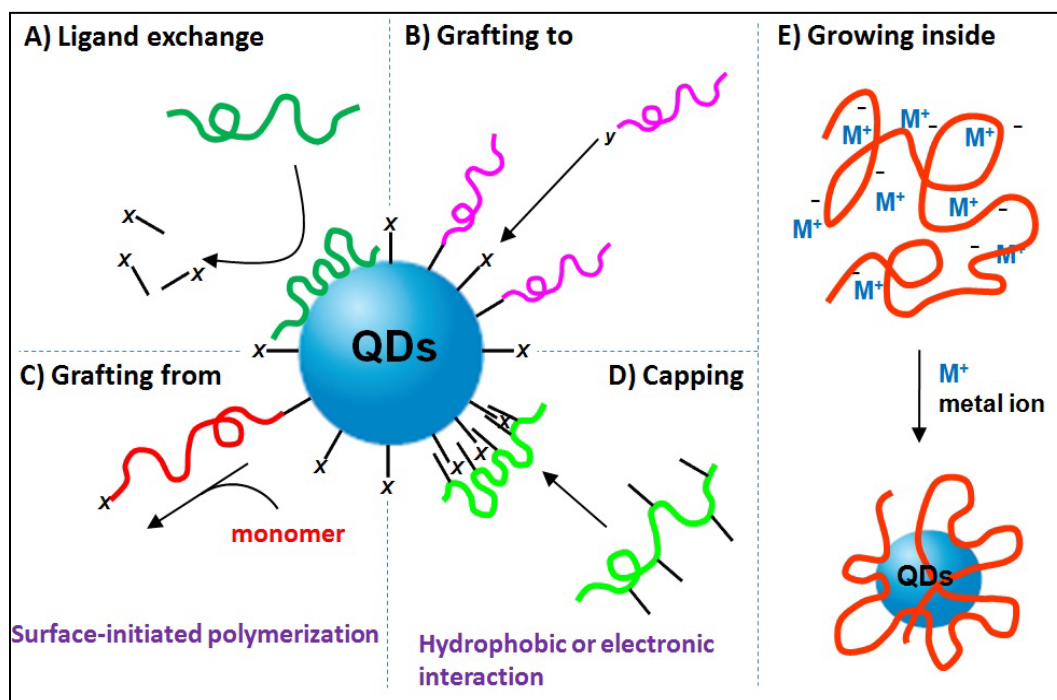


Fig. 6 Schematic summary of synthetic strategies for fabricating biocompatible polymer/QDs hybrid materials, categorized as A) exchanging ligand between polymer and QDs; (B) polymer grafting to QDs; (C) polymer grafting from QDs; (D) polymer capping onto QDs; (E) growing QDs within polymer template [83].

3.2 Exchanging ligand between polymer and QDs

Ligand exchange is the process of replacing existing as grown ligand with new biocompatible polymers. In order to passivate QDs to the polymers, polymers generally have functional anchor groups such as thiol, amine and carboxyl. For example thiol terminated poly(PEG) is a bio-compatible polymer that is used to prepare bio-compatible QDs fluorospores [84, 85]. Similar studies on bio-compatible polymers like thiol-PEG-peptide hybrid polymers [86], thiol terminated OH-poly (amidoamine) (OH-PAMAM) hyper-branched polymers [87], Amine-NH₂ modified poly(acrylic acid) (PAA) [88, 89], NH₂ functionalized poly (acryloyloxysuccinimide) (PAAS) [90], NH₂ modified PEG [91] by ligand exchange method have yielded positive results like increased pH responsiveness, great disparity, enhanced brightness and robust colloidal stability. Poly(2-(dimethy-lamino) ethyl methacrylate) (PDMAEMA) [92], a thermo-pH sensitive

polymer with tertiary amines is modified to encapsulate CdSe QDs in small loops through ligand exchange as shown in Fig. 7.

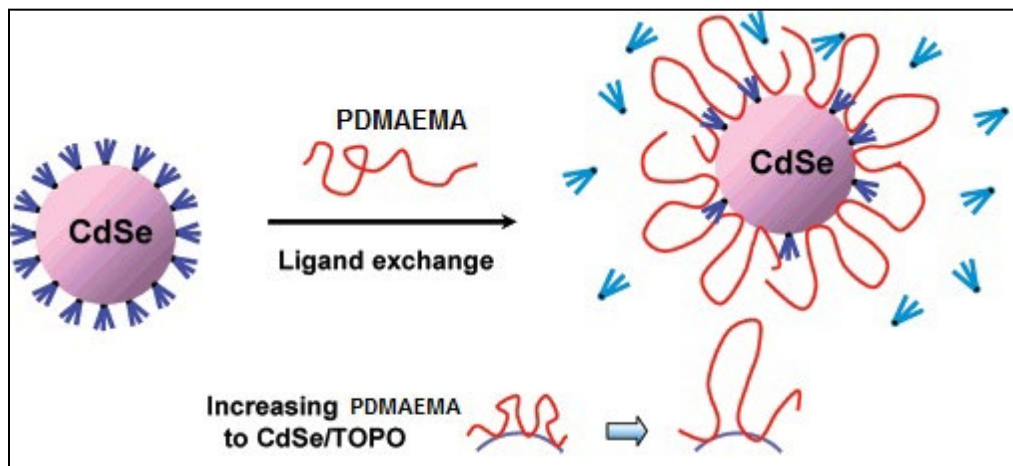


Fig. 7 Scheme of ligand exchange process of PDMAEMA with CdSe QDs [93].

3.3 Polymer grafting to QDs

In graft-to approach, the biocompatible polymers covalently attached to QDs surface using their functionalised anchor groups at the end of the polymer chain through ligand exchange. Skaff et al. [94] has attempted to develop a water soluble, PEG functionalized QD using grafting-to-method of ligand exchange using pyridine functionalized poly(ethylene glycol) (PEG) for TOPO on CdSe NC particles. The resulting polymer-QD is shown in Fig. 8. Similar attempts have been made by Peng et al. in generating biocompatible PEI/QDs with great water solubility using ligand exchange of hyper branched PEI to CdSe [95]. Also PEG/CdSe QDs are synthesized through 1-ethyl-3-(3-dimethylaminopropyl) carbodiimide/N-hydroxysuccinimide (EDC/NHS) reaction [95, 96].

3.4 Polymer grafting from QDs

In graft-from approach, the polymerization takes place from the ligands attached to the QD surface. Thus the polymers are grown outward from the QD surface. Some of the prominent polymerisation techniques used in polymer grafting are ring-opening polymerization [97], reversible addition-fragmentation chain transfer polymerization [98], nitroxide-mediated radical polymerization [99], atom transfer radical polymerization [100, 101] and oxyanionic vinyl polymerization [102].

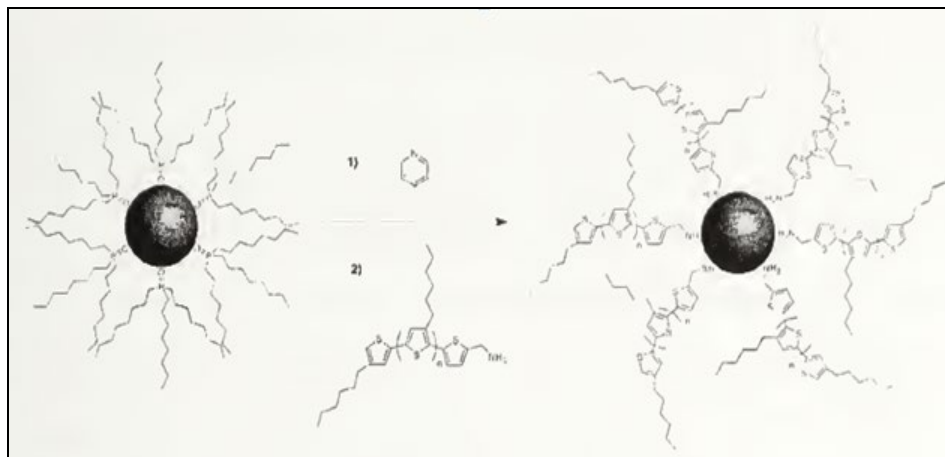


Fig. 8 Polymer graft-to QDs method of ligand exchange of TOPO-covered CdSe nanoparticles with PEG [94].

3.5 Polymer capping into QDs

Polymers are used as capping agents by hydrophobic or electronic interaction. It improves the stability of the QDs. Amphiphilic co-polymers promotes QDs dispersion in water by coupling the original QDs ligands with their hydrophobic segments. Comparing to graft-from and graft-to methods of polymerization, capping method provides more stability because of multiple interactions of QDs with the single polymer chain results in smaller hydrodynamic sizes of polymer-QDs in water. For example, hydrophobic core and QDs that remain stable in water are synthesized in amphiphilic PEG polymers [103-106].

3.6 QDs growth within polymer

In this method, QDs are directly grown inside the polymers containing metal-ion segments that are chemically transformed into QDs NC particle by reduction or precipitation reaction. For example PMMA/CdS and PAMAM/CdS are fabricated using PMMA polymeric microsphere [107, 108] and PAMAM dendrimer [109].

3.7 Challenges in biocompatible polymer/QDs

- Reduction in quantum yields of QD surfaces due to surface interaction of polymer with QD core.
- Further demand for smaller polymer/QDs for applications in cell level.
- Development of polymer/QDs that are colloidal stable over long-term, aggregation-free use in aqueous environment and thermally stable.

- Still toxicity of the QDs are not completely addressed.
- Retrieval of polymer-QDs from the body.

4. Applications of QD composites

QDs being semiconductor NCs due to their ability of high light absorption over wide spectrum range, luminescence nature have found wider applications in optoelectronics and bio-medical fields [110, 111]. The NCs are not soluble on aqueous medium and do not possess bio-compatibility. But synthesizing QDs using polymer-QDs encapsulation techniques with the functionalized groups like mercaptoacetic acid facilitates aqueous solubility [112]. In bio-medical area, its ability to control size and display broad spectrum of colors for a single excitation of QDs have found many application in bio-imaging, bio-sensing, and bio-assay applications.

4.1 Bio-imaging

The QDs which showing an emission wave length ranging from 700-900 nm can be used for biological imaging, because the QDs have near-infrared luminescent property has maximum depth of penetration in tissue and the interference of tissue auto fluorescence is minimum [113, 114]. Water soluble QDs that are paramagnetic coated are widely preferred for its luminescence in bio-imaging and magnetic resonance. They are also used as bio-markers in labelling cells and in identifying timorous cancerous cells. Hyun et al. [115] synthesized near infrared fluorescence imaging with water soluble PbS and PbSe QDs capped with carboxylic groups using ligand exchange method to label cells. Li et al. [116] used CdTe QDs core that are capped with 3-mercaptopropionic acid (3-MPA) for bio-imaging of salmonella typhimurium cells. Similarly, Mulder et al. [117] achieved labelling of HeLa cells using CdSe/ZnS QDs and also developed MRI detectable paramagnetic QDs conjugated with cyclic peptides that target human endothelial cells. Weissleder [118] provided clear vision in-vivo imaging of tissues and blood using InP and InAs QDs system in the near infrared region. Bio-imaging of salmonella typhimurium cells was made feasible using CdS QDs as core capped with 3-mercaptopropionic acid (MPA) [119]. Cao et al. claimed near infrared QDs with QD800 emission with a wavelength of 800nm detects cancer cells much better than conventional cancer recognition techniques [113]. Hyu et al. used carboxylic group functionalized PbSe QDs to bio-label imaging of human colon cancer cells [120].

4.2 Photo-thermal therapies

QDs embedded in matrix material have the ability to transfer heat to the surrounding environment when illuminated with the resonance wavelength. This photo-thermal effect

is effectively used in the transfer of drugs to the target cells. Polymers must be identified to be thermally stable. It results in many polymer-QDs drug delivery systems [121]. Okano et al. demonstrated photo-thermal ability of N-isopropylacrylamide and acrylamide that are stable at lower critical stability temperature (LCST) which is equivalent to that of the body temperature. But, further increase in LCST temperature results in the collapse of polymer-QD matrix system. The phase change results in the burst of the matrix that releases any soluble medium like drug in the system [122]. Photo-thermal ability of polymer QDs is effectively used in tumour ablation. The QD painted tumour cells are affectively killed when they exposed to near infra-red light without affecting the normal cell [123].

4.3 Opto-electric applications

The quantum size tunable semiconductor NCs have found its place in the development of many applications like light emitting diodes (LEDs) [124], photo-voltaics [125, 126], thermo-electric devices [127], etc.

4.3.1 QD LEDs

The first polymer-QDLEDs was reported by Colvin et al. [128] in 1994 by combining polymer-QD matrix of CdSe core shell and a soluble polymer-poly(p-phenylenevinylene) PPV derivative layer. Since then, CdSe/CdS has provided significant improvement in the advancement of LED [129]. Hybrid organic NC composites are unstable with metal conductivity and are subjected to organic degradation which limits its lifetime under high current conditions. The above limitations were overcome with the advent of non-contact polymers that forms photo-luminescence layer when combined with QD core [130, 131].

4.3.2 Polymer QD liquid crystal displays

The photo-emissivity property of QDs effectively converts backlight, a critical part of LCDs to emit basic colors of red, green and blue. Backlight of LCDs is so important, that it affects optical brightness efficiency, color distribution and viewing angle [132-135]. The LCD backlight is basically a blue QD layer that creates a basic blue background color. Red and green QDs are applied as a separate layer. The LCD backlight supplies energy to green and red QDs to their respective colors. The final image is created after passing through the color filter. QDs are highly efficient in creating highly saturated ultra-deep colors of splendid image quality with high brightness using less energy. The important features of QDs application of LCD is given as follows: i) Control over wavelength emission, ii) Size uniformity that determines its full width at half maximum, iii) High photo-luminescence efficiency, iv) Simple device configuration [136-144].

4.3.3 QD polymer photo-voltaic devices

QDs have found its application in the manufacturing of solar cells and slowly replace the conventional use of silicon which requires an extensive purification process. QD solar cells thus can be developed from inexpensive polymer materials at room temperature. For the application of QDs in solar cell, they are used as either photo sensitizer or as an electron receptor. For example poly (N-vinylcarbazole) [145,146] in polymer QD matrix is used to enhance photo-induced charged generation whereas poly (3-hexylthiophene), phenyl-C61-butyric acid methyl ester or poly(p-phenylene vinylene) is used for their excellent electron conductivity properties [147-150].

5. Metallic NCs

The QDs are classified into three groups based on the particle size, nature and composition of NC particle where their photo-luminescence emission band of QDs can be manipulated from UV to infrared regions (Fig. 9). Thus based on the binary alloys of atoms QDs are grouped as i) ZnS, CdS, CdSe, HgS (12-16 atoms), ii) GaAs, InP, InAs, GaN (13-15 atoms), and iii) PbTe, PbSe (14-16 atoms) [151, 152].

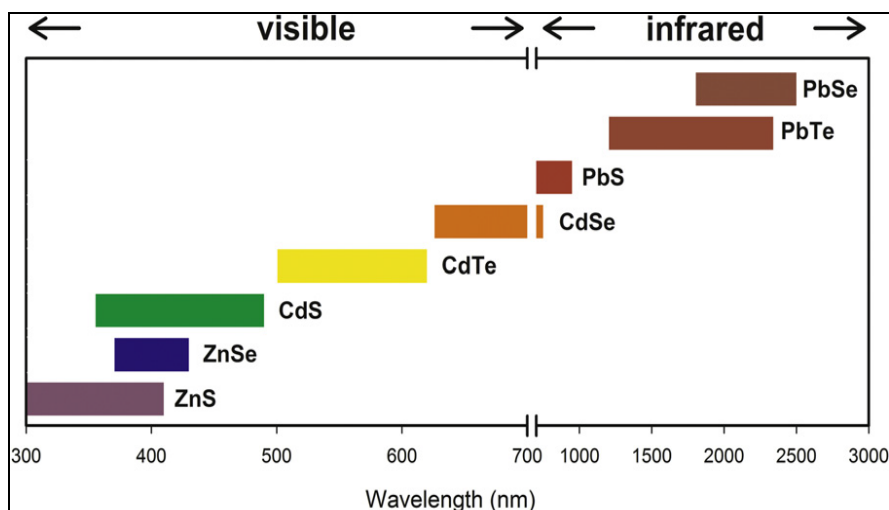


Fig. 9 QDs fluorescence emission wavelengths [153].

The study of metals as nano-materials is one of the favorable studies among the biologists, physicists and chemists in the area of nano-science to develop new nano-material for applications in the area of electronics, bio-medical, photo-voltaic, etc. [154]. Similar to the study of QDs of polymer, the focus of nano-materials is on the study of the properties of optical, chemical and electronic properties and its relationship between its structures. At quantum mechanics level, the normal bulk properties of the metals are found to be completely different, when their dimensions are reduced to Fermi wavelength

of electron [155, 156]. The transition of properties of metals at quantum level results in i) The continuum of electron state is destroyed, ii) Increase in size of the fraction of surface atoms. These changes at the quantum level results in the loss of bulk properties [157, 158]. Also, these metallic NCs show new properties of electric, optic and magnetic properties which contradict the conventional metallic properties. Some of the productive and distinctive properties which the metal NCs exhibit are Raman scattering effect enhanced by surface characteristics, local field enhancement by surface second harmonic generation and fast optical non-linearity in the third order [159-161]. Some of the important characteristic of NC metals are i) large surface-area-to-volume ratio, ii) molecular and metallic states will have specific electronic structure due to large surface energies transition, iii) plasmon excitation, iv) quantum confinement, v) short range ordering, vi) specific chemical properties and vii) excess electrons storing capability.

5.1 Classification of metallic NCs

The foundation of modern colloidal science was given by Michael Faraday in the nineteenth century with the study of gold-sol. Since, the inceptions of gold-sols, several metals were attempted in the production of NCs. Generally, metals possess excellent crystal structure that remains intact even at the nano-scale. The extraordinary stability of the metallic nano-clusters are attributed to the atomic or electronic shell closing due to which they are called as magic clusters. Some of the metals that are widely used as nano-clusters are copper (Cu), silver (Ag), gold (Au), nickel (Ni), palladium (Pd), platinum (Pt), aluminium (Al), iron (Fe), chromium (Cr), vanadium (V), titanium (W), selenium (Se), zinc (Zn), etc. Among the possible metal nano-clusters, the noble metals, Au and Ag are highly used for their excellent photo-luminescence properties. Though the quantum yield (QY) of these metals is low in earlier studies, the QY has been enhanced to 10^{-3} to 10^{-1} in the later studies [162].

5.2 Production of metallic NCs

In order to produce metal NCs in large scale and to be used for commercial purpose, the dispersion of metal NCs in the polymer matrix must be controlled. Generally, by reducing the metal ions of the metals, the metallic NCs are formed. But, aggregation of NCs is the major issue faced in the reduction of metal ion in aqueous solution. Aggregation results in the formation of large metal crystals which affects the quantum properties of metallic NCs [161]. Therefore, to improve their fluorescence properties, a suitable catalyst is added to the metallic NCs which acts as a stabilizer and prevents large NCs formation. Thus, to synthesize metallic colloid NCs, electro-static interactions across Debye double layer should be stable when stabilizing agents like surfactant and polymers are added [163, 164]. Thus the production of metallic NCs depends on the

methods that are i) reproducible, ii) ability to control the shape of the particles, iii) yielding monodisperse metallic nano-particles, iv) water soluble, v) environmental friendly, vi) use less number of reagents and vii) less waste generation.

5.2.1 Metallic NCs synthesis methods

Generally synthesis of metallic NCs involves two methods. One is breakdown (Top down) method where the solid is breakdown into ultrafine NC particles due to the application of external force. The other method is a buildup (bottom up) method which produces nano-particles based in atomic/molecular level transformations of atoms from gas or liquid medium. Some of the top down and bottom up approaches of producing metal NCs are given in Fig. 10.

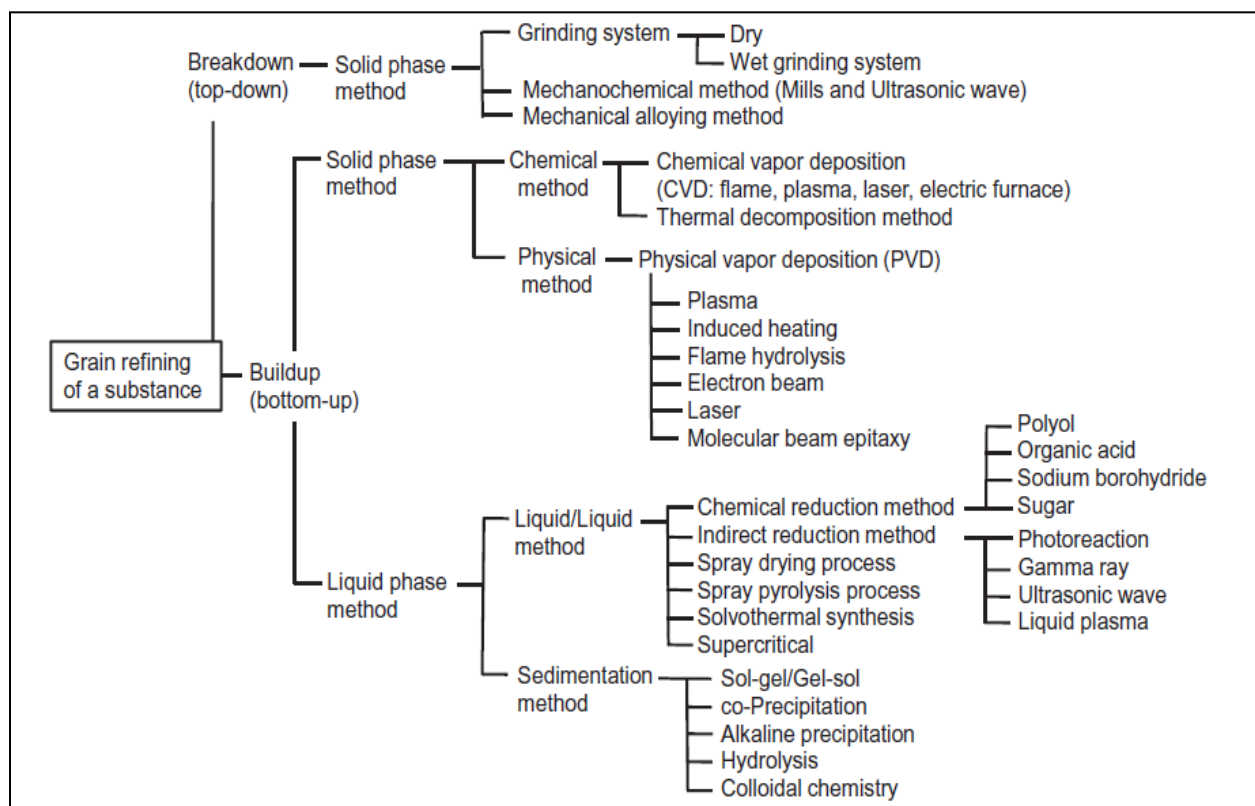


Fig. 10 Top Down and Bottom up approaches of synthesis of metallic NCs [165].

5.3 Applications of metallic nano-particles

The absorption ability of the material into the surface of metal nano-particles is determined by the factor called surface plasmon resonance (SPR). SPR is an optical effect which is used to measure the resonant oscillation of binding electrons in real time when stimulated by incident light [166]. SPR is an important technique that its ability to measure affinity and kinetics between inter-molecular interactions makes its wide use in color based bio-sensor applications, binding between DNA and protein, a protein and antibody, etc.

5.3.1 Silver NCs

Silver NC is widely used in metal QD applications owing to its high plasmon excitation. In the visible spectrum, its plasmon resonance can be tuned for any wavelength. With an Ag NC, the morphology that can be controlled are size and shape, refractive index medium, behaviour at solid solution interface etc. as shown in Fig. 11. Some of the applications of Ag colloidal QDs are represented in Fig. 12.

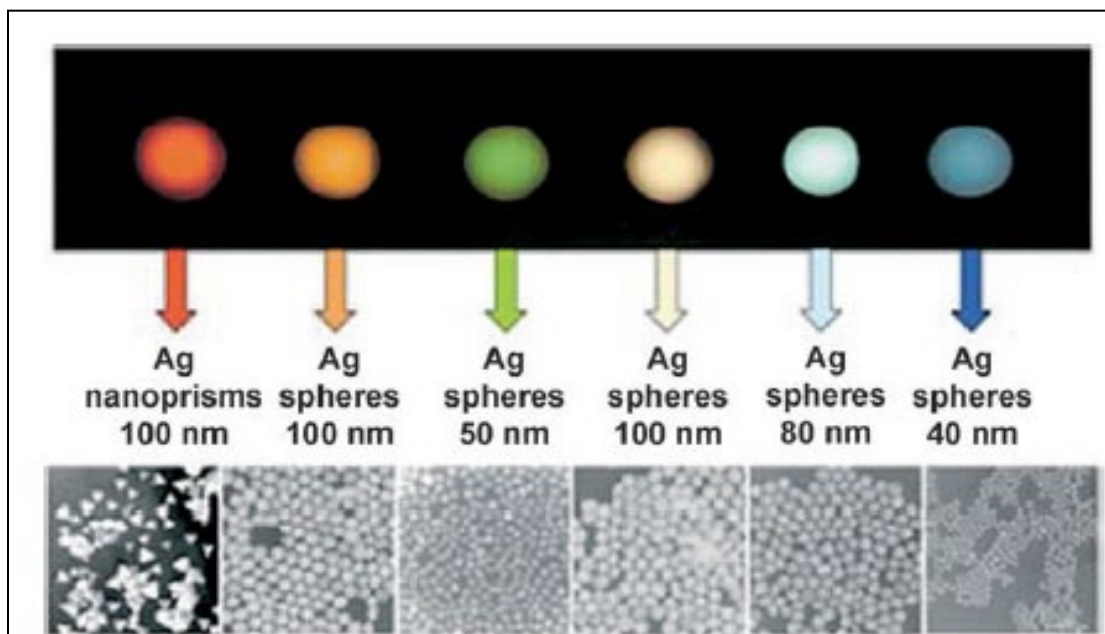


Fig. 11 Influence of Ag particles under SPR [167].

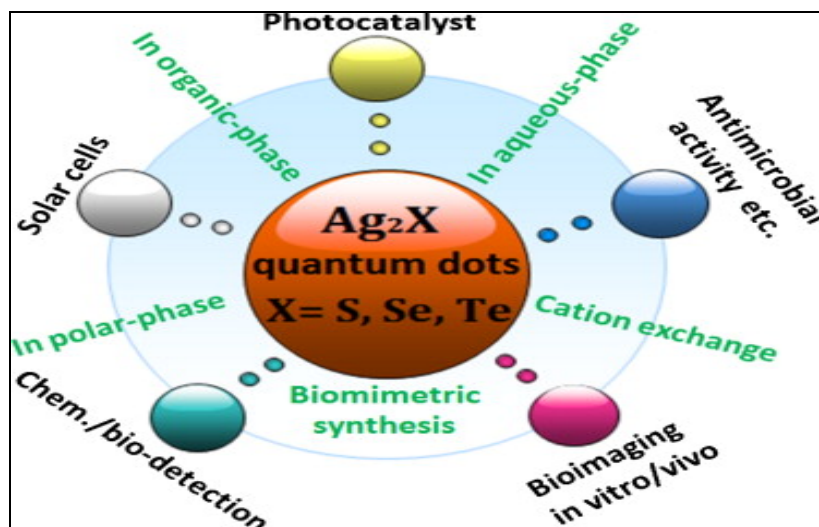


Fig. 12 Applications of Ag QDs [168].

5.3.2 Pbs QDs

The Pbs QDs exhibit broad absorption spectrum range, high peak-to-valley ratio (>4) and narrow fluorescence band emissions (<100 nm) owing to its size (2.5-8nm) and tunable emission wavelength (900-1600nm). It is widely used in infrared LEDs and in solar cells as light absorbers or infrared emitter [169]. i) Gold – DNA labelling, drug delivery , cancer therapy and microbial, ii) selenium – anticancer, antimicrobial, iii) palladium – biocatalysts, iv) copper – antimicrobial, v) platinum – anticancer, vi) silver – anticancer, antimicrobial, antiviral, vii) zinc oxide – cosmetic coating and viii) iron – anticancer, molecular imaging, cancer therapy.

Conclusion

This chapter summarizes the production, modification, and applications of QD@MOF composites for several industrial purposes. The production mechanisms such as crystallization, interfacial diffusion, micro-fluidic processing, and vapour deposition methods are discussed in detail. From the literature it is clearly observed that there is significant improvement by changing the microstructure, affinity, and pore size of the QD@MOF composites. The applications of QD@MOF composites including gas storage, separation, nano-filtration, stimuli-responsiveness, etc. are critically analyzed. The tremendous achievements in production, modification, and applications of QD@MOF have been achieved in recent years, still many challenges and opportunities exist for further research. We hope that understanding of production process, modification and applications of QD@MOF composites will be helpful for industrial

applications. In conclusion QD@MOF composites are an important type of material that has a bright future and the potential across several fields of research.

References

- [1] S. Kitagawa, R. Kitaura, S.-i. Noro, Functional porous coordination polymers, *Angew. Chem. Int. Ed.*, 43 (2004) 2334-2375. <https://doi.org/10.1002/anie.200300610>
- [2] H. Li, M. Eddaoudi, M. O'Keeffe, O.M. Yaghi, Design and synthesis of an exceptionally stable and highly porous metal-organic framework, *Nature*, 402 (1999) 276-279. <https://doi.org/10.1038/46248>
- [3] A.K. Cheetham, C.N.R. Rao, R.K. Feller, Structural diversity and chemical trends in hybrid inorganic–organic framework materials, *Chem. Commun.*, 0 (2006) 4780-4795. <https://doi.org/10.1039/B610264F>
- [4] J.-R.Li, R.J. Kuppler, H.-C.Zhou, Selective gas adsorption and separation in metal-organic frameworks, *Chem. Soc. Rev.* 38 (2009) 1477-1504. <https://doi.org/10.1039/b802426j>
- [5] J. Lee, O.K. Farha, J. Roberts, K.A. Scheidt, S.T. Nguyen, J.T. Hupp, Metal-organic framework materials as catalysts *Chem. Soc. Rev.* 38(2009) 1450-1459. <https://doi.org/10.1039/b807080f>
- [6] J.-R.Li, J. Sculley, H.-C. Zhou, Metal-organic frameworks for separations *Chem. Rev.* 112 (2011) 869-932. <https://doi.org/10.1021/cr200190s>
- [7] L.E. Kreno, K. Leong, O.K. Farha, M. Allendorf, R.P. Van Duyne, J.T. Hupp, Metal-organic framework materials as chemical sensors, *Chem. Rev.* 112 (2011) 1105-1125. <https://doi.org/10.1021/cr200324t>
- [8] P. Juzenas, W. Chen, Y.-P. Sun, M.A.N. Coelho, R. Generalov, N. Generalova, I.L. Christensen, Quantum dots and nanoparticles for photodynamic and radiation therapies of cancer, *Adv. Drug Deliver. Rev.* 60 (2008) 1600-1614. <https://doi.org/10.1016/j.addr.2008.08.004>
- [9] C.E. Probst, P. Zrazhevskiy, V. Bagalkot, X. Gao, Quantum dots as a platform for nanoparticle drug delivery vehicle design, *Adv. Drug Deliver. Rev.* 65 (2013) 703-718. <https://doi.org/10.1016/j.addr.2012.09.036>
- [10] J. Rabone, Y.-F. Yue, S.Y. Chong, K.C. Stylianou, J. Bacsá, D. Bradshaw, G.R. Darling, N.G. Berry, Y.Z. Khimyak, A.Y. Ganin, P. Wipar, J.B. Claridge, M.J. Rosseinsky, An adaptable peptide-based porous material, *Science*, 329 (2010) 1053-1057. <https://doi.org/10.1126/science.1190672>

- [11] A. Ghoufi, A. Subercaze, Q. Ma, P.G. Yot, Y. Ke, I. Puente-Orench, T. Devic, V. Guillerm, C. Zhong, C. Serre, G. Ferey, G. Maurin, Comparative Guest, Thermal, and Mechanical Breathing of the Porous Metal Organic Framework MIL-53(Cr): A Computational Exploration Supported by Experiments, *J. Phys. Chem. C*, 116 (2012) 13289-13295. <https://doi.org/10.1021/jp303686m>
- [12] Y. Sakata, S. Furukawa, M. Kondo, K. Hirai, N. Horike, Y. Takashima, H. Uehara, N. Louvain, M. Meilikhov, T. Tsuruoka, S. Isoda, W. Kosaka, O. Sakata, S. Kitagawa, Shape-memory nanopores induced in coordination frameworks by crystal downsizing, *Science*, 339 (2013) 193-196. <https://doi.org/10.1126/science.1231451>
- [13] T.D. Bennett, J. Sotelo, J.-C.Tan, S.A. Moggach, Mechanical properties of zeolitic metal-organic frameworks: mechanically flexible topologies and stabilization against structural collapse, *Cryst. Eng. Comm.* 17 (2015) 286-289. <https://doi.org/10.1039/C4CE02145B>
- [14] D. Bradshaw, A. Garai, J. Huo, Metal-organic framework growth at functional interfaces: thin films and composites for diverse applications, *Chem. Soc. Rev.* 41 (2012) 2344-2381. <https://doi.org/10.1039/C1CS15276A>
- [15] A. Betard, R.A. Fischer, Metal-Organic Framework Thin Films: From Fundamentals to Applications, *Chem. Rev.*, 112 (2012) 1055-1083. <https://doi.org/10.1021/cr200167v>
- [16] Y. Hu, X. Dong, J. Nan, W. Jin, X. Ren, N. Xu, Y.M. Lee, Metal-organic framework membranes fabricated via reactive seeding *Chem. Commun.* 47 (2011) 737-739. <https://doi.org/10.1039/C0CC03927F>
- [17] M.S. Denny, S.M. Cohen, In situ modification of metal-organic frameworks in mixed-matrix membranes, *Angew. Chem. Int. Ed.*, 54 (2015) 9029-9032. <https://doi.org/10.1002/anie.201504077>
- [18] J. Huo, J. Aguilera-Sigalat, S. El-Hankari, D. Bradshaw, Magnetic MOF microreactors for recyclable size-selective biocatalysis, *Chem. Sci.* 6 (2015) 1938-1943. <https://doi.org/10.1039/C4SC03367A>
- [19] A. Carne-Sanchez, I. Imaz, M. Cano-Sarabia, D. MasPOCH, A spray-drying strategy for synthesis of nanoscale metal-organic frameworks and their assembly into hollow superstructures, *Nat, Chem*, 5 (2013) 203-211. <https://doi.org/10.1038/nchem.1569>
- [20] Q.-L.Zhu, Q. Xu, Metal-organic framework composites, *Chem. Soc. Rev.* 43 (2014) 5468-5512. <https://doi.org/10.1039/C3CS60472A>

- [21] Ekimov, A. I.; Onushchenko, A. A. Quantum size effect in three-dimensional microscopic semiconductor crystals, *JETP Lett.* 34 (1981) 345–349.
- [22] Kastner, M. A. Artificial Atoms, *Physics Today* 46 (1) (1993) 24.
<https://doi.org/10.1063/1.881393>. <https://doi.org/10.1063/1.881393>
- [23] Ashoori, R. C. Electrons in artificial atoms, *Nature*, 379(6564) (1996) 413-419.
<https://doi.org/10.1038/379413a0>
- [24] Collier, C. P.; Vossmeier, T.; Heath, J. R. Nanocrystal superlattices, *Annual Review of Physical Chemistry*, 49 (1998) 371-404.
<https://doi.org/10.1146/annurev.physchem.49.1.371>
- [25] Yoffe, A.D. Semiconductor quantum dots and related systems: Electronic, optical, luminescence and related properties of low dimensional systems, *Advances in Physics*, 50(1) (2001) 1-208. <https://doi.org/10.1080/00018730010006608>
- [26] Brus L., Electron-electron and electron-hole interactions in small semiconductor crystallites: the size dependence of the lowest excited electronic state. *J Chem Phys* 80 (1984) 4403–44093. <https://doi.org/10.1063/1.447218>
- [27] Brus L., Electronic wave functions in semiconductor clusters: experiment and theory. *J Phys Chem* 90(12) (1986) 2555–2560. <https://doi.org/10.1021/j100403a003>
- [28] Sabaeian, Mohammad; Khaledi-Nasab, Ali, "Size-dependent intersubband optical properties of dome-shaped InAs/GaAs quantum dots with wetting layer". *Applied Optics*. 51 (18): 4176–4185. <https://doi.org/10.1364/AO.51.004176>
- [29] Khaledi-Nasab, Ali; Sabaeian, Mohammad; Sahrai, Mostafa; Fallahi, Vahid (2014). "Kerr nonlinearity due to intersubband transitions in a three-level InAs/GaAs quantum dot: the impact of a wetting layer on dispersion curves". *Journal of Optics*. 16 (5): 055004. <https://doi.org/10.1088/2040-8978/16/5/055004>
- [30] X. Michalet, F.F. Pinaud, L.A. Bentolila, J.M. Tsay, S. Doose, J.J. Li, G. Sundaresan, A.M. Wu, S.S. Gambhir, S. Weiss, Quantum dots for live cells, in vivo imaging, and diagnostics, *Science*, 307 (2005) 538-544.
<https://doi.org/10.1126/science.1104274>
- [31] P. Alivisatos, The use of nanocrystals in biological detection *Nat Biotech*, 22 (2004) 47-52. <https://doi.org/10.1038/nbt927>
- [32] R.C. Somers, M.G. Bawendi, D.G. Nocera, CdSe nanocrystal based chem-/bio-sensors *Chem. Soc. Rev.* 36 (2007) 579-591. <https://doi.org/10.1039/b517613c>

- [33] F. Chen, D. Gerion, Fluorescent CdSe/ZnS nanocrystal-peptide conjugates for long-term, nontoxic imaging and nuclear targeting in living cells, *Nano Lett.*, 4 (2004) 1827-1832. <https://doi.org/10.1021/nl049170q>
- [34] M.G. Bawendi, M.L. Steigerwald, L.E. Brus, The quantum mechanics of larger semiconductor clusters ("quantum dots"), *Annu. Rev. Phys. Chem.*, 41 (1990) 477-496. <https://doi.org/10.1146/annurev.pc.41.100190.002401>
- [35] U. Resch-Genger, M. Grabolle, S. Cavaliere-Jaricot, R. Nitschke, T. Nann, Quantum dots versus organic dyes as fluorescent labels, *Nat Meth*, 5(2008) 763-775. <https://doi.org/10.1038/nmeth.1248>
- [36] B.O. Dabbousi, J. Rodriguez-Viejo, F.V. Mikulec, J.R. Heine, H. Mattoussi, R. Ober, K.F. Jensen, M.G. Bawendi, (CdSe)ZnS core-shell quantum dots: synthesis and characterization of a size series of highly luminescent nanocrystallites, *J. Phys. Chem. B*, 101 (1997) 9463-9475. <https://doi.org/10.1021/jp971091y>
- [37] M.A. Hines, P. Guyot-Sionnest, Synthesis and characterization of strongly luminescing zns-capped cdse nanocrystals, *J. Phys. Chem.*, 100 (1996) 468-471. <https://doi.org/10.1021/jp9530562>
- [38] D.V. Talapin, A.L. Rogach, A. Kornowski, M. Haase, H. Weller, Highly luminescent monodisperse CdSe and CdSe/ZnS nanocrystals synthesized in a hexadecylamine-trioctylphosphine oxide-trioctylphosphine mixture, *Nano Lett.*, 1 (2001) 207-211. <https://doi.org/10.1021/nl0155126>
- [39] C.B. Murray, D.J. Norris, M.G. Bawendi, Synthesis and characterization of nearly monodisperse CdE (E = sulfur, selenium, tellurium) semiconductor nanocrystallites, *J. Am. Chem. Soc.*, 115 (1993) 8706-8715. <https://doi.org/10.1021/ja00072a025>
- [40] H. Shen, H. Wang, Z. Tang, J.Z. Niu, S. Lou, Z. Du, L.S. Li, High quality synthesis of monodisperse zinc-blende CdSe and CdSe/ZnS nanocrystals with a phosphine-free method, *Cryst.Eng Comm*, 11 (2009) 1733-1738. <https://doi.org/10.1039/b909063k>
- [41] J. Aguilera-Sigalat, S. Rocton, J.F. Sanchez-Royo, R.E. Galian, J. Perez-Prieto, Highly fluorescent and photostable organic- and water-soluble CdSe/ZnS core-shell quantum dots capped with thiols, *RSC Adv.*, 2(2012) 1632-1638. <https://doi.org/10.1039/C1RA01005K>
- [42] N.I. Hammer, T. Emrick, M.D. Barnes, Quantum dots coordinated with conjugated organic ligands: new nanomaterials with novel photophysics, *Nanoscale Res. Lett.* 2 (2007) 282-290. <https://doi.org/10.1007/s11671-007-9062-8>

- [43] B. Dubertret, P. Skourides, D.J. Norris, V. Noireaux, A.H. Brivanlou, A. Libchaber, In vivo imaging of quantum dots encapsulated in phospholipid micelles, *Science*, 298 (2002) 1759-1762. <https://doi.org/10.1126/science.1077194>
- [44] S.T. Selvan, Silica-coated quantum dots and magnetic nanoparticles for bioimaging applications, *Biointerphases*, 5 (2010) FA110-FA115. <https://doi.org/10.1116/1.3516492>
- [45] Wang F, Tan W B, Zhang Y, Fan X, Wang M, Upconverting rare-earth nanoparticles with a paramagnetic lanthanide complex shell for upconversion fluorescent and magnetic resonance dual-modality imaging, *Nanotechnology*, 2006, 17 R1.
- [46] Du D, Chen W, Cai J, Zhang J, Qu F and Li H, Development of Acetylcholinesterase biosensor based on CdTe quantum dots modified cysteamine self-assembled monolayers, *J. Electroanal. Chem.* 623 (2008) 81-85. <https://doi.org/10.1016/j.jelechem.2008.06.020>
- [47] Yu T, Shen J-S, Bai H-H, Guo L, Tang J-J, Jiang Y-B and Xie J-W, A photoluminescent nanocrystal-based signaling protocol highly sensitive to nerve agents and highly toxic organophosphate pesticides, *Analyst* 134 (2009) 2153-2157. <https://doi.org/10.1039/b915159c>
- [48] Periasamy A P, Umasankar Y and Chen S-M, Nanomaterials - Acetylcholinesterase enzyme matrices for organophosphorus pesticides electrochemical sensors: a review, *Sensors* 9 (2009) 4034-4055. <https://doi.org/10.3390/s90604034>
- [49] L. Shcherbyna, T. Torchynska. Si quantum dot structures and their applications, *Physica E: Low-dimensional Systems and Nanostructures*, 51 (2013) 65-70. <https://doi.org/10.1016/j.physe.2012.09.026>
- [50] W. Deng, E.M. Goldys, Chemical sensing with nanoparticles as optical reporters: from noble metal nanoparticles to quantum dots and upconverting nanoparticles, *Analyst* 139 (2014) 5321-5334. <https://doi.org/10.1039/C4AN01272K>
- [51] C. Kim, P. Ghosh, V.M. Rotello, Multimodal drug delivery using gold nanoparticles, *Nanoscale* 1 (2009) 61-67. <https://doi.org/10.1039/b9nr00112c>
- [52] Q.H. Tran, V.Q. Nguyen, A.-T. Le, Silver nanoparticles: synthesis, properties, toxicology, applications and perspectives, *Adv. Nat. Sci.: Nanosci. Nanotechnol.* 4 (2013) 033001/1–033001/20. <https://doi.org/10.1088/2043-6262/4/3/033001>

- [53] Averitt, R.D., Sarkar, D., Halas, N.J. Plasmon resonance shifts of Au-coated Au₂S nanoshells: insight into multicomponent nanoparticle growth, *Phys. Rev. Lett.* 78 (1997) 4217-4220. <https://doi.org/10.1103/PhysRevLett.78.4217>
- [54] Luis M. Liz-Marzán-Nanometals:formation and color, *Materials Today*, 7 (2004) 26-31. [https://doi.org/10.1016/S1369-7021\(04\)00080-X](https://doi.org/10.1016/S1369-7021(04)00080-X)
- [55] Oldenburg, S.J., Averitt, R.D., Westcott, S.L., Halas, N.J. Nanoengineering of optical, resonances.*Chem. Phys. Lett.* 288 (1998) 243-247. [https://doi.org/10.1016/S0009-2614\(98\)00277-2](https://doi.org/10.1016/S0009-2614(98)00277-2)
- [56] Sershen, S.R., Westcott, S.L., Halas, N.J., and West, J.L. Temperature-sensitive polymer-nanoshell composites for photothermally modulated drug delivery, *J. Biomed. Mater. Res.* 51 (2000) 293-298. [https://doi.org/10.1002/1097-4636\(20000905\)51:3<293::AID-JBM1>3.0.CO;2-T](https://doi.org/10.1002/1097-4636(20000905)51:3<293::AID-JBM1>3.0.CO;2-T)
- [57] Erik T. Thostenson, Chunyu Li, Tsu-Wei Chou, Nanocomposites in context,*Composites Science and Technology*, 65 (2005) 491–516. <https://doi.org/10.1016/j.compscitech.2004.11.003>
- [58] Suarez I, Gordillo H, Abargues R, Albert S, Martinez-Pastor J Photoluminescence waveguiding in CdSe and CdTe QDs–PMMA nanocomposite films. *Nanotechnology* 22 (2011) 435202–435209. <https://doi.org/10.1088/0957-4484/22/43/435202>
- [59] Zhu L, Yang S, Wang J, Wang C-F, Chen L, Chen S, Quantum-dot-embedded polymeric fiber films with photoluminescence and superhydrophobicity. *Mater Lett* 99 (2013) 54–56. <https://doi.org/10.1016/j.matlet.2012.03.118>
- [60] Tomczak N, Janczewski D, Han M, Vancso GJ, Designer polymer–quantum dot architectures. *Prog.Polym.Sci.* 34(5) (2009) 393–430. <https://doi.org/10.1016/j.progpolymsci.2008.11.004>
- [61] Dubois F, Mahler B, Dubertret B, Doris E, Mioskowski C A, Versatile strategy for quantum dot ligand exchange, *J Am ChemSoc* 129 (2007) 482-483. <https://doi.org/10.1021/ja067742y>
- [62] Wisher AC, Bronstein I, Chechik V, Thiolated PAMAM dendrimer-coated CdSe/ZnSe nanoparticles as protein transfection agents, *Chem. Commun.* 31 (2006) 1637-1639. <https://doi.org/10.1039/b518115a>
- [63] Selvan ST, Tan TT, Ying JY Robust, Non-Cytotoxic, Silica-coated CdSe quantum dots with efficient photoluminescence,*Adv Mater* 17 (2005)1620-1625. <https://doi.org/10.1002/adma.200401960>

- [64] Kim HC, Hong HG, Yoon C, Choi H, Ahn IS, Lee DC, Kim YJ, Lee K, Fabrication of high quantum yield quantum dot/polymer films by enhancing dispersion of quantum dots using silica particles. *J Colloid Interface Sci* 393 (2013)74–79. <https://doi.org/10.1016/j.jcis.2012.10.045>
- [65] Ullah MH, Kim J-H, Ha C-S, Highly transparent o- PDA functionalized ZnS-polymer nanocomposite thin films with high refractive index. *Mater Lett* 62 (15) (2008) 2249–2252. <https://doi.org/10.1016/j.matlet.2007.11.065>
- [66] Lawrence WG, Thacker S, Palamakumbura S, Riley KJ, Nagarkar VV, Quantum dot-organic polymer composite materials for radiation detection and imaging. *IEEE Trans Nucl. Sci* 59(1) (2012) 215–221. <https://doi.org/10.1109/TNS.2011.2178861>
- [67] Zhang H, Tang Y, Zhang J, Li M, Yao X, Li X, Yang B Manipulation of semiconductor nanocrystals growth in polymer soft materials. *Soft Matter* 5 (2009) 4113–4117. <https://doi.org/10.1039/b914213d>
- [68] F. Fleischhaker and R. Zentel, Photonic crystals from core-shell colloids with incorporated highly fluorescent quantum dots, *Chemistry of Materials*, 17 (2005) 1346-1351. <https://doi.org/10.1021/cm0481022>
- [69] Bradley, M.; Bruno, N.; Vincent, B. Distribution of CdSe quantum dots within swollen polystyrene microgel particles using confocal microscopy. *Langmuir* 21 (7) (2005) 2750–2753. <https://doi.org/10.1021/la047322r>
- [70] Han, M.; Gao, X.; Su, J. Z.; Nie, S. Quantum-Dot-Tagged Microbeads for Multiplexed Optical Coding of Biomolecules. *Nat. Biotechnol.* 19 (7) (2001) 631–635. <https://doi.org/10.1038/90228>
- [71] Li, M.; Zhang, H.; Zhang, J.; Wang, C.; Han, K.; Yang, B. Easy Preparation and Characterization of Highly Fluorescent Polymer Composite Microspheres from Aqueous CdTe Nanocrystals. *J. Colloid Interface Sci.* 300 (2) (2006) 564–568. <https://doi.org/10.1016/j.jcis.2006.04.031>
- [72] Kuang, M.; Wang, D.; Bao, H.; Gao, M.; Möhwald, H.; Jiang, M. Fabrication of multicolor-encoded microspheres by tagging semiconductor nanocrystals to hydrogel spheres. *Adv. Mater.* 17 (2) (2005) 267–270. <https://doi.org/10.1002/adma.200400818>
- [73] O'Brien, P.; Cummins, S. S.; Darcy, D.; Dearden, A.; Masala, O.; Pickett, N. L.; Ryley, S.; Sutherland, A. J. Quantum Dot-labelled polymer beads by suspension polymerisation. *Chem. Commun. (Camb)*. 1 (2003)2532–2533. <https://doi.org/10.1039/b307500a>

- [74] Sheng, W.; Kim, S.; Lee, J.; Kim, S.-W.; Jensen, K.; Bawendi, M. G. In-situ encapsulation of quantum dots into polymer microspheres. *Langmuir* 22 (8) (2006)3782–3790. <https://doi.org/10.1021/la051973l>
- [75] Yang, X.; Zhang, Y. Encapsulation of quantum nanodots in polystyrene and silica micro-/nanoparticles. *Langmuir*, 20 (14) (2004) 6071–6073. <https://doi.org/10.1021/la049610t>
- [76] Asua, J. M. Mapping the morphology of polymer-inorganic nanocomposites synthesized by miniemulsion polymerization. *Macromol. Chem. Phys.* 215 (5) (2014) 458–464. <https://doi.org/10.1002/macp.201300696>
- [77] Fleischhaker, F.; Zentel, R. Photonic crystals from core-shell colloids with incorporated highly fluorescent quantum dots. *Chem. Mater.* 17 (6) (2005) 1346–1351. <https://doi.org/10.1021/cm0481022>
- [78] Joumaa, N.; Lansalot, M.; Théretz, A.; Elaissari, A.; Sukhanova, A.; Artemyev, M.; Nabiev, I.; Cohen, J. H. M. Synthesis of quantum dot-tagged submicrometer polystyrene particles by miniemulsion polymerization. *Langmuir* 22 (4) (2006)1810–1816. <https://doi.org/10.1021/la052197k>
- [79] Michalet, X.; Pinaud, F.F.; Bentolila, L.A.; Tsay, J.M.; Doose, S.; Li, J.J.; Sundaresan, G.;Wu, A.M.; Gambhir, S.S.; Weiss, S. Quantum dots for live cells, in vivo imaging, and diagnostics, *Science* 307 (2005) 538-544. <https://doi.org/10.1126/science.1104274>
- [80] Rosenthal, S.J.; Chang, J.C.; Kovtun, O.; McBride, J.R.; Tomlinson, I.D. Biocompatible quantumdots for biological applications. *Chem. Biol.* 18 (2011) 10-24. <https://doi.org/10.1016/j.chembiol.2010.11.013>
- [81] Tomczak, N.; Jańczewski, D.; Han, M.; Vancso, G.J. Designer polymer-quantum dots architectures. *Prog. Polym. Sci.* 34 (2009) 393-430. <https://doi.org/10.1016/j.progpolymsci.2008.11.004>
- [82] Hezinger, A.F.E.; Teßmar, J.; Göpferich, A. Polymer coating of quantum dots-A powerful tool toward diagnostics and sensorics. *E. J. Pharm. Biopharm.* 68 (2008) 138-152. <https://doi.org/10.1016/j.ejpb.2007.05.013>
- [83] Lei Shen,Biocompatible polymer/quantum dots hybrid materials: current status and future developments, *J. Funct. Biomater.* 2 (2011)355-372. <https://doi.org/10.3390/jfb2040355>

- [84] Uyeda, H.T.; Medintz, I.L.; Jaiswal, J.K.; Simon, S.M.; Mattoussi, H. Synthesis of compact multidentate ligands to prepare stable hydrophilic quantum dot fluorophores. *J. Am. Chem. Soc.* 127(2005) 3870-3878. <https://doi.org/10.1021/ja044031w>
- [85] Yildiz, I.; McCaughan, B.; Cruickshank, S.F.; Callan, J.F.; Raymo, F.M. Biocompatible CdSe-ZnS core-shell quantum dots coated with hydrophilic polythiols. *Langmuir*, 25 (2009) 7090-7096. <https://doi.org/10.1021/la900148m>
- [86] Wu, Y.; Chakroborty, S.; Gropeanu, R.A.; Wilhelmi, J.; Xu, Y.; Shih Er, K.; Kuan, S.L.; Koynov, K.; Chan, Y.; Weil, T. pH-responsive quantum dots via an albumin polymer surface coating. *J. Am. Chem. Soc.* 132 (2010) 5012-5014. <https://doi.org/10.1021/ja909570v>
- [87] Wang, Y.A.; Li, J.J.; Chen, H.; Peng, X. Stabilization of inorganic nanocrystals by organic dendrons. *J. Am. Chem. Soc.* 124 (2002) 2293-2299. <https://doi.org/10.1021/ja016711u>
- [88] Mattheakis, L.C.; Dias, J.M.; Choi, Y.J.; Gong, J.; Bruchez, M.P.; Liu, J.; Wang, E. Optical coding of mammalian cells using semiconductor quantum dots. *Anal. Biochem.* 327 (2004) 200-208. <https://doi.org/10.1016/j.ab.2004.01.031>
- [89] Smith, A.M.; Nie, S. Minimizing the hydrodynamic size of quantum dots with multifunctional multidentate polymer ligands. *J. Am. Chem. Soc.* 130 (2008) 11278-11279. <https://doi.org/10.1021/ja804306c>
- [90] Potapova, I.; Mruk, R.; Hübner, C.; Zentel, R.; Basché, T.; Mews, A. CdSe/ZnS nanocrystals with dye-functionalized polymer ligands containing many anchor groups. *Angew. Chem. Int. Ed.* 44 (2005) 2437-2440. <https://doi.org/10.1002/anie.200462236>
- [91] Nikolic, M.S.; Krack, M.; Aleksandrovic, V.; Kornowski, A.; Förster, S.; Weller, H. Tailor-made ligands for biocompatible nanoparticles. *Angew. Chem. Int. Ed.* 45 (2006) 6577-6580. <https://doi.org/10.1002/anie.200602209>
- [92] Wang, X.; Dykstra, T.E.; Salvador, M.R.; Manners, I.; Scholes, G.D.; Winnik, M.A. Surface passivation of luminescent colloidal quantum dots with poly (dimethylaminoethyl ethacrylate) through a ligand exchange process. *J. Am. Chem. Soc.* 126 (2004) 7784-7785. <https://doi.org/10.1021/ja0489339>
- [93] Shen, L.; Soong, R.; Wang, M.; Lee, A.; Wu, C.; Scholes, G.D.; Macdonald, P.M.; Winnik, M.A. Pulsed field gradient NMR studies of polymer adsorption on colloidal CdSe quantum dots. *J. Phys.Chem. B* 112 (2008) 1626-1633. <https://doi.org/10.1021/jp0768975>

- [94] Skaff, H.; Emrick, T. The use of 4-substituted pyridines to afford amphiphilic, pegylated cadmium selenide nanoparticles, *Chem. Commun.* 9 (2003) 52-53. <https://doi.org/10.1039/b208718a>
- [95] Balazs, A.; Ginzburg, V. V.; Qui, F.; Peng, G.; Jasnow, D. Multi-Scale model for binary mixtures containing nanoscopic particles, *J. Phys. Chem. B* 104 (2000) 3411-3422. <https://doi.org/10.1021/jp993356+>
- [96] Ballou, B.; Lagerholm, B.C.; Ernst, L.A.; Bruchez, M.P.; Waggoner, A.S. Noninvasive imaging of quantum dots in mice. *Bioconjugate Chem.* 15 (2004) 79-86. <https://doi.org/10.1021/bc034153y>
- [97] Tan, S.J.; Jana, N.R.; Gao, S.; Patra, P.K.; Ying, J.Y. Surface-ligand-dependent cellular interaction, subcellular localization, and cytotoxicity of polymer-coated quantum dots. *Chem. Mater.* 22 (2010) 2239-2247. <https://doi.org/10.1021/cm902989f>
- [98] Carrot, G.; Rutot-Houzé, D.; Pottier, A.; Degée, P.; Hiborn, J.; Dubois, P. Surface-initiated ring-opening polymerization: A versatile method for nanoparticle ordering. *Macromolecules*, 35 (2002) 8400-8404. <https://doi.org/10.1021/ma020558m>
- [99] Skaff, H.; Emrick, T. Reversible addition fragmentation chain transfer (RAFT) polymerization from unprotected cadmium selenide nanoparticles. *Angew. Chem. Int. Ed.* 43 (2004) 5383-5386. <https://doi.org/10.1002/anie.200453822>
- [100] Sill, K.; Emrick, T. Nitroxide-mediated radical polymerization from CdSe nanoparticles. *Chem. Mater.* 16 (2004) 1240-1243. <https://doi.org/10.1021/cm035077b>
- [101] Farmer, S.; Patten, T.E. photoluminescent polymer/quantum dot composite nanoparticles. *Chem. Mater.* 13 (2001) 3920-3926. <https://doi.org/10.1021/cm010291q>
- [102] Esteves, A.C.C.; Bombalski, L.; Trindade, T.; Matyjaszewski, K.; Barros-Timmons, A. Polymer grafting from CdS quantum dots via AGET ATRP in miniemulsion. *Small* 3 (2007) 1230-1236. <https://doi.org/10.1002/sml.200600510>
- [103] Dubertret, B.; Skourides, P.; Norris, D.J.; Noireaux, V.; Brivanlou, A.H.; Libchaber, A. In vivo imaging of quantum dots encapsulated in phospholipid micelles. *Science* 298 (2002) 1759-1762. <https://doi.org/10.1126/science.1077194>
- [104] Gao, X.; Cui, Y.; Levenson, R.M.; Chung, L.W.K.; Nie, S. In vivo cancer targeting and imaging with semiconductor quantum dots. *Nat. Biotechnol.* 22 (2004) 969-975. <https://doi.org/10.1038/nbt994>
- [105] Boulmedais, F.; Bauchat, P.; Brienne, M.J.; Arnal, I.; Artzner, F.; Gacoin, T.; Dahan, M.; Marchi-Artzner, V. Water-soluble pegylated quantum dots: From a

- composite hexagonal phase to isolated micelles. *Langmuir*, 22 (2006) 9797-9803.
<https://doi.org/10.1021/la061849h>
- [106] Yu, W.W.; Chang, E.; Falkner, J.C.; Zhang, J.; Al-Somali, A.M.; Sayes, C.M.; Johns, J.; Drezek, R.; Colvin, V.L. Forming biocompatible and nonaggregated nanocrystals in water using amphiphilic polymers. *J. Am. Chem. Soc.* 129 (2007) 2871-2879. <https://doi.org/10.1021/ja067184n>
- [107] Capek, R.K.; Weber, M.; Eychmuller, A. Alternative incorporation of quantum dots in polymer microspheres. *Chem. Mater.* 22 (2010) 4912-4918.
<https://doi.org/10.1021/cm101004m>
- [108] Zhang, J.; Xu, S.; Kumacheva, E. Polymer microgels: Reactors for semiconductor, metal, and magnetic nanoparticles. *J. Am. Chem. Soc.* 126 (2004) 7908-7914.
<https://doi.org/10.1021/ja031523k>
- [109] Lemon, B.L.; Crooks, R.M. Preparation and characterization of dendrimer-encapsulated cds semiconductor quantum dots. *J. Am. Chem. Soc.* 122 (2000) 12886-12887. <https://doi.org/10.1021/ja0031321>
- [110] Bruchez, M., Moronne, M., Gin, P., Weiss, S., and Alivisatos, A.P. Semiconductor nanocrystals as fluorescent biological labels. *Science* 281 (1998) 2013–2016.
<https://doi.org/10.1126/science.281.5385.2013>
- [111] Chan, W.C., Maxwell, D.J., Gao, X., Bailey, R.E., Han, M., and Nie, S. Luminescent quantum dots for multiplexed biological detection and imaging, *Curr. Opin. Biotechnol.* 13 (2002) 40–46. [https://doi.org/10.1016/S0958-1669\(02\)00282-3](https://doi.org/10.1016/S0958-1669(02)00282-3)
- [112] Chan, W.C. and Nie, S. Quantum dot bioconjugates for ultrasensitive nonisotopic detection. *Science* 281 (1998) 2016–2018.
<https://doi.org/10.1126/science.281.5385.2016>
- [113] Cao Y, Yang K, Li Z, Zhao C, Shi C, Yang J. Near-infrared quantum-dot-based non-invasive in vivo imaging of squamous cell carcinoma U14. *Nanotechnology*. 21 (2010) 475104. <https://doi.org/10.1088/0957-4484/21/47/475104>
- [114] Jiang W, Singhal A, Zheng J, Wang C, Chan WCW. Optimizing the synthesis of red- to near-IR-emitting CdS-capped CdTe $x\text{Se}_{1-x}$ alloyed quantum dots for biomedical imaging. *Chem Mater*. 18 (2006) 4845- 4854.
<https://doi.org/10.1021/cm061311x>
- [115] Hyun BR, Chen H, Rey DA, Wise FW, Batt CA. Near-infrared fluorescence imaging with water-soluble lead salt quantum dots. *J Phys Chem*. 111 (2007) 5726-5730. <https://doi.org/10.1021/jp068455j>

- [116] Li H, Shih WY, Shih WH. Synthesis and characterization of aqueous carboxyl-capped CdS quantum dots for bioapplications. *Ind Eng Chem Res.* 46 (2007) 2013-2019. <https://doi.org/10.1021/ie060963s>
- [117] Mulder WJM, Koole R, Brandwijk RJ, Storm G, Chin PT, Strijkers GJ, de Mello Donegá C, et al. Quantum dots with a paramagnetic coating as a bimodal molecular imaging probe. *Nano Lett.* 6 (2006) 1-6. <https://doi.org/10.1021/nl051935m>
- [118] Weissleder, R. A clearer vision for in vivo imaging. *Nat. Biotechnol.* 19 (2001) 316–317. <https://doi.org/10.1038/86684>
- [119] Chem JM, Taniguchi S, Green M, Rizvi B, Seifalian A. The one-pot synthesis of core / shell / shell CdTe / CdSe / ZnSe quantum dots in aqueous media for in vivo deep tissue imaging. 9 (2011) 2877-2882. <https://doi.org/10.1039/c0jm03527k>
- [120] Hyun BR, Chen H, Rey DA, Wise FW, Batt CA. Near-infrared fluorescence imaging with water-soluble lead salt quantum dots. *J Phys Chem.* 111 (2007) 5726-5730. <https://doi.org/10.1021/jp068455j>
- [121] Sershen, S.R., Westcott, S.L., Halas, N.J., West, J.L. Temperature-sensitive polymernanoshell composites for photothermally modulated drug delivery. *J. Biomed. Mater. Res.* 51 (2000) 293–298. [https://doi.org/10.1002/1097-4636\(20000905\)51:3<293::AID-JBM1>3.0.CO;2-T](https://doi.org/10.1002/1097-4636(20000905)51:3<293::AID-JBM1>3.0.CO;2-T)
- [122] Okano, T., Bae, Y.H., Jacobs, H., and Kim, S.W. Thermally on–off switching polymers for drug permeation and release. *J. Control. Release* 11 (1990) 255–265. [https://doi.org/10.1016/0168-3659\(90\)90138-J](https://doi.org/10.1016/0168-3659(90)90138-J)
- [123] Hirsch, L.R., Stafford, R.J., Bankson, J.A., Sershen, S.R., Rivera, B., Price, R.E., Hazle, J.D., Halas, N.J., West, J.L. Nanoshell-mediated near infrared thermal therapy of tumors under magnetic resonance guidance. *Proc. Natl Acad. Sci. USA* 100 (2003) 13549–13554. <https://doi.org/10.1073/pnas.2232479100>
- [124] Colvin, V.L.; Schlamp, M.C. Alivisatos, A.P. Light-emitting diodes made from cadmium selenide nanocrystals and a semiconducting polymer. *Nature* 370 (1994) 354–357. <https://doi.org/10.1038/370354a0>
- [125] Zhou, Y.; Riehle, F.S.; Yuan, Y.; Schleiermacher, H.F.; Niggemann, M.; Urban, G.A.; Krueger, M. Improved efficiency of hybrid solar cells based on non-ligand exchanged CdSe quantum dots and poly (3-hexylthiophene). *Appl. Phys. Lett.* 96 (2010) 013304. <https://doi.org/10.1063/1.3280370>

- [126] Zhou, Y.; Eck, M.; Kruger, M. Bulk-heterojunction hybrid solar cells based on colloidal nanocrystals and conjugated polymers. *Energy Environ. Sci.* 3 (2010) 1851–1864. <https://doi.org/10.1039/c0ee00143k>
- [127] Wang, R.Y.; Feser, J.P.; Lee, J.-S.; Talapin, D.V.; Segalman, R.; Majumdar, A. Enhanced thermopower in PbSe nanocrystal quantum dot superlattices. *Nano Lett.* 8 (2008) 2283–2288. <https://doi.org/10.1021/nl8009704>
- [128] Colvin, V.L.; Schlamp, M.C. Alivisatos, A.P. Light-emitting diodes made from cadmium selenide nanocrystals and a semiconducting polymer. *Nature* 370 (1994) 354–357. <https://doi.org/10.1038/370354a0>
- [129] Schlamp, M.C.; Peng, X.; Alivisatos, A.P. Improved efficiencies in light emitting diodes made with CdSe/CdS core/shell type nanocrystals and a semiconducting polymer. *J. Appl. Phys.* 82 (1997) 5837–5842. <https://doi.org/10.1063/1.366452>
- [130] Lee, J.; Sundar, V.C.; Heine, J.R.; Bawendi, M.G.; Jesen, K.F. Full color emission from II-VI semiconductor quantum dot-polymer composites. *Adv. Mater.* 12 (2000) 1102–1105. [https://doi.org/10.1002/1521-4095\(200008\)12:15<1102::AID-ADMA1102>3.0.CO;2-J](https://doi.org/10.1002/1521-4095(200008)12:15<1102::AID-ADMA1102>3.0.CO;2-J)
- [131] Chung, W.; Park, K.; Yu, H.J.; Kim, B.; Kim, S.H. White emission using mixtures of CdSe quantum dots and PMMA as a phosphor. *Opt. Mater.* 32 (2010) 515–521. <https://doi.org/10.1016/j.optmat.2009.11.005>
- [132] S. Kobayashi, S. Mikoshiba, and S. Lim, *LCD Backlights*. New York, NY, USA: Wiley, 2009. <https://doi.org/10.1002/9780470744826>
- [133] T. Okumura, A. Tagaya, Y. Koike, M. Horiguchi, H. Suzuki, Highly efficient backlight for liquid crystal display having no optical films, *Appl. Phys. Lett.*, 83 (2003) 2515–2517. <https://doi.org/10.1063/1.1613051>
- [134] K. Kalantar, Modified functional light-guide plate for backlighting transmissive LCDs, *J. Soc. Inf. Display*, 11 (2003) 641–645. <https://doi.org/10.1889/1.1825692>
- [135] D. Feng, Y. Yan, X. Yang, G. Jin, and S. Fan, “Novel integrated lightguide plates for liquid crystal display backlight, *Journal of Optics A: Pure and Applied Optics*, 7 (2005) 111–117. <https://doi.org/10.1088/1464-4258/7/3/003>
- [136] E. Jang et al., White-light-emitting diodes with quantum dot color converters for display backlights, *Adv. Mater.*, 22 (2010) 3076–3080. <https://doi.org/10.1002/adma.201000525>
- [137] Z. Luo, Y. Chen, S. T. Wu, Wide color gamut LCD with a quantum dot backlight, *Opt. Express*, 21(2013) 26269–26284. <https://doi.org/10.1364/OE.21.026269>

- [138] S. Coe-Sullivan, W. Liu, P. Allen, J. S. Steckel, Quantum dots for LED downconversion in display applications, *ECS J. Solid State Sci. Technol.*, 2 (2013) R3026–R3030, 2013. <https://doi.org/10.1149/2.012302jss>
- [139] Y. Shirasaki, G. J. Supran, M. G. Bawendi, V. Bulovic, Emergence of colloidal quantum-dot light-emitting technologies, *Nat. Photon.*, 7 (2013) 13–23. <https://doi.org/10.1038/nphoton.2012.328>
- [140] J. S. Steckel et al., Quantum dot manufacturing requirements for the high volume LCD market, In *Proc. SID Symp. Dig. Tech. Papers*, 44 (2013) 943–945. <https://doi.org/10.1002/j.2168-0159.2013.tb06377.x>
- [141] Z. Luo, D. Xu, and S. T. Wu, Emerging quantum-dots-enhanced LCDs, *J. Display Technol.*, 10 (2014) 526–539. <https://doi.org/10.1109/JDT.2014.2325218>
- [142] K. Bourzac, Quantum dots go on display, *Nature*, 493 (2013) 283. <https://doi.org/10.1038/493283a>
- [143] J. S. Steckel et al., Quantum dots: The ultimate down-conversion material for LCD displays, *J. Soc. Inf. Display*, 23 (2015) 294–305. <https://doi.org/10.1002/jsid.313>
- [144] Q. Hong, K. C. Lee, Z. Luo, and S. T. Wu, High-efficiency quantum dot remote phosphor film, *Appl. Opt.* 54 (2015) 4617–4622. <https://doi.org/10.1364/AO.54.004617>
- [145] Wang, Y. Semiconductor nanocrystals in carrier-transporting polymers. charge generation and charge transport. *J. Lumin* 70 (1996) 48–59. [https://doi.org/10.1016/0022-2313\(96\)00043-9](https://doi.org/10.1016/0022-2313(96)00043-9)
- [146] Yang, C. L.; Wang, J. N.; Ge, W. K.; Wang, S. H.; Cheng, J. X.; Li, X. Y.; Yan, Y. J.; Yang, S. H. Significant enhancement of photoconductivity in truly two-component and chemically hybridized CdS-poly (n-vinylcarbazole) nanocomposites. *Appl. Phys. Lett.* 78 (2001) 760–762. <https://doi.org/10.1063/1.1345826>
- [147] Han, L.; Donghuan, Q.; Jiang, X.; Liu, Y.; Wang, L.; Chen, J.; Cao, Y. Synthesis of high quality zinc-blende CdSe nanocrystals and their application in hybrid solar cells. *Nanotechnology* 17 (2006) 4736–4742. <https://doi.org/10.1088/0957-4484/17/18/035>
- [148] Park, E.-K.; Kim, J.-H. J.-H.; Ji, I. A.; Choi, H. M.; Kim, J.-H. J.-H.; Lim, K.-T.; Bang, J. H.; Kim, Y.-S. Optimization of CdSe Quantum Dot Concentration in P3HT:PCBM Layer for the Improved Performance of Hybrid Solar Cells. *Microelectron. Eng.* 119 (2014) 169–173. <https://doi.org/10.1016/j.mee.2014.05.003>

- [149] Yin, J.; Kumar, M.; Lei, Q.; Ma, L.; Raavi, S. S. K.; Gurzadyan, G. G.; Soci, C. SmallSize Effects on Electron Transfer in P3HT/InP Quantum Dots. *J. Phys. Chem. C* 119 (2015) 26783–26792. <https://doi.org/10.1021/acs.jpcc.5b09397>
- [150] E. Bundgaard, S. E. Shaheen, F. C. Kerbs, D. S. Ginley,. Bulk heterojunctions based on a low band gap copolymer of thiophene and benzothiadiazole, *Solar Energy Materials & Solar Cells*, 91 (2007) 1631-1637. <https://doi.org/10.1016/j.solmat.2007.05.013>
- [151] Medintz, I.L., Clapp, A.R., Mattoussi, H., Goldman, E.R., Fisher, B., Mauro, J.M., Self-assembled nanoscale biosensors based on quantum dot FRET donors, *Nature Materials* 2 (2015) 630–638. <https://doi.org/10.1038/nmat961>
- [152] Medintz, I.L., Uyeda, H.T., Goldman, E.R., Mattoussi, H., Quantum dot bioconjugates for imaging, labelling and sensing, *Nature Materials* 4 (2005) 435–446. <https://doi.org/10.1038/nmat1390>
- [153] Francesc A. Esteve-Turrillas, Antonio Abad-Fuentes, Applications of quantum dots as probes in immunosensing of small-sized analytes, *Biosensors and Bioelectronics* 41 (2013) 12–29. <https://doi.org/10.1016/j.bios.2012.09.025>
- [154] V. Lindbergand B Hellsing, Metallic quantum dots, *J. Phys.: Condens. Matter* 17 (2005) S1075–S1094. <https://doi.org/10.1088/0953-8984/17/13/004>
- [155] Crommie M F, Lutz C P, Eigler D M. Confinement of electrons to quantum corrals on a metal surface, *Science* 262 (1993) 218-220. <https://doi.org/10.1126/science.262.5131.218>
- [156] Avouris P and Lyo I-W Observation of Quantum-Size Effects at Room Temperature on Metal Surfaces With STM, *Science*, 264 (1994) 942-945. <https://doi.org/10.1126/science.264.5161.942>
- [157] Rosetti, R.; Hull, R.; Gibson, J. M.; Brus, L. E. *J. Chem. Phys.* 1985, 82, 552. <https://doi.org/10.1063/1.448727>
- [158] Ricard, D.; Roussignol, P.; Flytzanis, Surface-mediated enhancement of optical phase conjugation in metal colloids, *C. Opt. Lett.* 10 (1985) 511-513. <https://doi.org/10.1364/OL.10.000511>
- [159] Nie, S.; Emory, S. R. Probing single molecules and single nanoparticles by surface-enhanced Raman scattering, *Science* 275 (1997) 1102-1106. <https://doi.org/10.1126/science.275.5303.1102>

- [160] Jang, N. H. The coordination chemistry of DNA nucleosides on gold nanoparticles as a probe by SERS, *Bull. Korean Chem. Soc.* 23 (2002) 1790-1800.
<https://doi.org/10.5012/bkcs.2002.23.12.1790>
- [161] Rodolphe Antoine, Pierre F. Brevet, Hubert H. Girault, Rodolphe Antoine, Pierre F. Brevet, Donald Bethell, David J. Schiffrin, Surface plasmon enhanced non-linear optical response of gold nanoparticles at the air/toluene interface, *Chem. Commun.*, 0 (1997) 1901-1902. <https://doi.org/10.1039/a704846g>
- [162] Mooradian A, Photoluminescence of metals, *Phys. Rev. Lett.* 22(5) (1969) 185–187. <https://doi.org/10.1103/PhysRevLett.22.185>
- [163] Diez I, Ras RHA Fluorescent silver nanoclusters, *Nanoscale*, 3 (2011) 1963–1970.
<https://doi.org/10.1039/c1nr00006c>
- [164] Belloni, Metal nanocolloids, *J. Curr. Opin. Colloid Interface Sci.* 1 (1996) 184-196.
[https://doi.org/10.1016/S1359-0294\(96\)80003-3](https://doi.org/10.1016/S1359-0294(96)80003-3)
- [165] Satoshi Horikoshi, Nick Serpone, Introduction to Nanoparticles,
<https://doi.org/10.1002/9783527648122.ch1>.
- [166] Robin J. White, Rafael Luque, Vitaliy L. Budarin James H. Clark, Duncan J. Macquarrie supported metal nanoparticles on porous materials. Methods and applications, *Chem. Soc. Rev.* 38 (2009) 481-494. <https://doi.org/10.1039/B802654H>
- [167] Juan M. Campelo, Diego Luna, Rafael Luque, Jose M. Marinas, Antonio A. Romero, Sustainable preparation of supported metal nanoparticles and their applications in catalysis Campelo –*Chem Sus Chem* 2 (2009) 18-45.
<https://doi.org/10.1002/cssc.200800227>
- [168] Rijun Gui, Hui Jin, Zonghua Wang, Lianjiang Tan, Aqueous synthesis of multidentate-polymer-capping Ag₂Se quantum dots with bright photoluminescence tunable in a second near-infrared biological window, *Coordination Chemistry Reviews*, 296 (2015) 91-124.
- [169] Wang X, Koleilat GI, Tang J, Liu H, Kramer IJ, et al. Tandem colloidal quantum dot solar cells employing a graded recombination layer. *Nature Photon* 5 (2011) 480–484. <https://doi.org/10.1038/nphoton.2011.123>

Chapter 5

Designing Metal-Organic-Framework for Clean Energy Applications

Shivy Mangal¹, S. Shanmuga Priya^{2*}, K.Sudhakar^{3,4,5}

^{1,2} Department of Chemical Engineering, Manipal Institute of Technology Manipal Academy of Higher Education(MAHE),Manipal, Karnataka, India

³ Faculty of Mechanical Engineering, Universiti Malaysia Pahang, 26600 Pahang, Malaysia

⁴ Energy Centre, Maulana Azad National Institute of Technology Bhopal, M.P., India

⁵ Automotive Engineering Centre, Universiti Malaysia Pahang, 26600 Pekan, Pahang, Malaysia

*shan.priya@manipal.edu

Abstract

Metal–organic frameworks (MOFs) are novel type of porous crystalline materials that have attracted increasing attention in clean energy applications due to their high surface area, permanent porosity, and controllable structures. Due to the extraordinarily massive extent of variability of both of constituents that make up metal organic frameworks, it seems that an inexhaustible quantity of MOFs could theoretically be designed and synthesized. The following chapter deals with various clean energy application of MOFs and their design considerations.

Keywords

Metal Organic Frameworks, Clean Energy, Carbon dioxide Capture, Hydrogen Storage, Harmful Gas Removal, Super Capacitors, Fuel Cells, Photo Catalysis

Contents

1.	Introduction.....	86
1.1	Introduction to MOF Composites & Derivatives	89
1.2	Chemistry of MOFs	90
2.	Applications of MOF in clean energy	91
2.1	Hydrogen Storage	91
2.2	Carbon dioxide capture.....	94

2.3	Methane storage.....	96
2.4	Electrical energy storage and conversion	99
2.5	MOFs for supercapacitor applications.....	100
2.6	NH₃ removal	101
2.7	Benzene removal	101
2.8	NO ₂ removal	102
2.9	Photocatalysis	102
Conclusion.....		104
References		104

1. Introduction

The global demand of energy resources has sky rocketed since the industrial revolution. Since then, the ever increasing dependency on natural resources in order to fulfill the energy demand has caused concerns over the continuous availability on natural resources and environmental problems that conventional energy sources possess to the environment including but not limited to climate change. As a result, development of sustainable energy sources has become an important topic not just from research perspective but also for the survival on this planet. Lot of efforts have been made in this area ranging from reducing dependence on fossil fuels to finding ways of generating and storing clean energy for future use. One of the results of devoted research in this field is Metal Organic Framework (MOF). Metal organic frameworks, also referred to as porous co-ordination polymers, are synthetic materials that are made up of organic linkers and metal ions. They are constructed by assembling together metal containing clusters and organic ligands such as carboxylates, sulfonates, tetrazolates etc. Merely by changing the species involved in constructing MOF, the structure and properties can be easily tailored. Such a freedom of selection has given rise to more 20,000 MOFs and counting. Fig. 1 shows the process of constructing MOF. Fig. 2 shows typical structure of an MOF. Fig. 3 depicts how to by just changing the metal center [3].

From Zn to Cr, a considerable change in the geometry of MOF is observed. Fig. 3(a) shows MOF-5 based on nets of linked Zn₄O tetrahedrons via 1,4-benzenedicarboxylate (1,4-BDC) ligands, appearing as a three-dimensional cubic network structure with interconnected pores diameter of 12 Å. Fig. 3(b) shows what happens when the metal unit is changed from Zn₄O to Cr₃O. A visible change in structure can easily be observed. Fig. 3(b) which is MIL101, contains giant cages with the diameter of 3 nm [1].

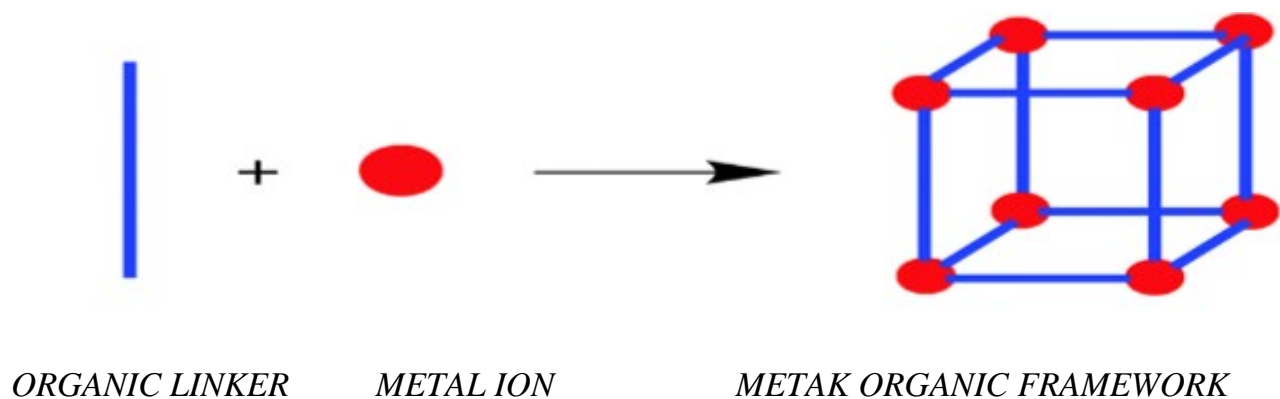


Figure 1. Schematic illustration of the process of MOF assembly

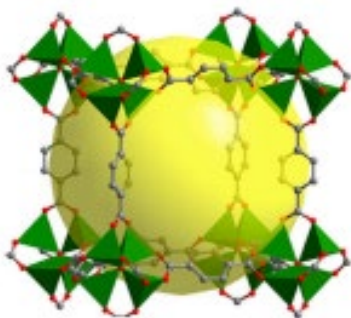


Figure 2. The structure of a typical MOF

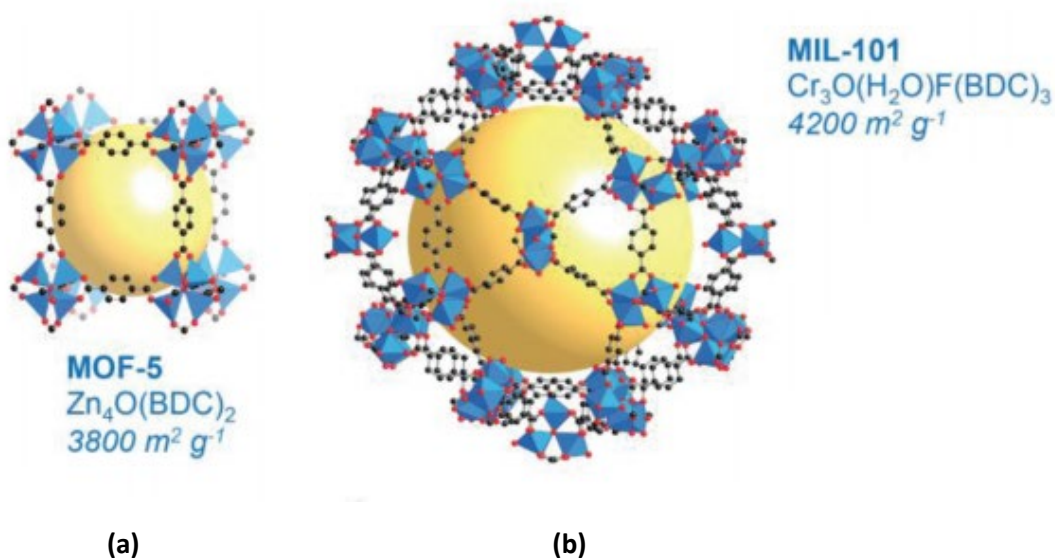


Figure 3. A comparison between the structures of MOF-5 and MIL101

MOFs have up to 90% of free volume i.e. they have ultra-high porosity, high surface area extending Langmuir surface area of $10000 \text{ m}^2 \text{ g}^{-1}$. This helps in applications such as sensing, drug delivery etc. Usually, porous MOFs show microporous characters ($<2 \text{ nm}$). MOFs will have a versatile functionality by the combination of metals components, organic linkers and combination of both. The high surface area, controllable pore sizes and low densities have allowed MOFs to find application as adsorbents, in gas storage, waste gas capture, photocatalytic applications, batteries, super capacitors as well as in chemical catalysis.

In order to please the present application of MOFs, it is important to boost its properties by introducing new functionalities. MOFs composites have one MOF and one or more different constituent materials. The properties of the constituent materials being different from the individual components, adds on to the performance of the MOFs. By combining the MOFs having good flexibility, high porosity and adaptivity with different functional materials having magnetic, catalytic and electrical properties can enhance the performance of the MOFs.

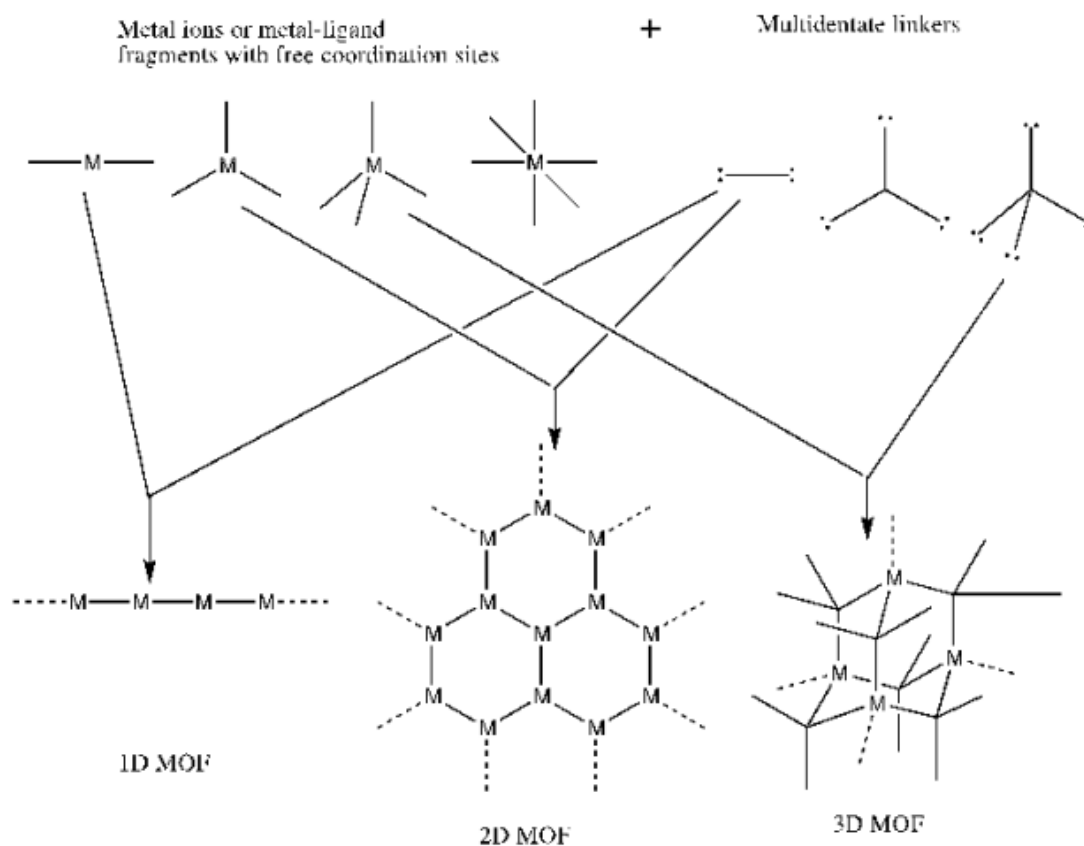


Figure 4. Basic building units of one-, two-, and three-dimensional MOFs.

As stated earlier, the metal centre and organic linker primarily determine the structural properties of MOFs however, in the synthesis, solvents and counterions are also used and they too play an important role.

The shape, length, and functional groups present in the organic linker also affect the structure of MOFs. The linkers commonly used are 4,4'-bipyridine (neutral ligands), polycarboxylates (anionic ligands). Polycarboxylates may be di, tri or tetra, or hexacarboxylates. The binding of a linker to the metal center may generate a one-dimensional (1D), two dimensional (2D) or three-dimensional (3D) arrangement, which depends on the metal center (Fig. 4) [4].

1.1 Introduction to MOF Composites & Derivatives

MOFs can be modelled to further enhance its performance or introduce a new functionality by incorporating various sorts of functional materials in it [33]. Such a compound is known as an MOF composite. So far, a number of MOF composites have been successfully prepared by assembling MOFs and various functional materials such as graphene, carbon nanotubes, metal oxides or even enzymes. Such composites have shown great performance in areas such as catalysis, photo-induced hydrogen generation, gas storage etc. In an MOF composite, the individual functions and properties of MOFs and the incorporated functional material combine together not just to provide multi-functionality but also exhibit physical and chemical properties that don't seem to be present in the individual elements. Thus we can say, such a mixture of MOF and functional material has extended the applications of MOFs to different fields.

We know that porous carbon, metal oxides, metal sulfides etc. are important inorganic materials that find application in the field of nanoscience as well as environmental applications. Nano porous carbon materials possess very high surface areas and large pore volumes. They also exhibit great mechanical and chemical stability. We know that MOFs possess an ordered structure and contain organic compounds. So, their carbonization results in nanoporous carbon structures having high surface area and large pore volumes. Pyrolysis of MOFs is another effective route for the fabrication of nano materials. Fig. 5 shows the inter-conversion between MOFs, MOFs composites and derivatives.

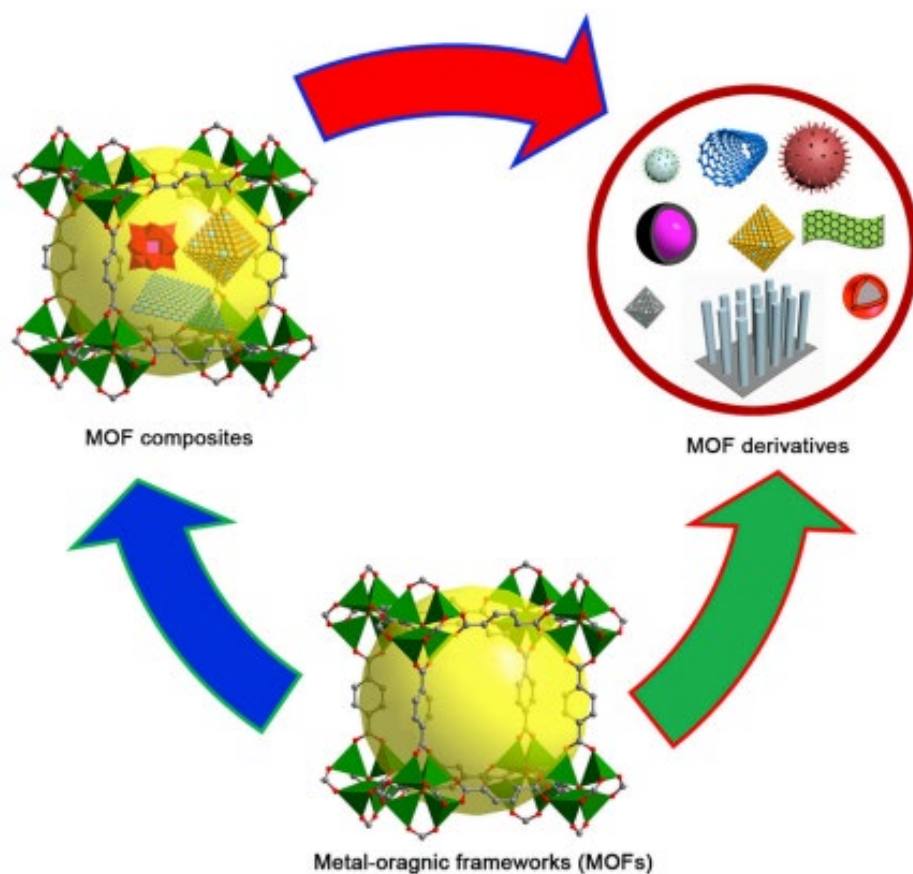


Figure 5. MOFs, MOF Composites, and MOF Derivatives and their interconversion.

1.2 Chemistry of MOFs

On the basis of the final structure of MOFs different processing techniques can be employed like, solvo-thermal process, electrochemical process, mechano-chemical process and slow diffusion. As mentioned in an earlier section, solvo-thermal process is usually opted for porous materials. As already mentioned, because of the two parts of the MOFs it provides a variety of combinations. This characteristic helps to synthesize very novel materials compared to silica, zeolite or hyper cross linked polymer particles [KAMI]. Most of the MOFs are prepared in pure N-N diethyl formamide (DEF) or N-N dimethyl formamide (DME). DEF and DME is decomposed at high temperature. This leads to the generation of the amine base. The amine base deprotonates the organic functionalities of the linker and forms the metal-organic clusters. Teflon lined caps can be used as they prevent solvent escape and also corrosion. Crystalline materials are formed by heating around 50-250° C. The solvent is removed from the crystals and later

submerge CHCl_3 , CH_2Cl_2 , methanol or some weakly coordinating solvents to extract DFM or DEM. If any water pores are detected they will also be removed. To fully vacate the pores, crystals are filtered, dried under vacuum at high temperature. The MOFs now formed are sensitive to moisture and air. It may compose or re-hydrate irreversibly in air.

There are few aspects that aids to increase the surface area of the MOFs, like, using fresh DEF and DME, filtering the reaction before heating, removing the excess gas in reaction solvent using N_2 . The above mentioned strategies will effectively minimize the crystal defects and improve the surface area.

From all these mentioned techniques, proper evacuation or activation must be done to serve the purpose. The next step after synthesis is to characterize the new MOFs for its different properties. The analytical techniques used are, Thermo gravimetric analysis (TGA), X-ray diffraction (XRD), IR, elemental microanalysis and surface area analysis [5][14][17].

2. Applications of MOF in clean energy

2.1 Hydrogen Storage

For long, hydrogen has been considered as a clean alternative to conventional energy sources because of its carbon free nature. It has also been considered as a replacement of hydrocarbon based fuel because it's oxidation only releases water as a byproduct thereby generating "zero emission". The energy density of hydrogen is thrice that of gasoline (on mass basis). Hydrogen's performance (fuel cell) is also twice as good as the internal combustion engine.

The greatest challenge that hydrogen faces in replacing fossil oil powered vehicles is that it lacks an efficient storage system. Therefore, if hydrogen storage could be efficiently achieved, then hydrogen will quickly replace gasoline in vehicles.

Ever since the capability of MOF as a storage medium for hydrogen has been reported, numerous MOFs have been evaluated for hydrogen storage applications and many of them have shown striking performance when compared with other porous materials.

There are two concepts which are used to describe hydrogen storage in MOFs namely excess adsorption and total adsorption. Excess adsorption is the amount of gas adsorbed that interacts with the framework. Total adsorption is the amount of gas adsorbed that interacts with the framework and stays in the pores when there is no gas-solid interaction. Mostly the data published in the journals is about excess hydrogen adsorption. However, total adsorption is also an important criterion with regards to hydrogen storage. XRD data

on MOF allows the estimation of total adsorption capacity based on excess hydrogen adsorption data.

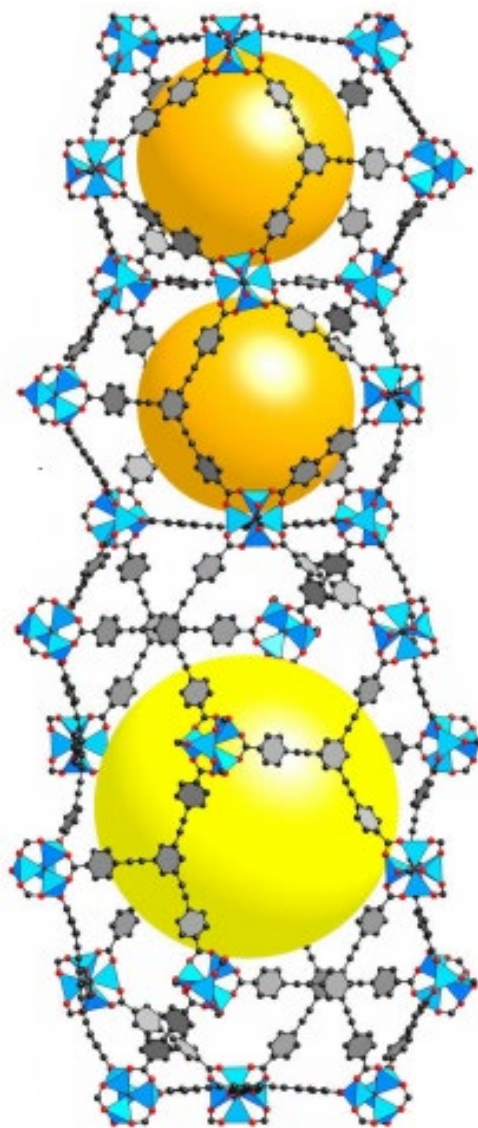


Figure 6. Structure of MOF-210.

Studies have shown that hydrogen uptake of porous MOFs at 77 K increases with the increase in their Langmuir surface areas. It has also been widely accepted that a high surface area is a primary requirement for hydrogen storage application of MOFs. However, it is not a sufficient factor that guarantees high hydrogen uptake capacity of MOFs. For instance, MOF-5 having Langmuir surface area of around 4400 m²/g shows higher hydrogen uptake of 0.076kg/kg at saturation which is much larger than that shown

by MOFs possessing higher surface areas in comparison to MOF-5 like MIL-101 which exhibits an uptake capacity of 0.061 kg/kg but has a surface area close to 6000 m²/g.

MOF-5 has been reported to show an uptake of 5wt % at 77 K and 90 bar. MOF-177 shows an uptake of 7.5 wt% at 77 K and 80 bar. Many strategies for increasing the hydrogen uptake capacity of MOFs have been explored. One such technique is embedding coordinatively unsaturated metal centres within MOF structure. Another technique is minimizing pore volume, doping alkali metals such as lithium or magnesium into the MOF framework.

Thus far, the highest hydrogen uptake capacity has been shown by MOF-210 (Zn₄O(BTE)₄/3(BPDC)). Fig. 6 shows the structure of MOF-210 [2][3][13][10][7].

Fig. 7 shows the hydrogen uptake of MOF-210 in comparison to MOF-205. Table 1 lists various MOFs with surface areas, excess and total hydrogen adsorption capacity

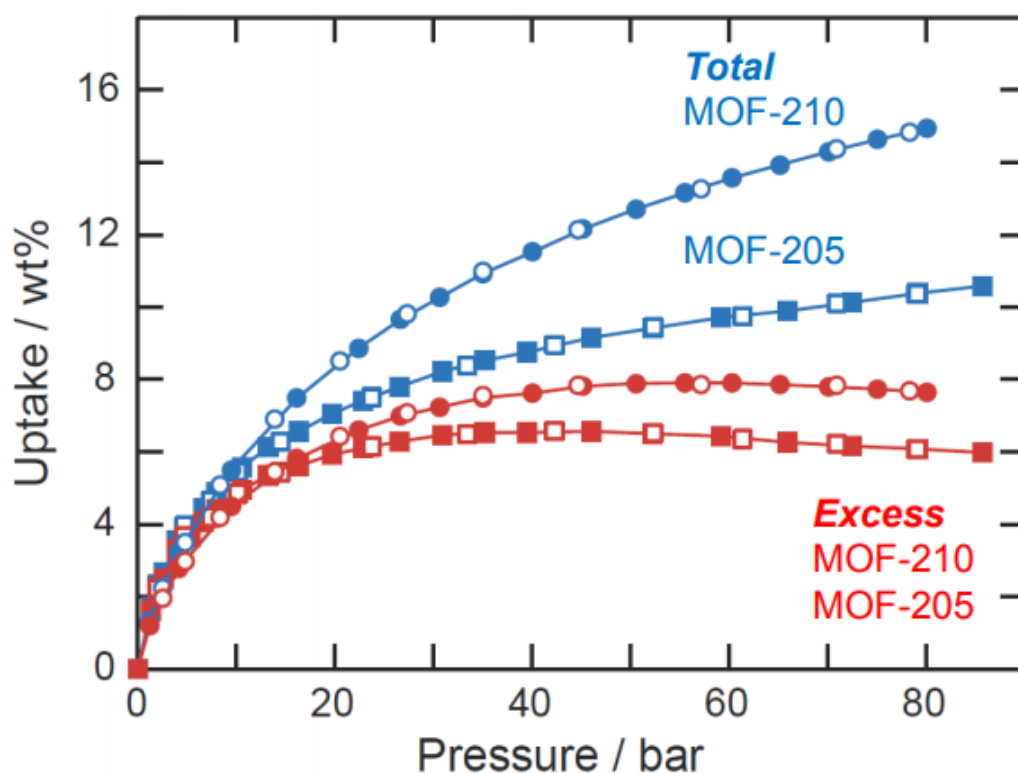


Figure 7. Comparison between excess and total hydrogen uptake of MOF-205 and MOF-210

Table 1. Various MOFs and their excess and total hydrogen uptake capacities.

Name	BET Surface area(m ² /g)	Excess Uptake capacity (wt%)	Total uptake capacity (wt%)	Total uptake capacity (g/L)
MOF-5	3800	7.1	9.6	63
MOF-177	4500	6.8	10.4	50
MOF-200	4530	6.9	14.0	36
MOF-205	4460	6.5	10.7	46
MOF-210	6240	7.9	15.0	44
UMCM-2	5200	6.5	11.0	50
NU-100	6143	9.0	14.1	41

2.2 Carbon dioxide capture

Global warming is a pressing concern today. It has drawn the attention of governing bodies and researchers and the realization of immediate corrective measures has opened new doors for exploration of ways to reduce CO₂ emission. Carbon dioxide is primarily generated as a result of fossil fuel combustion and due to the rapid consumption of fossil fuels worldwide, accumulation of CO₂ in the environment has reached alarming levels. To reduce further accumulation of carbon dioxide in the atmosphere, it is imperative to develop feasible carbon dioxide capture technologies. Currently these technologies are limited to scrubbing by amine. Which are not only costly but also inefficient. Vast development in MOFs technologies is generating increasing interest in using MOFs as carbon capture materials. MOFs have been focused at the forefront of this battle due to their high surface areas and variable pore geometries. Fig. 8 shows the schematic illustration of carbon dioxide capture by MOFs from a source having 2 components.

Yaghi et al. in their work have revealed that carbon dioxide uptake capacities in MOFs increase with increasing surface areas. MOF-177 has achieved an edge over some benchmark materials. Fig. 9 shows the dominance of MOF-177 over zeolite 13x an activated carbon material called MAXSORB.

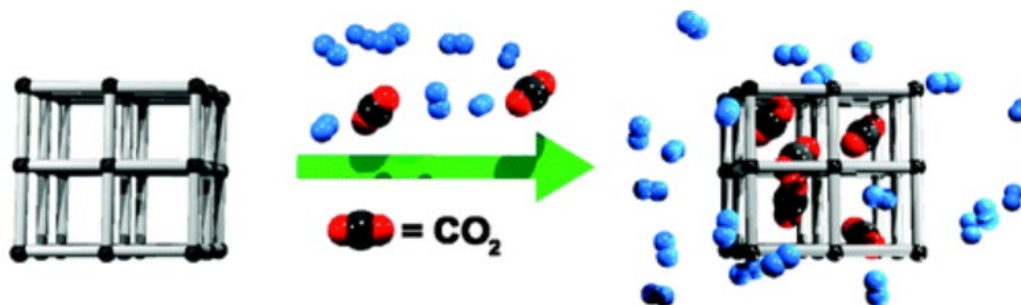


Figure 8. Schematic Illustration CO₂ capture using MOF.

Data has recently been published citing usage of MOF-74 a zinc based MOF and cobalt, nickel and magnesium based analogs in the uptake of CO₂ at low pressure [64]. The Mg-based analog of MOF-74 (Mg/DOBDC) was found to uptake 35 wt % CO₂ at 1 atm and room temperature. Fig. 10 shows the experimental CO₂ uptake in different MOFs at 0.1 bar and 298 K. We shall now discuss the synthesis of MOF-74 (Co-DOBDC) and (Mg/DOBDC) [3, 12].

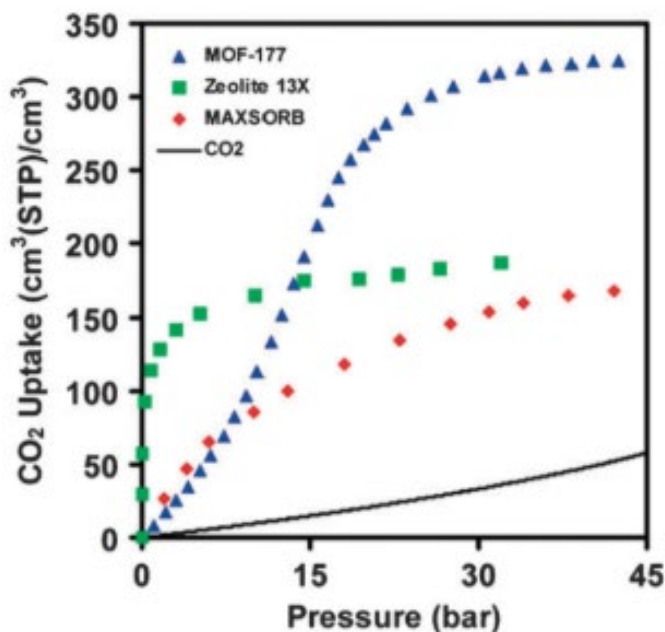


Figure 9. Comparison of carbon dioxide uptake of MOF-177 and some benchmark materials.

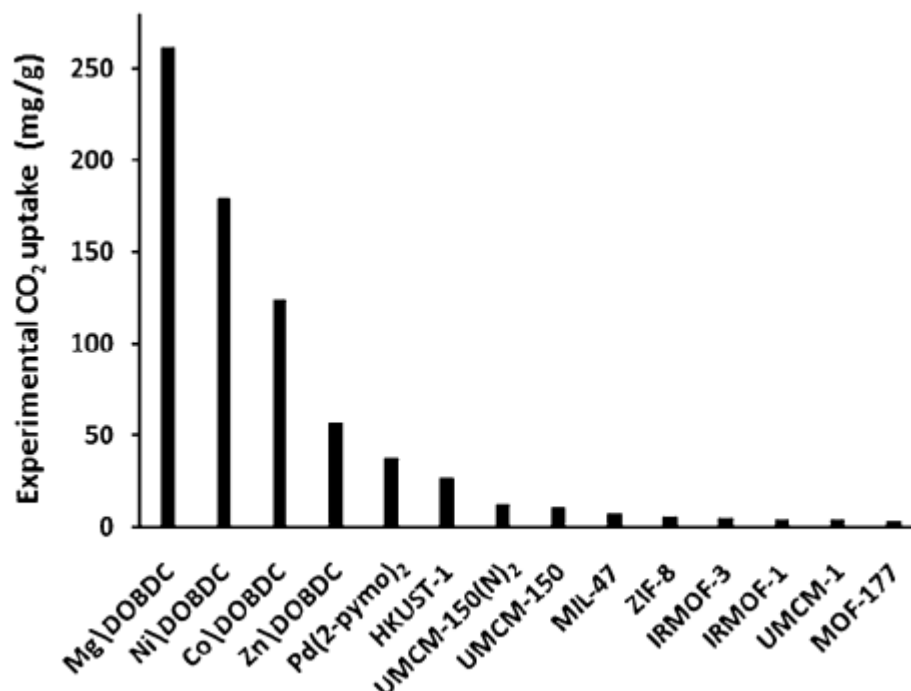


Figure 10. Comparison between carbon dioxide uptake capacities of different MOFs.

2.3 Methane storage

Like hydrogen, methane is one of the clean energy gases. Since methane exhibits high carbon to hydrogen ratio, it can provide much more energy than petroleum fuel. Methane containing natural gas deposits are more globally widespread than petroleum oil and its purification to an energy fuel is also much simpler as compared to purification of crude oil. Methane is also produced by decomposition of organic wastes. Methane has come across as a worthy alternative for mobile applications.

Compressed Natural Gas (CNG) vehicles are already popular. However, these vehicles store methane in high pressure cylinders which are dangerous as well as heavy. Development of better methane storage technology is highly required.

It is evident that a large number of MOFs have been explored as methane storage units. Some MOFs that have high storage capacities are listed in Table 2.

Table 2. Methane uptake of some selected MOFs at 298 K.

MOF	BET Surface area (m ² /g)	Total uptake (cm ³ /cm)	
		65 bar	80 bar
Cu-tbo-MOF-5	3971	199	214
MOF-519	2400	-	279
MOF-520	3290	-	231
Ni-MOF-74	1350	251	267
HKUST-1	1850	267	272
PCN-14	2000	230	250
UTSA-76	2820	257	-
NU-111	4930	205	-
NU-1100	4020	180	-
Al-soc-MOF-1	5585	196	221
NJZU-53	3034	241	-
ZJNU-50	3308	229	-
UTSA-80	2280	233	-

With reference to hydrogen storage, a number of factors currently affect the ability of MOF to adsorb methane such as surface area, pore volume, ligand functional group, etc. Farha et al. studied methane uptake of various MOFs and reported that HKUST-1 exhibits methane uptake capacity higher than any other MOF at room temperature. It is shown that the total uptake capacity of HKUST-1 is about 270 cm³/cm³ at 65 bar pressure. The reason of such a high uptake capacity exhibited by HKUST-1 was found by Brown et al. Methane adsorption data for HKUST-1 and its chromium based analog Cr₃(BTC)₂ reflects that when we alter the metal center there is little to no difference in the volumetric adsorption capacity. XRD data shows that primary adsorption sites are around the octahedral cage in the structure. Fig. 11 shows the structure of HKUST-1. Alteration of the HKUST-1 structure by substitution with Cu²⁺, Cr²⁺ to change the binding strength does not improve methane uptake capacity.

For use in mobile applications, MOF should possess high methane storage capacity and high methane deliverable capacity. He et al. in their study elongated the organic linker in NOTT-101 by introducing C triple bond. Such an assembly of elongated ligand gave rise

to NbO type MOF- ZJNU-50 having methane storage capacity of $229 \text{ cm}^3/\text{cm}^3$ at 298 K which is comparable to that of NOTT-101 which shows $237 \text{ cm}^3/\text{cm}^3$. However, the deliverable capacity of ZJNU-50 was larger than NOTT-101. He et al. also developed a new organic linker constructed ZJNU-53. The total volumetric uptake capacity of ZJNU-53 was found to be $241 \text{ cm}^3/\text{cm}^3$ at 298 K and 65 bar and the deliverable capacity at 298 K WAS $190 \text{ cm}^3/\text{cm}^3$. This data clearly shows ZJNU-53 has dominance over ZJNU-50 [2-3,9,11]. Fig. 12 shows the comparison of structure of *of* ZJNU-50 and ZJNU-53.

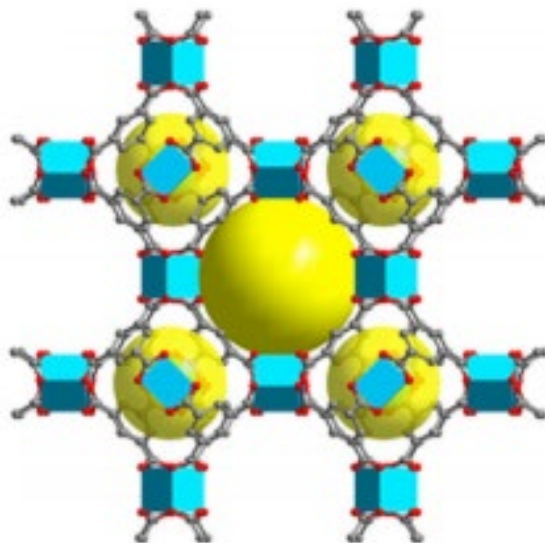


Figure 11. Structure of HKUST-1.

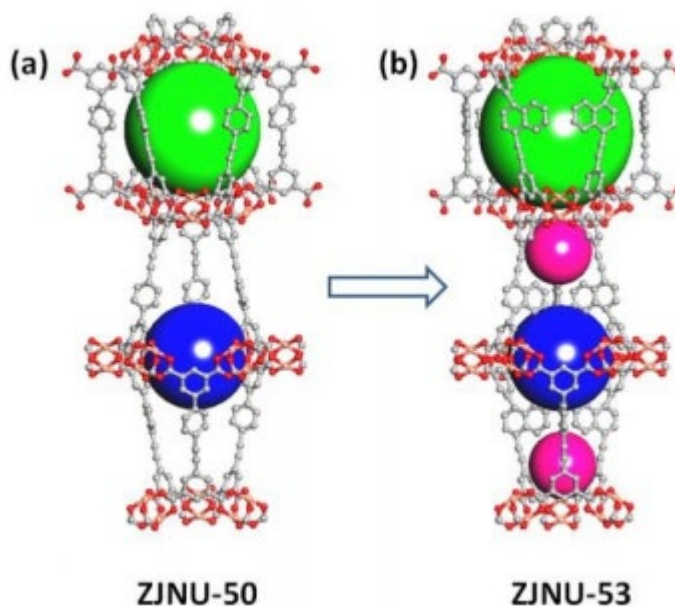


Figure 12. Comparison of structures of ZJNU-50 and ZJNU-53.

2.4 Electrical energy storage and conversion

2.4.1 Fuel cell

A fuel cell is a device which is used for electrochemical conversion. Each fuel cell is comprised of a cathode, an anode and an electrolyte that facilitates the movement of ions between cathode and anode. A typical example of fuel cell is Polymer Electrolyte Membrane fuel cell (PEMFC). In a PEMFC hydrogen is used as fuel which is delivered to the anode where it undergoes oxidation by anodic catalyst and produces electrons and protons. The protons move to the cathode side while electrons move through an external circuit. This electron movement thereby produces current. At the cathode in presence of catalyst water heat is released as a result of interaction between oxygen and electrons and protons. Fig.13 shows the assembly of PEMFC cell.

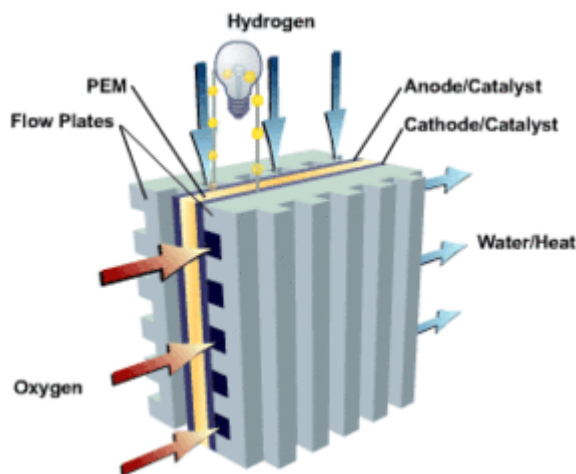


Figure 13. Typical assembly of a PEMFC cell.

MOFs can be custom made to exhibit high surface areas and well organized porous structure by selecting suitable metal ions and organic linkers. A suitable electro-chemical catalyst can thus be designed using MOFs.

MOFs as we know comprise of metal centers bound by organic linkers. By careful consideration of required functionality, MOFs with electrochemical properties can thus be designed. Lanqun et al. first demonstrated the use of MOF as an electrocatalyst in oxygen reduction reaction (ORR). Two copper based MOFs were synthesized viz. [copper (II) benzene-1,3,5-tricarboxylate] and [copper (II)-2,20 - bipyridinebenzene-

1,3,5-tricarboxylate]. The [copper (II)-2,20 -bipyridinebenzene-1,3,5-tricarboxylate] MOFs was found to show an excellent electrocatalytic activity towards 4e⁻ reduction of O₂. Based on the excellent catalytic performance of Cu-MOFs, some graphene and Cu-MOFs composites have been researched to overcome the poor electron-conduction properties of Cu-MOFs and further improve the catalytic activity and stability.

Maryam et al. developed graphene oxide based MOF having copper as the central metal. This composite exhibited good catalytic property. These composites exhibited little over potential and high current density for all the above mentioned electrocatalytic reactions and showed excellent stability in acidic medium [1,15].

2.5 MOFs for supercapacitor applications

Supercapacitors are next generation energy storage devices. They are known to possess high power energy and long cycle life. One such supercapacitor is EDLC (electrical double layer capacitor). They are made using carbon materials having high surface area and large pore sizes. MOFs and its derivatives show great potential and possible application in supercapacitors owing to their high surface areas, controllable pores and small sizes. Fig.14 shows a typical EDLC. MOFs can directly be used as electrodes in supercapacitors. Cobalt based MOF-5 was first used as electrode material for supercapacitor. In another study, different organic ligands having varied lengths were used to vary the pore size of cobalt based MOFs. The MOF which has longer organic linker exhibited larger pores, larger surface area, and highest capacitive properties.

Wei et al. used a layered structure of nickel based MOF as an electrode material for supercapacitors with large specific capacitance, high rate capability of 1127 and 668 F/g.

In another study, zirconium based MOF UiO66 was synthesized at different temperatures to obtain different particle sizes and varied degree of crystallization. The sample shows that lowest temperature exhibited smallest particle size and highest specific capacitance of around 1150 F/g.

Yaghi et al. designed zirconium based MOF (nMOF-867) exhibited capacitance of about 6 times higher that of commercial activated carbon [1,15]

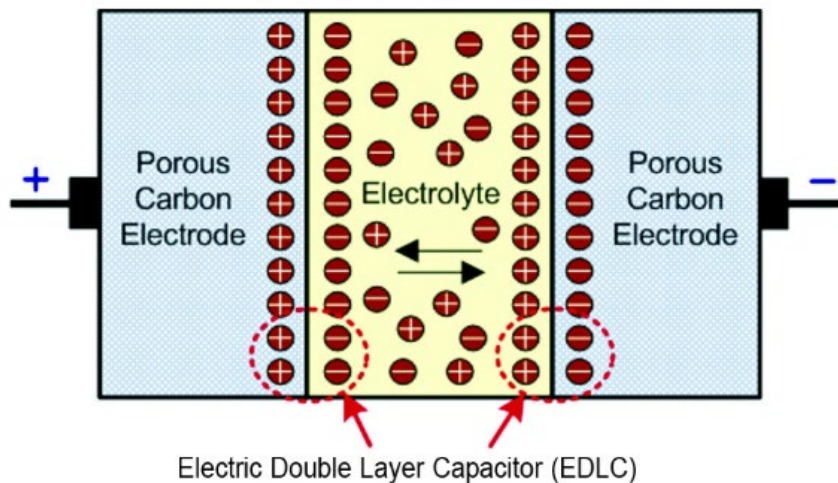


Figure 14. EDLC Supercapacitor

2.6 NH₃ removal

About 150 million tons of ammonia is produced globally each year. It is used as feed in many industries such as fertilizers industries, pharmaceutical industries and refrigeration. Large scale production and storage of ammonia is hazardous due to its toxic nature. Due to dangers associated with exposure to ammonia it is necessary to develop new materials for adsorptive removal of ammonia from air. MOFs are considered as good adsorbing agents for ammonia.

HKUST-1 has shown immense capabilities in this area. It can efficiently adsorb ammonia both under dry and humid conditions.

The working principle is the coordination of ammonia molecules to available Cu (II) sites. To increase the availability of Cu (II) sites, Farha et al. selected Cu₂(dobdc), having highest availability of Cu (II) sites (4.7 nm⁻³) of any known MOFs to absorb ammonia. Ammonia uptake capacity of Cu₂(dobdc) under 0 and 80% relative humidity was found to be 3.4 and 7.6 mmol g⁻¹ respectively. It is found that gravimetric uptake and number of NH₃ molecules per Cu site was found to be less than HKUST-1, the volumetric NH₃ uptake of Cu₂(dobdc) is 5.9 ammonia/ nm³ at 80% relative humidity, higher than that of HKUST-1 which is about 3.9 ammonia/nm³) [2,8].

2.7 Benzene removal

Benzene finds applications in a large number of chemical industries. But the presence of benzene causes emissions and poses great health risks. Reversible physical absorption within the framework of MOFs is a great strategy for benzene removal. MOFs

have been studied for benzene removal. Data present in literature has shown that adsorption capacity of HKUST-1 is about 9.5 mmol g^{-1} at 298 K and 1.0 kPa. Benzene uptake capacity of MIL-141 based on cesium was found to be 2.6 mmol g^{-1} at 303 K and 0.69 kPa. MOFs have also been studied for removal of benzene derivatives. Toulene adsorption capacity of SCUTC-18 was found to be $1.848 \text{ mmol g}^{-1}$ at 298 K and 3.405 kPa. Kirillov et al. in their study created a stable nanotubular zinc based MOF which was derived from biphenyl-3,5-dicarboxylic acid which shows great adsorption features. The adsorption amounts were quantitatively determined on the basis of NMR spectra as 1.08, 1.79, and 1.04 mg g^{-1} for benzene, *p*-xylene, and *m*-xylene, respectively. NMR spectroscopy data clearly shows that Zn-MOF could be effective for separation of benzene from toluene or xylene [8].

2.8 NO₂ removal

NO₂ is one of the major toxic pollutants harmful for all forms of life. MOFs have been extensively studied as NO₂ absorbing agents. Zirconium based MOFs are widely popular for this application due to their high chemical stability.

Bandosz et al. reported the synthesis zirconium based MOFs with slight modifications viz. introduction of an NH₂ group. The prepared samples could be used for NO₂ adsorption in both dry and humid conditions. It was found that water enhanced the NO₂ adsorption process. [2,8].

2.9 Photocatalysis

By the use of solar energy, many chemical processes like hydrogen production from water, air treatment, water treatment and organic synthesis is in practice. Thus all the process will be environmental friendly and avoid the toxic chemicals usage and their generation. Titanium dioxide (TiO₂) based materials are generally used as photocatalyst. There are several methods for the preparation of nano porous semiconductor based materials for photocatalytic application like, sol-gel method, hydrothermal method, spray-drying method and deposition method. All methods help to improve the catalytic performance of the photocatalyst by, metal doping, ligand modification and coupling with semiconductors and modification with carbon material.

Semiconductor photocatalytic procedures have shown great latent in sustainable treatment technologies in waste water treatment. It is believed that, ZnO is effective in removing the organic compounds from waste water. Another study was made by Zhang's group in 2016, which included preparation of Cu/CuO/C nanocomposites from the direct carbonization of Cu-BTC. The crew also studied the influence on CO oxidation. By controlling the heating rate and annealing temperature, the synthesized carbon

compressed Cu/Cu₂O catalyst achieved a complete CO conversion at 155°C and was stable up to 4 hours. The team also reported that around 500°C is the optimum annealing temperature for catalyst preparation. If the temperature is dropped below 500°C, that will lead to poor crystallinity. On the other hand if the temperature is raised above 500°C, this will cause agglomeration of the catalyst particle. This study shows that MOFs can be effectively adopted in CO₂ conversion by photocatalysis.

Adsorptive separation of CO₂ in MOFs: Like most of the porous materials, CO₂ absorption capacity is determined by the surface area of the MOFs. Compared to activated carbons and zeolites MOFs have larger surface area. The CO₂ gravimetric capacities of few selected MOFs are given in Table 3. The CO₂ loading ability of MOFs can be measured at different pressures and temperatures, a correlation between surface area and storage capacity. Yaghi *et al.* carried out the first study to see the relationship between MOFs surface area and CO₂ capacity. It was found that MOF-117 possesses largest surface area. It also has the highest CO₂ uptake at high pressure, i.e 60.6 wt% at 35 bar. More detailed information is listed in Table 3 below [17-20].

Table 3. CO₂ absorption capacities in selected MOFs.

Chemical Formula	Common Name	Surface area (m ² /g)		Capacity (wt%)	Pressure (bar)	Temp. (K)
		BET	Langmuir			
Zn ₄ O(BBC) ₂ (H ₂ O) ₃	MOF-200	4530	10400	70.9	50	298
Zn ₄ O(BBC) _{4/3} (NDC)	MOF-205	4460	6170	59.9	50	298
Zn ₄ O(BTE) _{4/3} (BPDC)	MOF-210	6240	10400	70.6	50	298
Mg ₂ (DOBDC)	Mg-MOF-74	1800	2060	35.2	1	298
Zn ₂ (BDC) ₂	MOF-2	345	-	12.3	35	298
Cu(BPTC)	MOF-505	1547	-	31.0	35	298
Zn ₂ (DOBDC)	Zn-MOF-74	816	-	31.4	35	298
Cu ₃ (BTC) ₂	HKUST-1	1781	-	32.0	35	298
Zn ₄ O(HPDC) ₃	IRMOF-11	2096	-	39.3	35	298
Zn ₄ O(C ₂ H ₄ BDC) ₃	IRMOF-6	2516	-	46.2	35	298
Zn ₄ O(NH ₂ BDC) ₃	IRMOF-3	2160	-	45.1	35	298
Zn ₄ O(BDC) ₃	IRMOF-1	2833	-	48.8	35	298
Zn ₄ O(BTB) ₃	MOF-177	4508	-	60.0	35	298
Cd(ANIC) ₂	Cd-ANIC-1	329.3	504.9	14.4	1	298
CO(ANIC) ₂	Co-ANIC-1	274.0	412.6	13.3	1	298

Conclusion

Metal organic frameworks find numerous applications in the field of clean energy. Due to the freedom that MOFs offer with respect to optimization as per requirement, they have proved to be worthy candidates in environmental applications. Since the structural and functional properties of MOFs can easily be modified a large number of derivatives and composites are frequently prepared that come out to be more efficient than their parent MOFs. Since their inception, MOFs have gone a long way and with time their applications are getting more diverse. MOFs might help us in solving the energy crisis that the world is currently facing and can turn out to be a boon for mankind.

Acknowledgement

The authors would like to acknowledge the gratitude to Manipal Institute of Technology, Manipal Academy of Higher Education, Manipal for providing all the support.

References

- [1] Yang Zhao, Zhongxin Song, Xia Li, Qian Sun, Niancai Cheng, Stephen Lawes, Xueliang Sun, Metal organic frameworks for energy storage and conversion, *Energy Storage Materials*.2 (2016) 35 - 62. <https://doi.org/10.1016/j.ensm.2015.11.005>
- [2] Bin Wang, Lin-Hua Xie, Xiaoqing Wang, XiaoMin Liu, Jinping Li, Jian-Rong Li, Applications of metal–organic frameworks for green energy and environment: New advances in adsorptive gas separation, storage and removal, *Green Energy & Environment* 3 (3) (2018) 191 - 228. <https://doi.org/10.1016/j.gee.2018.03.001>
- [3] Ma Shengqian, and Hong-Cai Zhou, Gas storage in porous metal organic frameworks for clean energy applications, *Chemical Communications* 46 (2010) 44 - 53. <https://doi.org/10.1039/B916295J>
- [4] Sandra Loera-Serna, Elba Ortiz, Chapter 4 Catalytic Applications of Metal-Organic Frameworks, *InTech*, 2016, pp. 2 – 29.
- [5] Sumbal Farid, Suzhen Ren, Ce Hao, MOF derived metal/carbon materials as oxygen evolution reaction catalysts, *Inorganic Chemistry Communications* 94 (2018) 57 – 74. <https://doi.org/10.1016/j.inoche.2018.06.008>
- [6] Troy Scott Blankenship II, Norah Balahmar, Robert Mokaya, Oxygen-rich microporous carbons with exceptional hydrogen storage capacity, *Nature Communications* 8 (2017) 1 – 12. <https://doi.org/10.1038/s41467-017-01633-x>

- [7] Yichao Lin, Chunglong Kong, Qiuju Zhang, Liang Chen, Metal-Organic Frameworks for Carbon Dioxide Capture and Methane Storage, *Advanced Energy Materials* 7(4) (2017) 1 – 29. <https://doi.org/10.1002/aenm.201601296>
- [8] Michael J. Katz, Ashlee J. Howarth, Peyman Z. Moghadam, Jared B. DeCoste, Randall Q. Snurr, Joseph T. Hupp, Omar K. Farha, High Volumetric uptake of ammonia using Cu-MOF74/Cu-CPO-27, *Dalton Transactions* 45 (2016) 4150 – 4153. <https://doi.org/10.1039/C5DT03436A>
- [9] Xin-Juan Hou, Peng He, Huiquan Li, Xingrui Wang, Understanding the Adsorption Mechanism of C_2H_2 , CO_2 , and CH_4 in Isostructural Metal–Organic Frameworks with Coordinatively Unsaturated Metal Sites, *The Journal of Physical Chemistry C* 117 (6) (2013) 2824 – 2834. <https://doi.org/10.1021/jp310517r>
- [10] D Saha, Z Wei, S Deng, Equilibrium, kinetics and enthalpy of hydrogen adsorption in MOF177, *International Journal of Hydrogen Energy* 33 (24) (2008) 7479-7488. <https://doi.org/10.1016/j.ijhydene.2008.09.053>
- [11] Guohai Xu, Bin Li, Hui Wu, Wei Zhou, Banglin Chen. Construction of ntt -Type Metal–Organic Framework from C_2 -Symmetry Hexacarboxylate Linker for Enhanced Methane Storage, *Crystal Growth & Design* 17 (9) (2017) 4795 – 4800. <https://doi.org/10.1021/acs.cgd.7b00737>
- [12] Kyriakos C. Stylianou, Wendy L. Queen. Recent Advances in Carbon Capture with Metal–Organic Frameworks, *CHIMIA International Journal for Chemistry* 69(5) (2015) 274 – 283. <https://doi.org/10.2533/chimia.2015.274>
- [13] Shengqian Ma. Gas adsorption applications of porous metal–organic frameworks, *Pure and Applied Chemistry* 81 (12)(2009) 2235- 2251. <https://doi.org/10.1351/PAC-CON-09-07-09>
- [14] Suh, Myunghyun Paik, Hye Jeong Park, Thazhe Kootteri Prasad, and Dae-Woon Hydrogen Storage in Metal–Organic Frameworks, *Chemical Reviews* 112 (2) (2012) 782 - 835. <https://doi.org/10.1021/cr200274s>
- [15] Xiuxiu Liu, Changdong Shi, Changwei Zhai, Meiling Cheng, Qi Liu, Guoxiu Wang. Cobalt Based Layered Metal–Organic Framework as an Ultrahigh Capacity Supercapacitor Electrode Material, *ACS Applied Materials & Interfaces* 8(7) (2016) 4585 -4591. <https://doi.org/10.1021/cr200274s>
- [16] Gómez-Gualdrón, Diego A., Christopher E. Wilmer, Omar K. Farha, Joseph T. Hupp, and Randall Q. Snurr, Exploring the Limits of Methane Storage and Delivery in

Nanoporous Materials, The Journal of Physical Chemistry C, 118(13) (2014) 6941 – 6951. <https://doi.org/10.1021/jp502359q>

- [17] Hu, J., Deng, M., Wang, H., Wang, X., Hu, Y., Jiang, H.-L., Jiang, J., Zhang, Q., Xie, Y., and Xiong, Y, Integration of an inorganic semiconductor with a metal–organic framework: a platform for enhanced gaseous photocatalytic reactions. *Advanced Materials* 26 (2014) 4783-4788. <https://doi.org/10.1002/adma.201400428>
- [18] Millward AR and Yaghi OM, Metal-organic framework with exceptionally high capacity for storage of carbon dioxide at room temperature, *Journal of American Chemical Society* 127 (2005) 17998-17999. <https://doi.org/10.1021/ja0570032>
- [19] J. Aguilera-Sigalat, D. Bradshaw, Synthesis and applications of meta-organic framework-quantum dot (QD@MOF) composites. *Coordination Chemistry Reviews* 307 (2015) 1 - 56. <https://doi.org/10.1016/j.ccr.2015.08.004>
- [20] P. Kumar, K. Vellingiri, K.-H. Kim, R.J.C. Brown, M.J. Manos, Modern progress in metal-organic frameworks and their composites for diverse applications. *Microporous and Mesoporous Materials* 253 (2017) 251 – 265. <https://doi.org/10.1016/j.micromeso.2017.07.003>

Chapter 6

Nanoporous Metal-Organic-Framework

Sameer Ahmad^{1*}, Afzal Ansari¹, Weqar Ahmad Siddiqi¹, M. Khursheed Akram²

¹Department of Applied Sciences and Humanities, Faculty of Engineering and Technology,
Jamia Millia Islamia, New Delhi-110025, India

²Applied Sciences and Humanities Section, University Polytechnic, Faculty of Engineering and
Technology, Jamia Millia Islamia, New Delhi-110025, India

* ahmad.sameer68@yahoo.com

Abstract

Nanoporous metal-organic frameworks (MOFs) are three-dimensional porous lattices of inorganic-organic linkers. These materials have tunable physiochemical properties such as high porosity, crystalline nature, chemical, thermal and mechanical stability as well. The fabrication of different MOFs can be approached by synthetic modification methods for instance modulated synthesis and post-synthetic modification. Synthetic modifications develop most stable functionalized MOFs materials, which play the most promising role in different fields such as gas separation, catalysis, gas storage, water treatment, and other different applications.

Keywords

Metal-Organic Frameworks, Stability, Porosity, Functionalization, Gas Separation, Catalysis

Contents

1. Introduction.....	108
1.1 Fundamental stabilities of nano MOFs.....	115
1.1.1 Chemical stability	115
1.1.2 In water medium	115
1.1.3 In acid/base condition	116
1.1.4 Thermal Stability	117
1.1.5 Mechanical Stability	118
1.2 Synthesis	119

1.2.1 Modulated synthesis	121
1.2.2 Post-synthetic modification (PSM)	123
1.3 Applications of MOFs	126
1.3.1 Gas separations and storage.....	126
1.3.2 Catalysis	128
1.3.2.1 Lewis acid catalysis	128
1.3.2.2 Bronsted acid catalysis.....	129
1.3.2.3 Redox Catalysis	129
1.3.2.4 Photocatalysis	129
1.3.2.5 Electrocatalysis	130
1.3.3 Water treatment	130
1.4 Other applications.....	131
1.4.1 Sensors	131
1.4.2 Supercapacitors.....	131
1.4.3 Biomedical applications.....	131
Conclusion.....	132
References	133

1. Introduction

Nanoporous metal-organic frameworks (MOFs) are crystalline coordination polymers (CPs) which are constructed by the linkage of inorganic metal ion and organic ligands through a chemical bond. Where, metal ion act as a center of MOF, is known as the primary building unit (PBU) and organic ligands known as secondary building units (SBUs) of the framework. The term “nanoporous” for metal-organic frameworks (MOFs) are referred to those porous materials which have pores diameter less than a hundred nanometers (<100nm) with 2D- or 3D-networks of the voids spaces, and resulted (Fig. 1) into a single entity with nanoscale measurement. Nanoporous metal-organic frameworks (MOFs) are considered to be a new generation hybrid materials, which are useful in most diverse fields based on their structural performance and physiochemical properties such as large pores surface area, unsaturated metal sites, exchangeable ligands and presence of their voids in its structure [1-2]. Nanoporous MOFs contains dozens of structural topologies on different scales, such as mesoporous (2-50 nm pore diameter) and microporous (<2nm pore diameter) scales for instance MCM-41, ZIF-MOFs, MIL-

100,101 and many others. While, the others conventional example of MOFs are Rho and sodalite (Fig. 2) that are well known for zeolites respectively, but effective performs than nanoporous MOFs materials[2-3].

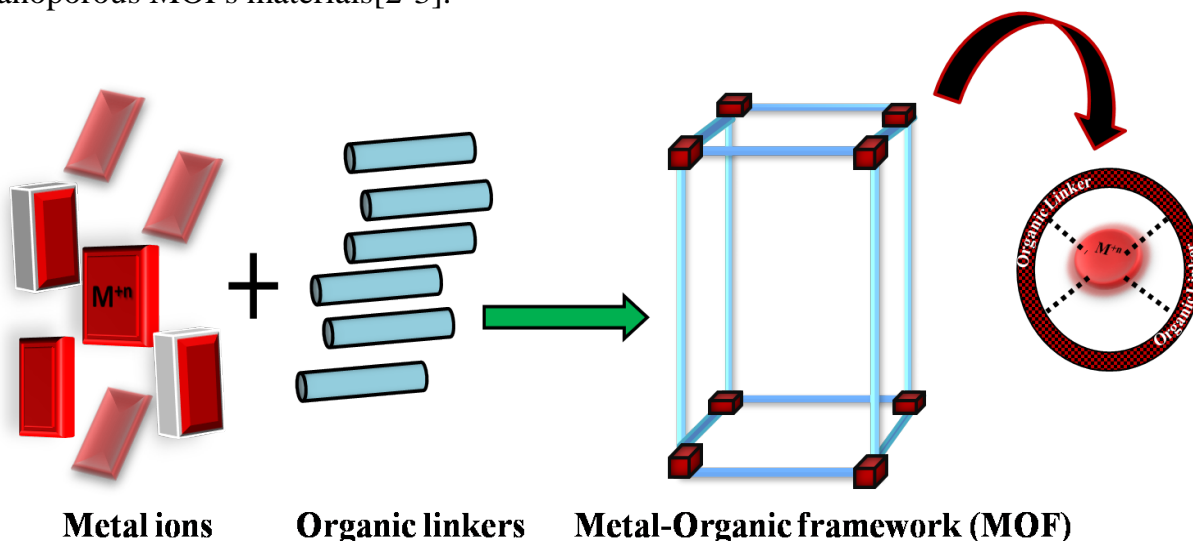


Figure 1: General representation of 3D-nanoporous metal-organic framework (MOF).

Due to the structural similarity with organometallic complexes they are considered to be as coordination polymers (PCs). Moreover, nano MOFs is to be consider different over others coordination polymers in terms of physiochemical properties and these differences are enlisted in (Table-1), as the key of structural differences between MOFs and other coordination polymer materials [4-5]. In the light of crystal shape arrangement, nano MOFs are classified into two types: crystalline and amorphous. The crystalline form shows an infinite arrangement of solids in regular long-range order while amorphous MOFs possess short-range order with the finite arrangement of the solids [5]. The crystalline nano MOFs exhibits large surface area up to $7000 \text{ m}^2\text{g}^{-1}$, and permanent free volume porosity up to 90% and low densities to 0.14 gcm^{-3} [3]. Nanoporous MOFs exhibits structural and functional tunability towards research and development for both engineers and scientists. These nanoporous materials have been used in expanding scope such as catalysis specific for heterogeneous fashion, energy storage, and gas separation but are also used for other practical applications including chemical sensing, biomedicine, photocatalysis and water treatment [6]. The crystalline nanoporous metal-organic frameworks (MOFs) expose some different properties over usually used coordination polymers (e.g. organo-metallic framework) and other molecular sieves as they are structurally flexible and multi-functional materials which are reliable for a useful physical characteristics like as photoluminescence, magnetism, and conductivity.

Table 1: Compare between physiochemical properties of zeolite and molecular sieves.

S.No.	Physiochemical properties	Dimensions
1.	Pore size	~4-12 Å ^o
2.	Pore shape	Circular and elliptical
3.	Surface nature	Hydrophobic for high silica, hydrophilic
4.	Voids volume	<50%

While, the conventional porous zeolites which are a well-recognized example of crystalline nanoporous MOFs material characterized on a micro-scale with pores size about (02 nm) in diameter. Usually, these microporous crystalline hybrids are three-dimensionally (3D) framework also and composed by tetrahedrons (T-atoms) of Silicon-oxides (SiO₄) and Aluminium-oxides (AlO₄) in the form of negatively charged lattices (Fig. 2). The negative charges on the lattices are balanced by central metal cations of the framework. There are more than 190 different most known zeolites form have been reviewed in literature, for example ZSM-5, zeolite-β, zeolites(X, Y, and A), silicalite-1 among others.

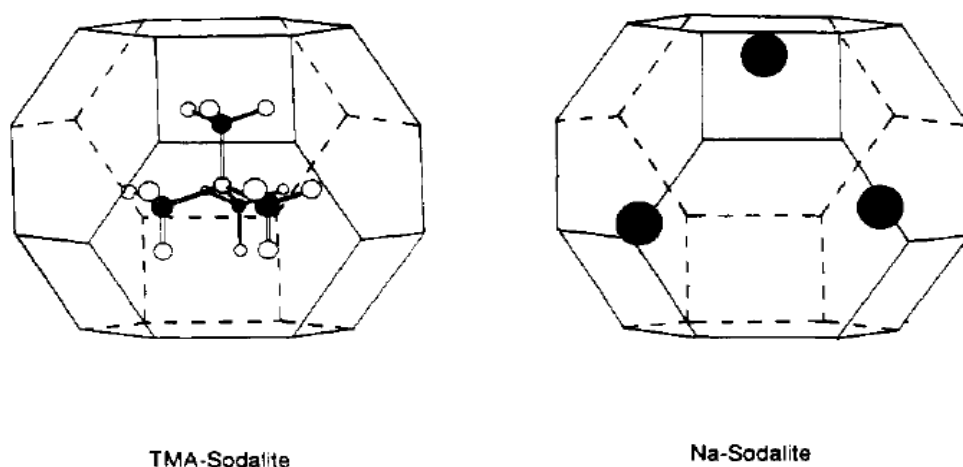


Figure 2: Three dimensional overview of porous zeolites lattices (sodalite) reuse with permission from ref-(11).

The well-oriented pores and voids spaces of the zeolites frameworks with transition metal cations account for redox activity and catalytic applications [2,7]. Henceforth, approximately forty (40) natural zeolites have been found where typical cations are alkali metals e.g. Na⁺, K⁺ and alkaline earth metal e.g. Ca²⁺, Ba²⁺ ions used in its framework

center. In contrast to characteristic zeolites, synthetic zeolites may contain both inorganic and natural cations, e.g., Na^+ , quaternary ammonium particles, and protons. Based on crystal size and symmetry of framework, the International Zeolite Association (IZA) assigned a three-letter code to each zeolite MOFs topology, for instance, ZSM-5, AlPO_4 -5, AlPO_4 -1, but MFI (Mobil number five) code especially used for some molecular sieves [7].

One of the most important example of nanoporous MOF materials are zeolitic imidazole frameworks (ZIFs) and assigned with an unique code up to twelve frameworks topologies such as ZIF-9 to ZIF-12 have been reported. ZIFs MOF are constructed by tetrahedral transition metal ions and imidazoles (IM) linkers, where IM linkers are replaced linkers instead of the tetrahedral Si-O and Al-O bonds of the aluminosilicate zeolites MOFs. Moreover, example of ZIFs are ZIF-1 to -4, -6 to -8 and -10 to -11 are known for zinc (Zn^{2+}) metal ion, ZIF-5 (Zn^{2+} and In^{2+}) and ZIF-9,-12 known for cobalt metal (Co^{2+}) ion, which can be synthesized by copolymerization process [8].



Imidazoles (IM) unit of the framework are formed by losing a proton from an imidazole molecule and make a bridge like M-IM-M link in MOF, where this unit (IM) combines with metal ions as similar to the Si-O-Si bond link of the zeolite structure. A large number of new groups of nonporous low symmetrical ZIFs have been reported which are structurally analogous to tetrahedral zeolite frameworks composed by Fe (II), Co (II), Cu (II) and Zn (II) metal ions (Fig. 3). Among these frameworks, two zeolitic IM-frameworks (ZIF-7,8) have a porous and symmetrical structure as similar to zeolites. Furthermore, other two zeolitic IM-framework ZIF-8 and -11 exhibits their permanent porous nature (Table-2) with high surface area (1,810 square meter/gram), chemical resistivity towards alkaline solutions and remarkable thermal stability up to 550°C which prevents ZIFs to degrade in various operating environments [8-10].

Table 2: Physiochemical properties of MOF ZIFs-8, 11 analyzed by X-ray diffraction (XRD) technique.

ZIF-n	ZIF-8	ZIF-11	Ref.
Pore diameter (\AA°)	11.6	14.6	[8]
Surface area (m^2/g)	1,948	1,677	
Pore volume (m^3/g)	0.664	0.580	

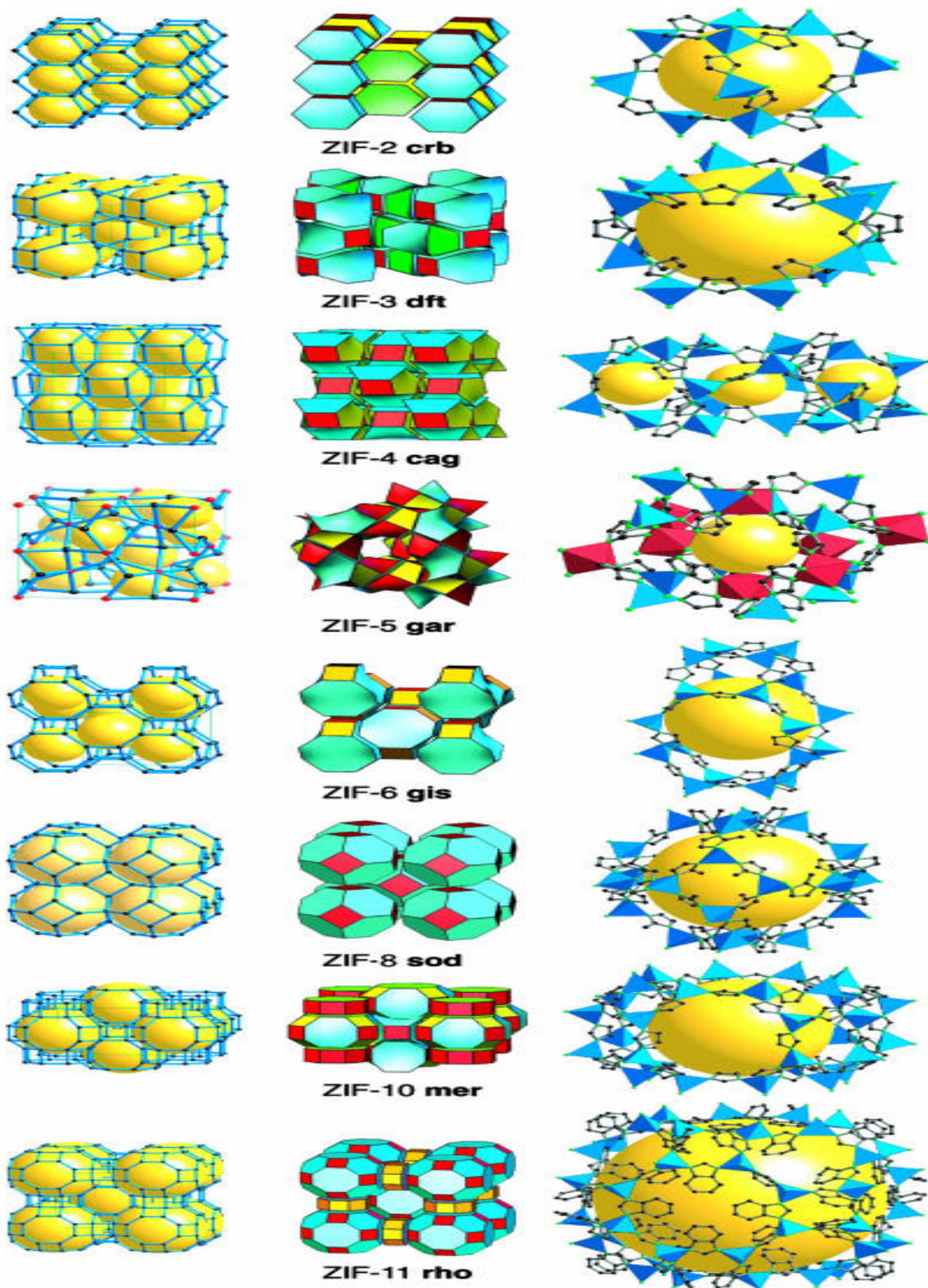


Figure 3: Schematic representation of different porous symmetrical ZIF- frameworks reuse with permission from ref. [8].

Due to the permanent porosity and surface area of two ZIFs-8 and -11 IM-compounds have been extensively used for the applications in catalysis, gas separation and storage etc. [11].

The connection among nanostructure and the macroscopic properties e.g. physiochemical properties (Table 3) of the nano-MOFs allow using as molecular sieves with size precisions under 1 \AA scale. It is not required every molecular sieve to be zeolites when its structure formed by other than silicon and aluminum [11]. There are two proposed mechanism utilized for Zeolite MOFs synthesis - (i) the solution transport system and (ii) the phase-change of the solids mechanism. There are other different synthesis strategies accessible for zeolites preparation which are discussed later in this chapter.

Another group of microporous MOF materials are Aluminium based crystalline nano-MOFs for instance aluminophosphate (AlPO)/silicoaluminophosphates (SAPO) frameworks these porous materials also known as molecular sieves. Usually, the Aluminium MOFs-(Al) exhibits oxophilic nature due to the presence of Al-O bonds in its structure. In contrast to porous zeolites frameworks where, Aluminium (Al) cations is encompassed in tetrahedron state, while in MOFs-(Al) frameworks this same cation (Al^{+3}) facilitated in octahedral state until now. Albeit, there are various Al-MOFs have been reported in terms of their unique codes for instance, MIL (Materiaux del institute Lavoisier), CAU (Christian-Albrechts Universitat) and DUT (Dresden University of Technology) which were designed by groups from the Universite de Versailles, France. In the light of Al-based MOFs abbreviations, there are different sort of microporous Al-MOFs derivatives reported, for example, MIL-100,118,120 CAU-1-NH₂, CAU-3, DUT-4,5 and among others. These all aluminium based MOFs demonstrate their favorable properties towards various applications as sensors, membranes for separation technique and gas storage and so forth. These favorable properties of MOFs-(Al) are:

- The Al-MOFs can be facilely synthesized in water
- Different Al-MOFs derivatives can be synthesized by direct synthesis and post-synthetic modification (PSM)
- Flexible, chemically and thermally stable

The chemistry of Aluminum (Al) based microporous crystalline MOFs can be modified by using different functional groups, for example, -Cl, -CH₃, -NO₂, -NH₂ etc. with different organic linkers, these functionalized MOFs-(Al) shows their temperature dependent structural flexibility in different operating conditions and utilized in diverse applications such catalysis, water treatment, gas storage and separation etc. While, temperature-dependent flexibility of MOFs-(Al) can be also observed without

functionalization of its organic linkers, but shows low performance than functionalized framework structures [12].

Table 3: Physiochemical properties of nano-MOFs and coordination polymers.

Properties difference between the MOFs and coordination polymers			
S.No	Name Properties	MOFs	Coordination polymer
1.	Nature of joint framework units	Polyatomic	Monatomic
2.	Nature of pores	Neutral	Charged
3.	Bond energy (kJ/mol)	362	150
4.	The dissociation energy of framework units (kJ/mol)	2200	400-600

In the structure of nano MOFs, the inorganic unit (metal ion) assumed as polar site while another organic linker unit assumed as a non-polar site and these both units are combined through strong bonds into a single entity. The central metal ion of MOFs can be alkali metal ion, transition metal ion or group of metals as discussed already. Furthermore, other inorganic metal and its mixture such as iron, silica, zeolite and many more are also used for the preparation of MOFs [5].



In emerging field of nano metal-organic frameworks around tens of thousands (10,000) highly ordered crystalline nano MOFs are constructed from 3p-(Al³⁺, Ga³⁺, In³⁺) cations, 3d-divalent metal ions (Zn²⁺, Cu²⁺, Co²⁺, Ni²⁺, Cd²⁺,....) and other 3d-metal ions (Sc³⁺, Ti⁴⁺, Cr³⁺, Fe³⁺, Zr⁴⁺ etc.) all these metal ions act as catalysis center of the MOF-cavity which are linked to organic ligands, where organic ligands may be in the form of carboxylate, phosphonates, imidazoles, phenolates etc. All these ligands performed as electron donor unit to centered metal ion [13-15]. In the formation of nano MOFs structure, the inorganic unit (metal ions) can be used with various different oxidation states which described the stability criteria, chemical reactivity of MOFs [13]. A general skeleton of nano MOF is presented in fig.1. which shows a rigid and packed 3D-building network [16].

1.1 Fundamental stabilities of nano MOFs

1.1.1 Chemical stability

The stability of MOFs exhibits its robustness in the working environments where chemical stability defined as the capacity of MOFs to keep up their stable framework in certain chemical conditions. The stability of MOF controlled by two methods such as Brunauer-Emmett-Teller (BET) N_2 -isotherm for the surface area and powder X-ray diffraction (PXRD) pattern which described the degree of crystallinity of the MOFs sample. There are two major factors which influence the strength of the MOFs-(a) an external factor as operating environment and (b) an internal factor which is MOF structure respectively [6].

1.1.2 In water medium

The stability of MOF is affected as it degrades in water media as response to progression series of substitution reactions, where organic linkers are replaced by water molecules or hydroxide ions (Fig. 4). In this particular way the direct substitution method to disallow this degradation and upgrade the robustness between the MOF coordinated linkers.

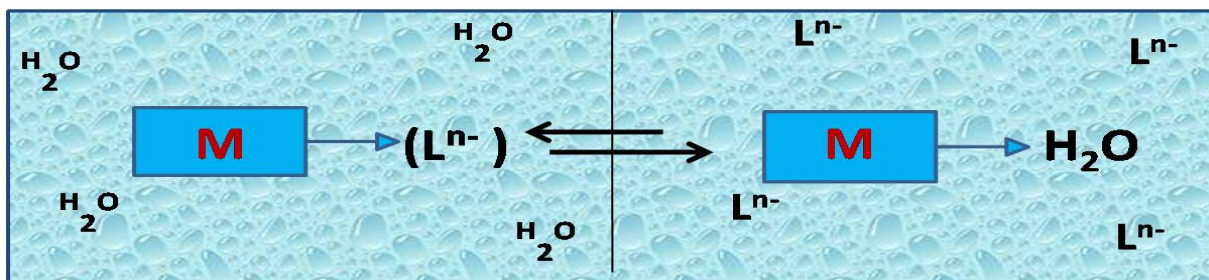


Figure 4: Proposed degradation mechanism of MOF in water.

In the light of Pearson's HSAB hypothesis to obtain most stable MOFs, researchers follow this concept to construct MOFs framework structure, with the interaction between hard Lewis bases (e.g.-carboxylate ligands) to hard Lewis acid (metal ions) or soft Lewis bases (e.g.-Azolates ligands) to soft Lewis acids. Followed by this guideline (Fig. 5) thousands of most stable nano MOFs were synthesized [6].

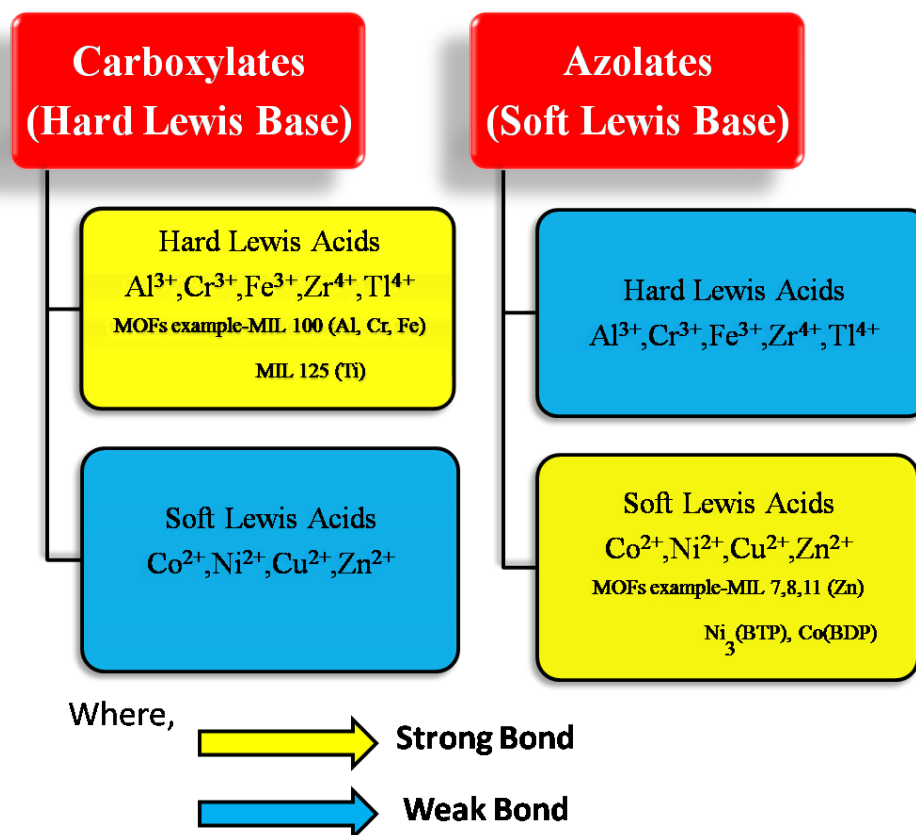


Figure 5: Rule to the manufacturing of stable MOFs as followed by HSAB hypothesis.

Moreover, the stability of MOFs is most challenging in aqua media where water molecule and hydroxide ion causes the degradation to MOFs in the form of ligands exchanging to each others. But it is clearly distinct in aqueous acid and base conditions, where an aqueous acid-base chemical condition imparts the different bond strengths between organic linkers and metals ions of the framework for instance carboxylates ligands (hard Lewis base) exhibit strong bond strength with high-valence metal ions (hard Lewis acid) in acidic solution, while weaker bonding occurs in base solutions and this same condition is reciprocal for those MOFs structure which consists azolates based ligands[8,17].

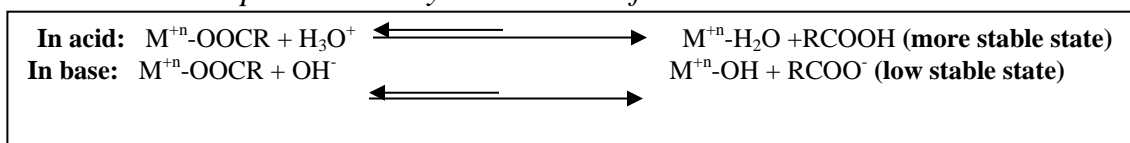
1.1.3 In acid/base condition

When nanoporous metal frameworks are used in various applications, the skeleton of nanoporous MOFs maintains structural functionalities and characteristics toward neutral aqueous media and acid/base condition. In the last few years researchers have focused on the chemical stability of nanoporous MOFs in different medium to understand the possible changes in its structure and attempting to develop high stable nanoporous MOFs buildings, but the stability of nanoporous metal-organic framework can be influenced by

multiple factors including the central metal ions nodes, organic ligands, metal-ligand bonds and geometry, hydrophobic nature of nanoporous surface, kinetic factors etc.[6].

The stability of the nanoporous MOFs completely depending upon the nature of bonding between metal ions and organic linkers, strong bonds provides higher stability. Hence, the stability of nanoporous MOFs is not limited to bond strength only, but it can be considered according to the Pearson's HSAB (hard and soft acids and bases) principle. In general, the metal-organic frameworks are formed by high valence metal clusters and carboxylate-based linkers which shows excellent stability in acidic medium, while same MOFs exhibits poor stability in the basic medium as presented in (Scheme 1) [16].

Scheme 1: Proposed stability mechanism of MOFs in Acid and Base medium.



In various applications of porous MOFs the different kind of stabilities associated with their functions individually, for example, chemical stabilities are important for hydrolytic process and thermal stabilities for gas storage and separation, water-desalination, ion exchange as well as catalytic activity. Furthermore, mechanical stability of MOFs plays an important role, when MOFs compacted and modified into pellets forms. It is also observed that the design and stability conflicts the MOFs structure, depending on the hydrous and anhydrous conditions with respect to temperature (<100°C) and (>100°C) respectively towards various applications such as hydrogen fuel cells, corrosive acidic gases separation from hydrocarbons, water treatment and in drug delivery system [3].

1.1.4 Thermal Stability

Thermal stability of MOFs described as the degradation of the bond between the metal nodes and organic linkers, when MOFs treated in the thermal atmosphere as followed by organic-linkers combustion. Consequently, thermal stability depends upon the number of organic-linkers which is bonded with each metal node in the framework structure [3]. Insight, there are important examples of most thermally stable MOFs for example-zirconium (Zr) based-MOFs are reported with increasing their connected organic linkers to zirconium metal node designed as MOF-808 (6-connected linkers), PCN-222/MOF-545 (8-connected linkers), MOF-802 (10-connected linkers) and UiO-66 among others. Usually, this stability increases with a number of organic linkers which are coordinated to each metal node of the framework (Fig. 6). In the MOFs structure, thermal spoilage can occur as MOF-graphitization, MOF-amorphization, dehydration at the metal node, and as

melting state [18-21]. During the graphitization process of organic linkers are degraded into useful residue materials. Simply, thermal stability increases with metal-ligand bond strength but at a critical point, this property disintegrates the most composition of organic linkers resultant into useful waste residue when MOF thermally treated [22].

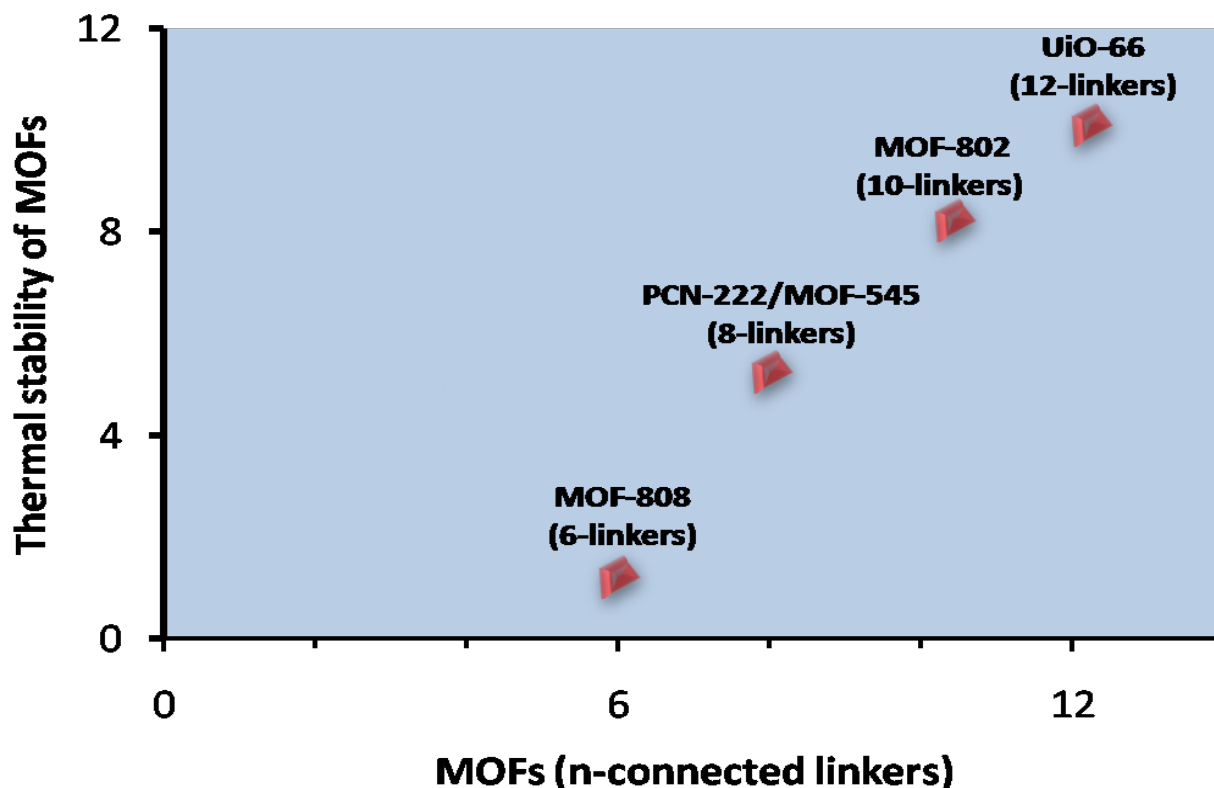


Figure 6: Proposed stability diagram for Zr-based MOFs with n-linkers.

Where, PCN=Porous coordination network, UiO=University of Oslo.

While, the dehydration occurs in MOF structures which have terminal monocarboxylate ligands or a pair of $-OH/H_2O$ groups at metal node so, this hydration resultant in the form of direct loss of water linkers via a condensation reaction between $-OH/H_2O$ groups of the framework [3-16].

1.1.5 Mechanical Stability

Nanoporous hybrid frameworks exhibit mechanical attributes either under pressure or vacuum condition towards various industrial and research applications [6]. Mostly, all MOFs possess extraordinary porosity which typically leads to decreasing its mechanical strength. Consequently, all MOFs are assumed less mechanical stable than zeolites based

MOFs due to the occurrence of the instability of its structure phases and partial collision of pores. However, MOFs blocks consist of various mechanical properties and their functioning which enhances its stability such as bulk modulus –resistance to constant compression, young modulus-resistance to linear elasticity along a particular axis of the framework [23].

According to computational studies, hafnium-based UiO-66(12-connected) MOF are reported as most mechanical stable with highest bulk and shear moduli of all MOFs structure, but not idealized (defect free) and stable as compare to MIL-140 MOF structure possess idealized framework [24]. While, based on valency concept the divalent zirconium-based MOFs have tunable stability in terms of its high coordination between metal and linkers. Conclusively, the presence of shorter ligands in MOFs blocks leads to better mechanical robustness [3,25-26]. There are various experimental techniques (table 3) used to measure the MOF mechanical properties such as nanoindentation, spectroscopic ellipsometry, high-pressure crystallography (HPC) and atomic force microscopy (AFM). These techniques are used to determine MOFs mechanical properties like Young modulus, MOFs hardness and bulk modulus [27-28].

Table 4: Useful techniques for MOFs mechanical stability determination.

S.N	Techniques	Applications
0.		
1.	Nanoindentation	Bulk modulus and Young's modulus
2.	Ellipsometry	Elastic modulus of MOF
3.	Atomic force microscopy (AFM)	Hardness, roughness and Young's modulus
4.	High-pressure X-ray crystallography (HPC)	Hydrostatic compression and bulk modulus

Usually, MOFs are considered to most mechanically stable withhold their porosity and solid phase nature under the loading process. Nanoporous MOFs has low order hardness over the dense frameworks, the low magnitude of hardness response to framework degradation under load environment[23,29].

1.2 Synthesis

Generally, nanoporous metal organic frameworks are synthesized by the coordination reaction between inorganic metal centers (vacant or labile site) and polydentate-organic

linkers, which form a well-defined structural framework. Based on the nature of the system used in chemical reaction either a single crystals framework or endless polymeric frameworks (Fig.7) are formed. The synthesized MOFs exhibit remarkable chemical and physical characteristics with respect to their molecular modifications during their fabrication process [30-31].

In general, synthesis of nanoporous framework allows a terminated chemical reaction between the inorganic unit and organic linkers to produce desired MOFs. There are various synthetic routes employed to synthesize the nanoporous frameworks, according to Stock and Biswas who provide the account of these synthetic methods including ultrasonic, microwave, electrochemical, solvothermal synthesis, sonochemical synthesis, microfluid-based synthesis and mechanochemical synthesis and many more (Fig.8).

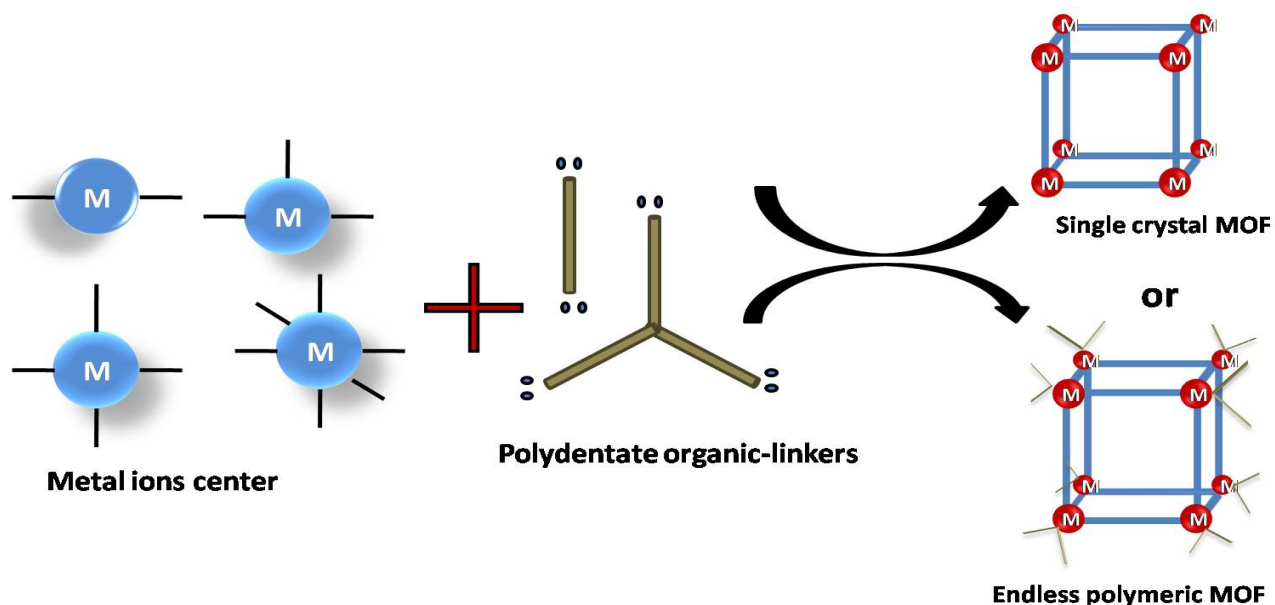


Figure 7: Proposed representation of MOFs synthesis.

While, Cohen et al provide an account of the latest method, the post-synthetic modification (PSM) which is an alternative route to modifications within the framework structure, through different functional groups on its ligands site. Other researchers Shai Yuan et al have reported modulated synthesis method to obtain a high crystalline single crystal of metal organic frameworks, which are discussed below [5-6,32].

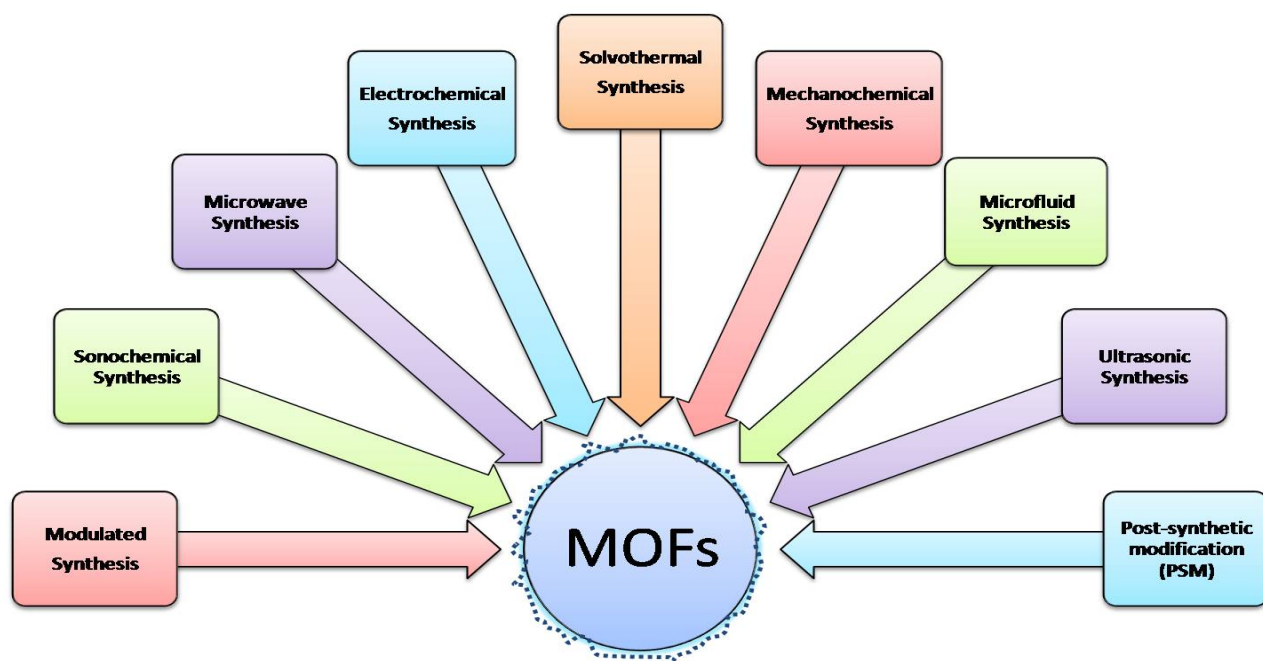


Figure 8: Different routes to synthesize nanoporous MOFs.

Hence, we highlight on two basic synthesis techniques which most followed by researchers that is “Modulated synthesis” and “Post-synthetic modification (PSM)” to obtain the desired structural metal organic frameworks.

1.2.1 Modulated synthesis

In the modulated synthesis method high crystalline MOFs are obtained. This method consist of two steps where an intermediate are formed among the initial and final step of the chemical reaction. The intermediate refer to as cluster (organic complex) formed by combination of metal ion and proposed organic linkers, these organic linkers also known as modulators. Modulated synthesis play an important role to regulate the bonding equilibrium in MOF structure by modulators in terms of complex form with metal ion or eliminate the proton of organic linkers at last step of the reaction. As a result, in modulated synthesis reaction the rate of nucleation is decreases with slow crystal formation which help to produce high crystalline (Fig. 9) MOFs structures [6].

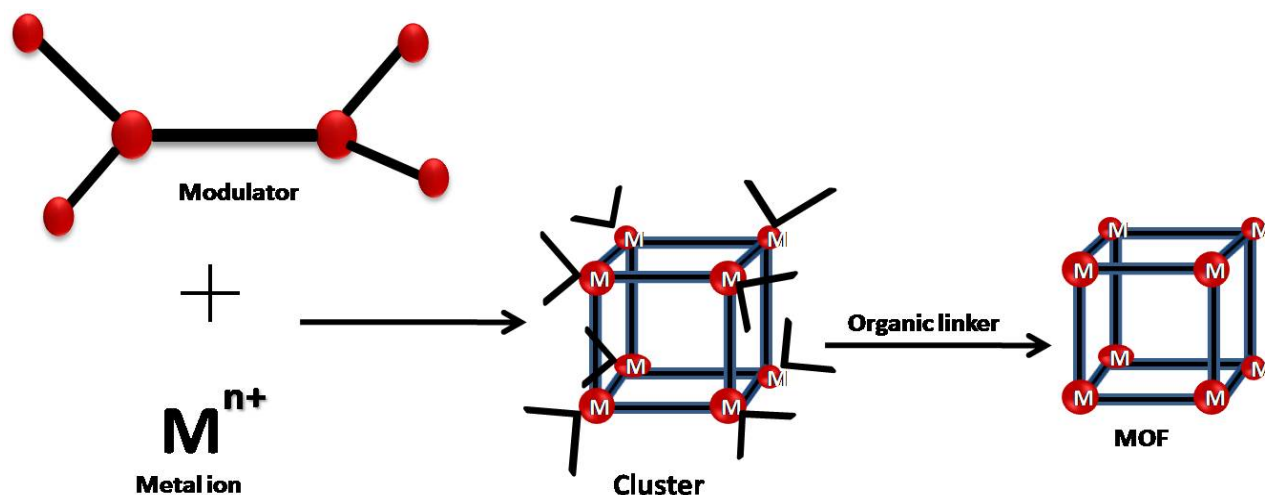


Figure 9: Schematic representation of modulated synthesis.

Indeed, various MOFs, containing divalent metal-based MOFs were synthesized by adding acids i.e. HBO_4 or HNO_3 as modulating agent to help to decrease the crystal growth and produce less predicted but desired MOF crystal structure. During, the reaction the added acids (modulating agent) function to suppress the proton of organic linkers at low pH level [33]. Therefore, the overall reaction between metal center, modulating agents and organic linkers are referred to as one-pot reaction with an intermediate step as hybrid cluster formation. For example, various metal-oxo clusters are formed by modulated synthesis and according to researcher Schaate et al. who reported first the zirconium (Zr) based MOF synthesized by this same method in 2011. While the formation of UiO-based MOFs are studied with monocarboxylic acid (modulating agent) in which the shape of MOF-crystal are variable as the amount of modulating agent is changed. Hence, in the modulated synthesis method different stable MOFs crystals are reported (scheme 2) which are produce from the intermediates of monocarboxylic acid-based clusters [34-37].

Scheme 2: Synthetic modulated stable MOFs with monocarboxylic acid linkers.

Clusters	MOFs
$[\text{Zr}_6(\mu_3\text{-OH})_4(\text{RCOO})_{12}]$	Zr-MOFs
$[\text{Fe}_3(\mu_3\text{-O})(\text{OH})(\text{H}_2\text{O})_2(\text{RCOO})_6]$	MIL-88(Fe)
$[\text{Ti}_8\text{O}_8(\text{RCOO})_{16}]$	MIL-125(Ti)

Guillerm et al. reported that in the development of zirconium based intermediate e.g.-[Zr₆(μ₃-O)₄(μ₃-OH)₄(methacrylate)₁₂] cluster to produce Zr-MOFs with UiO frameworks, which were confirmed by X-ray diffraction (XRD) analysis as a single crystal. During the reaction, the dicarboxylate linkers are added to the final product instead of methacrylate linkers which referred to as mimicing the strategic reaction route of modulated synthesis [6]. Many researchers are trying to develop this modulated synthetic route to produce different types of series of nano-MOFs for example [Fe₂M(μ₃-O)(H₂O)₃(RCOO)₆] cluster where (M = Fe²⁺, Co²⁺, Ni²⁺, Mn²⁺, Zn²⁺ etc.), and avoiding the formation of various intermediates clusters in other synthetic routes, while favoring preformed intermediate clusters to obtain the desired structural MOFs product in modulated synthesis [35].

1.2.2 Post-synthetic modification (PSM)

The first concept of post-synthetic modification (PSM) was reported in 1999 and later this term “PSM” was earn by researcher Wang and Cohen in 2007. The post-synthetic modification (PSM) method is a most attractive technique to fabricate stable MOFs structures as comparative to other existing traditional one-pot synthesis methods. The PSM route has been proven a unique tool to develop different kinds of stable MOFs structures with diverse modifications and obtain topologically analogous of MOF frameworks [6]. Post-synthetic method has attractive advantages over other available techniques due to various purpose [6,38-39]:

- Other present synthesis routes are limited to introduce diverse functionality in MOFs structure in presynthetically manner.
- Due to the presence of high porosity in MOFs structure, this modification help to functionalized various solids such as gold nanoparticles (NPs) and quantum dots (QDs) in terms of exterior and interior surface modifications.
- The PSM technique produce stable MOFs frameworks with maintain their porosity and crystallinity during modification process.

In the literature, the PSM techniques are reported with its three major classes: (i) covalent post-synthetic modification (CPSM), (ii) dative post-synthetic modification (DPSM) known as coordinate covalent modification and (iii) post-synthetic deprotection method. However, in all these modification approaches new chemical bonds are formed or split in the framework during modified operation which help to identify each of these modification classes [38,40]. In fact, the post-synthetic techniques has been a proven unique approach to prepare stable porous MOF framework with regular metal-organic linker robustness and containing unique characteristics such as high surface area and high crystallinity [38].

Covalent post-synthetic modification (CPSM) describes the modification of a component of the MOF through a modifying reagent in heterogeneous manner and forms a covalent bond between metal and linkers post-synthetically. The modifying reagent known as functional group such as alkynes, azides, amino groups and many more, usually handles as prefixed on the organic linkers of MOFs to promote the post-synthetic modification [6]. The amine-functionalized linkers, are UiO-66-NH₂ and ZnF-3,5-diamino-1,2,4-triazole (ZnF-Am₂TAZ) are the example of covalent PSM (Fig. 10). Besides these examples there are many more MOFs reported synthesized by covalent PSM for instance, MIL-53 (Al, Cr and Fe), MIL-101(Al, Cr and Fe) (see Fig.11, Fig.12) and UiO-66 [38,41-42].

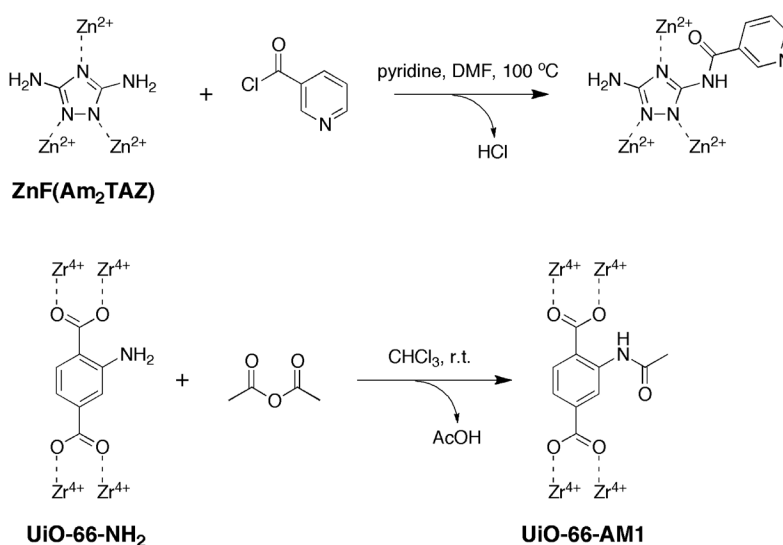


Figure 10: Covalent post-synthetic modification (PSM) of Zn-MOF and Ui-66-NH₂ copyright permission from ref. [38].

Covalent PSM has proven a tool for introducing diverse chemical functional groups over the surface of MOFs framework.

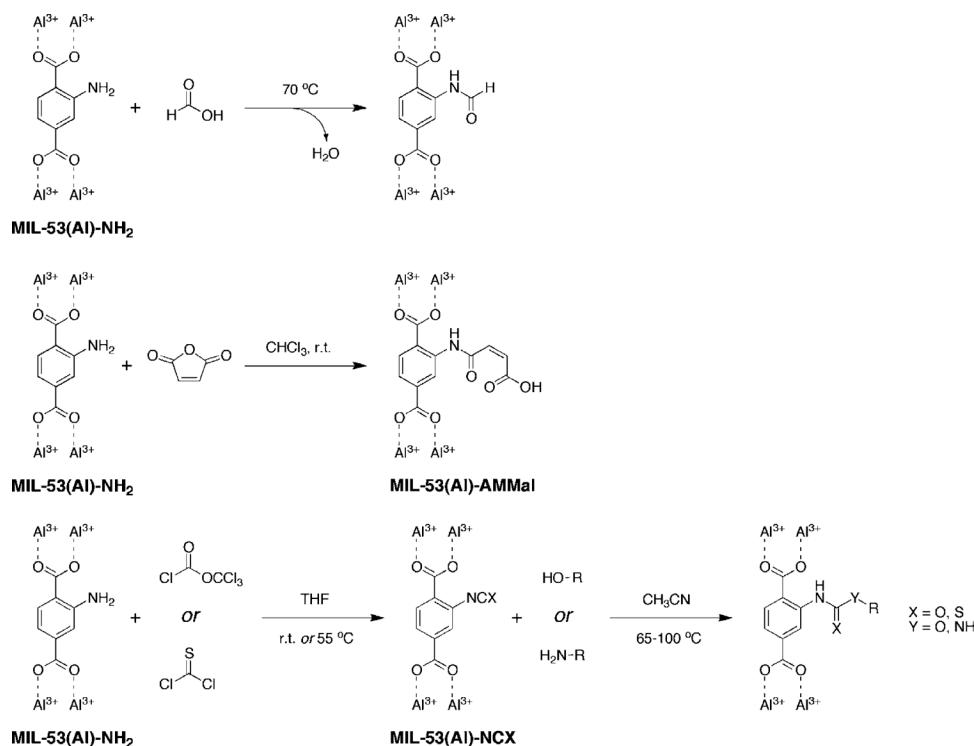


Figure 11: Covalent post-synthetic modification (PSM) of MIL-53(Al) copyright permission from ref. [38].

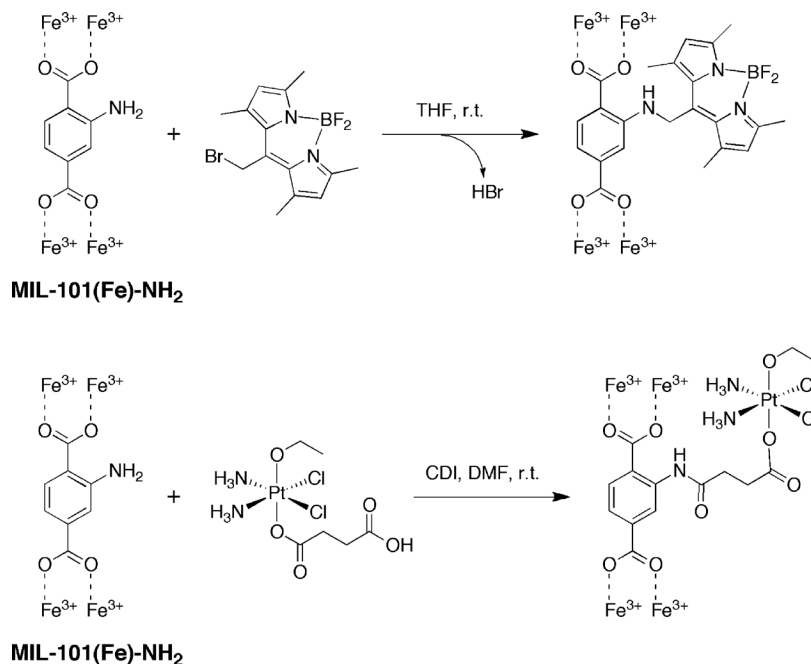


Figure 12: Covalent post-synthetic modification (PSM) of MOFs-101(Fe) reuse with permission from ref. [38].

Dative PSM define as similarly covalent PSM but there is dative or coordinate bond formed between metal and organic linkers. In this modification MOFs are functionalized where the linkers are metalated post-synthetically with soft metals ions such as Cu^{2+} , Pd^{2+} among others. For example, the MIL-101(Cr, Fe) are functionalized via pyridine groups to develop the $[\text{M}_3 (\mu_3\text{-O})(\text{COO})_6]$ ($\text{M}=\text{Cr}^{3+}$ or Fe^{3+}) MOF frameworks and play an important role towards catalytic activity. Indeed, there are various examples of the dative modifications which are used in different respective fields [6,38].

At last, the the post-synthetic deprotection (PSD) referred to as the chemical bonds (e.g., dative or covalent bonds) are split post-synthetically in MOF frameworks. In terms of bond splitting of MOF during the PSD reaction, which define as the introduction of chemical functionality in MOF block and build up stable MOF frameworks with different characteristics. Usually, it has been reported that the PSD technique is a less explored approach for functionalizing the MOFs as compared to covalent-PSM and dative modifications [38].

1.3 Applications of MOFs

1.3.1 Gas separations and storage

Many metal organic-frameworks exhibit a significant feasibility towards gas separation and gas storage via adsorption, distillation, extraction and membrane separations and other processes, for chemical industry and research applications [43], [44]. The separation processes of gas mixtures are depend upon adsorption capacities of different MOFs and their molecular pores size. In the light of environmental concerns the researchers have reported the selective adsorption and separation for light gases such as hydrogen (H_2), nitrogen (N_2), oxygen (O_2), carbon dioxide (CO_2) and methane (CH_4). In fact, the adsorption behavior of MOFs for light gases has to be determine through gas chromatography (GC) or other separation trending techniques such as selective adsorption isotherms [43]. There are various MOFs and their respective polymeric membranes have been reported, which are performed to separate different gases (Table 5) with respect to different parameters such as MOFs operating condition, gas selectivity and permeability [44].

Energy storage is another important application of MOFs frameworks, which is demonstrated as the energy storage adsorbed by the MOFs, which depends upon the porosity of the framework or volume of the pores in terms of volumetric gas storage. Although, some frameworks possess high surface area it does not translate to high efficient with high volumetric gas storage due to the presence of low densities pores of the MOFs. While, a perfect porous MOF for high gas storage applications need to exhibit

unique properties such as high densities of pores, and balanced internal pores functions as well [45,46].

Table 5: Role of different MOFs in gas separation copyright from ref. [44].

MOF/polymer	MOF loading	Permeability	Selectivity	Test conditions
MIL-53(Al)-NH ₂ /copolyimide ¹⁵³	10-15 wt. %	CO ₂ , 57-137	H ₂ /CH ₄ , 34.7 CO ₂ /CH ₄ , 35.8	35 °C, 3 bar
MIL-101(Al)-NH ₂ /copolyimide ¹⁵³	5-10 wt. %	CO ₂ , 53-151	H ₂ /CH ₄ , 67.3 CO ₂ /CH ₄ , 42.2	35 °C, 3 bar
ZIF-7/Pebax ¹⁵⁴	8-34 wt. %	CO ₂ , 41-145	CO ₂ /CH ₄ , 44 CO ₂ /N ₂ , 105	25 °C, 3.75 bar
Cu-bipy/PSF ¹⁵⁵	0-5 wt. %		H ₂ /CH ₄ , ~200 CH ₄ /N ₂ , ~10	35 °C, 1 bar
MIL-53(Al)-NH ₂ /PSF ¹⁵⁶	8-40 wt. %	CO ₂ , 5	CO ₂ /CH ₄ , ~25	35 °C, 3 bar
MIL-101/PSF ¹⁵⁷	0-24 wt. %	O ₂ , 6	O ₂ /N ₂ , 5-6	30 °C, 3 bar
HKUST-1/PSF ¹⁵⁸			H ₂ /CO ₂ , 7.2	25 °C, 2.75 bar

In terms of high efficiency and high volumetric gas storage there are well promising and high efficient MOFs reported for high volumetric gas storage for instance, a copper coordinated framework encoded as HKUST-1 with high surface area (1850 m² g⁻¹) reported by Chui et al., used for high volume storage for methane gas (CH₄) with methane storage capacity of 267 cm³ at room temperature and 65 bar pressure [47]. Whereas, researcher Hupp et al. has developed a balanced and high efficient porous (3,24-connected)-MOF NUI-111 with surface area (4930 m²/g) used for carbon dioxide (CO₂) storage at room temperature and 30 bar pressure [48]. At last, the highest

Hydrogen (H₂) storage capacity (176 mg/g) was reported for NU-100 MOF at low temperature 77 K and 56 bar pressure [44].

1.3.2 Catalysis

The application of metal organic-frameworks (MOFs) and their composites have promised and emerged as novel material in catalysis in different catalysis types (Fig.13) such as Lewis acid catalysis, Bronsted acid catalysis, Redox catalysis and Photocatalysis [6,44].

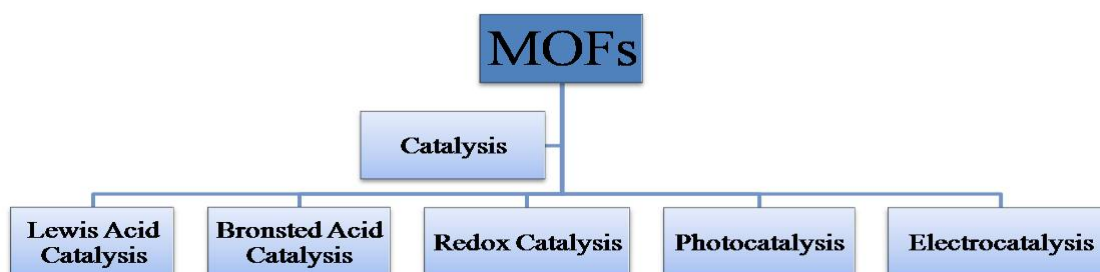


Figure 13: Role of MOFs in different types of catalysis reactions.

1.3.2.1 Lewis acid catalysis

In MOF structure the unsaturated metal centre have been found as Lewis acidic sites and act as catalyst. For solution phase catalysis, the acidic metal site interact with substrate and is able to replace the substrate molecule instead of solvent molecules. While, in gas state the catalytic activity proceed by heating or evacuation of the metal site to eliminate the bound solvent molecules. Studies have revealed that the most stable high-valence MOFs metal node provide essential Lewis acidic sites and catalyze a different kind of chemical reactions, such as α -pinene oxide isomerization, cyanosilylation of aldehydes, cycloaddition of CO₂ and epoxides, Friedel-Crafts reaction and Hetro-Diels-Alder reaction [49-52]. Some examples of stable MOFs for Lewis acid catalysis have been reported such as Fe³⁺-based MIL-(53,88,100 and 101), MIL-101(Cr), Zr-based UiO-66 i.e.- [Zr₆(μ_3 -O)₄(μ_3 -OH)₄(COO)₁₂], dimethyl 4-nitrophenyl phosphate (DMNP) based [Zr₆(μ_3 -O)₄(μ_3 -OH)₄(OH)₄(H₂O)₄(COO)₈] and many others are used for respective kind of chemical reactions [6].

1.3.2.2 Bronsted acid catalysis

The MOFs can be stimulated for catalytic reactions, with the addition of Bronsted acid for interior functionalization of MOF where it acts as catalyst. The porous frameworks with Bronsted acids have been examined for many different chemical reactions such as acetalization, Diels-Alder reaction, Friedel-Craft reaction and dehydration [53-56]. Bronsted acid can be introduced into MOF through the covalent interaction of Bronsted acid group to organic linkers of the framework. There are various examples of this kind of catalysis in which most efficient example reported as MIL-53,101(Cr) functionalized with sulfonic acid, which shows the high catalytic significance towards esterification of hydrocarbons i.e. n-butanol, and these MOF has turnover frequency (TOF) about 0.72 per minute [55].

1.3.2.3 Redox Catalysis

In this sort of catalysis the functionalized organic linkers i.e. metallo-linkers of the MOF act as catalyst and response to redox catalytic activity. For example UiO-66 framework functionalized with 3d-metals such as molybdenum (Mo), tungsten (W) and vanadium (V) for epoxidation of unsaturated hydrocarbons. Another example is metallation of Zr-MOFs with $[\text{Ir}(\text{COD})(\text{OMe})_2]$ (COD=1,5-cyclooctadiene), which act as catalyst for many organic reactions including silylation of aryl aldehydes and ketones, dehydrocoupling of amines and borylation of aryls C-H bonds [6].

1.3.2.4 Photocatalysis

Photocatalysis is the process in which solar energy directly convert into valuable chemical energy [57]. Metal organic-frameworks (MOFs) irradiated by visible light act photoresponsive towards various catalytic reactions. Amine functionalized titanium (Ti) based MOF i.e. MIL-125-NH₂ work as photoactive for carbon dioxide reduction and hydrogen gas production [58-59]. Gracia and co-workers first studied the water soluble photocatalyst UiO-66-NH₂ response to hydrogen generation in mixture of H₂O and CH₃OH when it irradiated at 300 nm wavelength. In the structure of MOF UiO-66-NH₂ the presence of amide group responsible for visible light absorption at 300 nm due to the bathochromic and auxochromic shift. In fact, the UiO-66-NH₂ MOF shows the better photocatalytic activity than non-functionalized UiO-66 framework towards carbon dioxide reduction and aerobic oxidation [60].

Another promising example is Chi et al. developed iron based MOF i.e. MIL-101 (Fe) and its amines derivatives which shows the excellent photocatalytic activity under visible light in various applications for instance oxygen evolution from water, removal of heavy metals from water, hydrogen evolution from water and many more [61].

1.3.2.5 Electrocatalysis

Electrocatalysis is the limited widespread application for the MOFs solid materials. Although, in research trending only Pt-based catalyst are employed as better electrocatalyst in energy devices due to its exclusive cost and low quantity. Metal organic-framework (MOFs) has been proven to be a better electrocatalyst for many electrochemical reactions due its adaptable nature. Molybdenum based MOF such as MoS_2 , Mo_2C employed as electrocatalyst in hydrogen evolution reaction because of its excellent stability in acidic medium. Another example was reported by Zhang et al. who introduced an alkaline stable electrocatalyst i.e. $[\text{Co}_2(\mu\text{-OH})_2(\text{BBTA})]$ BBTA= benzo bistriazole, for oxygen evolution from water [6,62].

1.3.3 Water treatment

There is limited literature evaluated on nano-MOFs for water treatment. The nano-porous MOF solid materials have been found as promising better solution for water treatment problems than other conventional porous materials such as zeolites, some polymer nanocomposites and charcoal. MOFs employed as better candidate for water treatment, due to its unique properties such as crystalline nature, permanent porosity, flexible structure, band-gap, and chemical-thermal stability [63,64]. MOFs work for water treatment followed by three major mechanism such as adsorption, photocatalytic degradation and via hydrogen generation from water [65]. Cu-based MOF i.e. HKUST-1 has been reported for removal of toxic sulfonamide antibiotics from waste water through adsorption mechanism, with adsorption capacity $384 \text{ mg}\cdot\text{g}^{-1}$ at room temperature [66]. Moreover, graphene oxide based MIL-68(In)- NH_2 (In-MOF/GO) reported for the degradation of rhodamine-B (RhB) dye from wastewater via adsorption process [67].

In another report the cobalt based MOF series for example- $[\text{Co}(\text{DPA})(\text{TPMP})]_n$, $\{[\text{Co}(\text{TPA})_{0.5}(\text{TPMP})_{0.5}]_n \cdot \text{H}_2\text{O}\}_n$, $[\text{Co}(\text{OBA})_{0.5}(\text{TPMP})]_n$, $[\text{Co}(\text{FBA})(\text{TPMP})]_n$, and where DPA = dipehnic acid, OBA = 4,40-oxybis(benzoicacid), FBA = 4,40 (hexafluoro-isopropylidene) bis(benzoic acid), and TPA = terephthalic acid, these Co-MOFs series play an important role in photocatalytic degradation of the contaminated organic dyes from wastewater [68].

In water desalination the MOFs exhibit tunable properties such as its hydrophobic pores, framework flexibility and nanoporous sieving nature, which allow them to be in membrane form for filtration of desalinated ions. In an investigation ZIF-8 membrane allow to remove salted ions e.g. Na^+ and Cl^- ions from water, due to its molecular sieving nature. Another example is MOF MIL-100,101(Fe) used to remove malachite green and methyl orange dyes from water, due to its high adsorption properties [69]. There are

many other examples of MOFs available for wastewater treatment but we reported only high efficient MOFs for important applications as earlier discussed.

1.4 Other applications

There are many others important applications reported of the porous metal organic frameworks (MOFs) for example, in sensor devices, supercapacitors, biomedical applications, batteries fabrications and many others.

1.4.1 Sensors

The sensing application of MOFs materials extended to detect the gases, explosives, liquids and small molecules. The key factor of MOF which makes it sensitive is high volume pore surface area and lower limit of detection of the MOF material. Others, factors which are responsible for its sensitivity are: variation in bond distance between metal centre and organic ligands of the framework and analyte interaction with the metal centre of the MOF. Lanthanides and transition metal based examples of MOFs which have been used for metal ion sensing are reported as- $\text{Eu}_2(\text{FMA})_2(\text{OX})(\text{H}_2\text{O})_4 \cdot 3.4\text{H}_2\text{O}$ (FMA = fumarate and Ox = oxalate), $[\text{Eu}(\text{PDA})_3\text{Mn}_{1.5}(\text{H}_2\text{O})_3] \cdot 3.5\text{H}_2\text{O}$ and $[\text{Tb}(\text{PDA})_3\text{Mn}_{1.5}(\text{H}_2\text{O})_3] \cdot 3.5\text{H}_2\text{O}$ (PDA = pyridine-2,6-dicarboxylic acid)[70].

1.4.2 Supercapacitors

Supercapacitors are those devices which store charges through adsorption of electrolyte ions on its electrode surface. The porous-MOFs works as supercapacitors on electron adsorption-desorption mechanism. Researcher Liu et al. reported an MOF composite [PFA/MOF-5] (PFA=paraformaldehyde) which shows a capacitance 258 farad per gram in sulfuric acid electrolyte at 0.25 ampere per gram current density. Another high capacitance example of nanoporous ZIF-8 reported with 214 farad per gram at 5 milivolt per second in presence of half (0.5) molar sulfuric acid as electrolyte [71].

1.4.3 Biomedical applications

Nanoporous MOFs also exhibits the promising role in biological applications including (Fig. 14) cancer therapy, drug delivery, biosensors, biomedical imaging etc. [5,6]. Nanoporous MOFs are most important materials useful in different cancers therapy, for example iron based MOFs (Fe_3O_4 -UiO-66) applied to delivering of anticancer agent in the human body [72]. Another example of nano-MOFs, which are useful for cancer treatment is magnesium based MOFs with silica coating i.e., $\text{Mn}_3(\text{BTC})_2(\text{H}_2\text{O})_6$ and $\text{Mn}(1,4\text{-BDC})(\text{H}_2\text{O})_2$ [73].

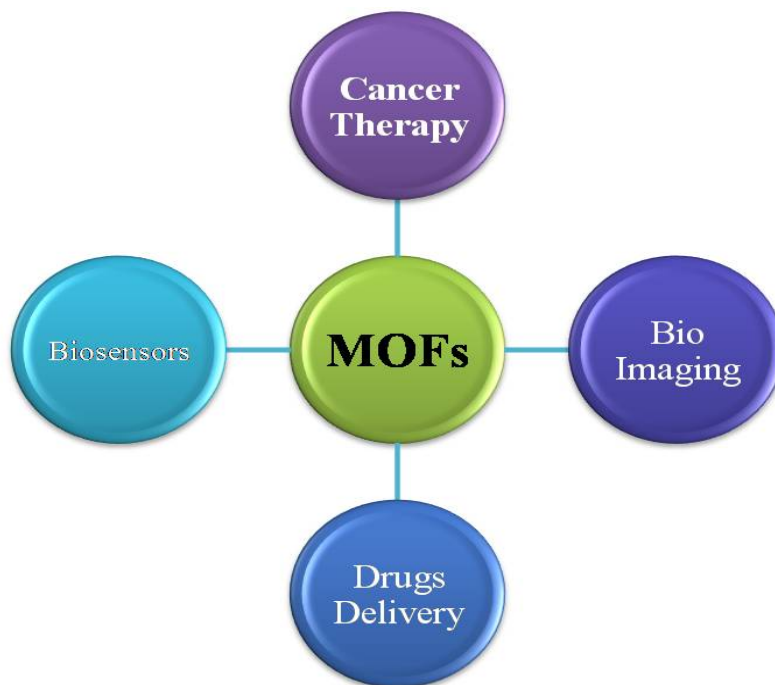


Figure16: An overview of MOFs applications in biomedical field.

In drug delivery system MOFs plays a significant role as drug delivery device to release the loaded drug to desired site, MOFs are able to load the drug due to their voids surface area. Iron based MOFs are helpful in drug delivery for instance BioMIL-1(Fe) helpful for higher loading of nicotine and HUKUST-1 MOFs useful to release the metronidazole drugs [74]. While, nanoporous MOFs $\text{Gd}(\text{BTC})(\text{H}_2\text{O})_3$ and $\text{Mn}_3(\text{BTC})_2(\text{H}_2\text{O})_6$ are useful in magnetic resonance imaging (MRI) technique, where MRI technique is useful for diagnose to diverse diseases in imaging sense [5].

Conclusion

In this chapter, we have tried to emphasize fundamental stabilities, synthesis, and applications of nanoporous metal-organic frameworks (MOFs). It has to be found that the desired stable nanoporous frameworks could be designed and synthesize through selecting the three main parameters, first by selecting an organic ligand with high ligancy power, secondly, is select a high valence metal ions and finally, framework satisfy the hard soft acid base (HSAB) hypothesis. Another parameter is the functionalization of organic ligands with suitable reagents which is also responsible for MOFs stability, towards in different working medium. For the fabrication of stable porous MOFs, there are usually, two techniques being adopted one is the post-synthetic method (PSM) and another is the modulated synthesis. Most of the studied porous MOFs are well

recognized for their different topologies for instance zirconium based MOFs, UiO-66, ZIFs, and MIL-100,101(Fe) and others. Usually, the nanoporous MOFs exhibits the most important properties such as high pores density surface area, crystalline nature, chemical, thermal and mechanical stabilities. Because of these unique properties, nanoporous MOFs have been utilized in diverse field such as gas separation, gas storage, catalysis, water treatment and for biological importance.

Finally, one point that needs to be addressed in brief is the stability of porous MOFs for a longer time under different conditions i.e. thermal, mechanical, the organic linkers of the framework tends to degrade as its self-degradation that would be the weakest factor for its commercial applications. We predict that in the next decade we will witness a rapid development of these nanoporous MOFs that might eventually end up with their multifunctional features and its diverse commercial applications, and that will undoubtedly contribute to a better understanding of the confined topic.

References

- [1] J. Ma *et al.*, “Bio-inspired method to fabricate poly-dopamine/reduced graphene oxide composite membranes for dyes and heavy metal ion removal,” *Polym. Adv. Technol.*, no. October 2017, pp. 941–950, 2017. <https://doi.org/10.1002/pat.4205>
- [2] N. Z. Logar and V. Kaučič, “From Catalysis and Hydrogen Storage to Wastewater Treatment [ceoliti netiro ūdēnu atīrīšani .pdf,” pp. 117–135, 2006.
- [3] A. J. Howarth *et al.*, “Chemical, thermal and mechanical stabilities of metal-organic frameworks,” *Nat. Rev. Mater.*, vol. 1, no. 15018, pp. 1–15, 2016. <https://doi.org/10.1038/natrevmats.2015.18>
- [4] H. Q. Hao, Z. J. Lin, S. Hu, W. T. Liu, Y. Z. Zheng, and M. L. Tong, “Nanoporous metal-organic framework comprising of 1D cobalt oxalate chains and flexible ligands exhibiting both dynamic gas adsorption and antiferromagnetic chain behaviours,” *CrystEngComm*, vol. 12, no. 7, pp. 2225–2231, 2010. <https://doi.org/10.1039/b927200c>
- [5] S. Beg *et al.*, “Nanoporous metal organic frameworks as hybrid polymer–metal composites for drug delivery and biomedical applications,” *Drug Discov. Today*, vol. 22, no. 4, pp. 625–637, 2017. <https://doi.org/10.1016/j.drudis.2016.10.001>
- [6] S. Yuan *et al.*, “Stable Metal–Organic Frameworks: Design, Synthesis, and Applications,” *Adv. Mater.*, vol. 30, no. 37, pp. 1–35, 2018. <https://doi.org/10.1002/adma.201870277>

- [7] M. Moliner *et al.*, “A New aluminosilicate molecular sieve with a system of pores between those of ZSM-5 and beta zeolite,” *J. Am. Chem. Soc.*, vol. 133, no. 24, pp. 9497–9505, 2011. <https://doi.org/10.1021/ja2015394>
- [8] K. S. Park *et al.*, “ZIFs - first synthesis,” *Proc. Natl. Acad. Sci.*, vol. 103, no. 27, pp. 10186–10191, 2006.
- [9] X. C. Huang, Y. Y. Lin, J. P. Zhang, and X. M. Chen, “Ligand-directed strategy for zeolite-type metal-organic frameworks: Zinc(II) imidazoles with unusual zeolitic topologies,” *Angew. Chemie - Int. Ed.*, vol. 45, no. 10, pp. 1557–1559, 2006. <https://doi.org/10.1002/anie.200503778>
- [10] F. Wikipedia, Repeated measures design Practice effects. 2007.
- [11] M. E. Davis and R. F. Lobo, “Zeolite and Molecular Sieve Synthesis,” *Chem. Mater.*, vol. 4, no. 4, pp. 756–768, 1992. <https://doi.org/10.1021/cm00022a005>
- [12] N. Stock, “Metal-Organic Frameworks: Aluminium-Based Frameworks,” *Encycl. Inorg. Bioinorg. Chem.*, no. iv, pp. 1–16, 2014. <https://doi.org/10.1002/9781119951438.eibc2197>
- [13] C. Soc, T. Devic, and C. Serre, “Chem Soc Rev,” pp. 6097–6115, 2014. <https://doi.org/10.1039/C4CS00081A>
- [14] H. Furukawa, K. E. Cordova, M. O. Keeffe, and O. M. Yaghi, “The Chemistry and Applications of Metal-Organic Frameworks The Chemistry and Applications of,” vol. 341, no. August, 2013. <https://doi.org/10.1126/science.1230444>
- [15] N. C. Burtch, J. Heinen, T. D. Bennett, D. Dubbeldam, and M. D. Allendorf, “Mechanical Properties in Metal – Organic Frameworks : Emerging Opportunities and Challenges for Device Functionality and Technological Applications,” vol. 1704124, pp. 1–18, 2018. <https://doi.org/10.1002/adma.201704124>
- [16] S. Yuan, J. S. Qin, C. T. Lollar, and H. C. Zhou, “Stable Metal-Organic Frameworks with Group 4 Metals: Current Status and Trends,” *ACS Cent. Sci.*, vol. 4, no. 4, pp. 440–450, 2018. <https://doi.org/10.1021/acscentsci.8b00073>
- [17] C. Serre *et al.*, “Very large breathing effect in the first nanoporous chromium(III)-based solids: MIL-53 or CrIII(OH)·{O2C-C6H4- CO2}·{HO2C-C6H4 - CO2H}x·H2Oy,” *J. Am. Chem. Soc.*, vol. 124, no. 45, pp. 13519–13526, 2002. <https://doi.org/10.1021/ja0276974>
- [18] D. Umeyama, S. Horike, M. Inukai, T. Itakura, and S. Kitagawa, “Reversible solid-to-liquid phase transition of coordination polymer crystals,” *J. Am. Chem. Soc.*, vol. 137, no. 2, pp. 864–870, 2015. <https://doi.org/10.1021/ja511019u>

- [19] Y. I. Fujiwara *et al.*, “Control of pore distribution of porous carbons derived from Mg²⁺ porous coordination polymers,” *Inorg. Chem. Front.*, vol. 2, no. 5, pp. 473–476, 2015. <https://doi.org/10.1039/C5QI00019J>
- [20] T. D. Bennett *et al.*, “Structure and properties of an amorphous metal-organic framework,” *Phys. Rev. Lett.*, vol. 104, no. 11, pp. 2–5, 2010. <https://doi.org/10.1103/PhysRevLett.104.115503>
- [21] J. K. Sun and Q. Xu, “Functional materials derived from open framework templates/precursors: Synthesis and applications,” *Energy Environ. Sci.*, vol. 7, no. 7, pp. 2071–2100, 2014. <https://doi.org/10.1039/c4ee00517a>
- [22] T. A. Makal, X. Wang, and H. C. Zhou, “Tuning the moisture and thermal stability of metal-organic frameworks through incorporation of pendant hydrophobic groups,” *Cryst. Growth Des.*, vol. 13, no. 11, pp. 4760–4768, 2013. <https://doi.org/10.1021/cg4009224>
- [23] H. Wu, T. Yildirim, and W. Zhou, “Exceptional mechanical stability of highly porous zirconium metal-organic framework UiO-66 and its important implications,” *J. Phys. Chem. Lett.*, vol. 4, no. 6, pp. 925–930, 2013. <https://doi.org/10.1021/jz4002345>
- [24] V. Guillerm *et al.*, “A series of isorecticular, highly stable, porous zirconium oxide based metal-organic frameworks,” *Angew. Chemie - Int. Ed.*, vol. 51, no. 37, pp. 9267–9271, 2012. <https://doi.org/10.1002/anie.201204806>
- [25] J. C. Tan, T. D. Bennett, and A. K. Cheetham, “Chemical structure, network topology, and porosity effects on the mechanical properties of Zeolitic Imidazolate Frameworks,” *Proc. Natl. Acad. Sci.*, vol. 107, no. 22, pp. 9938–9943, 2010. <https://doi.org/10.1073/pnas.1003205107>
- [26] A. Kuc, A. Enyashin, and G. Seifert, “Metal-organic frameworks: Structural, energetic, electronic, and mechanical properties,” *J. Phys. Chem. B*, vol. 111, no. 28, pp. 8179–8186, 2007. <https://doi.org/10.1021/jp072085x>
- [27] N. C. Burtch, J. Heinen, T. D. Bennett, D. Dubbeldam, and M. D. Allendorf, “Mechanical Properties in Metal–Organic Frameworks: Emerging Opportunities and Challenges for Device Functionality and Technological Applications,” *Adv. Mater.*, vol. 30, no. 37, pp. 1–18, 2018. <https://doi.org/10.1002/adma.201704124>
- [28] J. C. Tan and A. K. Cheetham, “Mechanical properties of hybrid inorganic-organic framework materials: Establishing fundamental structure-property relationships,” *Chem. Soc. Rev.*, vol. 40, no. 2, pp. 1059–1080, 2011. <https://doi.org/10.1039/c0cs00163e>

- [29] J. J. Low, P. Jakubczak, J. F. Abrahamian, S. A. Faheem, and R. R. Willis, "Virtual High Throughput Screening Confirmed Experimentally : Porous Coordination Polymer Hydration," no. 5, pp. 15834–15842, 2009. <https://doi.org/10.1021/ja9061344>
- [30] S. L. James, "Metal-organic frameworks," pp. 276–288, 2003. <https://doi.org/10.1039/b200393g>
- [31] J. Lei, R. Qian, P. Ling, L. Cui, and H. Ju, "Trends in Analytical Chemistry Design and sensing applications of metal – organic framework composites," *Trends Anal. Chem.*, vol. 58, pp. 71–78, 2014. <https://doi.org/10.1016/j.trac.2014.02.012>
- [32] C. Reviews, "Introduction to Metal – Organic Frameworks," pp. 673–674, 2012. <https://doi.org/10.1021/cr300014x>
- [33] C. V McGuire and R. S. Forgan, "The surface chemistry of metal – organic frameworks," pp. 5199–5217, 2015. <https://doi.org/10.1039/C4CC04458D>
- [34] T. Devic and C. Serre, "High valence 3p and transition metal based MOFs," *Chem. Soc. Rev.*, vol. 43, no. 16, pp. 6097–6115, 2014. <https://doi.org/10.1039/C4CS00081A>
- [35] D. Feng *et al.*, "metal – organic frameworks," pp. 1–8, 2014.
- [36] A. Schaate *et al.*, "Modulated Synthesis of Zr-Based Metal – Organic Frameworks : From Nano to Single Crystals," pp. 6643–6651, 2011. <https://doi.org/10.1002/chem.201003211>
- [37] C. Sanchez, K. J. Shea, S. Kitagawa, and L. Rozes, "Hybrid materials themed issue," no. 2, 2011.
- [38] S. M. Cohen, "Postsynthetic Methods for the Functionalization of Metal À Organic Frameworks," pp. 970–1000, 2012. <https://doi.org/10.1021/cr200179u>
- [39] R. Soc, "Surface modification , functionalization and bioconjugation of colloidal inorganic nanoparticles," pp. 1333–1383, 2010. <https://doi.org/10.1098/rsta.2009.0273>
- [40] C. Sanchez, K. J. Shea, S. Kitagawa, K. K. Tanabe, and S. M. Cohen, "Hybrid materials themed issue," no. 2, 2011.
- [41] S. Bauer, C. Serre, T. Devic, P. Horcajada, and N. Stock, "High-Throughput Assisted Rationalization of the Formation of Metal Organic Frameworks in the Iron (III) Aminoterephthalate Solvothermal System ´ rard Fe," vol. 47, no. 17, pp. 7568–7576, 2008. <https://doi.org/10.1021/ic800538r>
- [42] S. Couck, J. F. M. Denayer, G. V Baron, T. Re, and J. Gascon, "An Amine-Functionalized MIL-53 Metal - Organic Framework with Large Separation Power for CO 2 and CH 4," vol. 53, pp. 6326–6327, 2009. <https://doi.org/10.1021/ja900555r>

- [43] J. Li, J. Sculley, and H. Zhou, “Metal À Organic Frameworks for Separations,” pp. 869–932, 2012. <https://doi.org/10.1021/cr200190s>
- [44] S. Li and F. Huo, “Metal-organic framework composites: From fundamentals to applications,” *Nanoscale*, vol. 7, no. 17, pp. 7482–7501, 2015. <https://doi.org/10.1039/C5NR00518C>
- [45] O. Frameworks, “HHS Public Access,” vol. 134, no. 10, pp. 4517–4520, 2015.
- [46] A. Manuscript, “Energy & Environmental Science,” no. 207890, 2020.
- [47] B. Li, H. Wen, W. Zhou, and B. Chen, “Porous Metal – Organic Frameworks for Gas Storage and Separation: What, How, and Why?,” 2014. https://doi.org/10.1007/430_2014_159
- [48] C. H. Hendon, A. J. Rieth, M. D. Korzyn, and M. Dinca, “Grand Challenges and Future Opportunities for Metal – Organic Frameworks,” 2017. <https://doi.org/10.1021/acscentsci.7b00197>
- [49] P. Horcajada *et al.*, “Synthesis and catalytic properties of MIL-100 (Fe), an iron (III) carboxylate with large pores { ,,” vol. 100, pp. 2820–2822, 2007. <https://doi.org/10.1039/B704325B>
- [50] C. Sci *et al.*, “Catalysis Science & Technology Iron (III) metal – organic frameworks as solid Lewis acids for the isomerization of a -pinene oxide,” vol. 3, pp. 324–330, 2012. <https://doi.org/10.1039/C2CY00376G>
- [51] T. Liu, D. Feng, Y. Chen, L. Zou, M. Bosch, and S. Yuan, “Topology-Guided Design and Syntheses of Highly Stable Mesoporous Porphyrinic Zirconium Metal – Organic Frameworks with High Surface Area,” 2014. <https://doi.org/10.1021/ja5111317>
- [52] A. Henschel, K. Gedrich, and S. Kaskel, “Catalytic properties of MIL-101 w,” pp. 4192–4194, 2008. <https://doi.org/10.1039/b718371b>
- [53] A. Herbst, A. Khutia, and C. Janiak, “Brønsted Instead of Lewis Acidity in Functionalized MIL-101Cr MOFs for E ffi cient Heterogeneous (nano-MOF) Catalysis in the Condensation Reaction of Aldehydes with Alcohols,” vol. 3, 2014. <https://doi.org/10.1021/ic5006456>
- [54] Y. Zhang, K. Na, and O. M. Yaghi, “Superacidity in Sulfated Metal – Organic Framework-808,” 2014.
- [55] J. M. Chem *et al.*, “chemistry by active site engineering †,” pp. 10313–10321, 2012.

- [56] C. M. McGuirk *et al.*, “Turning On Catalysis: Incorporation of a Hydrogen-Bond-Donating Squaramide Moiety into a Zr Metal – Organic Framework,” 2014.
<https://doi.org/10.1021/ja511403t>
- [57] H. Li, Y. Yang, C. He, L. Zeng, and C. Duan, “Mixed-Ligand Metal–Organic Framework for Two-Photon Responsive Photocatalytic C–N and C–C Coupling Reactions,” *ACS Catal.*, vol. 9, pp. 422–430, 2018.
<https://doi.org/10.1021/acscatal.8b03537>
- [58] Y. Fu, D. Sun, Y. Chen, R. Huang, Z. Ding, and X. Fu, “Angewandte An Amine-Functionalized Titanium Metal – Organic Framework Photocatalyst with Visible-Light-Induced Activity for CO₂ Reduction **,” vol. 125, no. Figure 1, pp. 3364–3367, 2012. <https://doi.org/10.1002/anie.201108357>
- [59] Y. Horiuchi *et al.*, “Visible-Light-Promoted Photocatalytic Hydrogen Production by Using an Amino-Functionalized Ti (IV) Metal – Organic Framework,” no. Iv, 2012. <https://doi.org/10.1021/jp3046005>
- [60] C. Lollar, “platform for catalysis and biomimetics,” pp. 4231–4249, 2018.
- [61] C. G. Silva, I. Luz, F. X. Llabrós, and A. Corma, “Water Stable Zr – Benzenedicarboxylate Metal – Organic Frameworks as Photocatalysts for Hydrogen Generation,” pp. 11133–11138, 2010. <https://doi.org/10.1002/chem.200903526>
- [62] X. Lu *et al.*, “An Alkaline-Stable, Metal Hydroxide Mimicking Metal – Organic Framework for Efficient Electrocatalytic Oxygen Evolution,” 2016.
<https://doi.org/10.1021/jacs.6b03125>
- [63] P. Kumar, K. Kim, E. Kwon, and J. E. Szulejko, “management of air quality : advances and future,” pp. 345–361, 2016. <https://doi.org/10.1039/C5TA07068F>
- [64] P. Kumar, A. Pournara, K. Kim, V. Bansal, S. Rapti, and M. J. Manos, “Progress in Materials Science Metal-organic frameworks : Challenges and opportunities for ion-exchange / sorption applications,” *Prog. Mater. Sci.*, vol. 86, pp. 25–74, 2017.
<https://doi.org/10.1016/j.pmatsci.2017.01.002>
- [65] P. Kumar, V. Bansal, K. Kim, and E. E. Kwon, “Journal of Industrial and Engineering Chemistry Metal-organic frameworks (MOFs) as futuristic options for wastewater treatment,” *J. Ind. Eng. Chem.*, 2018.
<https://doi.org/10.1016/j.jiec.2017.12.051>
- [66] M. Rizwan, H. Rasool, H. Sun, V. Periasamy, M. O. Tadé, and S. Wang, “Journal of Colloid and Interface Science Excellent performance of copper based metal organic framework in adsorptive removal of toxic sulfonamide antibiotics from wastewater,” *J.*

Colloid Interface Sci., vol. 478, pp. 344–352, 2016.
<https://doi.org/10.1016/j.jcis.2016.06.032>

- [67] C. Yang, S. Wu, J. Cheng, and Y. Chen, “Indium-based metal-organic framework / graphite oxide composite as an efficient adsorbent in the adsorption of rhodamine B from aqueous solution,” *J. Alloys Compd.*, vol. 687, pp. 804–812, 2016.
<https://doi.org/10.1016/j.jallcom.2016.06.173>
- [68] V. A. Online and R. Mondal, “RSC Advances,” 2016.
- [69] M. R. Ryder and J. Tan, “Nanoporous metal organic framework materials for smart applications,” vol. 30, no. 13, 2014.
<https://doi.org/10.1179/1743284714Y.00000000550>
- [70] P. Kumar, A. Deep, and K. Kim, “Trends in Analytical Chemistry,” *Trends Anal. Chem.*, vol. 73, pp. 39–53, 2015. <https://doi.org/10.1016/j.trac.2015.04.009>
- [71] J. Zou *et al.*, “Ultrahigh-content nitrogen-decorated nanoporous carbon derived from metal organic frameworks and its application in supercapacitors,” *Electrochim. Acta*, vol. 271, pp. 599–607, 2018. <https://doi.org/10.1016/j.electacta.2018.03.200>
- [72] H. Zhao *et al.*, “Chemical Science,” pp. 5294–5301, 2016.
<https://doi.org/10.1039/C6SC01359G>
- [73] K. M. L. Taylor, W. J. Rieter, and W. Lin, “Manganese-Based Nanoscale Metal - Organic Frameworks for Magnetic Resonance Imaging,” pp. 14358–14359, 2008.
<https://doi.org/10.1021/ja803777x>
- [74] A. C. Mckinlay *et al.*, “Multirate delivery of multiple therapeutic agents from metal-organic frameworks from metal-organic frameworks,” vol. 124108, no. December, 2014. <https://doi.org/10.1063/1.4903290>

Chapter 7

Metal-Organic-Framework-Based Materials for Energy Applications

Ashwini P. Alegaonkar ^a, Vidya K. Kalyankar ^b, Prashant S. Alegaonkar ^{c*}

^a Department of Chemistry, Savitribai Phule Pune University (Formerly University of Pune), Ganeshkhind, Pune 411 007, MS, India

^c Department of Chemistry, Abasheb Graware College, Karve road, Pune

^c Department of Applied Physics, Defence Institute of Advance Technology, Girinagar, Pune 411 025, MS, India

Abstract

The ratio between the energy production and consumption will face vast difference by 2040. Currently in the electrical energy sector fulfilment of rising demands and balance between available conventional resources and consumption leads to a need of non-conventional development in sustainable renewable energy. The sources of energy like solar, fuel cell, hydrothermal, metal organic framework have been exploited as renewable sources. Among them, metal organic framework (MOF) is hosted as a potential alternative for renewable energy for many applications because of its tuneable porosity. MOF is a systematic repetitive arrangement of organic framework with metal ion at the centre. They are economic to synthesize, richness of metal ions reactivity boost to study different applications of MOF. Herein, we have discussed the MOF's of $\text{Ni}_3(\text{HITP})_2$ and $\text{Co}_3\text{O}_4\text{C}$ nanowire as sustainable renewable energy resources essentially applied as electro-catalysts in EDLC and OER mechanism toward energy storage application. This chapter includes brief survey of MOF, particularly the study of $\text{Ni}_3(\text{HITP})_2$ and $\text{Co}_3\text{O}_4\text{C}$ nanowire MOF. The chapter includes the synthesis and characterization of $\text{Ni}_3(\text{HITP})_2$ and $\text{Co}_3\text{O}_4\text{C}$ nanowire MOF. They are studied as alternative sources for renewable energy. It is studied with taking example of $\text{Ni}_3(\text{HITP})_2$ MOF with a perspective of supercapacitor while in former case $\text{Co}_3\text{O}_4\text{C}$ nanowire MOF as potential candidate in (Oxygen Evolution Reaction) OER process. We have concluded that MOF can be a good alternative as a renewable energy sources with above mentioned examples. In further sections the details are presented.

Keywords

Renewable Energy, $\text{Ni}_3(\text{HITP})_2$ MOF, Hybrid $\text{Co}_3\text{O}_4\text{C}$ Nanowire MOF, Super Capacitance, OER Process

Contents

1. Introduction.....	141
1.1 Role of MOF in supercapacitor	143
1.2 Role of MOF in oxygen evolution reaction (OER)	144
2. Synthesis of $\text{Ni}_3(\text{HITP})_2$ MOF	146
3. Characterization of $\text{Ni}_3(\text{HITP})_2$ MOF	147
4. $\text{Ni}_3(\text{HITP})_2\text{MOF}$ as supercapacitor electrode for EDLC :	151
5. Two electrode measurements	153
6. Electrochemical impedance (EIS) measurements	155
7. Device performance	155
8. Hybrid $\text{Co}_3\text{O}_4\text{C}$ nanowires electrode for OER process.....	159
9. Synthesis of hybrid $\text{Co}_3\text{O}_4\text{C}$ nanowires	160
10. Characterization of hybrid $\text{Co}_3\text{O}_4\text{C}$ nanowires	160
11. Hybrid $\text{Co}_3\text{O}_4\text{C}$ nanowires MOF electrode for oxygen evolution reaction.....	163
Conclusion.....	169
References	169

1. Introduction

The energy demand is increasing drastically with the globalization. A recent survey of Energy Information Administration (EIA) U.S.A. observed that, internationally consumption of total energy will rise up from 549 quadrillion British thermal units (Btu) to 815 quadrillion British thermal units (Btu). Total energy consumption will rise almost 48% by 2040. As a result the ratio of energy consumption to available energy resources has been declining from 96% to 88% [1,2]. In conventional energy resources, fossil fuel

is dominating clean resource for the sustainable energy which is easily available but it has implication on climate [3]. With increasing population the fossil fuels will accomplish only around 78% energy demand till 2040 [4]. Other sources such as natural gases and liquefied hydrocarbons are also used to meet the energy demand; however its use is restricted due to drawback like greenhouse gases [5]. Ultimately the developments in renewable energy sources are essential on a large scale to meet the energy demand and to save the environment. Different renewable energy sources such as solar, wind and hydro power technologies has been significantly implemented in different energy sectors and looking forward for clean and greenhouse gases free technology.

Particularly, the energy demand is high on electro-catalyst. The development in electro-catalyst as renewable energy source used in different electronic gadgets is having a crucial importance. Prominently, the energy generated or stored in chemical bond has been applied in metal-air batteries, water splitting, and fuel cells as a renewable energy [6-10].

Metal organic framework (MOF) also known as *Coordination polymer*, an important class of chemistry is an alternative as a renewable energy sources. Metal ions and organic ligands are bonded through coordination bond, hydrogen bonds, metallic bond or through van der Waals force of interaction and hold a large specific surface area (SSA). These molecular assemblies possess the definite structure, diverse scaffold, adjustable pore size with abundant active sites. As a result different MOF are widely used in variety of applications such as catalysis, gas adsorption and separation, drug delivery, imaging and sensors [11-13]. Besides this MOF and their derivatives are promising candidate in the field of electrochemical energy storage such as lithium ion batteries, fuel cells and supercapacitors etc. Due to high porosity and compositional tunability of MOF advantages to enhance the electrical capacitance over the other currently available carbon materials [14]. The Figure 1 shows schematic representation of MOF and its various applications.

Such a crystalline metal organic framework (MOF) can have a definite shape and size. It can be synthesized using different methods under controlled reaction conditions. These MOFs can be characterized by single crystal X-ray Diffraction pattern, FE- SEM, TEM and HRTEM images. Oxidation state of metal ion can be determined by X-ray XPS. The organic framework i.e. ligands can be characterized using Infrared spectroscopy (FT-IR), ^1H and ^{13}C nuclear magnetic spectroscopy and mass spectrometry.

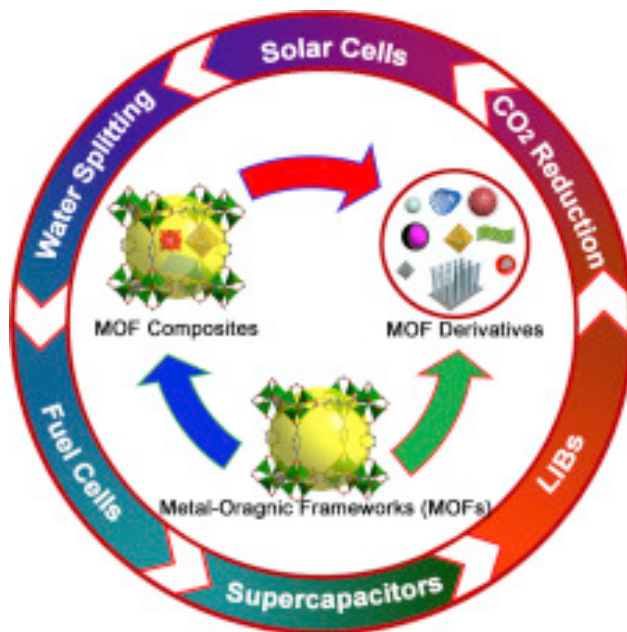


*Figure 1 Schematic representation of crystal structure of MOF with some applications
 [Reprinted with permission from (15)]*

1.1 Role of MOF in supercapacitor

Supercapacitors fascinated researchers for the last four decades. They are the most attractive source of energy storage in many electronic devices such as electronic communications, the emergent electric transportation industry, aerospace and many more. Ideally they should possess eco-friendly, high specific capacitance, high power density material, fast charge/discharge rate and long cycle life [15-23]. The energy storage mechanisms are electric double layer capacitance (EDLC) and pseudo capacitance [24-25]. In EDLC mechanism the movement of ions at the interface between electrodes and electrolytes take place, e.g. are carbon based material such as graphene, carbon nanotubes, activated carbon etc. [26-27]. In pseudo capacitance energy stores via reversible redox reaction between electrode and electrolyte, e.g. metal oxides like NiO₂, RuO₂, CoO₂, MnO₂ etc. or conductive polymers (Poly aniline, poly pyrrole etc.) [28-30].

Metal organic frameworks (MOFs) are porous crystalline molecular assemblies with definite coordination bond between organic ligand and metal centre. They hold high electrical conductivity and stability. The MOFs with high conductivity can be exploited for the development of supercapacitor electrode material [31-34]. Table 1 summarizes different MOFs materials as a supercapacitor enlists magnitude of specific capacitance.

Table 1 Summary of MOF and their magnitudes of specific capacitance.

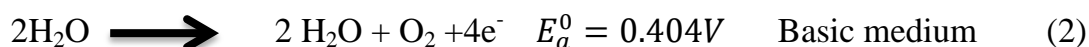
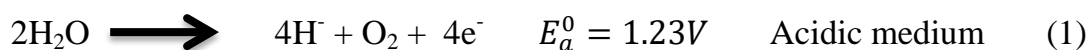
Sr. No.	MOF	Capacitive performance (Fg ⁻¹)	Ref
1	Co(H ₂ BPDC) i.e. 4,4-biphenyldicarboxylic acid	179.2	[35]
2	Ni(PTA) i.e. p-benzodicarboxylic acid	988	[36]
3	ZIF-67 i.e. Zeoliteimidazole framework	10.45	[37]
4	CIRMOF-3-950	239	[38]
5	ZIF-11	307	[39]
6	Zn-MOF	212	[40]
7	MOX-Fe (metal organic wet gel)	600	[41]
8	Carbon-ZSR	305	[42]
9	Co-MOF	150	[43]
10	Brick like Ce-MOF	502	[44]
11	Co ₃ O ₄	504	[45]
12	Ni-MOF	117	[46]

From the above, MOFs have proven to have good electrochemical properties and can be improved with change in metal ion, organic framework pore size with effective surface area. It also influences abundant active site and long cycle life. In aqueous media the electrical conductivity of MOFs is improved and boosts the electrical performance. In short, MOF's are economic with high electrical performance as energy storage and are a good alternative for the future. Furthermore, MOF has potential application towards oxygen evolution reaction.

1.2 Role of MOF in oxygen evolution reaction (OER)

As OER electro-catalysis find applications in various fields such as water splitting, metal-air batteries, fuel cells and many more. The catalyst used for OER electro-catalysis is a renewable energies source. A good example of this is metal-air batteries with portable size which can be used as electrochemical energy storage (EES). They have potential energy 40mJ/Kg like Li batteries [47]. Due to poor cycling ability they have limitations for practical application. In OER mechanism, production of molecular oxygen takes place at the expense of four electrons. It is a multistep process in acidic/basic/neutral medium.

In acidic or neutral medium, two water molecules were oxidized to form 4H^+ and O_2 molecules, whereas in basic medium, OH^- is converted into H_2O and O_2 . The equilibrium half-cell potential (E_a^0) for OER at 25°C and 1 atm are shown as follows in equation 1 and 2,



During the OER process as transport of four electrons takes place as a result energy gets accumulated in each step. This makes the process kinetically sluggish and results in large over potential. In order to scale up industrially the catalyst used in OER process should be with low potential, high stability, easy availability and economic.

Topologically the MOFs are divided into four categories viz. isorecticular metal-organic frameworks (IRMOFs), zeoliticimidazolate frameworks (ZIFs), Lavoisier frameworks (MILs) and pocket-channel frameworks (PCNs) [48]. Table 2 summarizes the various MOFs used in OER process and their electrode potential.

Table 2 Summary of MOFs used in OER process.

Sr. No.	MOF	Electrode potential (V)	Ref
1	Fe/Ni(BTC), BTC= 1,3,5, benzene tricarboxylate	0.5	[49]
2	Co(4,5-di(4'-carboxylphenyl) phthalic acid and 4,4'-bipyridine	-1.02	[50]
3	Co(4,5- di(4'-carboxylphenyl)phthalic acid and azene	0.62	[51]
4	MOF(Fe/Co)	0.90	[52]
5	Cu-MOF	1.19	[53]
6	Pb-TCPP,[Pb ₂ (H ₂ TCPP)]·4DMF·H ₂ O (H ₆ TCPP = 5,10,15,20-tetra(carboxylphenyl)porphyrin))	1.70	[54]

Among various MOF and their applications in vast different areas we have focused on two MOF structures namely $\text{Ni}_3(\text{HITP})_2$ that is $\text{Ni}_3(2,3,6,7,10,11\text{-hexaiminotriphenylene})_2$, and hybrid $\text{Co}_3\text{O}_4/\text{C}$ nanowires. This chapter reviews an application study of these two MOF as energy storage and OER study. The first part discusses the energy storage and the second part the OER study.

Part I: The synthesis of $\text{Ni}_3(2,3,6,7,10,11\text{-hexaiminotriphenylene})_2/(\text{Ni}_3(\text{HITP})_2)$ reported by Sheberla et al. in ref [55, 56]. They studied an electrochemical cell material. They used neat MOFs as active materials without any binders. The $\text{Ni}_3(\text{HITP})_2$ based MOF device shows higher aerial capacitance than that of most carbon-based materials with capacity retention greater than 90% over 10,000 cycles, in line with commercial devices. The established results for structural and compositional tunability of $\text{Ni}_3(\text{HITP})_2$ helps to design and synthesize the electrode material for the new generation of supercapacitors at the molecular level.

Part II: Hybrid $\text{Co}_3\text{O}_4\text{C}$ nanowires used as electro-catalyst for OER study with ultrahigh oxygen evolution and strong durability. This study is described in ref [57] by Ma et al. The $\text{Co}_3\text{O}_4\text{C}$ has nanowire array electrode configuration and in situ carbon incorporation is carried out. It leads to a large active surface area, enhanced mass/charge transport capability, easy release of oxygen gas bubbles, and strong structural stability. Furthermore, the hybrid $\text{Co}_3\text{O}_4\text{C}$ porous nanowire arrays can efficiently catalyse oxygen reduction reaction. A desirable four-electron pathway for reversible oxygen evolution and reduction process was observed. It is potentially useful for rechargeable metal-air batteries, regenerative fuel cells, and other important clean energy devices.

2. Synthesis of $\text{Ni}_3(\text{HITP})_2$ MOF

Nickel chloride hexahydrate ($\text{NiCl}_2 \cdot 6\text{H}_2\text{O}$) 6.6.mg (0.028 mmol) was dissolved in 5ml water and 0.3 ml concentrated aqueous ammonia (NH_4OH , 14 molL^{-1}). 2,3,6,7,10,11-hexaaminotriphenylene hexahydrochloride ($\text{HATP} \cdot 6\text{HCl}$) was used as organic framework for MOF synthesis. A solution of $\text{HATP} \cdot 6\text{HCl}$ 10 mg (0.019 mmol) in 5 ml of water was added to above prepared nickel solution. The reaction mixture was stirred for 2 hours at 65 °C in aerobic condition. A black powder was obtained as a product. Finally it is centrifuged, filtered, and washed with water under reflux for 36 hrs. Finally, the solid was heated at reflux in neat acetone for another 3 h and dried under vacuum at 150 °C. The scheme of synthesis is represented in Figure 2. The obtained $\text{Ni}_3(\text{HITP})_2$ is a 2-D graphene like analogue with intrinsic zero band gap. Further, the product of $\text{Ni}_3(\text{HITP})_2$ was characterized and used for future application.

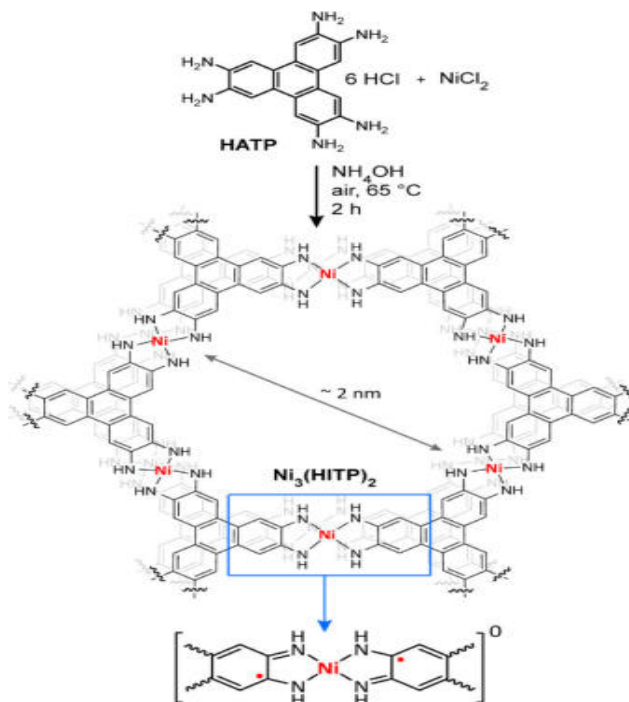


Figure 2 Scheme of synthesis of $\text{Ni}_3(\text{HITP})_2$ MOF (Reprinted with permission from [55])

3. Characterization of $\text{Ni}_3(\text{HITP})_2$ MOF

The characterization study of $\text{Ni}_3(\text{HITP})_2$ MOF was carried out by elemental analysis, X-ray Photoelectron spectroscopy (XPS), Powder X-ray Diffraction (PXRD) and SEM images. It is reported in [55].

The micro elemental analysis of $\text{Ni}_3(\text{HITP})_2$ for M, C, H, N, and Cl elements was calculated and matched with observed values. They are found to be: C: 53.84%; H: 3.12%; N: 20.83%; Cl: <0.02%. The thermo gravimetric analysis (TGA) of $\text{Ni}_3(\text{HITP})_2$ shown in Figure 3 (a) suggested that the loss of water at 150°C , the loss at $200\text{--}300^\circ\text{C}$ is due to organic moiety and above 500°C loss confirms the presence of Ni atom. The X-ray photoelectron spectroscopy (XPS) analysis data of $\text{Ni}_3(\text{HITP})_2$ from Figure 3 (b) indicates the presence of only Ni, C, N and O resonance peaks and water guest molecules but no anionic Cl^- was observed. High resolution XPS analysis showed only one type of Ni (2p) and N (1p) peak in spectra, also indicative of absence of Ni^{+2} and NH^{+4} species.

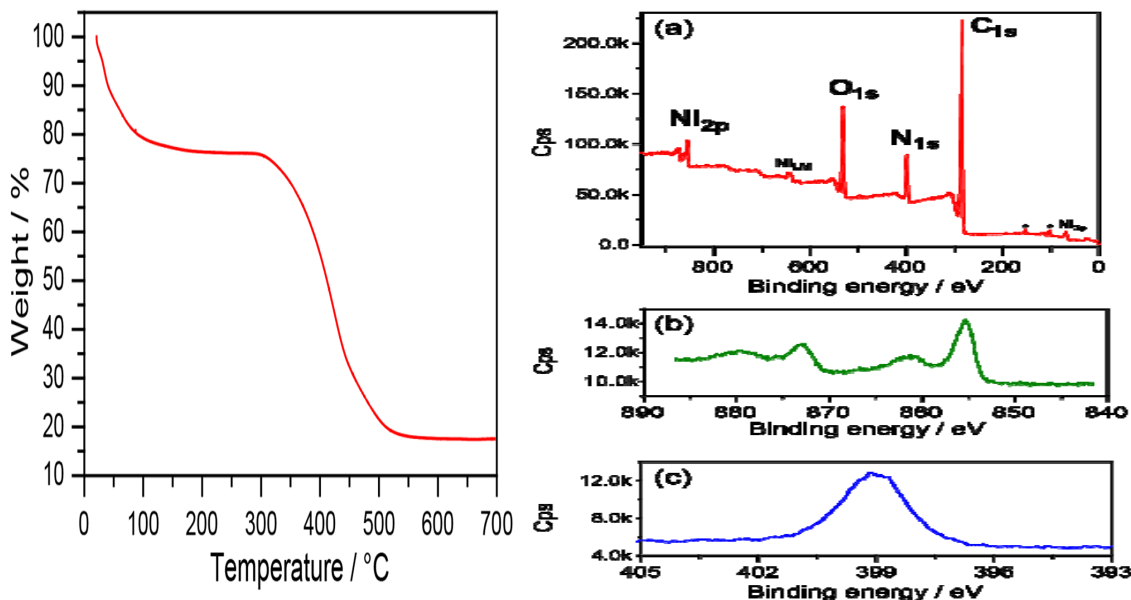


Figure 3 (a) TGA curve of $\text{Ni}_3(\text{HITP})_2$ MOF. (b) XPS spectra of the $\text{Ni}_3(\text{HITP})_2$ MOF electrode after the cyclic voltammetry experiment (Reprinted with permission from [55]).

Powder X-ray diffraction (PXRD) analysis of $\text{Ni}_3(\text{HITP})_2$ shows a crystalline structure with prominent peaks at $2\theta = 4.7^\circ$, 9.5° , 12.6° , and 16.5° , indicative of long-range order within the ab plane as shown in Figure 4(a). An additional, weaker and broader peak at $2\theta = 27.3^\circ$, corresponding to the [001] reflections indicates a poor long range coupling towards the plane c direction. This AB sequence stacking was further supported by DFT calculations. It is shown in 4(b). The calculations for potential energy of AB sequence plane in the 2D sheet were most stable as compared with the AA plane sequence. Finally in all, the PXRD, EXAFS, and DFT data suggested a hexagonal $\text{Ni}_3(\text{HITP})_2$ MOF structure with slipped-parallel stacking and unit cell parameters $a = b = 21.75 \text{ \AA}$ and $c = 6.66 \text{ \AA}$.

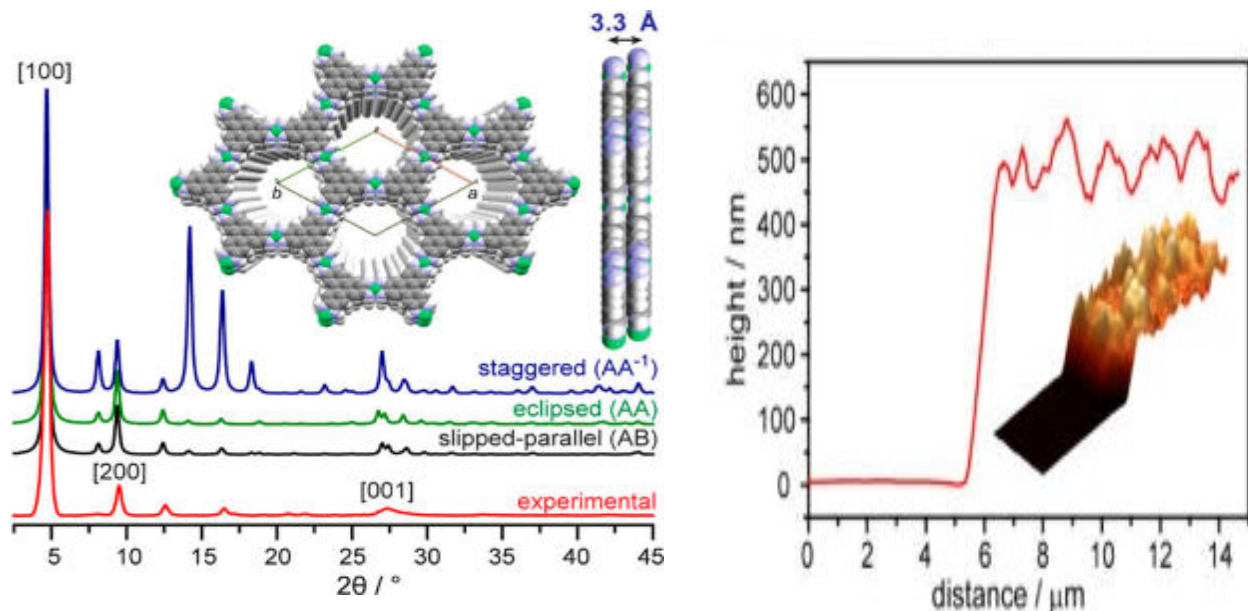


Figure 4 (a) Powder X-ray Diffraction Pattern of $\text{Ni}_3(\text{HITP})_2\text{MOF}$. (b) AFM thickness profile with AFM 3D image. (Reprinted with permission from [55]).

The Scanning electron microscopy (SEM) images were measured for both bulk material and thin films of thickness ~ 500 nm of $\text{Ni}_3(\text{HITP})_2$ with an excellent coverage on quartz substrate as shown in Figure 25.4 (a) and observed the microporous surface which was further supported with AFM microscopy for the electronic properties as shown in Figure 4 (b). UV-VIS Spectroscopy was performed for $\text{Ni}_3(\text{HITP})_2\text{MOF}$, exclusively the electronic absorption band at near IR region (λ_{max} 1400 nm) as shown in Figure 5 (b). Such a low electronic excitations commonly was observed in π conjugated organic molecules but very rarely observed in metal complexes. Consequently this property helps to explore the electronic property.

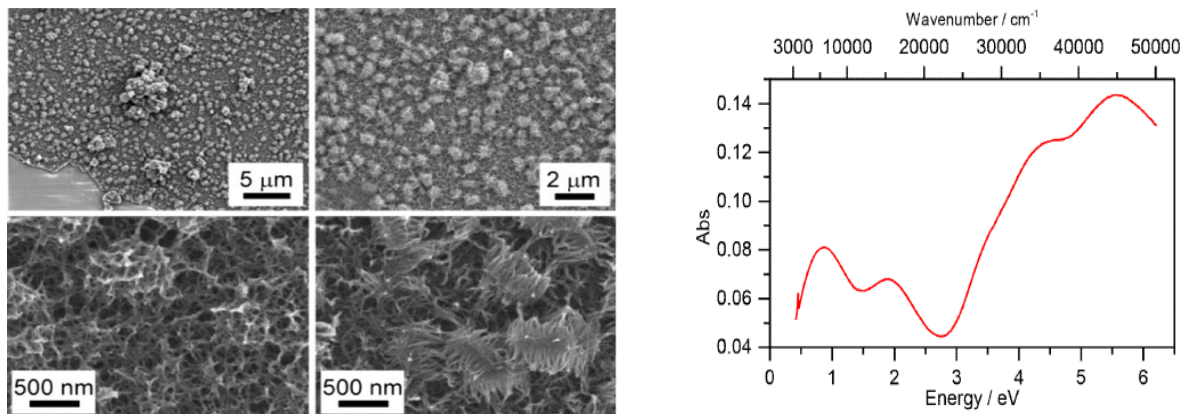


Figure 5 (a) FE-SEM images of $\text{Ni}_3(\text{HITP})_2\text{MOF}$ at various magnification (b) UV-Vis-NIR absorption of $\text{Ni}_3(\text{HITP})_2$ film on quartz slide (Reprinted with permission from [55]).

After characterization the film of $\text{Ni}_3(\text{HITP})_2$ was prepared on quartz substrate and conductivity was carried out consistently. The magnitude of conductivity is $40 \text{ S} \cdot \text{cm}^{-1}$ at room temperature, as measured by the van der Pauw method [58] as presented in Figure 6.

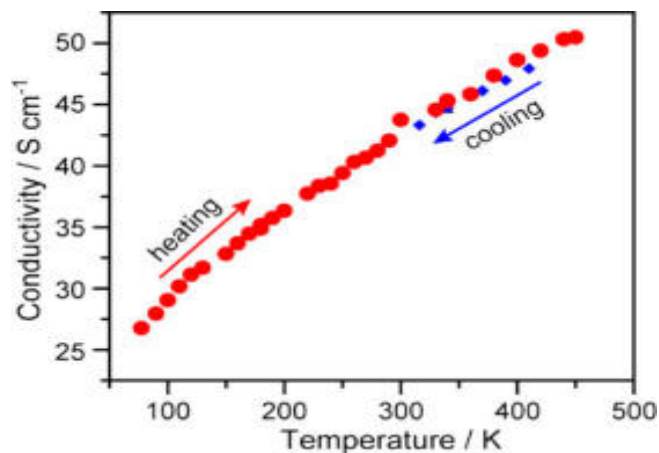


Figure 6 Variable-temperature van der Pauw conductivity measurement on a $\sim 500 \text{ nm}$ thick film on quartz of $\text{Ni}_3(\text{HITP})_2\text{MOF}$. (Reprinted with permission from [56]).

Figure 7 shows measurement of porosity and surface area determination using an apparent Brunauer-Emmett-Teller (BET). A porosity of π conjugated 2D stacked $\text{Ni}_3(\text{HITP})_2$ was measured 1.5nm diameter shown in figure 7 with cylindrical channel and surface area of $630 \text{ m}^2 \text{ g}^{-1}$, as determined from a N_2 adsorption isotherm at 77K [60]. Such a high conductivity and large surface area makes $\text{Ni}_3(\text{HITP})_2$ MOF competent over other carbon based materials in EDLCs.

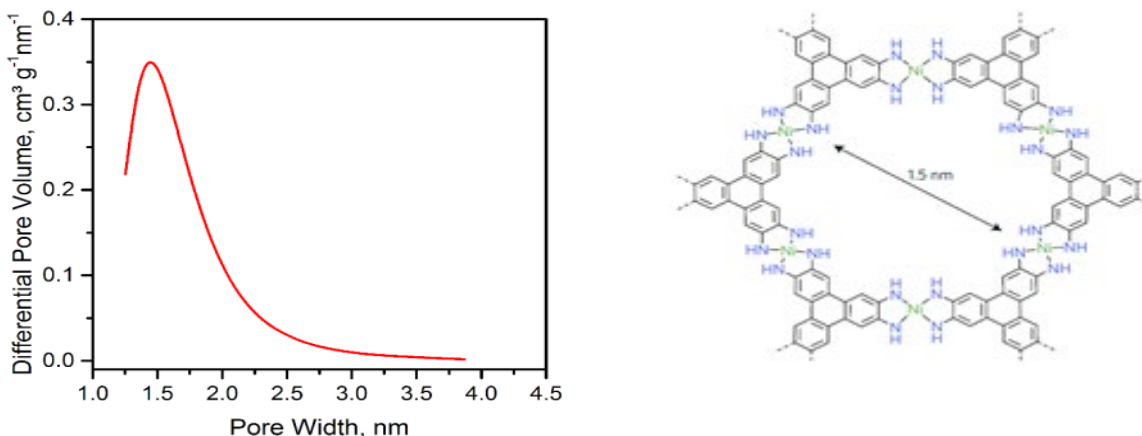


Figure 7 Porosity and Dubinin-Astakhov differential pore volume plot (Exponent = 1.8465). (Reprinted with permission from [55]).

4. $\text{Ni}_3(\text{HITP})_2$ MOF as supercapacitor electrode for EDLC :

Theoretical and experimental studies were further carried out on conductive $\text{Ni}_3(\text{HITP})_2$ for stable supercapacitor high areal capacitance. A relative to batteries, due to superior cyclability and high power density, electrochemical double layer capacitors (EDLCs) have emerged as an significant electrical energy storage technology that will play a crucial role in renewable energy sources, smart power grids, and electrical vehicles [59].

MOF of $\text{Ni}_3(\text{HITP})_2$ have a sufficient space (clear form Figure 7) to accommodate different electrolyte such as tetraethylammonium tetrafluoroborate, TEABF_4 even with their first solvation sphere in acetonitrile (ACN), a common organic solvent for EDLCs. The high conductivity and porosity which facilitates the easy movement of electrolyte with minimal volume changes on repeated charge/discharge cycles give good reason to explore the $\text{Ni}_3(\text{HITP})_2$ MOF as neat electrode material in ELDCs.

Cyclic Voltammetry of $\text{Ni}_3(\text{HITP})_2$ MOF was performed in three electrode cells in 1M $\text{TEABF}_4/\text{ACN}$ electrolyte having $\text{Ni}_3(\text{HITP})_2$ MOF powder pressed into Pt –mesh acts as a working electrode. The cyclic voltammogram (CV) is shown in Figure 8. It specifies absence of faradaic process when cycled cathodically in open circuit potential between 0.02 V and 0.6V or anodically between 0.02 and 0.5V. Indeed, a quasi-reversible oxidation process at approximately 0.7V was observed while scanning anodically past 0.5V indicative of capacitive behaviour of the electrode.

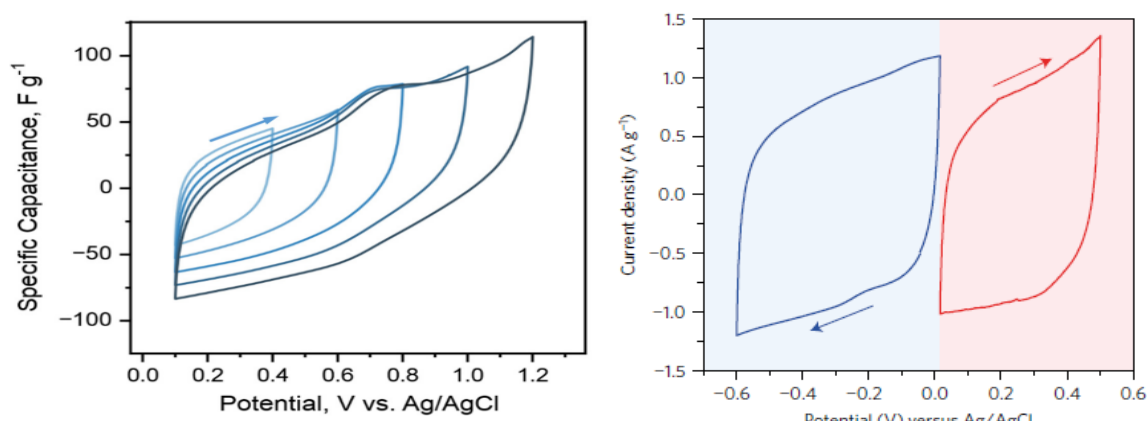


Figure 8 Cyclic voltammetry of $\text{Ni}_3(\text{HITP})_2$ MOF in a 3-electrode cell at a scan rate of 10 mV s⁻¹ with increasing potential limits in the positive direction. (Reprinted with permission from [56]).

Capacitive behaviour of electrode is studied with ex situ X-ray absorption spectroscopy (XAS) on 1V anodic polarization at Ni K-edge of $\text{Ni}_3(\text{HITP})_2$. The K-edge position of Ni was intact at 8,343eV indicating oxidation state and local coordination environment around Ni atoms doesn't undergo any change during the redox process. The quasi reversible oxidation at 0.7V is obtained due to the organic framework i.e. HITP moiety instead of Ni atoms which is also called as ligand based redox activity. An imine ($\text{C}=\text{N}$) functional group present in its organic framework i.e. HITP of $\text{Ni}_3(\text{HITP})_2$ is an active group which assist the redox mechanism. The labile π bonds very easily undergo resonance hybrid structure. Thus the pores as well as organic framework enhanced the electro catalytic activity. The electrolyte decomposition was studied by cycling anodically past 1.4V and cathodically 0.6V assist to determine the working potential window of 1.0V.

5. Two electrode measurements

In order to test its behaviour in the cell the two electrode symmetrical supercapacitor cell was prepared, an electrode of density $0.6\text{--}0.2\text{ gcm}^{-3}$ was prepared by pressing $\text{Ni}_3(\text{HITP})_2\text{MOF}$ powder into self-supported pellet at pressure of $100\text{ kg-force cm}^{-2}$. The characterization of this is carried out. Scanning electron microscopy (SEM) of pellet in Figure 9 shows the packed particle size of $0.5\text{--}0.2\text{ }\mu\text{m}$ of similar pores. The areal mass loading for each pellet was around 7 mg/cm^2 which in turn was adjusted to produce a cell with capacitance of at least 0.5 F . This is in fair deal with those used in commercial applications [61].

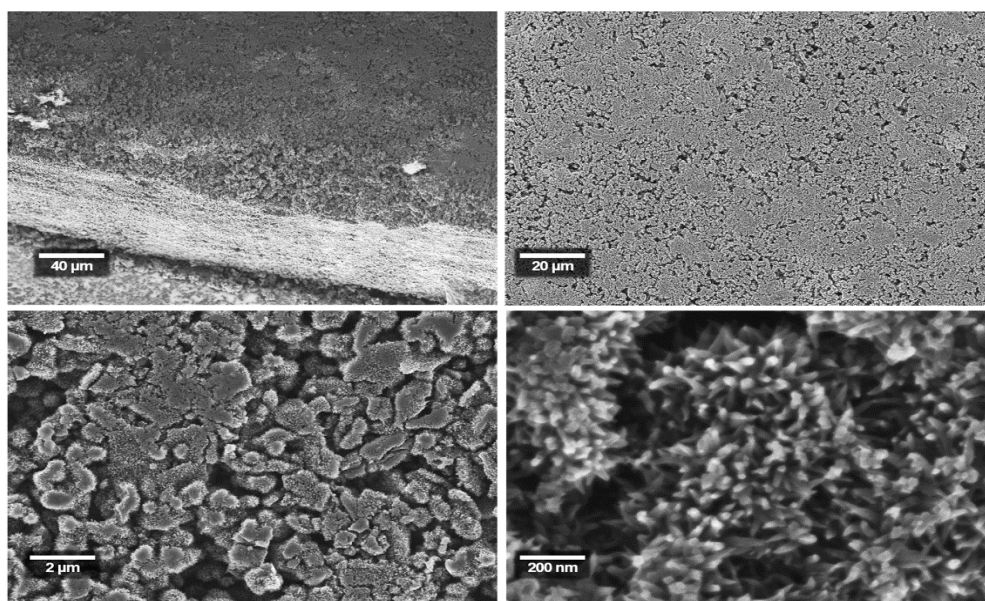


Figure 9 Top surface view of scanning electron micrographs of hand-pressed pellets of $\text{Ni}_3(\text{HITP})_2\text{MOF}$. (Reprinted with permission from [56]).

The CV measurement of charge and discharge cycle of symmetrical cell shows nearly rectangular and triangular traces respectively indicative of ideal capacitive behaviour as presented in Figure 10. The specific gravimetric capacitance of MOF was calculated 111 F/g at low current density 0.05 A/g . It is further compared with activated carbon, chemically reduced graphene, single walled carbon nanotubes etc. Like carbon materials with exception of holy graphene have gravimetric capacitance of 262 F/g (EMIMBF₄/ACN, 3.5 V , 1 A/g) [62]. The decrease can be attributed to decrease ion

accessibility and to pore surface which are made of long cylindrical pores and dense packing.

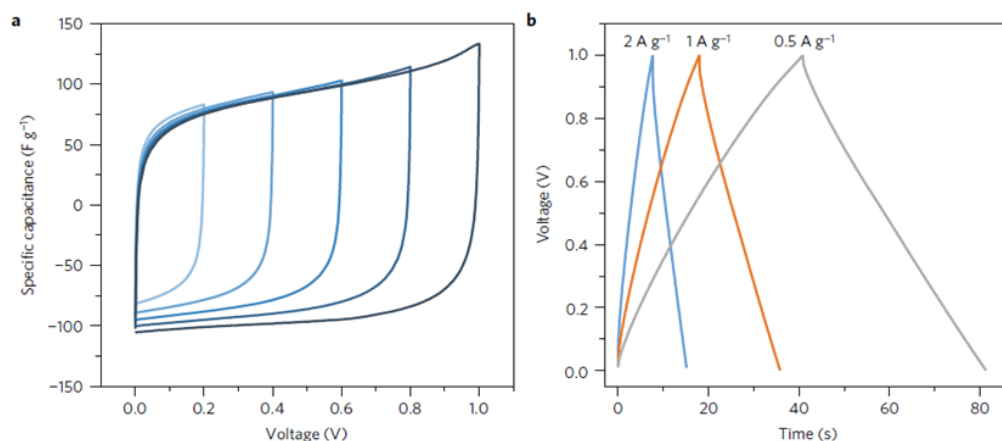


Figure 10 a. Cyclic voltammetry at a scan rate of 10mVs^{-1} at increasing cell voltage. b. Galvanostatic charge and discharge curves at current densities of 0.5, 1.0, 2.0 A g^{-1} . (Reprinted with permission from [56]).

The galvanostatic discharge curve (CD) at different current densities were calculated to obtain specific gravimetric capacitance of $\text{Ni}_3(\text{HITP})_2$ MOF in EDLC from Figure 11. It is obtained as 111 F g^{-1} at low discharge rate of 0.05 A , is higher compared with other carbon materials. The value of area capacitance obtained for $\text{Ni}_3(\text{HITP})_2$ MOF is $18\text{ }\mu\text{F cm}^{-2}$ for normalized specific area which is again much higher than any carbon material. This study clearly indicates that the rate capability of $\text{Ni}_3(\text{HITP})_2$ MOF electrode is proportional to the size of the pores.

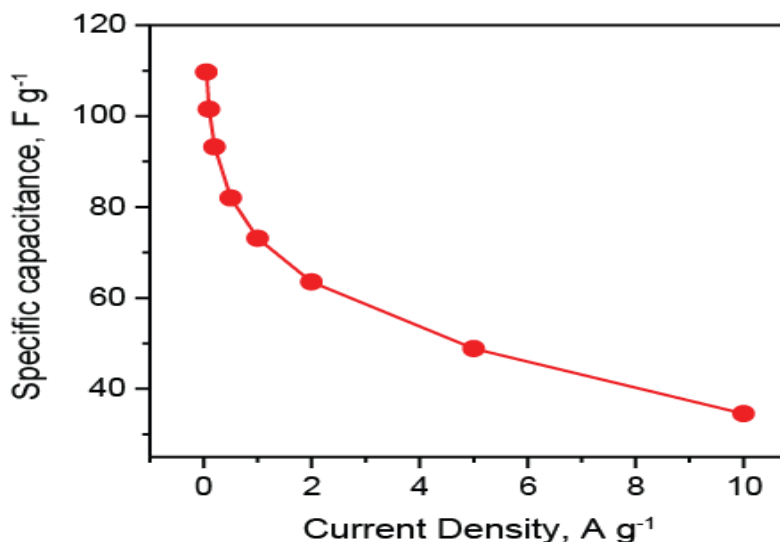


Figure 11 Gravimetric specific capacitance vs. current density obtained from constant current discharging over 1 V. (Reprinted with permission from [56]).

Equivalent series resistance (ESR) gives us an idea of total resistance of the electrolyte, membrane separator, internal resistance, current collector and resistance of the interface between active material and current collector [63]. The values of high ESR values reduces power of the cell which is related as,

$$P_{\max} = V^2 / 4 \times \text{ESR} \quad (3)$$

Where, V is the potential window.

ESR value for fully developed $\text{Ni}_3(\text{HITP})_2$ was obtained as low as $0.47 \, \Omega$ at regular current discharge which is less than graphene based supercapacitor under similar mass loading.

6. Electrochemical impedance (EIS) measurements

EIS measurements were performed in the frequency range between 62 kHz to 10 kHz. The Nyquist plot in such a low frequency range and the linear curve exhibiting of a Warburg transition frequency 3.5 Hz indicates high electrical conductivity of $\text{Ni}_3(\text{HITP})_2$ is predominantly due to electron transport in the active electrode which influences the cyclic rate. Figure 10 (b) shows capacitive retention up to 10,000 cycles. The cyclic stability of $\text{Ni}_3(\text{HITP})_2$ electrode shows excellent stability up to 10,000 cycles, but after shows reduction of 10% capacitance with no increase in ESR value.

7. Device performance

Device performance was studied by applying different pressures at the time of assembling the $\text{Ni}_3(\text{HITP})_2$ pellets. Figure 12 (a) indicates Nyquist plot and equivalence capacitance at different current densities. The pressure applied ($2.3 \, \text{ton force cm}^{-2}$) increases density of electrodes ($1.1 \pm 0.2 \, \text{g cm}^{-3}$) shows better packing. As a result decrease in gravimetric capacitance $107 \, \text{Fg}^{-1}$ with ESR of $0.8 \, \Omega$ but there is volumetric capacitance up to $118 \, \text{Fcm}^{-3}$ compared to $66 \, \text{Fcm}^{-3}$ for hand press pellets.

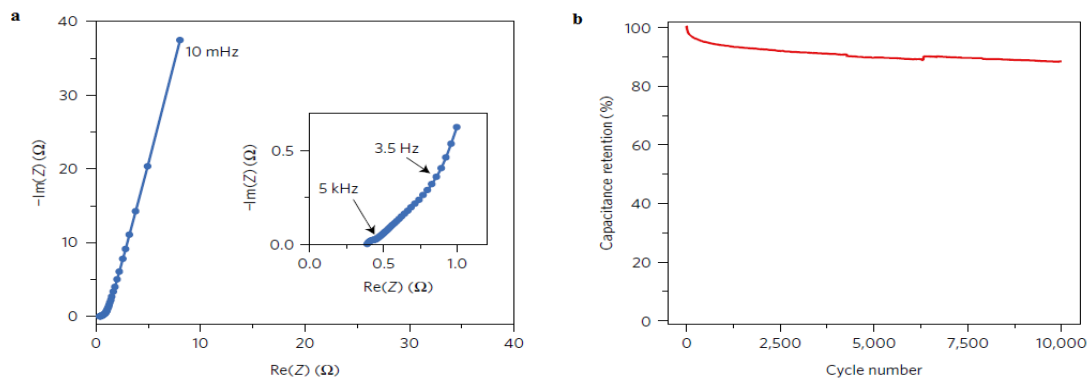


Figure 12 (a) Nyquist plot showing the imaginary part versus the real part of impedance in the 62 kHz–10 mHz range of high-frequency part (62 kHz–1 Hz). (b) Capacitance retention under repeated cycling at a current density of 2Ag^{-1} for 10,000 cycles. (Reprinted with permission from [56]).

Moreover, galvanostatic charge discharge was measured at different current densities. The reduced rate shows inter particle diffusion of electrolyte ion is restricted for denser pellet indicated from Figure 13(b). The EIS measurements also supports the Warburg region is extended and knee frequency is reduced to 0.3 Hz for denser pellets shown in Figure 13 (a).

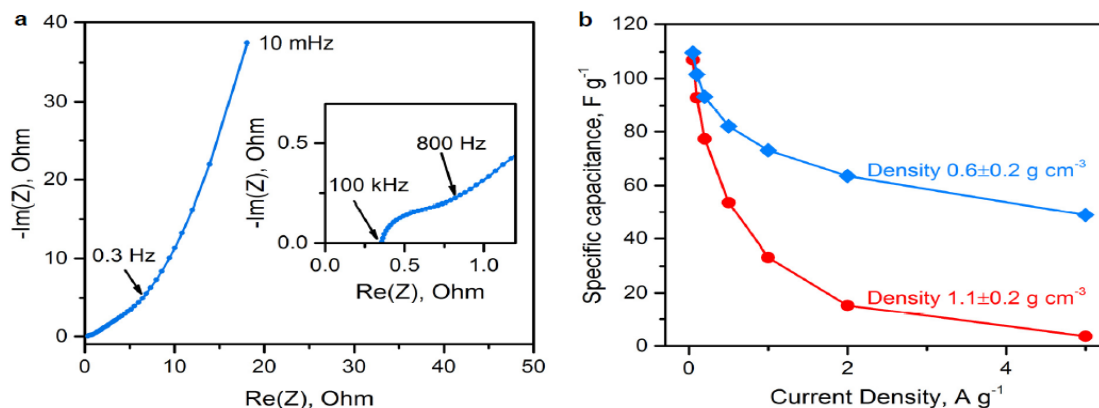


Figure 13 (a) Electrochemical impedance spectroscopy from 100 kHz to 10 mHz and (b) gravimetric specific capacitance vs. current density obtained from constant current discharging over 1V. (Reprinted with permission from [56]).

In a symmetric capacitor cell, capacitance loss before and after cycling at 1.5V is studied and shown in Figure 14 (a) and (b). The cell voltage window is 0 to 1.4V for before cycling (Figure 10 (a)) and 0 to 1V after cycling (Figure 11 (b)). This indicates the decay in capacitance is due to a purely faradic process after 5000 cycles but this loss has minimal effect on the ESR value which increased only by 0.43Ω after cycling at 1.5V.

To explore nature of interaction further individual potentials were measured on the positive and negative $\text{Ni}_3(\text{HITP})_2$ electrodes in a symmetrical cell by sandwiching reference Ag/AgCl electrode at scan rate 10mVs^{-1} shown in Figure 14. The measured potentials are less positive than electrolyte oxidation and less negative than irreversible reduction of cathode. Consequently it is clear that, electrolytic oxidation or faradic process is not involved in cyclic voltammetry. But a quasi faradic process may take place in cyclic voltammetry.

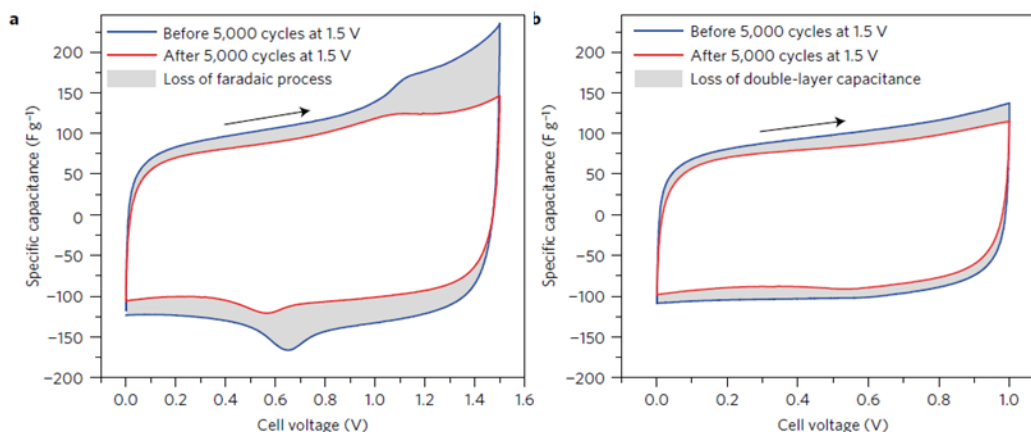


Figure 14 (a) cyclic voltammogram traces measured between 0 and 1.5V, showing pronounced loss of the Faradaic process (b) cyclic voltammogram traces between 0 and 1.0V, showing losses in double layer capacitance only. (Reprinted with permission from [56]).

Further, powder X-ray diffraction (PXRD) and X-ray photoelectron spectroscopy (XPS) were carried out to study stability. The crystallinity of $\text{Ni}_3(\text{HITP})_2$ electrode was maintained throughout the experiment and is shown in Figure 15 (a). The XPS analysis shown in Figure 15 (b) specifies slight shift in 0.5eV in Ni $2\text{P}_{3/2}$ peak of $\text{Ni}_3(\text{HITP})_2$ towards higher binding energies for both positive and negative electrodes. This can be attributed to a small change in the ligand field surrounding Ni atoms. This suggests of geometrical distortions of Ni and slight changes in stacking sequences of $\text{Ni}_3(\text{HITP})_2$.

Above 1V the faradic process is ligand based. Expectedly, cells made from $\text{Ni}_3(\text{HITP})_2$ degrade more precipitously only when cycled above 1.5V. This can be altered by changing metal so that it can work for higher potential.

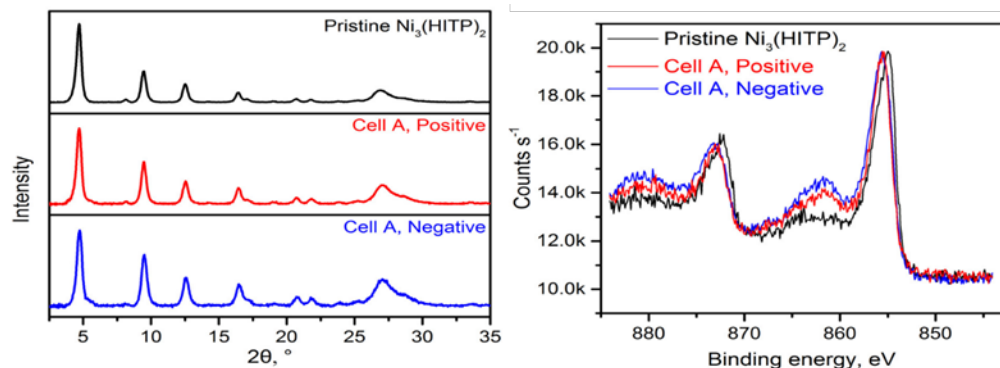


Figure 15 (a) PXRD of positive and negative electrodes of Cell A after 10,000 cycles at 2 Ag-1 between 0.0 V and 1.0 V followed by 5,000 cycles at 2Ag-1 between 0.0 V and 1.5 V. (b) X-ray photoelectron spectrum (Ni2p region) of positive and negative electrodes of Cell A after 10,000 cycles at 2 A g-1 between 0.0 V and 1.0 V followed by 5,000 cycles at 2 A g-1 between 0.0 V and 1.5 V. (Reprinted with permission from [56]).

The cell $\text{Ni}_3(\text{HITP})_2$ MOF undergo precipitation at negative electrode upon cycling above 1.5V. This degradation is due to an irreversible reductive process. It is indicative that at 1.5V capacitance loss of $\text{Ni}_3(\text{HITP})_2$ MOF is more pronounced. This is evidenced by spent $\text{Ni}_3(\text{HITP})_2$ MOF cathode showing a notable change in the Ni K-edge X-ray absorption near edge structure (XANES) Figure 16 (a) and X-ray absorption spectra of both electrode and pristine electrode as shown in Figure 16 (b)

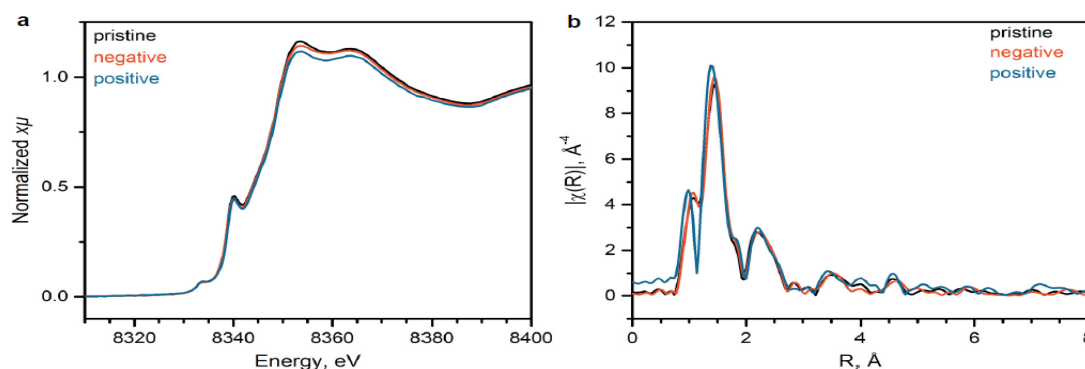


Figure 16 (a) X-ray absorption spectra Ni K-edge XANES and (b) k3-weighted Fourier transform of the EXAFS of $\text{Ni}_3(\text{HITP})_2$ MOF positive and negative electrodes of Cell B after cycling at 2 A g-1 between 0.0 V and 1.0 V over 10,000 cycles. (Reprinted with permission from [56]).

To summarize, conductive porous $\text{Ni}_3(\text{HITP})_2$ is a promising active electrode material prepared on reaction with Ni salt and HITP. This metal organic framework is an excellent electrode material for supercapacitor showing EDLCs behaviour. It has high surface area with low ESR value. Moreover compression of $\text{Ni}_3(\text{HITP})_2$ MOF powder gives high volumetric capacitance. The reported work on non-carbon centre material is a milestone and can be further tuned for future device architecture.

8. Hybrid $\text{Co}_3\text{O}_4\text{C}$ nanowires electrode for OER process

This is the wonderful example of MOF applied as electro-catalyst which renewable energy source through OER mechanism [57]. OER is nothing but for oxygen evolution reaction. OER mechanism plays a crucial role in many energy storage applications such as metal-air batteries, regenerative fuel cells etc. A suitable electro-catalyst can effectively accelerate the OER process by overcoming hassle of large over potentials generated between the electrodes. Many electro-catalyst comprises of noble metals (Ir/Ru) transition metals (Co, Ni, Fe and Mn etc.) and non-metals (N-doped graphitic carbon, graphitic carbon nitrides). They are used as either in the form of thin films or active material loaded on glossy carbon including Ni foam or some conductive substrates [64-67]. Moreover, synthesis of electro-catalyst involves various fabrication techniques like casting or coating involves polymeric binders results into irregular microstructure. However, they are not ideal for the multistep four electron transport of OER process. More recently many reports are available on nanowires as active electro-catalysts. e.g. $\text{Ni}_x\text{Co}_{3-x}\text{O}_4$ and $\text{Zn}_x\text{Co}_{3-x}\text{O}_4$ nanowires grown on Ti foils, Co_3O_4 nanowires grown on stainless steel surface, Ni substituted Co_3O_4 nanowires grown on Ni foam are the few illustrations of nanowires in OER electro-catalytic process [68, 69]. Due to effective pore size permits penetration of electrolyte and diffusion of ionic species is facilitated. With high stability and good electrical conductivity they possess great prospective in electrochemical cells particularly in OER process in alkaline media. This part of the chapter describes the use of $\text{Co}_3\text{O}_4\text{C}$ nanowires as electro-catalyst for OER mechanism [57].

9. Synthesis of hybrid $\text{Co}_3\text{O}_4\text{C}$ nanowires

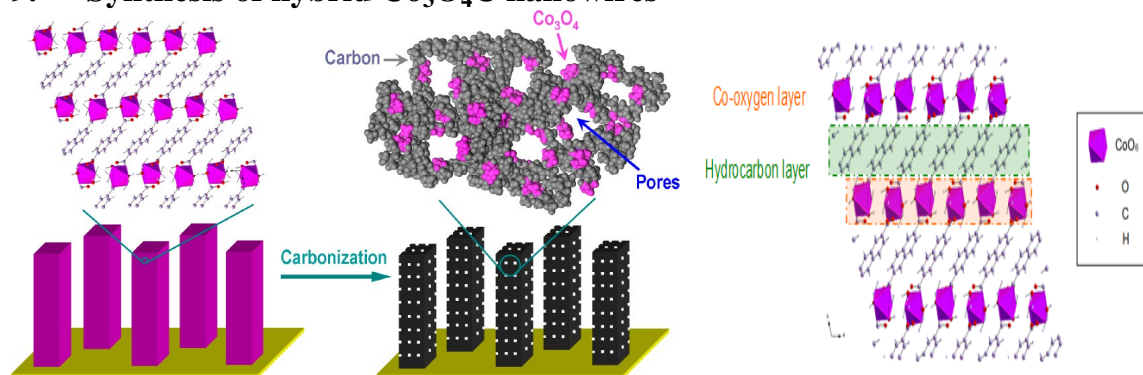


Figure 17 Scheme for synthesis of hybrid $\text{Co}_3\text{O}_4\text{C}$ nanowires MOF with its crystal structure. (Reprinted with permission from [57]).

Initially, di-potassium 2, 6-naphthalene-dicarboxylate and 0.3mmol of cobalt (II) acetate tetra hydrate were mixed in aqueous solution at room temperature under vigorous stirring. The reaction mixture was transferred into a Teflon lined stainless steel hydrothermal device. The Cu foil repeatedly rinsed with absolute alcohol and Milli-Q water through sonication treatment was immersed in hydrothermal. The other side of Cu foil is protected by applying nail polish layer to avoid nanowire array growth. The hydrothermal was sealed and maintained at 80 °C for 20h. After 20h, the autoclave cooled down to room temperature. The MOF composed of $\text{Co}(\text{C}_{12}\text{H}_6\text{O}_4)(\text{H}_2\text{O})_4$ grown on Cu foil, was subjected to repeated washing and drying under ambient conditions overnight. The Cu foil was further transferred into tube furnace and burnt under flowing N_2 atmosphere. Specifically it was gradually heated from room temperature to 400 °C with a ramp rate of 1 °C per min and maintained at 400 °C for 2h. Additionally, the temperature was further increased up to 600 °C and stabilized for another 4h. Finally cooled down to room temperature and resultant product hybrid Co_3O_4 -carbon porous nanowire arrays grown on Cu foil was obtained. The loading amount of nanowire arrays on Cu foil was approximately 0.2 mg cm^{-2} , which was determined by using the increased mass of Cu foil. These values were roughly consistent from batch to batch using the identical synthetic procedure.

10. Characterization of hybrid $\text{Co}_3\text{O}_4\text{C}$ nanowires

The morphology of synthesized hybrid $\text{Co}_3\text{O}_4\text{C}$ nanowires was determined by SEM, TEM and HRTEM images with X-ray mapping (EDS). The hybrid $\text{Co}_3\text{O}_4\text{C}$ was obtained in high yield with a smooth surface indicates that all Co_3O_4 and carbon species are

integrated in one. Layered crystalline structure of carbon is obtained by controlled deterioration and carbonization of naphthalene layers catalysed by Co species.

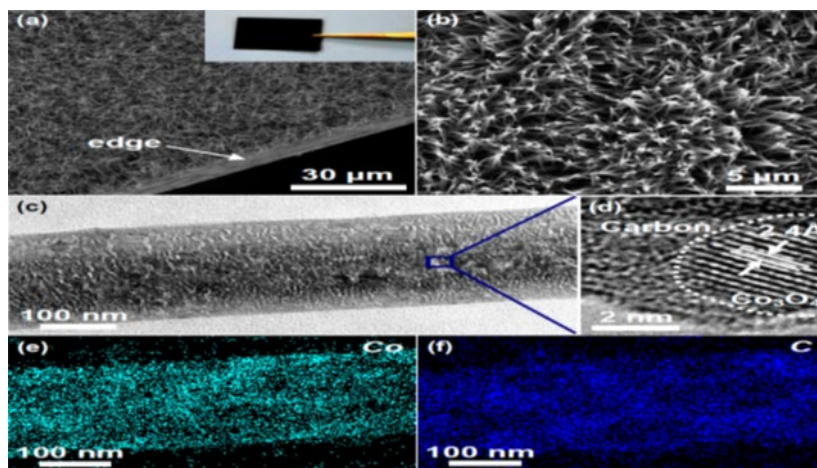


Figure 17 (a) and (b) SEM images (c) TEM image (d) HRTEM image (e) and (f) EDS mapping of hybrid $\text{Co}_3\text{O}_4\text{C}$ nanowires. (Reprinted with permission from [57]).

Figure 17 part (a) shows FESEM of black coloured hybrid Co MOF shown grown on Cu foil and part (c) shows transmission electron microscopy (TEM) a single nanowire having smooth surface of diameter $\sim 250\text{nm}$. A smooth surface indicates the homogenous arrangement of Co_3O_4 and carbon species with traces of Co_3O_4 crystals. Moreover high resolution transmission electron microscopy (HRTEM) image from part (d) of amorphous MOF identified lattice fringe space of 2.4 \AA corresponds to (311) plane of cubic Co_3O_4 spinel phase. On focusing at $\sim 5\text{nm}$ the pore size distribution curve was obtained and found a large surface area of $251 \text{ m}^2 \text{ g}^{-1}$ which is larger than any other Co-MOF. Further structural studied from part (e) and (f) shows EDS mapping indicates uniform distribution of Co and C species.

X-ray diffraction (XRD) pattern shown in Figure 18 (a) reveals the crystalline structure of $\text{Co}(\text{C}_{12}\text{H}_6\text{O}_4) \cdot (\text{H}_2\text{O})_4$ supports in situ carbonization with no traces of Co oxides. It also confirms the cubic spinel shaped structure (JCPDS No, 43-1003) with a broad shoulder peak in the range of $20\text{-}30^\circ$ shows presence of amorphous carbon species homogeneously distributed in nanowires that are formed in situ during the carbonization process (Figure 18 (b)). Moreover the N_2 adsorption isotherms is recorded for hybrid $\text{Co}_3\text{O}_4\text{C}$ -nanowires resembles slit like mesopores material supportive to TEM observations with crystalline structure of MOF. The N_2 adsorption isotherm recorded on $\text{Co}_3\text{O}_4\text{C}$ nano wires resembles

type IV with an H3 type hysteresis loop (Figure 18 (b)). The inset shows pore distribution, peak centred at ~ 5 nm and having a large surface area of $251 \text{ m}^2 \text{ g}^{-1}$. As a result highly porous hybrid nanowires from MOF via the carbonization process are formed. Thermo gravimetric analysis (TGA) studies shown in Figure 18 (c) indicates the weight loss of 3% below 200°C was due to water and gases, weight loss of 59.5% from 200 - 500°C was due to combustion of organic species with surface bonded oxygen containing functional groups. X-ray photoelectron spectra (XPS) of hybrid $\text{Co}_3\text{O}_4\text{C}$ -nanowires shown in Figure 18 (d). The deconvoluted peak of Co-2p profile shows the coexistence of Co^{2+} and Co^{3+} which includes two pairs of spin-orbit doublets indicating the coexistence of Co^{2+} and Co^{3+} and their four shakeup satellites. The shift in peak from 780eV to 781.2eV of Co_3O_4 species confirmed the formation and strong bonding between Co_3O_4 and carbon species. This resulted in the impaired electron density of Co atoms in $\text{Co}_3\text{O}_4\text{C}$ nano array. In short it revealed that homogeneously distributed and well-interacting nanocrystalline Co_3O_4 nanowires which is further studied as high-performance electro-catalysts study.

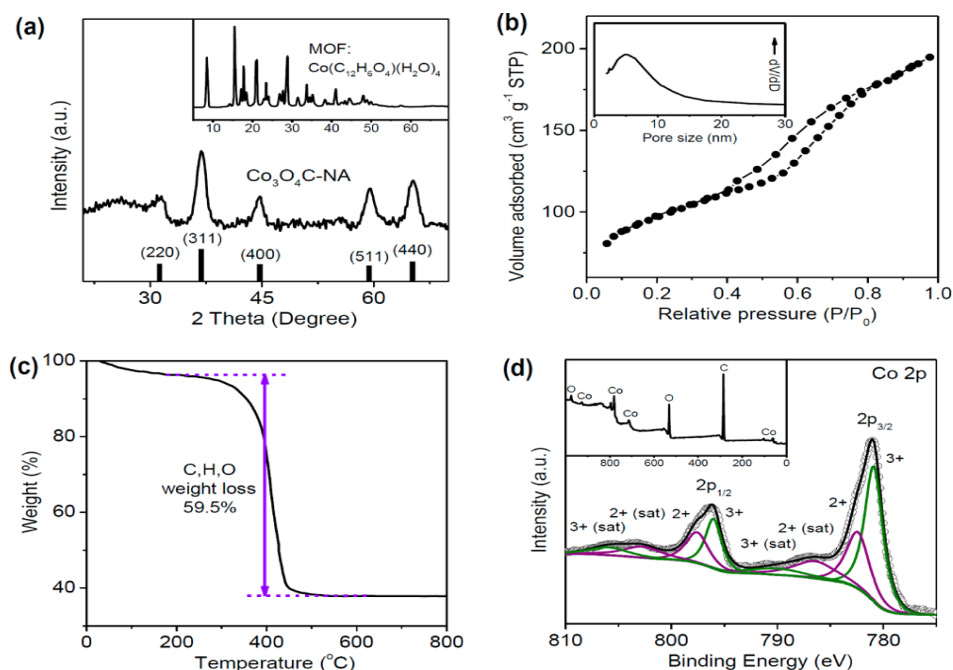


Figure 18 (a) XRD patterns of hybrid $\text{Co}_3\text{O}_4\text{C}$ -nanowires (b) N_2 adsorption isotherm and (inset) the corresponding pore size distribution of hybrid Co_3O_4 -nanowires. (c) TG curve of hybrid $\text{Co}_3\text{O}_4\text{C}$ -nanowires. (d) High-resolution XPS spectrum of the Co 2p core level of hybrid $\text{Co}_3\text{O}_4\text{C}$ -nanowires. (Reprinted with permission from [57]).

11. Hybrid Co₃O₄C nanowires MOF electrode for oxygen evolution reaction

Hybrid Co₃O₄C nanowires grown on Cu foil itself without any additives or substrates was used as working electrode for OER activity. During OER, a scan rate of 0.5mVs⁻¹ was preferred to reduce capacitive current. Alkaline (0.1M and 1M KOH) electrolytes were used over acidic solutions since hybrid Co₃O₄C nanowires have slight solubility in acidic medium and Cu foil exhibits negligible catalytic activity. A reversible hydrogen electrode (RHE) potential was measured and compared with reported Co-MOF. It was observed that there is high onset potential at 1.47 V with greatly enhanced OER activity compared with Co-MOF. It indicates enhanced catalytic activity due to compositional transformation of MOF to hybrid Co₃O₄C nanowires.

Figure 19 (a) shows the operating potential for OER activity of hybrid Co₃O₄C nanowires of current density 10.0 mA/cm² ($E_j = 10$) vs. RHE was 1.52 V. the operation potential is lower than that of IrO₂/C and many other noble metal catalysts at pH 14 [70-75].

The Tafel plot Figure 19 (b) shows the catalytic kinetics for the evolution of oxygen. The Tafel equation is as follows:

$$\eta = b \cdot \log (j / j_0) \quad (4)$$

Where η denotes the over potential, b denotes the Tafel slope, j denotes the current density, and j_0 denotes the exchange current density. The plot of over potential vs. $\log (j / j_0)$ is plotted and slope b ; Tafel slope is calculated. The hybrid Co₃O₄C nanowires shows low slope value (70 mV/decade) compared with other catalyst used for OER process. This specifies that the hybrid Co₃O₄ nanowire is highly active as a OER catalyst and favourable for reaction kinetics. Substantial durability in OER is an important criteria for energy conversion and storage systems. This is studied by the chronoamperometric response. Figure 19 (e) shows demonstrates chronoamperometric suggesting the high stability of Co₃O₄C nanowire, showing a slight anodic current attenuation of 6.5% within 30 h, whereas IrO₂/C displays a 4.7 times larger current attenuation of 30.4% indicating the apparent advantage of active materials directly grown on conductive substrates in comparison to the post coated catalysts on electrodes, because the latter suffer from peeling off during the evolution of a large amount of O₂ gas.

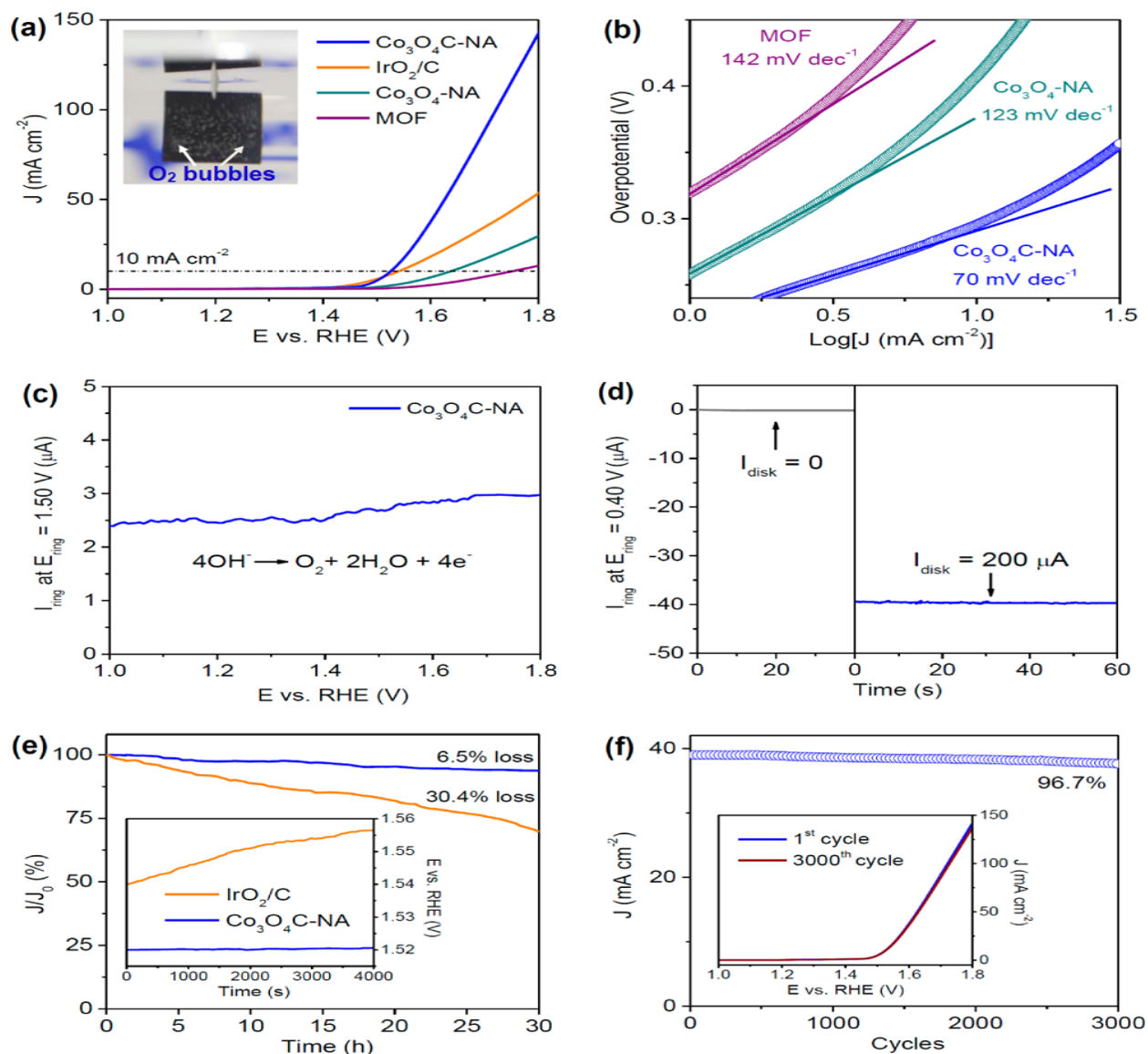


Figure 19 (a) Polarization curves. (b) Tafel plots of hybrid $\text{Co}_3\text{O}_4\text{C}$ nanowires, IrO_2/C , $\text{Co}_3\text{O}_4\text{C-NA}$, and the MOF in an O_2 -saturated 0.1 M KOH solution (scan rate 0.5 mV s⁻¹). (c) Ring current of hybrid $\text{Co}_3\text{O}_4\text{C}$ nanowires on an RRDE (1500 rpm) in O_2 -saturated 0.1 M KOH solution (ring potential 1.50 V). (d) Ring current of hybrid $\text{Co}_3\text{O}_4\text{C}$ nanowires on an RRDE (1500 rpm) in N_2 -saturated 0.1 M KOH solution (e) Chronoamperometric response at a constant potential of 1.52 V ($E_j=10$). Inset in (e): chronopotentiometric response at a constant current density of 10.0 mA cm⁻² of $\text{Co}_3\text{O}_4\text{C}$ nanowires in comparison to that of IrO_2/C . (f) Plot of the current density at 1.60 V recorded from the polarization curve of hybrid $\text{Co}_3\text{O}_4\text{C}$ nanowires vs the cycle number. (Reprinted with permission from [57]).

The XRD pattern of the catalyst after a 30 h reaction reveals no phase change in comparison to the fresh $\text{Co}_3\text{O}_4/\text{C}$ nano wires. This is indicative that the hybrid $\text{Co}_3\text{O}_4/\text{C}$ nanowire arrays are highly OER active and stable catalysts.

Moreover to probe the OER mechanism, a rotating ring disk electrode (RRDE) was constructed consisting of glossy carbon disc electrode and Pt ring electrode. During the experiment, hybrid $\text{Co}_3\text{O}_4/\text{C}$ nanowires is scrapped off from Cu foil, ultrasonically dispersed in water and isopropanol. Then they were coated onto RRDE using nafion binder. A scan rate of 0.5mV/s and rotation speed of 1500 rpm was applied for RRDE tests. To determine the OER mechanism, a constant ring potential of 1.50 V vs. RHE was applied specifically for formation of HO_2^- and further oxidation HO_2^- intermediates in O_2 saturated 0.1KOH at the surface. To calculate Faradaic efficiency of the system, the ring potential was held constant at 0.40V vs. RHE to decrease the O_2 evolution from the catalyst on the disk electrode in N_2 saturated 0.1M KOH solution. Figure 20 displays a continuous “OER (disk electrode) \rightarrow ORR (ring electrode) process”.

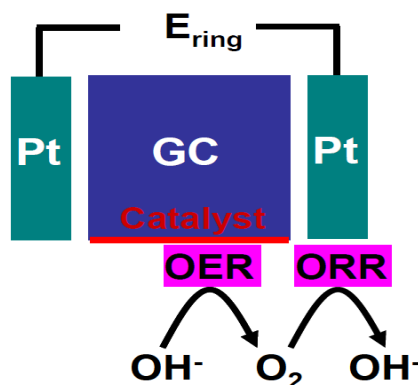


Figure 20 Schematic representation of the continuous OER (disk electrode) \rightarrow ORR (ring electrode) process initiated on a RRDE. (Reprinted with permission from [57]).

The Faradaic efficiency (ϵ) was calculated using formula,

$$\epsilon = I_r / (I_d N) \quad (5)$$

Where I_d is disk current, I_r is ring current and N is current collection efficiency of the RRDE. Figure 19 (c) shows ring current detected is $\sim 3\mu\text{A}$ which is of three order lower in magnitude (scale = mA) with H_2O_2 formation. This leads to the conclusion that the developed current originates only from water oxidation via four electron transfer

mechanism i.e. $4\text{OH}^- \rightarrow \text{O}_2$ and H_2O with generation of four electrons. In order to know faradaic efficiency ring current was plotted as shown in Figure 19 (d). The measured ring current is $\sim 3.9\mu\text{A}$ is indicative of oxidation current catalysed by hybrid $\text{Co}_3\text{O}_4\text{C}$ nanowires can be fully attributed to OER with Faradaic efficiency of 99.3%. In Figure 19 (e) the chronoamperometric response was studied to know stability. It revealed high stability with anodic current attenuation of 6.5% within 10h whereas IrO_2/C displays 4.7 times larger current attenuation of 30.4%. It has advantage over post coated catalyst. It does not peel off in evolution of Oxygen gas. The 3.3% anodic current loss is observed after 3000 continuous potential cycles (scan rate 100mV/s). So hybrid $\text{Co}_3\text{O}_4\text{C}$ nanowires are stable catalyst Figure 19 (f).

For practical application, the effective operation of hybrid $\text{Co}_3\text{O}_4\text{C}$ nanowires electrocatalyst was studied in concentrated electrolyte, 4M KCl. For this purpose, OER measurements were performed in a three-electrode glass cell. As synthesized nanowire arrays grown on Cu foil were directly used as the working electrode for electrochemical characterizations. The reference electrode was Ag/AgCl and the counter electrode was a platinum wire. The current density was normalized to the geometrical surface area and the measured potentials vs. Ag/AgCl were converted to a reversible hydrogen electrode (RHE) scale according to, Nernst equation as,

$$E_{\text{RHE}} = E_{\text{Ag/AgCl}} + 0.059 \times \text{pH} + 0.205 \quad (6)$$

A flow of O_2 was maintained over the electrolyte (0.1 M or 1M KOH) during electrochemical measurements in order to ensure the $\text{O}_2/\text{H}_2\text{O}$ equilibrium at 1.23 V vs. RHE. The polarization curves were recorded with the scan rate of 0.5mVs^{-1} . The working electrodes were scanned for several times until the signals were stabilized. The onset potentials were determined based on the beginning of the linear region in Tafel plots. The over potential was calculated as follows: (Provided $\text{O}_2/\text{H}_2\text{O}$ equilibrium at 1.23 V vs. RHE)

$$\eta = E (\text{vs. RHE}) - 1.23 \quad (7)$$

Electrochemical impedance spectrum (EIS) of hybrid $\text{Co}_3\text{O}_4\text{C}$ nanowires from Figure 21(a) shows a larger semi-circular diameter in low frequency region. This is attributed to smaller contact and charge transfer impedance of hybrid $\text{Co}_3\text{O}_4\text{C}$ nanowires. In 1M KOH, the high activity of hybrid $\text{Co}_3\text{O}_4\text{C}$ nanowires is well preserved showing a large current density and lower Tafel slope of 61mV/decade as shown in Figure 21(b) (in comparison

with 87 mV/decade of IrO_2/C) indicating the superior reaction kinetics of hybrid $\text{Co}_3\text{O}_4\text{C}$ nanowires.

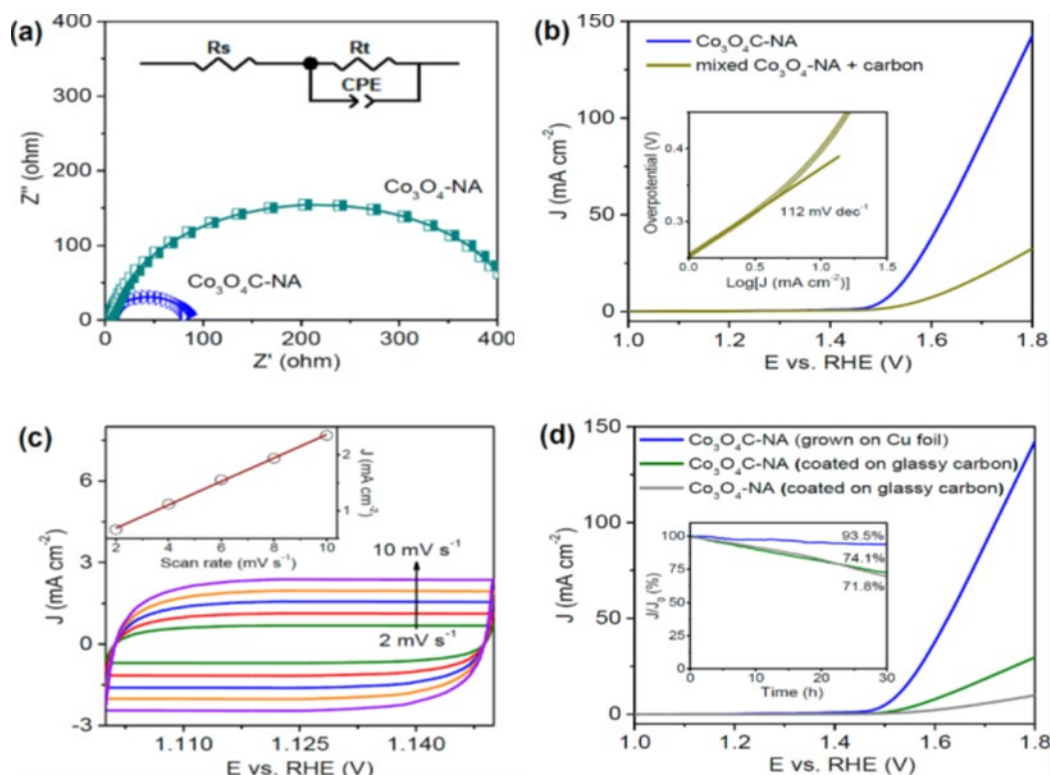


Figure 21 (a) EIS of hybrid $\text{Co}_3\text{O}_4\text{C}$ nanowires and hybrid $\text{Co}_3\text{O}_4\text{C}$ nanowires recorded at 1.60 V. (b) Polarization curves of hybrid $\text{Co}_3\text{O}_4\text{C}$ nanowires directly grown on Cu foil and physically mixed hybrid $\text{Co}_3\text{O}_4\text{C}$ nanowires and carbon powder coated on Cu foil. (c) Cyclic voltammograms (CVs) of hybrid $\text{Co}_3\text{O}_4\text{C}$ nanowires measured at different scan rates from 2 to 10 mV s^{-1} . (d) Polarization curves of hybrid $\text{Co}_3\text{O}_4\text{C}$ nanowires directly grown on Cu foil and hybrid $\text{Co}_3\text{O}_4\text{C}$ nanowires and hybrid $\text{Co}_3\text{O}_4\text{C}$ nanowires scraped off from Cu foil and coated on glassy-carbon electrodes. (Reprinted with permission from [57]).

In order to study rechargeable metal-air batteries, the reaction reversibility during oxygen evolution is significantly important. For this a polarization curve is recorded for the whole region of OER and ORR. It is shown in Figure 21 (d)

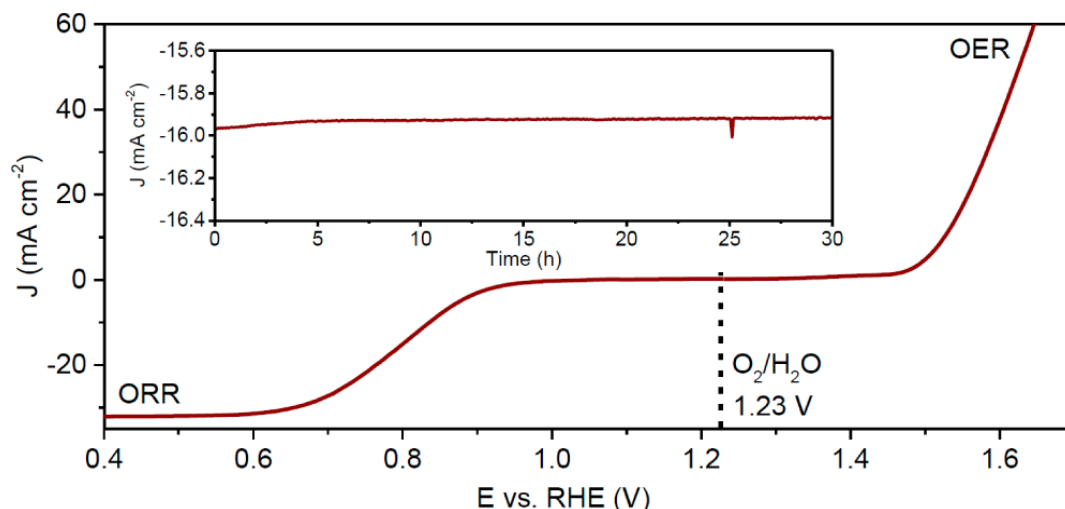


Figure 22 Polarization curve measured in O_2 -saturated 0.1 M KOH solution (scan rate 0.5 mV s^{-1}) for hybrid Co_3O_4C nanowires grown on Cu foil (directly used as the working electrode) in the whole region of OER and ORR. (Reprinted with permission from [70]).

The reversibility of OER \rightarrow ORR process was calculated by plotting polarization curve as shown in Figure 22. It exhibits a half wave potential ($E_{1/2}$) of 0.78V and Tafel slope of 89 mV. The overall electrode activity i.e. the difference between OER and ORR metrics ($\Delta E = E_{j=10} - E_{1/2}$) is obtained as 0.74V which is lower as compared with earlier reported electrodes, indicating that the hybrid Co_3O_4C nanowires is having an excellent reversible oxygen electrode nature. Further the electron transfer number is calculated from RRDE and reversible OER \rightarrow ORR process. An electron transfer number of 3.85–3.96 was confirmed in the potential range of 0.40 to 0.90V, showing the four-electron ORR pathway with few peroxide intermediates.

In a summary, The MOF hybrid Co_3O_4C nanowires directly grown on Cu foil possess higher OER activity with favourable kinetics and stronger durability as compared to reported electrocatalyst. The porous nature of hybrid Co_3O_4C nanowires electrode with in situ configuration with carbon leads to enlarge active surface area, strong structural durability with improve mass/ charge transport. The reversibility in OER \rightarrow ORR process an efficient four-electron pathway, hybrid Co_3O_4C nanowires are new reversible oxygen electrodes and are promising for direct use in metal–air batteries, fuel cells, water-splitting devices, and other key renewable energy systems.

Conclusion

The chapter is focused on two MOF of $(\text{Ni}_3(\text{HITP})_2$ that is $\text{Ni}_3(2,3,6,7,10,11\text{-hexaiminotriphenylene})_2$, and hybrid $\text{Co}_3\text{O}_4\text{C}$ nanowires. Their application study of $(\text{Ni}_3(\text{HITP})_2$ is dedicated to energy storage and that of hybrid $\text{Co}_3\text{O}_4\text{C}$ as an electro-catalyst to oxygen evolution reaction. Herein, Part-I discussed energy storage and Part-II of the chapter focuses on the OER study. The $(\text{Ni}_3(\text{HITP})_2$ based MOF device shows high aerial capacitance than that of most carbon-based materials with capacity retention greater than 90% over 10,000 cycles, in line with commercial devices. The established results for structural and compositional tunability of $\text{Ni}_3(\text{HITP})_2$ helps to design and synthesize the electrode material for the new generation of supercapacitors at the molecular level. The MOF based on $\text{Co}_3\text{O}_4\text{C}$ is nanowire array and in situ carbon incorporation is carried out. The electrode configuration possesses an active surface area, enhanced mass/charge transport capability, easy release of oxygen gas bubbles, and strong structural stability. Furthermore, the hybrid $\text{Co}_3\text{O}_4\text{C}$ porous nanowire arrays can efficiently catalyse oxygen reduction reaction. It is potentially useful for rechargeable metal-air batteries, regenerative fuel cells, and other important clean energy devices.

References

- [1] S. Chu, A. Majumdar, Opportunities and challenges for a sustainable energy future, *Nature* (2012), 488, 294-303. <https://doi.org/10.1038/nature11475>
- [2] U.S. Energy Information Administration, 2016.
- [3] World Energy Outlook 2015” (International Energy Agency, 2015). 4. “The Outlook for Energy: A View to 2040” (Exxon Mobil Corporation, 2015).
- [4] Lee, R. The outlook for population growth, *Science* (2011) 333, 569–573. <https://doi.org/10.1126/science.1208859>
- [5] Katsounaros, I., Cherevko, S., Zeradjanin, A. R., Mayrhofer, K. J. J. Dissolution of Platinum in the Operational Range of Fuel Cells. *Angew. Chem.*, (2014) 126, 104–124. <https://doi.org/10.1002/ange.201306588>.
- [6] D. Kim, K. K. Sakimoto, D. Hong, P. Yang, Artificial photosynthesis for sustainable fuel and chemical production, *Angew. Chem. Int. Ed.* (2015), 54, 3259-3266. <https://doi.org/10.1002/anie.201409116>
- [7] A. Tatin, J. Bonin, M. Robert, A Case for Electro fuels, *ACS Energy Lett.* 2016, 1, 1062-1064. <https://doi.org/10.1021/acsenergylett.6b00510>

- [8] 10 Gonzalez A, Goikolea E, Barrena JA, et al. Review on supercapacitors: technologies and materials. *Renew Sustain Energy Rev* (2016) 58, 1189–1206. <https://doi.org/10.1016/j.rser.2015.12.249>
- [9] J. R. McKone, S. C. Marinescu, B. S. Brunschwig, J. R. Winkler, H. B. Gray, Earth-abundant hydrogen evolution electrocatalysts, *Chem. Sci.* (2014)5, 865-878. <https://doi.org/10.1039/C3SC51711J>
- [10] R. Parsons, The rate of electrolytic hydrogen evolution and the heat of adsorption of hydrogen. *Trans. Faraday Soc.* (1958) 54, 1053–1063. <https://doi.org/10.1039/tf9585401053>
- [11] W. Zhang, W. Lai, R. Cao, Energy-related small molecule activation reactions: Oxygen Reduction and Hydrogen and Oxygen Evolution Reactions Catalyzed by Porphyrin- and Corrole-Based Systems, *Chem. Rev.* (2017) 117, 3717-3797. <https://doi.org/10.1021/acs.chemrev.6b00299>
- [12] Furukawa H, Cordova KE, O’Keeffe M. The chemistry and applications of metal organic frameworks. *Science.* (2013) 341, 1230444. <https://doi.org/10.1126/science.1230444>
- [13] Sun L, Campbell MG, Dincă M. Electrically conductive porous metal-organic frameworks. *Angew Chem Int Ed*, 2016, 55: 3566– 3579. <https://doi.org/10.1002/anie.201506219>
- [14] Georges Chedid and Ali Yassin, Recent Trends in Covalent and Metal Organic Frameworks for Biomedical Applications, *Nanomaterials* 2018, 8, 916. <https://doi.org/10.3390/nano8110916>
- [15] Hailong Wang, Qi-Long Zhu, Ruqiang Zou, and Qiang Xu, Metal-Organic Frameworks for Energy Applications, *Chem* (2017) 2, 52–80. <https://doi.org/10.1016/j.chempr.2016.12.002>
- [16] Ozkan S, Nguyen NT, Hwang I, et al. Highly conducting spaced TiO₂ nanotubes enable defined conformal coating with nanocrystalline Nb₂O₅ and high performance supercapacitor applications, *Small*, (2017) 13, 1603821. <https://doi.org/10.1002/sml.201603821>
- [17] Shi P, Li L, Hua L, et al. Design of amorphous manganese oxide@ multiwalled carbon nanotube fiber for robust solid-state supercapacitor. *ACS Nano*, (2017) 11, 444–452. <https://doi.org/10.1021/acsnano.6b06357>

- [18] Wang S, Liu N, Su J, et al. Highly stretchable and self-healable supercapacitor with reduced graphene oxide based fiber springs. *ACS Nano*, (2017) 11, 2066–2074. <https://doi.org/10.1021/acsnano.6b08262>
- [19] Gonzalez-Gaitan C, Ruiz-Rosas R, Nishihara H, et al. Successful functionalization of superporous zeolite templated carbon using aminobenzene acids and electrochemical methods. *Carbon*, (2016) 99, 157–166. <https://doi.org/10.1016/j.carbon.2015.12.006>
- [20] Li X, Zhao Y, Bai Y, et al. A non-woven network of porous nitrogen-doping carbon nanofibers as a binder-free electrode for supercapacitors. *Electrochim Acta*, (2017) 230, 445–453. <https://doi.org/10.1016/j.electacta.2017.02.030>
- [21] Dong L, Xu C, Li Y, et al. Flexible electrodes and supercapacitors for wearable energy storage: a review by category. *J Mater Chem A*, (2016) 4, 4659–4685. <https://doi.org/10.1039/C5TA10582J>
- [22] Huang C, Zhang J, Young NP, et al. Solid-state supercapacitors with rationally designed heterogeneous electrodes fabricated by large area spray processing for wearable energy storage applications. *Sci Rep*, (2016) 6, 25684. <https://doi.org/10.1038/srep25684>
- [23] Wang Y, Shi Z, Huang Y, et al. Supercapacitor devices based on graphene materials. *J Phys Chem C*, 2009, 113: 13103–13107. <https://doi.org/10.1021/jp902214f>
- [24] Ma W, Chen S, Yang S, et al. Hierarchical MnO₂ nanowire/graphene hybrid fibers with excellent electrochemical performance for flexible solid-state supercapacitors. *J Power Sources* (2016) 306, 481–488. <https://doi.org/10.1016/j.jpowsour.2015.12.063>
- [25] Wang D, Fang G, Xue T, et al. A melt route for the synthesis of activated carbon derived from carton box for high performance symmetric supercapacitor applications. *J Power Sources*, (2016) 307, 401–409. <https://doi.org/10.1016/j.jpowsour.2016.01.009>
- [26] Wu S, Zhu Y. Highly densified carbon electrode materials towards practical supercapacitor devices. *Sci China Mater*, (2017) 60, 25–38. <https://doi.org/10.1007/s40843-016-5109-4>
- [27] Sahu V, Shekhar S, Sharma RK, et al. Ultrahigh performance supercapacitor from lacey reduced graphene oxide nanoribbons, *ACS Appl Mater Interfaces* (2015) 7, 3110–3116. <https://doi.org/10.1021/am5071706>

- [28] Wang JG, Kang F, Wei B. Engineering of MnO₂-based nanocomposites for high-performance supercapacitors. *Prog Mater Sci*, (2015) 74, 51–124.
<https://doi.org/10.1016/j.pmatsci.2015.04.003>
- [29] Dhawale DS, Kim S, Park DH, et al. Hierarchically ordered porous CoOOH thin-film electrodes for high-performance supercapacitors. *Chem Electro Chem*, (2015) 2, 497–502. <https://doi.org/10.1002/celec.201402365>
- [30] Wang R, Luo Y, Chen Z, et al. The effect of loading density of nickel-cobalt sulfide arrays on their cyclic stability and rate performance for supercapacitors. *Sci China Mater*, (2016) 59, 629–638. <https://doi.org/10.1007/s40843-016-5074-y>
- [31] Choi KM, Jeong HM, Park JH, et al. Supercapacitors of nanocrystalline metal-organic frameworks. *ACS Nano*, (2014) 8, 7451–7457.
<https://doi.org/10.1021/nn5027092>
- [32] Sun L, Campbell MG, Dincă M. Electrically conductive porous metal-organic frameworks. *Angew Chem Int Ed*, (2016) 55, 3566– 3579.
<https://doi.org/10.1002/anie.201506219>
- [33] Zhang YZ, Cheng T, Wang Y, et al. A simple approach to boost capacitance: flexible supercapacitors based on manganese oxides@ MOFs via chemically induced in situ self-transformation. *Adv Mater*, (2016) 28, 5242–5248.
<https://doi.org/10.1002/adma.201600319>
- [34] Guan C, Zhao W, Hu Y, et al. Cobalt oxide and N-doped carbon nanosheets derived from a single two-dimensional metal-organic framework precursor and their application in flexible asymmetric supercapacitors. *Nanoscale Horiz*, (2017) 2, 99–105. <https://doi.org/10.1039/C6NH00224B>
- [35] Lee DY, Yoon SJ, Shrestha NK, et al. Unusual energy storage and charge retention in Co-based metal-organic-frameworks. *Micropor Mesopor Mater*, (2012) 153, 163–165. <https://doi.org/10.1016/j.micromeso.2011.12.040>
- [36] Yang J, Xiong P, Zheng C, et al. Metal-organic frameworks: a new promising class of materials for a high performance supercapacitor electrode. *J Mater Chem A*, (2014) 2, 16640–16644. <https://doi.org/10.1039/C4TA04140B>
- [37] Worrall SD, Mann H, Rogers A, et al. Electrochemical deposition of zeolitic imidazolate framework electrode coatings for supercapacitor electrodes. *Electrochim Acta*, (2016) 197, 228–240. <https://doi.org/10.1016/j.electacta.2016.02.145>

- [38] Jeon JW, Sharma R, Meduri P, et al. In situ one-step synthesis of hierarchical nitrogen-doped porous carbon for high-performance supercapacitors. *ACS Appl Mater Interfaces*, (2014) 6, 7214–7222. <https://doi.org/10.1021/am500339x>
- [39] Hao F, Li L, Zhang X, et al. Synthesis and electrochemical capacitive properties of nitrogen-doped porous carbon micropolyhedra by direct carbonization of zeolitic imidazolate framework-11. *Mater Res Bull*, (2015) 66, 88–95. <https://doi.org/10.1016/j.materresbull.2015.02.028>
- [40] Yu M, Zhang L, He X, et al. 3D interconnected porous carbons from MOF-5 for supercapacitors. *Mater Lett*, (2016) 172, 81–84. <https://doi.org/10.1016/j.matlet.2016.02.144>
- [41] Mahmood A, Zou R, Wang Q, et al. Nanostructured electrode materials derived from metal-organic framework xerogels for high-energy-density asymmetric supercapacitor. *ACS Appl Mater Interfaces*, (2016) 8, 2148–2157. <https://doi.org/10.1021/acsami.5b10725>
- [42] Liu X, Shi C, Zhai C, et al. Cobalt-based layered metal-organic framework as an ultrahigh capacity supercapacitor electrode material. *ACS Appl Mater Interfaces*, (2016) 8, 4585–4591. <https://doi.org/10.1021/acsami.5b10781>
- [43] Meng F, Fang Z, Li Z, et al. Porous Co_3O_4 materials prepared by solid-state thermolysis of a novel Co-MOF crystal and their superior energy storage performances for supercapacitors. *J Mater Chem A*, (2013) 1, 7235–7241. <https://doi.org/10.1039/c3ta11054k>
- [44] Maiti S, Pramanik A, Mahanty S. Extraordinarily high pseudocapacitance of metal organic framework derived nanostructured cerium oxide. *Chem Commun*, (2014) 50, 11717–11720. <https://doi.org/10.1039/c3ta11054k>
- [45] Salunkhe RR, Tang J, Kamachi Y, et al. Asymmetric supercapacitors using 3D nanoporous carbon and cobalt oxide electrode synthesized from a single metal-organic framework. *ACS Nano*, (2015) 9, 6288–6296. <https://doi.org/10.1021/acs.nano.5b01790>
- [46] Sheberla D, Bachman JC, Elias JS, et al. Conductive MOF electrodes for stable supercapacitors with high areal capacitance. *Nat Mater*, (2016) 16, 220–224. <https://doi.org/10.1038/nmat4766>
- [47] Courtney A. Downes, Smaranda C. Marinescu, Electrocatalytic Metal-Organic Frameworks for Energy Applications, *Chem sus chem*, (2017) 10, 4374-4392. <https://doi.org/10.1002/cssc.201701420>

- [48] D.-Y. Du, J.-S. Qin, S.-L. Li, Z.-M. Su, Y.-Q. Lan, Recent advances in porous polyoxometalate-based metal-organic framework materials. *Chem. Soc. Rev.* (2014) 43, 4615-4632. <https://doi.org/10.1039/C3CS60404G>
- [49] L. Wang, Y. Wu, R. Cao, L. Ren, M. Chen, X. Feng, J. Zhou, B. Wang, Fe/Ni metal-organic frameworks and their binder-free thin films for efficient oxygen evolution with low over potential. *ACS Appl. Mater. Interfaces*, (2016) 8, 16736-16743. <https://doi.org/10.1021/acsami.6b05375>
- [50] X.-F. Lu, P.-Q. Liao, J.-W. Wang, J.-X. Wu, X.-W. Chen, C.-T. He, J.-P. Zhang, G.-R. Li, X.-M. An Alkaline-Stable, Metal Hydroxide Mimicking Metal-Organic Framework for Efficient Electrocatalytic Oxygen Evolution. *Chen, J. Am. Chem. Soc.*, (2016) 138, 8336-8339. <https://doi.org/10.1021/jacs.6b03125>
- [51] M. Jiang, L. Li, D. Zhu, H. Zhang, X. Zhao, Oxygen reduction in the nanocage of metal-organic frameworks with an electron transfer mediator *J. Mater. Chem. A*, (2014) 2, 5323-5329. <https://doi.org/10.1039/C3TA15319C>
- [52] J.-Q. Shen, P.-Q. Liao, D.-D. Zhou, C.-T. He, J.-X. Wu, W.-X. Zhang, J.-P. Zhang, X.-M. Modular and Stepwise Synthesis of a Hybrid Metal-Organic Framework for Efficient Electrocatalytic Oxygen Evolution. *Chen, J. Am. Chem. Soc.* (2017) 139, 1778-1781. <https://doi.org/10.1021/jacs.6b12353>
- [53] P. M. Usov, S. R. Ahrenholtz, W. A. Maza, B. Stratakes, C. C. Epley, M. C. Kessinger, J. Zhu, A. J. Morris, Cooperative electrochemical water oxidation by Zr nodes and Ni-porphyrin linkers of a PCN-224 MOF thin film, *J. Mater. Chem. A*, (2016) 4, 16818-16823. <https://doi.org/10.1039/C6TA05877A>
- [54] F. Dai, W. Fan, J. Bi, P. Jiang, D. Liu, X. Zhang, H. Lin, C. Gong, R. Wang, L. Zhang, D. Sun, A lead-porphyrin metal-organic framework: gas adsorption properties and electrocatalytic activity for water oxidation, *Dalton. Trans.* (2016) 45, 61-65. <https://doi.org/10.1039/C5DT04025F>
- [55] Dennis Sheberla, Lei Sun, Martin A. Blood-Forsythe, Suleyman Er, Casey R. Wade, Carl K. Brozek, Alan Aspuru-Guzik, and Mircea Dinca, High electrical conductivity in $\text{Ni}_3(2,3,6,7,10,11\text{-hexaiminotriphenylene})_2$, a semiconducting metal-organic graphene analogue, *J. Am. Chem. Soc.*, (2014) 136 (25), 8859-8862. <https://doi.org/10.1021/ja502765n>
- [56] Dennis Sheberla, John C. Bachman, Joseph S. Elias, Cheng-Jun Sun, Yang Shao-Horn and Mircea Dinca, Conductive MOF electrodes for stable supercapacitors with high areal capacitance, *Nature materials*, (2017) 6, 220-225. <https://doi.org/10.1038/nmat4766>

- [57] Tian Yi Ma, Sheng Dai, Mietek Jaroniec, and Shi Zhang Qiao, Metal Organic Framework derived hybrid Co_3O_4 -Carbon porous nanowire arrays as reversible oxygen evolution electrodes, *J. Am. Chem. Soc.* (2014) 136, 13925–13931.
<https://doi.org/10.1021/ja5082553>
- [58] Ronald Chwang, B. J. Smith, C.R.Crowell, Contact size effects on the van der Pauw method for resistivity and Hall coefficient measurement, *Solid state electronics* (1974) 17, 1217-1312. [https://doi.org/10.1016/0038-1101\(74\)90001-X](https://doi.org/10.1016/0038-1101(74)90001-X)
- [59] Chmiola, J. et al. Anomalous increase in carbon capacitance at pore sizes less than 1 nanometer. *Science* (2006) 313, 1760-1763. <https://doi.org/10.1126/science.1132195>
- [60] Miner, E. M. et al. Electrochemical oxygen reduction catalysed by $\text{Ni}_3(\text{hexaiminotriphenylene})_2$. *Nat. Commun.* (2016) 7, 10942.
<https://doi.org/10.1038/ncomms10942>
- [61] Gogotsi, Y. & Simon, P. True performance metrics in electrochemical energy storage. *Science*, (2011) 334, 917- 918. <https://doi.org/10.1126/science.1213003>
- [62] Xu, Y. et al. Holey graphene frameworks for highly efficient capacitive energy storage. *Nat. Commun.* (2014) 5, 4554. <https://doi.org/10.1038/ncomms5554>
- [63] Taberna, P. L., Portet, C. & Simon, P. Electrode surface treatment and electrochemical impedance spectroscopy study on carbon/carbon supercapacitors. *Appl. Phys. A* (2006) 82, 639- 646. <https://doi.org/10.1007/s00339-005-3404-0>
- [64] Zhang Q, Chen H, Wang J, Xu D, Li X, Yang Y, Zhang K, Growth of hierarchical 3D mesoporous $\text{NiSi}_x/\text{NiCo}_2\text{O}_4$ Core/Shell Hetero structures on Nickel Foam for Lithium-Ion Batteries, *ChemSusChem* (2014) 7(8), 2325–2334.
<https://doi.org/10.1002/cssc.201402039>
- [65] Li, Y. G.; Wang, H. L.; Liang, Y. Y.; Wu, J. Z.; Zhou, J. G.; Wang, J.; Regier, T.; Wei, F.; Dai, H. J. An advanced Ni-Fe layered double hydroxide electrocatalyst for water oxidation, *J. Am. Chem. Soc.* (2013) 135, 8452–8455.
<https://doi.org/10.1021/ja4027715>
- [66] Jin, K.; Park, J.; Lee, J.; Yang, K. D.; Pradhan, G. K.; Sim, U.; Jeong, D.; Jang, H. L.; Park, S.; Kim, D.; Sung, N. E.; Kim, S. H.; Han, S.; Nam, K. T. Hydrated manganese(II) phosphate $(\text{Mn}_3(\text{PO}_4)_2 \cdot 3\text{H}_2\text{O})$ as a water oxidation catalyst. *J. Am. Chem. Soc.* (2014) 136, 7435–7443. <https://doi.org/10.1021/ja5026529>
- [67] Wang, J., Zhong, H. X., Qin, Y. L., Zhang, X. B. An efficient three-dimensional oxygen evolution electrode. *Angew. Chem.*, (2013) 125, 5356–5361.
<https://doi.org/10.1002/ange.201301066>

- [68] Wang D, Chen X, Evans DG. Well-dispersed $\text{Co}_3\text{O}_4/\text{Co}_2\text{MnO}_4$ nanocomposites as a synergistic bifunctional catalyst for oxygen reduction and oxygen evolution reactions, *Nanoscale*. (2013) 5, 5312-5315. <https://doi.org/10.1039/c3nr00444a>
- [69] Gong M, Zhou W, Tsai MC. Nanoscale nickel oxide/nickel heterostructures for active hydrogen evolution electrocatalysis. *Nature Communications*. (2014) 5, 1-6. <https://doi.org/10.1038/ncomms5695>
- [70] Y. Liang, Y. G. Li, H. L. Wang, J. G. Zhou, J. Wang, T. Regier, H. J. Dai, Co_3O_4 nanocrystals on graphene as a synergistic catalyst for oxygen reduction reaction. *Nat. Mater.* (2011) 10, 780–786. <https://doi.org/10.1038/nmat3087>
- [71] M. R. Gao, Y. F. Xu, J. Jiang, Y. R. Zheng, S. H. Yu, Water oxidation electrocatalyzed by an efficient $\text{Mn}_3\text{O}_4/\text{CoSe}_2$ nanocomposite, *J. Am. Chem. Soc.*(2012) 134, 2930–2933. <https://doi.org/10.1021/ja211526y>
- [72] X. Liu, Z. Chang, L. Luo, T. Xu, X. Lei, J. Liu, X. Sun, Non-precious cobalt oxalate microstructures as highly efficient electrocatalysts for oxygen evolution reaction. *Chem. Mater. A* (2014) 26, 1889–1895.
- [73] Y. Li, P. Hasin, Y. Wu, $\text{Ni}_x\text{Co}_{(3-x)}\text{O}_{(4)}$ nanowire arrays for electrocatalytic oxygen evolution. *Adv. Mater.* (2010) 22, 1926–1929. <https://doi.org/10.1002/adma.200903896>
- [74] B. Lu, D. Cao, P. Wang, G. Wang, Y. Gao, Oxygen evolution reaction on Ni-substituted Co_3O_4 nanowire array electrodes. *Int. J. Hydrogen Energy* (2011) 36, 72–78. <https://doi.org/10.1016/j.ijhydene.2010.09.056>
- [75] Y. Zhao, R. Nakamura, K. Kamiya, S. Nakanishi, K. Has himoto, Nitrogen-doped carbon nanomaterials as non-metal electrocatalysts for water oxidation. *Nat. Commun.* (2013) 4, 2390. <https://doi.org/10.1038/ncomms3390>

Chapter 8

Metal-Organic-Framework Composites as Proficient Cathodes for Supercapacitor Applications

Wei Ni^{1*}, Lingying Shi^{2*}

¹Panzhuhua University, Panzhuhua 617000, China

²College of Polymer Science and Engineering, State Key Laboratory of Polymer Materials Engineering, Sichuan University, Chengdu 610065, China

* niwei@iccas.ac.cn (W. Ni), shilingying@scu.edu.cn (L.Y. Shi)

Abstract

Metal-organic frameworks (MOFs) have garnered significant interest over the past two decades for next-generation electrochemical energy storage applications, especially for supercapacitors that combine the two features of high energy density of batteries and high power density of capacitors, owing to their high specific surface areas, controllable structures, and adjustable pore sizes. Herein we timely and comprehensively reviewed the impressive advancements achieved in recent years on MOFs and their composites for promising electrochemical capacitors (including supercapacitors, asymmetric supercapacitors and hybrid supercapacitors). The challenges and opportunities are also proposed for new breakthroughs in further development of MOF-based supercapacitors for ultimate practical applications.

Keywords

Metal-Organic Frameworks (MOFs), Composite, Supercapacitor, Hybrid Capacitor, Cathode

Contents

1. Introduction.....	178
2. MOFs: Structure, properties and strategies for SCs	179
3. Single-metal MOFs	182
4. Bimetal or doped MOFs.....	191
5. Hybrids and composites	195

6. Flexible or freestanding SCs.....	204
Conclusion and Perspectives.....	215
Acknowledgements.....	216
References	217

1. Introduction

To void the environmental pollution and forthcoming energy crisis, the application of clean and sustainable energy instead of fossil fuel has attracted huge attention. It is of great urgency and importance to develop various energy conversion and storage technologies and materials aimed at utilization of various clean energy sources [1-3]. Supercapacitors (SCs), or called electrochemical capacitors, are a new-type of energy storage equipment between rechargeable batteries and conventional capacitors, i.e., keeping the advantages of both high energy density and high power density as well as long-term cycling stability [4-8]. Notably, many significant breakthroughs for a new generation of supercapacitors have been reported in last years, related to theoretical understanding, material synthesis and device designs, e.g., microsupercapacitors (MSCs), flexible SCs, hybrid supercapacitors (HSCs) to bridge the performance gap between batteries, conventional supercapacitors and wearable electronics [5, 9-12]. Metal-organic frameworks (MOFs), as a new class of intrinsically porous inorganic-organic hybrid crystalline materials with well-defined structures, are acting as a superior candidate in this field in recent years based on their high surface area, controllable pore size and structures/topologies (based on versatile precursors with unrivalled degree of tunability and varied functionalities as well as systematic assembly/shaping techniques) and excellent electrochemical performances for next-generation electrochemical energy-storage (EES) devices [1, 4, 13-28]. Theoretically, MOFs can be excellent electrode materials due to their unique structures; more and more pioneering works based on pristine MOFs, so far, have been reported and there is an increasing trend of utilizing these MOFs as ideal supercapacitor electrodes [19, 29-31]. The direct utilization of pristine MOFs as a supercapacitor-active material is very promising, because the bare MOFs can offer more pseudocapacitive redox centers and a porous skeleton, facilitating fast ion diffusion; furthermore, the direct approach can provide more candidates for supercapacitor electrode materials [24, 32, 33].

Herein, significant advances in the recent development of MOFs for next-generation high-power clean energy applications are selectively reviewed, with special emphases shown to the applications of MOFs as platforms for emerging advanced supercapacitors.

Firstly, fundamental understanding of the mechanism is focused on the relationship between the structure, composition of MOFs-based electrode materials and their electrochemical performances. Secondly, some emerging electrode materials of MOFs are discussed, including single-metal, bimetal or doped MOFs, conductive MOFs, MOF-based hybrids/composites as well as their promising applications in supercapacitors, hybrid supercapacitors, and flexible/wearable supercapacitors. Finally, the future developments and key technical challenges are highlighted and discussed for further research in this thriving field.

2. MOFs: Structure, properties and strategies for SCs

Metal-organic frameworks (MOFs), also known as porous coordination polymers (PCPs), are a kind of crystalline materials formed via self-assembly of inorganic metal ions (or clusters) and organic ligands connected by coordination interactions; typically, transition-metal based MOFs show excellent electrochemical properties and have attracted wide research interest for use in next-generation EES systems especially for supercapacitors or hybrid capacitors [4, 15, 16, 34]. The capacitance of pristine MOFs comes from the redox reaction of center metal ions and the electrochemical double-layer capacitance (EDLC) on the large internal surface area [9, 35]. The extremely high porosity and openness as well as low density of MOFs structure would give high capacity for storage and robust cycling of ions, which shall make them a key role in high-performance electrochemical energy storage [15]. Moreover, nano-MOFs with tailorable size and morphology represent a new direction for conventional pristine MOFs [15, 17, 36-40].

The combination of the highly porous structure, structural tailorability and chemical versatility of MOFs, along with the low cost and availability for mass production, has provided plenty of opportunities for the preparation of MOFs and their composites [24, 30, 41]. As a new type of electrode material recently directly used in supercapacitors, studies on MOFs for such applications are emerging and more challenging [13, 42]. These MOFs suited for electrochemical supercapacitors, i.e., with enhanced conductivities (typical strategies are schematically shown in Fig. 1) [43], include single-transition-metal (e.g., Co- [44-59], Ni- [10, 60-74], Mn- [75], Zr-[76-79], Fe- [80, 81], In- [82], Zn- [83-85], Cd- [83], Cu- [59, 86-91], V- [92]; typical samples and their SCs performance are listed in Table 1), bimetallic or doped (e.g., Zn/Co- [93], Ni/Co- [94, 95], Zn-doped Ni- [96]) materials with varied structures/morphologies and the related hybrids/composites as well as flexible electrodes for extended applications [30, 43]. Besides, MOF-derived nanostructures or hybrids including carbonaceous materials and transition-metal oxides/chalcogenides are gaining momentum in electrochemical

conversion and storage field [4, 13, 14, 26, 34, 97-103], which will be referred to in detail in other chapters.

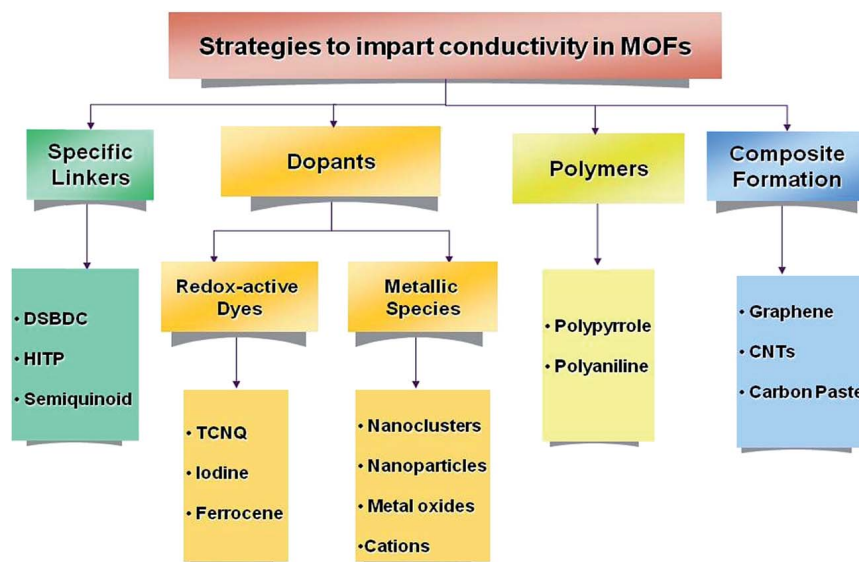


Figure 1 Flow diagram depicting different strategies for the development of conducting MOFs. Reprinted with permission from Ref. [43] Copyright 2018, The Royal Society of Chemistry.

Table 1. Typical single-metal MOF materials for supercapacitors. (abbr. 3-E, three-electrode; ML, mass loading; CD, current density; SR, scan rate; VR, voltage range; CR, capacitance retention; ED/PD, energy density/power density)

MOFs	Electrodes (ML [mg cm ⁻²])	CD (or SR) [A g ⁻¹] (VR) [V]	Capacitance [F g ⁻¹] (cycles, CR)	ED/PD [W h Kg ⁻¹ /W Kg ⁻¹]	Electrolyte	Refs.
MIL-100(Fe) <i>Fe(H₃BTC)</i>	3-E (vs MSE)	0.1 (-0.2 to 0.6)	58		0.1 M K ₂ SO ₄	[80]
Conductive Ni ₃ (HITP) ₂	SSC (7–13)	0.05/1 (0–1.0)	111/70 (18/11 μF cm ⁻²) (10000, >90%)		1 M TEABF ₄ /ACN	[107]
Conductive Ni-HAB MOFs	3-E (vs Ag/AgCl) (4)	1 mV s ⁻¹ (-0.75 to -0.25)	420 F g ⁻¹ (1.6 F cm ⁻²) (17 F cm ⁻² @65ML) (12000, 90%)		1 M KOH	[108]
		0.2 mV s ⁻¹ (-0.75 to -0.25)	760 F cm ⁻³ @9ML, (710@35ML, 460@65ML)			
Conductive Cu-HAB MOFs		1 mV s ⁻¹ (-0.55 to -0.1)	215 F g ⁻¹ 0.86 F cm ⁻²			

Pillared Ni-DMOF-ADC	3-E (vs Ag/AgCl) (1.9)	1/20/50 (0–0.45)	552/438/395		4 M KOH	[71]
	ASC (Ni-MOF//AC)	(0–1.5)	(16000, >98%)			
Co(TPA)	3-E (vs Ag/AgCl)	0.6 (0–0.5)	207 (1k, 98.5%)		1 M LiOH	[44]
[Co(HTATB)(dib)]·2H ₂ O	3-E (vs Hg/HgO) (0.4–0.6)	0.75/15	2405/1287 (3000, 93.5%; CE 92.2%)	83.5@187 44.7@3751	4 M KOH	[51]
Ni ₃ (btc) ₂ ·12H ₂ O	3-E (vs SCE)	1/5 (0–0.4)	726/314 (1k, 94.6%)		2 M KOH	[60]
	ASC (Ni-MOF//AC) (4/8)	0.25/1/5 (0.4–1.6)	86/66/49	16.5 Wh kg ⁻¹ (max)		
1D Ni-MOF nanorods (<i>salicylate ligand</i>)	3-E (vs Hg/HgO) (20)	1/2/5/10 (0–0.6)	1698/1385/1068/838 (1000, 94.8%)		6 M KOH	[62]
	ASC (Ni-MOF//graphene) (20//60)	1/3/5 (0–1.6)	166/142/119			
Spherical mesocrystal Ni-MOF (<i>assembled nanorods, folic acid ligand</i>)	3-E (vs Ag/AgCl) (1.5)	0.5/1/2/5/10 (0–0.45)	912/827/804/703/660 (2000, 89%)		1 M KOH	[110]
	ASC (Ni-MOF//AC)	1/2/5/10 (0–1.6)	78/67/54/51 (8000, 97.6%)	27.8@1001 18.0@9963		
2D Ni(PTA) [Ni ₃ (OH) ₂ (C ₈ H ₄ O ₄) ₂ (H ₂ O) ₄]·2H ₂ O	3-E (vs SCE) (5)	0.5/10 (0–0.35V)	1127/668 (3k, >90%)		6 M KOH	[61]
2D nanofakes of Ni-MOF assembly (<i>micro-sized particle</i>) (<i>ellagic acid ligand</i>)	3-E (vs Ag/AgCl)	0.5/1/2/5/10 (0–0.45)	1050/963/836/714/550 (1000, 89%)		1 M KOH	[72]
	ASC (Ni-MOF//AC)	1/2/5/10 (0–1.6)	88/79/68/58 (4000, 91.8%)	31.2@800 20.6@8017		
2D layered Ni-MOF	3-E (vs SCE)	1 (0–0.32)	123 (3000, 88.6%)		3 M KOH	[10]
		1/2/5/10	175/130/120/89 (3000, 93.0%)		3 M KOH + 0.1 M K ₄ Fe(CN) ₆	
	ASC (Ni-MOF//CNTs-COOH)	1/2/5/10 (0–1.4)	97/91/86/80 (3000, 90.6%)	55.8@7000		
Hierarchical porous Ni-MOF (flower-like; trimesic acid ligand)	3-E (vs SCE) (1.7)	1/30 (0–0.4)	1057/649 (2500, 70%)		3 M KOH	[111]
	ASC Ni-MOF//AC (1.7//2.4)	0.5/10 (0–1.4)	87/63	21.05@440 5.36@6030		

Layered structural Co-MOF nanosheets (PTA ligand)	3-E (vs SCE) (4–5)	1/20 (0–0.35)	2564/1164 (3000, 95.8%)		5 M KOH	[49]
Mn-LMOF $Mn(tfbdac)(bpy)(H_2O)_2$	3-E (vs SCE)	1/20 (0–0.5)	1098/396 (2000, 92.6%)		1 M KOH	[75]
		1/20 (0–0.5)	1178/424 (2000, 94.6%)		1 M LiOH	
Mesoporous In-MOF $In(BTTB)_{2/3}(OH)](NMF)_5(H_2O)_4$	3-E (vs SCE)	0.2/0.5/1/2/4/8 (–0.7 to 0.3)	150/92/81/72/64/56 (6000, ~100%)		6 M KOH	[82]
Mesoporous Co-MOF	3-E (vs Ag/AgCl)	0.5 (0–0.6)	231 (1000, 95.2%)		1 M LiOH	[47]
Hierarchical porous Zr-MOFs (HP-UiO-66) (BDC ligand)	3-E (vs Hg/HgO)	0.2/10 (0–0.45)	849/237		6 M KOH	[76]
	ASC (HP-UiO-66//PC) (2.8//2.9)	0.3/10 (0–1.6)	90/48 (2000, 68.8%)	32@240 16@7486		
Co-MOF nanoneedles (H_3BTC ligand)	3-E (vs Ag/AgCl) (4)	2/30 (0–0.45)	958/628 (3000, 92.3%)	24.4@429 16.1@6444	3 M KOH	[56]
Co-LMOF (Layered) $[Co(Hmt)(tfbdac)(H_2O)_2] \cdot (H_2O)_2$	3-E (vs SCE) (2.0–4.6)	1/2/4/8/20 (0–0.5)	2474/1978/1728/1514/1024 (2000, 94.3%)		1 M KOH	[46]
		1/2/5/10/20 (0–0.5)	1786/1348/922/736/592 (2000, 95%)		1 M LiOH	
Cu-LCP $Cu(hmt)(tfbdac)(H_2O)$	3-E (vs SCE)	1/2/20 (0–0.5)	1274/954/568 (2000, 88%)		1 M LiOH	[86]
		1/2/6/10/20 (0–0.5)	1102/950/658/534/328 (2000, 88.3%)		1 M KOH	
Rod-like V-MOF (MIL-47) $V^V(O)(bdc)$	3-E (vs SCE) (5)	0.5/1/2/5/10 (0–1.0)	573/521/517/505/495 (10 000, 92.8%; CE 99%)		1.0 M Na_2SO_4	[92]
	ASC (V-MOF//AC) (2//4)	0.5/1/2/5/10 (0–1.6)	132/125/119/111/103 (10 000, 92.1%)			
		0.5/1/2/5/10 $mA\ cm^{-2}$ (0–1.6)	147/123/107/93/78 $mF\ cm^{-2}$ (10 000, 93.6%)	6.72 $mWh\ cm^{-3}@70$.35 $mW\ cm^{-3}$	solid-state (Na_2SO_4 /PVA)	
Zn-MOF (ZnPIIm) $[Zn(HPO_4)(H_2PO_4)_2](ImH_2)_2$	SSC (0.6–0.8)	1/2/5 (0–1.6)	500/430/393 (4000, 91%)	41.3@7421	1 M H_2SO_4	[84]

3. Single-metal MOFs

Pristine MOFs for electrochemical supercapacitors require good charge transport coexisting with permanent porosity and high surface area; despite the fact that most

MOFs are electrical insulators, several materials in this class with highly conjugated ligands for long-range charge transport, i.e. conductive MOFs, have recently demonstrated excellent electrical conductivity and high charge mobility [43, 104-106]. Dincă and coworkers fabricated a high-electrical-conductivity Ni-MOF ($\text{Ni}_3(\text{HITP})_2$, HITP: 2,3,6,7,10,11-hexaiminotriphenylene) as a single-component electrode material without any other binders or conductive additives [107]. The conductive $\text{Ni}_3(\text{HITP})_2$ is made of π -conjugated organometallic layers possessing 1D pores, and these stacked conductive layers form nanotextured particles of 0.5–2 μm in diameter with extended cylindrical channels for electrolyte passage. It delivered a superior gravimetric capacitance of 111 F g^{-1} at the discharge rate of 50 mA g^{-1} , and an outstanding areal (i.e., surface area normalized) capacitance of 18 $\mu\text{F cm}^{-1}$ with high-capacity retention (>90%) over 10000 cycles, higher than that of most carbon-based materials including carbon nanotubes except holey graphene (Fig. 2 a–e). The high power density and superior cyclability, compared to batteries, have made it a new generation of supercapacitors beyond carbon-based materials with promising potential in the large-scale deployment of intermittent renewable energy sources, electrical vehicles, and smart power grids. Bao and coworkers further developed highly conductive 2D metal organic frameworks based on the hexaaminobenzene (HAB) ligand with excellent chemical stability, and therefore the HAB-based MOFs (i.e., Cu-/Ni-HAB MOFs) are compatible with aqueous electrolytes (both acidic and basic) in sharp contrast to conventional MOFs [108]. For miniaturized capacitive energy storage, volumetric and areal capacitances are more important metrics than gravimetric ones because of the constraints imposed by device volume and chip area. Through ligand selection in the conductive MOF design, e.g., small HAB ligand, it not only can obtain highly dense frameworks and hierarchical porous structure for further enhanced capacitive volumetric performance (with exceptionally high volumetric capacitance up to 760 F cm^{-3} , superior to those of most materials), but also achieve stable redox behavior and gravimetric capacitance over 400 F g^{-1} . Due to the small HAB-MOF particle size, the areal capacitance did not plateau and reached a high value of over 20 F cm^{-2} even with an increase in electrode thickness up to 360 μm (i.e., mass loading of 65 mg cm^{-2}). Moreover, the HAB MOF electrodes exhibited highly reversible redox behaviors and outstanding cycling stability with a capacitance retention of 90% even after 12000 cycles (Fig. 2 f–k). The structure tunability and designability of conductive MOFs will allow the further development of novel redox-active MOFs with even higher capacitances (viz., benefiting from the pseudocapacitive beyond the EDL charge-storage mechanism) and energy/power densities for the next generation of energy-storage applications.

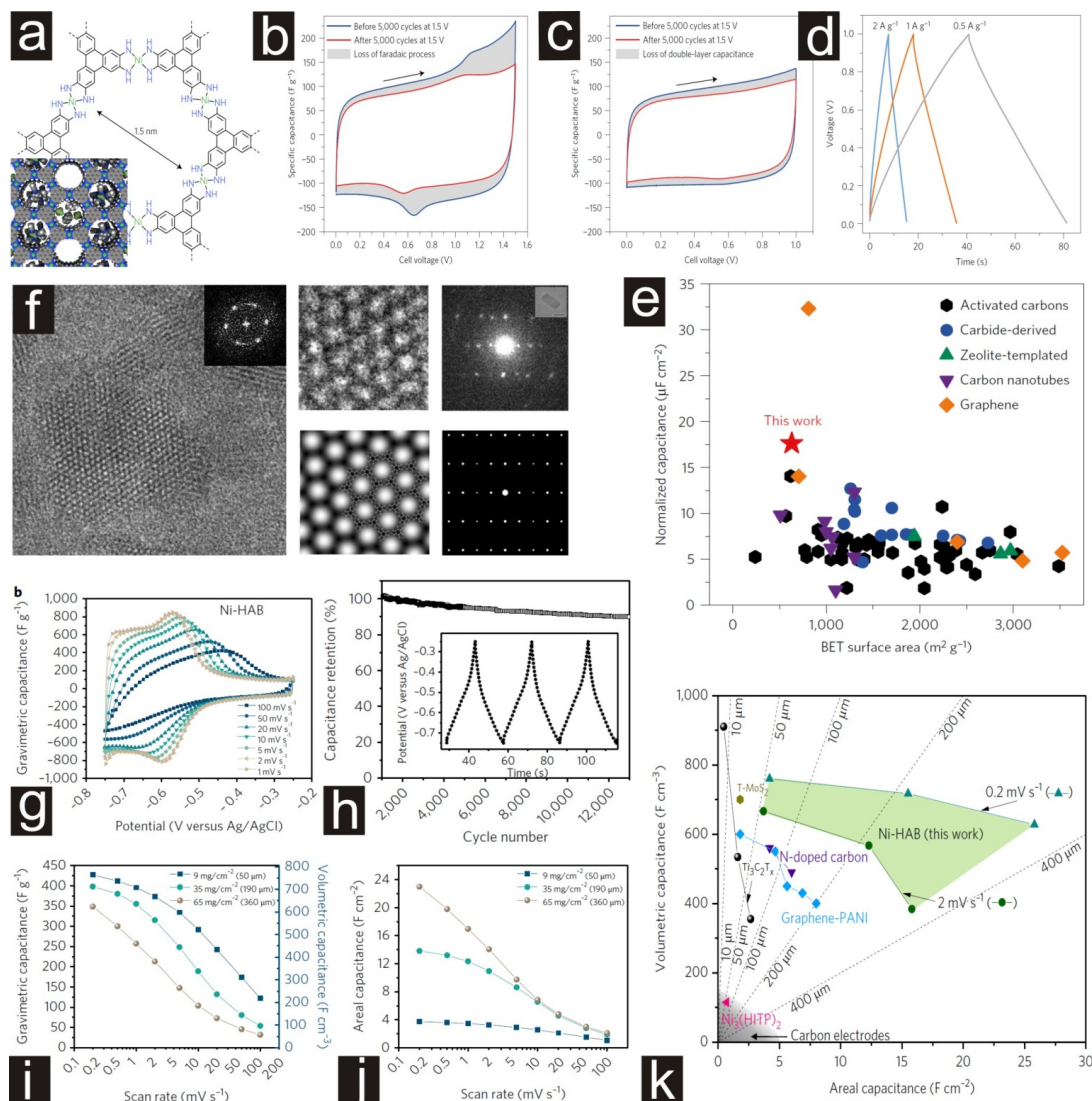


Figure 2 Structure and electrochemical behavior of conducting $\text{Ni}_3(\text{HITP})_2$. (a) Structural schematics (pore size of 1.5 nm). (b, c) Capacitance loss in a symmetric supercapacitor (organic electrolyte) at 1.5 V and 1.0 V, respectively, showing different capacitance loss processes, i.e., pronounced loss of Faradaic capacitance or EDLC loss only. (d) Galvanostatic charge–discharge (GCD) profiles. (e) Comparison of areal capacitances among various EDLC materials. Reprinted with permission from Ref. [107] Copyright 2016, Springer Nature. Structures and electrochemical behaviors of conducting HAB MOFs. (f) Structural characterization of Cu-HAB MOF (hexagonal pore packing of smaller pore size of 0.8 nm). Electrochemical performance of Ni-HAB pellet electrodes in aqueous three-electrode system (1 M KOH): (g) CV, (h) capacitance retention (10 A g^{-1}), inset GCD profiles, (i) gravimetric and volumetric rate performance, (j) areal rate performance with different weight loadings. (k) Comparison of the volumetric and areal capacitance of Ni-HAB additive-free electrodes (green area) with that of other materials. Reprinted with permission from Ref. [108] Copyright 2018, Springer Nature.

The large EDLC-type capacitance of MOFs is mainly ascribed to the extremely large surface area and unique porous structures, which allow facile diffusion of electrolyte ions through the micro- and mesopores [15, 35, 51, 58]; MOFs engineering at nanoscale will realize higher capacitance, better rate capacity, and even enhanced mechanical properties [56, 59, 62, 91, 109, 110]. For example, Xu et al. synthesized 1D Ni-MOF nanorods (with average length 900 nm, diameter 60 nm) via a facile hydrothermal process and utilized them as promising pseudo-capacitive electrode materials for supercapacitors [62]. The Ni-based MOF nanorods exhibited a superior specific capacitance (1698 F g^{-1} at 1 A g^{-1}), high rate capability (capacitances of 1698, 1385, 1068 and 838 F g^{-1} at 1, 2, 5 and 10 A g^{-1} , respectively) and good cycling stability (capacitance retention of 94.8% over 1000 cycles at 1 A g^{-1}). Furthermore, the constructed Ni-MOF nanorods/graphene asymmetric supercapacitor (ASC) exhibited outstanding capacitive performance with a specific capacitance of 166 F g^{-1} at a current density of 1 A g^{-1} and superior rate capability (119 F g^{-1} at 5 A g^{-1}). Moreover, the assembled micro-/nanoarchitectures may further enhance structural stability and improve the long-term cycling stability of ASCs thereof [110]. Pang and coworkers developed a simple process for the fabrication of rod-like vanadium metal-organic frameworks (MIL-47) [92]. The V-MOF as a cathode of SCs exhibits a maximum specific capacitance of 572 F g^{-1} at a current density of 0.5 A g^{-1} in aqueous three-electrode system as well as superior cycle life with almost no capacitance decay after 10000 cycles at a current density of 1 A g^{-1} (92.8% retention of the initial specific capacitance). More significantly, the assembled solid-state asymmetric supercapacitors (V-MOFs and activated carbon as the positive electrode and negative electrode materials, respectively) exhibited high capacity, great cycling stability (93.6% capacitance retention over 10 000 cycles), as well as high energy density of 6.72 mWh cm^{-3} at a power density of 70.35 mW cm^{-3} in the potential window of 0–1.6 V. This superior performance confirms that V-MOF electrodes are promising materials for applications in supercapacitors. Furthermore, making the V-MOFs size decrease to the nanoscale and combining the V-MOFs with high conductivity materials such as CNTs, graphene and conducting polymers will further enhance the performances.

Compared to bulk MOF crystals, two-dimensional (2D) MOF nanosheets or layer-structured MOFs exhibit larger surface areas and more accessible active sites on their surfaces due to the specific 2D morphology [17, 32, 38, 46, 86]. Thus, the 2D morphology/structure of MOFs or their assembled architectures will enhance the synergistic effect beyond huge internal surface area [49, 68, 69, 72, 111, 112]. For instance, Wei and coworkers synthesized a series of layered 2D MOFs (e.g., Ni-, Co-based) and studied the supercapacitive performance in an aqueous KOH electrolyte [49, 61]. The Ni-MOF-24 crystal exhibited a loosely packed sheet-like structure and was

composed of nanosheets of ca. 10 nm thick with the lattice fringe of ca. 0.93 nm (corresponding to the d_{100} -spacing) (Fig. 3 a–d). In a standard three-electrode system, the Ni-based MOF electrode could deliver high capacitances of 1127 and 668 F g⁻¹ at rates of 0.5 and 10 A g⁻¹, respectively, and >90% capacitance was retained after 3000 cycles. Accordingly, the maximum power and energy densities were 1750 W kg⁻¹ and 19.2 W h kg⁻¹, respectively [61]. By further controlling the ultrasonic time (post-treatment after hydrothermal synthesis), novel accordion-like Ni-MOF superstructure could be formed, i.e., the intersheet spacing was thus tuned. When used as electrode materials, the supercapacitors exhibited excellent electrochemical performance, e.g., the accordion-like Ni-MOF electrode exhibited specific capacitances of 1021, 988 and 823 F g⁻¹ in 3 M KOH solution at current densities of 0.7, 1.4 and 7.0 A g⁻¹, respectively, while maintaining outstanding cycling stability (capacitance retention of 96.5% after 5000 cycles at the current density of 1.4 A g⁻¹) (Fig. 3 e–i) [112]. And for the Co-based MOF electrode, it exhibited a maximum capacitance of 2564 F g⁻¹ at 1 A g⁻¹ (1164 F g⁻¹ at 20 A g⁻¹), and the capacitance retention kept at 95.8% after 3000 cycles [49]. These superior electrochemical properties (i.e. large capacitance, high-rate capability and cycling stability) may be related to the intrinsic characteristics of the transition-metal based MOF materials including the layered structure and favorable exposed facets. Zhu et al. fabricated a similar layered structure of Co-MOF, as a self-supported supercapacitor electrode it exhibited ultrahigh areal capacitance (13.6 F cm⁻² at 2 mA cm⁻²) and excellent rate performance (79.4% retention at a current density of 20 mA cm⁻²). As for an asymmetric supercapacitor (ASC) device, it demonstrates a high energy density of 1.7 mW h cm⁻² at a power density of 4.0 mW cm⁻² [48]. Hierarchical porous Ni-MOF constructed with nanosheets can further be controllably fabricated by a facile hydrothermal process with the existence of trimesic acid and nickel ions [111]. The hierarchical structure can not only supply more active sites but also prevent the 2D nanosheets from stacking during fast charge–discharge process for enhanced electrochemical properties. It can deliver an outstanding specific capacitance of 1057 F g⁻¹ at 1 A g⁻¹, good rate capability (649 F g⁻¹ even high up to 30 A g⁻¹), and keep 70% of its original value over 2500 cycles (at 10 A g⁻¹). Furthermore, the assembled ASCs based on the hierarchical porous Ni-MOF and activated carbon (AC) showed a specific capacitance of 87 F g⁻¹ at 0.5 A g⁻¹, and a high energy density of 21.05 Wh kg⁻¹ and power density of 6.03 kW kg⁻¹, which demonstrates promising applications in high performance supercapacitors.

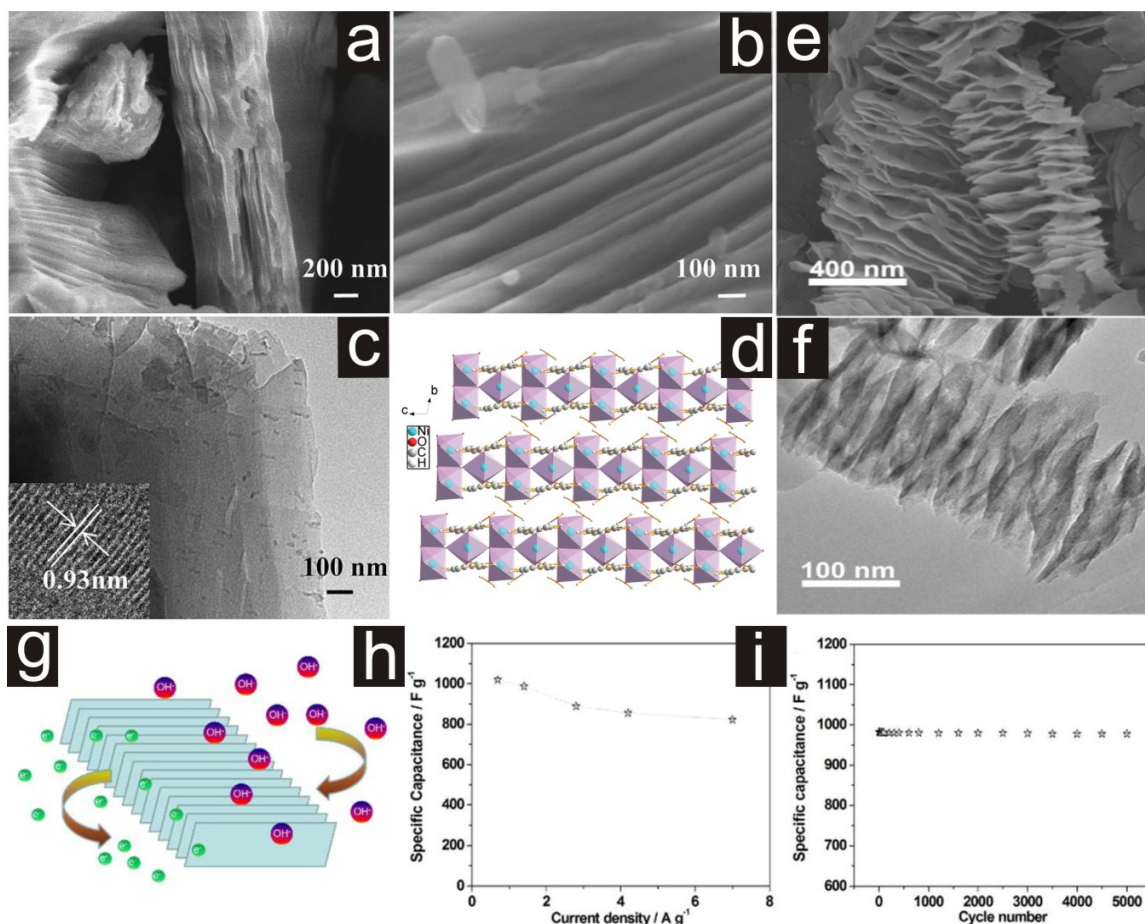


Figure 3 Structural illustration of a layered 2D Ni-based MOF: (a, b) SEM image, (c) TEM image, and (d) structural diagram. Reprinted with permission from Ref. [61] Copyright 2014, The Royal Society of Chemistry. Structure and electrochemical behavior of an accordion-like Ni-MOF: (e) SEM and (f) TEM images, (g) schematic model showing the possible charge–discharge process, (h) specific capacitances and (i) cycling profile (1.4 A g^{-1}). Reprinted with permission from Ref. [112] Copyright 2016, The Royal Society of Chemistry.

Mesoporous MOFs ($2 \text{ nm} < \text{pore size} < 50 \text{ nm}$), compared to the microporous (pore size $< 2 \text{ nm}$), will have faster molecular diffusion and mass transfer as well as enhanced accommodation for larger guest components or anchoring molecular functions [40, 50, 51, 82, 113]. For example, Du et al. developed a channel-type In-MOFs (mesoporous 437-MOF material with perfect 1-D hexagonal channels of ca. 3 nm pore size) and the physicochemical stability was further enforced via a combined approach of heating in boiling water followed by annealing (i.e., synergistic activation) (Fig. 4 a–f) [82]. The synergistic effects of the external and internal surfaces of the porous crystalline material endow the MOFs with better stability, which is a critical issue in practical applications of

MOFs. The hierarchical moderately-activated In(III) mesoMOF material with both thermal and chemical stability exhibited a higher recycling capability as SCs electrode. Another hierarchical porous Zr-MOF (HP-UiO-66) was fabricated using bimetallic Zn/Zr-MOFs as a precursor, subsequently wiping off Zr-MOFs [76]. When used as cathode materials for supercapacitors, the broad redox peaks indicate the enhanced pseudocapacitive behavior of HP-UiO-66 with a specific capacitance of 849 F g^{-1} at 0.2 A g^{-1} , which is 8 times higher than that of ordinary UiO-66 (101.5 F g^{-1}). The clearly enhanced electrochemical performance of HP-UiO-66 can be ascribed to the advantages of the hierarchical porous structure (including mesopores and micropores), pore volume, and sufficient surface defects from unsaturated Zr^{4+} as well as the facilitated ion or electrolyte diffusion at/near the surface of the electrode thereof. Furthermore, the assembled aqueous ASCs based on the HP-UiO-66 and biomass-derived porous carbon could deliver an energy density of 32 W h kg^{-1} at a power density of 240 W kg^{-1} (16 W h kg^{-1} at a power density of 7481 W kg^{-1}). This strategy may offer a general method for tailoring new type of hierarchical porous MOFs and the enhanced performance of MOFs-based SCs thereof. More interestingly, Xu and coworkers synthesized a controllable hierarchical meso- and microporous MOF in an ionic liquid (IL)/supercritical CO_2 (SC CO_2)/surfactant emulsion system, wherein CO_2 plays a dual effect during the synthesis, viz., CO_2 droplets were utilized as a soft template for the cores of nanospheres while CO_2 -swollen micelles induce mesopores on nanospheres (Fig. 4 g, h) [47]. And through changing CO_2 pressure, both the size and mesopore properties of nanospheres may be easily tuned. The Co-MOF exhibited a high specific capacitance of 230.5 F g^{-1} at 0.5 A g^{-1} by virtue of the interconnected nature of the hierarchically porous nanospheres.

Molecular length of organic linkers (or ligands) can be used to manipulate the pore size and surface area of MOFs, i.e., longer linkers incline to produce larger pores and larger surface area, and vice versa; also, different molecular dimensions of organic linkers may produce different surface architecture, channel topology/structure and the varied electrode surface thereof, which may be beneficial to electrochemical performance including higher capacitance [45, 65, 114]. Designing kinetically stable MOFs through ligand functionalization to overcome the structure collapse in aqueous electrolytes can effectively improve their supercapacitive performances [51, 71]. Qu et al. synthesized a series of nickel-based pillared DABCO-MOFs (abbr. DMOFs; DABCO: 1,4-diazabicyclo[2.2.2]-octane) of similar topologies, of which the DMOF-ADC with ADC (9,10-anthracenedicarboxylic acid) linker showed the best specific capacitances of 552, 438, and 395 F g^{-1} at current densities of 1, 20, and 50 A g^{-1} , respectively, while maintaining outstanding cycling stability for ASCs (capacitance retention >98% after 16000 cycles at 10 A g^{-1}) [71]. Wang et al. synthesized a novel polythreaded Co-based MOF by choosing a flexible N-donor ligand and a rigid multicarboxylate linker. The

maximum gravimetric capacitance of the nanorod electrode can reach 2405 F g^{-1} at 0.75 A g^{-1} with high Coulombic efficiency (92.2%), rate capability (53.5% after 20 times increase, i.e., 1287 F g^{-1} at 15.0 A g^{-1}), and good cycling performance (93.5% after 3000 cycles). The excellent electrochemical property may be benefiting from the 3D networks constructed by the 2D entangled layered structures that facilitating electron transport, providing sufficient interlayer spaces for the storage and diffusion of OH^- ions, and the small-size effect of the nanorods [51]. These works open a new channel for the application of water-stable MOFs in energy storage. In addition, the diffusion of electrolyte ions (e.g., OH^-) probably regulates the redox reaction during the period of the electrochemical process and thus results in distinct performances under various concentrations of electrolytes, viz., the electrolyte concentration will, even significantly, affect the maximum specific capacitance, maximum specific energy/power of the electrode, hence an optimized electrolyte and concentration is beneficial for the enhanced performances of SCs [51].

The electrochemical mechanisms for pristine MOF-based supercapacitors are noteworthy. Despite the fact that the transition-metal based MOFs, at the presence of alkaline aqueous solution during repeated cycling, may convert to highly functionalized metal hydroxides (not simple hydroxides as reported by some other works but, for example, turbostratic hydroxides highly functionalized with carbonate ions most likely incorporated in the interlayer spacing), the structure remained highly stable during charge–discharge processes. Meanwhile, the strong Faradaic redox peaks may come from intercalation and deintercalation of e.g., OH^- during electrochemical reaction, which leads to reversible valence state changes between e.g., transition-metal M^{2+} and M^{3+} ions. The excellent cycling stability of MOF-derived highly functionalized metal hydroxide based electrochemical capacitors can be attributed to the high structure stability of the converted material inherited from MOF structure. The MOF derived material inherited the external morphology from the MOF but with obvious volume shrinkage, probably attributed to the substitution effect of the ligand to OH^- units at the presence of alkali. Raman, FTIR and X-ray analyses reveal that the significant difference between the fresh MOF and cycled MOF, i.e., the rather weak M–ligand coordination bond will be broken during electrochemical charge storage and will be replaced by stronger M–OH ionic/covalent bond. Besides, the carboxyl group bonded on linker/ligand may be oxidized, forming carbonate ions incorporated between the turbostratic $\text{M}(\text{OH})_x$ layers. For water-stable MOFs, the evolved layered structure has a 3D nanostructure inherited from pristine MOFs, which provides a larger surface area and increases electrode–electrolyte contact area and decreases polarization of the electrode in charge–discharge cycles. Also, the low-crystalline nature of the structure with high structural disorder may

contribute to the high structural stability. Overall, the detailed mechanism of the structure change and the final structure of MOFs after the charge/discharge processes are still not very clear yet, and further more advanced characterization methods and in-depth studies are required [71].

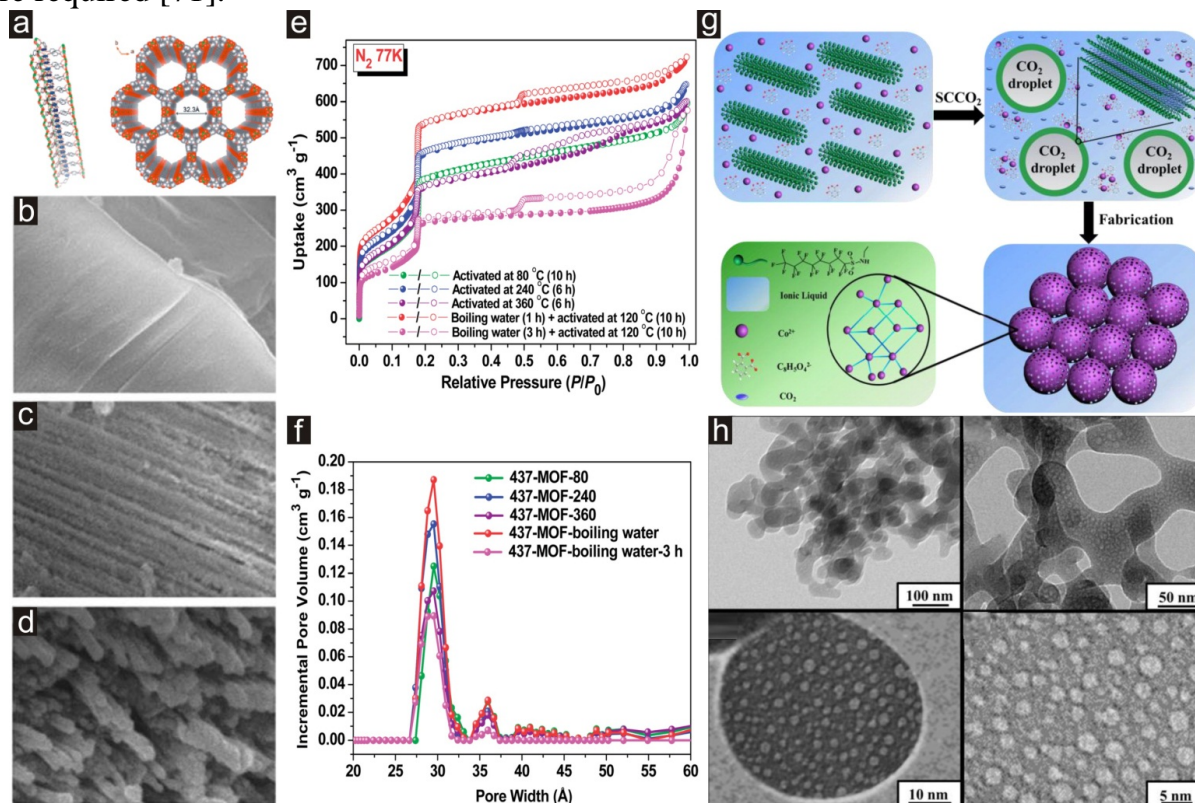


Figure 4 Channel-type mesoporous In-MOF via activating method. (a) Schematic views of the 3D framework with regular 1D hexagonal channels of 3.23 nm pore size. SEM images of (b) as-synthesized 437-MOF, and those after activation by boiling water (c) 1 h and (d) 3 h as well as the corresponding (e, f) N_2 sorption isotherms for the activated 437-MOFs at different conditions showing mesoporous features. Reprinted with permission from Ref. [82] Copyright 2014, The Royal Society of Chemistry. Surfactant-directed assembly of mesoporous Co-MOF in a switchable solution. (g) Schematic illustration for the formation of mesoporous Co-MOF in an ionic liquid (IL)/supercritical CO_2 (SC CO_2)/surfactant emulsion system, and (h) TEM images of the as-synthesized Co-MOF. Reprinted with permission from Ref. [47] Copyright 2015, The Royal Society of Chemistry.

Alkaline battery–supercapacitor hybrid deceives (ABSHDs) have been attracting great attention due to their combined advantages of both alkaline batteries and supercapacitors [10, 115]. 2D layered Ni-MOF has been demonstrated to have a high specific capacity and can further improve the energy storage through a novel strategy “synergistic effect between Ni-MOF and redox additives (e.g., $Fe(CN)_6^{4-}/Fe(CN)_6^{3-}$),” where the Ni-MOF

provides enough space for $\text{Fe}(\text{CN})_6^{4-}/\text{Fe}(\text{CN})_6^{3-}$ storage and diffusion, and $\text{Fe}(\text{CN})_6^{4-}/\text{Fe}(\text{CN})_6^{3-}$ acts as electrons relay during charge–discharge process by coupling the Ni(II)/Ni(III) in the Ni-MOF electrode. Thus, the assembled Ni-MOF//CNTs-COOH ABSHD in 3 M KOH and 0.1 M $\text{K}_4\text{Fe}(\text{CN})_6$ mixed electrolyte could achieve an extended voltage window of 1.4 V, resulting in a high energy density (55.8 W h kg^{-1}) and power density (7000 W kg^{-1}) simultaneously (Fig. 5) [10]. And it can broaden the applications of MOFs in energy storage devices and provide insightful guidelines for developing other redox additives to improve the performance of the electrochemical energy storage devices.

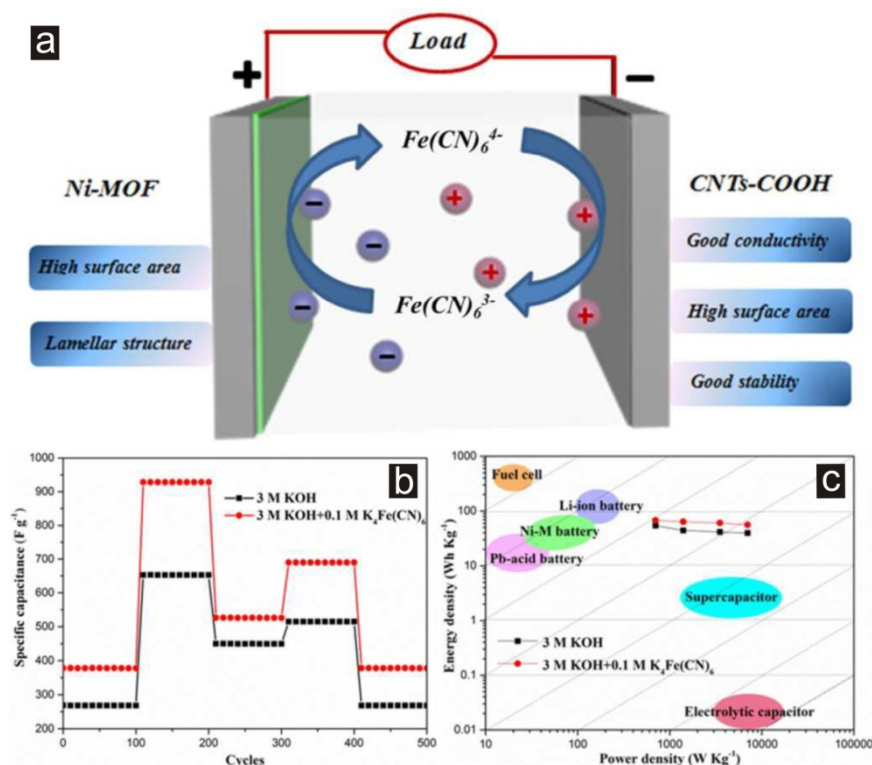


Figure 5 (a) Schematic illustration of an alkaline battery-supercapacitor hybrid device (ABSHD) containing Ni-MOF and CNTs-COOH as the positive and negative electrodes, respectively. (b) Rate performance and cycling stability of Ni-MOF via three-electrode system in 3 M KOH and in mixed electrolyte 3 M KOH + 0.1 M $\text{K}_4\text{Fe}(\text{CN})_6$ (redox additive), respectively. (c) Ragone plots of the ABSHD, exhibiting high energy density and power density approaching that of Li-ion batteries and supercapacitors. Reprinted with permission from Ref. [10] Copyright 2016, The Royal Society of Chemistry.

4. Bimetal or doped MOFs

Studies have shown that rational control of the shape and components of MOFs can optimize their electrochemical performances; to further enhance the capacitance, the

MOFs could be doped or partially substituted by heteroatoms for tailored internal space for better electrolyte/ions diffusion, smaller charge transfer resistance, or more stable crystal structure [9, 94, 96], such as Ni/Zn- [9, 96, 116], Ni/Co- [9, 94, 95, 117-119], Co/Mn- [120], Co/Fe- [121, 122], Zn/Co- [93, 123], Mn/Fe- [124], Fe/Ni- [125], Cr/Mg- [126], S/Ni- [127] MOFs (typical samples and their performance are listed in Table 2).

Table 2. Typical bimetal MOF materials for supercapacitors.

MOFs	Electrodes (ML [mg cm ⁻²])	CD (or SR) [A g ⁻¹] (VR) [V]	Capacitance [F g ⁻¹] (cycles, CR)	ED/PD [W h Kg ⁻¹ /W Kg ⁻¹]	Electrolyte	Refs.
Flower-like Co/Ni-MOF	3-E (vs SCE) (3)	1/10 (-0.2 to 0.4)	236/196		3 M KOH	[9]
	HSC (Co/Ni-MOF//CNTs-COOH)	1/2/5/10 (0-1.45)	212/187/148/99 (5000, 86%)	61.8@725 54.7@1450 43@3625 28.7@7250		
Flower-like Zn/Ni-MOF	3-E (vs SCE) (3)	1/10 (-0.2 to 0.4)	162/90 (3000, 89.1%)			
	HSC (Zn/Ni-MOF//CNTs-COOH)	1/2/5/10 (0-1.45)	183/170/123/90 (5000, 80%)	53.6@725 49.5@1450 36@3625 26.1@7250		
2D Ni/Co-MOF nanoflake-assembled spherical hollow microstructures	3-E (vs Ag/AgCl) (0.1)	0.5	530 (2000, 99.75%; 3000, 70.9%)		1 M LiOH	[95]
Co8-MOF-5 <i>Zn_{3.68}Co_{0.32}O(BDC)₃(DEF)_{0.7}</i>	MOF//CB	0.01 (0-1.2)	2 (1k, 92%)		0.1 M TBAPF ₆ /A CN	[93]
Zn-doped Ni-MOF <i>4.56%Zn-Ni(PTA)</i>	3-E (vs SCE) (5)	0.25/10 (0-0.35)	1620/854 (3k, 92%)		6 M KOH	[96]
Ni/Co-MOF (<i>Ni/Co=1/1</i>)	3-E (vs Ag/AgCl) (4-5)	1/2/5/10 (0-0.4)	1049/839/771/642 (5000, 97.4%)		3 M KOH	[117]
Ni/Co-MOF <i>Ni_{3-x}Co_x(BTC)₂·12H₂O (x=0.5)</i>	3-E (vs SCE) (5)	1/2/5/10 (0-0.4)	1067/972/870/780 (2500, 68.4%)		3 M KOH	[118]
Ni/Co-MOF (<i>BPDC ligand</i>)	3-E (vs Ag/AgCl) (2)	1/20 (0-0.4)	991/405 (1000, 56.2%; 3000, 55.8%; CE >98.0%)		2 M KOH	[119]
Dandelion-like Ni/Co-MOF (<i>H₃BTC ligand</i>)	3-E (vs SCE)	1/2/5/10/15 (0-0.5)	758/757/731/673/644 (5000, 75%)		2 M KOH	[94]
	ASC (Ni/Co-MOF//AC)	1/2/5 (0-1.6)	56/51/44 (5000, 85%)	20.9@800 15.8@4000		

Wei and coworkers improved the previously synthesized layered structural Ni-MOFs via Zn doping, and the Zn-doped Ni-based MOF materials with different amount of Zn (ranging from 2.28% to 9.12%) generally exhibited higher capacitance [96]. Amongst, the moderately doped Ni-MOF (4.56%) delivered the best specific capacitance, rate capability and cycling stability: the capacitances of 1620 and 854 F g⁻¹ were achieved at 0.25 and 10 A g⁻¹, respectively, the retention was maintained at over 91% after 3000 cycles, and maximum power and energy densities were 1750 W kg⁻¹ and 27.6 W h kg⁻¹, respectively. It is noteworthy to mention that the replacing of smaller Ni²⁺ ions (0.065 nm) with larger Zn²⁺ ions (0.074 nm) would shift the XRD characteristic peaks to a lower angle side and thus an enlarged interlayer distance (from 0.95 nm to 1.04 nm) for electrolyte diffusion and ions intercalation/deintercalation, also the morphology would evolve from nanoflakes into a microsphere structure composed of flake-like subunits (Fig. 6 a–e).

Xia et al. developed a facile two-step method to realize nanostructure engineering of 2D nanoflake MOFs [95]. The hollow structure of Ni/Co-MOF (i.e., 2D MOF nanoflake-assembled spherical microstructures) exhibited enhanced electrochemical performance in supercapacitors, e.g., high capacitance of 530 F g⁻¹ at 0.5 A g⁻¹ in 1 M LiOH aqueous solution, good rate capability, and robust cycling performance with almost no capacity fading after 2000 cycles (99.75 % capacitance retention) (Fig. 6 f–j). It highlights the significant role of tuning 2D nanoflake ensembles of MOFs in accelerating electron and charge transportation for optimizing energy storage and conversion devices.

Chen and coworkers developed an effective strategy to improve the conductivity of MOFs by partially substituting Ni²⁺ in the Ni-MOF with Co²⁺ or Zn²⁺ (viz., isomorphic substitutions during crystallization in the synthesis process) [9]. The flower-like mixed-metal (i.e., bimetal) organic frameworks showed superior (battery-type) electrochemical performance, which can be attributed not only to the favorable paths for charge transport due to the presence of free pores, but also to the enhanced EDLC capacitance at the enlarged specific surface area of the architecture. The cycling stability of the assembled hybrid supercapacitors (Co/Ni-MOFs//CNTs-COOH) was also enhanced due to the alleviation of phase transformation during electrochemical cycling tests; the Co/Ni-MOF//CNTs-COOH also presented an excellent energy density (49.5 W h kg⁻¹) and power density (1450 W kg⁻¹) simultaneously (Fig. 7). The bimetal-based hybrid supercapacitors provide a positive promising for the application of the MOF family in the advanced electrochemical energy storage field.

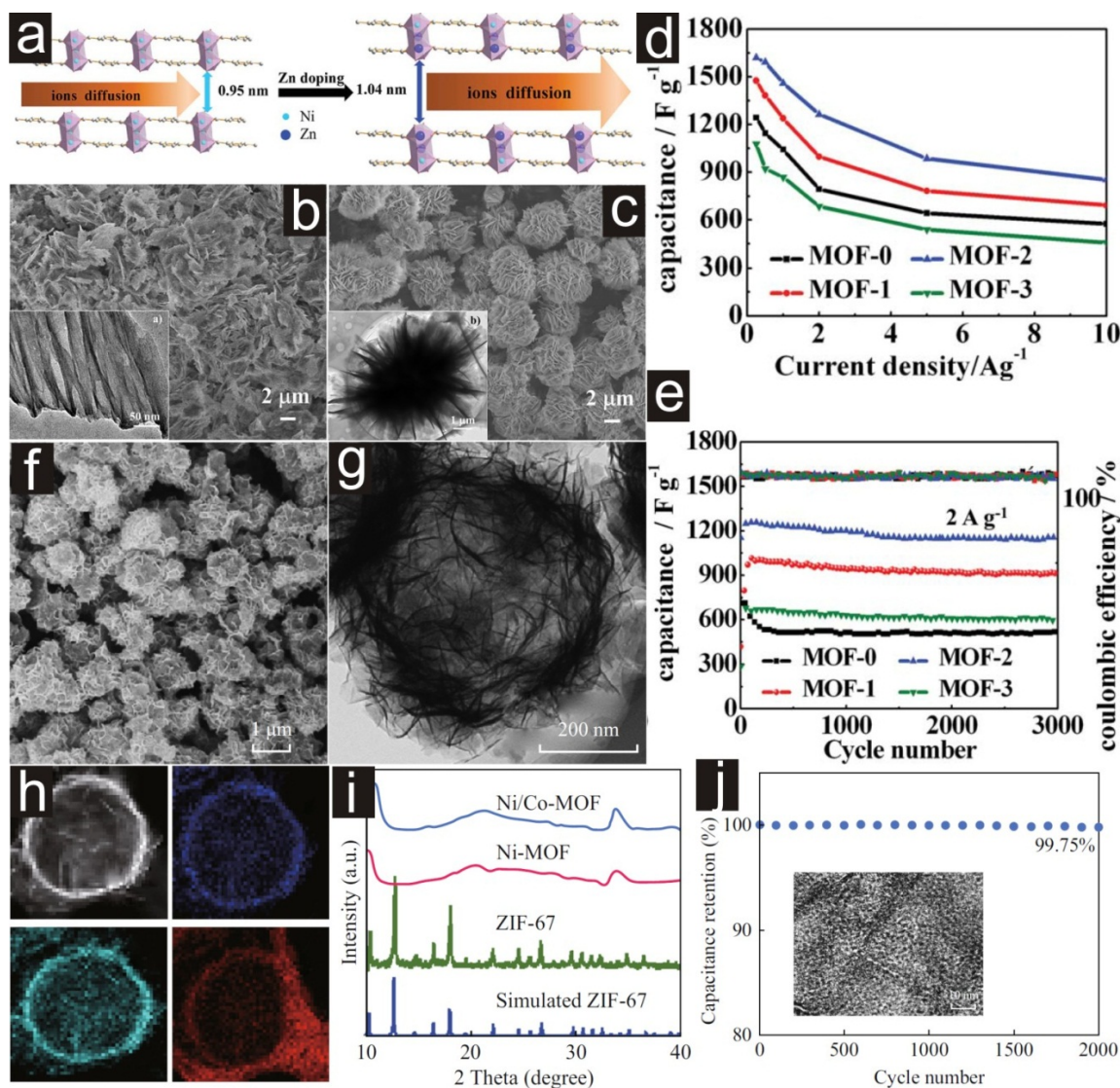


Figure 6 Structure and electrochemical performances of layered Zn-doped Ni-MOF. (a) A structural change mode for the Ni-MOF via Zn-doping. SEM and TEM images of (b) Ni-MOF and (c) Zn-doped Ni-MOF materials. (d) Specific capacitances, and (e) GCD cycling performance of Zn-doped Ni-MOF electrodes (MOF-1, 2, 3) compared with Ni-MOF (MOF-0). Reprinted with permission from Ref. [96] Copyright 2014, The Royal Society of Chemistry. Structure and electrochemical behavior of 2D bimetal Ni/Co-MOF nanoflake-assembled spherical hollow microstructure. (f) SEM, (g) TEM images, (h) elemental mapping, (i) XRD patterns, and (j) cycling performance (2 A g⁻¹, inset HRTEM image). Reprinted with permission from Ref. [95] Copyright 2017, Springer Nature.

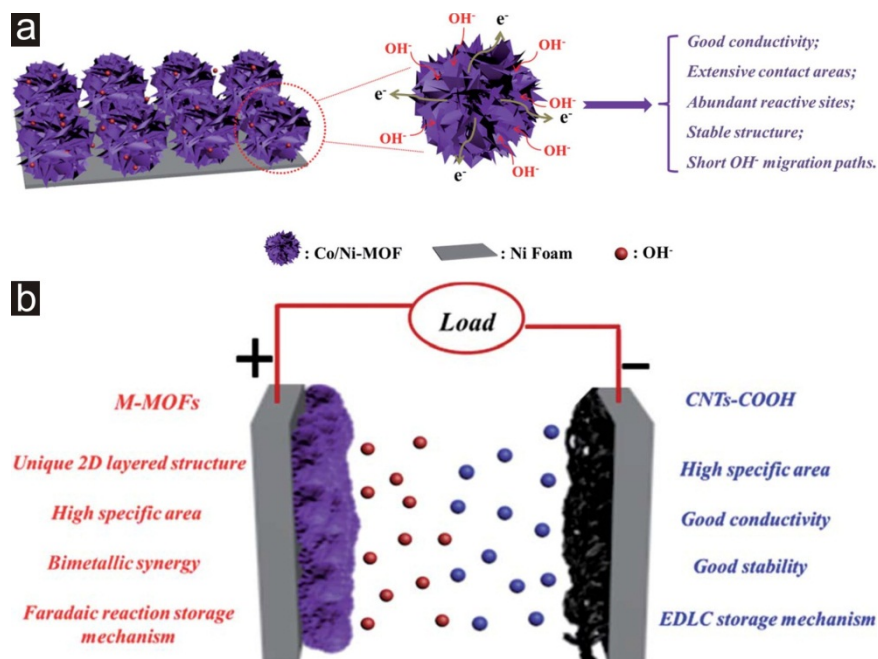


Figure 7 (a) Schematic diagram showing the advantages of ion and charge transfer in the Co/Ni-MOF electrode, and (b) an abstract illustration of hybrid supercapacitors containing mixed-/bimetallic MOFs and CNTs-COOHs, for example, as a positive and negative electrode, respectively. Reprinted with permission from Ref. [9] Copyright 2017, The Royal Society of Chemistry.

5. Hybrids and composites

Despite the high porosities, pure MOF supercapacitors usually exhibit low specific capacitance due to the poor conductivity; for real breakthroughs, combining their electrochemical properties with appropriate electronic and ionic conductivity will be required [13]. Integration of MOFs with a variety of functional materials (e.g., conductive or pseudocapacitive components) is a quite effective and feasible strategy to further improve MOF electrochemical performance or introduce new functionality for smart applications [15, 24, 30, 41]. In order to improve the conductivity of MOFs, the incorporation of MOFs with conductive materials, such as carbons (including mesoporous activated carbon [128, 129], carbon nanotubes [130-134], graphene [33, 131, 132, 135-147], graphene aerogels [148, 149], 3D carbon networks [150]), layered carbon nitride (CN) [151], nickel boride (Ni-B) [152], MXenes [153], Ag nanowires [154], conductive polymers [35, 155-164] or multiple synergistic materials [165-168] has been proved to be an effective strategy to enhance SCs performance (typical samples and their performance are listed in Table 3).

Table 3. Typical MOF-based hybrid/composite materials for supercapacitors.

MOFs	Electrodes (ML [mg cm ⁻²])	CD (or SR) [A g ⁻¹] (VR) [V]	Capacitance [F g ⁻¹] (cycles, CR)	ED/PD [W h Kg ⁻¹ /W Kg ⁻¹]	Electrolyte	Ref.
Cu-MOF/AC (1 <i>H</i> -imidazole ligand)	3-E (vs Ag/AgCl)	1/2/5 (0–0.8) 5/10/20/50/10 0 mV s ⁻¹	733/221/33 (2000, 85%) 753/593/470/333/ 245		1 M KOH	[129]
nMOF- 867/graphene film <i>Zr₆O₄(OH)₄(BPYDC)₆</i>	SSC (0.014) (thickness 2 μm)	0.88 mA cm ⁻³ (0–2.7)	726 (0.64 F cm ⁻³ ; 5.09 mF cm ⁻²) (10000, ~95%)	0.286 mWh cm ⁻³ @0.3 86 W cm ⁻³ 0.604 mWh cm ⁻³ (max) 1.097 W cm ⁻³ (max)	1 M (C ₂ H ₅) ₄ NBF ₄ / ACN	[33]
2D Co-MOF/Ag nanowires (A-CoL/Ag NC)	3-E (vs Hg/HgO) (4.6)	1/10 mA cm ⁻² (0–0.5)	1467/1060 mF cm ⁻² (1200, 98.9%)		3 M KOH	[154]
	ASC (A-CoL/Ag NC//AC)	1/10 mA cm ⁻² (0–1.6)	1534/865 mF cm ⁻² (7000, 97.2%)	110@760 63@6410	3 M KOH	
		1/10 mA cm ⁻² (0–1.6)	1080/470 mF cm ⁻² (7000, 95.2%)	151@790 70@7972	solid-state (KOH/PVA)	
Ni(H ₂ BDC)/CNTs	3-E (vs Ag/AgCl) (4)	0.5/10 (0–0.4)	1765/950		6 M KOH	[130]
	ASC (Ni- MOF/CNTs//rGO/C ₃ N ₄) (4.5 total)	0.5/20 (0.8–1.6)	103/46			
Flower-shaped MWCNTs@Ni(TA) (trimesic acid ligand)	3-E (vs Ag/AgCl) (2)	2/10 (0–0.45)	115/89 (5000, 81.6%)		2 M KOH	[134]
CNTs@Mn-MOF <i>Mn(C₈H₄O₄)(H₂O)₂</i> (<i>p</i> - benzenedicarboxylic acid ligand)	3-E (vs SCE) (1.2)	1 (0–1.0)	203 (3000, 88%)		1 M Na ₂ SO ₄	[133]
	SSC	0.25/0.5/1/2/5/ 10	50/49/48/41/31/23	6.9@123 1.3@2240		
ZIF-67/3D carbon network (3DCN) (ball-in-cage nanocomposite)	3-E (vs Hg/HgO) (1.5)	0.5/1/2/5/10 (–0.1 to 0.4)	119/116/101/83/6 9 (2000, 77.6%)		1 M KOH	[150]
	SSC (1.5)	0.5/10 (0–1.0)	69/56 (1500, 80.7%)	9.5@1006 7.8@2010		
Fe-ZIF/CN (Fe-doped ZIF/layered carbon nitride nano- sandwiches)	3-E (vs Ag/AgCl) (5)	1/20 (0–0.4)	1096/689 (2000, 90.7%)		6 M KOH	[151]
	SSC	1 (0–0.65)	123	11@400		
	ASC (Fe- ZIF/C//porous- C/CN) (2)	1/50 (0–1.6)	432/203	153@800 72@40000		

Ni-doped Zn-MOF/rGO	3-E (vs Ag/AgCl)	0.05 (0–0.5)	758 (1.28 F cm ⁻²)		1 M KOH	[171]
Ni-MOF@GO-3wt%	3-E (vs Ag/AgCl) (3)	1/20 (0–0.45)	2192/1074 (3000, 85.1%)		2 M KOH	[135]
Ni-pydc@EEG (NiEG) (<i>electrochemical exfoliated graphene</i>)	3-E (vs Ag/AgCl) (1.3)	1/5/10/20 (0–0.6)	1283/835/688/482 (3000, 93%)		0.5 M LiOH	[147]
	ASC (NiEG//EEG) (2//10)	1/2/5/10 (0–1.5)	69/65/59/46 (CE 90.1%)	21.5@750 14.5@750 0	solid-state (LiOH/PVA)	
Ni ₃ (HCOO) ₆ /rGO	3-E (vs Hg/HgO) (2)	5 mV s ⁻¹ (0–0.6)	940 (500, 96.28%)		1 M KOH	[136]
Ni-MOF/N-doped graphene (Ni-PDC@NG)	3-E (vs Hg/HgO) (1–1.5)	1/40 (0–0.65)	735/390 (14000, 85.3%; 6000, 97.9%)	21.7@801 9.8@1603 6	1 M LiOH	[140]
Graphene@Prussian blue (G@PB)	3-E (vs SCE) (2.0)	0.5/1 (0–1.1)	445/388 (5000, 97.2%)	74.8@550 0	0.5 M Na ₂ SO ₄	[131]
	ASCs: G@PB//AC (total 13)	0.5/5 (0–1.8V)	44.6/16.1 (5000, 87.5%)	20.1@450 10.7@270 0		
Cu-MOF/rGO	3-E (vs Ag/AgCl)	1.6/8 (–0.5 to 0.7)	685/486 (1000, 91.91%)	137@4800	1 M Na ₂ SO ₄	[139]
Nanoflower-like Cu-MOF/POAP film Cu ₂ (2- <i>mpinh</i>) ₂ Cl ₂ (H ₂ O)	3-E (vs Ag/AgCl)	1/4/8 (–0.5 to 0.5)	315/~295/~265 (1000, 90%)		0.1 M HClO ₄	[156]
Nanoflower-like Cu-MOF/POAP film Cu(<i>btec</i>) _{0.5} DMF		1 (–0.5 to 0.5)	241 (1000, 91%)			[158]
ZIF-67/POAP film			724 (1000, >90%)			[159]
GO/ZIF-67/POAP film			825 (1000, 90%)	115@500		[167]
GO/ZIF-8/POAP film			670	112@601		
Flower-like Zn/Ni-MOF@PPy	3-E (vs SCE) (3)	1/2/5/10 (0–0.4)	202/198/174/86 (3000, 94.4%)		3 M KOH	[160]
	HSC (Zn/Ni-MOF@PPy//CNTs-COOH)	1/2/5/10 (0–1.4)	203/187/145/102 (3000, 91.8%; 5000, 78.8%)	55.3@699 50.9@133 8 39.5@348 5 35.4@559 0		
Rod-like HKUST-1@PANI (MOF-199)	3-E (vs Ag/AgCl) (2)	1/10 (0.05–0.50)	270/205		6 M KOH	[163]
	ASC (HKUST-1@PANI/rGO)	0.5/10 (0–1.5)	20.0/5.1 (2000, 87%)	6.22@375 1.58@749 7		
ZIF-67/GO-2wt%	3-E (vs SCE) (2.5)	5/100 mV s ⁻¹ (–0.3 to 0.4)	100/57		6 M KOH	[141]
		1/20 (–0.3 to 0.35)	71/46 (1000, 150%)			

ZIF-8/GO	3-E (vs SCE)	5/50 mV s ⁻¹ (0–0.6)	160/56		6 M KOH	[143]	
		1 (0–0.4)	95				
ZIF-67/GO		1 (0–0.4)	202				
ZIF-67/rGO	3-E (vs Ag/AgCl)	5 mV s ⁻¹ (–0.3 to 0.25)	218		6 M KOH	[142]	
		1 (–0.3 to 0.25)	210 (1000, 80%)				
MIL-88-Fe/graphene aerogel <i>GAMOF</i> (Fe ³⁺)	3-E (vs SCE) (2.64)	20 (0–1.0)	353 (10000; 74.4%)	36@588 27@4300	1 M H ₂ SO ₄	[148]	
Co-MOF/MXene@Ni-foam	3-E (vs Ag/AgCl) (2.9)	3 mA cm ⁻² (0–0.4)	3741 (18.7 F cm ⁻²) (3000, 92.1%)		3 M KOH	[153]	
Co-MOF/graphene nanosheets (CoBTC MOF rods/GNC)	3-E (vs Ag/AgCl)	0.25 (–0.1 to 0.45)	608 (2000, 94.9%)	49.8@102 6 26.7@205 0	1 M KOH	[144]	
	SSC (2.0)	0.25/2/4/8/10 (–0.1 to 1.3)	183/162/149/116/ 98 (2000/5000, 98.4%/92.2%)				
Ce-MOF/GO	3-E (vs Ag/AgCl) (2.0)	1 (–0.2 to 0.4)	234	12.0@449 7	3 M KOH	[132]	
			2221	111@4497	3 M KOH + 0.2 M K ₃ Fe(CN) ₆		
Ce-MOF-CNT			130		3 M KOH		
			1367		3 M KOH + 0.2 M K ₃ Fe(CN) ₆		
Ni ₃ (NO ₃) ₂ (OH) ₄ @U IO-66 (Zr-MOF)	3-E (vs SCE) (4.9)	5/30 mV s ⁻¹ (–0.2 to 0.6)	992/398	88.1@198 0 35.4@477 0	6 M KOH	[179]	
Ni ₂ CO ₃ (OH) ₂ @ZIF-67	3-E (vs Ag)	5/30 mV s ⁻¹ (–0.15 to 0.4)	1037/697		6 M KOH	[180]	
		5 mA cm ⁻² (–0.15 to 0.4)	1029 (1600, 79.8%)				
Ni ₂ CO ₃ (OH) ₂ /ZIF-8 (Zn(N ₂ C ₄ H ₆) ₂)	3-E (vs Ag) (4.65)	5/30 mV s ⁻¹	851/417		6 M KOH	[182]	
NiC ₂ O ₄ /ZIF-67 (nickel oxalate)	3-E (vs Ag) (4.65)	5/30 mV s ⁻¹ (–0.2 to 0.35)	1020/574 (2000, 73%)		6 M KOH	[181]	
SnO ₂ quantum dots@ZIF-8	3-E (vs Ag)	5/100 mV s ⁻¹ (0–0.6)	931/182		6 M KOH	[183]	
Ultrathin Cu-MOF@δ-MnO ₂ nanosheets	3-E (vs Hg/HgO) (1)	1 (0–1.05)	667		1 M Na ₂ SO ₄	[186]	
	ASC (Cu-MOF@δ-MnO ₂ //AC)	1/2/4/10/20 (0–2.0)	340/297/264/210/ 152 (6000, 95%)				

For example, Pang and coworkers incorporated the 2D amorphous Co-MOF with silver nanowires (Ag NWs) for an integrated nanocomposite (A-CoL/Ag NC) by one-step solution agitation at room temperature [154]. The hybrid with enhanced conductivity

provides sufficient contact between active material and electrolyte, and facilitates ions/electrons transfer, resulting in high specific capacitance, great rate capacity, high output potential, and long-term cycle stability. As a supercapacitor cathode, it demonstrated a superior specific capacitance high up to 1467 mF cm^{-2} at 1.0 mA cm^{-2} , and 1060 mF cm^{-2} even at 10.0 mA cm^{-2} in a three-electrode system. The aqueous A-CoL/Ag NC//AC asymmetric supercapacitor (ASC) with activated carbon as anode could deliver a maximum energy density of 110 W h kg^{-1} at 760 W kg^{-1} and a maximum power density of 6410 W kg^{-1} at 63 W h kg^{-1} in 3 M KOH . And the solid-state ASC based on A-CoL/Ag NC//AC exhibited a broad operated potential window of $0\text{--}1.6 \text{ V}$, long cycle life (95.2% capacitance retention after cycling 7000 cycles), as well as an energy density of 151 W h kg^{-1} (at 790 W kg^{-1}), and a power density of 7972 W kg^{-1} (at 70 W h kg^{-1}). The well-synthesized nanocomposite of 2D MOFs and 1D metal nanowires provides another novel way to synthesize prominent electrode materials for supercapacitors. Wen et al. developed a solvothermal method to grow Ni-MOF on the CNTs surface for a durable ASC with Ni-MOF/CNTs and reduced graphene oxides/graphitic carbon nitride (rGO/g- C_3N_4) as the cathode and anode electrodes [130]. In the Ni-MOF/CNT composites, CNTs serve as a robust backbone, whose surface can be easily modified for facilitating the uniform growth of Ni-MOF on their surface. Excellent conductivity of CNTs provides low ionic diffusion resistance and can work as a current collector to shorten the path length of electron transport. The synergistic effects of CNTs and the Ni-MOF will also buffer the large volume change of active species and keep electrode stability in long-term cycling beyond the enhanced capacitance and rate capacity (e.g., 1765 F g^{-1} at 0.5 A g^{-1} , 1.6 time higher than that of the pure Ni-MOF; 950 F g^{-1} at high up to 10 A g^{-1}). The electrochemical performance of the ASC, evaluated at a working voltage of 1.6 V in 6 M KOH aqueous electrolyte, exhibited a high energy density of 36.6 W h kg^{-1} at a power density of 480 W kg^{-1} , and an excellent long cycle life along with 95% capacitance retention over 5000 cycles. Those excellent electrochemical performances encouraged much interest in investigating the possibility of using MOF-based composites for promising applications in asymmetric aqueous supercapacitors.

Recently, 2D graphene has become a promising candidate for supercapacitors or their vital component as conductive frameworks owing to the exceptional characteristics on structural, electronic, thermal, electrochemical, and mechanical aspects [23, 169, 170]. Herein, researchers have attempted to develop a series of composite by incorporating MOFs and graphene-based materials, which leads to a surprising enhancement in conductivity, structural stability and electrochemical performance [23]. For example, Majumder and coworkers synthesized Ni-doped MOF-5/rGO, and the concept of the SCs composite electrode is shown in Fig. 8a [171].

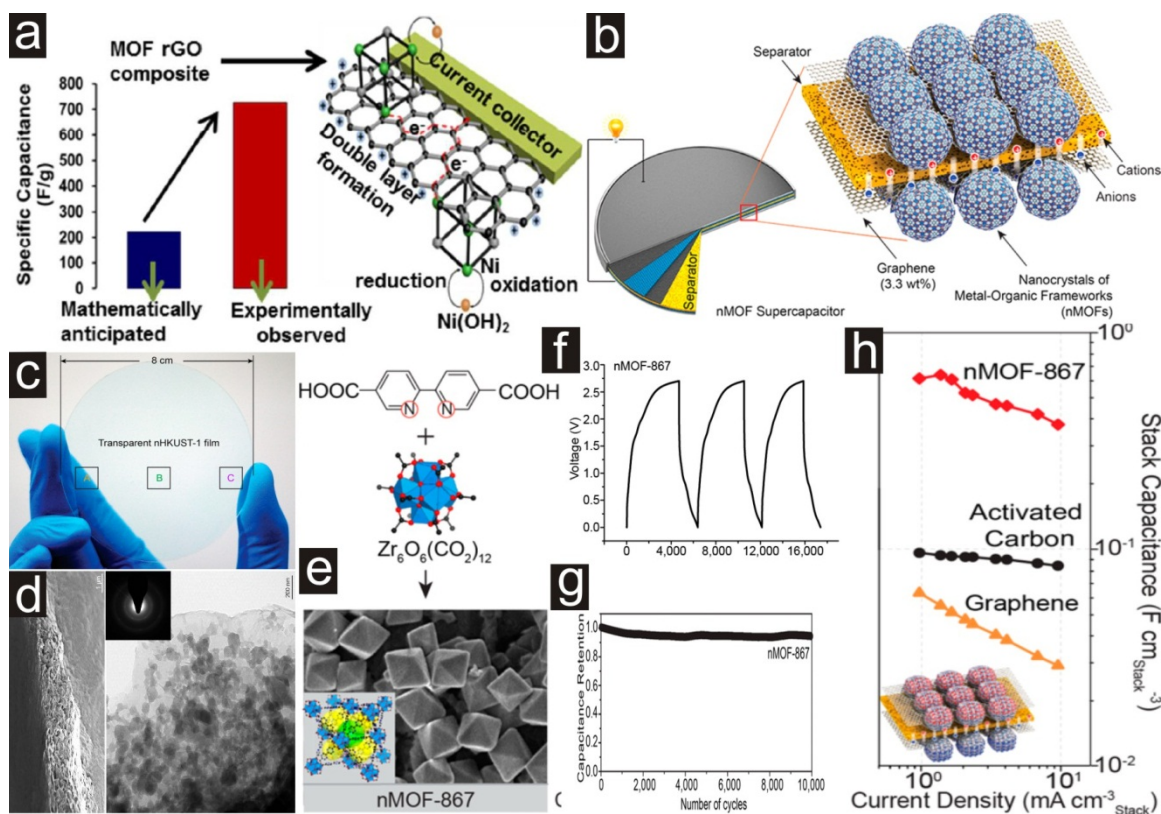


Figure 8 (a) Concept for incorporation of graphene to form a conducting composite electrode material with efficient charge transfer processes and enhanced electrochemical capacitance via synergistic effect (more than the sum of its parts). Reprinted with permission from Ref. [171] Copyright 2015, American Chemical Society. (b) Construct for nMOF supercapacitors via MOF nanocrystals doped with graphene and incorporated into devices. (c) A large, transparent nMOFs (e.g., nHKUST-1) composite film on a quartz substrate (8 cm in diameter), and (d) SEM and TEM images of the composite film (2 μm in thickness). (e) Synthesis of nMOFs (e.g., nMOF-867) crystal structures, (f) the charge-discharge profile and (g) life cycle for nMOF-867, and (h) the corresponding volumetric stack capacitance compared to activated carbon and graphene. Reprinted with permission from Ref. [33] Copyright 2014, American Chemical Society.

The efficient charge transfer process of the electrode was attributed to the synergistic effect of the distributed Ni centers in the MOF-5 and interconnected graphene nanosheets. The capacitance of this composite (MOF-5 50% and rGO 50%) is almost 3 times larger than the algebraic sum of contributions from the Faradaic capacitance of Ni-doped MOF-5 and EDLC capacitance of rGO; as an energy storage device it realized an energy density of 37.8 Wh kg⁻¹ at a power density of 227 W kg⁻¹, and exhibited superior stability during cycling. Choi et al. synthesized a series of nanocrystalline MOFs (nMOFs) with different metals, ligands, and structures [33]. Of which, the Zr-MOF

(nMOF-867) based supercapacitor (with ~3 wt% graphene) manifests the highest performance with stack and areal capacitance of 0.64 and 5.09 mF cm⁻², respectively (about 6 times that of the SCs made from the benchmark commercial activated carbon materials), and the calculated gravimetric capacitance of nMOF-867 is 726 F g⁻¹. Meanwhile, it exhibits outstanding durability over 10000 cycles as well as superior energy/power densities with extended exposure to the maximum voltage of 0–2.7 V (Fig. 8 b–h).

Graphene aerogel (GA) is an ideal conductive substrate characterized by its 3D conducting graphene network, which offers an opportunity to optimize the ionic diffusion in graphene-based electrodes for capacitors due to its low density, high compressibility, high specific surface area, and excellent electrical conductivity; thus it is suitable to support redox nanoparticles for high-performance supercapacitors [148, 149, 169]. Hu and coworkers reported a growth-oriented Fe-based MOF (MIL-88-Fe) synergized with graphene aerogel composite and its application for supercapacitor [148]. A typical morphology of such 3D composite graphene aerogels is given in Fig. 9a (inset), showing well dispersed MOF crystals grown on the graphene surface or wrapped by the sheets of graphene. MIL-88-Fe was in-situ grown at (002) lattice plane on the surface of graphene via a one-step solvothermal method. It is proved that MOF could affect the EDLC characteristics of composites with abundant interspace of GA. Compared with randomly distributed MOF (in 3D graphene/ZIF-8 composite, Fig. 9 a–c) [149], the oriented MOF/GA composite demonstrates the advantage of higher gravimetric capacitance, faster charge/discharge rate, and more reliable cycling stability. The specific capacitance of MOF/GA composites was as high as 353 F g⁻¹ at 20 A g⁻¹, and the retention ratio was 74.4% over 10000 cycles [148].

The introduction of carbon network as well as low temperature can reduce the size of MOF crystals for fast and effective redox reaction as well as the enhanced conductivity [150, 172, 173]. Zhao and coworkers designed a Co-based zeolitic imidazolate framework (ZIF-67) polyhedron in-situ integrated into three-dimensional carbon network (3DCN) to construct a Ball-in-Cage (BIC) nanoarchitecture [150]. The introduced 3DCN acting as the electronic pathway will provide the nucleation sites of MOF particles; and the further growth of which is thus confined by the size effect of 3DCN. The BIC frame can not only control the MOF particle size, but also ensure a high electron conductivity of the integrate structure (Fig. 9 d–k). The as-prepared BIC electrode for supercapacitors displays an enhanced capacitance and greater rate performance. The space-confined effect of 3DCN on the MOF crystalline size could be expected to be a promising method to improve the electrochemical performance of pristine MOFs in the future.

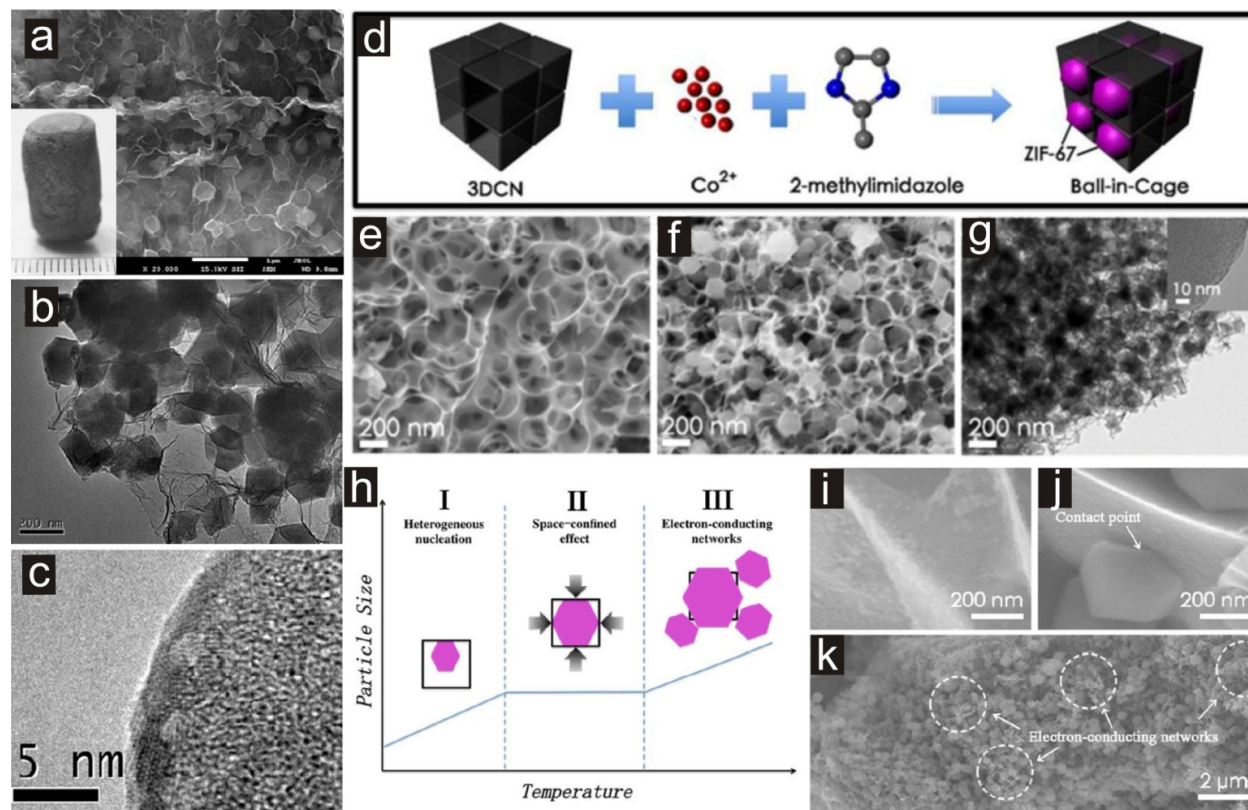


Figure 9 (a) SEM and (b, c) TEM images of the as-prepared 3D graphene/ZIF-8 composite (3D G-ZIF8) with different magnifications (inset, photograph of the aerogel composite; bulk density 25 mg cm^{-3}). Reprinted with permission from Ref. [149]

Copyright 2014, Elsevier. (d) Schematic illustration of Ball-in-Cage (BIC) synthesis process via in-situ integration of ZIF-67 into 3D carbon network (3DCN) to construct a BIC composite nanostructure. (e) SEM image of 3DCN, (f) SEM and (g) TEM images of the as-synthesized BIC composite. (h) The role of 3DCN in the fabrication of BIC nanostructure (viz., formation mechanism), i.e., stage I, heterogeneous nucleation effect followed by MOF particles growth with increasing synthesis temperature; stage II, space-confinement effect; stage III, larger MOF particles extending critical size while electronic pathways maintained. The corresponding structures in three stages: (i) heterogeneous nucleation MOFs at the surface of 3DCN, (j) the contact point of MOFs particle and the carbon layer, and (k) the electron-conducting networks of 3DCN in the composite electrodes. Reprinted with permission from Ref. [150] Copyright 2017, The Royal Society of Chemistry.

By incorporation of conducting polymers, Wang et al. fabricated a ZIF-67 nanocrystals electrochemically interweaved with polyaniline (PANI) for enhanced conductivity [35]. The deposited PANI, which directly interconnected the MOF interior surface and the external circuit to boost electron transportation, together with the MOF exhibited an

enhanced areal capacitance of 2146 mF cm^{-2} at 10 mV s^{-1} . Chen and coworkers developing an “oxidant-free additive (i.e., oxygen in air)” synthetic strategy for polypyrrole (PPy) coated Zn/Ni-MOF composite electrodes, which exhibited enhanced specific capacity and cycling stability [160]. The “trade-off effect” between the ion diffusion kinetics and electrical conductivity was optimized with different loadings of PPy. As an excellent positive electrode for hybrid supercapacitors, it exhibited a higher energy density (50.9 W h kg^{-1}), power density (1338 W kg^{-1}) and long-life cycling performance (retaining 91.8% of the value at 10 A g^{-1} after 3000 cycles) simultaneously. This synthetic method for composites may be suitable for coating a variety of conductive polymers on other layer-like crystal structural MOFs.

Utilization of redox additives in the electrolyte is another approach to enhance the specific capacitance of electrode materials via redox reactions of the additives between the electrode and electrolyte interfaces; the effect of the migration of redox species between the electrode/electrolyte interface is thus a primary characteristic to improve the pseudocapacitance and cyclic stability [132, 174-177]. Ramachandran et al. fabricated cerium MOF based composites (Ce-MOF/GO and Ce-MOF/CNT), and compared the KOH and KOH + $\text{K}_3\text{Fe}(\text{CN})_6$ electrolytes [132]. Notably, it is found that the introduction of redox additives (e.g., via the faradic redox reaction of $\text{Fe}(\text{CN})_6$ with redox pair of $[\text{Fe}(\text{CN})_6]^{3-}/[\text{Fe}(\text{CN})_6]^{4-}$) directly gives additional pseudocapacitance contributions to the electrode, due to the facilitated multiple redox activities during electrochemical process and the decreased charge transfer resistance of KOH electrolyte which allows fast electron transportation [174].

Another effective strategy to enhance the capacitance is the combination of MOFs with pseudocapacitive materials including transition-metal compounds [168, 178-184]. For example, Zr-MOFs (UIO-66) are a kind of crystalline porous material with controllable porous structure and potential strong thermal stability up to 773 K [185]. By incorporation with $\text{Ni}_3(\text{NO}_3)_2(\text{OH})_4$, the composite ($\text{Ni}_3(\text{NO}_3)_2(\text{OH})_4@\text{Zr-MOF}$) as pseudocapacitor material facilitates interfacial charge transport and provides short diffusion paths for ions, which results in a high specific capacitance. A maximum specific capacitance of 992 F g^{-1} was obtained from cyclic voltammetry (CV) at a scan rate of 5 mV s^{-1} , which is higher than that of the separate components as electrode material [179]. Xu et al. synthesized controllable ultrathin Cu-MOF@ $\delta\text{-MnO}_2$ nanosheets for 2.0 V neutral aqueous (Na_2SO_4) electrolyte-based electrochemical capacitors that involve activated carbon as the counter electrode of ASCs [186]. The as-prepared nanoparticle/nanosheet composite combines the advantages of the porous Cu-MOF and the functional ultrathin $\delta\text{-MnO}_2$ nanosheets. It showed a large increase in performance with a high specific capacitance of 340 F g^{-1} at a current density of 1 A g^{-1} , and cycling

stability for 6000 cycles with only 5% drop compared to the initial capacitance (Fig. 10). The superior performance during the charging–discharging process can be attributed to the existence of 2D nanostructures, which prevent electronic conduction while allowing ionic conduction. In addition, polyoxometalates (POMs), as early transition-metal anionic clusters, have been widely explored in catalysis, electrochemistry, and energy storage and conversion because of their advantages such as redox properties, stability, and diversity as well as large electronic transfer capability. Thus, taking the synergistic advantages of MOFs and POMs, i.e., polyoxometalate-based MOFs (POMOFs) supercapacitors with high performance based on two types of materials may be attractive candidates for supercapacitors and will be a promising research field [168].

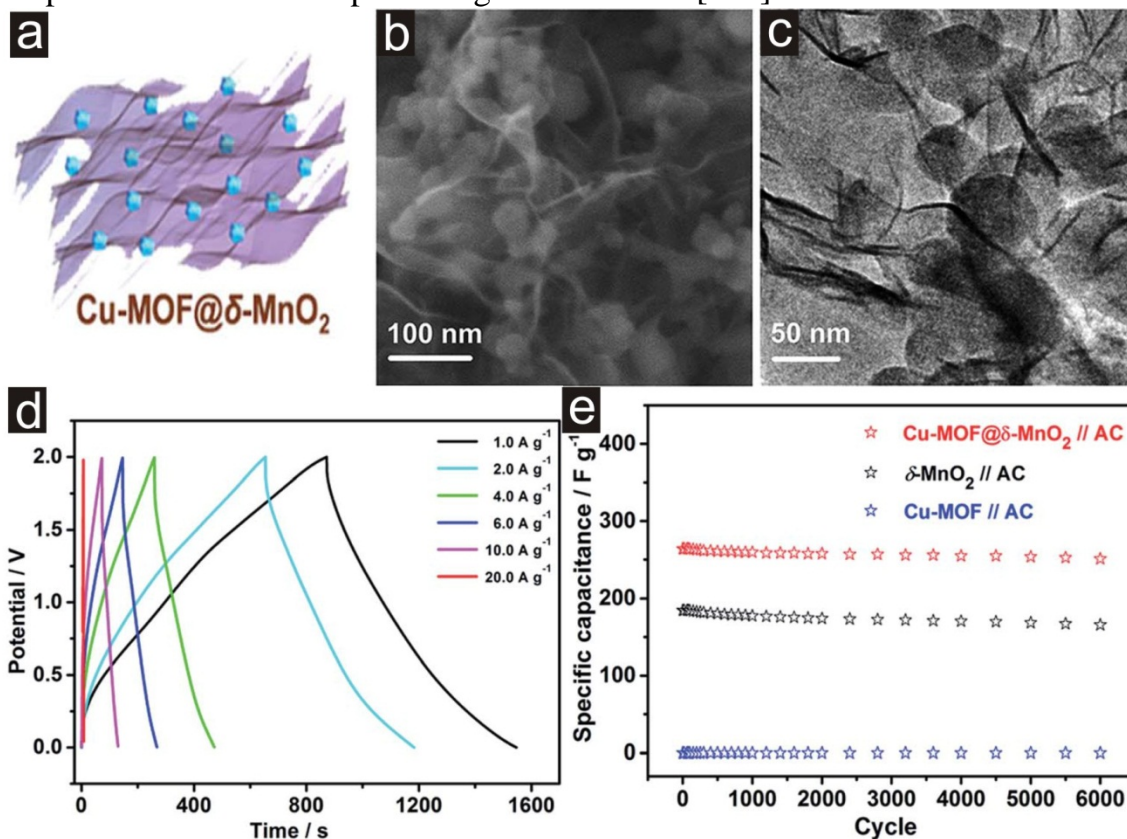


Figure 10 (a) Schematic illustration, (b) SEM and (c) TEM images of ultrathin Cu-MOF@δ-MnO₂ nanosheets. (d) GCD curves of Cu-MOF@δ-MnO₂//AC ASC, and (e) charge–discharge cycling of various (Cu-MOF@δ-MnO₂//AC, δ-MnO₂//AC, Cu-MOF//AC) ASC devices at 4 A g⁻¹ in 1 M Na₂SO₄ aqueous electrolyte. Reprinted with permission from Ref. [186] Copyright 2018, The Royal Society of Chemistry.

6. Flexible or freestanding SCs

Among these various developed SCs, flexible supercapacitors (FSCs), especially flexible solid-state supercapacitors (FSSCs), are considered to be promising candidates for

electrochemical energy storage toward light-weight, safe, eco-friendly, and easy-to-handle devices since they avoid using liquid electrolyte and can be easily folded or attached to any surfaces [35], which have raised extensive attention owing to recent significant breakthroughs in modern wearable electronics [187]. Despite exceptional advantages for supercapacitors, MOFs are mostly nonconductive, and as a result, it is challenging to build effective flexible or free-standing SCs based on pristine MOFs but incorporation with other conductive additives or frameworks including carbon (fiber) cloth [188, 189], carbon fiber paper [109, 190], electrospun carbon nanofibers [191, 192], carbon nanotube film [193-195], graphite paper [196], graphene paper [32], Pt-PET film [112, 178], or synergistic multiple components (e.g., hybrid systems of conductive polymers, graphene, CNTs, carbon paper, textile, fibers metal foil/wire or polymer-based substrates) [35, 165, 187, 191, 193-195, 197-204], with typical samples and their performance listed in Table 4.

Table 4. Typical flexible MOF-based electrodes for supercapacitors.

MOFs	Electrodes (ML [mg cm ⁻²])	CD (or SR) [A g ⁻¹] (VR) [V]	Capacitance [F g ⁻¹] (cycles, CR)	ED/PD [W h Kg ⁻¹ /W Kg ⁻¹]	Electrolyte	Refs.
CFP@TM-nanorods (<i>Ni-MOF nanorods on carbon fiber paper</i>)	TM-nanorods 3-E (vs Ag/AgCl) (6)	1/20 (0– 0.45)	862/790 (13600, 80.8%)		2 M KOH	[190]
	TM-NPCs (derived carbon) 3-E (vs Ag/AgCl)	1/20 (–1.0 to 0)	330/290 (10000, 97.8%)			
	HSC (TM- nanorods//TM-NPCs)	1/2/4/10/ 20 (0–1.5)	161/149/135/116/ 102 (10000, 83.2%; CE ~100%)	47.1@101 8 29.8@171 04		
Cu-TCPP nanosheets@PPy (<i>on carbon paper</i>)	3-E (vs Ag/AgCl) (0.6)	1/10 (0–0.7)	496/283 (3000, ~70%)		0.5 M H ₂ SO ₄	[204]
	SSC (0.4)	2 (1.6 mA cm ⁻²) (0–0.9)	240 (~48 mF cm ⁻²) (3000, 68.5%)	0.29 mWh cm ⁻³ @270 mW cm ⁻³	solid-state (H ₂ SO ₄ /P VA)	
PPNF@MOF hybrids (<i>Ni-MOF nanosheets on electrospun PAN nanofibers</i>)	3-E (vs Hg/HgO)	0.5/5 (0–0.5)	703/302 (10 000, ~100%; CE>97%)		3 M KOH	[192]
	CNFs@Ni hybrid (derived)	0.5 (–1.0 to 0)	102			
	ASC (PPNF@MOF//CNFs @Ni)	2/5/10 (0–1.5)	165/53/25	51.4@150 0 7.8@7497	solid-state (KOH/PV A)	
CC@PANI/UiO-66	SSC	0.5/1 (0–0.8)	886/647 (5000, 91%)	78.8@200	solid-state (H ₂ SO ₄ /P VA)	[203]

Conductive Cu-CAT NWAs (<i>nanowire arrays on carbon fiber paper</i>)	3-E (vs Ag/AgCl)	0.5/10 (0–0.5)	134/202 (5000, 80%)		3 M KCl	[109]
	SSC (0.5)	0.5 (0–0.8V)	120 (22 $\mu\text{F cm}^{-2}$) (5000, >85%)	2.6@200	solid-state (KCl/PVA)	
ZIF-67/PPy tubes-28wt% (<i>on graphite paper</i>)	3-E (vs Ag/AgCl) (1)	0.5/20 (0–0.6)	554/243		1 M Na_2SO_4	[196]
	SSC (10)	0.4 mA cm^{-2} (0–0.6)	226 mF cm^{-2}		solid-state (PVA/ Na_2SO_4)	
CC/ZIF-67/PPy (<i>on carbon cloth</i>)	3-E (vs Hg/HgO)	1 mA cm^{-2} (–0.2 to 0.4)	284 (181 mF cm^{-2}) (40000, 100.7%)		6 M KOH	[188]
MnO_x -MHCF Nanocubes (<i>on Pt-PET film</i>)	3-E (vs SCE) (5) (on nickel foam)	10 (0–0.8)	1200 (10000, >94.7)		1.0 M Na_2SO_4	[178]
	HSC (MnO_x -MHCF//AC)	0.5 mA cm^{-2} (0–1.3)	175 mF cm^{-2} (10000, 94.5%)	5.1 mW h cm^{-3} (210 W h kg^{-1})	solid-state (KOH/PV A)	
Accordion-like Ni-MOF [$\text{Ni}_3(\text{OH})_2(\text{C}_8\text{H}_4\text{O}_4)_2(\text{H}_2\text{O})_4 \cdot 2\text{H}_2\text{O}$] (PTA ligand; <i>on Pt-PET film</i>)	3-E (vs Hg/HgO) (on Ni foam; 5)	0.7/1.4/7.0 (0–0.45)	1021/988/823 (5000, 96.5%)		3 M KOH	[112]
	ASC (Ni-MOF//AC) (4//12)	1.0 mA cm^{-2} (0–1.2)	230 mF cm^{-2} (5000, 92.8%)	4.18 mWh cm^{-3} (max) 231.2 mW cm^{-3} (max)	solid-state (KOH/PV A)	
2D MOF/rGO paper	ASC (2D Co-MOF/rGO paper//2D Ni-MOF/rGO paper)	1.2 mA cm^{-2} (0–1.8)	426.5 mF cm^{-2} 22.45 F cm^{-3} (3000, 93.3%)	1.87 mWh cm^{-3} (35.5 $\mu\text{Wh cm}^{-2}$) 250 mW cm^{-3} (4.75 mWh cm^{-2})	solid-state (H_2SO_4 /PVA)	[32]

Wang and coworkers designed a new strategy for achieving high performance SCs and overcoming the insulating problems of MOFs by electrochemically interweaving MOF crystals with a conductive PANI via electrochemical deposition, where the isolated MOF crystals deposited on the carbon cloth (CC) were interconnected and linked up by the chains of PANI that acted as bridges for electrons transportation between the external circuit and the internal surface of MOFs [35]. A synergistic effect revealed that the deposited PANI could not only efficiently improve the conductivity of MOFs but also enhance Faradaic processes across the interface, i.e., the hybrid-structured electrode took the advantages of both high capacitance originated from the MOFs and effective pseudocapacitance from PANI. An unprecedented high areal capacitance of 2146 mF cm^{-2}

at 10 mV s^{-1} in a three-electrode system and a power density of 0.833 W cm^{-3} at a current density of 0.05 mA cm^{-2} were achieved for the flexible solid-state symmetric SCs based on MOFs (ZIF-67), reaching a record value among all MOF-based FSCs and superior to those of most FSCs based on CNPs, CNTs, graphene, conductive polymers, and metal oxides (Fig. 11).

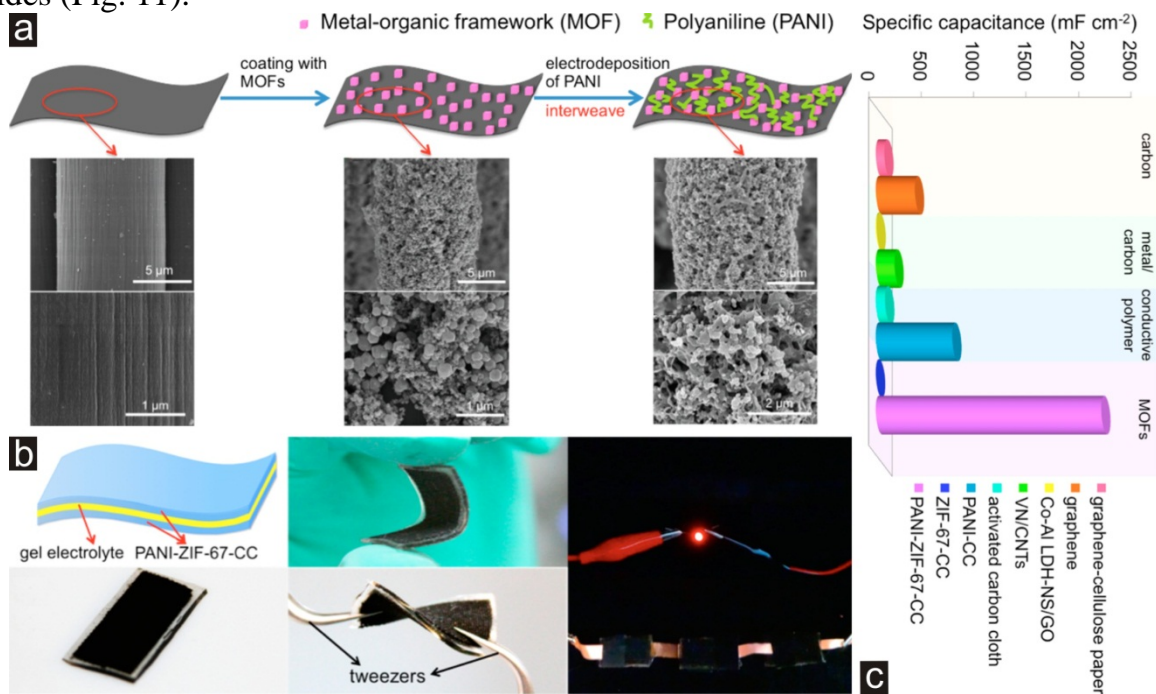


Figure 11 (a) Schematic illustration of the two-step fabrication process of flexible conductive porous electrode (PANI-ZIF-67-CC) by interweaving MOF crystals with PANI chains, and the corresponding SEM images. (b) Schematic illustration and photo of PANI-ZIF-67-CC flexible solid-state SC device. (c) Comparison of areal capacitances on typical reported SCs. Reprinted with permission from Ref. [35] Copyright 2015, American Chemical Society.

Conductive MOFs are a new class of promising microporous electrode materials for supercapacitors, compared to the conventional MOFs as electrode materials with intrinsically poor electrical conductivity [104, 109, 205]. Li et al. demonstrated the possibility to apply one of conductive MOFs (i.e., conductive Cu-CAT; conductivity as high as 20 S m^{-1} [205]) in a high-performance solid-state supercapacitor, where the highly oriented crystalline nanowire arrays (NWAs) of conductive MOF material (supported on carbon fiber paper) as integrated electrodes without conductive additives and binders [109]. By taking advantage of the nanostructure (irregularly shaped crystallite) and making full use of the high porosity and excellent conductivity, the symmetric solid-state supercapacitor can achieve a superior areal capacitance ($\approx 22 \text{ μF cm}^{-2}$) and rate performance, beyond most previously reported values for other MOF-

based supercapacitors or comparable to those of carbon-based symmetric solid-state supercapacitors (Fig. 12).

Recently, design and fabrication of hybrid supercapacitors (HSCs) has emerged as an alternative and effective strategy to enhance the energy storage capability of conventional SCs, i.e., assembling a battery-type positive electrode material with high specific capacitance and a capacitive negative electrode material with high rate capability and cyclability into a single device for narrowing the gap between batteries and SCs [11, 190, 206, 207].

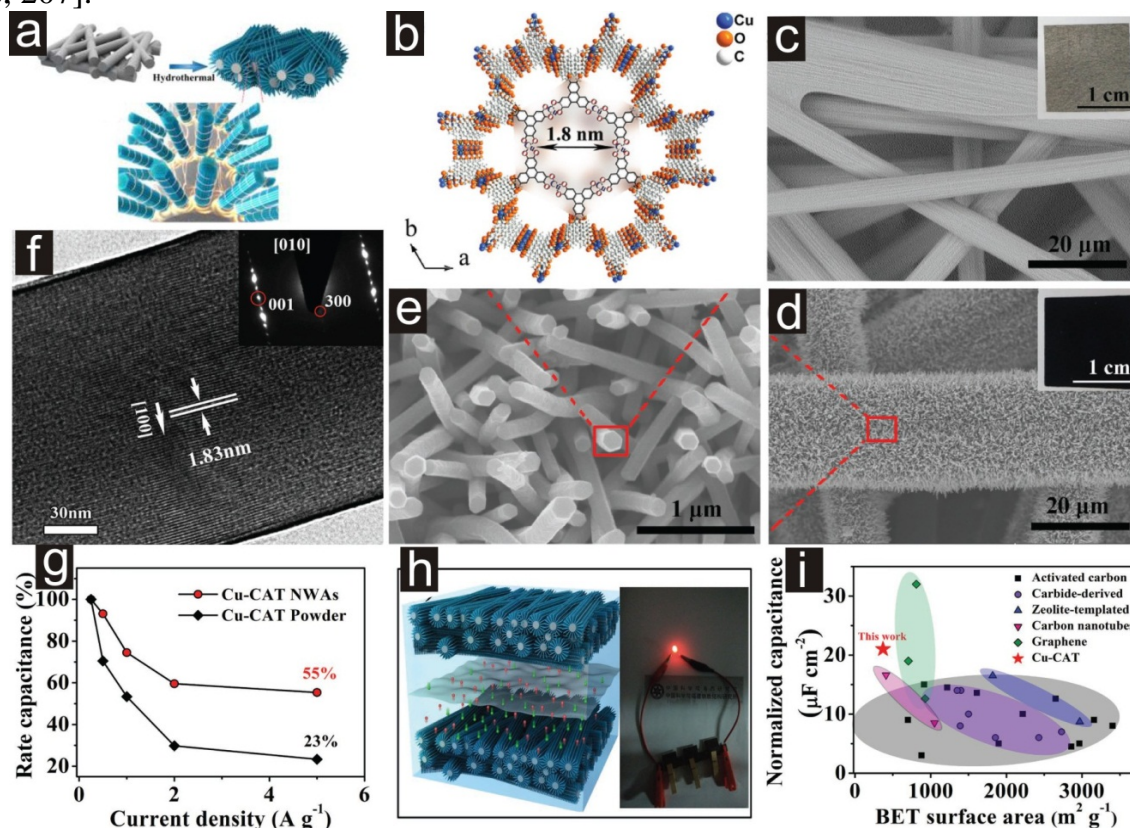


Figure 12 (a) Schematic illustration of the formation of conductive Cu-CAT NWAs on carbon fiber paper. (b) Crystal structure of Cu-CAT viewed along the c-axis. (c) SEM and photographic image (inset) of the carbon fiber paper. (d, e) SEM and photographic image (inset) of the Cu-CAT NWAs growing on carbon fiber paper. (f) TEM images of Cu-CAT nanowire (inset SAED pattern). Device performances of Cu-CAT NWA-based supercapacitor: (g) rate performance, (h) structure of the symmetric solid-state supercapacitor and the corresponding photograph of a proto, and (i) performance comparison of Cu-CAT NWAs and carbon materials based symmetric solid-state supercapacitors. Reprinted with permission from Ref. [109] Copyright 2017, WILEY-VCH.

Although the broadened voltage window and enhancement of both energy density/power densities for HSCs, researchers have encountered practical issues in finding proper positive/negative materials to match well with each other. Xu et al. developed a general and effective approach to design and prepare a flexible MOFs-based supercapacitor device via fabricating in-situ network of ZIF-67 particles connected by conductive PPy nanotubes [196]. The as-prepared ZIF-PPy hybrids demonstrated high gravimetric specific capacitance of 554 F g^{-1} at a current density of 0.5 A g^{-1} and excellent stability (90.7% capacitance retention over 10000 cycles, compared to that of 70.6% for ZIF-67 and 55.0% for PPy) as well as a high areal specific capacitance of 2.33 F cm^{-2} in a three-electrode system. For the symmetric supercapacitor (SSC) with ZIF-PPy on flexible graphite electrodes and PVA/ Na_2SO_4 as gel electrolyte, it exhibited stable performance between 0–0.6 V and a high areal specific capacitance of 226 mF cm^{-2} , which is a superior value compared with previously reported MOF-based flexible supercapacitors and has high potential for applications in flexible/wearable electronics (Fig. 13).

Zhang et al. designed flexible supercapacitors based on manganese oxides@MOFs via a simple approach to boost capacitance [178]. The metal oxides were introduced into the MOF systems through a very simple one-step chemically induced self-transformation process, e.g., in which the starting materials bimetallic MHCF nanocubes (manganese hexacyanoferrate hydrate, a classical Prussian blue analogue with Mn ions located at the outside of the unit cell) were evolved into MHCF– MnO_x by adding NH_4F . The hybrid product inherits the crystal structure of pristine MHCF, with a possible amorphous or weakly crystalline coating layer of MnO_x ($\text{MnO}/\text{Mn}_2\text{O}_3$), i.e., MnO_x “nanoflowers” distributed on the surface of each individual MHCF cubes. By forming intimate connection between the pseudocapacitive materials and MOFs, the performance of the composite can be remarkably increased. The MnO_x –MHCF hybrid in three-electrode system exhibited a threefold increase in terms of specific capacitance and rate capacitance compared to the pristine MOF ($\approx 1200 \text{ F g}^{-1}$ vs $\approx 300 \text{ F g}^{-1}$ at 10 A g^{-1}) or twofold increase to MnO_x ($\approx 400 \text{ F g}^{-1}$ at 10 A g^{-1}), in addition to the outstanding long-term cycling stability ($>94.7\%$ of its initial capacitance after 10000 cycles at 10 A g^{-1}). To further investigate the MnO_x –MHCF hybrid for practical applications, especially for flexible energy storage, a flexible solid-state-hybrid-supercapacitor (SSHC) device was fabricated based on MnO_x –MHCF as cathode and activated carbon as anode, Pt-coated polyethylene terephthalate (PET) substrate as the flexible conductive substrate, and PVA/KOH as the solid electrolyte. Areal capacitance is more relevant in the case of flexible/wearable energy storage devices; the calculated maximum areal capacitances of the SSHC were 175 to 127 mF cm^{-2} at the current density ranging from 0.5 to 5.0 mA cm^{-2} ; also the device exhibited good flexibility, lightweight characteristic and

outstanding stability (with capacitance retention of $\approx 94.5\%$ after 10000 cycles at 5.0 mA cm^{-2}) as well as a maximum volumetric energy density of 5.1 mW h cm^{-3} (210 W h kg^{-1}) (Fig. 14). The enhanced capacitance and increased conductivity of the electrode contribute to the outstanding performance of the device with significantly superior performance among recent reported state-of-the-art flexible supercapacitors.

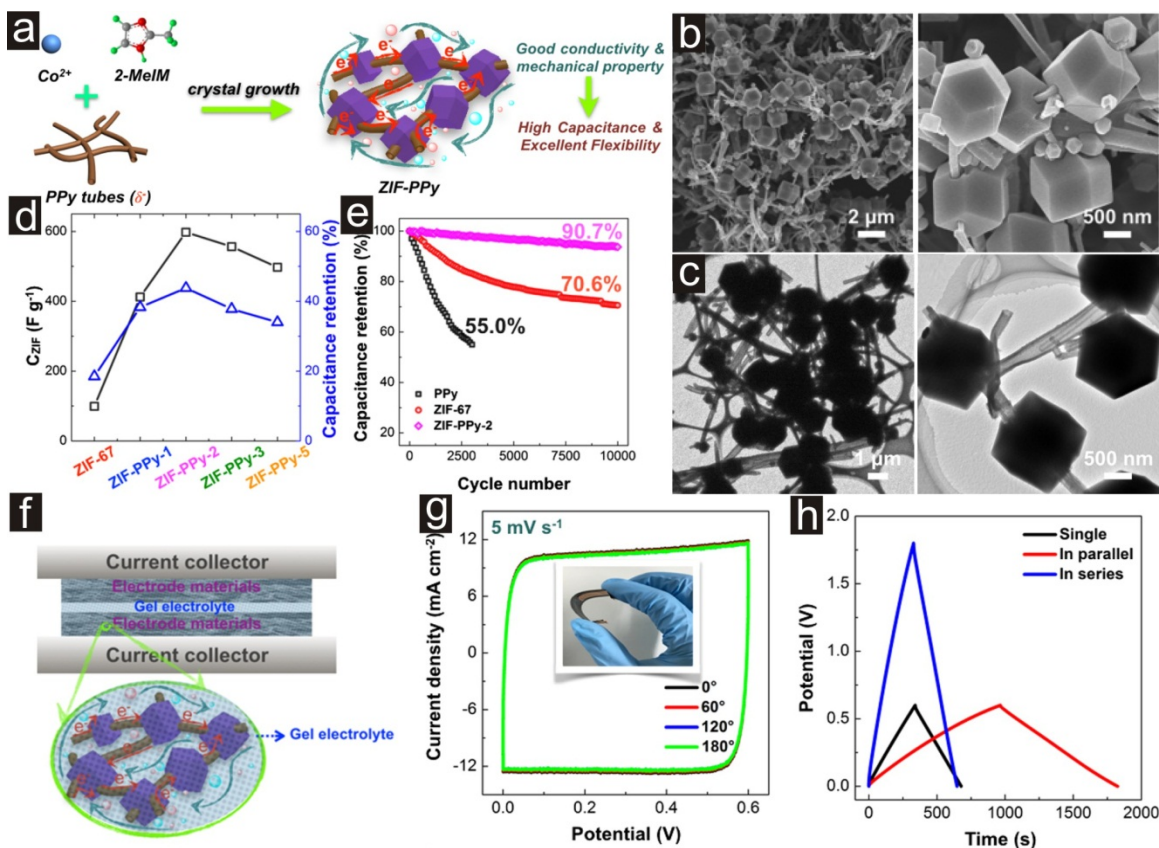


Figure 13 (a) Schematic illustration of the procedure for fabrication of 3D networked ZIF-PPy hybrids. (b) SEM and (c) TEM images of typical ZIF-PPy hybrids. (d) Capacitance and capacitance retention of ZIF-67 and various ZIF-PPy hybrids. (e) Comparison of the cycling performance of PPY, ZIF-67, and typical ZIF-PPy at 20 A g^{-1} . (f) Schematic representation of a flexible supercapacitor device based on ZIF-PPy electrodes and gel electrolyte, and the corresponding (g) CV curves subjected to different bending angles and (h) GCD curves with different device configurations. Reprinted with permission from Ref. [196] Copyright 2017, American Chemical Society.

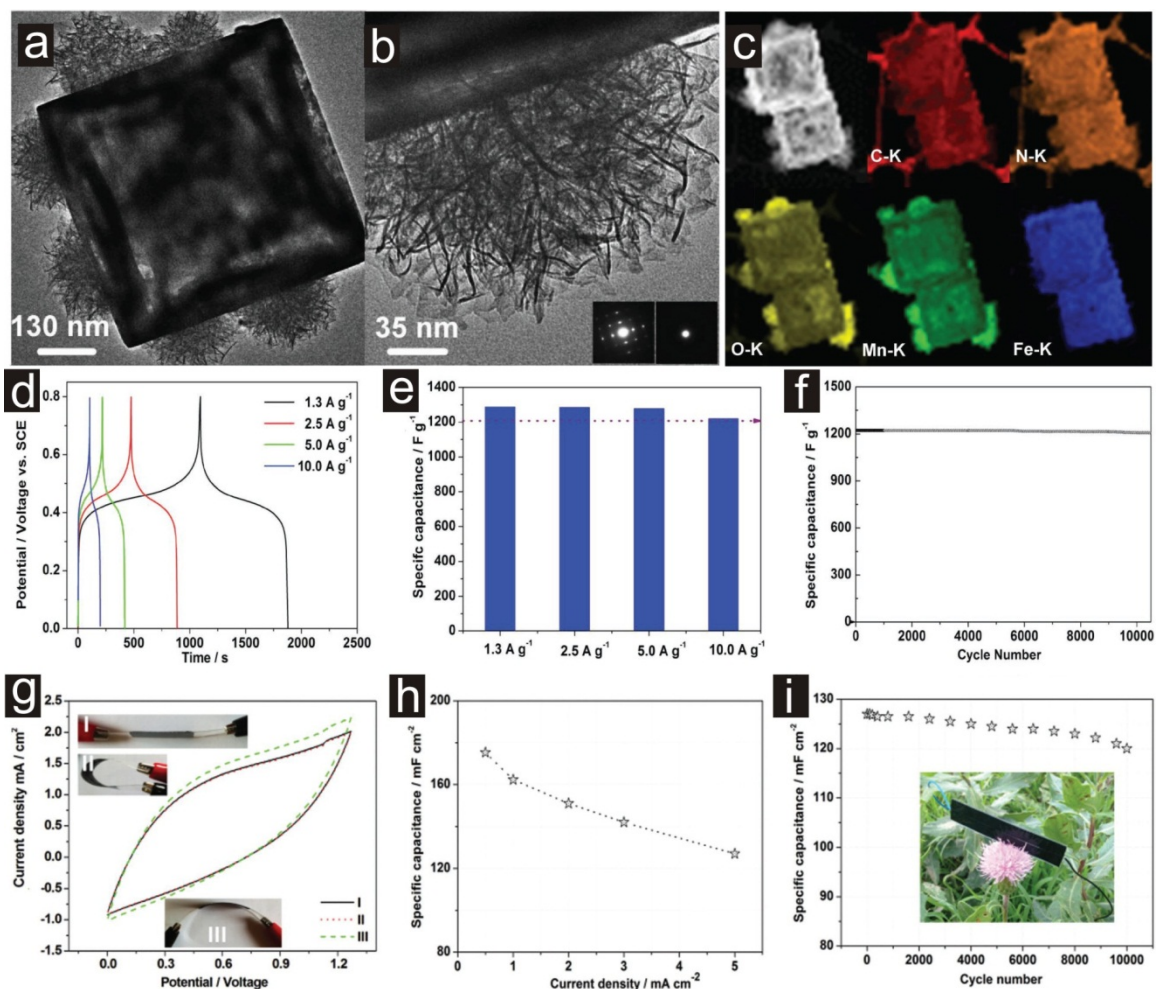


Figure 14 (a, b) TEM images of MnO_x-MHCF hybrid and SAED patterns (insets, left: nanocube, right: “flowers”). (c) EDS mappings for different elements in MnO_x-MHCF. Electrochemical behaviors of as-synthesized MnO_x-MHCF electrode in a three-electrode cell using 1 M Na₂SO₄ solution as electrolyte: (d) GCD curves, (e) specific capacitances, (f) cycling performance. Electrochemical performance of flexible supercapacitor based on MnO_x-MHCF (positive) and activated carbon (negative) active materials. (g) CV curves of the device under different bending angles, (h) specific capacitances, (i) cycling performance (5 mA cm⁻²). Reprinted with permission from Ref. [178] Copyright 2016, WILEY-VCH.

Among various MOFs with tunable structures and exceptional porosities, water stable pillared MOFs with dual ligands have been reported to exhibit high supercapacitor performance [190]. Qu et al. developed a “One-for-All” strategy to fabricate pillared MOF nanorods as precursor for both positive/negative electrodes of high-performance hybrid supercapacitor (HSC) [190]. The pillared MOF nanorods directly grown on carbon

fiber paper (CFP@TM-nanorods) function as the positive electrode of HSC under alkaline electrolyte and the calcinated N-doped hierarchical porous carbon nanorods (CFP@TM-NPCs) are utilized as the negative counter-electrode. TM-nanorods demonstrated much enhanced supercapacitor performances (862 F g^{-1} at 1 A g^{-1} and 790 F g^{-1} at 20 A g^{-1} ; capacitance retention of 80.8% after 13600 cycles at 10 A g^{-1}) when tested within 0–0.45 V, making it an ideal positive electrode material. Meanwhile, TM-NPCs were produced from a one-step heat treatment of TM-nanorods for an outstanding negative electrode material (330 F g^{-1} at 1 A g^{-1} and 290 F g^{-1} at 20 A g^{-1} ; high capacitance retention of 97.8% even after 10000 cycles at 10 A g^{-1}). As a hybrid device, the TM-nanorods//TM-NPCs device exhibits a wide voltage window of 1.5 V with a high sloping discharge plateau between 1.0–1.2 V along with outstanding energy/power densities (e.g., energy density of 47.1 W h kg^{-1} at a power density of 1018 W kg^{-1} and retaining 29.8 W h kg^{-1} at elevated working power of 17104 W kg^{-1}) and long-term cycling stability (retaining 83.2% of the initial capacitance after 10000 cycles at high current density of 10 A g^{-1} with columbic efficiencies of around 100%), indicating its great potential in practical applications (Fig. 15). The as-described “One-for-All” strategy will be widely applicable and highly reproducible in producing MOF-based electrode materials for HSC applications, which may shorten the gap between experimental synthesis and practical application of MOFs in fast energy storage [190, 192].

Device-level editability and programmability of flexible supercapacitors are highly desirable for the development of advanced portable and miniaturized electronics [32]. Cheng et al. demonstrated flexible highly conductive 2D-MOF/rGO papers through the electrostatic self-assembly of intrinsically electronegative GO sheets and electropositive MOF sheets followed by subsequent reduction processes [32]. The 2D-MOF/rGO hybrid paper with high mechanical robustness, tensile strength, and flexibility efficiently alleviates the self-restacking of rGO, and enhances the electrical conductivity of MOF structure. Based on different metal ions of MOFs, the cathode (Co-MOF/rGO) and anode (Ni-MOF/rGO) assembled flexible all-solid-state ASCs can achieve high energy densities due to the expanded voltage windows of the devices, demonstrating an outstanding volumetric energy density of $1.87 \text{ mW h cm}^{-3}$ and an ultrahigh volumetric power density of 250 mW cm^{-3} . Moreover, the operations of micro-SCs with artistically designed patterns are demonstrated (Fig. 16). Due to the improved electrochemical performances and edibility of the SCs, the ASCs based on 2D-MOF/rGO hybrid papers may pave a way for the development of scalable high-performance portable and stylish micro-sized integrated energy storage devices.

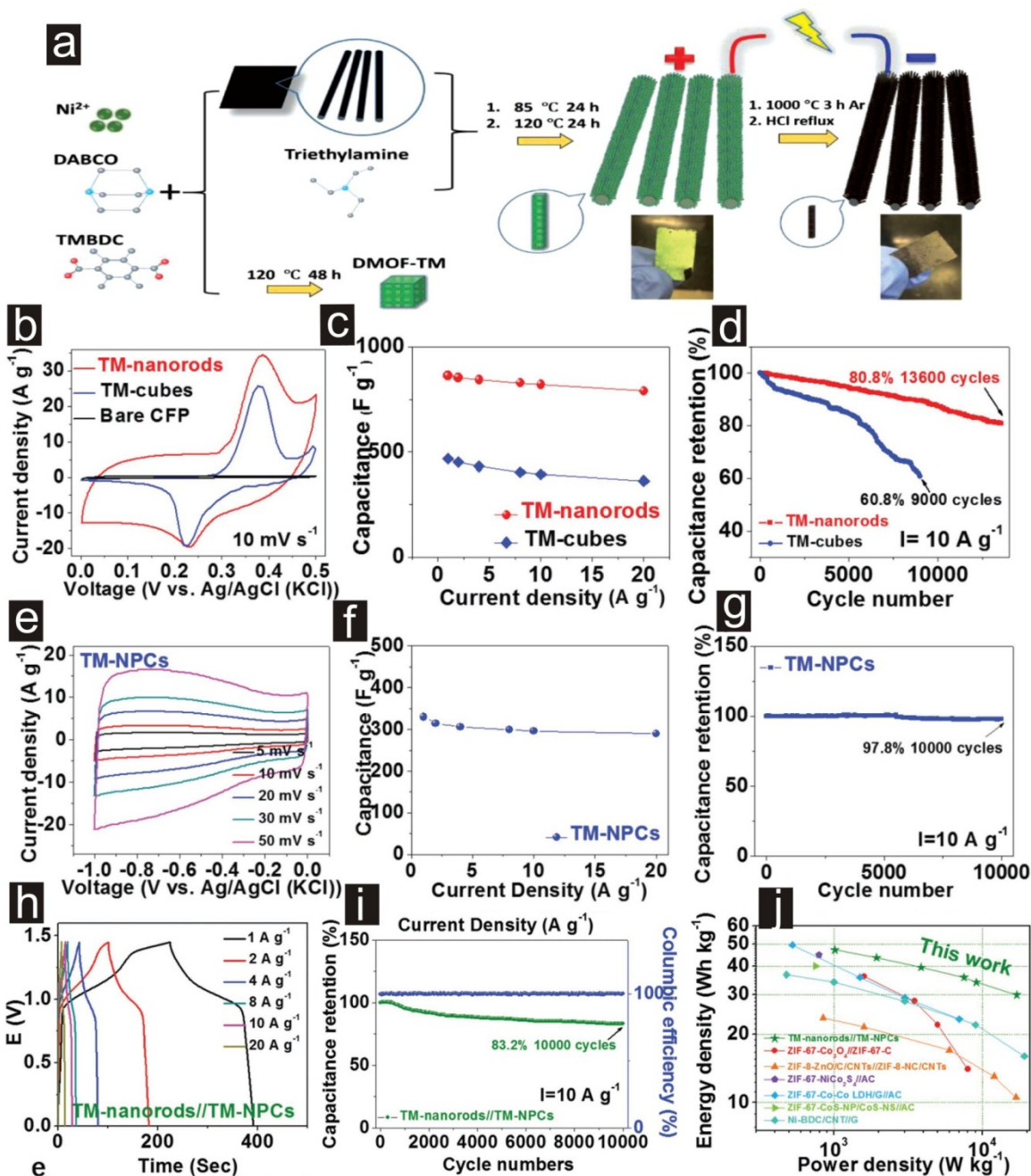


Figure 15 (a) Design and synthesis schematic of the "One-for-All" TM-nanorods//TM-NPCs hybrid supercapacitor (HSC) device. Three-electrode performances of (b–d) TM-nanorods and (e–g) TM-NPCs: (b) CV curves, (c) specific capacitances, and (d) cycling performance of TM-nanorods; (e) CV curves, (f) specific capacitances, (g) cycling performance of TM-NPCs. HSC performances of TM-nanorods//TM-NPCs: (h) GCD curves; (i) cycling performance, and (j) Ragone plots of the TM-nanorods//TM-NPCs and some reported MOF-derived HSCs. Reprinted with permission from Ref. [190] Copyright 2018, WILEY-VCH.

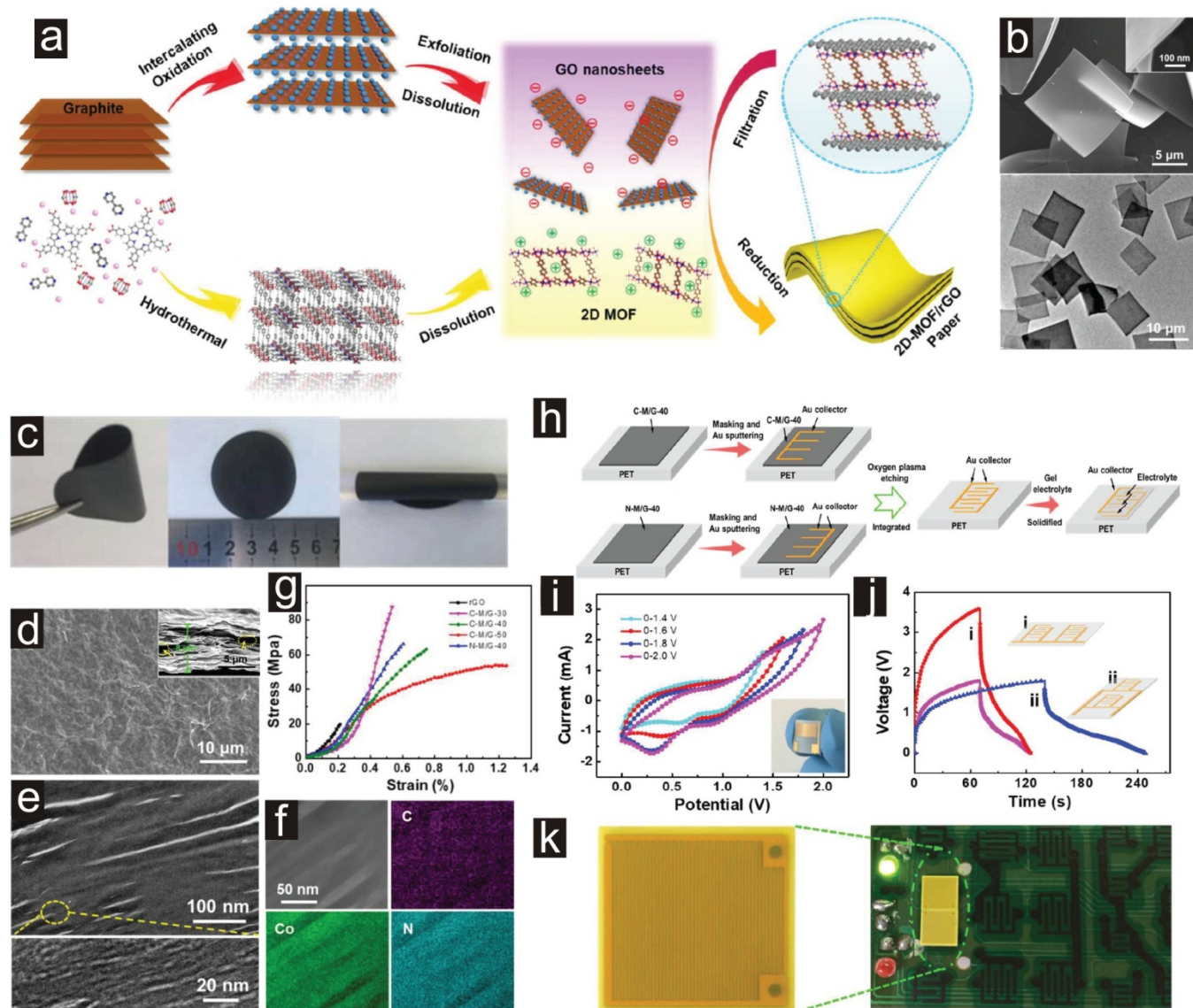


Figure 16 (a) Schematic illustration of the synthesis process of 2D-MOF/rGO paper. (b) SEM and TEM images of the as-synthesized 2D Co-MOF nanosheets. Characterization of flexible, free-standing 2D-MOF/rGO hybrid papers: (c) Photographs, (d, e) top-view and cross-sectional SEM images, (f) STEM image and the corresponding EDX elemental mapping images, and (g) enhanced mechanical properties (e.g., tensile strength, Young's modulus) of various 2D-MOF/rGO hybrid papers due to the hybridization (or interaction) between rGO and 2D-MOF. Fabrication and characterization of the in-plane flexible micro-supercapacitors: (h) Schematic of the process in the preparation of asymmetric micro-SCs devices (Co-MOF/graphene/Ni-MOF/graphene) on a PET substrate, (i) CV, (j) GCD curves for the as-designed flexible micro-SCs, and (k) integrated micro-SCs into a printed circuit board (PCB). Reprinted with permission from Ref. [32] Copyright 2018, The Royal Society of Chemistry.

Conclusion and Perspectives

In summary, the novel MOFs have attracted great attention and huge research interest as an emerging material for electrochemical energy storage especially for supercapacitors. The design and synthesis of conductive MOF composites are a promising and low-cost strategy to produce novel materials bearing a set of combined properties superior to those of the individual components. Alternatively, intrinsically conductive MOFs are a new class of promising electrode materials for energy storage applications in recent years. In future, much work should focus on overcoming some major challenges such as higher energy density, longer cycling performance, and higher mass loading of the active materials. However, given that MOFs possess well-established structure and property tunability, it will provide a great prospect for developing MOFs as an ideal class of electrode materials for supercapacitors. Several ongoing research hotspots and future trends of MOFs for high-performance supercapacitors are listed as follows:

- i) The structural design and controlling of the morphology, surface area, particle size and pore properties need to be further investigated for optimizing performances. The nanostructuring is an efficient way; together with the enhanced specific surface area and pore properties, it will provide more electroactive sites for higher and faster energy storage. Doping with heteroatoms may also tune the structures and improve the electrochemical behaviors thereof. The dissolution of the MOF electrodes, especially during the reduction process, which may severely limit the cycling stability of the electrode, should be further investigated and suppressed. Besides the enhancing of electrical conductivity and ion insertion via tailoring the structure or pore size, the compatibility between these MOFs and the electrolyte should also be considered, thus the optimization of MOF composition and electrolytes are so much beneficial. The introduction of redox additives into the electrolyte will directly give additional pseudocapacitance contributions to the electrode.
- ii) As an efficient strategy to improve the conductivity of MOFs, the integration of highly conductive components will not only embody the advantages of all constituents but also overcome the drawbacks of individual components to combine both the high energy density and high power density features. Carbon nanomaterials, especially graphene and 3D carbon networks, will provide versatile platforms for integrating MOFs for acting as most effective electrodes of supercapacitors or hybrid capacitors.
- iii) Asymmetric capacitors or hybrid capacitors are optional solutions to achieve higher energy and power density synchronously. By designing the electrolytes (especially the non-aqueous electrolytes) for optimum electrochemical performances, high-voltage operation and the higher energy/power densities thereof may be obtained without

compromising long-term cycling stability (or lifetime). Despite some critical factors for optimizing pseudocapacitive MOFs, it is quite promising for high-rate capability electrodes to couple with the capacitive (carbon) negative electrode when used in asymmetric (hybrid) devices for practical applications.

iv) Flexible solid-state supercapacitors (FSSCs) are stylish frontrunners in energy storage device technology and have attracted extensive attention owing to recent significant breakthroughs in modern wearable electronics. Although some encouraging progress has been made on flexible supercapacitors, their high energy density, mechanical robustness, bending-tolerant property, and performances under various severe service conditions, such as being seriously cut, bent, and heavily loaded, are still limited; excellent mechanical properties of electrodes are required for FSSCs to guarantee the stable energy output in wearable devices; several other intractable problems, especially for wearable applications, such as the potential risks of catching fire or corrosion, short cycling life, rather long charging time, and the difficulties in meeting the rigid requirement for various forming factors are also concerned. Micro-supercapacitors with editable properties (e.g., on-chip or in-plane flexible micro-SCs with folding, cutting, and stretching advantages) have emerged as favorable alternatives or complements to micro-batteries, not only because of the intrinsic characteristics of supercapacitors, but also due to their high compatibility with flexible application scenarios and miniaturized features.

Acknowledgements

This work was supported by the National Natural Science Foundation of China (Grant Nos. 51403193, 51403132) and Open Project Foundation of the Beijing National Laboratory for Molecular Sciences (2016).

Abbreviations: AC, activated carbon; ACN, acetonitrile; ASC, asymmetric supercapacitor; CB, carbon black; CC, carbon (fiber) cloth; CE, coulombic efficiency; CNTs, carbon nanotubes; HSC, hybrid supercapacitor; MSE, mercury-mercurous sulfate electrode; MWCNTs, multi-walled carbon nanotubes; SCE, saturated calomel electrode; SSC, symmetric supercapacitor. Ligands: $(C_2H_5)_4NBF_4$, tetraethylammonium tetrafluoroborate; *bdc*, 1,4-benzenedicarboxylate; *BPDC*, 4,4'-biphenyldicarboxylic; *bpy*, 4,4'-bipyridine; *BPYDC*, 2,2'-bipyridine-5,5'-dicarboxylate; *dib*, 1,4-di(1H-imidazol-1-yl)butane; *H₂BDC*, 1,4-dicarboxybenzene; *H₂tfbdc*, 2,3,5,6-tetrafluoroterephthalic acid; *H₃BTC*, 1,3,5-benzenetricarboxylic acid (trimesic acid); *H₃BTTB*, 4,4',4''-[benzene-1,3,5-triyl-tris(oxy)]tribenzoic acid; *H₄btec*, 1,2,4,5-benzenetetracarboxylate acid; *HAB*, hexaaminobenzene; *HITP*, 2,3,6,7,10,11-hexaiminotriphenylene; *Hmt*, hexamethylenetetramine; *HTATB*, 4,4',4''-s-triazine-2,4,6-triyl-tribenzoic acid; *mpinh*, 2-methylpyridinecarboxaldehyde isonicotinohydrazide; *PDC*, 3,5-pyridinedicarboxylic

acid; *POAP*, poly(ortho-aminophenol); *PTA*, p-benzenedicarboxylic acid; *pydc*, pyridine-2,6-dicarboxylate; *TBAPF₆*, tetrabutylammonium hexafluorophosphate; *TCPP*, 5,10,15,20-tetrakis(4-carboxyphenyl)porphyrin; *TEABF₄*, tetraethylammonium tetrafluoroborate; *TPA*, terephthalic acid.

References

- [1] S.-L. Li, Q. Xu, Metal–organic frameworks as platforms for clean energy, *Energy Environ. Sci.* **6** (2013) 1656-1683. <https://doi.org/10.1039/c3ee40507a>
- [2] Z. Wei, L. Wang, M. Zhuo, W. Ni, H. Wang, J. Ma, Layered Tin Sulfide and Selenide Anode Materials for Li- and Na-ion Batteries, *J. Mater. Chem. A* **6** (2018) 12185-12214. <https://doi.org/10.1039/C8TA02695E>
- [3] J. Huang, Z. Wei, J. Liao, W. Ni, C. Wang, J. Ma, Molybdenum and tungsten chalcogenides for lithium/sodium-ion batteries: Beyond MoS₂, *J. Energy Chem.* (2018). <https://doi.org/10.1016/j.jechem.2018.09.001>
- [4] S. Zheng, X. Li, B. Yan, Q. Hu, Y. Xu, X. Xiao, H. Xue, H. Pang, Transition-metal (Fe, Co, Ni) based metal-organic frameworks for electrochemical energy storage, *Adv. Energy Mater.* **7** (2017) 1602733. <https://doi.org/10.1002/aenm.201602733>
- [5] F. Wang, X. Wu, X. Yuan, Z. Liu, Y. Zhang, L. Fu, Y. Zhu, Q. Zhou, Y. Wu, W. Huang, Latest advances in supercapacitors: from new electrode materials to novel device designs, *Chem. Soc. Rev.* **46** (2017) 6816-6854. <https://doi.org/10.1039/C7CS00205J>
- [6] W. Ni, B. Wang, J. Cheng, X. Li, Q. Guan, G. Gu, L. Huang, Hierarchical foam of exposed ultrathin nickel nanosheets supported on chainlike Ni-nanowires and the derivative chalcogenide for enhanced pseudocapacitance, *Nanoscale* **6** (2014) 2618-2623. <https://doi.org/10.1039/C3NR06031D>
- [7] W. Ni, J. Cheng, X. Li, G. Gu, L. Huang, Q. Guan, D. Yuan, B. Wang, Polymeric cathode materials of electroactive conducting poly (triphenylamine) with optimized structures for potential organic pseudo-capacitors with higher cut-off voltage and energy density, *RSC Adv.* **5** (2015) 9221-9227. <https://doi.org/10.1039/C4RA14401E>
- [8] W. Raza, F. Ali, N. Raza, Y. Luo, K.-H. Kim, J. Yang, S. Kumar, A. Mehmood, E.E. Kwon, Recent advancements in supercapacitor technology, *Nano Energy* **52** (2018) 441-473. <https://doi.org/10.1016/j.nanoen.2018.08.013>

- [9] Y. Jiao, J. Pei, D. Chen, C. Yan, Y. Hu, Q. Zhang, G. Chen, Mixed-metallic MOF based electrode materials for high performance hybrid supercapacitors, *J. Mater. Chem. A* 5 (2017) 1094-1102. <https://doi.org/10.1039/C6TA09805C>
- [10] Y. Jiao, J. Pei, C. Yan, D. Chen, Y. Hu, G. Chen, Layered nickel metal-organic framework for high performance alkaline battery-supercapacitor hybrid devices, *J. Mater. Chem. A* 4 (2016) 13344-13351. <https://doi.org/10.1039/C6TA05384J>
- [11] D.P. Dubal, O. Ayyad, V. Ruiz, P. Gomez-Romero, Hybrid energy storage: the merging of battery and supercapacitor chemistries, *Chem. Soc. Rev.* 44 (2015) 1777-1790. <https://doi.org/10.1039/C4CS00266K>
- [12] Z. Wu, L. Li, J.-m. Yan, X.-b. Zhang, Materials design and system construction for conventional and new-concept supercapacitors, *Adv. Sci.* 4 (2017) 1600382. <https://doi.org/10.1002/advs.201600382>
- [13] A. Morozan, F. Jaouen, Metal organic frameworks for electrochemical applications, *Energy Environ. Sci.* 5 (2012) 9269-9290. <https://doi.org/10.1039/c2ee22989g>
- [14] X. Cao, C. Tan, M. Sindoro, H. Zhang, Hybrid micro-/nano-structures derived from metal-organic frameworks: preparation and applications in energy storage and conversion, *Chem. Soc. Rev.* 46 (2017) 2660-2677. <https://doi.org/10.1039/C6CS00426A>
- [15] H. Wang, Q.-L. Zhu, R. Zou, Q. Xu, Metal-Organic Frameworks for Energy Applications, *Chem* 2 (2017) 52-80. <https://doi.org/10.1016/j.chempr.2016.12.002>
- [16] H. Furukawa, K.E. Cordova, M. O'Keeffe, O.M. Yaghi, The chemistry and applications of metal-organic frameworks, *Science* 341 (2013) 1230444. <https://doi.org/10.1126/science.1230444>
- [17] W. Zhao, J. Peng, W. Wang, S. Liu, Q. Zhao, W. Huang, Ultrathin two-dimensional metal-organic framework nanosheets for functional electronic devices, *Coord. Chem. Rev.* 377 (2018) 44-63. <https://doi.org/10.1016/j.ccr.2018.08.023>
- [18] Y. Zhao, Z. Song, X. Li, Q. Sun, N. Cheng, S. Lawes, X. Sun, Metal organic frameworks for energy storage and conversion, *Energy Storage Mater.* 2 (2016) 35-62. <https://doi.org/10.1016/j.ensm.2015.11.005>
- [19] L. Wang, Y. Han, X. Feng, J. Zhou, P. Qi, B. Wang, Metal-organic frameworks for energy storage: Batteries and supercapacitors, *Coord. Chem. Rev.* 307 (2016) 361-381. <https://doi.org/10.1016/j.ccr.2015.09.002>

- [20] Y. Xu, Q. Li, H. Xue, H. Pang, Metal-organic frameworks for direct electrochemical applications, *Coord. Chem. Rev.* 376 (2018) 292-318.
<https://doi.org/10.1016/j.ccr.2018.08.010>
- [21] F.-S. Ke, Y.-S. Wu, H. Deng, Metal-organic frameworks for lithium ion batteries and supercapacitors, *J. Solid State Chem.* 223 (2015) 109-121.
<https://doi.org/10.1016/j.jssc.2014.07.008>
- [22] G. Xu, P. Nie, H. Dou, B. Ding, L. Li, X. Zhang, Exploring metal organic frameworks for energy storage in batteries and supercapacitors, *Mater. Today* 20 (2017) 191-209. <https://doi.org/10.1016/j.mattod.2016.10.003>
- [23] Y. Zheng, S. Zheng, H. Xue, H. Pang, Metal-organic frameworks/graphene-based materials: Preparations and applications, *Adv. Funct. Mater.* 28 (2018) 1804950.
<https://doi.org/10.1002/adfm.201804950>
- [24] Z. Liang, C. Qu, W. Guo, R. Zou, Q. Xu, Pristine metal–organic frameworks and their composites for energy storage and conversion, *Adv. Mater.* 30 (2018) 1702891.
<https://doi.org/10.1002/adma.201702891>
- [25] J. Zhou, B. Wang, Emerging crystalline porous materials as a multifunctional platform for electrochemical energy storage, *Chem. Soc. Rev.* 46 (2017) 6927-6945.
<https://doi.org/10.1039/C7CS00283A>
- [26] Z. Xie, W. Xu, X. Cui, Y. Wang, Recent progress in metal–organic frameworks and their derived nanostructures for energy and environmental applications, *ChemSusChem* 10 (2017) 1645-1663. <https://doi.org/10.1002/cssc.201601855>
- [27] B. Valizadeh, T.N. Nguyen, K.C. Stylianou, Shape engineering of metal–organic frameworks, *Polyhedron* 145 (2018) 1-15. <https://doi.org/10.1016/j.poly.2018.01.004>
- [28] Y. Zhao, J. Liu, M. Horn, N. Motta, M. Hu, Y. Li, Recent advancements in metal organic framework based electrodes for supercapacitors, *Sci. China Mater.* 61 (2018) 159-184. <https://doi.org/10.1007/s40843-017-9153-x>
- [29] S. Zheng, H. Xue, H. Pang, Supercapacitors based on metal coordination materials, *Coord. Chem. Rev.* 373 (2018) 2-21.
<https://doi.org/10.1016/j.ccr.2017.07.002>
- [30] S. Sundriyal, H. Kaur, S.K. Bhardwaj, S. Mishra, K.-H. Kim, A. Deep, Metal-organic frameworks and their composites as efficient electrodes for supercapacitor applications, *Coord. Chem. Rev.* 369 (2018) 15-38.
<https://doi.org/10.1016/j.ccr.2018.04.018>

- [31] W. Du, Y.-L. Bai, J. Xu, H. Zhao, L. Zhang, X. Li, J. Zhang, Advanced metal-organic frameworks (MOFs) and their derived electrode materials for supercapacitors, *J. Power Sources* 402 (2018) 281-295. <https://doi.org/10.1016/j.jpowsour.2018.09.023>
- [32] J. Cheng, S. Chen, D. Chen, L. Dong, J. Wang, T. Zhang, T. Jiao, B. Liu, H. Wang, J.-J. Kai, D. Zhang, G. Zheng, L. Zhi, F. Kang, W. Zhang, Editable asymmetric all-solid-state supercapacitors based on high-strength, flexible, and programmable 2D-metal-organic framework/reduced graphene oxide self-assembled papers, *J. Mater. Chem. A* 6 (2018) 20254-20266. <https://doi.org/10.1039/C8TA06785F>
- [33] K.M. Choi, H.M. Jeong, J.H. Park, Y.-B. Zhang, J.K. Kang, O.M. Yaghi, Supercapacitors of nanocrystalline metal-organic frameworks, *ACS Nano* 8 (2014) 7451-7457. <https://doi.org/10.1021/nn5027092>
- [34] W. Xia, A. Mahmood, R. Zou, Q. Xu, Metal-organic frameworks and their derived nanostructures for electrochemical energy storage and conversion, *Energy Environ. Sci.* 8 (2015) 1837-1866. <https://doi.org/10.1039/C5EE00762C>
- [35] L. Wang, X. Feng, L. Ren, Q. Piao, J. Zhong, Y. Wang, H. Li, Y. Chen, B. Wang, Flexible solid-state supercapacitor based on a metal-organic framework interwoven by electrochemically-deposited PANI, *J. Am. Chem. Soc.* 137 (2015) 4920-4923. <https://doi.org/10.1021/jacs.5b01613>
- [36] Z. Zhang, Y. Chen, X. Xu, J. Zhang, G. Xiang, W. He, X. Wang, Well-defined metal-organic framework hollow nanocages, *Angew. Chem. Int. Ed.* 53 (2014) 429-433. <https://doi.org/10.1002/anie.201308589>
- [37] D. Liu, J. Wan, G. Pang, Z. Tang, Hollow metal-organic-framework micro/nanostructures and their derivatives: Emerging multifunctional materials, *Adv. Mater.* 0 (2019) 1803291. <https://doi.org/10.1002/adma.201803291>
- [38] M. Zhao, Q. Lu, Q. Ma, H. Zhang, Two-dimensional metal-organic framework nanosheets, *Small Methods* 1 (2017) 1600030. <https://doi.org/10.1002/smtd.201600030>
- [39] P. Kumar, K.-H. Kim, V. Bansal, P. Kumar, Nanostructured materials: A progressive assessment and future direction for energy device applications, *Coord. Chem. Rev.* 353 (2017) 113-141. <https://doi.org/10.1016/j.ccr.2017.10.005>
- [40] H.-Y. Guan, R.J. LeBlanc, S.-Y. Xie, Y. Yue, Recent progress in the syntheses of mesoporous metal-organic framework materials, *Coord. Chem. Rev.* 369 (2018) 76-90. <https://doi.org/10.1016/j.ccr.2018.05.001>
- [41] Q.-L. Zhu, Q. Xu, Metal-organic framework composites, *Chem. Soc. Rev.* 43 (2014) 5468-5512. <https://doi.org/10.1039/C3CS60472A>

- [42] B. Li, M. Zheng, H. Xue, H. Pang, High performance electrochemical capacitor materials focusing on nickel based materials, *Inorg. Chem. Front.* 3 (2016) 175-202. <https://doi.org/10.1039/C5QI00187K>
- [43] S.K. Bhardwaj, N. Bhardwaj, R. Kaur, J. Mehta, A.L. Sharma, K.-H. Kim, A. Deep, An overview of different strategies to introduce conductivity in metal–organic frameworks and miscellaneous applications thereof, *J. Mater. Chem. A* 6 (2018) 14992-15009. <https://doi.org/10.1039/C8TA04220A>
- [44] D.Y. Lee, S.J. Yoon, N.K. Shrestha, S.-H. Lee, H. Ahn, S.-H. Han, Unusual energy storage and charge retention in Co-based metal–organic-frameworks, *Microporous Mesoporous Mater.* 153 (2012) 163-165. <https://doi.org/10.1016/j.micromeso.2011.12.040>
- [45] D.Y. Lee, D.V. Shinde, E.-K. Kim, W. Lee, I.-W. Oh, N.K. Shrestha, J.K. Lee, S.-H. Han, Supercapacitive property of metal–organic-frameworks with different pore dimensions and morphology, *Microporous Mesoporous Mater.* 171 (2013) 53-57. <https://doi.org/10.1016/j.micromeso.2012.12.039>
- [46] X. Liu, C. Shi, C. Zhai, M. Cheng, Q. Liu, G. Wang, Cobalt-based layered metal–organic framework as an ultrahigh capacity supercapacitor electrode material, *ACS Appl. Mater. Interfaces* 8 (2016) 4585-4591. <https://doi.org/10.1021/acsami.5b10781>
- [47] H. Yu, D. Xu, Q. Xu, Dual template effect of supercritical CO₂ in ionic liquid to fabricate a highly mesoporous cobalt metal–organic framework, *Chem. Commun.* 51 (2015) 13197-13200. <https://doi.org/10.1039/C5CC04009D>
- [48] G. Zhu, H. Wen, M. Ma, W. Wang, L. Yang, L. Wang, X. Shi, X. Cheng, X. Sun, Y. Yao, A self-supported hierarchical Co-MOF as a supercapacitor electrode with ultrahigh areal capacitance and excellent rate performance, *Chem. Commun.* 54 (2018) 10499-10502. <https://doi.org/10.1039/C8CC03669A>
- [49] J. Yang, Z. Ma, W. Gao, M. Wei, Layered structural Co-based mof with conductive network frames as a new supercapacitor electrode, *Chem. Eur. J.* 23 (2017) 631-636. <https://doi.org/10.1002/chem.201604071>
- [50] X.-Y. Hou, X. Wang, S.-N. Li, Y.-C. Jiang, M.-C. Hu, Q.-G. Zhai, Gas uptake and supercapacitor performance of a highly connected porous Co-metal–organic framework induced by ligand bulk, *Cryst. Growth Des.* 17 (2017) 3229-3235. <https://doi.org/10.1021/acs.cgd.7b00215>
- [51] K. Wang, X. Wang, D. Zhang, H. Wang, Z. Wang, M. Zhao, R. Xi, H. Wu, M. Zheng, Interpenetrated nano-MOFs for ultrahigh-performance supercapacitors and excellent dye adsorption performance, *CrystEngComm* 20 (2018) 6940-6949. <https://doi.org/10.1039/C8CE01067F>

- [52] Z.-X. Li, G. Ye, J. Han, Y. Yang, K.-Y. Zou, X. Wang, X.-L. Wang, X.-F. Gou, 1D–3D mixed-ligand frameworks with an unusual dmp topology tuned by intersection angles of isomeric benzenedicarboxylates: magnetic properties, gas-dependent calcination-thermolysis and energy storage performances, *Dalton Trans.* 44 (2015) 9209-9220. <https://doi.org/10.1039/C5DT00963D>
- [53] S.D. Worrall, H. Mann, A. Rogers, M.A. Bissett, M.P. Attfield, R.A.W. Dryfe, Electrochemical deposition of zeolitic imidazolate framework electrode coatings for supercapacitor electrodes, *Electrochim. Acta* 197 (2016) 228-240. <https://doi.org/10.1016/j.electacta.2016.02.145>
- [54] S. Prakash, P. Muthuraja, K. Balamurugan, J. Anandha Raj, P. Manisankar, Porous cobalt metal-organic framework with ultracapacitor activity, *Mater. Lett.* 222 (2018) 8-11. <https://doi.org/10.1016/j.matlet.2018.03.087>
- [55] R. Rajak, M. Saraf, A. Mohammad, S.M. Mobin, Design and construction of a ferrocene based inclined polycatenated Co-MOF for supercapacitor and dye adsorption applications, *J. Mater. Chem. A* 5 (2017) 17998-18011. <https://doi.org/10.1039/C7TA03773B>
- [56] R. Ramachandran, C. Zhao, D. Luo, K. Wang, F. Wang, Morphology-dependent electrochemical properties of cobalt-based metal organic frameworks for supercapacitor electrode materials, *Electrochim. Acta* 267 (2018) 170-180. <https://doi.org/10.1016/j.electacta.2018.02.074>
- [57] X. Liu, H.L. Valentine, W.-P. Pan, Y. Cao, B. Yan, 2D metal–organic frameworks: Syntheses, structures, and electrochemical properties, *Inorg. Chim. Acta* 447 (2016) 162-167. <https://doi.org/10.1016/j.ica.2016.03.048>
- [58] W. Xuan, R. Ramachandran, C. Zhao, F. Wang, Influence of synthesis temperature on cobalt metal-organic framework (Co-MOF) formation and its electrochemical performance towards supercapacitor electrodes, *J. Solid State Electrochem.* 22 (2018) 3873-3881. <https://doi.org/10.1007/s10008-018-4096-7>
- [59] D. Zhang, H. Shi, R. Zhang, Z. Zhang, N. Wang, J. Li, B. Yuan, H. Bai, J. Zhang, Quick synthesis of zeolitic imidazolate framework microflowers with enhanced supercapacitor and electrocatalytic performances, *RSC Adv.* 5 (2015) 58772-58776. <https://doi.org/10.1039/C5RA08226A>
- [60] L. Kang, S.-X. Sun, L.-B. Kong, J.-W. Lang, Y.-C. Luo, Investigating metal-organic framework as a new pseudo-capacitive material for supercapacitors, *Chin. Chem. Lett.* 25 (2014) 957-961. <https://doi.org/10.1016/j.cclet.2014.05.032>

- [61] J. Yang, P. Xiong, C. Zheng, H. Qiu, M. Wei, Metal-organic frameworks: a new promising class of materials for a high performance supercapacitor electrode, *J. Mater. Chem. A* **2** (2014) 16640-16644. <https://doi.org/10.1039/C4TA04140B>
- [62] J. Xu, C. Yang, Y. Xue, C. Wang, J. Cao, Z. Chen, Facile synthesis of novel metal-organic nickel hydroxide nanorods for high performance supercapacitor, *Electrochim. Acta* **211** (2016) 595-602. <https://doi.org/10.1016/j.electacta.2016.06.090>
- [63] J. Luo, X. Yang, S. Wang, Y. Bi, A. Nautiyal, X. Zhang, Facile synthesis of nickel-based metal organic framework [Ni₃(HCOO)₆] by microwave method and application for supercapacitor, *Funct. Mater. Lett.* **11** (2018) 1850030. <https://doi.org/10.1142/S1793604718500303>
- [64] C.M. Liao, J.C. Zhao, B.H.J. Tang, A.M. Tang, Y.H. Sun, J.L. Xu, Electrochemical performance of M-3(BTC)(2)center dot 12H(2)O (M=Co, Ni, and Zn) for supercapacitors, *J. New Mater. Electrochem. Syst.* **15** (2012) 79-82. <https://doi.org/10.14447/jnmes.v15i2.74>
- [65] K. Wang, Z. Wang, X. Wang, X. Zhou, Y. Tao, H. Wu, Flexible long-chain-linker constructed Ni-based metal-organic frameworks with 1D helical channel and their pseudo-capacitor behavior studies, *J. Power Sources* **377** (2018) 44-51. <https://doi.org/10.1016/j.jpowsour.2017.11.087>
- [66] C. Feng, C.-P. Lv, Z.-Q. Li, H. Zhao, H.-H. Huang, A porous 2D Ni-MOF material with a high supercapacitive performance, *J. Solid State Chem.* **265** (2018) 244-247. <https://doi.org/10.1016/j.jssc.2018.06.019>
- [67] C. Shi, X. Wang, Y. Gao, H. Rong, Y. Song, H.-J. Liu, Q. Liu, Nickel metal-organic framework nanoparticles as electrode materials for Li-ion batteries and supercapacitors, *J. Solid State Electrochem.* **21** (2017) 2415-2423. <https://doi.org/10.1007/s10008-017-3591-6>
- [68] S. Gao, Y. Sui, F. Wei, J. Qi, Q. Meng, Y. He, Facile synthesis of cuboid Ni-MOF for high-performance supercapacitors, *J. Mater. Sci.* **53** (2018) 6807-6818. <https://doi.org/10.1007/s10853-018-2005-1>
- [69] C. Zhang, Q. Zhang, K. Zhang, Z. Xiao, Y. Yang, L. Wang, Facile synthesis of a two-dimensional layered Ni-MOF electrode material for high performance supercapacitors, *RSC Adv.* **8** (2018) 17747-17753. <https://doi.org/10.1039/C8RA01002A>
- [70] Q. Hu, L. Qin, J. Lei, X.-X. Tan, G. Ni, Y.-Q. Wang, J. Li, F.-H. Cao, Nitrogen-rich metal-organic framework: Dye adsorptions and electrochemical performance, *Polyhedron* **151** (2018) 33-36. <https://doi.org/10.1016/j.poly.2018.05.014>

- [71] C. Qu, Y. Jiao, B. Zhao, D. Chen, R. Zou, K.S. Walton, M. Liu, Nickel-based pillared MOFs for high-performance supercapacitors: Design, synthesis and stability study, *Nano Energy* 26 (2016) 66-73. <https://doi.org/10.1016/j.nanoen.2016.04.003>
- [72] Q. Li, W. Teng, L. Han, R. Liu, 2D Nanoflakes of metal-polyphenolic coordination assembly for high-performance supercapacitor, *Inorg. Chem. Commun.* 90 (2018) 51-56. <https://doi.org/10.1016/j.inoche.2018.02.005>
- [73] C. Liao, Y. Zuo, W. Zhang, J. Zhao, B. Tang, A. Tang, Y. Sun, J. Xu, Electrochemical performance of metal-organic framework synthesized by a solvothermal method for supercapacitors, *Russ. J. Electrochem.* 49 (2013) 983-986. <https://doi.org/10.1134/S1023193512080113>
- [74] F. Zhang, G. Zhang, H. Yao, Z. Gao, X. Chen, Y. Yang, Scalable in-situ growth of self-assembled coordination supramolecular network arrays: A novel high-performance energy storage material, *Chem. Eng. J.* 338 (2018) 230-239. <https://doi.org/10.1016/j.cej.2018.01.003>
- [75] X. Wang, X. Liu, H. Rong, Y. Song, H. Wen, Q. Liu, Layered manganese-based metal-organic framework as a high capacity electrode material for supercapacitors, *RSC Adv.* 7 (2017) 29611-29617. <https://doi.org/10.1039/C7RA04374K>
- [76] W. Gao, D. Chen, H. Quan, R. Zou, W. Wang, X. Luo, L. Guo, Fabrication of hierarchical porous metal-organic framework electrode for aqueous asymmetric supercapacitor, *ACS Sustainable Chem. Eng.* 5 (2017) 4144-4153. <https://doi.org/10.1021/acssuschemeng.7b00112>
- [77] Q. Lu, Y. Tan, W. Ye, B. Tang, Preparation and performance of Zr-MOF with different particle sizes, *Battery Bimonthly* 45 (2015) 252-254.
- [78] F. Yang, W. Li, B. Tang, Facile synthesis of amorphous UiO-66 (Zr-MOF) for supercapacitor application, *J. Alloys Compd.* 733 (2018) 8-14. <https://doi.org/10.1016/j.jallcom.2017.10.129>
- [79] Y. Tan, W. Zhang, Y. Gao, J. Wu, B. Tang, Facile synthesis and supercapacitive properties of Zr-metal organic frameworks (UiO-66), *RSC Adv.* 5 (2015) 17601-17605. <https://doi.org/10.1039/C4RA11896K>
- [80] N. Campagnol, R. Romero-Vara, W. Deleu, L. Stappers, K. Binnemans, D.E. De Vos, J. Fransaer, A hybrid supercapacitor based on porous carbon and the metal-organic framework MIL-100(Fe), *ChemElectroChem* 1 (2014) 1182-1188. <https://doi.org/10.1002/celec.201402022>
- [81] L. Zhou, Z. Yang, C. Li, B. Chen, Y. Wang, L. Fu, Y. Zhu, X. Liu, Y. Wu, Prussian blue as positive electrode material for aqueous sodium-ion capacitor with

- excellent performance, RSC Adv. 6 (2016) 109340-109345.
<https://doi.org/10.1039/C6RA21500A>
- [82] M. Du, M. Chen, X.-G. Yang, J. Wen, X. Wang, S.-M. Fang, C.-S. Liu, A channel-type mesoporous In(iii)–carboxylate coordination framework with high physicochemical stability for use as an electrode material in supercapacitors, J. Mater. Chem. A 2 (2014) 9828-9834. <https://doi.org/10.1039/C4TA00963K>
- [83] Y. Gong, J. Li, P.-G. Jiang, Q.-F. Li, J.-H. Lin, Novel metal (II) coordination polymers based on N, N'-bis-(4-pyridyl) phthalamide as supercapacitor electrode materials in an aqueous electrolyte, Dalton Trans. 42 (2013) 1603-1611.
<https://doi.org/10.1039/C2DT31965A>
- [84] N. Phattharasupakun, J. Wutthiprom, S. Kaenket, T. Maihom, J. Limtrakul, M. Probst, S.S. Nagarkar, S. Horike, M. Sawangphruk, A proton-hopping charge storage mechanism of ionic one-dimensional coordination polymers for high-performance supercapacitors, Chem. Commun. 53 (2017) 11786-11789.
<https://doi.org/10.1039/C7CC07490E>
- [85] Y.Y. Kannangara, U.A. Rathnayake, J.-K. Song, Redox active multi-layered Zn-pPDA MOFs as high-performance supercapacitor electrode material, Electrochim. Acta 297 (2019) 145-154. <https://doi.org/10.1016/j.electacta.2018.11.186>
- [86] Q. Liu, X. Liu, C. Shi, Y. Zhang, X. Feng, M.-L. Cheng, S. Su, J. Gu, A copper-based layered coordination polymer: synthesis, magnetic properties and electrochemical performance in supercapacitors, Dalton Trans. 44 (2015) 19175-19184. <https://doi.org/10.1039/C5DT02918J>
- [87] R. Ramachandran, C. Zhao, D. Luo, K. Wang, F. Wang, Synthesis of copper benzene-1, 3, 5-tricarboxylate metal organic frameworks with mixed phases as the electrode material for supercapacitor applications, Appl. Surf. Sci. 460 (2018) 33-39.
<https://doi.org/10.1016/j.apsusc.2017.11.271>
- [88] L. Yu, X. Wang, M. Cheng, H. Rong, Y. Song, Q. Liu, A Three-Dimensional Copper Coordination Polymer Constructed by 3-Methyl-1H-pyrazole-4-carboxylic Acid with Higher Capacitance for Supercapacitors, Cryst. Growth Des. 18 (2018) 280-285. <https://doi.org/10.1021/acs.cgd.7b01219>
- [89] X. Xiong, L. Zhou, W. Cao, J. Liang, Y. Wang, S. Hu, F. Yu, B. Li, Metal–organic frameworks based on halogen-bridged dinuclear-Cu-nodes as promising materials for high performance supercapacitor electrodes, CrystEngComm 19 (2017) 7177-7184.
<https://doi.org/10.1039/C7CE01840A>
- [90] G. Wang, T. Chen, S. Li, H. Pang, H. Ma, A coordination polymer based on dinuclear (pyrazinyl tetrazolate) copper(ii) cations and Wells–Dawson anions for high-

- performance supercapacitor electrodes, *Dalton Trans.* 46 (2017) 13897-13902.
<https://doi.org/10.1039/C7DT02230A>
- [91] M.H. Zhu, X.M. Wu, B.T. Niu, D. Guo, H.X. Guo, Facile mechanochemical green fabrication of CuBr(tu)(3) nanowires as electrochemical supercapacitor electrodes, *Chin. J. Struct. Chem.* 37 (2018) 1155-1159.
- [92] Y. Yan, Y. Luo, J. Ma, B. Li, H. Xue, H. Pang, Facile synthesis of vanadium metal-organic frameworks for high-performance supercapacitors, *Small* 14 (2018) 1801815. <https://doi.org/10.1002/smll.201801815>
- [93] R. Díaz, M.G. Orcajo, J.A. Botas, G. Calleja, J. Palma, Co8-MOF-5 as electrode for supercapacitors, *Mater. Lett.* 68 (2012) 126-128.
<https://doi.org/10.1016/j.matlet.2011.10.046>
- [94] S. Gao, Y. Sui, F. Wei, J. Qi, Q. Meng, Y. Ren, Y. He, Dandelion-like nickel/cobalt metal-organic framework based electrode materials for high performance supercapacitors, *J. Colloid Interface Sci.* 531 (2018) 83-90.
<https://doi.org/10.1016/j.jcis.2018.07.044>
- [95] H. Xia, J. Zhang, Z. Yang, S. Guo, S. Guo, Q. Xu, 2D MOF Nanoflake-Assembled Spherical Microstructures for Enhanced Supercapacitor and Electrocatalysis Performances, *Nano-Micro Lett.* 9 (2017) 43. <https://doi.org/10.1007/s40820-017-0144-6>
- [96] J. Yang, C. Zheng, P. Xiong, Y. Li, M. Wei, Zn-doped Ni-MOF material with a high supercapacitive performance, *J. Mater. Chem. A* 2 (2014) 19005-19010.
<https://doi.org/10.1039/C4TA04346D>
- [97] B.N. Bhadra, A. Vinu, C. Serre, S.H. Jhung, MOF-derived carbonaceous materials enriched with nitrogen: Preparation and applications in adsorption and catalysis, *Mater. Today* (2018). <https://doi.org/10.1016/j.mattod.2018.1010.1016>
- [98] R.R. Salunkhe, Y.V. Kaneti, Y. Yamauchi, Metal-organic framework-derived nanoporous metal oxides toward supercapacitor applications: Progress and prospects, *ACS Nano* 11 (2017) 5293-5308. <https://doi.org/10.1021/acsnano.7b02796>
- [99] B.Y. Guan, X.Y. Yu, H.B. Wu, X.W. Lou, Complex nanostructures from materials based on metal-organic frameworks for electrochemical energy storage and conversion, *Adv. Mater.* 29 (2017) 1703614. <https://doi.org/10.1002/adma.201703614>
- [100] Y. Li, Y. Xu, W. Yang, W. Shen, H. Xue, H. Pang, MOF-derived metal oxide composites for advanced electrochemical energy storage, *Small* 14 (2018) 1704435. <https://doi.org/10.1002/smll.201704435>

- [101] L. Lux, K. Williams, S. Ma, Heat-treatment of metal–organic frameworks for green energy applications, *CrystEngComm* 17 (2015) 10-22.
<https://doi.org/10.1039/C4CE01499E>
- [102] X. Li, S. Zheng, L. Jin, Y. Li, P. Geng, H. Xue, H. Pang, Q. Xu, Metal-Organic Framework-Derived Carbons for Battery Applications, *Adv. Energy Mater.* (2018) 1800716. <https://doi.org/10.1002/aenm.201800716>
- [103] M.H. Yap, K.L. Fow, G.Z. Chen, Synthesis and applications of MOF-derived porous nanostructures, *Green Energy Environ.* 2 (2017) 218-245.
<https://doi.org/10.1016/j.gee.2017.05.003>
- [104] L. Sun, M.G. Campbell, M. Dincă, Electrically conductive porous metal–organic frameworks, *Angew. Chem. Int. Ed.* 55 (2016) 3566-3579.
<https://doi.org/10.1002/anie.201506219>
- [105] A. Vlad, A. Balducci, Porous materials get energized, *Nat. Mater.* 16 (2017) 161-162. <https://doi.org/10.1038/nmat4851>
- [106] P.F. Li, B. Wang, Recent development and application of conductive MOFs, *Isr. J. Chem.* 58 (2018) 1010-1018. <https://doi.org/10.1002/ijch.201800078>
- [107] D. Sheberla, J.C. Bachman, J.S. Elias, C.-J. Sun, Y. Shao-Horn, M. Dincă, Conductive MOF electrodes for stable supercapacitors with high areal capacitance, *Nat. Mater.* 16 (2016) 220-224. <https://doi.org/10.1038/nmat4766>
- [108] D. Feng, T. Lei, M.R. Lukatskaya, J. Park, Z. Huang, M. Lee, L. Shaw, S. Chen, A.A. Yakovenko, A. Kulkarni, J. Xiao, K. Fredrickson, J.B. Tok, X. Zou, Y. Cui, Z. Bao, Robust and conductive two-dimensional metal–organic frameworks with exceptionally high volumetric and areal capacitance, *Nat. Energy* 3 (2018) 30-36.
<https://doi.org/10.1038/s41560-017-0044-5>
- [109] W.-H. Li, K. Ding, H.-R. Tian, M.-S. Yao, B. Nath, W.-H. Deng, Y. Wang, G. Xu, Conductive metal–organic framework nanowire array electrodes for high-performance solid-state supercapacitors, *Adv. Funct. Mater.* 27 (2017) 1702067.
<https://doi.org/10.1002/adfm.201702067>
- [110] J. Zhao, Q. Li, L. Han, R. Liu, Spherical mesocrystals from self-assembly of folic acid and nickel(II) ion for high-performance supercapacitors, *J. Colloid Interface Sci.* 538 (2019) 142-148. <https://doi.org/10.1016/j.jcis.2018.11.088>
- [111] P. Du, Y. Dong, C. Liu, W. Wei, D. Liu, P. Liu, Fabrication of hierarchical porous nickel based metal-organic framework (Ni-MOF) constructed with nanosheets as novel pseudo-capacitive material for asymmetric supercapacitor, *J. Colloid Interface Sci.* 518 (2018) 57-68. <https://doi.org/10.1016/j.jcis.2018.02.010>

- [112] Y. Yan, P. Gu, S. Zheng, M. Zheng, H. Pang, H. Xue, Facile synthesis of an accordion-like Ni-MOF superstructure for high-performance flexible supercapacitors, *J. Mater. Chem. A* 4 (2016) 19078-19085. <https://doi.org/10.1039/C6TA08331E>
- [113] Q.-R. Fang, T.A. Makal, M.D. Young, H.-C. Zhou, Recent advances in the study of mesoporous metal-organic frameworks, *Comments Inorg. Chem.* 31 (2010) 165-195. <https://doi.org/10.1080/02603594.2010.520254>
- [114] C.R. Rawool, S.P. Karna, A.K. Srivastava, Enhancing the supercapacitive performance of Nickel based metal organic framework-carbon nanofibers composite by changing the ligands, *Electrochim. Acta* 294 (2019) 345-356. <https://doi.org/10.1016/j.electacta.2018.10.093>
- [115] T. Wei, M. Zhang, P. Wu, Y.-J. Tang, S.-L. Li, F.-C. Shen, X.-L. Wang, X.-P. Zhou, Y.-Q. Lan, POM-based metal-organic framework/reduced graphene oxide nanocomposites with hybrid behavior of battery-supercapacitor for superior lithium storage, *Nano Energy* 34 (2017) 205-214. <https://doi.org/10.1016/j.nanoen.2017.02.028>
- [116] W. Li, H. Yao, G. Zhang, Y. Yang, A Ni/Zn bi-metallic coordination supramolecular network applied for high performance energy storage material, *Electrochim. Acta* 228 (2017) 233-240. <https://doi.org/10.1016/j.electacta.2017.01.066>
- [117] H. Gholipour-Ranjbar, M. Soleimani, H.R. Naderi, Application of Ni/Co-based metal-organic frameworks (MOFs) as an advanced electrode material for supercapacitors, *New J. Chem.* 40 (2016) 9187-9193. <https://doi.org/10.1039/C6NJ01449F>
- [118] S. Zhao, L. Zeng, G. Cheng, L. Yu, H. Zeng, Ni/Co-based metal-organic frameworks as electrode material for high performance supercapacitors, *Chin. Chem. Lett.* (2019). <https://doi.org/10.1016/j.ccllet.2018.10.018>
- [119] X. Wang, Q. Li, N. Yang, Y. Yang, F. He, J. Chu, M. Gong, B. Wu, R. Zhang, S. Xiong, Hydrothermal synthesis of NiCo-based bimetal-organic frameworks as electrode materials for supercapacitors, *J. Solid State Chem.* 270 (2019) 370-378. <https://doi.org/10.1016/j.jssc.2018.11.038>
- [120] S.H. Kazemi, B. Hosseinzadeh, H. Kazemi, M.A. Kiani, S. Hajati, Facile synthesis of mixed metal-organic frameworks: Electrode materials for supercapacitors with excellent areal capacitance and operational stability, *ACS Appl. Mater. Interfaces* 10 (2018) 23063-23073. <https://doi.org/10.1021/acsami.8b04502>
- [121] N. Sun, Y. Wang, W. Wei, Z. Song, W. Liu, Synthesis of CoFe Prussian blue analogue nanocubes and its supercapacitive performance, *Electron. Compon. Mater.* 37 (2018) 35-39.

- [122] H. Yu, H. Xia, J. Zhang, J. He, S. Guo, Q. Xu, Fabrication of Fe-doped Co-MOF with mesoporous structure for the optimization of supercapacitor performances, *Chin. Chem. Lett.* 29 (2018) 834-836. <https://doi.org/10.1016/j.cclet.2018.04.008>
- [123] S.-H. Lee, S. Choi, Bimetallic zeolitic imidazolate frameworks for symmetric electrical double-layer supercapacitors with aqueous electrolytes, *Mater. Lett.* 207 (2017) 129-132. <https://doi.org/10.1016/j.matlet.2017.07.055>
- [124] H. Wang, Z. Huang, H. Zhao, F. Zhang, C. Xu, Q. Fu, H. Tao, H. Li, J. Ma, Electrochemical performance of $\text{Fe}_x\text{Mn}_{1-x}$ -based metal-organic frameworks as electrode materials for supercapacitors, *J. Mater. Sci.: Mater. Electron.* 29 (2018) 19819-19824. <https://doi.org/10.1007/s10854-018-0109-7>
- [125] Y.W. Sui, D.L. Zhang, Y.P. Han, Z. Sun, J.Q. Qi, F.X. Wei, Y.Z. He, Q.K. Meng, Electrochemical potential enhancement of supercapacitors by synthesizing advanced electrode materials using Ni doped Fe metal-organic frameworks, *Nanosci. Nanotechnol. Lett.* 9 (2017) 1567-1571. <https://doi.org/10.1166/nnl.2017.2511>
- [126] A. Farisabadi, M. Moradi, S. Borhani, S. Hajati, M.A. Kiani, S.A. Tayebifard, Synthesis and electrochemical properties of Mg-doped chromium-based metal organic framework/reduced graphene oxide composite for supercapacitor application, *J. Mater. Sci.: Mater. Electron.* 29 (2018) 8421-8430. <https://doi.org/10.1007/s10854-018-8853-2>
- [127] L. Yue, H. Guo, X. Wang, T. Sun, H. Liu, Q. Li, M. Xu, Y. Yang, W. Yang, Non-metallic element modified metal-organic frameworks as high-performance electrodes for all-solid-state asymmetric supercapacitors, *J. Colloid Interface Sci.* 539 (2019) 370-378. <https://doi.org/10.1016/j.jcis.2018.12.079>
- [128] O. Fleker, A. Borenstein, R. Lavi, L. Benisvy, S. Ruthstein, D. Aurbach, Preparation and properties of metal organic framework/activated carbon composite materials, *Langmuir* 32 (2016) 4935-4944. <https://doi.org/10.1021/acs.langmuir.6b00528>
- [129] E. Elanthamilan, S. Rajkumar, R. Rajavalli, J.P. Merlin, Cost effective synthesis of a copper-1H-imidazole@activated carbon metal organic framework as an electrode material for supercapacitor applications, *New J. Chem.* 42 (2018) 10300-10308. <https://doi.org/10.1039/C8NJ01927D>
- [130] P. Wen, P. Gong, J. Sun, J. Wang, S. Yang, Design and synthesis of Ni-MOF/CNT composites and rGO/carbon nitride composites for an asymmetric supercapacitor with high energy and power density, *J. Mater. Chem. A* 3 (2015) 13874-13883. <https://doi.org/10.1039/C5TA02461G>

- [131] S.-C. Wang, M. Gu, L. Pan, J. Xu, L. Han, F.-Y. Yi, The interlocked in situ fabrication of graphene@prussian blue nanocomposite as high-performance supercapacitor, *Dalton Trans.* 47 (2018) 13126-13134.
<https://doi.org/10.1039/C8DT02331J>
- [132] R. Ramachandran, W. Xuan, C. Zhao, X. Leng, D. Sun, D. Luo, F. Wang, Enhanced electrochemical properties of cerium metal-organic framework based composite electrodes for high-performance supercapacitor application, *RSC Adv.* 8 (2018) 3462-3469. <https://doi.org/10.1039/C7RA12789H>
- [133] Y. Zhang, B. Lin, Y. Sun, X. Zhang, H. Yang, J. Wang, Carbon nanotubes@metal-organic frameworks as Mn-based symmetrical supercapacitor electrodes for enhanced charge storage, *RSC Adv.* 5 (2015) 58100-58106.
<https://doi.org/10.1039/C5RA11597C>
- [134] Q. Wang, Q. Wang, B. Xu, F. Gao, F. Gao, C. Zhao, Flower-shaped multiwalled carbon nanotubes@nickel-trimesic acid MOF composite as a high-performance cathode material for energy storage, *Electrochim. Acta* 281 (2018) 69-77.
<https://doi.org/10.1016/j.electacta.2018.05.159>
- [135] Y. Zhou, Z. Mao, W. Wang, Z. Yang, X. Liu, In-situ fabrication of graphene oxide hybrid ni-based metal-organic framework (Ni-MOFs@GO) with ultrahigh capacitance as electrochemical pseudocapacitor materials, *ACS Appl. Mater. Interfaces* 8 (2016) 28904-28916. <https://doi.org/10.1021/acsami.6b10640>
- [136] R.R. Fu, M. Luo, Y.H. Ma, S. Yang, Preparation and supercapitance of Ni-3(HCOO)(6)/reduced graphene oxide electrode materials, *Chem. J. Chin. Univ.-Chin.* 37 (2016) 1485-1490.
- [137] M. Luo, Y. Dou, H. Kang, Y. Ma, X. Ding, B. Liang, B. Ma, L. Li, A novel interlocked Prussian blue/reduced graphene oxide nanocomposites as high-performance supercapacitor electrodes, *J. Solid State Electrochem.* 19 (2015) 1621-1631. <https://doi.org/10.1007/s10008-015-2785-z>
- [138] M. Zhang, C. Hou, A. Halder, J. Ulstrup, Q. Chi, Interlocked graphene-Prussian blue hybrid composites enable multifunctional electrochemical applications, *Biosens. Bioelectron.* 89 (2017) 570-577. <https://doi.org/10.1016/j.bios.2016.02.044>
- [139] M. Saraf, R. Rajak, S.M. Mobin, A fascinating multitasking Cu-MOF/rGO hybrid for high performance supercapacitors and highly sensitive and selective electrochemical nitrite sensors, *J. Mater. Chem. A* 4 (2016) 16432-16445.
<https://doi.org/10.1039/C6TA06470A>
- [140] G. Zhang, F. Zhang, H. Yao, Z. Liu, Y. Yang, A nickel coordination supramolecular network synergized with nitrogen-doped graphene as an advanced

- cathode to significantly boost the rate capability and durability of supercapacitors, *J. Mater. Chem. A* **5** (2017) 19036-19045. <https://doi.org/10.1039/C7TA05667B>
- [141] W. Cao, M. Han, L. Qin, Q. Jiang, J. Xu, Z. Lu, Y. Wang, Synthesis of zeolitic imidazolate framework-67 nanocube wrapped by graphene oxide and its application for supercapacitors, *J. Solid State Electrochem.* **23** (2019) 325-334. <https://doi.org/10.1007/s10008-018-4138-1>
- [142] A. Hosseini, A. Amjad, R. Hosseinzadeh-Khanmiri, E. Ghorbani-Kalhor, M. Babazadeh, E. Vessally, Nanocomposite of ZIF-67 metal-organic framework with reduced graphene oxide nanosheets for high-performance supercapacitor applications, *J. Mater. Sci.: Mater. Electron.* **28** (2017) 18040-18048. <https://doi.org/10.1007/s10854-017-7747-z>
- [143] W. Zhang, Y. Tan, Y. Gao, J. Wu, J. Hu, A. Stein, B. Tang, Nanocomposites of zeolitic imidazolate frameworks on graphene oxide for pseudocapacitor applications, *J. Appl. Electrochem.* **46** (2016) 441-450. <https://doi.org/10.1007/s10800-016-0921-9>
- [144] N.S. Punde, C.R. Rawool, A.S. Rajpurohit, S.P. Karna, A.K. Srivastava, Hybrid composite based on porous cobalt-benzenetricarboxylic acid metal organic framework and graphene nanosheets as high performance supercapacitor electrode, *ChemistrySelect* **3** (2018) 11368-11380. <https://doi.org/10.1002/slct.201802721>
- [145] Z. Wang, C. Gao, Y. Liu, D. Li, W. Chen, Y. Ma, C. Wang, J. Zhang, Electrochemical performance and transformation of Co-MOF/reduced graphene oxide composite, *Mater. Lett.* **193** (2017) 216-219. <https://doi.org/10.1016/j.matlet.2017.01.121>
- [146] X.Y. Hou, X.L. Yan, X. Wang, S.N. Li, Y.C. Jiang, M.C. Hu, Q.G. Zhai, Excellent supercapacitor performance of robust nickel-organic framework materials achieved by tunable porosity, inner-cluster redox, and in situ fabrication with graphene oxide, *Cryst. Growth Des.* **18** (2018) 6035-6045. <https://doi.org/10.1021/acs.cgd.8b00881>
- [147] Z. Wang, H. Yao, F. Zhang, W. Li, Y. Yang, X. Lu, Electro-synthesized Ni coordination supermolecular-networks-coated exfoliated graphene composite materials for high-performance asymmetric supercapacitors, *J. Mater. Chem. A* **4** (2016) 16476-16483. <https://doi.org/10.1039/C6TA06974F>
- [148] L. Liu, Y. Yan, Z. Cai, S. Lin, X. Hu, Growth-oriented Fe-based MOFs synergized with graphene aerogels for high-performance supercapacitors, *Adv. Mater. Interfaces* **5** (2018) 1701548. <https://doi.org/10.1002/admi.201701548>
- [149] C. Li, C. Hu, Y. Zhao, L. Song, J. Zhang, R. Huang, L. Qu, Decoration of graphene network with metal-organic frameworks for enhanced electrochemical

- capacitive behavior, *Carbon* 78 (2014) 231-242.
<https://doi.org/10.1016/j.carbon.2014.06.076>
- [150] X. Deng, S. Zhu, J. Li, L. Ma, F. He, E. Liu, C. He, C. Shi, Q. Li, N. Zhao, Ball-in-cage nanocomposites of metal-organic frameworks and three-dimensional carbon networks: synthesis and capacitive performance, *Nanoscale* 9 (2017) 6478-6485.
<https://doi.org/10.1039/C7NR01548H>
- [151] L. Ma, H. Fan, K. Fu, Y. Zhao, Metal-organic framework/layered carbon nitride nano-sandwiches for superior asymmetric supercapacitor, *ChemistrySelect* 1 (2016) 3730-3738. <https://doi.org/10.1002/slct.201601053>
- [152] Z. Li, Y. Gao, J. Wu, W. Zhang, Y. Tan, B. Tang, Synthesis and electrochemical characterization of Ni-B/ZIF-8 as electrode materials for supercapacitors, *Electron. Mater. Lett.* 12 (2016) 645-650. <https://doi.org/10.1007/s13391-016-6149-3>
- [153] R. Ramachandran, K. Rajavel, W. Xuan, D. Lin, F. Wang, Influence of Ti₃C₂T_x (MXene) intercalation pseudocapacitance on electrochemical performance of Co-MOF binder-free electrode, *Ceram. Int.* 44 (2018) 14425-14431.
<https://doi.org/10.1016/j.ceramint.2018.05.055>
- [154] M. Zhao, Q. Zhao, J. Qiu, X. Lu, G. Zhang, H. Xue, H. Pang, Amorphous cobalt coordination nanolayers incorporated with silver nanowires: A new electrode material for supercapacitors, *Part. Part. Syst. Charact.* 34 (2017) 1600412.
<https://doi.org/10.1002/ppsc.201600412>
- [155] Z. Li, Y. Guo, X. Wang, W. Ying, D. Chen, X. Ma, X. Zhao, X. Peng, Highly conductive PEDOT:PSS threaded HKUST-1 thin films, *Chem. Commun.* 54 (2018) 13865-13868. <https://doi.org/10.1039/C8CC07591C>
- [156] A. Ehsani, M. Bigdeloo, M.Y. Ansari, B. Mirtamizdoust, A.A. Heidari, M. Hadi, H.M. Shiri, Nanocomposite of conjugated polymer/nano-flowers Cu(II) metal-organic system with 2-methylpyridinecarboxaldehyde isonicotinohydrazide as a novel and hybrid electrode material for highly capacitive pseudocapacitors, *Bull. Chem. Soc. Jpn.* 91 (2018) 617-622. <https://doi.org/10.1246/bcsj.20170391>
- [157] A. Ehsani, J. Khodayari, M. Hadi, H.M. Shiri, H. Mostaanzadeh, Nanocomposite of p-type conductive polymer/Cu (II)-based metal-organic frameworks as a novel and hybrid electrode material for highly capacitive pseudocapacitors, *Ionics* 23 (2017) 131-138. <https://doi.org/10.1007/s11581-016-1811-1>
- [158] M. Naseri, L. Fotouhi, A. Ehsani, S. Dehghanpour, Facile electrosynthesis of nano flower like metal-organic framework and its nanocomposite with conjugated polymer as a novel and hybrid electrode material for highly capacitive pseudocapacitors, *J. Colloid Interface Sci.* 484 (2016) 314-319. <https://doi.org/10.1016/j.jcis.2016.09.001>

- [159] F. Boorboor Ajdari, E. Kowsari, A. Ehsani, P-type conductive polymer/zeolitic imidazolate framework-67 (ZIF-67) nanocomposite film: Synthesis, characterization, and electrochemical performance as efficient electrode materials in pseudocapacitors, *J. Colloid Interface Sci.* 509 (2018) 189-194. <https://doi.org/10.1016/j.jcis.2017.08.098>
- [160] Y. Jiao, G. Chen, D. Chen, J. Pei, Y. Hu, Bimetal-organic framework assisted polymerization of pyrrole involving air oxidant to prepare composite electrodes for portable energy storage, *J. Mater. Chem. A* 5 (2017) 23744-23752. <https://doi.org/10.1039/C7TA07464F>
- [161] W. Ji, L. Feng, R. Hao, W. Pei, Study on the design and performance of Nano nHKUST-1/PANI electrode as supercapacitors, *Journal of Shaanxi Normal University. Natural Science Edition* 45 (2017) 59-65.
- [162] S.B. Aliev, D.G. Samsonenko, E.A. Maksimovskiy, E.O. Fedorovskaya, S.A. Sapchenko, V.P. Fedin, Polyaniline-intercalated MIL-101: selective CO₂ sorption and supercapacitor properties, *New J. Chem.* 40 (2016) 5306-5312. <https://doi.org/10.1039/C5NJ03477A>
- [163] E.A. Jafari, M. Moradi, S. Borhani, H. Bigdeli, S. Hajati, Fabrication of hybrid supercapacitor based on rod-like HKUST-1@polyaniline as cathode and reduced graphene oxide as anode, *Physica E* 99 (2018) 16-23. <https://doi.org/10.1016/j.physe.2018.01.007>
- [164] Q. Chen, S. Lei, P. Deng, X. Ou, L. Chen, W. Wang, Y. Xiao, B. Cheng, Direct growth of nickel terephthalate on Ni foam with large mass-loading for high-performance supercapacitors, *J. Mater. Chem. A* 5 (2017) 19323-19332. <https://doi.org/10.1039/C7TA05373H>
- [165] L. Wang, H. Yang, G. Pan, L. Miao, S. Chen, Y. Song, Polyaniline-Carbon Nanotubes@Zeolite Imidazolate Framework-67-Carbon Cloth Hierarchical Nanostructures for Supercapacitor Electrode, *Electrochim. Acta* 240 (2017) 16-23. <https://doi.org/10.1016/j.electacta.2017.04.035>
- [166] Y. Zou, Q. Wang, C. Xiang, Z. She, H. Chu, S. Qiu, F. Xu, S. Liu, C. Tang, L. Sun, One-pot synthesis of ternary polypyrrole-Prussian-blue-graphene-oxide hybrid composite as electrode material for high-performance supercapacitors, *Electrochim. Acta* 188 (2016) 126-134. <https://doi.org/10.1016/j.electacta.2015.11.123>
- [167] F.B. Ajdari, E. Kowsari, A. Ehsani, Ternary nanocomposites of conductive polymer/functionalized GO/MOFs: Synthesis, characterization and electrochemical performance as effective electrode materials in pseudocapacitors, *J. Solid State Chem.* 265 (2018) 155-166. <https://doi.org/10.1016/j.jssc.2018.05.038>

- [168] H.-N. Wang, M. Zhang, A.M. Zhang, F.-C. Shen, X.-K. Wang, S.-N. Sun, Y.-J. Chen, Y.-Q. Lan, polyoxometalate-based metal–organic frameworks with conductive polypyrrole for supercapacitors, *ACS Appl. Mater. Interfaces* 10 (2018) 32265-32270. <https://doi.org/10.1021/acsami.8b12194>
- [169] J. Ji, Y. Li, W. Peng, G. Zhang, F. Zhang, X. Fan, Advanced Graphene-Based Binder-Free Electrodes for High-Performance Energy Storage, *Adv. Mater.* 27 (2015) 5264-5279. <https://doi.org/10.1002/adma.201501115>
- [170] F. Bonaccorso, L. Colombo, G. Yu, M. Stoller, V. Tozzini, A.C. Ferrari, R.S. Ruoff, V. Pellegrini, Graphene, related two-dimensional crystals, and hybrid systems for energy conversion and storage, *Science* 347 (2015) 1246501. <https://doi.org/10.1126/science.1246501>
- [171] P.C. Banerjee, D.E. Lobo, R. Middag, W.K. Ng, M.E. Shaibani, M. Majumder, Electrochemical capacitance of Ni-doped metal organic framework and reduced graphene oxide composites: more than the sum of its parts, *ACS Appl. Mater. Interfaces* 7 (2015) 3655-3664. <https://doi.org/10.1021/am508119c>
- [172] S. Chen, W. Xing, J. Duan, X. Hu, S.Z. Qiao, Nanostructured morphology control for efficient supercapacitor electrodes, *J. Mater. Chem. A* 1 (2013) 2941-2954. <https://doi.org/10.1039/C2TA00627H>
- [173] F. Miao, C. Shao, X. Li, K. Wang, N. Lu, Y. Liu, Three-dimensional freestanding hierarchically porous carbon materials as binder-free electrodes for supercapacitors: high capacitive property and long-term cycling stability, *J. Mater. Chem. A* 4 (2016) 5623-5631. <https://doi.org/10.1039/C6TA00830E>
- [174] Q. Wang, F.N. Yong, Z.H. Xiao, X.Y. Chen, Z.J. Zhang, Simply incorporating an efficient redox additive into KOH electrolyte for largely improving electrochemical performances, *J. Electroanal. Chem.* 770 (2016) 62-72. <https://doi.org/10.1016/j.jelechem.2016.03.037>
- [175] M. Zhang, G. Wang, L. Lu, T. Wang, H. Xu, C. Yu, H. Li, W. Tian, Improving the electrochemical performances of active carbon-based supercapacitors through the combination of introducing functional groups and using redox additive electrolyte, *J. Saudi Chem. Soc.* 22 (2018) 908-918. <https://doi.org/10.1016/j.jscs.2018.02.001>
- [176] C. Zhao, T. Deng, X. Xue, L. Chang, W. Zheng, S. Wang, Development of novel and ultrahigh-performance asymmetric supercapacitor based on redox electrode-electrolyte system, *Electrochim. Acta* 231 (2017) 495-501. <https://doi.org/10.1016/j.electacta.2017.02.083>
- [177] Y. Tian, M. Liu, R. Che, R. Xue, L. Huang, Cooperative redox-active additives of anthraquinone-2,7-disulphonate and K₄Fe(CN)₆ for enhanced performance of active

- carbon-based capacitors, *J. Power Sources* 324 (2016) 334-341.
<https://doi.org/10.1016/j.jpowsour.2016.05.086>
- [178] Y.-Z. Zhang, T. Cheng, Y. Wang, W.-Y. Lai, H. Pang, W. Huang, A simple approach to boost capacitance: Flexible supercapacitors based on manganese oxides@MOFs via chemically induced in situ self-transformation, *Adv. Mater.* 28 (2016) 5242-5248. <https://doi.org/10.1002/adma.201600319>
- [179] Z. Li, Y. Tan, W. Zhang, B. Tang, Flower-like Ni₃(NO₃)₂(OH)₄@Zr-metal organic framework (UiO-66) composites as electrode materials for high performance pseudocapacitors, *Ionics* 22 (2016) 2545-2551. <https://doi.org/10.1007/s11581-016-1887-7>
- [180] Y. Gao, J. Wu, W. Zhang, Y. Tan, J. Gao, B. Tang, J. Zhao, Synthesis of nickel carbonate hydroxide@zeolitic imidazolate framework-67 (Ni₂CO₃(OH)₂@ZIF-67) for pseudocapacitor applications, *J. Appl. Electrochem.* 45 (2015) 541-547. <https://doi.org/10.1007/s10800-015-0795-2>
- [181] Y. Gao, J. Wu, W. Zhang, Y. Tan, J. Gao, J. Zhao, B. Tang, Synthesis of nickel oxalate/zeolitic imidazolate framework-67 (NiC₂O₄/ZIF-67) as a supercapacitor electrode, *New J. Chem.* 39 (2015) 94-97. <https://doi.org/10.1039/C4NJ01719F>
- [182] Y. Gao, J. Wu, W. Zhang, Y. Tan, J. Gao, B. Tang, J. Zhao, Synthesis of nickel carbonate hydroxide/zeolitic imidazolate framework-8 as a supercapacitors electrode, *RSC Adv.* 4 (2014) 36366-36371. <https://doi.org/10.1039/C4RA04474F>
- [183] Y. Gao, J. Wu, W. Zhang, Y. Tan, J. Zhao, B. Tang, The electrochemical performance of SnO₂ quantum dots@zeolitic imidazolate frameworks-8 (ZIF-8) composite material for supercapacitors, *Mater. Lett.* 128 (2014) 208-211 <https://doi.org/10.1016/j.matlet.2014.04.175>
- [184] Y. Wang, Q. Chen, Dual-layer-structured nickel hexacyanoferrate/MnO₂ composite as a high-energy supercapacitive material based on the complementarity and interlayer concentration enhancement effect, *ACS Appl. Mater. Interfaces* 6 (2014) 6196-6201. <https://doi.org/10.1021/am5011173>
- [185] J.H. Cavka, S. Jakobsen, U. Olsbye, N. Guillou, C. Lamberti, S. Bordiga, K.P. Lillerud, A new zirconium inorganic building brick forming metal organic frameworks with exceptional stability, *J. Am. Chem. Soc.* 130 (2008) 13850-13851. <https://doi.org/10.1021/ja8057953>
- [186] J. Xu, Y. Wang, S. Cao, J. Zhang, G. Zhang, H. Xue, Q. Xu, H. Pang, Ultrathin Cu-MOF@ δ -MnO₂ nanosheets for aqueous electrolyte-based high-voltage electrochemical capacitors, *J. Mater. Chem. A* 6 (2018) 17329-17336. <https://doi.org/10.1021/ja8057953>

- [187] D.P. Dubal, N.R. Chodankar, D.-H. Kim, P. Gomez-Romero, Towards flexible solid-state supercapacitors for smart and wearable electronics, *Chem. Soc. Rev.* 47 (2018) 2065-2129. <https://doi.org/10.1039/C7CS00505A>
- [188] Y.Z. Liu, N. Xu, W.C. Chen, X.L. Wang, C.Y. Sun, Z.M. Su, Supercapacitor with high cycling stability through electrochemical deposition of metal-organic frameworks/polypyrrole positive electrode, *Dalton Trans.* 47 (2018) 13472-13478. <https://doi.org/10.1039/C8DT02740D>
- [189] H. Yao, F. Zhang, G. Zhang, Y. Yang, A new hexacyanoferrate nanosheet array converted from copper oxide as a high-performance binder-free energy storage electrode, *Electrochim. Acta* 294 (2019) 286-296. <https://doi.org/10.1016/j.electacta.2018.10.056>
- [190] C. Qu, Z. Liang, Y. Jiao, B. Zhao, B. Zhu, D. Dang, S. Dai, Y. Chen, R. Zou, M. Liu, "One-for-all" strategy in fast energy storage: Production of pillared MOF nanorod-templated positive/negative electrodes for the application of high-performance hybrid supercapacitor, *Small* 14 (2018) 1800285. <https://doi.org/10.1002/sml.201800285>
- [191] Y. Mengyao, Z. Xin, Z. Junxian, T. Wenjun, L. Jie, D. Jie, Z. Qinghua, Flexible all-solid-state supercapacitors of polyaniline nanowire arrays deposited on electrospun carbon nanofibers decorated with MOFs, *Nanotechnology* 30 (2019) 085404. <https://doi.org/10.1002/sml.201800285>
- [192] D. Tian, X. Lu, Y. Zhu, M. Li, C. Wang, Fabrication of two-dimensional metal-organic frameworks on electrospun nanofibers and their derived metal doped carbon nanofibers for an advanced asymmetric supercapacitor with a high energy density, *J. Power Sources* 413 (2019) 50-58. <https://doi.org/10.1016/j.jpowsour.2018.12.014>
- [193] D. Fu, H. Zhou, X.-M. Zhang, G. Han, Y. Chang, H. Li, Flexible solid-state supercapacitor of metal-organic framework coated on carbon nanotube film interconnected by electrochemically -codeposited PEDOT-GO, *ChemistrySelect* 1 (2016) 285-289. <https://doi.org/10.1002/slct.201600084>
- [194] H. Li, D. Fu, X.-M. Zhang, G. Han, F. Zhang, Facile preparation of varisized ZIF-8 and ZIF-8/polypyrrole composites for flexible solid-state supercapacitor, *ChemistrySelect* 2 (2017) 7530-7534. <https://doi.org/10.1002/slct.201701607>
- [195] D. Fu, H. Li, X.-M. Zhang, G. Han, H. Zhou, Y. Chang, Flexible solid-state supercapacitor fabricated by metal-organic framework/graphene oxide hybrid interconnected with PEDOT, *Mater. Chem. Phys.* 179 (2016) 166-173. <https://doi.org/10.1016/j.matchemphys.2016.05.024>

- [196] X. Xu, J. Tang, H. Qian, S. Hou, Y. Bando, M.S.A. Hossain, L. Pan, Y. Yamauchi, Three-dimensional networked metal–organic frameworks with conductive polypyrrole tubes for flexible supercapacitors, *ACS Appl. Mater. Interfaces* 9 (2017) 38737-38744. <https://doi.org/10.1021/acsami.7b09944>
- [197] K. Qi, R. Hou, S. Zaman, Y. Qiu, B.Y. Xia, H. Duan, Construction of metal–organic framework/conductive polymer hybrid for all-solid-state fabric supercapacitor, *ACS Appl. Mater. Interfaces* 10 (2018) 18021-18028. <https://doi.org/10.1021/acsami.8b05802>
- [198] P. Srimuk, S. Luanwuthi, A. Krittayavathananon, M. Sawangphruk, Solid-type supercapacitor of reduced graphene oxide-metal organic framework composite coated on carbon fiber paper, *Electrochim. Acta* 157 (2015) 69-77. <https://doi.org/10.1016/j.electacta.2015.01.082>
- [199] L. Zhang, Y. Zhang, S. Huang, Y. Yuan, H. Li, Z. Jin, J. Wu, Q. Liao, L. Hu, J. Lu, S. Ruan, Y.-J. Zeng, Co₃O₄/Ni-based MOFs on carbon cloth for flexible alkaline battery-supercapacitor hybrid devices and near-infrared photocatalytic hydrogen evolution, *Electrochim. Acta* 281 (2018) 189-197. <https://doi.org/10.1016/j.electacta.2018.05.162>
- [200] Q. Wang, L. Shao, Z. Ma, J. Xu, Y. Li, C. Wang, Hierarchical porous PANI/MIL-101 nanocomposites based solid-state flexible supercapacitor, *Electrochim. Acta* 281 (2018) 582-593. <https://doi.org/10.1016/j.electacta.2018.06.002>
- [201] Y.-N. Liu, L.-N. Jin, H.-T. Wang, X.-H. Kang, S.-W. Bian, Fabrication of three-dimensional composite textile electrodes by metal-organic framework, zinc oxide, graphene and polyaniline for all-solid-state supercapacitors, *J. Colloid Interface Sci.* 530 (2018) 29-36. <https://doi.org/10.1016/j.jcis.2018.06.062>
- [202] C. Zhu, Y. He, Y. Liu, N. Kazantseva, P. Saha, Q. Cheng, ZnO@MOF@PANI core-shell nanoarrays on carbon cloth for high-performance supercapacitor electrodes, *J. Energy Chem.* 35 (2019) 124-131. <https://doi.org/10.1016/j.jechem.2018.11.006>
- [203] L. Shao, Q. Wang, Z. Ma, Z. Ji, X. Wang, D. Song, Y. Liu, N. Wang, A high-capacitance flexible solid-state supercapacitor based on polyaniline and Metal-Organic Framework (UiO-66) composites, *J. Power Sources* 379 (2018) 350-361. <https://doi.org/10.1016/j.jpowsour.2018.01.028>
- [204] H. Yao, F. Zhang, G. Zhang, H. Luo, L. Liu, M. Shen, Y. Yang, A novel two-dimensional coordination polymer-polypyrrole hybrid material as a high-performance electrode for flexible supercapacitor, *Chem. Eng. J.* 334 (2018) 2547-2557. <https://doi.org/10.1016/j.cej.2017.12.013>

- [205] M. Hmadeh, Z. Lu, Z. Liu, F. Gándara, H. Furukawa, S. Wan, V. Augustyn, R. Chang, L. Liao, F. Zhou, E. Perre, V. Ozolins, K. Suenaga, X. Duan, B. Dunn, Y. Yamamoto, O. Terasaki, O.M. Yaghi, New porous crystals of extended metal-catecholates, *Chem. Mater.* 24 (2012) 3511-3513. <https://doi.org/10.1021/cm301194a>
- [206] G. Wang, L. Zhang, J. Zhang, A review of electrode materials for electrochemical supercapacitors, *Chem. Soc. Rev.* 41 (2012) 797-828. <https://doi.org/10.1039/C1CS15060J>
- [207] P. Pazhamalai, K. Krishnamoorthy, S. Sahoo, S.J. Kim, High-energy aqueous Li-ion hybrid capacitor based on metal-organic-framework-mimicking insertion-type copper hexacyanoferrate and capacitive-type graphitic carbon electrodes, *J. Alloys Compd.* 765 (2018) 1041-1048. <https://doi.org/10.1016/j.jallcom.2018.06.249>

Chapter 9

Metal-Organic Frameworks and their Therapeutic Applications

Fulya Gülbağça¹, Anish Khan^{2,3,*}, Fatih Şen^{1,*}

¹Sen Research Group, Department of Biochemistry, Faculty of Arts and Science, Dumlupınar University, Evliya Çelebi Campus, 43100 Kütahya, Turkey.

²Chemistry Department, Faculty of Science, King Abdulaziz University, Jeddah-21589, P.O. Box 80203, Saudi Arabia

³Center of Excellence for Advanced Materials Research, King Abdulaziz University, Jeddah 21589, P.O. Box 80203, Saudi Arabia

* fatih.sen@dpu.edu.tr, anishkhan@gmail.com

Abstract

Metal-organic frameworks (MOFs), which can be used in numerous applications such as gas storage, gas/steam separation, sensor, catalysis, imaging, luminescence, medication and biomedical applications in the nanotechnology field, have attracted a lot of attention. MOFs with unique physical and chemical properties are linked to both organic and inorganic components by the coordination of polydentate organic binders and metal ions. Through these features specific to MOFs; Gives new perspectives on materials science, nanomedicine, biology, and drug distribution. In addition, biodegradability, porosity, high loading capacity, and surface modification properties are the main advantages of the new generation technologies. This chapter highlights various MOF types, their properties, and applications in various biomedical disciplines, with a particular focus on drug delivery and theranostics.

Keywords

Metal-Organic Frameworks, Biosensors, Therapeutic Applications, Nanomedicine, Antibacterial, Drug Delivery

Contents

1. Introduction.....	240
2. Metal-organic frameworks	241

2.1 Usage areas of metal-organic frameworks	244
2.1.1 Controlled drug release.....	245
2.1.2 Antibacterial activity of MOFs.....	249
2.1.3 Biomedicine	256
2.1.4 Chemical sensors	257
Conclusions and recommendations	267
References	268

1. Introduction

The nanomaterials field includes sub-areas that work on or develop materials with nanoscale dimensions. The nanomaterials used in nanotechnology application areas are defined by their structural dimensions of 1-100 nm. The pore diameters of these materials are between 1-1000 nm [1–5]. The nanomaterials, which have quite a lot of use, have unique features. These features; large surface area, wide pore volume, can be adjusted according to the desired properties. Nanomaterials with a larger surface area and pore volume were discovered in 1990, and these nanomaterials were named as Metal-Organic Frameworks or MOFs. MOF's; contain metal compounds and provide the integrity of the organic binders which bind the metal compounds in its contents. The privileged features of MOFs; With its large surface area and pore volume, flexible lattice structure, and magnetic properties, is actively used in many fields such as catalysis, separation of pollutants and gas storage, as well as controlled drug release for medical applications [6–7].

MOFs that add perspective to new generation technologies for the nanotechnology field are generally used with hybrid matrix membranes. Surface area and pore sizes are the most essential elements to determine the properties of MOFs in gas adsorption. MOFs often have hybrid matrix membranes and sometimes individual use. Materials such as UiO-66, ZIF-8, and HKUST-1 are the most investigated MOF structures in the gas storage area. In the applications studied, the MOF pores are filled with solvent molecules, and the solvents are removed. In this case, structural collapse may occur. The deterioration of mesoporous MOF structures is difficult compared to microporous. Despite the highly porous structure of MOFs, they pass into each other in order to increase the efficiency of the cages and in this case, the pore size decreases. This can sometimes be beneficial or can be harmful.

2. Metal-organic frameworks

The porous materials having high surfaces in terms of the technologies of chemical processes have always been of great importance and interest. In recent years, the use of these porous materials in the industrial field has been based on solid carbon and inorganic based materials. Apart from the use of these materials, Omar Yaghi worked on new and different materials in the 1990s and synthesized some of its organic groups and Metal Organic Frameworks (MOF).

MOF structures are formed by the bonding of polyfunctional organic molecules with metal ions (M^{+}) in one, two or three dimensions. The focus of research in recent years has been MOFs. Research on MOFs has been accelerated due to the changeable pore diameters of MOFs, large surface areas, variable geometric structures, and easy processability. Thanks to these characteristics of MOFs, they are suitable for use in a wide range of areas such as gas storage, gas separation, radiation, magnetism, catalyst, and drug release. The synthesis of different MOFs can be achieved by the use of different metal and ligand combinations, alteration of the synthesis method, and modification of the substances used in the synthesis [8]. Methods and methods of synthesis of MOFs are given in Table 1.

In addition, factors such as solubility, anions, and temperature change the structural characteristics of MOFs, the length of the bond and the angular properties of the bonding. MOF structures have recently attracted the attention of researchers. The source of this interest is the MOFs, as well as their interesting molecular structures, and their outstanding application in the future thanks to these features. It is expected that it will have a revolutionary impact on the chemical process technology by combining the properties of metal-organic frameworks with the highest internal surface area, pore volume, flexible lattice structure, adsorption capacity and the class of materials having the characteristic of chirality and magnetism. The large surface areas of MOFs have become more preferred due to their outstanding properties such as high pore volume, flexible cage structures, and gas adsorption capacity [18].

In order to explain the nano-sized structure of MOFs, it is necessary first to understand the Secondary Building Units (SBU). The SBUs, which are important organic binders, may change their structure when forming MOFs. The organic binders (linker) in the structure of MOFs have an effect on the volume of the pores and the area of adsorption.

Table 1. *Synthesis methods of MOFs.*

Name of the Method	Critical Attributes	Ref
Microwaveassisted synthesis method	It gives an advantage of shorter reaction time for synthesis to produce the MOFs with high monodispersity and possesses a high degree of applicability in the industrial set-up. Widely used in organic synthesis of MOFs	[9–11]
Spray drying method	It tends to yield end products with highly crystalline appearance, advantage of producing MOFs with desired shapes and architectures. It is an advanced method for synthesizing MOFs by aerosol casting	[12]
Microfluidic synthesis method	It produces monodispersed structures with nanocrystalline and nanofiber appearance. It aids in producing MOFs with desired hierarchy in a continuous manner	[13–14]
Microemulsion synthesis technique	It is a suitable technique for particle shaping. It allows control over shape, size, and polydispersity of the MOFs	[15]
Direct coupling synthesis technique	It provides synthesis of MOFs by direct reaction between the metal ions with organic linkers	[16–17]
Electrospinning synthesis technique	It is used for producing MOF formulations from the porous MOF polymer composites to produce the nanofibers	[18]
Hydrothermal synthesis technique	It is quite feasible in the organic synthesis of MOFs partially soluble in water at higher temperature	[19–20]
Solvothermal synthesis technique	It is useful for preparing the crystalline MOFs readily dissolvable in water	[21]

In addition to the various physical and chemical properties of MOFs, the geometry of the interconnections of the metal clusters and the organic binders can be changed to impart controllable polarity [22]. These features are desired to be gained; in particular, the volume of the pores, the specific area of BET and the ability to absorb. The length of the organic binders changes the adsorption property of MOFs. In case of increasing the

length of the organic binders, the density and volume of the pores can be increased. In addition, isotherm structures can affect the pore size of MOFs. The lattice flexibility of the MOFs can be affected by changing the metal ions. The most desirable feature of MOFs is the catalyst and storage capacity. The first microporous MOFs with a surface area of 310 m²/g was achieved in 1998. Since then, several studies have been carried out on the surface area of MOFs and continue to be dense. Among the studies that the researchers have included in the literature so far, there are many MOF studies with a surface area larger than 1000 m²/g. The synthesis of porous MOFs is based on the solvent to be removed in practice. While the solvent molecules that occupy the pores are removed, structural collapse may occur in MOFs. Providing the pores of the mesh structure of MOFs that remain intact according to the microporous MOFs is more difficult in mesoporous MOFs. Although MOFs use binders designed to provide the desired large pores to increase efficiency, sometimes the cage structures enter into each other. In such cases, the pore sizes are significantly reduced. However, this is desirable in some applications. This is because nested cages perform better in H₂ storage, etc. applications [23].

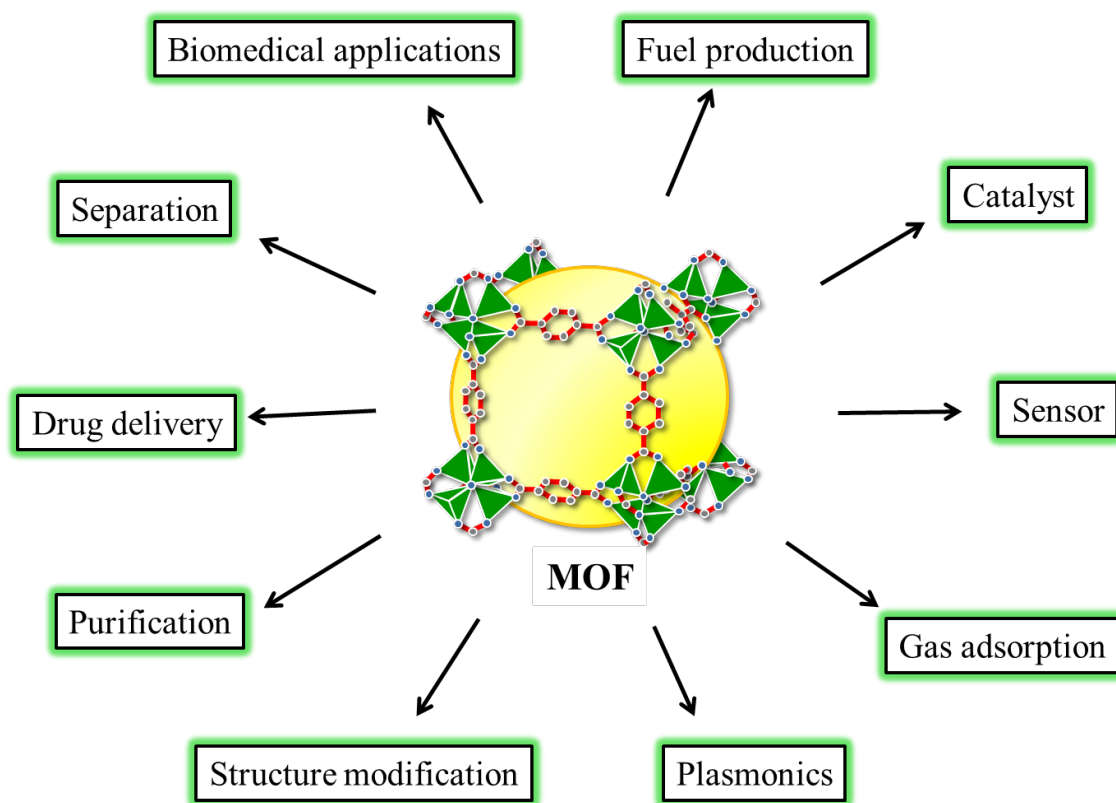


Fig 1. Usage areas of MOFs.

2.1 Usage areas of metal-organic frameworks

With its flexible mesh, large porous, high internal surface area, the MOFs have a wide range of application areas (Fig 1). The pores they have in terms of using MOFs provide significant advantages. MOFs are preferred for phase purification, separation, and storage due to the greatest advantages provided by large pore volumes. Apart from these, it is used in the fields of controlled drug release systems, drug storage and natural gas processes as well as a catalyst, magnetic material, sensor tool and nanomaterials in various fields (Table 2).

Table 2. Some Bio-MOFs and their potential applications.

BioMOF	Biomolecules	Auxiliary ligand	Potential application	Refs.
PCN-530	Adenine	TATB, 4,4',4''-s-triazine-2,4,6-triyl-tribenzoate	Molecular recognition	[24–26]
(Et4N)[Cd3(ade)2(ipa)2Br] 3MeOH_3.5DMA	Adenine	Isophthalic acid	Separation hydrocarbons	
(Et4N)[Cd3(ade)2(thb)2Cl]_3MeOH_3.5DMA	Adenine	2,5-Thiophenedicarboxylic acid	-	
Zn4(5-mtz)6(L-Ala)2_2(DMF)	L-Ala = L-alanine			
Zn4(5-mtz)6(L-Ala)2_2(DMF)	L-Ala = L-alanine	5-Hmtz, 5-methyltetrazole	Molecular recognition and separation enantiomers	[27]
Zn4(5-mtz)6(D-Ala)2_2(DMF)	D-Ala = D-alanine			
Zn4(5-mtz)6(L-Ser)2_2(DMF)	L-Ser = L-serine			
Zn4(5-mtz)6(L-Val)2_2(DMF)	L-Val = L-valine			
CuII(GHG)	GHG = Gly-L-His-Gly,	-	Separation for chiral drugs	[28–32]
BioMOF-100	Adenine	4,4'-Biphenyldicarboxylic acid	Drug release	
ZnBTCA	Adenine	BTC, benzene-1,3,5-tricarboxyl	Drug release	
ZnBDCA	Adenine	BDC, benzene-1,3-dicarboxylate	Molecular recognition and detection	

PCN-222	TCPP, Meso-tetra(4-carboxyphenyl)porphyrin	-	Photocatalytic water treatment, electrochemical sensor	[33–36]
γ -CD MOF	γ -CD, γ -Cyclodextrin	-	Separation of chiral aromatic alcohols	
CZJ-6	5,10,15,20-Tetrakis-(3,5-dicarboxyphenyl)porphine	-	Biomimetic catalysis	
MOF-1201, MOF-1203	L-lactate	Acetate	Food safety detection	

bdh-Zn-T122Hferritin	Ferritin	Benzene-1,4-dihydroxamic acid	Enzymatic catalysis	[37–39]
15 Ferritin–MOFs	Ferritin	Benzenehydroxamic acid	-	
[Zn ₁₆ (H ₂ O) ₈ (Mn ^{III} Cl-OCPP) ₄]	5,10,15,20-Tetrakis(3,5-biscarboxylphenyl)porphyrin	-	Olefins epoxidation catalysis	

2.1.1 Controlled drug release

In recent years, various methods have been used to increase the effectiveness of traditional treatment methods. The nanoparticle-based treatment method has been emphasized with the development of technology. In particular, in the last two decades, these small-molecule therapy methods that are of interest to the researchers can be controlled by controlled drug release systems in order to reduce the inconvenience.

In this respect, MOF's shape structure, pore size, and chemical properties can be adjusted, it has a wide range of chemical composition, so there are countless possibilities for selecting the compound to be used in the biomedical application, having a large surface area and ensuring the encapsulation of different drugs. Therefore, MOFs have a very important place in controlled drug release [40–42] (Table 3).

Table 3. *MOFs used in various drug delivery applications.*

MOFs	Drugs	Key Findings	Ref.
HKUST-1 (Cu)	NIM	Higher drug-loading with an extended drug release profile	[43–45]
MIL-53(Cr), MIL-53(Fe)	IBU	Zero order extended release for 3 weeks	
UiO-66(Zr)	CAF, IBU	Higher drug payload vis-à-vis conventional systems	
H3 BTC	DOX	Zn-BTX-DOX had better drug release profile vis-a-vis Fe-BTCDOX composite	[44–48]
MIL-100	Gem-MP	Higher drug loading (B30 wt%) vis-a-vis amorphous form	
MIL-53, MIL-100	IBU	Enhanced analgesic and antiinflammatory activity	
Fe ₃ O ₄ _UiO66	BSF, AZT-Tp, DOX, CDV	Improved therapeutic efficacy	[49–52]
Fe-MIL-88A	Iron	Simulating enzyme activity	
Fe-MIL-88A	ART	High drug in vitro release coupled with pH-sensitive properties	
MIL-101(Fe)	ESCP	A high drug loading of 13 wt% was observed	[44–48–53–55]
MIL-100 (Fe)	DOX	Higher theranostic potential against HT-29 (human adenosarcoma cells)	
Zn(BDC)(H ₂ O) ₂	NT recognition	A highly sensitive approach to detect NT	
Zn (BIX)	CAM, DAU	High drug encapsulation efficiency (21%) with extended release for 8 h	

MOF-15 (Cu)	5-FU	Extended 24 h drug release vis-a-vis pure drug	[44–59]
CuBTC(Cu)	5-FU	Extended 48 h release vis-a-vis pure drug	
MIL-100 (Fe)	CDV	High (42%) drug-loading	
MIL-101_NH2 (Fe)	CDV	High drug-loading efficacy	
ZrMOFs	PT, CPT	Drug-loaded MOF had higher antineoplastic potential vis-a-vis free drug	
UiO-66	5-FU	Light-activated release of drug from UiO-66	[60–63]
ZIF-8	DOX	DOX@ZIF-8 exhibited higher anticancer potential compared to pure drug	
ZIF-8 (Zn)	5-FU	Exceptionally high degree of drug loading	
MOF-1 (Zn)	5-FU	High drug-loading	

The use of MOFs as nano-sized (nMOF) for therapeutic use, therefore reducing their size will make it more suitable for use as drug carriers. Although nMOFs are promising for drug delivery, their impact on living things is still not fully understood. In order to be suitable for the use of nMOF'ların many developments and extensive research is required to occur [64]. Figure 2 shows the formation of MOF and drug loading schematically.

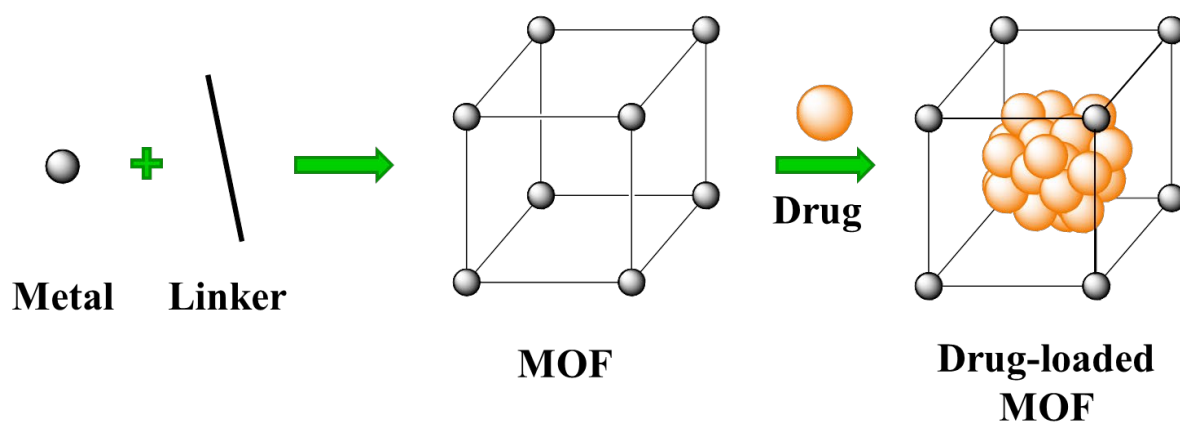


Fig 2. MOF formation and drug loading.

MOFs must be biocompatible for use in the biomedical field. This means that the toxic effect on the body should be reduced. While some metals are found in large amounts in the body, the presence of small amounts of chromium and some metals in the body can

create toxic effects. In the experiments, it was shown that iron metal, a component of hemoglobin, was about 22 micrometers in blood plasma and did not cause any toxicity.

The MIL (Materials of Institute Lavoisier) group, which was the first to investigate the drug transport potential of MOFs, was prepared with triple-valent metals bonded to the MOF's MIL-class carboxylic acid bridging binders. According to the researchers, the large hopper MIL (25-34 Å²), high surface areas (3100-5900 m²/g) and functional groups placed in the cage led to the use of the drug as the carrier systems [65]. Table 4 shows the other studies.

Table 4. *nMOF release kinetics of encapsulated drugs.*

MOF	Drug	Loading (wt%)	Release		Ref.
			% (PBS)	t(h)	
UiO	Cisplatin	12	20 (H ₂ O) 75 (PBS)	8	[66–68]
MIL-100(Fe)	Azidothymidine triphosphate	100	75	8	
M-CPO-27(Ni)	Nitric oxide	3	100	0.5	
	Metronidazole	11	100	6	[69–72]
MIL-100(Fe)	Busulfan	25	60	0.5	
AS1411-UCNPs@	Doxorubicin	17	18	96	
UiO-66	Alendronate	100	43 (pH 7.4) 59 (pH 5.5)	60	[62–73–74]
SiO ₂ -MIL-101-NH ₂	Ethoxysuccinato-cisplatin	12	-	72	
[Ni ₈ (μ ₄ -OH) ₄ (μ ₄ -OH ₂) ₂ -(μ ₄ ,4'-(buta-1,3-diyne-1,4-diyl)bispirazolato) ₆] _n	RAPTA-C	100	<20	15	
[(CH ₃) ₂ NH ₂][Zn(TATAT) _{2/3}]. 3DMF·H ₂ O	5-Fluorouracil	22	42	8	[75–76]
MG-Gd-pDBI	Doxorubicin	12	22 (pH 7.4) 44 (pH 5)	120	
PAA @ZIF-8	Doxorubicin	95	37 (pH 7.4) 78 (pH 5)	60	
ZIF-8	Camptothecin	2	50	1	[75–76]
MIL-100(Fe)	Topotecan	33	16	24	

The storage capacity of MOFs varies depending on the pore size. For example, chromium-based MIL-101 and MIL-100 and ibuprofen storage and release properties were investigated. In this chapter, the MIL-101 exhibited a storage capacity of 1,376 g ibuprofen / g MOF and 0.347 g ibuprofen / g MOF storage capacity for MIL-100. Since the most serious difference between these two materials is the pore size, it is thought that this also causes the difference in storage capacities. MIL-101 has a larger pore size with units of 12 700 and 20 600 Å[°], while it has been reported to have MIL-100 8200 and 12 700 Å[°] units [65].

MIL-53, which has a more flexible structure than other types of MOFs, was investigated for controlled drug release. The MIL-53 (Cr) showed a storage capacity of 0.220 g ibuprofen / g MOF, while the less toxic MIL-53 (Fe) showed storage capacity with 0.210 g ibuprofen / g MOF. In order to investigate the release kinetics of these drugs, they were kept in artificial body fluid (SBF) at 37 ° C. All drug delivery was carried out in three weeks. According to these results, the long release time of the drug was reported to be related to the flexibility of the cage structure and the strong interaction between the drug and cage [65].

MOFs with a low water solubility (hydrophobic), such as the MIL class, are ideal for encapsulation of drug molecules. MOFs can have hydrophobic pores or can be designed to carry a positive or negative charge. Such MOFs can provide the encapsulation of drugs by utilizing opposite charges. For an anionic MOF containing parabiphenyldicarboxylic acid, cationic zinc (II) ions were developed. It was also investigated the status of anionic MOF in the storage and release of cationic drugs in a biological fluid [65–77–78].

2.1.2 Antibacterial activity of MOFs

In the studies, silver, zinc, copper, and cobalt metals were used as common metals in MOF structures. While antibacterial activities of these metals were analyzed as Gram-positive/negative, especially *Escherichia coli* (E. Coli) and *Staphylococcus aureus* (S. aureus) bacteria strains were used.

MOF applications in the nanomedicine field can be divided into two categories:

- (a) MOFs as a delivery tool (with large pore sizes for drug encapsulation),
- (b) MOFs are having bioactive drug molecules in their structures (Table 5) and (Table 6) [79][80].

Table 5. *Antibacterial studies on MOF structures.*

Compound	Metal	Linker	Ref
[Ag ₂ (O-IPA)(H ₂ O)(H ₃ O)]	Ag	5-hydroxyisophthalic	[81–83]
Co-TDM	Co	Tetrakis[(3,5-dicarboxyphenyl)-oxamethyl] methane	
BioMIL-5	Zn	Azelaic Acid	
[Ag ₅ (PYDC) ₂ (OH)]	Ag	Pyridine-3,5-dicarboxylic acid	[81–85]
Ag ₃ (3-phosphonobenzoate)	Ag	3-Phosphono benzoate	
ZIF-67	Co	2-Methylimidazolate	
Co-SIM-1	Co	4-Methyl-5-imidazolecarboxaldehyde	
[(AgL)ClO ₄] ₂ H ₂ O	Ag	Tris(4-pyridylduryl)borane	[86–87]
CuBTC	Cu	Benzene-1,3,5-tricarboxylic acid	
[(AgL)NO ₃] ₂ H ₂ O	Ag	Tris(4-pyridylduryl)borane	
[(AgL)CF ₃ SO ₃] ₂ H ₂ O	Ag	Tris(4-pyridylduryl)borane	

Synthesis of the 2D framework by Wang et al. [Cd(Norf)(ClO₄)(H₂O)] was reported as an example of active ligands with bioactive MOFs in 2004. Norfloxacin (H-Norf), which is used as a ligand in this structure, is an antimicrobial drug [88]. In order to investigate the MOFs, the classification according to the metals of the MOF was made. In any case, MOFs with drug encapsulation capacity and bioactive drug molecules have also been reported. Table 6 shows the inhibition site, minimal inhibitory concentration (MIC) and minimum bactericidal concentration (MBC) parameters used in antimicrobial activity investigations.

Table 6. Advanced MOF studies.

<p>MOF: HKUST1 $\text{Cu}_3(\text{BTC})_2(\text{H}_2\text{O})_3$</p>	<p>Metal: Cu^{2+} Ligand: Benzene-1,3,5-tricarboxylic acid Pore size (Å): 9-6 Type of bacteria: S. Aureus, E. Coli, PAO1 MIC ($\mu\text{g mL}^{-1}$): 100, 25, 50 Other method: Zone diameter for S.aureus: 6.5–7.5, E. coli: 7.5–8 (mm) Coordination Sphere: Cu_2O_5</p>	<p>MOF: HKUST1 $\text{Cu}_3(\text{BTC})_2(\text{H}_2\text{O})_3$</p>	<p>Metal: Cu^{2+} Ligand: Benzene-1,3,5-tricarboxylic acid Drug encapsulated: AITC Pore size (Å): 9-6 Coordination Sphere: Cu_2O_5</p>	[89–92]
<p>MOF: MBioF (Glu-Cu^{+2}) $[\text{Cu}(\text{Glu})(\text{H}_2\text{O})]$</p>	<p>Metal: Cu^{2+} Ligand: DL-Glutamic acid Type of bacteria: S. aureus and E. coli Other method: When bacteria (S. Aureus and E. coli) treated by nanofibers, the surface of them became rough and wrinkled Coordination Sphere: Lack of crystal structure</p>	<p>MOF: Cu-SURMOF 2 $[\text{Cu}_2(\text{bdc})_2]\text{n}$</p>	<p>Metal: Cu^{2+} Ligand: 1,4-Benzene dicarboxylic Acid Pore size (Å): 11 Type of bacteria: Cobetia marina Other method: Fluorescence microscopy images showed many damaged bacteria (Cobetia marina) after 2 h incubation with Cu-SURMOF 2 Coordination Sphere: Cu_2O_5</p>	
<p>MOF: $[\text{Cu}(\text{L-Arg})$ $2(\text{m-4,4boy})]$ $\text{Cl}2.3\text{H}_2\text{O}]1$</p>	<p>Metal: Cu^{2+} Ligand: L-Arginine Pore size (Å): Forming Hbonded Chiral channels: 4.8-4.5 Type of bacteria: Gram-positive and gram-negative bacteria strains and fungia MIC ($\mu\text{g mL}^{-1}$): MIC<15 M Coordination Sphere: CuO_2N_4</p>	<p>MOF: MOF-74(Zn) $\text{Zn}_2(\text{DHBDC})(\text{DMF})_2 \cdot (\text{H}_2\text{O})_2$</p>	<p>Metal: Zn^{2+} Ligand: 2,5-Dihydroxyterephthalate Drug encapsulated: AITC Pore size (Å): 5.5×10 Coordination Sphere: ZnO_6</p>	[92–96–97]
<p>MOF: RPM6-Zn $[\text{Zn}_3(\text{bpdc})_3(\text{apy})] \cdot 3.08\text{DMF}$</p>	<p>Metal: Zn^{2+} Ligand: bpdc: biphenyl-4,40 dicarboxylate, apy1-4,4'-azobispyridine Drug encapsulated: AITC Pore size (Å): 7×20 Coordination Sphere: ZnO_6</p>	<p>MOF: ZIF-8 $\text{Zn}(\text{mim})_2$, where mim = 2-methylimidazolot</p>	<p>Metal: Zn^{+2} Ligand: 2-Methyl imidazole Pore size (Å): 11.6 Type of bacteria: S. Mutans Other method: The morphology of S. mutans changed to a globular shape, and the bacterial membranes were partially Decomposed Coordination Sphere: ZnN_4</p>	[92–98–101]

MOF: ZIF-8@I

$\text{Zn}(\text{mim})_2$
where mim = 2-methylimidazolate

Metal: Zn^{2+}

Ligand: Methyl imidazole

Drug encapsulated: Iodine

Type of bacteria: S. epidermidis, S. aureus and E. coli

Other method: All three bacterial cells were killed at ZIF-8@I dosage of 0.2 g/L within 3 min. At the same dosage, 100% killing effective rate of S. epidermidis and S. Aureus was achieved at 2 min and 3 min was required for E. coli

Coordination Sphere: ZnN_4

MOF: ZIF-8@FA@Van
 $\text{Zn}(\text{mim})_2$,
where mim = 2-methylimidazolate

Metal: Zn^{2+}

Ligand: 2-Methyl imidazole

Drug encapsulated: Vancomycin

Type of bacteria: S. Aureus E. Coli

MIC($\mu\text{g mL}^{-1}$): 8,-

MBC($\mu\text{g mL}^{-1}$): 16,-

Coordination Sphere: ZnO_4

[102–103]

MOF: BioMIL-5

$\text{Zn}(\text{C}_6\text{O}_4\text{H}_{14})$

Metal: Zn^{2+}

Ligand: Azelaic acid (AzA)

Pore size (Å): Lack of pore

Type of bacteria: S. Aureus S. Epidermidis

MIC($\mu\text{g mL}^{-1}$): 1,7-1,7

MBC($\mu\text{g mL}^{-1}$): 4,3-4,3

Coordination Sphere: ZnO_4

MOF: Zn-MOF
(3) $\{[\text{Zn}(\mu_4\text{hzba})_2, 4(\text{H}_2\text{O})]_n\}$

Metal: Zn^{+2}

Ligand: 4-Hydrazinbenzoate

Pore size (Å): 18.58×14.83

Interpenetrated Structure

Type of bacteria: S. Aureus

Other method: Average inhibition diameter against S. aureus 14.6 ± 3.1 mm

Coordination Sphere: tetracoordinate (ZnO_2N_2) and the other is hexacoordinated (ZnO_4N_2)

[104–105]

MOF: Co-SIM-1

$[\text{Co}(\text{C}_5\text{H}_5\text{N}_3\text{O})_2]$
= $[\text{Co}(4\text{-Me-5-CHOIm})_2]$

Metal: Co^{2+}

Ligand: 4-Methyl-5-imidazolecarboxyaldehyde ((4-Me-5-CHOIm)

Pore size (Å): Cage size of SIM-1 is 8 Å with pore aperture <3.4 Å

Type of bacteria: Pseudomonas putida, E. Coli

Other method: 15 mm inhibition Diameter

Coordination Sphere: CoN_4

MOF: ZIF-67
 $\text{Co}(\text{Hmim})_2$

Metal: Co^{2+}

Ligand: Benzene-1,3,5-tricarboxylic acid

Pore size (Å): da: 3.4 dp: 11.6b

Type of bacteria: Pseudomonas putida, E. Coli

Other method: 15 mm inhibition Diameter

Coordination Sphere: Cu_2O_5

[85–106–108]

MOF: MOF-53(Fe)@Van
 $\text{Fe}(\text{OH})(\text{BDC})$

Metal: Fe^{+3}

Ligand: Terephthalic acid (H2BDC)

Drug encapsulated: vancomycin

Pore size (Å): 16.1

Type of bacteria: S. Aureus

Other method: The number of viable bacterial colony forming units (cfus) for the control group was 296, cfus for MOF-53@Van with concentrations of 25, 50, 100, and 200 $\mu\text{g mL}^{-1}$ was 201, 142, 70, and 2, Respectively

Coordination Sphere: FeO_6

MOF: $\text{Ag}_3(3\text{-phosphonobenzoate})$

Metal: Ag^+

Ligand: 3-Phosphonobenzoic acid

Pore size (Å): 1-D channels 4×12.4

Type of bacteria: S. aureus

E. Coli, P. Aeruginosa

MBC($\mu\text{g mL}^{-1}$): 50–75, 50, 20–30

Coordination Sphere: Ag1: Ag_2O_4

Ag2: Ag_5O_3

Ag3: Ag_5O_3

Ag4: Ag_2O_4

Ag5: Ag_5O_4

Ag6: Ag_2O_4

[84–109]

**MOF: PES-
PANCMA-PEI-
Ag**

Metal: Ag⁺
Ligand: Poly (acrylonitrile-comaleic acid) (PANCMA)
Pore size (Å): 0.08 ± 0.015 mm
Other method: Inhibition zone: 2.5–3mm

**MOF: Si@PEI-
Ag⁺-Ag_{2n}
(BTEC)_{n/2} films
or Si@PEI-Ag_{2n}
(BTEC)_{n/2}**

Metal: Ag⁺
Ligand: H4BTEC = 1,2,4,5-benzenetetracarboxylic acid
Pore size (Å): 4.8×4.2
Type of bacteria: E. Coli
Other method: Results showed that both Si@PEI-Ag⁺-Ag_{2n} (BTEC)_{n/2} films and Si@PEI-Ag_{2n} (BTEC)_{n/2} films can destroy more than 90% of bacteria (E. coli) after 2 min and 99% after 30 min
Coordination Sphere: Ag1: Ag₂O₃
Ag2: Ag₂O₄

[110–112]

**MOF:
[(AgL)NO₃].2H₂O**

Metal: Ag⁺
Ligand: Tris-(4-pyridylduryl)borane
Pore size (Å): Void space: 46.4%
Type of bacteria: S. Aureus, E. Coli
MIC(μg mL⁻¹): 297-300
Other method: Inhibition zone (mm): S. aureus: 16 E. coli: 13
Coordination Sphere: AgN₃O₂

**MOF:
[(AgL)CF₃SO₃].2H₂O**

Metal: Ag⁺
Ligand: Tris-(4-pyridylduryl)borane
Pore size (Å): Void space: 43.6%
Type of bacteria: S. Aureus, E. Coli
MIC(μg mL⁻¹): 307-300
Other method: Inhibition zone (mm): S. aureus: 16, E. coli: 15
Coordination Sphere: AgN₃

[84]

**MOF:
[(AgL)ClO₄].2H₂O**

Metal: Ag⁺
Ligand: Tris-(4-pyridylduryl)borane
Pore size (Å): Void space: 21.7%
Type of bacteria: S. Aureus, E. Coli
MIC(μg mL⁻¹): 293-308
Other method: Inhibition zone (mm): S. aureus: 19, E. coli: 15
Coordination Sphere: AgN₃

**MOF:
[Ag(NO₃)(μ₃-
PTAdO)]_n**

Metal: Ag⁺
Ligand: 1,3,5-Triaza-7-phosphaadamantane-7-oxide (PTA@O)
Pore size (Å): 6.8×3, 9.9×3.9
Type of bacteria: E. Coli, P. Aeruginosa, S. Aureus, C. Albicans
MIC(μg mL⁻¹): 6, 7, 20,30
Coordination Sphere: AgO₃N₂

[84–113]

**MOF: [Ag₂(μ₂-
SO₄)(μ₂-PTAdO)
(H₂O)]_n**

Metal: Ag⁺
Ligand: 1,3,5-Triaza-7-phosphaadamantane-7-oxide (PTA = O)
Pore size (Å): 4.6×6.3, 6.3×6.4
Type of bacteria: E. Coli, P. Aeruginosa, S. Aureus, C. Albicans
MIC(μg mL⁻¹): 6, 6, 20,20
Coordination Sphere: Ag1: AgO₂N₂
Ag2: AgO₃N

**MOF: Ag(μ₃-
PTALS)]_n(NO₃)_n.
nH₂O**

Metal: Ag⁺
Ligand: 1,3,5-Triaza-7-phosphaadamantane-7- sulfide (PTA@S)
Pore size (Å): 4.7×9.2, 6.2×5.2
Type of bacteria: E. Coli, P. Aeruginosa, S. Aureus, C. Albicans
MIC(μg mL⁻¹): 4, 5, 20,30
Coordination Sphere: AgN₂S

[113–114]

<p>MOF: [Ag₄(m₄-PTALS)(m₅-PTALS)(m₂-SO₄)₂(H₂O)₂]_n.2nH₂O</p>	<p>Metal: Ag⁺ Ligand: 1,3,5-Triaza-7-phosphaadamantane-7-sulfide (PTA = S) Pore size (Å): 3.2×11.5 Type of bacteria: E. Coli, P. Aeruginosa, S. Aureus, C. Albicans MIC(μg/mL⁻¹): 20,20, 40, 60 Coordination Sphere: Ag1: AgNOS₂, Ag2: AgNOS₂, Ag3: AgNO₂S, Ag4: AgNOS</p>	<p>MOF: [Ag₂(μ-PTA)₂(μ-suc)]_n.2nH₂O</p>	<p>Metal: Ag⁺ Ligand: 1,3,5-Triaza-7-phosphaadamantane (PTA), Succinic acid (H₂suc) Pore size (Å): 10.6×5.1 Type of bacteria: E. Coli, P. Aeruginosa, S. Aureus, C. Albicans MIC(μg/mL⁻¹): 6, 20, 6, 40 Coordination Sphere: AgPON</p>	[114–115]
<p>MOF: [Ag₂(μ-PTA)₂(μ₄-adip)]_n.2nH₂O</p>	<p>Metal: Ag⁺ Ligand: ,3,5-Triaza-7-phosphaadamantane (PTA), Adipic acid (H₂adip) Pore size (Å): 4×7 Type of bacteria: E. Coli, P. Aeruginosa, S. Aureus, C. Albicans MIC(μg/mL⁻¹): 6, 20, 40 Coordination Sphere: Ag₂O₂PN</p>	<p>MOF: [Ag₂(μ₄-PTA)(μ₄-mal)]_n</p>	<p>Metal: Ag⁺ Ligand: 1,3,5-Triaza-7-phosphaadamantane (PTA), Malonic acid (H₂mal) Pore size (Å): 4×5.8, 3.4×4.8 Type of bacteria: E. Coli, P. Aeruginosa, S. Aureus, C. Albicans MIC(μg/mL⁻¹): 7, 6, 8, 30 Coordination Sphere: Ag1: AgO₂PN, Ag2: AgN₂O₂</p>	[115]
<p>MOF: [[Ag₄(μ₄-pzdc)2(μ-en)]₂.H₂O]_n</p>	<p>Metal: Ag⁺ Ligand: Pyrazine-2,3-dicarboxylate (pzdc), ethylenediamine (en) Pore size (Å): 4.2×7.3 Type of bacteria: E. Coli, P. Aeruginosa, S. Aureus, C. Albicans MIC(μg/mL⁻¹): 36, 63, 18–36, 36–63 Coordination Sphere: Ag1: AgO₂PN, Ag2: AgN₂O₂</p>	<p>MOF: [Ag₂(O-IPA)(H₂O).(H₂O)]</p>	<p>Metal: Ag⁺ Ligand: HO-H₂IPA (5-hydroxyisophthalic acid) Pore size (Å): 4.5×4.8, 3.4×8 Type of bacteria: E. Coli, S. aureus MIC(μg/mL⁻¹): 5–10, 10–15 Other method: Inhibition zone (mm): S. aureus: 16 E. coli: 20 Coordination Sphere: Ag1: Ag₂O₄, Ag2: Ag₃O₃</p>	[81–116]
<p>MOF: [Ag₅(PYDC)₂(OH)]</p>	<p>Metal: Ag⁺ Ligand: H₂PYDC (pyridine-3, 5-dicarboxylic acid) Pore size (Å): 3.5×4.5 Type of bacteria: E. Coli, S. aureus MIC(μg/mL⁻¹): 10–15, 15–20 Other method: Inhibition zone (mm): S. aureus: 14 E. coli: 17 Coordination Sphere:Ag1: AgO₃, Ag2: AgO₃N, Ag3: AgO₄</p>	<p>MOF: Ag₇(bte)₄(H₂O)-(HP₂W^{VI}₁₆W^V₂O₆₂)]₂.2H₂O</p>	<p>Metal: Ag⁺ Ligand: P₂W₁₈(bte = 1,2-bis(1,2,4-triazol-1-yl)ethane, btb = 1,4-bis(1,2,4-triazol-1-yl)butane) Type of bacteria: E. Coli, S. aureus Coordination Sphere: AgN₂O₃, AgN₂O₂, AgN₃O, Ag₂N₂O, Ag₂NO₂</p>	[81–117]

<p>MOF: $\text{Ag}_7(\text{btp})_5(\text{HP}_2\text{W}^{\text{V}}_{16}\text{W}^{\text{V}}_{2}\text{O}_{62})\cdot\text{H}_2\text{O}$</p>	<p>Metal: Ag^+ Ligand: $\text{P}_2\text{W}_{18}\text{btp}$ = 1,3-bis (1,2,4-triazol-1-yl)propane Type of bacteria: E. Coli, S. aureus Other method: Inhibition zone was slightly larger than Ag^+ ions Coordination Sphere: $\text{Ag}_2\text{N}_2\text{O}_2$, AgN_2O_2, Ag_2N_2</p>	<p>MOF: $[\text{Ag}_4(\text{btb})_{3.5}(\text{P}_2\text{W}_{18}\text{O}_{62})\cdot(\text{H}_2\text{btb})\cdot 2\text{H}_2\text{O}]$</p>	<p>Metal: Ag^+ Ligand: $\text{P}_2\text{W}_{18}\text{btb}$ = 1,4-bis (1,2,4-triazol-1-yl)butane) Pore size (Å): Diameter of the cage:18.5 Type of bacteria: E. Coli, S. aureus Other method: Showed almost identical inhibition zone values with Ag^+ Coordination Sphere: AgN_2O_3, AgN_2O_2, AgN_3, AgN_2O</p>	[117]
<p>MOF: $[\text{Co}_4(\text{H}_2\text{O})_2(\text{TDM})(\text{H}_2\text{O})_8]$</p>	<p>Metal: Co-TDM (20) Ligand: Tetrakis [(3,5-dicarboxyphenyl)-oxamethyl]methane (H_8TDM) Pore size (Å): Dumbbellshaped Open channels 11×6 Type of bacteria: E. Coli MBC($\mu\text{g mL}^{-1}$): 10–15, In a short incubation time period (<60 min) Coordination Sphere: CoO_6 Cobalt Coordination geometry is octahedral</p>	<p>MOF: $[\text{Ni}_2(\text{HL}2)_4(4,4'\text{-bipy})\cdot(\text{H}_2\text{O})_2\cdot 4\text{H}_2\text{O}]$</p>	<p>Metal: Ni^{2+} Ligand: 3-Phenyl-1H-pyrazole-4-carboxylic acid = H_2L^2 Pore size (Å): Channel size: 8.27×6.17 Type of bacteria: S. Aureus, C. Albicans, B. Subtilis, E. Coli, P. Aeruginosa MIC($\mu\text{g mL}^{-1}$): 12.5, 12.5, 25, 12.5, 12.5 Coordination Sphere: NiO_2N_4</p>	[82–118]
<p>MOF: $[\text{Co}(\text{HL}^2)_2(4,4'\text{-bipy})]$</p>	<p>Metal: Co^{2+} Ligand: 3-Phenyl-1H-pyrazole-4-carboxylic acid = H_2L^2 Pore size (Å): Channel size: 8.71×11.43 Type of bacteria: S. Aureus, C. Albicans, B. Subtilis, E. Coli, P. Aeruginosa MIC($\mu\text{g mL}^{-1}$): 12.5, 6.5, 25, 12.5, 12.5 Coordination Sphere: CoO_2N_4</p>	<p>MOF: $[\text{Ni}(\text{NPTA})(4,4'\text{-bipy})(\text{H}_2\text{O})_n]$</p>	<p>Metal: Ni^{2+} Ligand: Nitrophthalic acid (H_2NPTA) and 4,4-bipyridine (4,40-bipy) Pore size (Å): Window size: 11.5×13.8 Type of bacteria: S. Aureus, E. Coli MIC($\mu\text{g mL}^{-1}$): 12.5, 6.5, 25, 12.5, 12.5 Other method: Inhibition zone: E. coli: 14 mm, S. aureus: 12mm Coordination Sphere: NiO_4N_2</p>	[118–119]
<p>MOF: $[\text{Mn}(\text{Fbtz})_2\text{Cl}_2]_n$</p>	<p>Metal: Mn^{2+} Ligand: 1,4-bis (1,2,4-triazole-1-ylmethyl)-2,3,5,6-tetrafluorobenzene (Fbtz) Pore size (Å): 1-D Rhombic channels along the [010], direction, 11.9×14 Type of bacteria: B. Subtilis, S. Aureus, E. Coli, P. Fluorescence MIC($\mu\text{g mL}^{-1}$): 1.56, 0.78, 25, 12.5 Other method: Inhibition zone: E. coli: 14 mm, S. aureus: 12mm Coordination Sphere: 25 and 26 are Isostructural MnN_4Cl_2</p>	<p>MOF: $[\text{Co}(\text{Fbtz})_2\text{Cl}_2]_n$</p>	<p>Metal: Co^{2+} Ligand: 1,4-Bis (1,2,4-triazole-1-ylmethyl)-2,3,5,6-tetrafluorobenzene (Fbtz) Pore size (Å): 25 and 26 are Isostructural Type of bacteria: B. Subtilis, S. Aureus, E. Coli, P. Fluorescence MIC($\mu\text{g mL}^{-1}$): 3.13, 1.56, 12.50, 3.13 Coordination Sphere: MnN_4Cl_2</p>	[120]

<p>MOF: $\{[\text{Co}(\text{Fbtz})_2\text{Cl}_2] \cdot \text{CH}_2\text{Cl}_2 \cdot \text{H}_2\text{O}\}_n$</p>	<p>Metal: Co^{2+} Ligand: Fbtz Pore size (Å): 11.5×9.4, 5×8 Type of bacteria: B. Subtilis, S. Aureus, E. Coli, P. Fluorescence MIC($\mu\text{g mL}^{-1}$): 1.56, 1.56, 12.5, 6.25 Coordination Sphere: 27×29 are isostructural CoN_4Cl_2</p>	<p>MOF: $\{[\text{Fe}(\text{Fbtz})_2\text{Cl}_2] \cdot \text{CH}_2\text{Cl}_2 \cdot 2\text{H}_2\text{O}\}_n$</p>	<p>Metal: Fe^{2+} Ligand: Fbtz Pore size (Å): 27×29 are isostructural Type of bacteria: B. Subtilis, S. Aureus, E. Coli, P. Fluorescence MIC($\mu\text{g mL}^{-1}$): 0.78, 1.56, 0.78, 0.78 Coordination Sphere: CoN_4Cl_2</p>	[120]
<p>MOF: $\{[\text{Cu}(\text{Fbtz})_2\text{Cl}_2] \cdot 4\text{H}_2\text{O}\}_n$</p>	<p>Metal: Cu^{2+} Ligand: Fbtz Pore size (Å): 27×29 are isostructural Type of bacteria: B. Subtilis, S. Aureus, E. Coli, P. Fluorescence MIC($\mu\text{g mL}^{-1}$): 1.56, 3.13, 1.56, 1.56 Coordination Sphere: CoN_4Cl_2</p>	<p>MOF: $\{[\text{Cu}_2(\text{Fbtz})(\text{OAc})_4] \cdot 2\text{H}_2\text{O}\}_n$</p>	<p>Metal: Cu^{2+} Ligand: Fbtz Pore size (Å): A helical chain running in the [0 1 0] direction. And these two-D helices are surrounded by each other and make a doublestranded helical array Type of bacteria: B. Subtilis, S. Aureus, E. Coli, P. Fluorescence MIC($\mu\text{g mL}^{-1}$): 3.13, 6.25, >100, 25 Coordination Sphere: Coordination sphere: $\text{Cu}_2\text{O}_4\text{N}$</p>	

2.1.3 Biomedicine

Recently, the use of MOFs in the biomedicine field has increased. The reason for this increase is due to the high loading capacity, structural diversity, and biodegradability of the nanoscale MOFs. Conservation and molecular therapeutics, gas signaling molecules (gasotransmitter), bio-sensors, cell and virus manipulation, biocatalysis and biobanking are the emerging applications of MOFs [121–124].

In recent years, MOFs have been widely used in therapeutic compounds and controlled release systems because of their high surface area with large pore sizes. For the first time in 2006, Horcajada and his colleagues pointed out that MOFs have a considerable capacity from the drug-hosting feature [44]. Thanks to ibuprofen encapsulation and the mesoporosity of MOFs, it is possible to obtain 60% efficiency from MIL-100 and MIL-101 materials.

An et al. have used the porous anionic metal-organic framework (bio-MOF-1) using adenine for the release and storage of procainamide HCl, an important cationic antiarrhythmic drug [125]. It is an example of drug delivery systems that are activated by cation based on MOFs in this study. In another study, Hu et al. developed MOF-74-Fe (III) with the oxidation of MOF-74-Fe (II) which is neutral as a cationic drug carrier [126].

In this study, the cationic MOF-74-Fe (III) developed by Hu et al. proved that MOFs could be a drug delivery host with a loading capacity of about 15.9% by weight for the controlled release ibuprofen anions. In another study, 2 (DSCP / disuccinatocisplatin) containing 3(H₂O) 12 and 46.7% Pt-based drugs with high degradable Pt nanoparticles were delivered to cancer cells by Rieter et al. [75]. Meng et al. synthesized a dual-stimulating MOF with the supramolecular complexation of UiO-68-azobenzene (β -CD-coated UiO-68-azo) with CD-CD ligands [127].

Research on MOF for applications in the biomedical field, although still new, has shown unique advantages and great potential. Recently, it is believed that these widespread studies on MOFs will be a target for drug suppliers in the future.

2.1.4 Chemical sensors

The structure of the MOFs can be adjusted and regulated, making them usable in chemical sensors. Generally, the incorporation of the guest molecule for MOF hosts causes luminescence change. By incorporating MOF materials into many different chemical functionalities, MOFs have been extended to detect applications for biomolecules, metal ions, explosives and environmental toxins (Fig 3) [128–134]. Nagarkar et al. Successfully synthesized fluorescent MOF [Cd(NDC/2,6-naphthalene dicarboxylic acid) 0.5 (PCA/4-pyridinecarboxylic acid)] from NDC and PCA ligands, and very much for the 2,4,6-trinitrophenol (TNP) have shown that it is a sensitive detector. The sensitivity of the fluorescent MOF in this study consists of the electrostatic interactions between the TNP and the fluorophore as well as the electron and energy transfer mechanisms. Zhang et al. made MOFs functional with the amine (UIO-66-NH) for DNA detection testing. In this study, it was found that hydrogen bond interaction is very important for single-stranded DNA (ssDNA) and UIO-66-NH-amino group control. However, the complementarity of detection systems and selectivity and reproducibility for distinguishable DNA sequences and single base mismatch studies indicated that IO-66-NH had no activity [135].

Jiang et al. synthesized the zirconium-porphyrin skeleton PCN-225. This MOF prepared by Jiang et al. has found that the fluorescence intensity changes with pH and the most sensitive range for the density response are between 7 and 10 [136]. Zhan et al. used ZnO nanorods to provide Zn. The ions and the resulting ZnO® ZIF-8 nanorods for the formation of ZIF-8 showed a very selective photoelectrochemical reaction for hydrogen peroxide in the serious buffer solution [137].

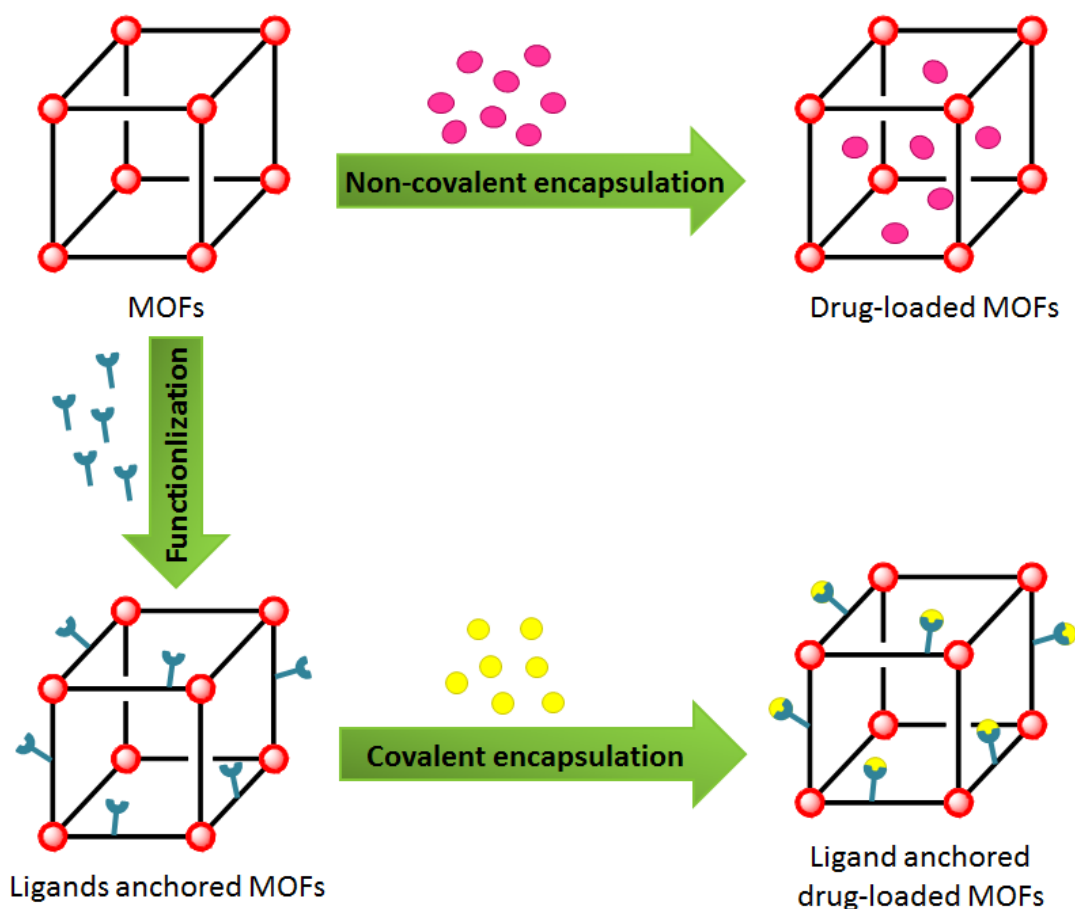


Fig 3. Biosensor studies on MOF structures.

Organic explosives and antibiotics, one of the major pollutants in wastewater, are difficult to detect because they are small. For this reason, Wang et al. have synthesized Zr-based MOF (iso-Zr (IV)). They synthesized $6\text{O}4(\text{OH})8(\text{H}_2\text{O})4(\text{CTTA})8/3(\text{AMA}-12, \text{H}, 3\text{CTTA} = 5' - (4\text{-carboxyphenyl}) - 2', 4', 6'\text{-trimethyl} - [1,1' : 3', 1' \text{-phenyl}] - 4,4' \text{-dicarboxylic acid})$ and $\text{Zr}_6\text{O}_4(\text{OH})_8(\text{H}_2\text{O})_4(\text{TT1A})_8/3(\text{AMA}-13, \text{H}, 3\text{TTIA} = 6, 6', 6 \text{ And } (2, 4, 6\text{-trimethylbenzene-1,3,5-triyl}) \text{ tris } (2\text{-naphthoic acid}))$ are water resistant and highly fluorescent [138]. Thanks to the fluorescence of these MOFs, they have been selected to detect nitrofurazone (NZF) selectively and nitrofurantoin (NFT) antibiotics in small amounts of wastewater and 2,4,6-trinitrophenol (TNP) and 4-nitrophenol (4-NP). Due to this characteristic of MOFs, they have been useful in both water quality monitoring and wastewater treatment. Research on the enzymatic studies of MOFs in the biomedicine field is given in the table below (Table 7).

Table 7. *Nanoenzyme studies on MOF structures.*

Application for colorimetric sensing		Ref
Nanozyme: MIL-53 (Fe)	Targets: H ₂ O ₂ Linear range: 0.95-19 μM LOD: 0.13 μM	[139-140]
Nanozyme: MIL-53 (Fe)	Targets: H ₂ O ₂ Linear range: 0.25-20 μm LOD: - μM	
Nanozyme: Fe-MIL-88A	Targets: H ₂ O ₂ Linear range: 2-20.3 μM LOD: 0.56 μM	[141-142]
Nanozyme: MIL-68(Fe)	Targets: H ₂ O ₂ Linear range: 3-40 μM LOD: 0.256 μM	
Nanozyme: MIL-100(Fe)	Targets: H ₂ O ₂ Linear range: 3-40 μM LOD: 0.155 μM	[141-142]
Nanozyme: Cu-MOF	Targets: H ₂ O ₂ Linear range: 10-50 μM LOD: 1.37 μM	
Nanozyme: Cuehemin MOFs	Targets: H ₂ O ₂ Linear range: 0.001-1 μM LOD: 0.42 μM	[143-144]
Nanozyme: MOF(Co/2Fe)	Targets: H ₂ O ₂ Linear range: 10-100 μM LOD: 5 μM	
Nanozyme: glycine-MIL-53(Fe)	Targets: H ₂ O ₂ Linear range: 0.1-10 μM LOD: 49 nM	[145-146]
Nanozyme: Hemin@MIL-101(Al)NH ₂	Targets: H ₂ O ₂ Linear range: 5-200 μM LOD: - μM	

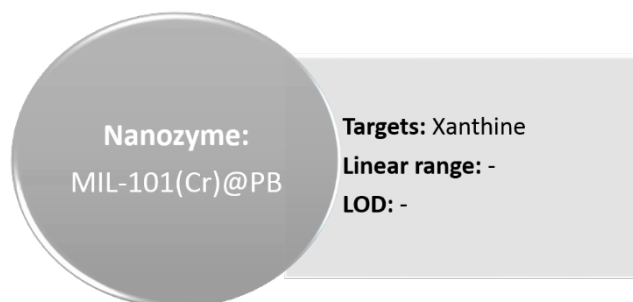
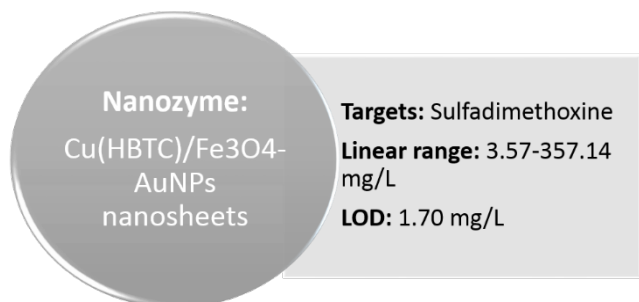
<p>Nanozyme: Fe₃O₄@MIL-100(Fe)</p>	<p>Targets: H₂O₂ Linear range: 0.2-30 μM LOD: 0.089 μM</p>	<p>Nanozyme: Cu(HBTC)/Fe₃O₄-AuNPs nanosheets</p>	<p>Targets: H₂O₂ Linear range: 2.86-71.43 nM LOD: -</p>	[147-148]
<p>Nanozyme: PB/MIL-101(Fe)</p>	<p>Targets: H₂O₂ Linear range: 2.4-100 μM LOD: 0.15 μM</p>	<p>Nanozyme: BHb@ZIF-8</p>	<p>Targets: H₂O₂ Linear range: 0-800 μM LOD: 1μM</p>	[149-150]
<p>Nanozyme: GOx@mZIF-8</p>	<p>Targets: H₂O₂ Linear range: 1.2 μM-0.1 μM LOD:</p>	<p>Nanozyme: CuNPs@C</p>	<p>Targets: H₂O₂ Linear range: 1 μM-1 μM LOD: 64.12 nM</p>	[151-152]
<p>Nanozyme: FeP nanocubes</p>	<p>Targets: H₂O₂ Linear range: 2-130 μM LOD: 0.62 μM</p>	<p>Nanozyme: CoNPs/MC</p>	<p>Targets: H₂O₂ Linear range: 0.1-20 μM LOD: 77 nM</p>	[153-154]
<p>Nanozyme: HAP@MIL-100(Fe)</p>	<p>Targets: H₂O₂ Linear range: 0.95-28.57 μM LOD: -</p>	<p>Nanozyme: MIL-53(Fe)</p>	<p>Targets: Glucose Linear range: 0.25-20 μM LOD: 0.25 μM</p>	[140-155]

<p>Nanozyme: Fe-MIL-88NH₂</p>	<p>Targets: Glucose Linear range: 2-300 μM LOD: 0.48 μM</p>	[143-156]
<p>Nanozyme: Cuehemin MOFs</p>	<p>Targets: Glucose Linear range: 0.01-3 μM LOD: 6.9 μM</p>	
<p>Nanozyme: glycine-MIL-53(Fe)</p>	<p>Targets: Glucose Linear range: 0.25-10 μM LOD: 0.13 μM</p>	[145-146]
<p>Nanozyme: Hemin@MIL-101(Al)NH₂</p>	<p>Targets: Glucose Linear range: 10-300 μM LOD: -</p>	
<p>Nanozyme: Cu(HBTC)/Fe₃O₄-AuNPs nanosheets</p>	<p>Targets: Glucose Linear range: 12.86-257.14 μM LOD: -</p>	[148-157]
<p>Nanozyme: AuNPs@2D MOFs</p>	<p>Targets: Glucose Linear range: 10-300 μM LOD: 8.5 μM</p>	
<p>Nanozyme: PB/MIL-101(Fe)</p>	<p>Targets: Glucose Linear range: 0.1-1.0 μM LOD: 0.4 μM</p>	[149-151]
<p>Nanozyme: GOx@mZIF-8</p>	<p>Targets: Glucose Linear range: 0.005-0.15 μM LOD: 1.9 μM</p>	
<p>Nanozyme: Cu@C-500</p>	<p>Targets: Glucose Linear range: 50-350 μM LOD: 320 nM</p>	[158-159]
<p>Nanozyme: GOx@ZIF-8 (NiPd)</p>	<p>Targets: Glucose Linear range: 0.01-0.3 μM LOD: 9.2 μM</p>	

<p>Nanozyme: HAP@MIL-100(Fe)</p>	<p>Targets: Glucose Linear range: 2-50 μM LOD: -</p>	[154-155]
<p>Nanozyme: CoNPs/MC</p>	<p>Targets: Glucose Linear range: 0.25-30 μM LOD: 156 nM</p>	
<p>Nanozyme: GOx/hemin@ZIF-8</p>	<p>Targets: Glucose Linear range: 0-250 μM LOD: 1.7 μM</p>	[139-160]
<p>Nanozyme: MIL-53(Fe)</p>	<p>Targets: AA Linear range: 28.6-190 μM LOD: 15 μM</p>	
<p>Nanozyme: Fe-MIL-88A</p>	<p>Targets: AA Linear range: 2.57-10.1 μM LOD: 1.03 μM</p>	[141-161]
<p>Nanozyme: MIL-68(Fe)</p>	<p>Targets: AA Linear range: 30-485 μM LOD: 6 μM</p>	
<p>Nanozyme: MIL-100(Fe)</p>	<p>Targets: AA Linear range: 30-485 μM LOD: 6 μM</p>	[141-152]
<p>Nanozyme: CuNPs@C</p>	<p>Targets: AA Linear range: 0.01-1 μM LOD: 1.41 μM</p>	
<p>Nanozyme: HAP@MIL-100(Fe)</p>	<p>Targets: AA Linear range: 9.52-142.86 μM LOD: -</p>	[155-162]
<p>Nanozyme: Ce-MOF</p>	<p>Targets: Cys Linear range: 0-40 μM LOD: 0.135 μM</p>	

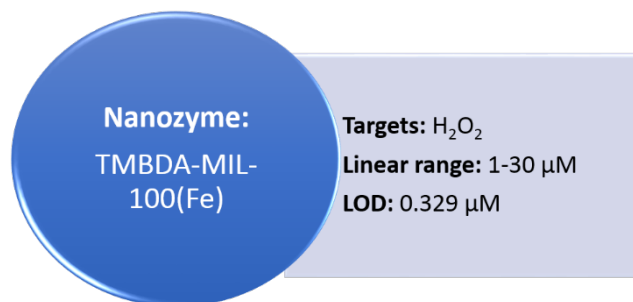
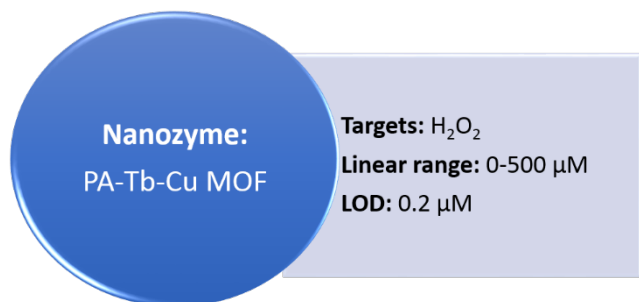
<p>Nanozyme: Ce-MOF</p>	<p>Targets: Cys Linear range: 0-1.0 μM LOD: 0.150 μM</p>	[163-164]
<p>Nanozyme: UIO-66(NH₂)</p>	<p>Targets: Cys Linear range: 5-120 μM LOD: 0.306 μM</p>	
<p>Nanozyme: Ce-MOF</p>	<p>Targets: GSH Linear range: 0-40 μM LOD: 0.129 μM</p>	[162-163]
<p>Nanozyme: Ce-MOF</p>	<p>Targets: GSH Linear range: 0-1.0 μM LOD: 0.132 μM</p>	
<p>Nanozyme: UIO-66(NH₂)</p>	<p>Targets: GSH Linear range: 5-120 μM LOD: 0.310 μM</p>	[164]
<p>Nanozyme: UIO-66(NH₂)</p>	<p>Targets: Hcy Linear range: 5-120 μM LOD: 0.330 μM</p>	
<p>Nanozyme: Ce-MOF</p>	<p>Targets: Hcy Linear range: 0-40 μM LOD: 0.143 μM</p>	[162-163]
<p>Nanozyme: Ce-MOF</p>	<p>Targets: Hcy Linear range: 0-1.0 μM LOD: 0.125 μM</p>	
<p>Nanozyme: Fe₃O₄@MIL-100(Fe)</p>	<p>Targets: Cholesterol Linear range: 2-50 μM LOD: 0.8 μM</p>	[147-165]
<p>Nanozyme: MIL-53(Fe)</p>	<p>Targets: Uric acid Linear range: 4.5-60 μM LOD: 1.3 μM</p>	

<p>Nanozyme: Fe-MIL-88NH₂</p>	<p>Targets: Dopamine Linear range: 0.05-30 μM LOD: 50 nM</p>	[166-167]
<p>Nanozyme: Cu/GMP MOF</p>	<p>Targets: Epinephrine Linear range: 5-50 mg/mL LOD: 0.41 mg/mL</p>	
<p>Nanozyme: BHb@ZIF-8</p>	<p>Targets: Phenol Linear range: 0-200 μM LOD: 1μM</p>	[150-168]
<p>Nanozyme: Pt NP@UiO-66-NH₂</p>	<p>Targets: Hg²⁺ Linear range: 0-10 nM LOD: 0.35 nM</p>	
<p>Nanozyme: PCuS</p>	<p>Targets: Hg²⁺ Linear range: 3.0-40 μM LOD: 0.22 μM</p>	[169-170]
<p>Nanozyme: Fe-MIL-101</p>	<p>Targets: Cancer cell Linear range: 50-500 cell LOD: 10 cell</p>	
<p>Nanozyme: Fe-MIL-88A</p>	<p>Targets: Thrombin Linear range: 10-80 nM LOD: 0.8 nM</p>	[171-172]
<p>Nanozyme: Cu-MOF</p>	<p>Targets: S. aureus Linear range: 50-10,000 CFU/mL LOD: 20 CFU/mL</p>	
<p>Nanozyme: Cu-MOF</p>	<p>Targets: ALP Linear range: 1-34 U/L LOD: 0.19 U/L</p>	[173-174]
<p>Nanozyme: Au@Fe-MIL-88(Fe)</p>	<p>Targets: HIV DNA Linear range: 30-150 nM LOD: 11.4 nM</p>	

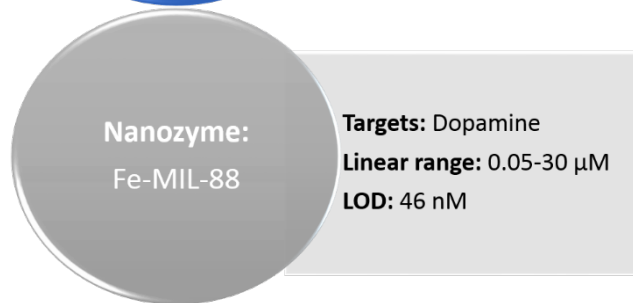
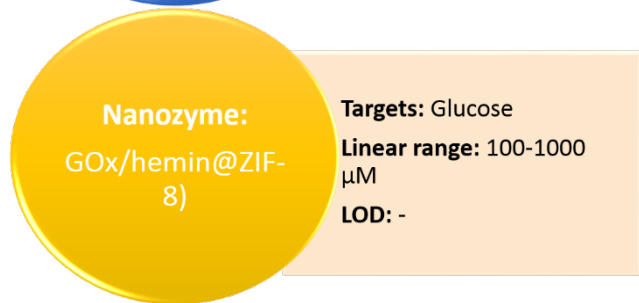


[148-175]

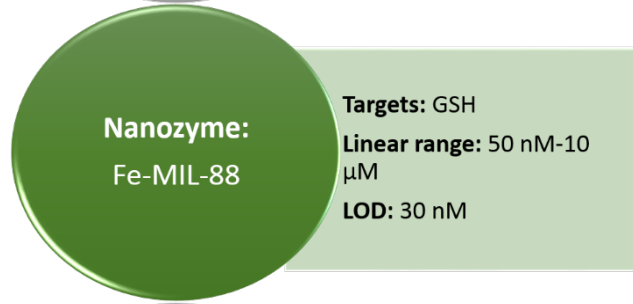
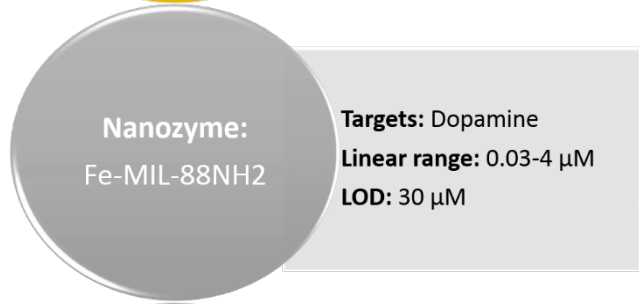
Applications for fluorescent sensing



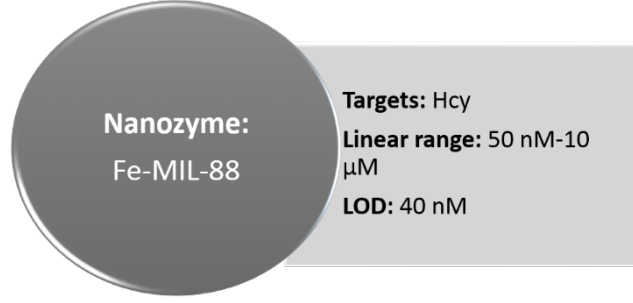
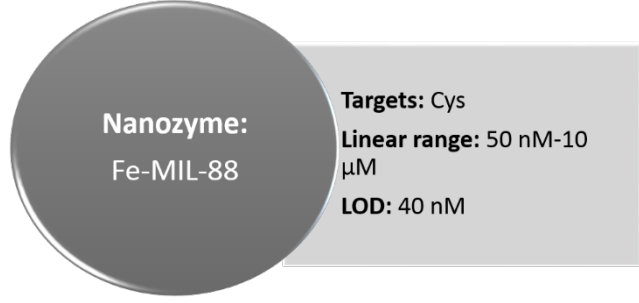
[176-177]



[160-178]



[166-179]



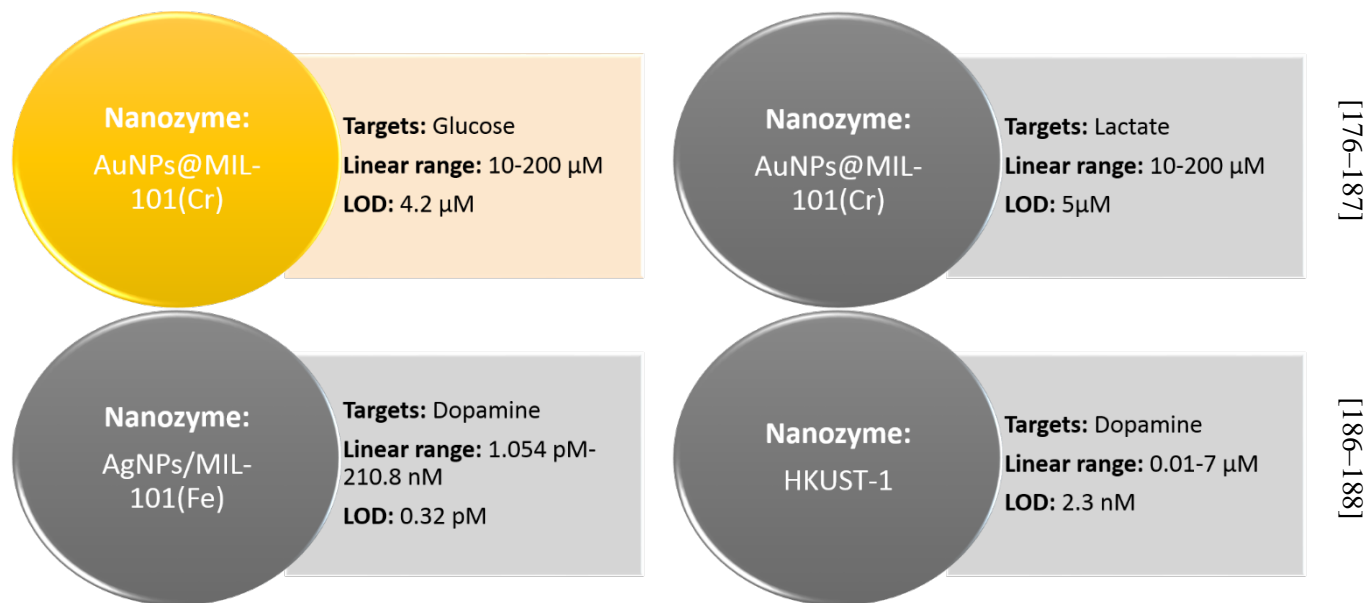
[179]

Nanozyme: HKUST-1	Targets: Thiamine Linear range: 4-700 μM LOD: 1 μM	Nanozyme: 2D Zn-TCPP(Fe)	Targets: Heparin Linear range: 0.1-10 mg/mL LOD: 15 ng/mL	[180-181]
-----------------------------	---	------------------------------------	--	-----------

Applications for chemiluminescent sensing

<div>Nanozyme: MIL-53(Fe)</div>	<div>Targets: H₂O₂ Linear range: 0.06-10 μM LOD: 0.02 μM</div>	<div>Nanozyme: Fe-MIL-88NH₂</div>	<div>Targets: H₂O₂ Linear range: 0.1-10 μM LOD: 0.025 μM</div>	[182-183]
<div>Nanozyme: Hemin@HKUST-1</div>	<div>Targets: H₂O₂ Linear range: 5-1000 μM LOD: 2μM</div>	<div>Nanozyme: Fe₃O₄/MIL-101(Fe)</div>	<div>Targets: H₂O₂ Linear range: 5-150 nM LOD: 3.7 nM</div>	[184-185]
<div>Nanozyme: MIL-53(Fe)</div>	<div>Targets: Glucose Linear range: 0.1-10 μM LOD: 0.05 μM</div>	<div>Nanozyme: Hemin@HKUST-1</div>	<div>Targets: Glucose Linear range: 7.5-70 μM LOD: 7μM</div>	[182-184]
<div>Nanozyme: TMBDA-MIL-100(Fe)</div>	<div>Targets: Acetylcholine Linear range: 0.1-10 μM LOD: 0.036 μM</div>	<div>Nanozyme: Fe₃O₄/MIL-101(Fe)</div>	<div>Targets: Glucose Linear range: 5-100 nM LOD: 4.9 nM</div>	[185-186]

Applications for SERS sensing



Conclusions and recommendations

Recently, research into MOFs has proven that MOFs are a good carrier for biomedical applications and especially for drug delivery. However, the use of MOFs in industrial production is still a major source of concern. This is due to the cost of production of MOFs, biocompatibility, biodegradability, and solvent-related toxicity. In addition to this, more comprehensive and detailed researches should be done through in vitro cell lines and other molecular biology studies, animal models and clinical studies for the use of MOFs in biological systems.

As a result, MOFs, which have a large surface area in therapeutic applications as in all areas, are used as catalysts in various reactions due to their small pores of less than 1 nm. MOFs were found to be more efficient and advantageous than micro-porous heterogeneous catalysts such as zeolites. The biggest reason for this is the large surface area of the MOF nanoparticles. The high metal content of the MOFs used in nanoreactors and their wide porous structure are met by the shape and selectivity of the catalysts. The metal ion set for the therapeutic applications in the examples given shows a stable catalytic activity with the binder of MOF. The organic binders of some MOFs may not benefit because they are not fully compatible with metals. However, by adjusting the pore volumes according to the reactions to be used, catalytic activity can be imparted. The size, shape and selective catalytic activity of MOFs whose pores can be adjusted according to the reaction to be used in theory depends on the presence of active transition metal centers.

References

1. B. Şen, A. Aygün, T. O. Okyay, A. Şavk, R. Kartop, & F. Şen, Monodisperse Palladium Nanoparticles Assembled on Graphene Oxide with The High Catalytic Activity and Reusability in The Dehydrogenation of Dimethylamine-borane. *International Journal of Hydrogen Energy*, **43** (2018) 20176–20182. <https://doi.org/10.1016/j.ijhydene.2018.03.175>.
2. J. Tian, J. Xu, F. Zhu, T. Lu, C. Su, & G. Ouyang, Application of nanomaterials in sample preparation. *Journal of Chromatography A*, **1300** (2013) 2–16. <https://doi.org/10.1016/J.CHROMA.2013.04.010>.
3. S. Ertan, F. Şen, S. Şen, & G. Gökağaç, Platinum nanocatalysts prepared with different surfactants for C1–C3 alcohol oxidations and their surface morphologies by AFM. *Journal of Nanoparticle Research*, **14** (2012) 922–934. <https://doi.org/10.1007/s11051-012-0922-5>.
4. B. Sen, A. Şavk, & F. Sen, Highly Efficient Monodisperse Pt Nanoparticles Confined in The Carbon Black Hybrid Material for Hydrogen Liberation. *Journal of Colloid and Interface Science*, **520** (2018) 112–118. <https://doi.org/10.1016/j.jcis.2018.03.004>.
5. R. Ayranci, G. Başkaya, M. Güzel, S. Bozkurt, F. Şen, & M. Ak, Carbon Based Nanomaterials for High Performance Optoelectrochemical Systems. *ChemistrySelect*, **2** (2017) 1548–1555. <https://doi.org/10.1002/slct.201601632>.
6. S. Akocak, B. Şen, N. Lolak, A. Şavk, M. Koca, S. Kuzu, & F. Şen, One-Pot Three-Component Synthesis of 2-Amino-4H-Chromene Derivatives by Using Monodisperse Pd Nanomaterials Anchored Graphene Oxide as Highly Efficient and Recyclable Catalyst. *Nano-Structures & Nano-Objects*, **11** (2017) 25–31. <https://doi.org/10.1016/j.nanoso.2017.06.002>.
7. Y. Yıldız, S. Kuzu, B. Sen, A. Savk, S. Akocak, & F. Şen, Different Ligand Based Monodispersed Pt Nanoparticles Decorated with rGO As Highly Active and Reusable Catalysts for The Methanol Oxidation. *International Journal of Hydrogen Energy*, **42** (2017) 13061–13069. <https://doi.org/10.1016/j.ijhydene.2017.03.230>.
8. Y. Liu, Z. U. Wang, & H.-C. Zhou, Recent advances in carbon dioxide capture with metal-organic frameworks. *Greenhouse Gases: Science and Technology*, **2** (2012) 239–259. <https://doi.org/10.1002/ghg.1296>.
9. S. H. Jung, J. Lee, & J.-S. Chang, Microwave synthesis of a nanoporous hybrid material, MIL-100(Cr). *Bulletin of the Korean Chemical Society*, **26** (2005) 880–881. <https://doi.org/10.5012/bkcs.2005.26.6.880>.

10. Z. N. and & R. I. Masei*, Rapid Production of Metal–Organic Frameworks via Microwave-Assisted Solvothermal Synthesis. (2006).
<https://doi.org/10.1021/JA0635231>.
11. J.-S. Choi, W.-J. Son, J. Kim, & W.-S. Ahn, Metal–organic framework MOF-5 prepared by microwave heating: Factors to be considered. *Microporous and Mesoporous Materials*, **116** (2008) 727–731.
<https://doi.org/10.1016/J.MICROMESO.2008.04.033>.
12. A. Carné-Sánchez, I. Imaz, M. Cano-Sarabia, & D. Maspoch, A spray-drying strategy for synthesis of nanoscale metal–organic frameworks and their assembly into hollow superstructures. *Nature Chemistry*, **5** (2013) 203–211.
<https://doi.org/10.1038/nchem.1569>.
13. M. Faustini, J. Kim, G.-Y. Jeong, J. Y. Kim, H. R. Moon, W.-S. Ahn, & D.-P. Kim, Microfluidic Approach toward Continuous and Ultrafast Synthesis of Metal–Organic Framework Crystals and Hetero Structures in Confined Microdroplets. *Journal of the American Chemical Society*, **135** (2013) 14619–14626.
<https://doi.org/10.1021/ja4039642>.
14. C. M. Doherty, D. Buso, A. J. Hill, S. Furukawa, S. Kitagawa, & P. Falcaro, Using Functional Nano- and Microparticles for the Preparation of Metal–Organic Framework Composites with Novel Properties. *Accounts of Chemical Research*, **47** (2014) 396–405. <https://doi.org/10.1021/ar400130a>.
15. W. Shang, X. Kang, H. Ning, J. Zhang, X. Zhang, Z. Wu, G. Mo, X. Xing, & B. Han, Shape and Size Controlled Synthesis of MOF Nanocrystals with the Assistance of Ionic Liquid Microemulsions. *Langmuir*, **29** (2013) 13168–13174.
<https://doi.org/10.1021/la402882a>.
16. F. LLABRESIXAMENA, O. CASANOVA, R. GALIASSOTAILLEUR, H. GARCIA, & A. CORMA, Metal organic frameworks (MOFs) as catalysts: A combination of Cu²⁺ and Co²⁺ MOFs as an efficient catalyst for tetralin oxidation. *Journal of Catalysis*, **255** (2008) 220–227. <https://doi.org/10.1016/j.jcat.2008.02.011>.
17. K. A. Mocniak, I. Kubajewska, D. E. M. Spillane, G. R. Williams, & R. E. Morris, Incorporation of cisplatin into the metal–organic frameworks UiO66-NH₂ and UiO66 – encapsulation vs. conjugation. *RSC Advances*, **5** (2015) 83648–83656.
<https://doi.org/10.1039/C5RA14011K>.
18. N. Stock & S. Biswas, Synthesis of Metal-Organic Frameworks (MOFs): Routes to Various MOF Topologies, Morphologies, and Composites. *Chemical Reviews*, **112** (2012) 933–969. <https://doi.org/10.1021/cr200304e>.

19. B. Gomez-Lor, E. Gutiérrez-Puebla, M. Iglesias, * M. A. Monge, and C. Ruiz-Valero, & N. Snežko, In₂(OH)₃(BDC)1.5 (BDC = 1,4-Benzendicarboxylate): An In(III) Supramolecular 3D Framework with Catalytic Activity. (2002). <https://doi.org/10.1021/IC0111482>.
20. A. K. Cheetham, C. N. R. Rao, & R. K. Feller, Structural diversity and chemical trends in hybrid inorganic–organic framework materials. *Chem. Commun.*, **0** (2006) 4780–4795. <https://doi.org/10.1039/B610264F>.
21. P. Pachfule, R. Das, P. Poddar, & R. Banerjee, Solvothermal Synthesis, Structure, and Properties of Metal Organic Framework Isomers Derived from a Partially Fluorinated Link. *Crystal Growth & Design*, **11** (2011) 1215–1222. <https://doi.org/10.1021/cg101414x>.
22. J. Kim, B. Chen, T. M. Reineke, H. Li, M. Eddaoudi, D. B. Moler, M. O’Keeffe, & O. M. Yaghi, Assembly of metal-organic frameworks from large organic and inorganic secondary building units: New examples and simplifying principles for complex structures. *Journal of the American Chemical Society*, **123** (2001) 8239–8247. <https://doi.org/10.1021/ja010825o>.
23. R. J. Kuppler, D. J. Timmons, Q.-R. Fang, J.-R. Li, T. A. Makal, M. D. Young, D. Yuan, D. Zhao, W. Zhuang, & H.-C. Zhou, Potential applications of metal-organic frameworks. *Coordination Chemistry Reviews*, **253** (2009) 3042–3066. <https://doi.org/10.1016/J.CCR.2009.05.019>.
24. M. Zhang, W. Lu, J.-R. Li, M. Bosch, Y.-P. Chen, T.-F. Liu, Y. Liu, & H.-C. Zhou, Design and synthesis of nucleobase-incorporated metal–organic materials. *Inorganic Chemistry Frontiers*, **1** (2014) 159. <https://doi.org/10.1039/c3qi00042g>.
25. H.-R. Fu & J. Zhang, Flexible Porous Zinc–Pyrazole–Adenine Framework for Hysteretic Sorption of Light Hydrocarbons. *Crystal Growth & Design*, **15** (2015) 1210–1213. <https://doi.org/10.1021/cg5016093>.
26. Y.-P. He, N. Zhou, Y.-X. Tan, F. Wang, & J. Zhang, Synthesis of metal-adeninate frameworks with high separation capacity on C₂/C₁ hydrocarbons. *Journal of Solid State Chemistry*, **238** (2016) 241–245. <https://doi.org/10.1016/J.JSSC.2016.03.043>.
27. M.-Y. Li, F. Wang, Z.-G. Gu, & J. Zhang, Synthesis of homochiral zeolitic metal–organic frameworks with amino acid and tetrazolates for chiral recognition. *RSC Advances*, **7** (2017) 4872–4875. <https://doi.org/10.1039/C6RA27069G>.
28. J. Navarro-Sánchez, A. I. Argente-García, Y. Moliner-Martínez, D. Roca-Sanjuán, D. Antypov, P. Campíns-Falcó, M. J. Rosseinsky, & C. Martí-Gastaldo, Peptide

- Metal–Organic Frameworks for Enantioselective Separation of Chiral Drugs. *Journal of the American Chemical Society*, **139** (2017) 4294–4297.
<https://doi.org/10.1021/jacs.7b00280>.
29. XianLi An & XiGeng Zheng, Post-training corticosterone opposingly modulates fear conditioning of high and low anxiety rats. *Proc. 2012 IEEE-EMBS Int. Conf. Biomed. Heal. Informatics* (IEEE, 2012), pp. 604–607.
<https://doi.org/10.1109/BHI.2012.6211655>.
30. H. Cai, M. Li, X.-R. Lin, W. Chen, G.-H. Chen, X.-C. Huang, & D. Li, Spatial, Hysteretic, and Adaptive Host-Guest Chemistry in a Metal-Organic Framework with Open Watson-Crick Sites. *Angewandte Chemie International Edition*, **54** (2015) 10454–10459. <https://doi.org/10.1002/anie.201502045>.
31. R. W. Sun, M. Zhang, D. Li, Z. Zhang, H. Cai, M. Li, Y. Xian, S. W. Ng, & A. S. Wong, Dinuclear Gold(I) Pyrrolidinedithiocarbamate Complex: Cytotoxic and Antimigratory Activities on Cancer Cells and the Use of Metal–Organic Framework. *Chemistry – A European Journal*, **21** (2015) 18534–18538.
<https://doi.org/10.1002/CHEM.201503656>.
32. H. Cai, L.-L. Xu, H.-Y. Lai, J.-Y. Liu, S. W. Ng, & D. Li, A highly emissive and stable zinc(ii) metal–organic framework as a host–guest chemopalette for approaching white-light-emission. *Chemical Communications*, **53** (2017) 7917–7920.
<https://doi.org/10.1039/C7CC03350H>.
33. J. Du, C.-H. Yuen, X. Li, K. Ding, G. Du, Z. Lin, C. T. Chan, & J. Ng, Tailoring Optical Gradient Force and Optical Scattering and Absorption Force. *Scientific reports*, **7** (2017) 18042. <https://doi.org/10.1038/s41598-017-17874-1>.
34. K. J. Hartlieb, J. M. Holcroft, P. Z. Moghadam, N. A. Vermeulen, M. M. Algaradah, M. S. Nassar, Y. Y. Botros, R. Q. Snurr, & J. F. Stoddart, CD-MOF: A Versatile Separation Medium. *Journal of the American Chemical Society*, **138** (2016) 2292–2301. <https://doi.org/10.1021/jacs.5b12860>.
35. M. Zhao & C.-D. Wu, Biomimetic Activation of Molecular Oxygen with a Combined Metalloporphyrinic Framework and Co-catalyst Platform. *ChemCatChem*, **9** (2017) 1192–1196. <https://doi.org/10.1002/cctc.201601606>.
36. J. Yang, C. A. Trickett, S. B. Alahmadi, A. S. Alshammari, & O. M. Yaghi, Calcium I -Lactate Frameworks as Naturally Degradable Carriers for Pesticides. *Journal of the American Chemical Society*, **139** (2017) 8118–8121.
<https://doi.org/10.1021/jacs.7b04542>.

37. P. A. Sontz, J. B. Bailey, S. Ahn, & F. A. Tezcan, A Metal Organic Framework with Spherical Protein Nodes: Rational Chemical Design of 3D Protein Crystals. *Journal of the American Chemical Society*, **137** (2015) 11598–11601. <https://doi.org/10.1021/jacs.5b07463>.
38. J. B. Bailey, L. Zhang, J. A. Chiong, S. Ahn, & F. A. Tezcan, Synthetic Modularity of Protein–Metal–Organic Frameworks. *Journal of the American Chemical Society*, **139** (2017) 8160–8166. <https://doi.org/10.1021/jacs.7b01202>.
39. X.-L. Yang & C.-D. Wu, Metalloporphyrinic Framework Containing Multiple Pores for Highly Efficient and Selective Epoxidation. *Inorganic Chemistry*, **53** (2014) 4797–4799. <https://doi.org/10.1021/ic500531k>.
40. M. Hamidi, K. Rostamizadeh, & M. A. Shahbazi, Hydrogel Nanoparticles in Drug Delivery. *Intelligent Nanomaterials: Processes, Properties, and Applications*, **60** (2012) 583–624. <https://doi.org/10.1002/9781118311974.ch15>.
41. J. R. Heath & M. E. Davis, Nanotechnology and Cancer. *Annual Review of Medicine*, **59** (2008) 251–265. <https://doi.org/10.1146/annurev.med.59.061506.185523>.
42. Z. Zhang, L. Wang, J. Wang, X. Jiang, X. Li, Z. Hu, Y. Ji, X. Wu, & C. Chen, Mesoporous Silica-Coated Gold Nanorods as a Light-Mediated Multifunctional Theranostic Platform for Cancer Treatment. *Advanced Materials*, **24** (2012) 1418–1423. <https://doi.org/10.1002/adma.201104714>.
43. F. Ke, Y.-P. Yuan, L.-G. Qiu, Y.-H. Shen, A.-J. Xie, J.-F. Zhu, X.-Y. Tian, & L.-D. Zhang, Facile fabrication of magnetic metal–organic framework nanocomposites for potential targeted drug delivery. *Journal of Materials Chemistry*, **21** (2011) 3843. <https://doi.org/10.1039/c0jm01770a>.
44. P. Horcajada, C. Serre, M. Vallet-Regí, M. Sebban, F. Taulelle, & G. Férey, Metal–Organic Frameworks as Efficient Materials for Drug Delivery. *Angewandte Chemie International Edition*, **45** (2006) 5974–5978. <https://doi.org/10.1002/anie.200601878>.
45. D. Cunha, M. Ben Yahia, S. Hall, S. R. Miller, H. Chevreau, E. Elkaïm, G. Maurin, P. Horcajada, & C. Serre, Rationale of Drug Encapsulation and Release from Biocompatible Porous Metal–Organic Frameworks. *Chemistry of Materials*, **25** (2013) 2767–2776. <https://doi.org/10.1021/cm400798p>.
46. M. C. Das, Q. Guo, Y. He, J. Kim, C.-G. Zhao, K. Hong, S. Xiang, Z. Zhang, K. M. Thomas, R. Krishna, & B. Chen, Interplay of Metalloligand and Organic Ligand to

- Tune Micropores within Isostructural Mixed-Metal Organic Frameworks (M'MOFs) for Their Highly Selective Separation of Chiral and Achiral Small Molecules. *Journal of the American Chemical Society*, **134** (2012) 8703–8710. <https://doi.org/10.1021/ja302380x>.
47. C. Adhikari & A. Chakraborty, Smart Approach for In Situ One-Step Encapsulation and Controlled Delivery of a Chemotherapeutic Drug using Metal-Organic Framework-Drug Composites in Aqueous Media. *ChemPhysChem*, **17** (2016) 1070–1077. <https://doi.org/10.1002/cphc.201501012>.
48. V. Rodriguez-Ruiz, A. Maksimenko, R. Anand, S. Monti, V. Agostoni, P. Couvreur, M. Lampropoulou, K. Yannakopoulou, & R. Gref, Efficient “green” encapsulation of a highly hydrophilic anticancer drug in metal–organic framework nanoparticles. *Journal of Drug Targeting*, **23** (2015) 759–767. <https://doi.org/10.3109/1061186X.2015.1073294>.
49. P. Horcajada, T. Chalati, C. Serre, B. Gillet, C. Sebrie, T. Baati, J. F. Eubank, D. Heurtaux, P. Clayette, C. Kreuz, J.-S. Chang, Y. K. Hwang, V. Marsaud, P.-N. Bories, L. Cynober, S. Gil, G. Férey, P. Couvreur, & R. Gref, Porous metal–organic-framework nanoscale carriers as a potential platform for drug delivery and imaging. *Nature Materials*, **9** (2010) 172–178. <https://doi.org/10.1038/nmat2608>.
50. W. Wang, L. Wang, Z. Li, & Z. Xie, BODIPY-containing nanoscale metal–organic frameworks for photodynamic therapy. *Chemical Communications*, **52** (2016) 5402–5405. <https://doi.org/10.1039/C6CC01048B>.
51. S. Keskin & S. Kızılel, Biomedical Applications of Metal Organic Frameworks. *Industrial & Engineering Chemistry Research*, **50** (2011) 1799–1812. <https://doi.org/10.1021/ie101312k>.
52. R. M. P. Colodrero, K. E. Papathanasiou, N. Stavgianoudaki, P. Olivera-Pastor, E. R. Losilla, M. A. G. Aranda, L. León-Reina, J. Sanz, I. Sobrados, D. Choquesillo-Lazarte, J. M. García-Ruiz, P. Atienzar, F. Rey, K. D. Demadis, & A. Cabeza, Multifunctional Luminescent and Proton-Conducting Lanthanide Carboxyphosphonate Open-Framework Hybrids Exhibiting Crystalline-to-Amorphous-to-Crystalline Transformations. *Chemistry of Materials*, **24** (2012) 3780–3792. <https://doi.org/10.1021/cm302381k>.
53. K. M. L. Taylor-Pashow, J. Della Rocca, Z. Xie, S. Tran, & W. Lin, Postsynthetic Modifications of Iron-Carboxylate Nanoscale Metal–Organic Frameworks for Imaging and Drug Delivery. *Journal of the American Chemical Society*, **131** (2009) 14261–14263. <https://doi.org/10.1021/ja906198y>.

54. J. Kirsch, C. Siltanen, Q. Zhou, A. Revzin, & A. Simonian, Biosensor technology: recent advances in threat agent detection and medicine. *Chemical Society Reviews*, **42** (2013) 8733. <https://doi.org/10.1039/c3cs60141b>.
55. I. Imaz, M. Rubio-Martínez, L. García-Fernández, F. García, D. Ruiz-Molina, J. Hernando, V. Puentes, & D. Maspoch, Coordination polymer particles as potential drug delivery systems. *Chemical Communications*, **46** (2010) 4737. <https://doi.org/10.1039/c003084h>.
56. H.-N. Wang, X. Meng, G.-S. Yang, X.-L. Wang, K.-Z. Shao, Z.-M. Su, & C.-G. Wang, Stepwise assembly of metal–organic framework based on a metal–organic polyhedron precursor for drug delivery. *Chemical Communications*, **47** (2011) 7128. <https://doi.org/10.1039/c1cc11932j>.
57. F. R. S. Lucena, L. C. C. de Araújo, M. do D. Rodrigues, T. G. da Silva, V. R. A. Pereira, G. C. G. Militão, D. A. F. Fontes, P. J. Rolim-Neto, F. F. da Silva, & S. C. Nascimento, Induction of cancer cell death by apoptosis and slow release of 5-fluoracil from metal-organic frameworks Cu-BTC. *Biomedicine & Pharmacotherapy*, **67** (2013) 707–713. <https://doi.org/10.1016/J.BIOPHA.2013.06.003>.
58. M. Filippousi, S. Turner, K. Leus, P. I. Siafaka, E. D. Tseligka, M. Vandichel, S. G. Nanaki, I. S. Vizirianakis, D. N. Bikiaris, P. Van Der Voort, & G. Van Tendeloo, Biocompatible Zr-based nanoscale MOFs coated with modified poly(ϵ -caprolactone) as anticancer drug carriers. *International Journal of Pharmaceutics*, **509** (2016) 208–218. <https://doi.org/10.1016/J.IJPHARM.2016.05.048>.
59. K. E. deKrafft, W. S. Boyle, L. M. Burk, O. Z. Zhou, & W. Lin, Zr- and Hf-based nanoscale metal–organic frameworks as contrast agents for computed tomography. *Journal of Materials Chemistry*, **22** (2012) 18139. <https://doi.org/10.1039/c2jm32299d>.
60. M. Nazari, M. Rubio-Martinez, G. Tobias, J. P. Barrio, R. Babarao, F. Nazari, K. Konstas, B. W. Muir, S. F. Collins, A. J. Hill, M. C. Duke, & M. R. Hill, Metal-Organic-Framework-Coated Optical Fibers as Light-Triggered Drug Delivery Vehicles. *Advanced Functional Materials*, **26** (2016) 3244–3249. <https://doi.org/10.1002/adfm.201505260>.
61. H. Zheng, Y. Zhang, L. Liu, W. Wan, P. Guo, A. M. Nyström, & X. Zou, One-pot Synthesis of Metal–Organic Frameworks with Encapsulated Target Molecules and Their Applications for Controlled Drug Delivery. *Journal of the American Chemical Society*, **138** (2016) 962–968. <https://doi.org/10.1021/jacs.5b11720>.

62. C.-Y. Sun, C. Qin, X.-L. Wang, G.-S. Yang, K.-Z. Shao, Y.-Q. Lan, Z.-M. Su, P. Huang, C.-G. Wang, & E.-B. Wang, Zeolitic imidazolate framework-8 as efficient pH-sensitive drug delivery vehicle. *Dalton Transactions*, **41** (2012) 6906. <https://doi.org/10.1039/c2dt30357d>.
63. C. Wang, D. Liu, & W. Lin, Metal–Organic Frameworks as A Tunable Platform for Designing Functional Molecular Materials. *Journal of the American Chemical Society*, **135** (2013) 13222–13234. <https://doi.org/10.1021/ja308229p>.
64. W. J. Rieter, K. M. L. Taylor, H. An, W. Lin, & W. Lin, Nanoscale Metal–Organic Frameworks as Potential Multimodal Contrast Enhancing Agents. *Journal of the American Chemical Society*, **128** (2006) 9024–9025. <https://doi.org/10.1021/ja0627444>.
65. R. C. Huxford, J. Della Rocca, & W. Lin, Metal–organic frameworks as potential drug carriers. *Current Opinion in Chemical Biology*, **14** (2010) 262–268. <https://doi.org/10.1016/J.CBPA.2009.12.012>.
66. X. Zhu, J. Gu, Y. Wang, B. Li, Y. Li, W. Zhao, & J. Shi, Inherent anchorages in UiO-66 nanoparticles for efficient capture of alendronate and its mediated release. *Chem. Commun.*, **50** (2014) 8779–8782. <https://doi.org/10.1039/C4CC02570A>.
67. T. Baati, P. Horcajada, R. Gref, P. Couvreur, & C. Serre, Quantification of fumaric acid in liver, spleen and urine by high-performance liquid chromatography coupled to photodiode-array detection. *Journal of Pharmaceutical and Biomedical Analysis*, **56** (2011) 758–762. <https://doi.org/10.1016/J.JPBA.2011.07.011>.
68. R. E. Morris & P. S. Wheatley, Gas Storage in Nanoporous Materials. *Angewandte Chemie International Edition*, **47** (2008) 4966–4981. <https://doi.org/10.1002/anie.200703934>.
69. V. Agostoni, T. Chalati, P. Horcajada, H. Willaime, R. Anand, N. Semiramo, T. Baati, S. Hall, G. Maurin, H. Chacun, K. Bouchemal, C. Martineau, F. Taulelle, P. Couvreur, C. Rogez-Kreuz, P. Clayette, S. Monti, C. Serre, & R. Gref, Towards an Improved anti-HIV Activity of NRTI via Metal-Organic Frameworks Nanoparticles. *Advanced Healthcare Materials*, **2** (2013) 1630–1637. <https://doi.org/10.1002/adhm.201200454>.
70. W. Lin, W. J. Rieter, & K. M. L. Taylor, Modular Synthesis of Functional Nanoscale Coordination Polymers. *Angewandte Chemie International Edition*, **48** (2009) 650–658. <https://doi.org/10.1002/anie.200803387>.

71. K. Deng, Z. Hou, X. Li, C. Li, Y. Zhang, X. Deng, Z. Cheng, & J. Lin, Aptamer-mediated up-conversion core/MOF shell nanocomposites for targeted drug delivery and cell imaging. *Scientific reports*, **5** (2015) 7851. <https://doi.org/10.1038/srep07851>.
72. P. F. Gao, L. L. Zheng, L. J. Liang, X. X. Yang, Y. F. Li, & C. Z. Huang, A new type of pH-responsive coordination polymer sphere as a vehicle for targeted anticancer drug delivery and sustained release. *Journal of Materials Chemistry B*, **1** (2013) 3202. <https://doi.org/10.1039/c3tb00026e>.
73. B. S. Luisi, K. D. Rowland, & B. Moulton, Coordination polymer gels: synthesis, structure and mechanical properties of amorphous coordination polymers. *Chemical Communications*, **0** (2007) 2802. <https://doi.org/10.1039/b703768f>.
74. W. Yuan, A. L. Garay, A. Pichon, R. Clowes, C. D. Wood, A. I. Cooper, & S. L. James, Study of the mechanochemical formation and resulting properties of an archetypal MOF: Cu₃(BTC)₂ (BTC = 1,3,5-benzenetricarboxylate). *CrystEngComm*, **12** (2010) 4063. <https://doi.org/10.1039/c0ce00486c>.
75. W. J. Rieter, K. M. Pott, K. M. L. Taylor, & W. Lin, Nanoscale Coordination Polymers for Platinum-Based Anticancer Drug Delivery. *Journal of the American Chemical Society*, **130** (2008) 11584–11585. <https://doi.org/10.1021/ja803383k>.
76. H. Ren, L. Zhang, J. An, T. Wang, L. Li, X. Si, L. He, X. Wu, C. Wang, & Z. Su, Polyacrylic acid@zeolitic imidazolate framework-8 nanoparticles with ultrahigh drug loading capability for pH-sensitive drug release. *Chem. Commun.*, **50** (2014) 1000–1002. <https://doi.org/10.1039/C3CC47666A>.
77. I. Abánades Lázaro & R. S. Forgan, Application of zirconium MOFs in drug delivery and biomedicine. *Coordination Chemistry Reviews*, **380** (2019) 230–259. <https://doi.org/10.1016/J.CCR.2018.09.009>.
78. G. Choi, T.-H. Kim, J.-M. Oh, & J.-H. Choy, Emerging nanomaterials with advanced drug delivery functions; focused on methotrexate delivery. *Coordination Chemistry Reviews*, **359** (2018) 32–51. <https://doi.org/10.1016/J.CCR.2018.01.007>.
79. N. J. Hinks, A. C. McKinlay, B. Xiao, P. S. Wheatley, & R. E. Morris, Metal organic frameworks as NO delivery materials for biological applications. *Microporous and Mesoporous Materials*, **129** (2010) 330–334. <https://doi.org/10.1016/J.MICROMESO.2009.04.031>.
80. S. R. Miller, D. Heurtaux, T. Baati, P. Horcajada, J.-M. Grenèche, & C. Serre, Biodegradable therapeutic MOFs for the delivery of bioactive molecules. *Chemical Communications*, **46** (2010) 4526. <https://doi.org/10.1039/c001181a>.

81. X. Lu, J. Ye, D. Zhang, R. Xie, R. F. Bogale, Y. Sun, L. Zhao, Q. Zhao, & G. Ning, Silver carboxylate metal–organic frameworks with highly antibacterial activity and biocompatibility. *Journal of Inorganic Biochemistry*, **138** (2014) 114–121. <https://doi.org/10.1016/J.JINORGBIO.2014.05.005>.
82. W. Zhuang, D. Yuan, J.-R. Li, Z. Luo, H.-C. Zhou, S. Bashir, & J. Liu, Highly Potent Bactericidal Activity of Porous Metal-Organic Frameworks. *Advanced Healthcare Materials*, **1** (2012) 225–238. <https://doi.org/10.1002/adhm.201100043>.
83. C. Tamames-Tabar, D. Cunha, E. Imbuluzqueta, F. Ragon, C. Serre, M. J. Blanco-Prieto, & P. Horcajada, Cytotoxicity of nanoscaled metal–organic frameworks. *J. Mater. Chem. B*, **2** (2014) 262–271. <https://doi.org/10.1039/C3TB20832J>.
84. M. Berchel, T. Le Gall, C. Denis, S. Le Hir, F. Quentel, C. Elléouet, T. Montier, J.-M. Rueff, J.-Y. Salaün, J.-P. Haelters, G. B. Hix, P. Lehn, & P.-A. Jaffrès, A silver-based metal–organic framework material as a ‘reservoir’ of bactericidal metal ions. *New Journal of Chemistry*, **35** (2011) 1000. <https://doi.org/10.1039/c1nj20202b>.
85. S. Aguado, J. Quirós, J. Canivet, D. Farrusseng, K. Boltes, & R. Rosal, Antimicrobial activity of cobalt imidazolate metal–organic frameworks. *Chemosphere*, **113** (2014) 188–192. <https://doi.org/10.1016/J.CHEMOSPHERE.2014.05.029>.
86. Y. Liu, X. Xu, Q. Xia, G. Yuan, Q. He, & Y. Cui, Multiple topological isomerism of three-connected networks in silver-based metal–organoboron frameworks. *Chemical Communications*, **46** (2010) 2608. <https://doi.org/10.1039/b923365b>.
87. C. Chiericatti, J. C. Basilico, M. L. Zapata Basilico, & J. M. Zamaro, Novel application of HKUST-1 metal–organic framework as antifungal: Biological tests and physicochemical characterizations. *Microporous and Mesoporous Materials*, **162** (2012) 60–63. <https://doi.org/10.1016/J.MICROMESO.2012.06.012>.
88. Y.-C. Wang, H. Zhao, Q. Ye, Z.-F. Chen, R.-G. Xiong, & H.-K. Fun, Novel 2D supramolecular array based on antibacterial drug norfloxacin. *Inorganica Chimica Acta*, **357** (2004) 4303–4308. <https://doi.org/10.1016/J.ICA.2004.05.036>.
89. A. R. Abbasi, K. Akhbari, & A. Morsali, Dense coating of surface mounted CuBTC Metal–Organic Framework nanostructures on silk fibers, prepared by layer-by-layer method under ultrasound irradiation with antibacterial activity. *Ultrasonics Sonochemistry*, **19** (2012) 846–852. <https://doi.org/10.1016/J.ULTSONCH.2011.11.016>.
90. H. S. Rodríguez, J. P. Hinestroza, C. Ochoa-Puentes, C. A. Sierra, & C. Y. Soto, Antibacterial activity against *Escherichia coli* of Cu-BTC (MOF-199) metal-organic

- framework immobilized onto cellulosic fibers. *Journal of Applied Polymer Science*, **131** (2014) n/a-n/a. <https://doi.org/10.1002/app.40815>.
91. F. N. Azad, M. Ghaedi, K. Dashtian, S. Hajati, & V. Pezeshkpour, Ultrasonically assisted hydrothermal synthesis of activated carbon–HKUST-1-MOF hybrid for efficient simultaneous ultrasound-assisted removal of ternary organic dyes and antibacterial investigation: Taguchi optimization. *Ultrasonics Sonochemistry*, **31** (2016) 383–393. <https://doi.org/10.1016/J.ULTSONCH.2016.01.024>.
92. E. Lashkari, H. Wang, L. Liu, J. Li, & K. Yam, Innovative application of metal-organic frameworks for encapsulation and controlled release of allyl isothiocyanate. *Food Chemistry*, **221** (2017) 926–935. <https://doi.org/10.1016/J.FOODCHEM.2016.11.072>.
93. F. Pu, X. Liu, B. Xu, J. Ren, & X. Qu, Miniaturization of Metal-Biomolecule Frameworks Based on Stereoselective Self-Assembly and Potential Application in Water Treatment and as Antibacterial Agents. *Chemistry - A European Journal*, **18** (2012) 4322–4328. <https://doi.org/10.1002/chem.201103524>.
94. M. P. Arpa Sancet, M. Hanke, Z. Wang, S. Bauer, C. Azucena, H. K. Arslan, M. Heinle, H. Gliemann, C. Wöll, & A. Rosenhahn, Surface anchored metal-organic frameworks as stimulus responsive antifouling coatings. *Biointerphases*, **8** (2013) 29. <https://doi.org/10.1186/1559-4106-8-29>.
95. M. Hanke, H. K. Arslan, S. Bauer, O. Zybaylo, C. Christophis, H. Gliemann, A. Rosenhahn, & C. Wöll, The Biocompatibility of Metal–Organic Framework Coatings: An Investigation on the Stability of SURMOFs with Regard to Water and Selected Cell Culture Media. *Langmuir*, **28** (2012) 6877–6884. <https://doi.org/10.1021/la300457z>.
96. A. Wojciechowska, A. Gągor, W. Zierkiewicz, A. Jarząb, A. Dylong, & M. Duczmal, Metal–organic framework in an l-arginine copper(ii) ion polymer: structure, properties, theoretical studies and microbiological activity. *RSC Advances*, **5** (2015) 36295–36306. <https://doi.org/10.1039/C5RA02790J>.
97. Nathaniel L. Rosi, Jaheon Kim, Mohamed Eddaoudi, Banglin Chen, and Michael O’Keeffe, & Omar M. Yaghi, Rod Packings and Metal–Organic Frameworks Constructed from Rod-Shaped Secondary Building Units. (2005). <https://doi.org/10.1021/JA045123O>.
98. H. Wang, E. Lashkari, H. Lim, C. Zheng, T. J. Emge, Q. Gong, K. Yam, & J. Li, The moisture-triggered controlled release of a natural food preservative from a

- microporous metal–organic framework. *Chemical Communications*, **52** (2016) 2129–2132. <https://doi.org/10.1039/C5CC09634K>.
99. K. S. Park, Z. Ni, A. P. Côté, J. Y. Choi, R. Huang, F. J. Uribe-Romo, H. K. Chae, M. O’Keeffe, & O. M. Yaghi, Exceptional chemical and thermal stability of zeolitic imidazolate frameworks. *Proceedings of the National Academy of Sciences of the United States of America*, **103** (2006) 10186–10191. <https://doi.org/10.1073/pnas.0602439103>.
100. J. Chen, X. Zhang, C. Huang, H. Cai, S. Hu, Q. Wan, X. Pei, & J. Wang, Osteogenic activity and antibacterial effect of porous titanium modified with metal-organic framework films. *Journal of Biomedical Materials Research Part A*, **105** (2017) 834–846. <https://doi.org/10.1002/jbm.a.35960>.
101. F.-X. Coudert, Molecular Mechanism of Swing Effect in Zeolitic Imidazolate Framework ZIF-8: Continuous Deformation upon Adsorption. *ChemPhysChem*, **18** (2017) 2732–2738. <https://doi.org/10.1002/cphc.201700463>.
102. A.-N. Au-Duong & C.-K. Lee, Iodine-loaded metal organic framework as growth-triggered antimicrobial agent. *Materials Science and Engineering: C*, **76** (2017) 477–482. <https://doi.org/10.1016/J.MSEC.2017.03.114>.
103. A. R. Chowdhuri, B. Das, A. Kumar, S. Tripathy, S. Roy, & S. K. Sahu, One-pot synthesis of multifunctional nanoscale metal-organic frameworks as an effective antibacterial agent against multidrug-resistant *Staphylococcus aureus*. *Nanotechnology*, **28** (2017) 095102. <https://doi.org/10.1088/1361-6528/aa57af>.
104. C. Tamames-Tabar, E. Imbuluzqueta, N. Guillou, C. Serre, S. R. Miller, E. Elkaïm, P. Horcajada, & M. J. Blanco-Prieto, A Zn azelate MOF: combining antibacterial effect. *CrystEngComm*, **17** (2015) 456–462. <https://doi.org/10.1039/C4CE00885E>.
105. J. Restrepo, Z. Serroukh, J. Santiago-Morales, S. Aguado, P. Gómez-Sal, M. E. G. Mosquera, & R. Rosal, An Antibacterial Zn-MOF with Hydrazinebenzoate Linkers. *European Journal of Inorganic Chemistry*, **2017** (2017) 574–580. <https://doi.org/10.1002/ejic.201601185>.
106. A. M. Marti, M. Van, & K. J. Balkus, Tuning the crystal size and morphology of the substituted imidazole material, SIM-1. *Journal of Porous Materials*, **21** (2014) 889–902. <https://doi.org/10.1007/s10934-014-9840-5>.
107. S. Aguado, C.-H. Nicolas, V. Moizan-Baslé, C. Nieto, H. Amrouche, N. Bats, N. Audebrand, & D. Farrusseng, Facile synthesis of an ultramicroporous MOF tubular

- membrane with selectivity towards CO₂. *New J. Chem.*, **35** (2011) 41–44.
<https://doi.org/10.1039/C0NJ00667J>.
108. R. Banerjee, A. Phan, B. Wang, C. Knobler, H. Furukawa, M. O’Keeffe, & O. M. Yaghi, High-throughput synthesis of zeolitic imidazolate frameworks and application to CO₂ capture. *Science (New York, N.Y.)*, **319** (2008) 939–43.
<https://doi.org/10.1126/science.1152516>.
109. R. Singleton, J. Bye, J. Dyson, G. Baker, R. M. Ranson, & G. B. Hix, Tailoring the photoluminescence properties of transition metal phosphonates. *Dalton Transactions*, **39** (2010) 6024. <https://doi.org/10.1039/c000531b>.
110. J. A. Prince, S. Bhuvana, V. Anbharasi, N. Ayyanar, K. V. K. Boodhoo, & G. Singh, Self-cleaning Metal Organic Framework (MOF) based ultra filtration membranes--a solution to bio-fouling in membrane separation processes. *Scientific reports*, **4** (2014) 6555. <https://doi.org/10.1038/srep06555>.
111. W. Li, S. Zhou, S. Gao, S. Chen, M. Huang, & R. Cao, Spatioselective Fabrication of Highly Effective Antibacterial Layer by Surface-Anchored Discrete Metal-Organic Frameworks. *Advanced Materials Interfaces*, **2** (2015) 1400405.
<https://doi.org/10.1002/admi.201400405>.
112. D. Sun, R. Cao, W. Bi, J. Weng, M. Hong, & Y. Liang, Syntheses and characterizations of a series of silver-carboxylate polymers. *Inorganica Chimica Acta*, **357** (2004) 991–1001. <https://doi.org/10.1016/J.ICA.2003.10.010>.
113. A. M. Kirillov, S. W. Wieczorek, A. Lis, M. F. C. Guedes da Silva, M. Florek, J. Król, Z. Staroniewicz, P. Smoleński, & A. J. L. Pombeiro, 1,3,5-Triaza-7-phosphaadamantane-7-oxide (PTA=O): New Diamondoid Building Block for Design of Three-Dimensional Metal–Organic Frameworks. *Crystal Growth & Design*, **11** (2011) 2711–2716. <https://doi.org/10.1021/cg200571y>.
114. S. W. Jaros, P. Smoleński, M. F. C. Guedes da Silva, M. Florek, J. Król, Z. Staroniewicz, A. J. L. Pombeiro, & A. M. Kirillov, New silver BioMOFs driven by 1,3,5-triaza-7-phosphaadamantane-7-sulfide (PTA and antimicrobial activity. *CrystEngComm*, **15** (2013) 8060. <https://doi.org/10.1039/c3ce40913a>. □ S): synthesis
115. S. W. Jaros, M. F. C. Guedes da Silva, M. Florek, M. C. Oliveira, P. Smoleński, A. J. L. Pombeiro, & A. M. Kirillov, Aliphatic Dicarboxylate Directed Assembly of Silver(I) 1,3,5-Triaza-7-phosphaadamantane Coordination Networks: Topological Versatility and Antimicrobial Activity. *Crystal Growth & Design*, **14** (2014) 5408–5417. <https://doi.org/10.1021/cg500557r>.

116. O. Z. Yeşilel, G. Günay, C. Darcan, M. S. Soylu, S. Keskin, & S. W. Ng, An unusual 3D metal–organic framework, $\{[\text{Ag}_4(\mu_4\text{-pzdc})_2(\mu\text{-en})_2]\cdot\text{H}_2\text{O}\}_n$: C–H \cdots Ag, N–H \cdots Ag and (O–H) \cdots Ag interactions and an unprecedented coordination mode for pyrazine-2,3-dicarboxylate. *CrystEngComm*, **14** (2012) 2817. <https://doi.org/10.1039/c2ce06603c>.
117. X. Wang, D. Zhao, A. Tian, & J. Ying, Three 3D silver-bis(triazole) metal–organic frameworks stabilized by high-connected Wells–Dawson polyoxometallates. *Dalton Transactions*, **43** (2014) 5211. <https://doi.org/10.1039/c3dt53437e>.
118. C.-B. Liu, Y.-N. Gong, Y. Chen, & H.-L. Wen, Self-assembly and structures of new transition metal complexes with phenyl substituted pyrazole carboxylic acid and N-donor co-ligands. *Inorganica Chimica Acta*, **383** (2012) 277–286. <https://doi.org/10.1016/J.ICA.2011.11.015>.
119. X. Lu, J. Ye, L. Zhao, Y. Lin, & G. Ning, Synthesis, structure, magnetism and antibacterial properties of a 2-D nickel(II) metal–organic framework based on 3-nitrophthalic acid and 4,4'-bipyridine. *Journal of Coordination Chemistry*, **67** (2014) 1133–1140. <https://doi.org/10.1080/00958972.2014.910773>.
120. Z.-H. Zhang, Q.-Q. Zhang, S. Feng, Z.-J. Hu, S.-C. Chen, Q. Chen, & M.-Y. He, Fluorinated metal–organic frameworks of 1,4-bis(1,2,4-triazol-1-ylmethyl)-2,3,5,6-tetrafluorobenzene: synergistic interactions of ligand isomerism and counteranions. *Dalton Trans.*, **43** (2014) 646–655. <https://doi.org/10.1039/C3DT52211C>.
121. T. Drake, P. Ji, & W. Lin, Site Isolation in Metal–Organic Frameworks Enables Novel Transition Metal Catalysis. *Accounts of Chemical Research*, **51** (2018) 2129–2138. <https://doi.org/10.1021/acs.accounts.8b00297>.
122. P. Horcajada, R. Gref, T. Baati, P. K. Allan, G. Maurin, P. Couvreur, G. Férey, R. E. Morris, & C. Serre, Metal–Organic Frameworks in Biomedicine. *Chemical Reviews*, **112** (2012) 1232–1268. <https://doi.org/10.1021/cr200256v>.
123. M.-X. Wu & Y.-W. Yang, Metal-Organic Framework (MOF)-Based Drug/Cargo Delivery and Cancer Therapy. *Advanced Materials*, **29** (2017) 1606134. <https://doi.org/10.1002/adma.201606134>.
124. C. Doonan, R. Riccò, K. Liang, D. Bradshaw, & P. Falcaro, Metal–Organic Frameworks at the Biointerface: Synthetic Strategies and Applications. *Accounts of Chemical Research*, **50** (2017) 1423–1432. <https://doi.org/10.1021/acs.accounts.7b00090>.

125. J. An, S. J. Geib, & N. L. Rosi, Cation-Triggered Drug Release from a Porous Zinc–Adeninate Metal–Organic Framework. *Journal of the American Chemical Society*, **131** (2009) 8376–8377. <https://doi.org/10.1021/ja902972w>.
126. Q. Hu, J. Yu, M. Liu, A. Liu, Z. Dou, & Y. Yang, A Low Cytotoxic Cationic Metal–Organic Framework Carrier for Controllable Drug Release. *Journal of Medicinal Chemistry*, **57** (2014) 5679–5685. <https://doi.org/10.1021/jm5004107>.
127. X. Meng, B. Gui, D. Yuan, M. Zeller, & C. Wang, Mechanized azobenzene-functionalized zirconium metal-organic framework for on-command cargo release. *Science Advances*, **2** (2016) e1600480. <https://doi.org/10.1126/sciadv.1600480>.
128. W. P. Lustig, S. Mukherjee, N. D. Rudd, A. V. Desai, J. Li, & S. K. Ghosh, Metal–organic frameworks: functional luminescent and photonic materials for sensing applications. *Chemical Society Reviews*, **46** (2017) 3242–3285. <https://doi.org/10.1039/C6CS00930A>.
129. B. Chen, S. Xiang, & G. Qian, Metal–Organic Frameworks with Functional Pores for Recognition of Small Molecules. *Accounts of Chemical Research*, **43** (2010) 1115–1124. <https://doi.org/10.1021/ar100023y>.
130. L. E. Kreno, K. Leong, O. K. Farha, M. Allendorf, R. P. Van Duyne, & J. T. Hupp, Metal–Organic Framework Materials as Chemical Sensors. *Chemical Reviews*, **112** (2012) 1105–1125. <https://doi.org/10.1021/cr200324t>.
131. Z. Hu, B. J. Deibert, & J. Li, Luminescent metal–organic frameworks for chemical sensing and explosive detection. *Chem. Soc. Rev.*, **43** (2014) 5815–5840. <https://doi.org/10.1039/C4CS00010B>.
132. B. Yan, Lanthanide-Functionalized Metal–Organic Framework Hybrid Systems To Create Multiple Luminescent Centers for Chemical Sensing. *Accounts of Chemical Research*, **50** (2017) 2789–2798. <https://doi.org/10.1021/acs.accounts.7b00387>.
133. F.-Y. Yi, D. Chen, M.-K. Wu, L. Han, & H.-L. Jiang, Chemical Sensors Based on Metal-Organic Frameworks. *ChemPlusChem*, **81** (2016) 675–690. <https://doi.org/10.1002/cplu.201600137>.
134. S. S. Nagarkar, B. Joarder, A. K. Chaudhari, S. Mukherjee, & S. K. Ghosh, Highly Selective Detection of Nitro Explosives by a Luminescent Metal–Organic Framework. *Angewandte Chemie International Edition*, **52** (2013) 2881–2885. <https://doi.org/10.1002/anie.201208885>.

135. H.-T. Zhang, J.-W. Zhang, G. Huang, Z.-Y. Du, & H.-L. Jiang, An amine-functionalized metal–organic framework as a sensing platform for DNA detection. *Chem. Commun.*, **50** (2014) 12069–12072. <https://doi.org/10.1039/C4CC05571C>.
136. H.-L. Jiang, D. Feng, K. Wang, Z.-Y. Gu, Z. Wei, Y.-P. Chen, & H.-C. Zhou, An Exceptionally Stable, Porphyrinic Zr Metal–Organic Framework Exhibiting pH-Dependent Fluorescence. *Journal of the American Chemical Society*, **135** (2013) 13934–13938. <https://doi.org/10.1021/ja406844r>.
137. W. Zhan, Q. Kuang, J. Zhou, X. Kong, Z. Xie, & L. Zheng, Semiconductor@Metal–Organic Framework Core–Shell Heterostructures: A Case of ZnO@ZIF-8 Nanorods with Selective Photoelectrochemical Response. *Journal of the American Chemical Society*, **135** (2013) 1926–1933. <https://doi.org/10.1021/ja311085e>.
138. B. Wang, X.-L. Lv, D. Feng, L.-H. Xie, J. Zhang, M. Li, Y. Xie, J.-R. Li, & H.-C. Zhou, Highly Stable Zr(IV)-Based Metal–Organic Frameworks for the Detection and Removal of Antibiotics and Organic Explosives in Water. *Journal of the American Chemical Society*, **138** (2016) 6204–6216. <https://doi.org/10.1021/jacs.6b01663>.
139. L. Ai, L. Li, C. Zhang, J. Fu, & J. Jiang, MIL-53(Fe): A Metal–Organic Framework with Intrinsic Peroxidase-Like Catalytic Activity for Colorimetric Biosensing. *Chemistry - A European Journal*, **19** (2013) 15105–15108. <https://doi.org/10.1002/chem.201303051>.
140. W. Dong, X. Liu, W. Shi, & Y. Huang, Metal–organic framework MIL-53(Fe): facile microwave-assisted synthesis and use as a highly active peroxidase mimetic for glucose biosensing. *RSC Advances*, **5** (2015) 17451–17457. <https://doi.org/10.1039/C4RA15840G>.
141. J.-W. Zhang, H.-T. Zhang, Z.-Y. Du, X. Wang, S.-H. Yu, & H.-L. Jiang, Water-stable metal–organic frameworks with intrinsic peroxidase-like catalytic activity as a colorimetric biosensing platform. *Chem. Commun.*, **50** (2014) 1092–1094. <https://doi.org/10.1039/C3CC48398C>.
142. E.-L. Zhou, C. Qin, P. Huang, X.-L. Wang, W.-C. Chen, K.-Z. Shao, & Z.-M. Su, A Stable Polyoxometalate-Pillared Metal–Organic Framework for Proton-Conducting and Colorimetric Biosensing. *Chemistry - A European Journal*, **21** (2015) 11894–11898. <https://doi.org/10.1002/chem.201501515>.
143. F. Liu, J. He, M. Zeng, J. Hao, Q. Guo, Y. Song, & L. Wang, Cu–hemin metal-organic frameworks with peroxidase-like activity as peroxidase mimics for

- colorimetric sensing of glucose. *Journal of Nanoparticle Research*, **18** (2016) 106.
<https://doi.org/10.1007/s11051-016-3416-z>.
144. H. Yang, R. Yang, P. Zhang, Y. Qin, T. Chen, & F. Ye, A bimetallic (Co/2Fe) metal-organic framework with oxidase and peroxidase mimicking activity for colorimetric detection of hydrogen peroxide. *Microchimica Acta*, **184** (2017) 4629–4635. <https://doi.org/10.1007/s00604-017-2509-4>.
145. W. Dong, L. Yang, & Y. Huang, Glycine post-synthetic modification of MIL-53(Fe) metal–organic framework with enhanced and stable peroxidase-like activity for sensitive glucose biosensing. *Talanta*, **167** (2017) 359–366.
<https://doi.org/10.1016/J.TALANTA.2017.02.039>.
146. F.-X. Qin, S.-Y. Jia, F.-F. Wang, S.-H. Wu, J. Song, & Y. Liu, Hemin@metal–organic framework with peroxidase-like activity and its application to glucose detection. *Catalysis Science & Technology*, **3** (2013) 2761.
<https://doi.org/10.1039/c3cy00268c>.
147. Y. Wu, Y. Y. Ma, G. Xu, F. Wei, Y. Y. Ma, Q. Song, X. Wang, T. Tang, Y. Song, M. Shi, X. Xu, & Q. Hu, Metal-organic framework coated Fe₃O₄ magnetic nanoparticles with peroxidase-like activity for colorimetric sensing of cholesterol. *Sensors and Actuators B: Chemical*, **249** (2017) 195–202.
<https://doi.org/10.1016/J.SNB.2017.03.145>.
148. B. Tan, H. Zhao, W. Wu, X. Liu, Y. Zhang, & X. Quan, Fe₃O₄-AuNPs anchored 2D metal–organic framework nanosheets with DNA regulated switchable peroxidase-like activity. *Nanoscale*, **9** (2017) 18699–18710.
<https://doi.org/10.1039/C7NR05541B>.
149. F. Cui, Q. Deng, & L. Sun, Prussian blue modified metal–organic framework MIL-101(Fe) with intrinsic peroxidase-like catalytic activity as a colorimetric biosensing platform. *RSC Advances*, **5** (2015) 98215–98221.
<https://doi.org/10.1039/C5RA18589K>.
150. Y. Yin, C. Gao, Q. Xiao, G. Lin, Z. Lin, Z. Cai, & H. Yang, Protein-Metal Organic Framework Hybrid Composites with Intrinsic Peroxidase-like Activity as a Colorimetric Biosensing Platform. *ACS Applied Materials & Interfaces*, **8** (2016) 29052–29061. <https://doi.org/10.1021/acsami.6b09893>.
151. C. Hou, Y. Wang, Q. Ding, L. Jiang, M. Li, W. Zhu, D. Pan, H. Zhu, & M. Liu, Facile synthesis of enzyme-embedded magnetic metal–organic frameworks as a reusable mimic multi-enzyme system: mimetic peroxidase properties and colorimetric sensor. *Nanoscale*, **7** (2015) 18770–18779. <https://doi.org/10.1039/C5NR04994F>.

152. H. Tan, C. Ma, L. Gao, Q. Li, Y. Song, F. Xu, T. Wang, & L. Wang, Metal-Organic Framework-Derived Copper Nanoparticle@Carbon Nanocomposites as Peroxidase Mimics for Colorimetric Sensing of Ascorbic Acid. *Chemistry - A European Journal*, **20** (2014) 16377–16383. <https://doi.org/10.1002/chem.201404960>.
153. W. Yang, J. Hao, Z. Zhang, & B. Zhang, Metal–organic frameworks-derived synthesis of porous FeP nanocubes: An effective peroxidase mimetic. *Journal of Colloid and Interface Science*, **460** (2015) 55–60. <https://doi.org/10.1016/J.JCIS.2015.08.032>.
154. W. Dong, Y. Zhuang, S. Li, X. Zhang, H. Chai, & Y. Huang, High peroxidase-like activity of metallic cobalt nanoparticles encapsulated in metal–organic frameworks derived carbon for biosensing. *Sensors and Actuators B: Chemical*, **255** (2018) 2050–2057. <https://doi.org/10.1016/J.SNB.2017.09.013>.
155. F.-F. Chen, Y.-J. Zhu, Z.-C. Xiong, & T.-W. Sun, Hydroxyapatite Nanowires@Metal-Organic Framework Core/Shell Nanofibers: Templated Synthesis, Peroxidase-Like Activity, and Derived Flexible Recyclable Test Paper. *Chemistry - A European Journal*, **23** (2017) 3328–3337. <https://doi.org/10.1002/chem.201604813>.
156. Y. L. Liu, X. J. Zhao, X. X. Yang, & Y. F. Li, A nanosized metal–organic framework of Fe-MIL-88NH₂ as a novel peroxidase mimic used for colorimetric detection of glucose. *The Analyst*, **138** (2013) 4526. <https://doi.org/10.1039/c3an00560g>.
157. Y. Huang, M. Zhao, S. Han, Z. Lai, J. Yang, C. Tan, Q. Ma, Q. Lu, J. Chen, X. Zhang, Z. Zhang, B. Li, B. Chen, Y. Zong, & H. Zhang, Growth of Au Nanoparticles on 2D Metalloporphyrinic Metal-Organic Framework Nanosheets Used as Biomimetic Catalysts for Cascade Reactions. *Advanced Materials*, **29** (2017) 1700102. <https://doi.org/10.1002/adma.201700102>.
158. Q. Wang, X. Zhang, L. Huang, Z. Zhang, & S. Dong, GOx@ZIF-8(NiPd) Nanoflower: An Artificial Enzyme System for Tandem Catalysis. *Angewandte Chemie International Edition*, **56** (2017) 16082–16085. <https://doi.org/10.1002/anie.201710418>.
159. Y. Song, D. Cho, S. Venkateswarlu, & M. Yoon, Systematic study on preparation of copper nanoparticle embedded porous carbon by carbonization of metal–organic framework for enzymatic glucose sensor. *RSC Advances*, **7** (2017) 10592–10600. <https://doi.org/10.1039/C7RA00115K>.
160. H. Cheng, L. Zhang, J. He, W. Guo, Z. Zhou, X. Zhang, S. Nie, & H. Wei, Integrated Nanozymes with Nanoscale Proximity for in Vivo Neurochemical

- Monitoring in Living Brains. *Analytical Chemistry*, **88** (2016) 5489–5497.
<https://doi.org/10.1021/acs.analchem.6b00975>.
161. C. Gao, H. Zhu, J. Chen, & H. Qiu, Facile synthesis of enzyme functional metal-organic framework for colorimetric detecting H₂O₂ and ascorbic acid. *Chinese Chemical Letters*, **28** (2017) 1006–1012.
<https://doi.org/10.1016/J.CCLET.2017.02.011>.
162. Y. Xiong, S. Chen, F. Ye, L. Su, C. Zhang, S. Shen, & S. Zhao, Synthesis of a mixed valence state Ce-MOF as an oxidase mimetic for the colorimetric detection of biothiols. *Chemical Communications*, **51** (2015) 4635–4638.
<https://doi.org/10.1039/C4CC10346G>.
163. R. Dalapati, B. Sakthivel, M. K. Ghosalya, A. Dhakshinamoorthy, & S. Biswas, A cerium-based metal–organic framework having inherent oxidase-like activity applicable for colorimetric sensing of biothiols and aerobic oxidation of thiols. *CrystEngComm*, **19** (2017) 5915–5925. <https://doi.org/10.1039/C7CE01053B>.
164. Z. Hu, X. Jiang, F. Xu, J. Jia, Z. Long, & X. Hou, Colorimetric sensing of bithiols using photocatalytic UiO-66(NH₂) as H₂O₂-free peroxidase mimics. *Talanta*, **158** (2016) 276–282. <https://doi.org/10.1016/J.TALANTA.2016.05.040>.
165. J. Lu, Y. Xiong, C. Liao, & F. Ye, Colorimetric detection of uric acid in human urine and serum based on peroxidase mimetic activity of MIL-53(Fe). *Analytical Methods*, **7** (2015) 9894–9899. <https://doi.org/10.1039/C5AY02240A>.
166. C. ZHAO, Y. LIU, & Y. LI, Colorimetric and Fluorometric Assays for Dopamine with a Wide Concentration Range Based on Fe-MIL-88NH₂; Metal-organic Framework. *Analytical Sciences*, **31** (2015) 1035–1039.
<https://doi.org/10.2116/analsci.31.1035>.
167. H. Liang, F. Lin, Z. Zhang, B. Liu, S. Jiang, Q. Yuan, & J. Liu, Multicopper Laccase Mimicking Nanozymes with Nucleotides as Ligands. *ACS Applied Materials & Interfaces*, **9** (2017) 1352–1360. <https://doi.org/10.1021/acsami.6b15124>.
168. H. Li, H. Liu, J. Zhang, Y. Cheng, C. Zhang, X. Fei, & Y. Xian, Platinum Nanoparticle Encapsulated Metal–Organic Frameworks for Colorimetric Measurement and Facile Removal of Mercury(II). *ACS Applied Materials & Interfaces*, **9** (2017) 40716–40725. <https://doi.org/10.1021/acsami.7b13695>.
169. Y. Xiong, L. Su, H. Yang, P. Zhang, & F. Ye, Fabrication of copper sulfide using a Cu-based metal organic framework for the colorimetric determination and the

- efficient removal of Hg^{2+} in aqueous solutions. *New Journal of Chemistry*, **39** (2015) 9221–9227. <https://doi.org/10.1039/C5NJ01348H>.
170. D. Chen, B. Li, L. Jiang, D. Duan, Y. Li, J. Wang, J. He, & Y. Zeng, Highly efficient colorimetric detection of cancer cells utilizing Fe-MIL-101 with intrinsic peroxidase-like catalytic activity over a broad pH range. *RSC Advances*, **5** (2015) 97910–97917. <https://doi.org/10.1039/C5RA18115A>.
171. Y. Wang, Y. Zhu, A. Binyam, M. Liu, Y. Wu, & F. Li, Discovering the enzyme mimetic activity of metal-organic framework (MOF) for label-free and colorimetric sensing of biomolecules. *Biosensors and Bioelectronics*, **86** (2016) 432–438. <https://doi.org/10.1016/J.BIOS.2016.06.036>.
172. S. Wang, W. Deng, L. Yang, Y. Tan, Q. Xie, & S. Yao, Copper-Based Metal–Organic Framework Nanoparticles with Peroxidase-Like Activity for Sensitive Colorimetric Detection of *Staphylococcus aureus*. *ACS Applied Materials & Interfaces*, **9** (2017) 24440–24445. <https://doi.org/10.1021/acsami.7b07307>.
173. C. Wang, J. Gao, Y. Cao, & H. Tan, Colorimetric logic gate for alkaline phosphatase based on copper (II)-based metal-organic frameworks with peroxidase-like activity. *Analytica Chimica Acta*, **1004** (2018) 74–81. <https://doi.org/10.1016/J.ACA.2017.11.078>.
174. Y. L. Liu, W. L. Fu, C. M. Li, C. Z. Huang, & Y. F. Li, Gold nanoparticles immobilized on metal–organic frameworks with enhanced catalytic performance for DNA detection. *Analytica Chimica Acta*, **861** (2015) 55–61. <https://doi.org/10.1016/J.ACA.2014.12.032>.
175. L. Su, Y. Xiong, H. Yang, P. Zhang, & F. Ye, Prussian blue nanoparticles encapsulated inside a metal–organic framework via in situ growth as promising peroxidase mimetics for enzyme inhibitor screening. *Journal of Materials Chemistry B*, **4** (2016) 128–134. <https://doi.org/10.1039/C5TB01924A>.
176. A. H. Valekar, B. S. Batule, M. Il Kim, K.-H. Cho, D.-Y. Hong, U.-H. Lee, J.-S. Chang, H. G. Park, & Y. K. Hwang, Novel amine-functionalized iron trimesates with enhanced peroxidase-like activity and their applications for the fluorescent assay of choline and acetylcholine. *Biosensors and Bioelectronics*, **100** (2018) 161–168. <https://doi.org/10.1016/J.BIOS.2017.08.056>.
177. Z. Qi, L. Wang, Q. You, & Y. Chen, PA-Tb-Cu MOF as luminescent nanoenzyme for catalytic assay of hydrogen peroxide. *Biosensors and Bioelectronics*, **96** (2017) 227–232. <https://doi.org/10.1016/J.BIOS.2017.05.013>.

178. C. Zhao, Z. Jiang, R. Mu, & Y. Li, A novel sensor for dopamine based on the turn-on fluorescence of Fe-MIL-88 metal-organic frameworks–hydrogen peroxide–o-phenylenediamine system. *Talanta*, **159** (2016) 365–370. <https://doi.org/10.1016/J.TALANTA.2016.06.043>.
179. Z. J. Sun, J. Z. Jiang, & Y. F. Li, A sensitive and selective sensor for biothiols based on the turn-on fluorescence of the Fe-MIL-88 metal–organic frameworks–hydrogen peroxide system. *The Analyst*, **140** (2015) 8201–8208. <https://doi.org/10.1039/C5AN01673H>.
180. H. Tan, Q. Li, Z. Zhou, C. Ma, Y. Song, F. Xu, & L. Wang, A sensitive fluorescent assay for thiamine based on metal-organic frameworks with intrinsic peroxidase-like activity. *Analytica Chimica Acta*, **856** (2015) 90–95. <https://doi.org/10.1016/J.ACA.2014.11.026>.
181. H. Cheng, Y. Liu, Y. Hu, Y. Ding, S. Lin, W. Cao, Q. Wang, J. Wu, F. Muhammad, X. Zhao, D. Zhao, Z. Li, H. Xing, & H. Wei, Monitoring of Heparin Activity in Live Rats Using Metal–Organic Framework Nanosheets as Peroxidase Mimics. *Analytical Chemistry*, **89** (2017) 11552–11559. <https://doi.org/10.1021/acs.analchem.7b02895>.
182. X. Yi, W. Dong, X. Zhang, J. Xie, & Y. Huang, MIL-53(Fe) MOF-mediated catalytic chemiluminescence for sensitive detection of glucose. *Analytical and Bioanalytical Chemistry*, **408** (2016) 8805–8812. <https://doi.org/10.1007/s00216-016-9681-y>.
183. Y. Li, X. You, & X. Shi, Enhanced Chemiluminescence Determination of Hydrogen Peroxide in Milk Sample Using Metal–Organic Framework Fe–MIL–88NH₂ as Peroxidase Mimetic. *Food Analytical Methods*, **10** (2017) 626–633. <https://doi.org/10.1007/s12161-016-0617-0>.
184. F. Luo, Y. Lin, L. Zheng, X. Lin, & Y. Chi, Encapsulation of Hemin in Metal–Organic Frameworks for Catalyzing the Chemiluminescence Reaction of the H₂O₂ – Luminol System and Detecting Glucose in the Neutral Condition. *ACS Applied Materials & Interfaces*, **7** (2015) 11322–11329. <https://doi.org/10.1021/acsami.5b01706>.
185. X. Qian Tang, Y. Dan Zhang, Z. Wei Jiang, D. Mei Wang, C. Zhi Huang, & Y. Fang Li, Fe₃O₄ and metal–organic framework MIL-101(Fe) composites catalyze luminol chemiluminescence for sensitively sensing hydrogen peroxide and glucose. *Talanta*, **179** (2018) 43–50. <https://doi.org/10.1016/j.talanta.2017.10.049>.

186. Q. Zhu, Y. Chen, W. Wang, H. Zhang, C. Ren, H. Chen, & X. Chen, A sensitive biosensor for dopamine determination based on the unique catalytic chemiluminescence of metal–organic framework HKUST-1. *Sensors and Actuators B: Chemical*, **210** (2015) 500–507. <https://doi.org/10.1016/J.SNB.2015.01.012>.
187. Y. Hu, H. Cheng, X. Zhao, J. Wu, F. Muhammad, S. Lin, J. He, L. Zhou, C. Zhang, Y. Deng, P. Wang, Z. Zhou, S. Nie, & H. Wei, Surface-Enhanced Raman Scattering Active Gold Nanoparticles with Enzyme-Mimicking Activities for Measuring Glucose and Lactate in Living Tissues. *ACS Nano*, **11** (2017) 5558–5566. <https://doi.org/10.1021/acsnano.7b00905>.
188. Z. Jiang, P. Gao, L. Yang, C. Huang, & Y. Li, Facile in Situ Synthesis of Silver Nanoparticles on the Surface of Metal–Organic Framework for Ultrasensitive Surface-Enhanced Raman Scattering Detection of Dopamine. *Analytical Chemistry*, **87** (2015) 12177–12182. <https://doi.org/10.1021/acs.analchem.5b03058>.

Chapter 10

Significance of Metal Organic Frameworks Consisting of Porous Materials

R. Kumar^{1*}, A. Arul Marcel Moshi², S.R. Sundara Bharathi², S. Sivaganesan¹,
C. Dhanasekaran¹, P. Senthamaraikannan³, S.S. Saravanakumar³, Anish Khan⁴

¹ Department of Mechanical Engineering, Vels Institute of Science, Technology & Advanced Studies, Pallavaram, Chennai, Tamil Nadu, India, Pin- 600117

² Department of Mechanical Engineering, National Engineering College, Kovilpatti, Tamil Nadu, India, Pin- 628503

³ Department of Mechanical Engineering, Kamaraj College of Engineering and Technology, Virudhunagar, Tamil Nadu, India, Pin- 625701

⁴ Department of Chemistry, Faculty of Science, King Abdulaziz University, Jeddah 21589, Saudi Arabia

*mepcokumar@gmail.com

Abstract

Metal-organic framework materials are adjustable and highly porous materials and they are sensitive to air and resistant to structural collapse upon heating. MOFs are often crystalline. Over the past 50 decades, porous materials have been focused with substantial attention. The attracting feature of MOFs is their porosity that allows the diffusion of guest molecules into the bulk structure. MOFs are one among the most extremely focused material types, which are formed by combining inorganic units with organic units through strong bonds (reticular synthesis). The strong bonds between the inorganic units (metal ions or clusters) and the organic linkers (building units) offer an unparalleled chemical diversity and pore environments to the entire structure. The inherent structural characteristics and the flexibility of MOFs with the geometry of their constituents, size and functionality have led to the extensive study on more than twenty thousand different forms of MOFs. These materials have pulled towards a great deal of attention in the past ten years; and the increase in the number of papers published in this area during recent years is remarkable. Metal Organic Frameworks are typically structured in such a way that the porosity is more than 50% of their entire crystal volume. The surface area values of such Metal Organic Frameworks normally range between 1000 and 10,000 m²/g, which is more than the values of regular porous materials like carbons and zeolites. Due to the unique chemical and structural properties, MOFs are utilized in various kinds of

real time applications such as separation of gases, storage of gases, catalysis, drug delivery, etc.

Keywords

Metal Organic Framework (MOF), Zeolites, activated Carbon, Porous Materials, Organic Linkers, Gas Separation and Drug Delivery

Contents

1. Introduction.....	291
1.1 Definition of porosity	293
2. Inferences obtained from the wide range of relevant research articles	294
2.1 Introduction to porous MOFs	294
2.2 Zeolites – an amorphous & inorganic porous material	294
2.3 Activated carbon – an organic porous material	295
2.4 Formation of pores in MOFs	295
2.5 Types of pores.....	295
2.6 Characterization of porous MOFs	297
2.7 Checking for permanent porosity	297
2.8 Advantages of MOF porous materials.....	298
2.9 Porous MOFs in separation of gases	298
2.10 Nanoporous MOFs.....	299
Conclusion.....	300
References	301

1. Introduction

Materials having porous nature are abundantly available in the nature in variety of forms. Few porous materials are mentioned in Figure 1. Metal organic frameworks (MOFs) are a new class of hybrid porous solids, which are potentially a type of prominent porous adsorbents; and they can exist in an empty guest free state as well [43].

MOFs are defined by Yaghi et al. as porous structures made up with coordinative bonding between metal ions and organic linkers [62]. MOFs have grown to the leading

domain of solid-state chemistry [23, 63]. This special case of crystalline materials presents a high degree of functional and structural tenability [65, 66] which is not possible with other traditional porous materials like Zeolites and activated carbons [23].

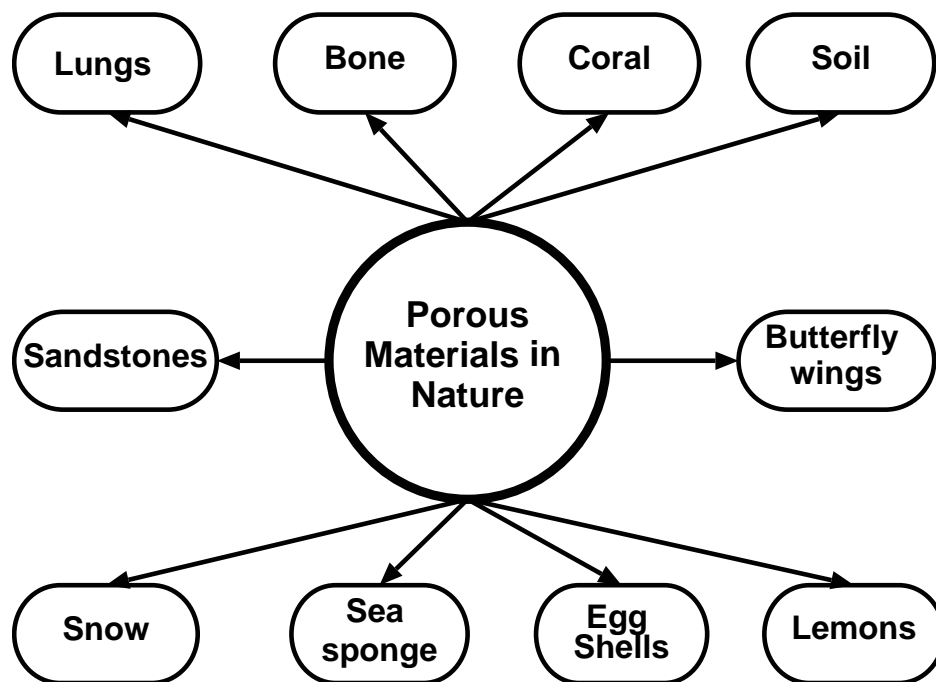


Figure.1 Materials with porous nature [63].

Even though the general porous materials are having many valuable attributes, [44] techniques for controlling the individual crystal locations and coatings with particularly designed size of pores and their arrangement cum distribution are not yet optimized [68]. Among all kinds of porous materials, MOFs are a special kind of ultra-porous materials with extraordinary accessible surface area because of the framework generated by the inorganic nodes and organic compounds [62, 69]. These surface areas are having the range between 1000 to 10,000 m²/g, which exceed the values of other porous materials such as carbons, zeolites and mesoporous based oxides [13]. Few commonly used products being artificially made up with porous nature are illustrated in figure 2.

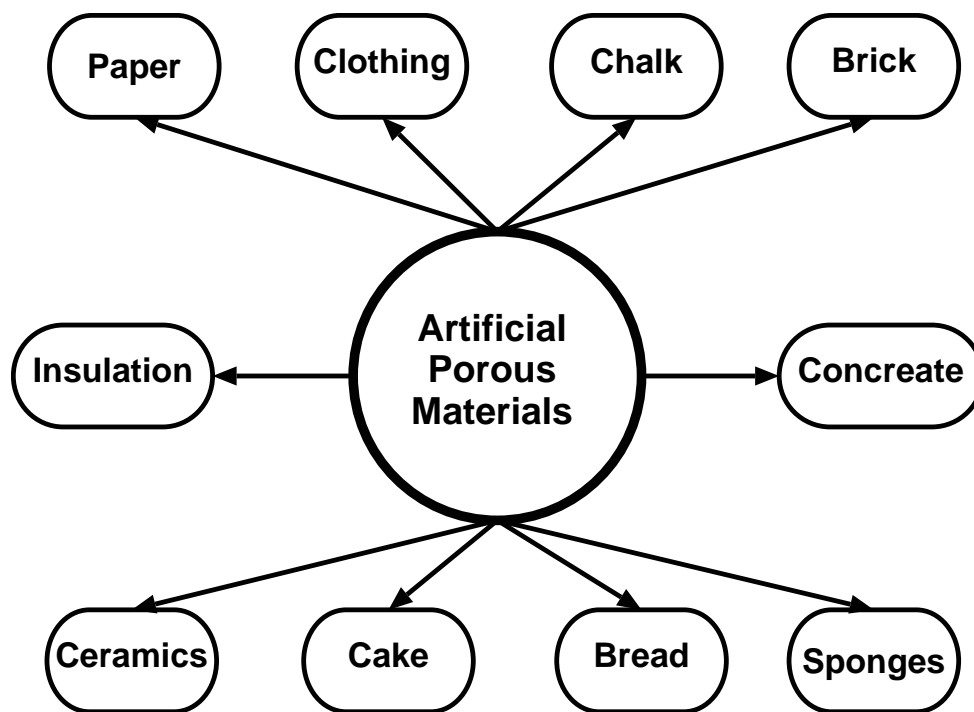


Figure 2 Artificially developed common porous materials [44].

It is a significant note that MOFs are termed by many names such as porous coordination networks, porous coordination polymers, etc. The faster rate of growth could be noted there in the past previous years over the synthesis, characterization and analysis on metal-organic frameworks (MOFs). These kinds of materials are produced in such a way with permanent porosity [1]. The flexibility with the MOFs is that their Secondary Building Units (SBUs) and organic linkers can be varied, which has led to the formation of thousands of MOF compounds. In specific, they have been extensively used in energy domain including fuel cell technology, super capacitors and catalytic convertors [3-4]. In order to utilize the positive features of both inorganic and organic porous compounds, porous hybrids (MOFs) are being generated which are stable, ordered and having high surface areas.

1.1 Definition of porosity

Porosity of any solid material can be realized with the presence of cavities, void space or/and inter-channels. Materials consisting of a regular organic - inorganic hybrid framework and acting as a regular porous structure with pores of size range 0.2×10^9 to 100×10^9 m are called as nanoporous materials [44].

2. Inferences obtained from the wide range of relevant research articles

Various research articles published related with porous for MOF materials have been referred and the important things are presented in this sub chapter.

2.1 Introduction to porous MOFs

At present, MOF chemistry has grown well enough to the peak where the chemical composition, structure of the compounds, specific functionality and nature of porosity of a metal-organic structure can be made for the desired application. This exclusive control over the assembly of compounds propel this area further into a new domain area for synthetic chemistry in which further more sophisticated materials may be approached. For example, materials can be visualized which have

- i. compartments combined together which operate separately, but their function is of integrated;
- ii. ability to perform simultaneous operations; and,
- iii. Dexterity to count, classify, and code data [5].

In the recent years, researchers have carried out extensive works on crystalline extended structures [6-7]. Even though these structures are extended crystal structures and not having large detached molecules like polymers, they are dubbed coordination “polymers”—Metal Organic Frameworks [8]. Because, these structures are constructed from long organic linkers which are surrounded by a void space. MOFs are known to have the potential to be permanently porous like in the case of zeolites. The porosity of Metal Organic Frameworks was investigated in the 1990s by forcibly sending gas molecules into the narrow openings at high pressure [9].

2.2 Zeolites – an amorphous & inorganic porous material

Zeolites are ideal type of structures which belong to the group of purely inorganic materials; which make a benchmark in the field of solid state porous materials. Zeolites are readily rehydrated and dehydrated which make to use them in various commercial areas [44]. Porous materials include a wide range of applications in the industries such as catalysis and absorption. Zeolites are most perfect examples among the group of crystalline alumino-silicate materials with interlinked pores of size 4 to 13A [14, 15]. In comparison with Zeolites, activated carbons have high degree of porosity and specific surface area. Activated Carbon also belongs to amorphous porous materials, which rules a major area of the market of solid state porous materials [16].

Inorganic porous frameworks exhibit a highly ordered structure (e.g. zeolites). Synthesis processes often require an organic or inorganic template with strong interactions between the template formed during the process and inorganic framework. As the outcome,

elimination of the template can to get collapsed in the framework. Inorganic frameworks are also influenced by many factors such as lack of diversity. On the other hand, inorganic frameworks are being used in applications like catalysis and separation of gases [23].

2.3 Activated carbon – an organic porous material

Porous materials are being utilized widely in gas storage, adsorption based gas and vapor separation, selective catalysis, storage and delivery of drugs, and as templates in the synthesis of low geometric materials [21]. Conventionally, porous materials are of either inorganic or organic type. Possibly, the most general organic type porous material is activated carbon which is normally produced by decomposing carbon rich materials at high temperature condition. Activated carbon has high surface area and good degree of adsorption capability; but, it does not have an ordered structure. Though activated carbon has the lack of order, porous carbon materials are being used in many application areas including the separating and storing gases, purifying water, and removing and recovering solvents [22].

2.4 Formation of pores in MOFs

Pores are known to be the voids present within the porous materials while removing the guest molecules [26]. Even though MOFs are being constructed by combining inorganic and organic compounds to have large number of pores, frameworks will often merge with one another to improve the packing efficiency [27]. In such cases, the sizes of the pores are considerably reduced, but this would also be useful for few applications. In fact, merged frameworks are being deliberately produced; and this phenomenon has been found to be useful in improving the performance. Example: in the storage of H₂ [28]. Assessment of porous materials has currently paid attention on the adsorption of pure methane. Even though methane is the major constituent (95%), commercial natural gas contains other impurities also including 3.2 % of ethane, 0.2 % of propane and 0.5 % of carbon dioxide [29]. Porous carbon materials, especially carbon nanotubes and activated carbons, are the most focused kinds of porous materials for storing methane [30].

2.5 Types of pores

The adhesion of the guest molecules and the surface of the adsorbent as well as the relationship between the adsorbent's surface and guest molecules play needful roles in predicting the characteristics of the porous structures; and which is majorly ruled by the shape and size of the pores. In the physical system, pores are categorized based on their sizes as listed shown in the figure 3.

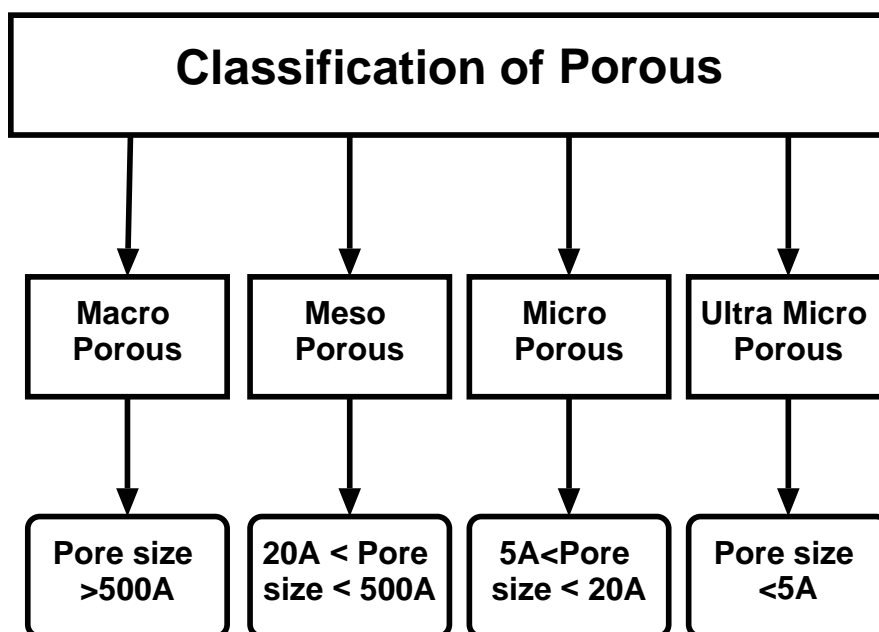


Figure 3 Types of pores based on pore size [67].

Liu et al. stated that microporous systems can be used in upgrading the energy density. Also, they have reported that mesoporous systems are used to improve the power density [67]. It is possible to have a flexible structure just by altering the inorganic or organic linkers [64].

Microporous materials are used in valuable applications like redox catalysts and in petroleum industry and in the synthesis of chemical items for different kinds of shape selective transformation and detachment processes. They create the fundamentals of new environment friendly technologies which involve cheaper and more efficient for performing chemical reactions. Transition metal modified microporous molecular filters with alumino-silicate and alumino-phosphate frameworks accelerate a wide range of artificially effective oxidizing transformations with impurity free oxidants like hydrogen peroxide under comparably light conditions, providing the advantage of recovering and recycling complex structures. MOFs are utilized in significant number of applications in waste treatment activities including detachment of heavy metals and radioactive species, ammonia, various kinds of phosphates and harmful gasses from soil, water and air because of having unique structural and physico chemical characteristics. In the earlier times, silica-aluminium based zeolite microporous materials were mainly used. In the recent days, several types of microporous materials are being produced with the aid of metal oxides, metal phosphates and inorganic-organic hydride materials [31].

2.6 Characterization of porous MOFs

As clearly explained, pore engineering is a powerful path to direct the structure and functionality of pores, which drastically promote the development of metal organic frameworks for recognizing differential molecules. It can be able to engineer the pores of metal organic frameworks by tuning their sizes or channels, functional sites and surface areas to achieve unique MOF materials to be utilized for specific gas separations [37].

This special characteristic makes metal organic frameworks unique regarding their structural properties, and which offers the desirable potential to use in different sectors. The comparably easiest production method of metal organic frameworks is one of the main reasons that they are a better choice for different applications. Their chemical properties, customized pore structure and thermal stability make them preferable for sound application domains such as separation of specific gases [39], catalysis [40] and conduction of protons [41]. Metal Organic Frameworks are usually characterized with the help of powder XRD (X-Ray Diffraction Method), surface area analysis, EM (Electron Microscopy), thermogravimetric analysis for predicting thermal stability of various constituents and Fourier Transform Infrared (FTIR) technique to characterize the molecules and atomic structures. Since Metal Organic Frameworks hold the nature of both crystalline materials as well as highly porous materials, usually powder X-ray diffraction (PXRD) is being used to characterize the adsorption measurements, phase purity and crystalline nature to check for the porosity [42].

2.7 Checking for permanent porosity

In order to ensure the permanent porosity, it needs determination of reversible gas sorption isotherms at low temperatures and low pressure conditions. Nevertheless, as we stated at that time [10], it was become a common place to mention the materials as “open framework” and “porous” though such validation was missing. The ultimate proof for permanent porosity of Metal Organic Frameworks can be obtained by estimating the carbon dioxide and nitrogen isotherms on layered zinc terephthalate metal organic framework [10]. The overall order of porosity in microporous molecular sieve depends on the template molecule, composition of inorganic materials, the condition of reaction and the formation mechanism.

A predominant advancement in the chemistry of metal organic frameworks happened in 1999 when the synthesis, determination of single crystal structure using x-ray diffraction, and low temperature – low pressure gas sorption characteristics were described for the first powerful porous MOF [11]. In order to prepare MOFs with further higher surface area, which require an increased storage space per weight of the component, that phenomenon is termed as ultrahigh porosity. Organic linkers with large length offer

larger storage space and more number of adsorption sites within a given component. Nevertheless, the more space within the framework makes it liable to make impregnating structures, in which two or more crystal frameworks get increased in size and mutually twirled together). By making metal organic frameworks whose topology obstructs impregnation, it can be effectively prevented from impregnation, which will require the further framework to be with a different topology [12, 13].

2.8 Advantages of MOF porous materials

The common advantages of MOF porous materials are presented in figure 4. The foremost advantage of metal organic framework porous materials is that the quantity of possible combinations of organic and inorganic parts to make the resulting expected structures is so excellent [17]. Moreover, MOFs hold some unique properties like luminescence [19] and magnetism [18] in comparison with other porous materials.

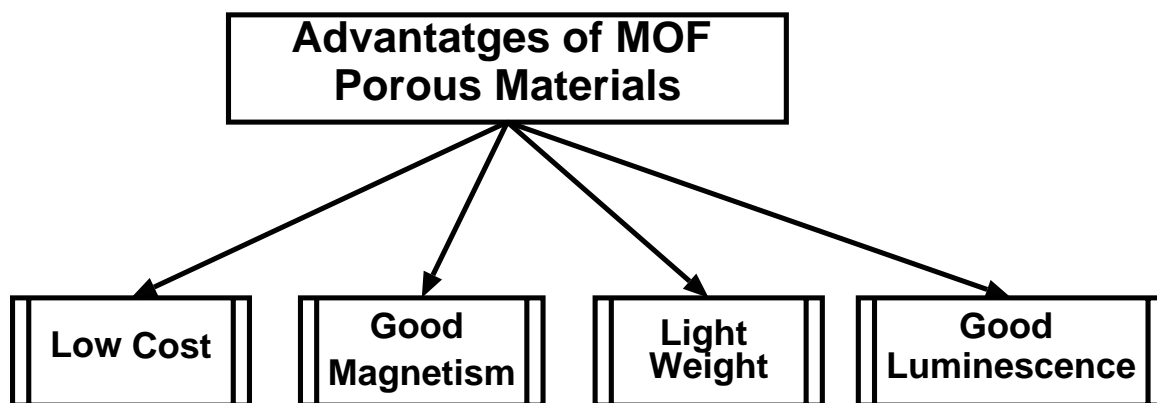


Figure 4 Common advantages of MOF porous materials [17].

MOFs have other few advantages such as low cost design, light weight, etc., which can probably be used to decrease the growing carbon dioxide level in the atmosphere due to burning of fossil fuels [65].

A tank charged with a porous adsorbent permits storing of a gas at a very low pressure than the similar tank without adsorbent. Thus, tanks with high pressure and multi stage compressors can be modified by providing a safe cum economical gas storage method. Many number of gas storage analyzes have been performed on porous adsorbents such as carbon nanotubes, activated carbon and zeolites [31].

2.9 Porous MOFs in separation of gases

As already discussed, MOF materials play vital roles in many application areas. Major application areas of MOF materials are tabulated in table 1.

Table 1. General application areas of MOF porous materials [10].

Sl.No	Application Area	Description
1	Pollution control	Low cost and light weight MOF porous materials are used to reduce the CO ₂ level in atmosphere.
2	Gas storage and separation	CO ₂ capture and CO ₂ separation from CH ₄ and N ₂ light HC separation, isomers separation, noble gases separation etc., are performed with the help of MOF porous materials.
3	Drug delivery	MOF porous materials are used to provide the therapeutic amount of drug to the proper site in the body to achieve promptly and to maintain the desired drug concentration.
4	Catalysis	MOF porous materials are being employed to catalyze transformations of existing petrochemical feedstocks.

The insight of the first few porous metal organic frameworks with permanent porosity implemented by gas adsorption analyzes significantly facilitated the development of these novel adsorbents for storing and separating gases [10, 32]. For separating specific gases, the early researchers conducted tests based on single component adsorption and/or desorption isotherm prediction of pure gases. The accumulation of sorption information (from number of metal organic frameworks) exhibited a positive potential for purification and separation of vapor or gas mixtures. However, normally separation of mixtures of gases with the help of metal organic frameworks was hardly understood until gas chromatography (a new evaluating method) was introduced into this field in the year 2005 [33]. In 2007, experimental fixed bed breakthrough also was applied on the prediction of separation of metal organic frameworks [34].

Based on these technologies, MOFs have revealed real separation of gas mixtures from their intrinsic porous properties. In turn, breakthrough experiment became a powerful tool for evaluating the separation of MOFs that can imitate the industrial process which cannot be implemented by a simple static – single component gas sorption analysis. Then, number of significant and challenging separations such as capturing CO₂, separating CO₂ from nitrogen or methane, separating light hydrocarbons, separating isomers, separating noble gases etc., have been accomplished by utilizing the unique MOFs as adsorbent materials [35-36].

2.10 Nanoporous MOFs

Currently, nanoporous materials are being focused with the view of nanoscience and nanotechnology that is an ever green multi-disciplinary domain of analysis, which

attracted lots of effort in R & D around the world. Nanoporous materials (as a subset of nanostructured materials) possess unique surface, structural, and chemical properties which show their importance in various sectors such as ion exchange [45], separation [46], catalysis [47], gas storage [48, 49&50], Li ion batteries [51], biological molecular isolation [52] and purification fields because of their flexible frameworks, uniform pore size, controlled chemistry and high internal surface area. In the recent years, porous materials are also extensively used in optical transparency, [53] photovoltaic solar cells [54], nanogenerators [55], nanotechnology [56], sensors [57], optoelectronic devices [58], biomedical imaging [59] and biomedical sciences [60]. However, they are capable of interacting with the atoms, ions and molecules at their surfaces as well as throughout the portion of the materials [44].

Hence, nanoporous materials also hold scientific technological and importance due to their flexibility to interact with atoms, ions and molecules on their large interior surfaces and in the pore space of nanometer size. They provide new opportunities in many areas including inclusion chemistry and guest-host synthesis [61].

Conclusion

The detailed description on porosity of Metal organic frameworks is presented in this chapter. The following salient points have been discussed throughout the chapter.

- Metal Organic frameworks are obtained by combining inorganic and organic contents with the help of strong bonds.
- Porous materials are naturally occurred. In addition to that, materials with porous nature are being intentionally artificially produced such as brick, concrete, cake, sponge, etc.,
- MOFs can be produced with comparable porosity with Zeolites and activated carbon.
- Characterization methods used to characterize the porous MOF materials have been elaborately discussed.
- MOFs possess high degree of structural and functional tenability.
- Porous MOF materials hold many advantages such as good magnetism, light weight, low cost and good luminescence.
- Due to the porous nature, MOFs are used in applications such as gas separation, gas storage, catalysis, drug delivery, etc.,

References

- [1] O.M. Yaghi, M.O. Keeffe, N.W. Ockwig, H.K. Chae, M. Eddaoudi, J. Kim, Reticular synthesis and the design of new materials. *Nature* 423 (2003) 705-714. <https://doi.org/10.1038/nature01650>
- [2] H.C. Zhou, J.R. Long, O.M. Yaghi, Introduction to metal-organic frameworks, *Chem. Rev.* 112 (2012) 673-674. <https://doi.org/10.1021/cr300014x>
- [3] U. Mueller, M. Schubert, F. Teich, H. Puetter, K.S. Arndt, J. Pastre, Metal-organic frameworks-prospective industrial applications. *J. Mater. Chem.* 16 (2006) 626-636. <https://doi.org/10.1039/B511962F>
- [4] M. Jacoby, Heading to market with MOFs, *Chem. Eng. News* 86 (2008) 13-16. <https://doi.org/10.1021/cen-v086n034.p013>
- [5] H. Deng, C.J. Doonan, H. Furukawa, R.B. Ferreira, J. Towne, C.B. Knobler, B. Wang, O.M. Yaghi, Multiple functional groups of varying ratios in metal-organic frameworks, *Science* 327 (2010) 846-850. <https://doi.org/10.1126/science.1181761>
- [6] A. F. Wells, *Structural Inorganic Chemistry* (Oxford Univ. Press, New York, 1984).
- [7] Y. Kinoshita, I. Matsubara, T. Higuchi, Y. Saito, The crystal structure of Bis(adiponitrilo)copper(I) nitrate, *Bull. Chem. Soc. Jpn.* 32 (1959) 1221-1226. <https://doi.org/10.1246/bcsj.32.1221>
- [8] O. M. Yaghi, H. Li, Hydrothermal synthesis of a metal-organic framework containing large rectangular channels, *J. Am. Chem. Soc.* 117 (1995) 10401-10402. <https://doi.org/10.1021/ja00146a033>
- [9] M. Kondo, T. Yoshitomi, H. Matsuzaka, S. Kitagawa, K. Seki, Three-dimensional framework with channelling cavities for small molecules: [M₂(4,4'-bpy)₃(NO₃)₄·xH₂O]_n (M = Co, Ni, Zn), *Angew. Chem. Int. Ed. Engl.* 36 (1997) 1725-1727. <https://doi.org/10.1002/anie.199717251>
- [10] H. Li, M. Eddaoudi, T. L. Groy, O. M. Yaghi, Establishing microporosity in open metal-organic frameworks: Gas sorption isotherms for Zn(BDC) (BDC = 1,4-benzenedicarboxylate), *J. Am. Chem. Soc.* 120 (1998) 8571-8572. <https://doi.org/10.1021/ja981669x>
- [11] H. Li, M. Eddaoudi, M. O'Keeffe, O. M. Yaghi, Design and synthesis of an exceptionally stable and highly porous metal-organic framework. *Nature* 402 (1999) 276-279. <https://doi.org/10.1038/46248>

- [12] H.K. Chae, D.Y.S. Perez, J. Kim, Y.B. Go, M. Eddaoudi, A.J. Matzger, M.O. Keefte, O.M. Yaghi, A route to high surface area, porosity and inclusion of large molecules in crystals, *Nature* 427 (2004) 523-527. <https://doi.org/10.1038/nature02311>
- [13] H. Furukawa, K.E. Cordova, M. O'Keeffe, O. Yaghi, The chemistry and applications of metal-organic frameworks, *Science* 341(2013) 974-986. <https://doi.org/10.1126/science.1230444>
- [14] Z.Y Gu, C.X. Yang, N. Chang, X.P. Yan, Metal-organic frameworks for analytical chemistry: from sample collection to chromatographic separation, *Acc. Chem. Res.* 45 (2012) 734-745. <https://doi.org/10.1021/ar2002599>
- [15] J.R.Li, J.Sculley, H.C. Zhou, Metal-organic frameworks for separations.*Chem. Rev.* 112 (2012) 869-932. <https://doi.org/10.1021/cr200190s>
- [16] R.C. Bansal, M. Goyal, Activated Carbon Adsorption from Solutions, In *Activated Carbon Adsorption*, CRC Press (2005) 145-199. <https://doi.org/10.1201/9781420028812.ch3>
- [17] S. Ma, Gas adsorption applications of porous metal-organic frameworks. *Pure Appl. Chem.* 81 (2009) 2235-2251. <https://doi.org/10.1351/PAC-CON-09-07-09>
- [18] Y.F Zeng, X. Hu, F.C Liu, X.H.Bu, Azido-mediated systems showing different magnetic behaviors, *Chem. Soc. Rev.* 38 (2009) 469-480. <https://doi.org/10.1039/B718581M>
- [19] M.D Allendorf, C.A.Bauer, R.K. Bhakta, R.J. Thouk, Luminescent metal organic frameworks, *Chem. Soc. Rev.* 38 (2009) 1330-1352. <https://doi.org/10.1039/b802352m>
- [20] J. Rouquerol, D. Avinr, H. Everett, C. Fairbridge, M. Haynes, N. Pernicone, J.D. F. Ramsay, K.S.W. Sing, K.K.Unger, Guidelines for the characterization of porous solids, *Stud. Surf. Sci. Catal.* 87 (1994) 1-9. [https://doi.org/10.1016/S0167-2991\(08\)63059-1](https://doi.org/10.1016/S0167-2991(08)63059-1)
- [21] J.R. Li, R.J. Kuppler, H.C. Zhou, Selective gas adsorption and separation in metal-organic frameworks *Chem. Soc. Rev.* 38 (2009) 1477. <https://doi.org/10.1039/b802426j>
- [22] S.M. Manocha, Porous carbons, *Sadhana* 28 (2003) 335-348. <https://doi.org/10.1007/BF02717142>
- [23] G. Ferey, Hybrid porous solids: past, present, future, *Chem. Soc. Rev.* 37 (2008) 191-214. <https://doi.org/10.1039/B618320B>

- [24] P. Horcajada, C. Serre, G. Maurin, N.A. Ramsahye, F. Balas, M. Vallet-Regi, M. Sebban, F. Taulelle, G. Ferey, Flexible porous metal-organic frameworks for a controlled drug delivery, *J. Am. Chem. Soc.* 130 (2008) 6774-6780.
<https://doi.org/10.1021/ja710973k>
- [25] Y.K. Park, S.B. Choi, H. Kim, K. Kim, B.H. Won, K. Choi, J.S. Choi, W.S. Ahn, N. Won, S. Kim, D.H. Jung, S.H. Choi, G.H. Kim, S.S. Cha, Y.H. Jhon, J.K. Yang, J. Kim, Crystal structure and guest uptake of a mesoporous metal-organic framework containing cages of 3.9 and 4.7 nm in diameter, *Angew. Chem. Int. Ed. Engl.* 46 (2007) 8230-8233. <https://doi.org/10.1002/anie.200702324>
- [26] K.S.W. Sing, D.H. Everett, R.A.W. Haul, L. Moscou, R.A. Pierotti, J. Rouquerol, T. Siemieniowska, Physical and biophysical chemistry division commission on colloid and surface chemistry including catalysis, *Pure Appl. Chem.* 57 (1985) 603-619.
<https://doi.org/10.1351/pac198557040603>
- [27] S.R. Batten, S.M. Neville, D.R. Turner, *Coordination polymers: design, analysis and application*, Royal Society of Chemistry, Cambridge, (2009) 1-424.
- [28] S. Ma, J. Eckert, P.M. Forster, J.W. Yoon, Y.K. Hwang, J.S. Chang, C.D. Collier, J.B. Parise, H.C. Zhou, Further investigation of the effect of framework catenation on hydrogen uptake in metal-organic frameworks, *J. Am. Chem. Soc.* 130 (2008) 15896-15902. <https://doi.org/10.1021/ja803492q>
- [29] W.E. Liss, W.H. Thrasher, G.F. Steinmetz, P. Chowdiah, A. Attari, Variability of natural gas composition in select major metropolitan areas of the United States, (1992) PB92-224617.
- [30] S.H. Yeon, S. Osswald, Y. Gogotsi, J.P. Singer, J.M. Simmons, J.E. Fischer, M.A. Lillo-Rodenas, A.L. Solano, Enhanced methane storage of chemically and physically activated carbide-derived carbon, *J. Power Sourc.* 191 (2009) 560-567.
<https://doi.org/10.1016/j.jpowsour.2009.02.019>
- [31] S. A. Jenekhe, X. L. Chen, Self-assembly of ordered microporous materials from rod-coil block copolymers, *Science* 283 (1999) 372-375.
<https://doi.org/10.1126/science.283.5400.372>
- [32] S.S.Y. Chui, S.M.F. Lo, J.P.H. Charmant, A.G. Orpen, I.D. Williams, A chemically functionalized nanoporous material $[\text{Cu}_3(\text{TMA})_2(\text{H}_2\text{O})_3]$, *Science* 283 (1999) 1148-1150. <https://doi.org/10.1126/science.283.5405.1148>
- [33] B. Chen, C. Liang, J. Yang, D.S. Contreras, Y.L. Clancy, E.B. Lobkovsky, O.M. Yaghi, S. Dai, *Angew.* A microporous metal-organic framework for gas-

chromatographic separation of alkanes, *Chem. Int. Ed.* 45 (2006) 1390-1393.

<https://doi.org/10.1002/anie.200502844>

[34] P.S. Bárcia, F. Zapata, J.A.C. Silva, A.E. Rodrigues, B. Chen, Kinetic separation of hexane isomers by fixed-bed adsorption with a microporous metal–organic framework, *J. Phys. Chem.* 111(2007) 6101–6103. <https://doi.org/10.1021/jp0721898>

[35] Z. Bao, G. Chang, H. Xing, R. Krishna, Q. Ren, B. Chen, Potential of microporous metal–organic frameworks for separation of hydrocarbon mixtures, *Energy Environ. Sci.* 9(2016) 3612–3641. <https://doi.org/10.1039/C6EE01886F>

[36] K. Adil, Y. Belmabkhout, R.S. Pillai, A. Cadiau, P.M. Bhatt, A.H. Assen, G. Maurin, M. Eddaoudi, Gas/vapour separation using ultra-microporous metal-organic frameworks: insights into the structure/separation relationship, *Chem. Soc. Rev.* 46 (2017) 3402–3430. <https://doi.org/10.1039/C7CS00153C>

[37] Y. Cui, B. Li, H. He, W. Zhou, B. Chen, G. Qian, Metal–organic frameworks as platforms for functional materials, *Acc. Chem. Res.* 49 (2016) 483–493. <https://doi.org/10.1021/acs.accounts.5b00530>

[38] B. Li, H.M. Wen, W. Zhou, B. Chen, Porous Metal–organic frameworks for gas storage and separation: what, how, and why?, *J. Phys. Chem. Lett.*, 5(2014)3468-3479. <https://doi.org/10.1021/jz501586e>

[39] A. Car, C. Stropnik, K.V. Peinemann, Hybrid membrane materials with different metal–organic frameworks (MOFs) for gas separation, *Desalination*, 200(2006)424-426. <https://doi.org/10.1016/j.desal.2006.03.390>

[40] F.X.L.I. Xamena, A. Abad, A. Corma, H. Garcia, MOFs as catalysts: Activity, reusability and shape-selectivity of a Pd-containing MOF, *J. Catal.* 250(2007)294-298. <https://doi.org/10.1016/j.jcat.2007.06.004>

[41] K.S. Park, Z. Ni, A.P. Cote, J.Y. Choi, R. Huang, F.J.U. Romo, H.K. Chae, M. O'keeffe, O.M. Yaghi, Exceptional chemical and thermal stability of zeoliticimidazolate frameworks. *Proc. Natl. Acad. Sci.* 103(2006) 10186-10191. <https://doi.org/10.1073/pnas.0602439103>

[42] N. L. Rosi, J. Eckert, M. Eddaoudi, D. T. Vodak, J. Kim, M. O'Keefe and O.M. Yaghi, Hydrogen storage in microporous metal-organic frameworks, *Science* 300 (2003) 1127-1129. <https://doi.org/10.1126/science.1083440>

[43] C. Prestipino, L. Regli, J. G. Vitillo, F. Bonino, A. Damin, C. Lamberti, A. Zecchina, P. L. Solari, K. O. Kongshaug, S. Bordiga, Local Structure of Framework Cu(II) in HKUST-1 Metallorganic Framework: Spectroscopic Characterization upon

Activation and Interaction with Adsorbates, *Chem. Mater.* 18 (2006)1337-1346.
<https://doi.org/10.1021/cm052191g>

[44] M.E. Davis, Ordered porous materials for emerging applications, *Nature* 417 (2002) 813-821. <https://doi.org/10.1038/nature00785>

[45] A.K. Patra, A. Dutta, A. Bhaumik, Self-assembled mesoporous γ -Al₂O₃, spherical nanoparticles and their efficiency for the removal of arsenic from water, *J. Hazard. Mater.* (2012) 170-177. <https://doi.org/10.1016/j.jhazmat.2011.11.056>

[46] M. Hartmann, Ordered mesoporous materials for bioadsorption and biocatalysis, *Chem. Mater.* 17 (2005) 4577-4593. <https://doi.org/10.1021/cm0485658>

[47] A. Taguchi, F. Schiith, Ordered mesoporous materials in catalysis *Micropor. Mesopor. Mater.* 77 (2005) 1-45. <https://doi.org/10.1016/j.micromeso.2004.06.030>

[48] D.J. Tranchemontagne, K.S. Park, H. Furukawa, J. Eckert, C. B. Knobler, O. M Yaghi, Hydrogen storage in new metal-organic frameworks, *J. Phy. Chem. C* 776 (2012)13143-13151. <https://doi.org/10.1021/jp302356q>

[49] A.Dutta, M. Pramanik, A. K. Patra, M. Nandi, H. Uyama, A.Bhaumik, Hybrid porous tin (IV) phosphonate: an efficient catalyst for adipic acid synthesis and a very good adsorbent for CO₂ uptake, *Chem. Commun.* 48 (2012)6738-6740.
<https://doi.org/10.1039/c2cc32298f>

[50] M. Nandi, K. Okada, A. Dutta, A. Bhaumik, J. Maruyama, D.Derks, H.Uyama, , Unprecedented CO₂ uptake over highly porous N-doped activated carbon monoliths prepared by physical activation, *Chem. Commun.* 48 (2012) 10283-10285.
<https://doi.org/10.1039/c2cc35334b>

[51] H.Liu,Z. Bi, X.-G. Sun, R. R. Unocic, M. P. Paranthaman, S.Dai, G. M. Brown, Mesoporous TiO₂-B microspheres with superior rate performance for lithium ion batteries, *Adv. Mater.* 23 (2011) 3450-3454. <https://doi.org/10.1002/adma.201100599>

[52] H. Wu, S. Zhang, J.Zhang, G.Liu, J.Shi, L.Zhang, X.Cui, M. Ruan, Q.He, W.Bu, A hollow-core, magnetic, and mesoporous double-shell nanostructure: In situ decomposition/reduction synthesis, bioimaging, and drug-delivery properties, *Adv. Fund. Mater.* 21(2011)1850-1862. <https://doi.org/10.1002/adfm.201002337>

[53] B.J. Scott, G. Wirnsberger, G.D. Stucky, Mesoporous and Mesostructured Materials for Optical Applications, *Chem. Mater.*13(2001)3140-3150.
<https://doi.org/10.1021/cm0110730>

- [54] S.E.Habas, H.A.S, Platt, M.F.A. M.Van Hest, D.S. Ginley, Low-cost inorganic solar cells: from ink to printed device, *Chem. Rev.* **110**(2010)6571-6594.
<https://doi.org/10.1021/cr100191d>
- [55] A.Stein, B.J.Melde, R.C. Schroden, Hybrid inorganic–organic mesoporous silicates-nanosopic reactors coming of age, *Adv. Mater.* **12** (2000)1403-1419.
[https://doi.org/10.1002/1521-4095\(200010\)12:19<1403::AID-ADMA1403>3.0.CO;2-X](https://doi.org/10.1002/1521-4095(200010)12:19<1403::AID-ADMA1403>3.0.CO;2-X)
- [56] I.W. Hamley, Nanotechnology with soft materials, *Angew.Chem. Int. Ed. Engl.* **42** (2003) 1692-1712. <https://doi.org/10.1002/anie.200200546>
- [57] D. Mao, J. Yao, X. Lai, M. Yang, J. Du, and D. Wang, Hierarchically mesoporous hematite microspheres and their enhanced formaldehyde-sensing properties, *Small* **7** (2011)578-582. <https://doi.org/10.1002/smll.201001728>
- [58] R.C.Hayward, P.A. Henning, B.F.Chmelka, G.D. Stucky, The current role of mesostructures in composite materials and device fabrication, *Micropor. Mesopor.Mater.* **44-45** (2001)619-624. [https://doi.org/10.1016/S1387-1811\(01\)00242-6](https://doi.org/10.1016/S1387-1811(01)00242-6)
- [59] S.Wang, Ordered mesoporous materials for drug delivery, *Micropor. Mesopor.Mater.* **117** (2009) 1-9. <https://doi.org/10.1016/j.micromeso.2008.07.002>
- [60] M.Vallet-Regi, F.Balas, D.Arcos, Mesoporous materials for drug delivery, *Angew.Chem. Int. Ed.Engl* **46** (2007)7548-7558.
<https://doi.org/10.1002/anie.200604488>
- [61] Y.Wan, H.Yang, D.Zhao, Host–Guest chemistry in the synthesis of ordered nonsiliceousmesoporous materials, *Ace. Chem. Res.* **39** (2006) 423-432.
<https://doi.org/10.1021/ar050091a>
- [62] S.L. James, Metal organic frameworks, *Chem. Soc. Rev.* **32** (2003) 276–288.
<https://doi.org/10.1039/b200393g>
- [63] M. Eddaoudi, D. B. Moler, H. L. Li, B. L. Chen, T. M. Reineke, M. O’Keeffe, O. M. Yaghi, Modular chemistry: secondary building units as a basis for the design of highly porous and robust metal-organic carboxylate frameworks, *Acc. Chem. Res.* **34** (2001) 319–330. <https://doi.org/10.1021/ar000034b>
- [64] I. Spanopoulos, I. Bratsos, C. Tampaxis, A. Kourtellaris, A. Tasiopoulos, G. Charalambopoulou, T.A. Steriotis, P.N. Trikalitis, Enhanced gas-sorption properties of a high surface area, ultramicroporous magnesium formate, *Cryst. Eng. Comm.* **17** (2015) 532-539. <https://doi.org/10.1039/C4CE01667J>

- [65] Z.J. Lin, J. Lu, M. Hong, R. Cao, Metal–organic frameworks based on flexible ligands (FL-MOFs): structures and applications, *Chem. Soc. Rev.*, 43 (2014) 5867-5895. <https://doi.org/10.1039/C3CS60483G>
- [66] W. Lu, Z. Wei, Z.-Y. Gu, T.-F. Liu, J. Park, J. Park, J. Tian, M. Zhang, Q. Zhang, T. Gentle Iii, M. Bosch, H.- C. Zhou, Tuning the structure and function of metal-organic frameworks via linker design, *Chem. Soc. Rev.* 43 (2014) 5561-5593. <https://doi.org/10.1039/C4CS00003J>
- [67] B. Liu, H. Shioyama, H. Jiang, X. Zhang, Q. Xu, Metal–organic framework (MOF) as a template for syntheses of nanoporous carbons as electrode materials for supercapacitor, *Carbon*, 48 (2010) 456-463. <https://doi.org/10.1016/j.carbon.2009.09.061>
- [68] P. Falcaro, D. Buso, A. J. Hill, C. M. Doherty, Patterning techniques for metal organic frameworks, *Adv. Mater.* 24 (2012) 3153–3168. <https://doi.org/10.1002/adma.201200485>
- [69] S.I. Noro and S. Kitagawa, *The supramolecular chemistry of organic-inorganic hybrid materials*, ed. John Wiley & Sons, Inc., (2010) 235–269. <https://doi.org/10.1002/9780470552704.ch7>

Chapter 11

Metal Organic Frameworks (MOF's) for Biosensing and Bioimaging Applications

Fulya Gülbağça¹, Kubilay Arıkan¹, Kemal Cellat¹, Anish Khan^{2,3}, Fatih Şen^{1*}

¹Sen Research Group, Department of Biochemistry, Faculty of Arts and Science, Dumlupınar University, Evliya Çelebi Campus, 43100 Kütahya, Turkey.

²Chemistry Department, Faculty of Science, King Abdulaziz University, Jeddah-21589, P.O. Box 80203, Saudi Arabia

³Center of Excellence for Advanced Materials Research, King Abdulaziz University, Jeddah 21589, P.O. Box 80203, Saudi Arabia

* fatih.sen@dpu.edu.tr

Abstract

Metal-organic-frameworks (MOFs) formed by combining between intermetallic ion bonds and organic bridge ligands are a class of nanomaterials. Due to their privileges such as structural porosity, flexibility, controllable synthesis, MOFs have been used in many applications and have shown a high-efficiency in biological detection and imaging. When compared with other nanomaterials, the MOF structures are foreseen for biological applications due to their biodegradability and compatibility advantages. Recently, MOF structures have been instrumental in the introduction of new generation technologies in clinical diagnoses such as detection of small biomolecules, DNA, RNA, enzyme activity, Magnetic Resonance Imaging (MRI) and Computed Tomography (CT). In this chapter, recent advances in biosensing and bio-imaging are reported in research for MOF.

Keywords

Biosensing and Bioimaging, Metal-Organic Frameworks, Enzymatic-MOF, Fluorescence, Computed Tomography, Magnetic Resonance Imaging

Contents

1.	Introduction.....	309
2.	In vitro MOF complex sensors	316
2.1	DNA-RNA-MOF complex sensor.....	316

2.2	Enzyme-MOF complex	319
2.2.1	Enzymatic-MOF complex	319
2.2.2	Non-enzymatic-MOF complex.....	320
2.3	Fluorescent-MOF complex.....	321
3.	In-vivo MOF complex sensors	330
3.1	MR complex	330
3.2	CT complex	331
	Conclusions and recommendations.....	334
	References	335

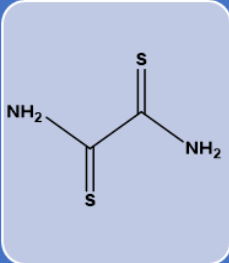
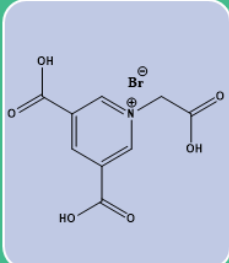
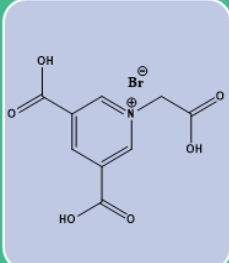
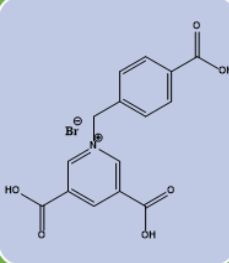
1. Introduction

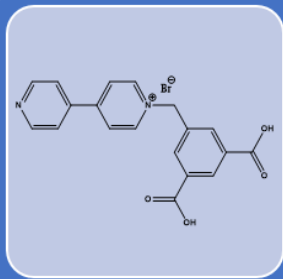
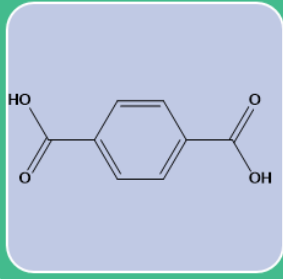
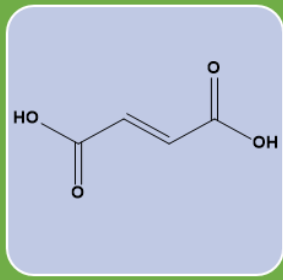
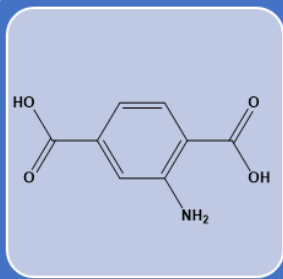
In recent years, metal-organic frameworks (MOFs) have been widely used in bioimmobilization support nanomaterials. Due to excellent porosity, multiple functionalities, stability, and wide surface area privileges, MOFs are highly appreciated for biological applications. Development of MOFs as biocatalysts; provides many advantages for new MOF-enzyme units such as recyclability, accessibility to more sites and high loading capacity [1–2]. In this section, it is aimed to discuss the recent studies on the biological applications of MOFs and the different approaches used in the development of MOF-enzyme biocatalytic supports.

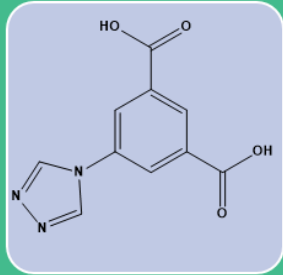
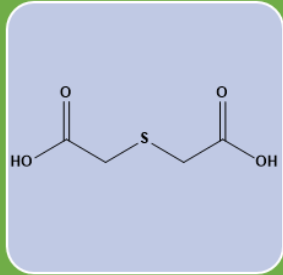
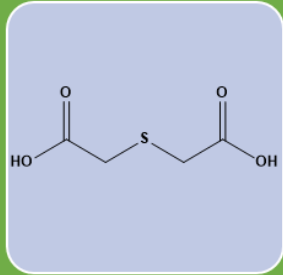
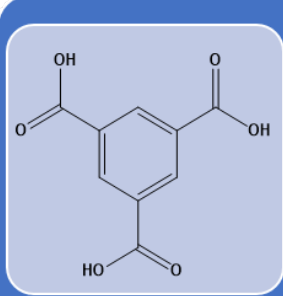
MOFs have been developed for an advanced level in clinical applications, in biosensing and bio-imaging analyzes to provide highly sensitive examinations. The manufacture of functional materials is of considerable importance, as examinations that result in sensitive detection are desired.

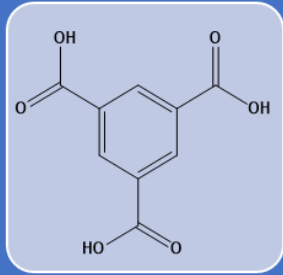
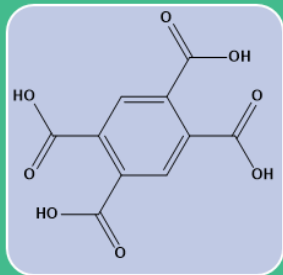
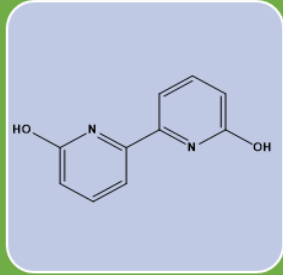
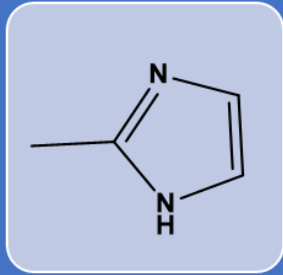
Firstly, in the design of biosensors, catalysts; graphene oxide (GO), metallic and silica nanoparticles, metal-organic frames (MOFs) and quantum dots are widely used [3–42]. MOFs with special functions have attracted considerable attention because they can recognize some particular molecules in the biosensor field [43–44]. The MOFs, which are the pioneers in comprehensive work, gave positive feedback in almost all of the studies (*Table 1*).

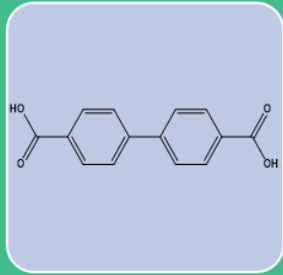
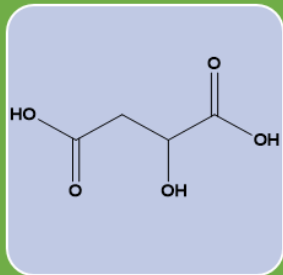
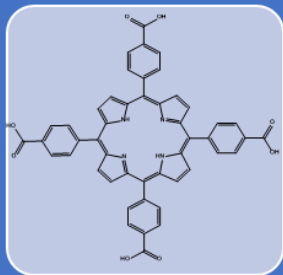
Table 1. Biosensing/sensing applications of MOFs.

	<p>Ligand abbreviation: H4DToA</p> <ul style="list-style-type: none"> • Metal: Cu²⁺ • MOF formula : [Cu(H2DToA)]_n • Surface area (m₂/g): - • Pore size (Å): 6 • Sensing targets: HIV DNA and thrombin, Protease • Roles of MOFs: Fluorescence quenching platform 	[45–47]
	<p>Ligand abbreviation: H3CmDcp</p> <p>Metal: Cu²⁺</p> <p>MOF formula : [Cu₃(CmDcp)₂(dps)₄(H₂O)₄(SO₄)_n]</p> <p>Surface area (m₂/g): 348</p> <p>Pore size (Å): 9.7 - 16.6</p> <p>Sensing targets: HIV DNA and SUDV RNA</p> <p>Roles of MOFs: Fluorescence Quenching platform</p>	
	<p>Ligand abbreviation: H3CmDcp</p> <p>Metal: Dy³⁺</p> <p>MOF formula : {[Dy(CmDcp)(H₂O)₃] (NO₃).2H₂O}_n</p> <p>Roles of MOFs: Fluorescence Quenching platform</p>	
	<p>Ligand abbreviation: H₃CbDcpBr</p> <p>Metal: Zn²⁺</p> <p>MOF formula : {[Zn(HCbDcp)₂].H₂O}_n</p> <p>Sensing targets: Fluorescence quenching platform</p> <p>Roles of MOFs: HIV DNA</p>	[50]

	<p>Ligand abbreviation: H₃CbdcpBr</p> <p>Metal: Zn²⁺</p> <p>MOF formula : {[Zn(HCbdcp)]₂·H₂O}_n</p> <p>Sensing targets: Fluorescence quenching platform</p> <p>Roles of MOFs: HIV DNA</p>	<p>[51]</p>
	<p>Ligand abbreviation: H₃CbdcpBr</p> <p>Metal: Cr³⁺</p> <p>MOF formula : [Cr₃F(H₂O)₂(BDC)₃·nH₂O]_n (MIL-101)</p> <p>Surface area (m₂/g): 5900</p> <p>Pore size (Å): 14.7 - 16</p> <p>Sensing targets: Fluorescence quenching platform</p> <p>Roles of MOFs: DNA</p>	<p>[52–53]</p>
	<p>Ligand abbreviation: FA</p> <p>Metal: Fe³⁺</p> <p>MOF formula : [Fe₃O(FA)₃Clz·3H₂O]_n (MIL-88A)</p> <p>Surface area (m₂/g): 347</p> <p>Pore size (Å): 5 - 7</p> <p>Sensing targets: Fluorescence quenching platform</p> <p>Roles of MOFs: DNA</p>	<p>[54–57]</p>
	<p>Ligand abbreviation: NH₂-BDC</p> <p>Metal: Zr⁴⁺</p> <p>MOF formula : [Zr₆O₄(OH)₄ (BDC-NH₂)₆]_n (UiO-66-NH₂)</p> <p>Surface area (m₂/g): 615</p> <p>Pore size (Å): 6,11</p> <p>Sensing targets: Fluorescence quenching platform</p> <p>Roles of MOFs: DNA</p>	<p>[58]</p>

	<p>Ligand abbreviation: TIA</p> <p>Metal: Gd³⁺</p> <p>MOF formula : [[Gd(TIA)(HCOO)]_n]</p> <p>Sensing targets: Fluorescence quenching platform</p> <p>Roles of MOFs: DNA and Hg₂⁺</p>	<p>[59]</p>
	<p>Ligand abbreviation: TDA</p> <p>Metal: Eu³⁺</p> <p>MOF formula : {[Eu₂(TDA)₃].2H₂O}_n</p> <p>Sensing targets: Fluorescence quenching platform</p> <p>Roles of MOFs: ROS</p>	<p>[60–61]</p>
	<p>Ligand abbreviation: TDA</p> <p>Metal: La³⁺</p> <p>MOF formula : {[La₂(TDA)₃].2H₂O}_n</p> <p>Sensing targets: Fluorescence quenching platform</p> <p>Roles of MOFs: DNA</p>	<p>[60–61]</p>
	<p>Ligand abbreviation: H3BTC</p> <p>Metal: Cu²⁺</p> <p>MOF formula : [Cu₃(BTC)₂(H₂O)₃]_n (HKUST-1)</p> <p>Surface area (m₂/g): 692</p> <p>Pore size (Å): 9</p> <p>Sensing targets: Fluorescence quenching platform, Catalyzer, MIP</p> <p>Roles of MOFs: DNA, Dopamine, H₂O₂, Protein</p>	<p>[62–68]</p>

	<p>Ligand abbreviation: H3BTC</p> <p>Metal: Fe³⁺</p> <p>MOF formula : [Fe₃F(H₂O)₂O(BTC)₂.nH₂O]_n [MIL-100(Fe)]</p> <p>Surface area (m₂/g): 1350</p> <p>Pore size (Å): 25- 29</p> <p>Sensing targets: Immobilization matrice</p> <p>Roles of MOFs: Glucose</p>	
	<p>Ligand abbreviation: H4BTEC</p> <p>Metal: Al³⁺</p> <p>MOF formula : {Al(OH)[H₂BTEC]₃ (H₂O/H₄BTEC)}_n (MIL-121)</p> <p>Surface area (m₂/g): 181</p> <p>Sensing targets: Fluorescent probe</p> <p>Roles of MOFs: Hippuric acid</p>	<p>[69–70]</p>
	<p>Ligand abbreviation: H2BPDC</p> <p>Metal: Eu³⁺ and Tb³⁺</p> <p>MOF formula : Eu_{0.6059}Tb_{0.3941}-ZMOF (MZMOF-3)</p> <p>Sensing targets: Fluorescent probe</p> <p>Roles of MOFs: Lysophosphatidic Acid</p>	<p>[71]</p>
	<p>Ligand abbreviation: MeIM</p> <p>Metal: Zn²⁺⁺</p> <p>MOF formula : [Zn(MeIM)₂]_n (ZIF-8)</p> <p>Surface area (m₂/g): 1079</p> <p>Pore size (Å): 3.4 - 11.6</p> <p>Sensing targets: Mimetic multienzyme</p> <p>Roles of MOFs: Glucose ,Oxidase</p>	<p>[72–75]</p>

	<p>Ligand abbreviation: BPDC</p> <p>Metal: Zn²⁺</p> <p>MOF formula : [Zn₈(ad)₄(BPDC)₆O.2Me₂NH₂, 8DMF, 11H₂O]_n (bio-MOF-1)</p> <p>Surface area (m₂/g): 943</p> <p>Sensing targets: Fluorescent probe</p> <p>Roles of MOFs: Dipicolinic acid</p>	<p>[76–77]</p>
	<p>Ligand abbreviation: Mal</p> <p>Metal: Cu²⁺</p> <p>MOF formula : {[Cu(Mal)(bpy)]_2H₂O}_n</p> <p>Pore size (Å): 4.25 - 9.95</p> <p>Sensing targets: Fluorescence quenching platform</p> <p>Roles of MOFs: Amino acids</p>	<p>[78]</p>
	<p>Ligand abbreviation: TCPP</p> <p>Metal: Zr⁴⁺</p> <p>MOF formula : [Zr₆(μ₃-OH)₈(OH)₈-(TCPP)₂]_n (PCN-222)</p> <p>Surface area (m₂/g): 2217</p> <p>Pore size (Å): 13 - 32</p> <p>Sensing targets: Catalyzer</p> <p>Roles of MOFs: Phosphoprotein</p>	<p>[79]</p>

Yaghi et al. also indicated to coordination networks or coordination polymers (CPs). Combined with inorganic binders and organic binder molecules, MOF, which is a hybrid material, provides the first step in the sensors that adapt to new generation technologies for fluorescent or luminescent production as well as porosity, controllability and flexibility properties, heterogeneous catalysis, gas storage, chemical detection, and biological applications. In these applications, the MOF is considered to be the most suitable one because of the presence of metal and ligand units in the fluorescent sensors [80–82]. Those, which provide the best possible fluorescent emission, for example, organic ligands containing aromatic and conjugated moieties. In addition, metal ions such as lanthanides in MOF may also contribute to photoluminescence. The loading of various molecules into the MOF structures, the content of the structures is proportional to the fluorescence intensity. Considering this, many studies have been carried out to develop

the MOF design, and there has been significant progress in the perception of gases, explosives, solvents, and biomolecules. The results of the study show very promising progress. Many MOF complexes exhibit low cytotoxicity, which is necessary for in vivo conditions. When MOF structures are reduced to nano size, nano-scale MOFs (nMOFs) occur. nMOFs are advantageous structures which are suitable for many utilizing areas. Since nMOFs are structures that are suitable for biodegradation, they are removed from the environment immediately after the task ends. NMOFs with these superior properties have become ideal structures for biosensing and bio-imaging. It can be examined the researches on MOF structures under four main topics; **DNA-RNA sensing, Enzyme-MOF complex, Flurosans Complex, MR / CT Complex.**

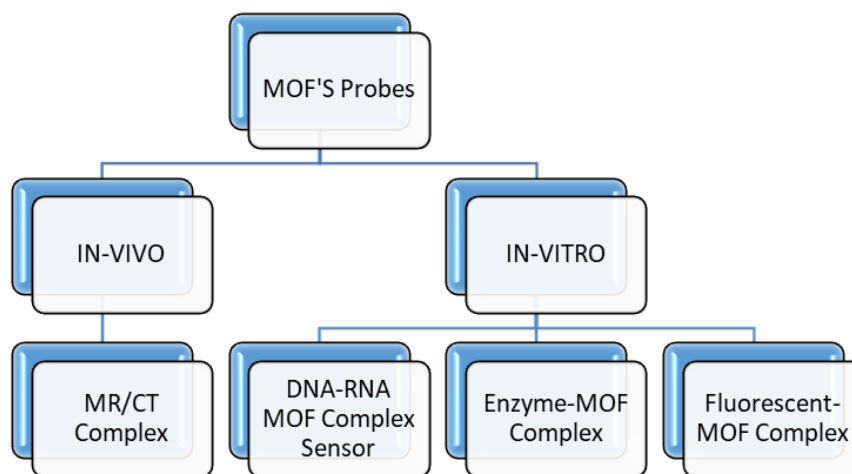
In Vivo Studies

- In studies of living tissues, MOF structures are used as ‘**extinguishers of fluorophores**’ in DNA or adenosine detection by attenuation of labeled DNA probes [83].
- MOF structures with fluorescent intensity are affected by target biomolecules [1];
- They are used in the unlabeled perception of biomolecules as a result of their combination with MOF structures as the key-lock model of bio enzymes.

In Vitro Studies

- Based on cell culture studies, MOF structures can be used in imaging applications such as **computed tomography (CT)** and **Magnetic Resonance Imaging (MRI)**.

Table 2. MOFs probes.



In researches carried out for MOF structures used in biosensing applications, it is clear that many types of MOF structures can be created and developed. Progressive multifunctional MOFs have shown many privileges in biosensing and bio-imaging. The development of MOF structures is significant for adaptation to new generation technologies for biosensors and biomarkers. However, besides the opportunities provided by the MOF structures, the challenges that need to be addressed [81–84–85]. With this researches, it is thought that MOFs will be developed and inspected in the field of bioscience and bio-imaging with a wider perspective.

2. In vitro MOF complex sensors

2.1 DNA-RNA-MOF complex sensor

The bases in the nucleotide unit are divided into two groups according to their ring structure. In the purine group, there is a double heterocyclic ring, while the pyrimidine group has a single heterocyclic ring. According to the sugar type, nucleic acids are divided into two groups as deoxyribonucleic acid (DNA) and ribonucleic acid (RNA). They are found in all living organisms and have important functions, such as coding, translation, and expression of genetic information [86]. DNA bases are Adenine (A), Guanine (G), Cytosine (C) and Thymine (T). The amount of Adenine (A) and Thymine (T) in the DNA molecule and Guanine (G) and Cytosine (C) were determined to be equal. The DNA molecule is also an interesting material in its applications due to its chemical stability, synthesis, and its unique design. Discoveries and extensive studies of metal-mediated natural and artificial base pairs significantly expand the design possibility of functional DNA molecules. The mercury-mediated T-T base pair ($\text{T-Hg}^{+2}\text{T}$) has been investigated for more than fifty years. Recent studies have shown that the Hg^{+2} ion is bound to the T pair, making the DNA duplex selectively was stranded significantly. Based on this case, DNA-based Hg^{+2} sensors were developed [87]. In addition to experimental studies, quantum chemical calculations can provide molecular-scale information about zeolite-adsorbate interactions, and also model the energetic changes and dynamics of important reactions in the channels and pores of zeolite catalysts [88]. Ag-DNA complexes have fluorophore properties. These alternative biomolecules have become an active research topic in recent years [86–89]. These probes are also used for precise and specific DNA detection. They are also seen as optical chromophore because they have various electronic spectra and wide emission intensities. Water-stable Ag-DNA complexes are used to elucidate the basic properties of metal molecules stabilized by microgels, peptides and DNA oligomers. These complexes are involved in the determination of various metal ions, molecular imaging and biological labeling. The theoretical calculations of Ag-DNA base pairs were performed by DFT and TD-DFT

methods. As a result of the calculations, Agn (n = 1-6) clusters were found to bind to the DNA molecule via nitrogen in base pairs [90]. The formation of Metallo-DNA complexes with metal-mediated base pairs allows the development of the genetic coding language and the formation of functionalized new DNA constructs. For example, metal modified DNA complexes contain information of pre-designed metallic structures, and metal-mediated base pairs reflect the properties of the metal to the DNA helix. As a result, there are many applications such as the design of sensors sensitive to various analytes, extraction of logic gates of Metallo-DNA structures, asymmetric catalysis, modified load transfer applications, etc. In recent years, many studies have been carried out on sensor studies. Metal-mediated nucleic acids can also be used in enantioselective catalysis. One of the studies in this area is on the Diels Alder reaction. Enantioselective Cu (II) -catalyzed Diels-Alder reaction was performed using copper-based DNA base pairs. Covalent binding is a general method of interacting DNA for the design of interactive anti-cancer drugs. DNA and chelate-forming platinum complexes typically exhibit anticancer activity. Many ruthenium (II) polypyridyl complexes have significant spectroscopic properties and relatively low toxicity. These complexes are used as ideal diagnostic agents because they are good DNA intercalators. Besides ruthenium, cobalt, gold, palladium and platinum metals are also used for this purpose. The design and synthesis of multifunctional nanomaterials can be used in biomedical applications, particularly in drug delivery and gene therapy as shown in Table 2 and 3. The production of porous particles for delivering bioactive molecules to living cells is an important target for the development of powerful tools for nanoparticles. Zeolite nanocrystals were used as multifunctional nanoparticles for the simultaneous transport of DNA oligonucleotides and organic molecules to living cells. While the multifunctional zeolite pore system was prepared by filling it with guest molecules, the DNA was electrostatically adsorbed to the surface. The kinetics of release of DNA and guest molecules into living cells has been investigated to prove the multidrug distribution capability of the system and the results obtained have been concluded that a new prototype can be created in this field.

Table 3. *MOF studies in the detection of biomolecules.*

	MOF types	MOF	Application type	Limit of detection (mM/ppm/ppb)	Ref.
Miscellaneous biosensing applications	Composite MOF structures	UiO-66-NH ₂ encapsulated metal ions (Cd ²⁺ or Pb ²⁺) and aptamer	Multiplex antibiotic detection	OTC - 0.18 pM KAN - 0.15 pM	[91–95]
		MOF-5	Sensing of BSA	-	
	Transition metal MOFs	Chitosan-immobilized Cu-MOFs and tyrosinase	Biosensing of bisphenols	15-33 nM	
		Ir-Zn ₆ MOFs	Biosensing of glucose	0.05mM	
	Heterometallic MOFs	Ir-Cd-Eggshell membrane-GOx layer	Biosensing of glucose	0.01mM	

Sensing of enzymes and proteins	REM MOFs	UiO-66-NH2	Detection of Hg ²⁺ ions using FAMlabeled ss-DNA	17.6 nM	[96–102]
	Transition metal MOFs	ATP-Ce-Tris	Artificial peroxidase-like activity and detection of H ₂ O ₂	0.6 nM	
		La-atp	Label-free assay of polyphenol oxidase	0.00012 U mL ⁻¹	
		HKUST-1	Detection of thiamine with intrinsic peroxidase-like activity	-	
	Heterometallic MOFs	Eu@Sc-MOFs	Detection of PS biomarker PGA in serum and urine	4.16 ppb	
	Composite MOF	Ru-PEI@ZIF-8 complex	Assay for telomerase activity	11 cells	
	structures	ZIF-8@BHB composites	Peroxidase-like activity and detection of H ₂ O ₂ and phenol	1.0 μM for each analyte	
Sensing of nucleic acids	Transition metal MOFs	Cd(L) ₂ (HDMA) ₂ (DMF)(H ₂ O) ₃ and Zn(L) ₂ (HDMA) ₂ (DMF)(H ₂ O) ₆	Nucleic Acid Detection	0.05 nM	[46–48–103]
		[Cu ₃ (Cmdcp) ₂ (dps) ₄ (H ₂ O) ₄ (SO ₄) _n] MOFs	Detection of HIV 1 ds-DNA and SUDV RNA Sequences	HIV DNA – 196 pM SUDV RNA – 73 pM	
		Cu(H ₂ dtoa)	Detection of HIV DNA and thrombin	DNA – 3Nm Thrombin – 1.3 nM	
LMOFs for bioimaging	REM MOFs	[Yb-PVDC-3]; [Yb-PVDC-1]	Cellular uptake and NIR Imaging	50	[104–108]
		Gd-MOF	MRI and cellular targeting	-	
		DBP-UiO	PDT of head and neck cancer	-	
	Heterometallic MOFs	Eu ³⁺ /Tb ³⁺ :Gd(BDC) _{1.5} (H ₂ O) ₂	Multimodal contrast imaging	-	
	Transition metal MOFs	MIL-101 (Fe ₃ -(μ ₃ -O)Cl(H ₂ O) ₂ (BDC) ₃)	Cisplatin Prodrug delivery and Br-BODIPY encapsulation for targeted imaging	-	
	Composite MOF structures	Gd(BDC) _{1.5} (H ₂ O) ₂ @SiO ₂ NPs	Controlled release of metal ions	-	
LMOFs as nanoreactors	REM MOFs	Tb-MOFs	Nanoreactor for the catalytic reaction of microperoxidase-11	-	[109–110]
	Transition metal MOFs	ZIF-8	Cytochrome C encapsulation	-	

2.2 Enzyme-MOF complex

The detection of macromolecules in biological applications is quite complicated. The fact that MOF structures have a very porous structure, elasticity, and fast decay properties make them compatible with enzymes and proteins. MOF structures used in many fields have become quite important for protein/enzyme sensors.

2.2.1 Enzymatic-MOF complex

In recent years, research has shown that enzyme biosensors are suitable in terms of sensitivity and cost, making them a focus of interest. The problems encountered in the immobilization of the substrate used in the experimental process, such as denaturation, transfer irregularity are the major problems in the development of enzyme biosensors. Solving these problems will accelerate the development of enzyme-based biosensors. In these biosensors, the main solution is installing the experimental enzyme most efficiently and improving the support matrix efficiently.

The organic binders in the content of MOF structures, which has the excellent porosity and the large surface area, are seen in Fig. 1.

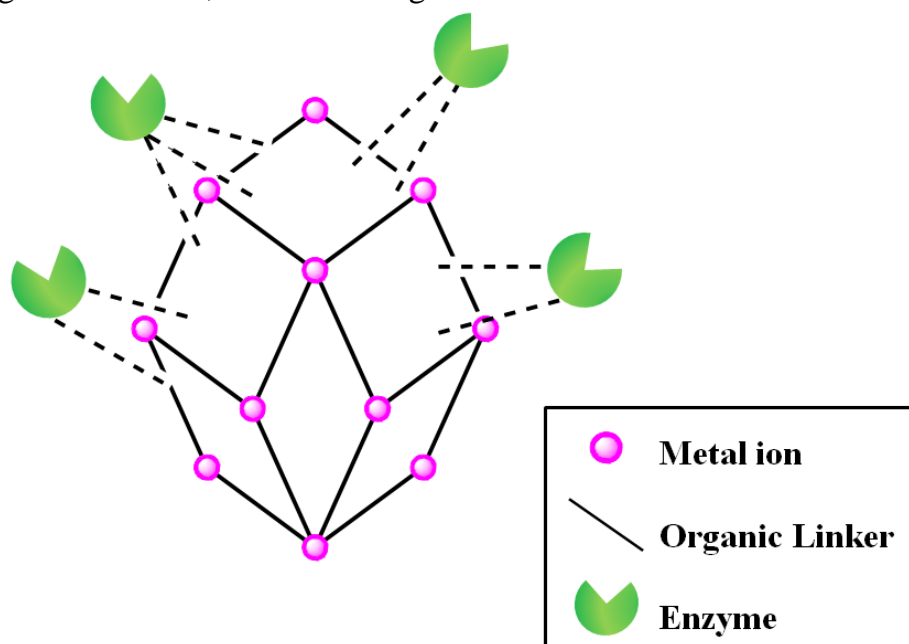


Fig. 1. Enzyme immobilization of MOFs.

More importantly, the porosity of MOFs shows excellent conductivity and stability. In the studies, Fe_2O_3 is mostly emphasized as semiconductor oxide, which becomes prominent with its environmentally friendly feature, and positive results have been obtained in many application such as being an anticorrosive agent, lithium-ion battery,

pigment, and sensor. In addition, the porous Fe_2O_3 nanomaterial can give a better reaction with biomolecules due to its advanced chemical properties.

Recent studies have focused on various methods on the synthesis of Fe_2O_3 . For example, Chen et al. tried to increase the lithium storage capacity of Fe_2O_3 by designing a multi-walled carbon nanotube with Fe_2O_3 nanoparticles [111]. Lou et al. produced a redox etching method for carbon-coated α - Fe_2O_3 nanoparticles using MnO_2 nanoparticles [112]. When looking at the content of research, the synthesis of carbon Fe_2O_3 contains complex, time-consuming and costly synthesis. If homogenous synthesis of Fe_2O_3 material can be achieved in the best way, the performance to be obtained will also increase. As a result, it will be the essence of nanomaterials and a new approach to the production of safe and sensitive biosensors.

In the development of enzyme biosensors studies, paraoxonase, which is a pesticide harmful to human health used in agriculture and hydrogen peroxide (H_2O_2), which is the target molecule that induces oxidative damage and affects cellular mechanisms is used [113–114]. In the development of enzyme-based biosensors, the detection of heme proteins produced by various metals [115] is interested; however, the MOFs [116], polymers [117] and graphene [118], etc used in the detection of H_2O_2 attracted attention. Although the studies become advanced level, some problems, such as enzyme denaturation, stability, and reproducibility deficiencies have still hampered the development of sensors.

For the formation of two-enzyme biosensors, direct calcination of $\text{Fe}_2\text{O}_3@\text{C}$, Fe-BTC was performed for immobilization of Mb/AChE on CPE and mixed with IL/NF to form two stable composite films used respectively. $\text{Fe}_2\text{O}_3@\text{C}$ material used to immobilize proteins and enzymes was found to contain highly active regions and performed high-performance electron transfer. In experimental studies, both sensors showed high sensitivity in detecting H_2O_2 and paraoxonase, and a low deviation was observed, such as 1.7×10^{-7} M and 1.2×10^{-14} M, respectively. The results show that $\text{Fe}_2\text{O}_3@\text{C}$ can provide better conjugation with biological compounds, improve electrochemical properties, and a successful electrode material for the production of multidirectional biosensors [119–123].

2.2.2 Non-enzymatic-MOF complex

Due to superior features of MOFs [124–125] produced for electron catalysis and photon catalysis, applications can be expanded in many fields such as luminescence [126], drug delivery [127], molecular recognition [128], proton and ion transmission [129–130]. Positive responses were obtained in Mn^+ molecule studies with MOF structures; Oxidation/reduction reactions of the target molecules were also carried out. Many

biomolecules have been studied for the application of MOF structures in the detection of toxic chemicals. Applications developed through MOF structures are still not enough due to high costs, low catalytic activity, low sensitivity, low linear range and low stability [131]. Studies on glucose [132–133], H_2O_2 [131–132–134–137], glutathione [138], tryptophan [139] and L-cysteine [140] have been insufficient. In order to improve the studies on the detection of biomolecules, it is necessary to eliminate the obstacles and shortcomings. When viewed from the glucose-related window, which is the energy source of the body, it can be used in the production of energy for normal activities [141]. Numerous studies have been conducted to address metal oxides [133] and metal nanoparticles to improve the non-enzymatic oxidation applications of glucose due to the many disadvantages [141–143]. When these studies are considered, Ni is more advantageous than other nanoparticles with its nontoxicity, low cost and high sensitivity [144–148].

2.3 Fluorescent-MOF complex

A wide range of research has been carried out in MOFs since the discovery of synthesis methods and the extension of their application areas (*Fig. 2*).

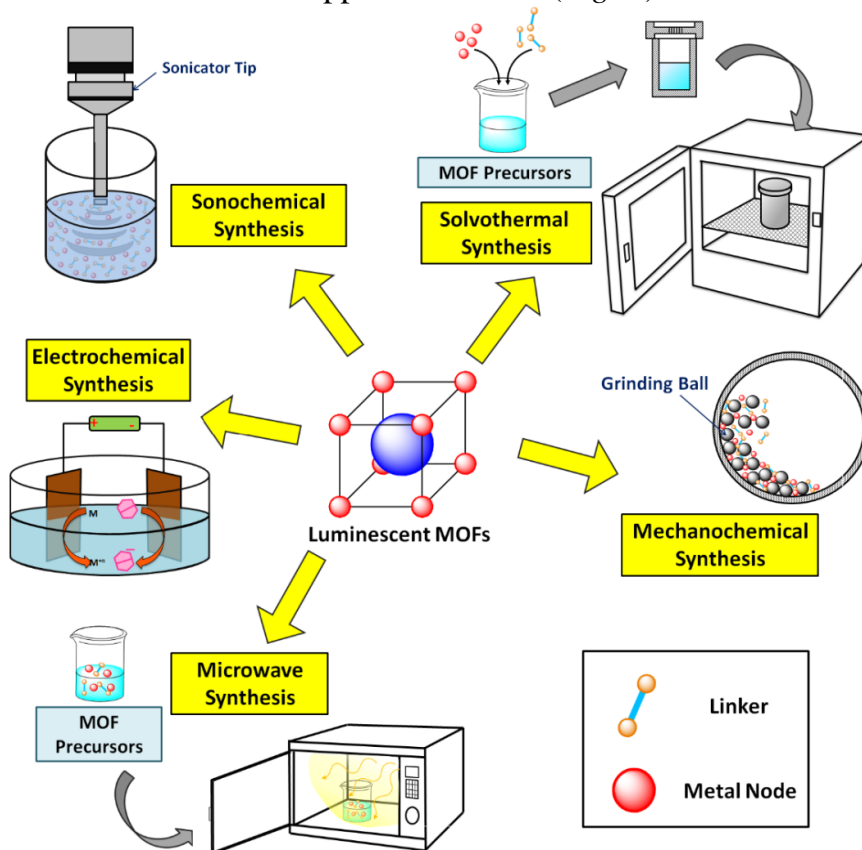


Fig 2. MOF synthesis diagram.

The simplified Jablonski diagram shows that the fluorophore (F) is stimulated by the singlet evoked electronic state (S1) and generates the induced fluorophore (F1). Fluorescence occurs when the F1 basic singlet returns with electronic emission (S0) photon emission. However, F1 can spin in a variety of ways, such as S0 a non-radiative relaxation and phosphorescence. Fluorescence damping is another important process that competes with fluorescence, where the intensity and/or life of the fluorescence falls as a result of interaction with a second molecule (F) with a damper (Q) (quencher). These interactions include stimulated state interaction, molecular rearrangement, energy transfer, charge transfer, basic state complex formation, and dynamic collision.

In fluorescence probe design for metal ions, the use of organic fluorophores and a specific chelating agent (receptor) as a fluorescent signal transducer is a common method. In this method, the metal receptor coordination will inform the presence of metal cation by causing excitation and emission maximum change, fluorescence intensity or lifetime. For the design of fluorescence probes, the interactions between the receptor and the fluorophore molecules are very important. Photo-induced electron transfer (PET) [149–151], fluorescence resonance energy transfer (FRET), photo-induced charge transfer (PCT) [151] and photo-induced excimer/exciple formation from conventional mechanisms are very common mechanisms for constructing the structure of probe molecules [152–153]. On the other hand, various methods have been investigated in the probe design such as aggregation-induced emission (AIE) and metal ion coordination inhibited excited-state intramolecular proton transfer (ESIPT) [154].

The most widely used mechanism in the design of fluorescent probes is the PET mechanism [150]. Classic metal cation PET probes are composed of three parts: spacer, ionophore, and fluorophore. While fluorophores form the electron acceptor moiety, the ionophore is usually electron donor moiety, such as containing amino groups. For the free probe, the electron that occupies the highest-filled molecular orbital (HOMO) is the lowest null molecular orbitale (LUMO) elevation by the excitation of the excitation photon. If the HOMO energy of the fluorophore is slightly lower than the ionophore, the electron within the ionophore HOMO will pass through the range to the HOMO of the evoked fluorophore. Hence, the transition of the excited electron from the fluorophore LUMO to the fluorophore HOMO will be prevented. This damping effect of fluorescence is called PET. When the ionophore is bonded to the target metal ion by a coordination bond, the energy range between the two HOMOs varies from positive to negative, by the metal coordination of the ionophore due to the HOMO level drop, and the fluorescence of the probe. This is defined as increased fluorescence (MCHEF) based on metal chelate formation. This is based on the release of the metal complex resulting from the relaxation of the state of the organic fluorophore stimulated by $\pi-\pi^*$. At the same time, one of the

reasons for the blockage of the PET procedure may be the protonation of the ionophore. The PET mechanism has been thoroughly addressed in the last thirty years, and several metal ion PET probes have been reported. In addition, PET probes may not be operated due to some deficiencies. For example, near-infrared (NIR) fluorescence probes are currently preferred than those with shorter excitation/emission wavelengths, because they have higher tissue penetration and lower phototoxicity. This results in a reduction of the energy range and reduces the efficiency of the free probe damping of the PET process [155]. Therefore, factors such as increasing of low analyte emission and high background fluorescence affect the NIR probes that work with the PET mechanism. Accordingly, designs of IR activated turn-on NIR probes with low background fluorescence are still challenging. Furthermore, metals with a certain weight, such as Hg^{+2} , may cause fluorescence damping with a number of mechanisms [156–160], and in the d-orbitals, non-matching metal-metal ions are capable of absorbing organic fluorophore emissions with unpaired electrons as seen in Cu^{+2} [161]. Therefore, changing the metal paramagnetic structure and the spin-orbital coupling by changing the ionophore and spacer structures and the detailed adjustment of the metal coordination is very important in the design of turn-on PET probes. Recently, two-photon stimulating probe with practical bioimaging applications with the PET mechanism has attracted the attention of researchers.

S. Lee et al. reported a new and easily prepared rhodamine-based Hg^{+2} sensor containing the pyridine unit and presented its structural characterization. This rhodamine derivative (RP) sensor can detect Hg^{+2} in $\text{CH}_3\text{CN}:\text{H}_2\text{O}$ (7:3, v/v) with both a significant color change and switch-on fluorescence [162]. D.-H. Kim et al. Have presented a promising analytical approach to detect Hg (II) in water without organic co-solvents and to detect a simple amino acid-based fluorescent sensor in living cells [163]. H. Zhu and others have developed a sensitive and selective fluorescence method to detect mercury ion in an aqueous medium containing a small amount of non-ionic surfactant [164].

C. Wang et al. have developed a new single-molecule FRET-based fluorescence sensor that can detect (ratiometric) and reversibly detect Hg^{+2} in aqueous solutions [165]. A. Han et al. have developed a new water-soluble fluorescent sensor that displays sensitive, selective and rapid fluorescence attenuation of Hg^{+2} ion in pH = 5.0 buffer solution [166]. L. Xu et al. have developed a new turn-on probe based on photochromic bisthenylene-rhodamine 6G that can detect Hg^{+2} with obvious color and fluorescence changes [167]. Li et al. performed the design and synthesis of the 1,8-naphthalimide derivative M1 containing the thiourea unit in the imidazole nitrogen for selective determination of the Hg^{+2} ion. In addition, Hg^{+2} recognition characteristics of the substance were investigated by UV-vis and fluorescence spectroscopy [168]. R. Kavitha et al. have developed a

simple, low-cost, efficient and water-soluble 2HNQ: β -CD that can be used for specific determination of transition metal ions. This chemo sensor shows high selectivity and sensitivity to toxic Hg^{+2} ions in neutral aqueous media [169]. M. Wang et al. developed a new 2,4-dichloroquinazoline-based chemosensor with selectivity, sensitivity in Hg^{+2} ion buffer solution. Background metals showed little or no interference in the detection of Hg^{+2} ion [170].

S. Liu et al. performed the design and synthesis of a series of near IR fluorescence probes. A wide range of absorption and emission bands of probes is possible by connecting different aromatic substituents to the aza-BODIPY unit. The probes exhibit emission damping and color change in solution in the presence of Hg^{+2} [171]. D. Udhayakumari et al. have synthesized Schiff bases that act as a sensitive chemical sensor. They investigated the chemical properties of the sensors in the aqueous analyte solution. They stated that the sensors could detect Fe^{+2} , Cu^{+2} , Hg^{+2} , Cr^{+2} ions with significant color changes in the presence of other metals [172].

N. Wanichacheva et al. performed the design and synthesis of a new FRET fluorescence sensor. For the determination of Hg^{+2} ion, the two rhodamine B fluorophores were bound by hydrazide [173]. N. Wanichacheva et al. have synthesized two new fluorescence sensors for use in Hg^{+2} ion detection. The sensing mechanism of the sensors is realized by covalently bonding the rhodamine-6G moieties of 2-[3-(2-aminoethylsulfanyl) propylsulfanyl] ethanamine to one and two units [174]. R. Puingam and others have synthesized a new rhodamine 6G derivative sensor to determine heavy metal. The sensor reported that it selectively selects Hg^{+2} ions in the presence of other metals in the aqueous medium [175]. X. Wang et al. have synthesized two new hydrazide-based fluorescence probes to be used for the determination of Cu^{+2} and Hg^{+2} ions. These chemosensors show higher affinity and selectivity to Cu^{+2} and Hg^{+2} ions than various other metals [176].

Table 4. Various MOF applications.

							Ref.
[Eu(PDC)1.5(DMF)]·(DMF) 0.5·(H ₂ O)0.5	320	590, 615	Na ⁺ , K ⁺ Mg ²⁺ , Mn ²⁺ , Cd ²⁺ , Cu ²⁺	5D ₀ →5F ₁ , 5D ₀ →5F ₁	0.2 – 89.4	Binding of pyridyl nitrogen atoms to Cu ²⁺	[177–181]
ZnMGO composite	310	442	Cu ²⁺	n-n*	3.07×10 ⁴	Effective electronic transition followed by the collapse of the framework	
[Tb ₃ (L) ₂ (HCOO)(H ₂ O) ₅]	~327	491, 545, 585, and 621	Cu ²⁺	5D ₄ →7F ₆ , 5D ₄ →7F ₅ , 5D ₄ →7F ₄ , 5D ₄ →7F ₃ ,	0.2×10 ⁴ (Cu) 70 ppm (nM)	Presence of bare Lewis basic sites	
BPEI-CQDs/ZIF-8 composites	360	440	Cu ²⁺	-	80 pM	Synergic effect of accumulation and quenching	
[[Eu ₂ (abtc)1.5(H ₂ O) ₃ -(DMA)]·H ₂ O·DMA] _n	365	470–490	Cu ²⁺	-	529	Diffusion of Cu ²⁺ into the adoptable channels or interlayer of MOF	

MOF	Excitation Wavelength (nm)	Emission Wavelength (nm)	Target Analyte	Emission/ Excitation transition	limit of detection [Stern– Volmer constant (K _{sv}) M ⁻¹ /ppm/ppb]	Mechanism
-----	----------------------------	--------------------------	----------------	---------------------------------	---	-----------

$[\text{Ln}_4(\mu_3\text{-OH})_4(\text{BPDC})_3(\text{BPDCA})_0.5(\text{H}_2\text{O})_6]\text{ClO}_4 \cdot 5\text{H}_2\text{O}]_n$ (Ln=Tb and Gd)	300	489, 544, 583, and 622	Cu^{2+}	$5\text{D}_0 \rightarrow 5\text{F}_1$ (J=6-3)	344.9 ± 10.2	Weak interaction of metal ions with Lewis basic sites of the MOF	[182–184]
$\text{Eu}_2(\text{FMA})_2(\text{OX})(\text{H}_2\text{O})_4 \cdot 4\text{H}_2\text{O}$	394	591, 616, 650 and 692	Cu^{2+}	$5\text{D}_0 \rightarrow 7\text{F}_1$, $5\text{D}_0 \rightarrow 7\text{F}_2$, $5\text{D}_0 \rightarrow 7\text{F}_3$, $5\text{D}_0 \rightarrow 7\text{F}_4$	528.7	The binding of Cu^{2+} with the Lewis basic carboxylate oxygen sites within the pore surface of MOF	
Eu [HODA]	305	614	Fe^{3+}	$5\text{D}_0 \rightarrow 7\text{F}_2$	2.09×10^4	Possible coordination to the uncoordinated carboxyl groups of MOFs	
$[\text{Zn}_2(\text{TPC4A})(\text{DMF})(\text{H}_2\text{O})_4] \cdot 3\text{H}_2\text{O}$ (1) and $[(\text{CH}_3)_2\text{NH}_2]_2[\text{Zn}(\text{TNC4A})] \cdot 4\text{H}_2\text{O}$ (2)	395 and 322	325, 371 nm	Fe^{2+} and Fe^{3+}	$\pi^* \rightarrow \pi$ or $\pi^* \rightarrow n$	-	Size effect of the guest molecules	[76–185]
Bio-MOF-1	365	415	Ln^{3+}	-	-	A phonon-assisted mechanism from either the triplet state or a metal-to-ligand charge transfer state of the sensitizer or an internal double-electron transfer mechanism	
Eu[BDC-NH ₂][DMF]	333	579, 593, 614, 650, and 697	Li^+ , Mn^{2+} , Zn^{2+} , Cd^{2+} , Ni^{2+} , Cu^{2+} , Fe^{2+} , Fe^{3+} , and Al^{3+}	$5\text{D}_0 \rightarrow 7\text{F}_J$ (J=0-4)	$(0.0019-3.8) \times 10^4$	Interaction between metal cations and organic ligands	[186–188]
$[(\text{CH}_3)_2\text{NH}_2]_2[\text{Eu}_6(\mu_3\text{-OH})_8(\text{BDC-F})_6(\text{H}_2\text{O})_6]$	277	580, 595, 616, 654, and 693	Cr^{2+} and Fe^{3+}	$5\text{D}_0 \rightarrow 7\text{F}_J$ (J=0-4)	9690 and 7520	Synergic effect of donor groups and non-radiative vibrations	
Eu-BDC-NH ₂ MOFs	278	592, 615, 700	Co^{2+}	$5\text{D}_0 \rightarrow 7\text{F}_2$	0.7M	Cyanocobalamin induced turn on fluorescence	

Eu ₂ [BDC]3(H ₂ O) ₂ ·(H ₂ O) ₂	315	590, 617 and 698	Nitro aromatic Explosives	5D ₀ →7F ₂	-	Competition between absorption the light source energy and the electronic interaction between analytes and BDC moieties
[Cd ₃ (TPT) ₂ (DMF) ₂ ·(H ₂ O) _{0.5}	333	390	Picric acid	-	6.56×10 ⁴	The polarizability of PA in an ethanol solution and π-π interaction between the analytes and host framework
[Cu(L)(I)] ₂ n·2nDMF·nMeCN	418	728	Nitro aromatic Explosives, Heterocycles	mixed iodide (I) to Cu(I) charge transfer and [3d→4s/4p] Cu ₂ I ₂ core-centered transition	-	Resonance energy transfer, which is reasonable for the confinement of analytes in the pores of the MOF
Tb+3@NENU-522 ([Zn ₄ O(L) ₃ (H ₂ O) ₂] ₃ -[Zn ₄ O(L) ₃] ₃ •xDMF)	333	489, 545, 588, and 622	Nitro aromatic Explosives	5D ₄ →7F _J (J=3-6)	80-2000 ppm	Energy transfer from the electron-donating groups to electron-deficient species
Eu MOF/CdSe QDs	300	550, 590, 615, 650, and 700	TNT	5D ₀ →7F _J (J=0-4)	3 ppb	Interaction between analyte and organic ligand
Tb[BTC]	300	544	DNT	5D ₄ →7F ₀ , 5D ₄ →7F ₃ , 5D ₄ →7F ₄ , 5D ₄ →7F ₅	23 ppm	Surface area related to the properties of the dopant
UiO-66-NH ₂	328	431	Nitrobenzene	π→π* transition of missing linker induced Zr clusters	0.91 ppm	Electron transfer from the excited missing linker induced sites
[Cd(atc)(H ₂ O) ₂] _n	352	424	Parathion	-	1 ppb	Bioconjugation
Zn ₃ (BTC) ₂ ·12H ₂ O	327	414	Organ amines	-	-	Interaction between open metal sites and guest molecules, diffusion of analyte into the channel

[189–197]

Eu [HODA]	305	614	Methanol	5D0→7F2	6.4 ppb	Weakening of the energy transfer of HODA3- in the presence of analyte	[184–198–202]
ZIF-8	-	-	Methanol, propylene, benzene, toluene, and styrene	-	29-99 ppb	-	
UiO-66-NH ₂	328	431	Formaldehyde	$\pi \rightarrow \pi^*$ transition of missing linker induced Zr clusters	4 ppm	Non-covalent bond formation between analyte and ligand units of the MOF	
[Eu ₂ (μ_2 -pzdc)(μ_4 -pzdc)(μ_2 -ox)(H ₂ O) ₄]	308	591, 614, 649, and 695	Acetone	-	5.75 vol%	Hydrogen bonding interactions between coordinated water molecules and acetone	
Yb(BPT)(H ₂ O)(DMF)1.5(H ₂ O)1.25	304	980	Acetone	-	5 vol%	Diffusion-controlled process	
Ag ⁺ /Eu ³⁺ :UiO-66(Zr)-(COOH)	330	613	Formaldehyde	5D0→7FJ (J=0-4)	-	Interaction with Ag ⁺ and its induced luminescence change	
[[Eu ₂ (L) ₃ (DMF) ₂].DMF.MeOH]	294	592, 616, 652 and 704	Polychlorinated benzenes	-	-	Self-adsorption or energy transfer process	[181–203]
[[Eu ₂ (abtc)1.5(H ₂ O) ₃ -(DMA)].H ₂ O.DMA] _n	365	470-490	Benzaldehyde	-	0–7.9%	OeH...O hydrogen bonds between benzaldehyde and MOF	

[Eu ₂ (phen) ₂ (fdc) ₃ ·2(H ₂ O)] _n	344	613.5	H ₂ S, CO ₂ , CH ₄ , and C ₂ H ₆	5D ₀ →7F _J (J=0-4)	-	Affinity of gaseous molecules with the surface of the MOF	[204–207]
Eu: In-BTC	285	618	Thiols	5D ₀ →7F ₀ , 5D ₀ →7F ₁ , 5D ₀ →7F ₂ , 5D ₀ →7F ₄	-	Coordination binding of coordinatively unsaturated metal centers	
Zn ₂ (TCPE) and Mg(H ₂ DHBDc)	350	487 and 511	Ammonia		-	Differential strength of analyte binding to the Zn ²⁺ ions in the Zn ₂ (O ₂ C-) ₄	
Cu-TCA	350	430	NO	π→π* transition of triphenylamine	-	The coordination of NO to the Cu(II) ions of the MOF reduces Cu ²⁺ centers to Cu ⁺	
Al-MIL-101-NH ₂	396	451	pH Sensor	-	pH=4	Proton transfer mechanism	[208–210]
JXNU-3(Tb)	327	544	pH Sensor	5D ₄ →7F ₅	-	Energy transfer from ligand to metal ion	
Nd _{0.577} Yb _{0.423} BDC-F	808	Yb ³⁺ =980 Nd ³⁺ =890, 1060, and 1350	Heat Sensing		0.816% K-1	Thermally-driven phonon assisted transfer mechanism	

3. In-vivo MOF complex sensors

3.1 MR complex

Magnetic resonance imaging (MRI) is the most common medical imaging technique for tissue contrast resolution in routine clinical use. Specifically, the acuity of showing soft tissues indicates that many diseases can be accurately visualized. In addition, the ability to show vessels without any intervention or medication in some cases eliminates the need for conventional angiography. MR angiography can be used to show all vascular body structures. In addition, functional images, 3D images, and moving images are possible to diagnose using MRI. MRI does not contain X heat that can be harmful due to its magnetic field strength. With this feature, it can be used for diagnostic purposes in infants and pregnant women. In radiological diagnostic methods, the best method of separating soft tissues from each other is the MRI method which can detect water protons in high molar concentration [211].

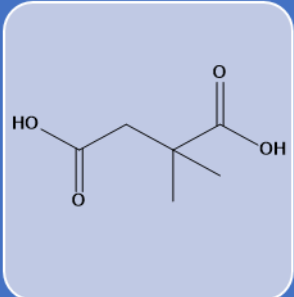
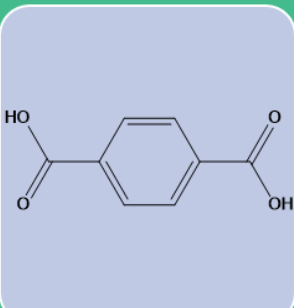
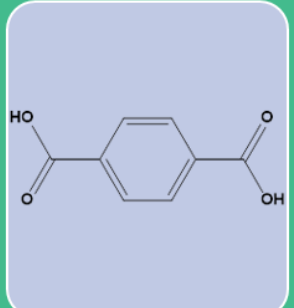
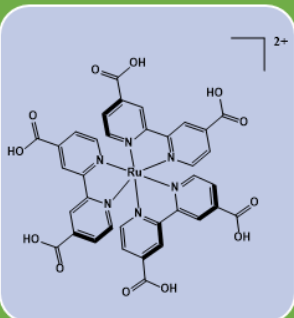
Materials for aligning the magnetic field are superparamagnetic materials, and nanoparticles such as iron oxide are used [212]. The relaxation value of the efficacy of an MRI contrast agent is expressed as r_1 in the positive state, while in the negative state it is expressed as r_2 . The smaller the particle size corresponds to the higher the relaxation (r_1) value, which means the relaxation values of the NPs are inversely proportional to their size. With the development of nano-scale metal organic frames (nMOFs), many studies are showing that the relaxation of magnetic nanoparticles has been improved (table 4) [213–214]. For example, in a study on the development of nanocrystalline-antibody probe systems, it has been reported that a synthetic nanocrystalline model system, which is synthetically controlled, achieves high efficiency in the detection of breast cancer cells by MRI [215]. It has also been reported that the use of MnFe_2O_3 nanocrystals is used in vivo MRI experiments in mice by the development of an antibody conjugate (Herceptin) in which cancer cells can be targeted [216]. Hybrid NPs with gold nanostructures have been reported for in vivo MRI showing good MRI signal in hepatoma. Here, each section provides a distinct signal that improves detection. The efficacy of nMOFs containing Gd^{+3} as the T1-weighted contrast agent was first reported [213]. They showed that samples 3 and 4 had a greater order than that of Omniscan, a small molecule contrast agent clinically used in 3T. Since the toxicity of nMOFs containing Gd^{+3} was uncertain, Mn-based nMOF was developed for T1-weighted contrast enhancement. In terms of toxicity, Mn^{+2} ions are reported to have a strong MRI contrast agent as well as having a lower than free Gd^{+3} [217].

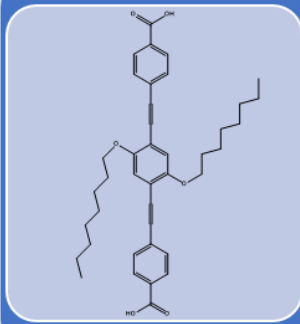
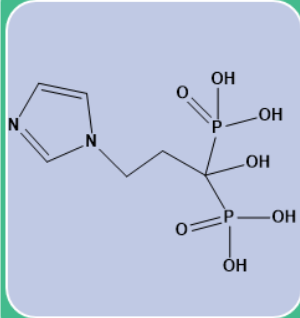
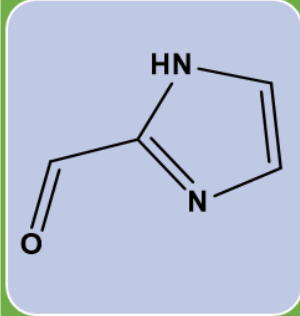
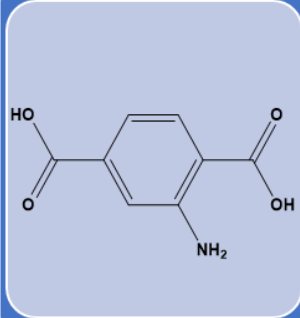
3.2 CT complex

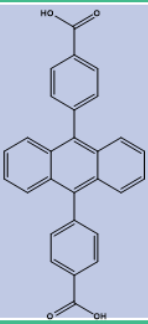
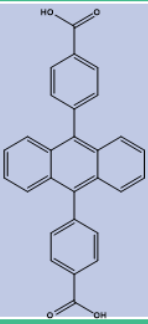
The CT imaging, which is based on the weakening of the X-rays, provides optimum 3D images in the spatial resolution [218]. As CT contrast agents, elements such as bismuth, barium, and iodine are typically used. However, they must be used in high doses to achieve efficient results. According to recent research, nMOF structures were produced and iodixanol, a contrast agent containing Zn^{+2} (18), Cu^{+2} (17) and I4 BDC, was reported to have slightly higher X-ray attenuation. The contributions of metal centers cause high nanoparticle attenuation. Therefore, nMOFs used for CT imaging must provide a platform that will contain other higher Z elements.

Typically, the use of special detectors that count the spectral CT single X-ray photons and divide their energies into more than three energy windows (compartments) is completely different from the integration of detectors for conventional and dual energy CT. The identification of K-edge discontinuities in the attenuation section of some metals and the quantitative determination without background signal can be made by a plurality of selective energy measurements. So far, K-edge has been explored for several heavy metals such as gold and bismuth [219–220]. In a phantom study, the potential use of iodine and gadolinium for the simultaneous visualization of two metals is shown [221]. Unlike blood pool contrast agents, a unique challenge in the design and synthesis of the targeted spectral CT agent is the necessity of very high metal content (about 500,000 metal atoms/nanoparticles) to obtain measurable concentrations with the density of the given binding regions [220]. Although iodine is the cornerstone of CT contrast agents in traditional blood pooling, low K-margin of iodine ($Z = 53$, $k = 33.2$ keV), for spectral CT applications in humans, suffers from photon hunger and ultimately through modeling to achieve poor yield [222]. Although gold ($Z = 79$, $k = 80.7$ keV) is attractive with K-edge energy and high atomic numbers, the cost of this precious metal, which is necessary for human diagnostic studies, excludes the translation into the clinic.

Table 5. Bioimaging applications of MOFs.

	<p>Ligand abbreviation: C₆H₁₀O₄</p> <p>Metal: Mn²⁺</p> <p>MOF formula : [Mn(C₆H₈O₄) (H₂O)]_n (MnDMS)</p> <p>Preparation approach): Ultrasonic exfoliation</p> <p>MOF particle size: ~200 nm</p> <p>Imaging Applications: DNA and RNA</p>	DNA and RNA [223–224]
	<p>Ligand abbreviation: BDC</p> <p>Metal: Gd³⁺</p> <p>MOF formula : [Gd (BDC)_{1.5}(H₂O)₂]_n</p> <p>Preparation approach): Reverse microemulsion process</p> <p>MOF particle size: 155 ± 30 nm</p> <p>Imaging Applications: MRI and CT</p>	MRI RNA and CT [107–225–227]
	<p>Ligand abbreviation: BDC</p> <p>Metal: Zr⁴⁺</p> <p>MOF formula : Zr₆O₄(OH)₄ (BDC)₆]_n (UiO-66)</p> <p>Preparation approach): Solvothermal method</p> <p>MOF particle size: ~125 nm</p> <p>Surface area (m₂/g): 621</p> <p>Pore size (Å): 12.2</p> <p>Imaging Applications: RNA</p>	
	<p>Ligand abbreviation: Lru</p> <p>Metal: Gd³⁺</p> <p>MOF formula : [L_{Ru}—Gd_{1.3}—(H₂O)₇]_n [Gd—Ru NCPs]</p> <p>Preparation approach): Hydrothermal method</p> <p>MOF particle size: ~100 nm</p> <p>Imaging Applications: MRI</p>	MRI [228]

	<p>Ligand abbreviation: OPEA</p> <p>Metal: Gd³⁺</p> <p>MOF formula : {[Gd(OPE)(NO₃) (H₂O)₂]-H₂O}_n</p> <p>Preparation approach): Solvothermal method</p> <p>MOF particle size: Diameter: 50–100 nm; Length: 0.5–0.8 μm</p> <p>Surface area (m₂/g): 293</p> <p>Pore size (Å): <20</p> <p>Imaging Applications: MRI</p>	MRI [229]
	<p>Ligand abbreviation: ZA</p> <p>Metal: Mn²⁺</p> <p>MOF formula : Mnbisphosphonate NCP</p> <p>Preparation approach): Microwave reaction</p> <p>MOF particle size: 55.8 ± 4.2 nm</p> <p>Imaging Applications: MRI</p>	MRI [230]
	<p>Ligand abbreviation: 2-ICA</p> <p>Metal: Zn²⁺</p> <p>MOF formula : Zn(C₄H₃N₂O)₂ ZIF-90</p> <p>Preparation approach): Surface modification</p> <p>MOF particle size: 64 nm</p> <p>Surface area (m₂/g): 1270</p> <p>Pore size (Å): 11.2</p> <p>Imaging Applications: MRI</p>	MRI [231– 232]
	<p>Ligand abbreviation: NH₂-BDC</p> <p>MOF formula : [Zn₄O(H₂-BDC)₃]_n IRMOF-3</p> <p>Preparation approach): Surface modification</p> <p>MOF particle size: 250 nm</p> <p>Surface area (m₂/g): 3124</p> <p>Imaging Applications: MRI</p>	MRI [233– 234]

	<p>Ligand abbreviation: H₂L</p> <p>Metal: Zr⁺⁴</p> <p>MOF formula : Zr-UiO</p> <p>Preparation approach): Solvothermal method</p> <p>MOF particle size: 50–200 nm</p> <p>Surface area (m₂/g): 2776</p> <p>Pore size (Å): 6–12</p> <p>Imaging Applications: CT</p>
	<p>Ligand abbreviation: H₂L</p> <p>Metal: Hf⁺⁴</p> <p>MOF formula : Hf-UiO</p> <p>Preparation approach): Solvothermal method</p> <p>MOF particle size: 50–200 nm</p> <p>Surface area (m₂/g): 2187</p> <p>Pore size (Å): 6–12</p> <p>Imaging Applications: CT</p>

CT
 [235–
 236]

Table 5. Bioimaging applications of MOFs.

Conclusions and recommendations

In this chapter, we focused on studies carried out in the field of biosensing and bio-imaging, which have an important place in the nanotube of MOF structures. Biological probes, designed with MOF structures, show superior properties such as excellent porosity and self-degradability. These privileges provide the using of MOF structures in various areas. The fact that they can react with the biological molecules in the nanomedicine field and create a key lock model provides a great advantage in adapting to new generation technologies. In addition, the non-toxic properties of MOF structures, low cytotoxicity, and rapid degradability indicate that they are extremely useful in biological compatibility. nMOF structures, which are synthesized in nanoscale, can be one step ahead with their excellent biocompatibility.

MOF structures have been developed for the detection of DNA, RNA and small biomolecules by fluorescent quenching, but are still in the early stages, and further research is needed. Recent studies have focused on the synthesis of MOF structures as contrast agents for MRI and CT applications. It is thought that nano sizes should be further reduced in order to endocytose the MOF structures by cells in the visualization of

living cells and tissues. Therefore, the morphology of MOF structures is very important for living systems.

For clinical diagnostic research, it is necessary to evaluate MOFs toxicologically. Since the toxicity of MOF structures still arouses concern, in vivo activities, metabolism pathways should be systematically examined. In this context, one of the possible solutions is considered the choice of low-toxic metal ions and ligands.

References

1. W. Ma, X. Li, Y. Bai, & H. Liu, Applications of metal-organic frameworks as advanced sorbents in biomacromolecules sample preparation. *TrAC Trends in Analytical Chemistry*, **109** (2018) 154–162. <https://doi.org/10.1016/j.trac.2018.10.003>
2. L. Jiao, J. Y. R. Seow, W. S. Skinner, Z. U. Wang, & H.-L. Jiang, Metal–organic frameworks: Structures and functional applications. *Materials Today*, (2018)
3. G. Başkaya, Y. Yıldız, A. Savk, T. O. Okyay, S. Eriş, H. Sert, & F. Şen, Rapid, Sensitive, and Reusable Detection of Glucose by Highly Monodisperse Nickel Nanoparticles Decorated Functionalized Multi-Walled Carbon Nanotubes. *Biosensors and Bioelectronics*, **91** (2017) 728–733. <https://doi.org/10.1016/j.bios.2017.01.045>
4. Y. Koskun, A. Şavk, B. Şen, & F. Şen, Highly Sensitive Glucose Sensor Based on Monodisperse Palladium Nickel/Activated Carbon Nanocomposites. *Analytica Chimica Acta*, **1010** (2018) 37–43. <https://doi.org/10.1016/j.aca.2018.01.035>
5. H. Göksu, B. Çelik, Y. Yıldız, F. Şen, & B. Kılbaş, Superior Monodisperse CNT-Supported CoPd (CoPd@CNT) Nanoparticles for Selective Reduction of Nitro Compounds to Primary Amines with NaBH₄ in Aqueous Medium. *ChemistrySelect*, **1** (2016) 2366–2372. <https://doi.org/10.1002/slct.201600509>
6. B. Sen, B. Demirkan, B. Şimşek, A. Savk, & F. Sen, Monodisperse Palladium Nanocatalysts for Dehydrocoupling of Dimethylamineborane. *Nano-Structures & Nano-Objects*, **16** (2018) 209–214. <https://doi.org/10.1016/j.nanoso.2018.07.008>
7. B. Şen, B. Demirkan, A. Savk, R. Kartop, M. S. Nas, M. H. Alma, S. Sürdem, & F. Şen, High-performance graphite-supported ruthenium nanocatalyst for hydrogen evolution reaction. *Journal of Molecular Liquids*, **268** (2018) 807–812. <https://doi.org/10.1016/j.molliq.2018.07.117>
8. B. Şen, A. Aygün, T. O. Okyay, A. Şavk, R. Kartop, & F. Şen, Monodisperse Palladium Nanoparticles Assembled on Graphene Oxide with The High Catalytic Activity and Reusability in The Dehydrogenation of Dimethylamine-borane. *International Journal of Hydrogen Energy*, **43** (2018) 20176–20182.

- <https://doi.org/10.1016/j.ij.> *International Journal of Hydrogen Energy*, **43** (2018) 20176–20182. <https://doi.org/10.1016/j.ijhydene.2018.03.175>
9. Z. Daşdelen, Y. Yıldız, S. Eriş, & F. Şen, Enhanced electrocatalytic activity and durability of Pt nanoparticles decorated on GO-PVP hybriide material for methanol oxidation reaction. *Applied Catalysis B: Environmental*, **219** (2017) 511–516. <https://doi.org/10.1016/j.apcatb.2017.08.014>
 10. B. Şahin, E. Demir, A. Aygün, H. Gündüz, & F. Şen, Investigation of The Effect Of Pomegranate Extract And Monodisperse Silver Nanoparticle Combination on MCF-7 Cell Line. *Journal of Biotechnology*, **260** (2017) 79–83. <https://doi.org/10.1016/j.jbiotec.2017.09.012>
 11. E. Demir, B. Sen, & F. Sen, Highly Efficient Pt Nanoparticles and f-MWCNT Nanocomposites Based Counter Electrodes for Dye-sensitized Solar Cells. *Nano-Structures & Nano-Objects*, **11** (2017) 39–45. <https://doi.org/10.1016/j.nanoso.2017.06.003>
 12. E. Demir, A. Savk, B. Sen, & F. Sen, A Novel Monodisperse Metal Nanoparticles Anchored Graphene Oxide as Counter Electrode for Dye-Sensitized Solar Cells. *Nano-Structures and Nano-Objects*, **12** (2017) 41–45. <https://doi.org/10.1016/j.nanoso.2017.08.018>
 13. S. Akocak, B. Şen, N. Lolak, A. Şavk, M. Koca, S. Kuzu, & F. Şen, One-Pot Three-Component Synthesis of 2-Amino-4H-Chromene Derivatives by Using Monodisperse Pd Nanomaterials Anchored Graphene Oxide as Highly Efficient and Recyclable Catalyst. *Nano-Structures & Nano-Objects*, **11** (2017) 25–31. <https://doi.org/10.1016/j.nanoso.2017.06.002>
 14. Y. Yıldız, S. Kuzu, B. Sen, A. Savk, S. Akocak, & F. Şen, Different ligand based monodispersed Pt nanoparticles decorated with rGO as highly active and reusable catalysts for the methanol oxidation. *International Journal of Hydrogen Energy*, **42** (2017) 13061–13069. <https://doi.org/10.1016/j.ijhydene.2017.03.230>
 15. S. Bozkurt, B. Tosun, B. Sen, S. Akocak, A. Savk, M. F. Ebeoğlu, & F. Sen, A Hydrogen Peroxide Sensor Based on TNM Functionalized Reduced Graphene Oxide Grafted with Highly Monodisperse Pd Nanoparticles. *Analytica Chimica Acta*, **989** (2017) 88–94. <https://doi.org/10.1016/j.aca.2017.07.051>
 16. B. Şen, N. Lolak, Ö. Paralı, M. Koca, A. Şavk, S. Akocak, & F. Şen, Bimetallic PdRu/graphene oxide based Catalysts for one-pot three-component synthesis of 2-amino-4H-chromene derivatives. *Nano-Structures & Nano-Objects*, **12** (2017) 33–40. <https://doi.org/10.1016/J.NANOSO.2017.08.013>

17. B. Sen, S. Kuzu, E. Demir, S. Akocak, & F. Sen, Monodisperse palladium–nickel alloy nanoparticles assembled on graphene oxide with the high catalytic activity and reusability in the dehydrogenation of dimethylamine–borane. *International Journal of Hydrogen Energy*, **42** (2017) 23276–23283.
<https://doi.org/10.1016/j.ijhydene.2017.05.113>
18. B. Sen, S. Kuzu, E. Demir, S. Akocak, F. S.-I. J. of, & undefined 2017, Polymer-graphene hybride decorated Pt nanoparticles as highly efficient and reusable catalyst for the dehydrogenation of dimethylamine–borane at room. *Elsevier*, (n.d.)
19. R. Ayranci, G. Baskaya, M. Guzel, S. Bozkurt, M. Ak, A. Savk, & F. Sen, Enhanced optical and electrical properties of PEDOT via nanostructured carbon materials: A comparative investigation. *Nano-Structures and Nano-Objects*, **11** (2017) 13–19. <https://doi.org/10.1016/j.nanoso.2017.05.008>
20. B. Sen, S. Kuzu, E. Demir, T. Onal Okyay, & F. Sen, Hydrogen Liberation from The Dehydrocoupling of Dimethylamine–borane at Room Temperature by Using Novel and Highly Monodispersed RuPtNi Nanocatalysts Decorated with Graphene Oxide. *International Journal of Hydrogen Energy*, **42** (2017) 23299–23306.
<https://doi.org/10.1016/j.ijhydene.2017.04.213>
21. B. Sen, S. Kuzu, E. Demir, S. Akocak, F. Sen, B. Şen, S. Kuzu, E. Demir, F. Akocak, SüleymanŞSen, B. Sen, S. Kuzu, E. Demir, S. Akocak, F. Şen, F. Akocak, SüleymanŞSen, B. Sen, S. Kuzu, E. Demir, S. Akocak, F. Sen, B. Şen, S. Kuzu, E. Demir, F. Akocak, SüleymanŞSen, B. Sen, S. Kuzu, E. Demir, S. Akocak, F. Sen, B. Şen, S. Kuzu, E. Demir, S. Akocak, & F. Şen, Highly Monodisperse RuCo Nanoparticles Decorated on Functionalized Multiwalled Carbon Nanotube with The Highest Observed Catalytic Activity in The Dehydrogenation of Dimethylamine–borane. *International Journal of Hydrogen Energy*, **42** (2017) 23292–23298. <https://doi.org/10.1016/j.ijhydene.2017.06.032>
22. B. Gezer, H. Sert, T. Onal Okyay, S. Bozkurt, G. Başkaya, B. Şahin, C. Ulutürk, & F. Sen, Reduced graphene oxide (rGO) as highly effective material for the ultrasound assisted boric acid extraction from ulexite ore. *Chemical Engineering Research and Design*, **117** (2017) 542–548. <https://doi.org/10.1016/j.cherd.2016.11.007>
23. Y. Yildiz, E. Erken, H. Pamuk, H. Sert, & F. Sen, Monodisperse Pt Nanoparticles Assembled on Reduced Graphene Oxide: Highly Efficient and Reusable Catalyst for Methanol Oxidation and Dehydrocoupling of Dimethylamine-Borane (DMAB). *Journal of nanoscience and nanotechnology*, **16** (2016) 5951–8
24. E. Erken, H. Pamuk, Ö. Karatepe, G. Başkaya, H. Sert, O. M. Kalfa, & F. Şen, New Pt(0) Nanoparticles as Highly Active and Reusable Catalysts in the C1–C3 Alcohol Oxidation and the Room Temperature Dehydrocoupling of Dimethylamine-

- Borane (DMAB). *Journal of Cluster Science*, **27** (2016) 9–23.
<https://doi.org/10.1007/s10876-015-0892-8>
25. B. Sen, S. Kuzu, E. Demir, E. Yıldırım, & F. Sen, Highly efficient catalytic dehydrogenation of dimethyl ammonia borane via monodisperse palladium–nickel alloy nanoparticles assembled on PEDOT. *International Journal of Hydrogen Energy*, **42** (2017) 23307–23314. <https://doi.org/10.1016/J.IJHYDENE.2017.05.115>
26. B. Şen, B. Demirkan, A. Şavk, S. Karahan Gülbay, & F. Şen, Trimetallic PdRuNi Nanocomposites Decorated on Graphene Oxide: A Superior Catalyst for The Hydrogen Evolution Reaction. *International Journal of Hydrogen Energy*, **43** (2018) 17984–17992. <https://doi.org/10.1016/j.ijhydene.2018.07.122>
27. H. Sert, Y. Yıldız, T. Onal Okyay, B. Sen, B. Gezer, S. Bozkurt, G. Ba, F. Sen, Y. Yıldız, T. O. Okyay, B. Sen, B. Gezer, S. Bozkurt, G. Başkaya, & F. Sen, Activated Carbon Furnished Monodisperse Pt Nanocomposites as a Superior Adsorbent for Methylene Blue Removal from Aqueous Solutions. *Journal of Nanoscience and Nanotechnology*, **17** (2017) 4799–4804. <https://doi.org/10.1166/jnn.2017.13776>
28. H. Goksu, H. Sert, B. Kilbas, & F. Sen, Recent Advances in the Reduction of Nitro Compounds by Heterogenous Catalysts. *Current Organic Chemistry*, **21** (2017) 794–820. <https://doi.org/10.2174/1385272820666160525123907>
29. R. Ulus, Y. Yıldız, S. Eriş, B. Aday, F. Şen, & M. Kaya, Functionalized Multi-Walled Carbon Nanotubes (f-MWCNT) as Highly Efficient and Reusable Heterogeneous Catalysts for the Synthesis of Acridinedione Derivatives. *ChemistrySelect*, **1** (2016) 3861–3865. <https://doi.org/10.1002/slct.201600719>
30. B. Aday, H. Pamuk, M. Kaya, & F. Sen, Graphene Oxide as Highly Effective and Readily Recyclable Catalyst Using for the One-Pot Synthesis of 1,8-Dioxoacridine Derivatives. *Journal of Nanoscience and Nanotechnology*, **16** (2016) 6498–6504. <https://doi.org/10.1166/jnn.2016.12432>
31. T. Demirci, B. Çelik, Y. Yıldız, S. Eriş, M. Arslan, F. Sen, & B. Kilbas, One-pot synthesis of Hantzsch dihydropyridines using a highly efficient and stable PdRuNi@GO catalyst. *RSC Advances*, **6** (2016) 76948–76956. <https://doi.org/10.1039/C6RA13142E>
32. Y. Yıldız, İ. Esirden, E. Erken, E. Demir, M. Kaya, & F. Şen, Microwave (Mw)-assisted Synthesis of 5-Substituted 1H-Tetrazoles via [3+2] Cycloaddition Catalyzed by Mw-Pd/Co Nanoparticles Decorated on Multi-Walled Carbon Nanotubes. *ChemistrySelect*, **1** (2016) 1695–1701. <https://doi.org/10.1002/slct.201600265>
33. H. Sert, Y. Yıldız, T. O. Okyay, B. Gezer, Z. Dasdelen, B. Sen, & F. Sen, Monodisperse Mw-Pt NPs@VC as Highly Efficient and Reusable Adsorbents for

- Methylene Blue Removal. *Journal of Cluster Science*, **27** (2016) 1953–1962.
<https://doi.org/10.1007/s10876-016-1054-3>
34. Y. Yıldız, H. Pamuk, Ö. Karatepe, Z. Dasdelen, & F. Sen, Carbon black hybrid material furnished monodisperse platinum nanoparticles as highly efficient and reusable electrocatalysts for formic acid electro-oxidation. *RSC Advances*, **6** (2016) 32858–32862. <https://doi.org/10.1039/C6RA00232C>
35. B. Çelik, G. Başkaya, H. Sert, Ö. Karatepe, E. Erken, F. Şen, B. Celik, G. Baskaya, H. Sert, O. Karatepe, E. Erken, & F. Sen, Monodisperse Pt(0)/DPA@GO nanoparticles as highly active catalysts for alcohol oxidation and dehydrogenation of DMAB. *International Journal of Hydrogen Energy*, **41** (2016) 5661–5669.
<https://doi.org/10.1016/j.ijhydene.2016.02.061>
36. E. Erken, Y. Yıldız, B. Kilbaş, & F. Şen, Synthesis and Characterization of Nearly Monodisperse Pt Nanoparticles for C 1 to C 3 Alcohol Oxidation and Dehydrogenation of Dimethylamine-borane (DMAB). *Journal of Nanoscience and Nanotechnology*, **16** (2016) 5944–5950. <https://doi.org/10.1166/jnn.2016.11683>
37. S. Eris, Z. Daşdelen, Y. Yıldız, & F. Sen, Nanostructured Polyaniline-rGO decorated platinum catalyst with enhanced activity and durability for Methanol oxidation. *International Journal of Hydrogen Energy*, **43** (2018) 1337–1343.
<https://doi.org/10.1016/J.IJHYDENE.2017.11.051>
38. B. Şahin, A. Aygün, H. Gündüz, K. Şahin, E. Demir, S. Akocak, & F. Şen, Cytotoxic Effects of Platinum Nanoparticles Obtained from Pomegranate Extract by The Green Synthesis Method on The MCF-7 Cell Line. *Colloids and Surfaces B: Biointerfaces*, **163** (2018) 119–124. <https://doi.org/10.1016/j.colsurfb.2017.12.042>
39. İ. Gulçin, P. Taslimi, A. Aygün, N. Sadeghian, E. Bastem, O. I. Kufrevioglu, F. Turkan, & F. Şen, Antidiabetic and antiparasitic potentials: Inhibition effects of some natural antioxidant compounds on α -glycosidase, α -amylase and human glutathione S-transferase enzymes. *International Journal of Biological Macromolecules*, **119** (2018) 741–746. <https://doi.org/10.1016/J.IJBIOMAC.2018.08.001>
40. S. Günbatar, A. Aygun, Y. Karataş, M. Gülcan, & F. Şen, Carbon-nanotube-based Rhodium Nanoparticles as Highly-Active Catalyst for Hydrolytic Dehydrogenation of Dimethylamineborane at Room Temperature. *Journal of Colloid and Interface Science*, **530** (2018) 321–327. <https://doi.org/10.1016/j.jcis.2018.06.100>
41. B. Aday, Y. Yıldız, R. Ulus, S. Eris, F. Sen, & M. Kaya, One-Pot, Efficient and Green Synthesis of Acridinedione Derivatives Using Highly Monodisperse Platinum Nanoparticles Supported with Reduced Graphene Oxide. *New Journal of Chemistry*, **40** (2016) 748–754. <https://doi.org/10.1039/C5NJ02098K>

42. B. Sen, A. Şavk, E. Kuyuldar, S. Karahan Gülbay, & F. Sen, Hydrogen Liberation from The Hydrolytic Dehydrogenation of Hydrazine Borane in Acidic Media. *International Journal of Hydrogen Energy*, **43** (2018) 17978–17983.
<https://doi.org/10.1016/j.ijhydene.2018.03.225>
43. N. M. Iverson, P. W. Barone, M. Shandell, L. J. Trudel, S. Sen, F. Sen, V. Ivanov, E. Atolia, E. Farias, T. P. McNicholas, N. Reuel, N. M. A. Parry, G. N. Wogan, & M. S. Strano, In vivo Biosensing via Tissue-localizable Near-infrared-fluorescent Single-walled Carbon Nanotubes. *Nature Nanotechnology*, **8** (2013) 873–880.
<https://doi.org/10.1038/nnano.2013.222>
44. P. Sennequier, Signal conditioning for electrochemical sensors. (2017) 1–27
45. H. Kitagawa, Y. Nagao, M. Fujishima, R. Ikeda, & S. Kanda, Highly proton-conductive copper coordination polymer, H₂dtoaCu (H₂dtoa=dithiooxamide anion). *Inorganic Chemistry Communications*, **6** (2003) 346–348.
[https://doi.org/10.1016/S1387-7003\(02\)00749-9](https://doi.org/10.1016/S1387-7003(02)00749-9)
46. X. Zhu, H. Zheng, X. Wei, Z. Lin, L. Guo, B. Qiu, & G. Chen, Metal–organic framework (MOF): a novel sensing platform for biomolecules. *Chemical Communications*, **49** (2013) 1276. <https://doi.org/10.1039/c2cc36661d>
47. W. Yang, G. Zhang, W. Weng, B. Qiu, L. Guo, Z. Lin, & G. Chen, Signal on fluorescence biosensor for MMP-2 based on FRET between semiconducting polymer dots and a metal organic framework. *RSC Adv.*, **4** (2014) 58852–58857.
<https://doi.org/10.1039/C4RA12478B>
48. S.-P. Yang, S.-R. Chen, S.-W. Liu, X.-Y. Tang, L. Qin, G.-H. Qiu, J.-X. Chen, & W.-H. Chen, Platforms Formed from a Three-Dimensional Cu-Based Zwitterionic Metal–Organic Framework and Probe ss-DNA: Selective Fluorescent Biosensors for Human Immunodeficiency Virus 1 ds-DNA and Sudan Virus RNA Sequences. *Analytical Chemistry*, **87** (2015) 12206–12214.
<https://doi.org/10.1021/acs.analchem.5b03084>
49. L. Qin, L.-X. Lin, Z.-P. Fang, S.-P. Yang, G.-H. Qiu, J.-X. Chen, & W.-H. Chen, A water-stable metal–organic framework of a zwitterionic carboxylate with dysprosium: a sensing platform for Ebolavirus RNA sequences. *Chemical Communications*, **52** (2016) 132–135. <https://doi.org/10.1039/C5CC06697B>
50. H.-Q. Zhao, G.-H. Qiu, Z. Liang, M.-M. Li, B. Sun, L. Qin, S.-P. Yang, W.-H. Chen, & J.-X. Chen, A zinc(II)-based two-dimensional MOF for sensitive and selective sensing of HIV-1 ds-DNA sequences. *Analytica Chimica Acta*, **922** (2016) 55–63. <https://doi.org/10.1016/J.ACA.2016.03.054>

51. H.-Q. Zhao, S.-P. Yang, N.-N. Ding, L. Qin, G.-H. Qiu, J.-X. Chen, W.-H. Zhang, W.-H. Chen, & T. S. A. Hor, A zwitterionic 1D/2D polymer co-crystal and its polymorphic sub-components: a highly selective sensing platform for HIV ds-DNA sequences. *Dalton Transactions*, **45** (2016) 5092–5100.
<https://doi.org/10.1039/C5DT04410C>
52. J. M. Fang, F. Leng, X. J. Zhao, X. L. Hu, & Y. F. Li, Metal–organic framework MIL-101 as a low background signal platform for label-free DNA detection. *The Analyst*, **139** (2014) 801–806. <https://doi.org/10.1039/C3AN01975F>
53. G. Férey, C. Mellot-Draznieks, C. Serre, F. Millange, J. Dutour, S. Surblé, & I. Margiolaki, A chromium terephthalate-based solid with unusually large pore volumes and surface area. *Science (New York, N.Y.)*, **309** (2005) 2040–2.
<https://doi.org/10.1126/science.1116275>
54. H. Tan, G. Tang, Z. Wang, Q. Li, J. Gao, & S. Wu, Magnetic porous carbon nanocomposites derived from metal-organic frameworks as a sensing platform for DNA fluorescent detection. *Analytica Chimica Acta*, **940** (2016) 136–142.
<https://doi.org/10.1016/J.ACA.2016.08.024>
55. R. Mejia-Ariza, J. Rosselli, C. Breukers, A. Manicardi, L. W. M. M. Terstappen, R. Corradini, & J. Huskens, DNA Detection by Flow Cytometry using PNA-Modified Metal-Organic Framework Particles. *Chemistry (Weinheim an der Bergstrasse, Germany)*, **23** (2017) 4180–4186. <https://doi.org/10.1002/chem.201605803>
56. C. Serre, C. Mellot-Draznieks, S. Surblé, N. Audebrand, Y. Filinchuk, & G. Férey, Role of solvent-host interactions that lead to very large swelling of hybrid frameworks. *Science (New York, N.Y.)*, **315** (2007) 1828–31.
<https://doi.org/10.1126/science.1137975>
57. T. Chalati, P. Horcajada, R. Gref, P. Couvreur, & C. Serre, Optimisation of the synthesis of MOF nanoparticles made of flexible porous iron fumarate MIL-88A. *J. Mater. Chem.*, **21** (2011) 2220–2227. <https://doi.org/10.1039/C0JM03563G>
58. H.-T. Zhang, J.-W. Zhang, G. Huang, Z.-Y. Du, & H.-L. Jiang, An amine-functionalized metal–organic framework as a sensing platform for DNA detection. *Chem. Commun.*, **50** (2014) 12069–12072. <https://doi.org/10.1039/C4CC05571C>
59. S.-N. Zhao, L.-L. Wu, J. Feng, S.-Y. Song, & H.-J. Zhang, An ideal detector composed of a 3D Gd-based coordination polymer for DNA and Hg²⁺ ion. *Inorganic Chemistry Frontiers*, **3** (2016) 376–380. <https://doi.org/10.1039/C5QI00252D>
60. H.-S. Wang, J. Li, J.-Y. Li, K. Wang, Y. Ding, & X.-H. Xia, Lanthanide-based metal-organic framework nanosheets with unique fluorescence quenching properties

- for two-color intracellular adenosine imaging in living cells. *NPG Asia Materials*, **9** (2017) e354–e354. <https://doi.org/10.1038/am.2017.7>
61. H.-S. Wang, W.-J. Bao, S.-B. Ren, M. Chen, K. Wang, & X.-H. Xia, Fluorescent Sulfur-Tagged Europium(III) Coordination Polymers for Monitoring Reactive Oxygen Species. *Analytical Chemistry*, **87** (2015) 6828–6833. <https://doi.org/10.1021/acs.analchem.5b01104>
62. P. Ling, J. Lei, L. Zhang, & H. Ju, Porphyrin-Encapsulated Metal–Organic Frameworks as Mimetic Catalysts for Electrochemical DNA Sensing via Allosteric Switch of Hairpin DNA. *Analytical Chemistry*, **87** (2015) 3957–3963. <https://doi.org/10.1021/acs.analchem.5b00001>
63. S. S.-Y. Chui, S. M.-F. Lo, J. P. H. Charmant, A. G. Orpen, & I. D. Williams, A chemically functionalizable nanoporous material. *Science (New York, N.Y.)*, **283** (1999) 1148–50. <https://doi.org/10.1126/SCIENCE.283.5405.1148>
64. Q. Zhu, Y. Chen, W. Wang, H. Zhang, C. Ren, H. Chen, & X. Chen, A sensitive biosensor for dopamine determination based on the unique catalytic chemiluminescence of metal–organic framework HKUST-1. *Sensors and Actuators B: Chemical*, **210** (2015) 500–507. <https://doi.org/10.1016/J.SNB.2015.01.012>
65. Q. Wang, Y. Yang, F. Gao, J. Ni, Y. Zhang, & Z. Lin, Graphene Oxide Directed One-Step Synthesis of Flowerlike Graphene@HKUST-1 for Enzyme-Free Detection of Hydrogen Peroxide in Biological Samples. *ACS Applied Materials & Interfaces*, **8** (2016) 32477–32487. <https://doi.org/10.1021/acsami.6b11965>
66. T. Guo, Q. Deng, G. Fang, D. Gu, Y. Yang, & S. Wang, Upconversion fluorescence metal-organic frameworks thermo-sensitive imprinted polymer for enrichment and sensing protein. *Biosensors and Bioelectronics*, **79** (2016) 341–346. <https://doi.org/10.1016/J.BIOS.2015.12.040>
67. S.-H. Huo & X.-P. Yan, Metal–organic framework MIL-100(Fe) for the adsorption of malachite green from aqueous solution. *Journal of Materials Chemistry*, **22** (2012) 7449. <https://doi.org/10.1039/c2jm16513a>
68. S. Patra, T. Hidalgo Crespo, A. Permyakova, C. Sicard, C. Serre, A. Chaussé, N. Steunou, & L. Legrand, Design of metal organic framework–enzyme based bioelectrodes as a novel and highly sensitive biosensing platform. *Journal of Materials Chemistry B*, **3** (2015) 8983–8992. <https://doi.org/10.1039/C5TB01412C>
69. J.-N. Hao & B. Yan, Recyclable lanthanide-functionalized MOF hybrids to determine hippuric acid in urine as a biological index of toluene exposure. *Chemical Communications*, **51** (2015) 14509–14512. <https://doi.org/10.1039/C5CC05219J>

70. C. Volkringer, T. Loiseau, N. Guillou, G. Férey, M. Haouas, F. Taulelle, E. Elkaim, & N. Stock, High-Throughput Aided Synthesis of the Porous Metal–Organic Framework-Type Aluminum Pyromellitate, MIL-121, with Extra Carboxylic Acid Functionalization. *Inorganic Chemistry*, **49** (2010) 9852–9862.
<https://doi.org/10.1021/ic101128w>
71. S.-Y. Zhang, W. Shi, P. Cheng, & M. J. Zaworotko, A Mixed-Crystal Lanthanide Zeolite-like Metal–Organic Framework as a Fluorescent Indicator for Lysophosphatidic Acid, a Cancer Biomarker. *Journal of the American Chemical Society*, **137** (2015) 12203–12206. <https://doi.org/10.1021/jacs.5b06929>
72. Y. Wang, C. Hou, Y. Zhang, F. He, M. Liu, & X. Li, Preparation of graphene nano-sheet bonded PDA/MOF microcapsules with immobilized glucose oxidase as a mimetic multi-enzyme system for electrochemical sensing of glucose. *Journal of Materials Chemistry B*, **4** (2016) 3695–3702. <https://doi.org/10.1039/C6TB00276E>
73. G. Lu & J. T. Hupp, Metal–Organic Frameworks as Sensors: A ZIF-8 Based Fabry–Pérot Device as a Selective Sensor for Chemical Vapors and Gases. *Journal of the American Chemical Society*, **132** (2010) 7832–7833.
<https://doi.org/10.1021/ja101415b>
74. Y. Pan, Y. Liu, G. Zeng, L. Zhao, & Z. Lai, Rapid synthesis of zeolitic imidazolate framework-8 (ZIF-8) nanocrystals in an aqueous system. *Chemical Communications*, **47** (2011) 2071. <https://doi.org/10.1039/c0cc05002d>
75. K. Wang, N. Li, J. Zhang, Z. Zhang, & F. Dang, Size-selective QD@MOF core-shell nanocomposites for the highly sensitive monitoring of oxidase activities. *Biosensors and Bioelectronics*, **87** (2017) 339–344.
<https://doi.org/10.1016/J.BIOS.2016.08.026>
76. J. An, C. M. Shade, D. A. Chengelis-Czegan, S. Petoud, & N. L. Rosi, Zinc-Adeninate Metal–Organic Framework for Aqueous Encapsulation and Sensitization of Near-infrared and Visible Emitting Lanthanide Cations. *Journal of the American Chemical Society*, **133** (2011) 1220–1223. <https://doi.org/10.1021/ja109103t>
77. Y. Zhang, B. Li, H. Ma, L. Zhang, & Y. Zheng, Rapid and facile ratiometric detection of an anthrax biomarker by regulating energy transfer process in bio-metal-organic framework. *Biosensors and Bioelectronics*, **85** (2016) 287–293.
<https://doi.org/10.1016/J.BIOS.2016.05.020>
78. W. Li & D. Cosker, Video interpolation using optical flow and Laplacian smoothness. *Neurocomputing*, **220** (2017) 236–243.
<https://doi.org/10.1016/J.NEUCOM.2016.04.064>

79. G.-Y. Zhang, Y.-H. Zhuang, D. Shan, G.-F. Su, S. Cosnier, & X.-J. Zhang, Zirconium-Based Porphyrinic Metal–Organic Framework (PCN-222): Enhanced Photoelectrochemical Response and Its Application for Label-Free Phosphoprotein Detection. *Analytical Chemistry*, **88** (2016) 11207–11212.
<https://doi.org/10.1021/acs.analchem.6b03484>
80. Z. Hu, B. J. Deibert, & J. Li, Luminescent metal–organic frameworks for chemical sensing and explosive detection. *Chem. Soc. Rev.*, **43** (2014) 5815–5840.
<https://doi.org/10.1039/C4CS00010B>
81. Y. Zhang, S. Yuan, G. Day, X. Wang, X. Yang, & H.-C. Zhou, Luminescent sensors based on metal-organic frameworks. *Coordination Chemistry Reviews*, **354** (2018) 28–45. <https://doi.org/10.1016/j.ccr.2017.06.007>
82. D. Kukkar, K. Vellingiri, K.-H. Kim, & A. Deep, Recent progress in biological and chemical sensing by luminescent metal-organic frameworks. *Sensors and Actuators B: Chemical*, **273** (2018) 1346–1370.
<https://doi.org/10.1016/j.snb.2018.06.128>
83. W. Morris, W. E. Briley, E. Auyeung, M. D. Cabezas, & C. A. Mirkin, Nucleic Acid–Metal Organic Framework (MOF) Nanoparticle Conjugates. *Journal of the American Chemical Society*, **136** (2014) 7261–7264.
<https://doi.org/10.1021/ja503215w>
84. B. Valizadeh, T. N. Nguyen, & K. C. Stylianou, Shape engineering of metal–organic frameworks. *Polyhedron*, **145** (2018) 1–15.
<https://doi.org/10.1016/j.poly.2018.01.004>
85. H. Cai, Y.-L. Huang, & D. Li, Biological metal–organic frameworks: Structures, host–guest chemistry and bio-applications. *Coordination Chemistry Reviews*, **378** (2019) 207–221. <https://doi.org/10.1016/j.ccr.2017.12.003>
86. J. T. Petty, C. Fan, S. P. Story, B. Sengupta, A. St. John Iyer, Z. Prudowsky, & R. M. Dickson, DNA Encapsulation of 10 Silver Atoms Producing a Bright, Modulatable, Near-Infrared-Emitting Cluster. *The Journal of Physical Chemistry Letters*, **1** (2010) 2524–2529. <https://doi.org/10.1021/jz100817z>
87. R. Dahm, Discovering DNA: Friedrich Miescher and the early years of nucleic acid research. *Human Genetics*, **122** (2008) 565–581. <https://doi.org/10.1007/s00439-007-0433-0>
88. Y. Nakazaki, N. Goto, & T. Inui, Simulation of dynamic behaviors of simple aromatic hydrocarbons inside the pores of a pentasil zeolite. *Journal of Catalysis*, **136** (1992) 141–148. [https://doi.org/10.1016/0021-9517\(92\)90113-V](https://doi.org/10.1016/0021-9517(92)90113-V)

89. P. Shah, A. Rørvig-Lund, S. Ben Chaabane, P. W. Thulstrup, H. G. Kjaergaard, E. Fron, J. Hofkens, S. W. Yang, & T. Vosch, Design Aspects of Bright Red Emissive Silver Nanoclusters/DNA Probes for MicroRNA Detection. *ACS Nano*, **6** (2012) 8803–8814. <https://doi.org/10.1021/nn302633q>
90. R. Srivastava, Complexes of DNA bases and Watson–Crick base pairs interaction with neutral silver Ag_n ($n = 8, 10, 12$) clusters: a DFT and TDDFT study. *Journal of Biomolecular Structure and Dynamics*, **36** (2018) 1050–1062. <https://doi.org/10.1080/07391102.2017.1310059>
91. M. Chen, N. Gan, Y. Zhou, T. Li, Q. Xu, Y. Cao, & Y. Chen, An electrochemical aptasensor for multiplex antibiotics detection based on metal ions doped nanoscale MOFs as signal tracers and RecJf exonuclease-assisted targets recycling amplification. *Talanta*, **161** (2016) 867–874. <https://doi.org/10.1016/J.TALANTA.2016.09.051>
92. P. Kumar, A. Deep, A. K. Paul, & L. M. Bharadwaj, Bioconjugation of MOF-5 for molecular sensing. *Journal of Porous Materials*, **21** (2014) 99–104. <https://doi.org/10.1007/s10934-013-9752-9>
93. X. Lu, X. Wang, L. Wu, L. Wu, Dhanjai, L. Fu, Y. Gao, & J. Chen, Response Characteristics of Bisphenols on a Metal–Organic Framework-Based Tyrosinase Nanosensor. *ACS Applied Materials & Interfaces*, **8** (2016) 16533–16539. <https://doi.org/10.1021/acsami.6b05008>
94. Y.-A. Chen, F.-J. Tsai, Y.-T. Zeng, J.-C. Wang, C. P. Hong, P.-H. Huang, H.-L. Chuang, S.-Y. Lin, C.-T. Chan, Y.-C. Ko, Y.-C. Chou, T.-L. Lin, G.-H. Lee, & M.-L. Ho, Fast and Effective Turn-on Paper-based Phosphorescence Biosensor for Detection of Glucose in Serum. *Journal of the Chinese Chemical Society*, **63** (2016) 424–431. <https://doi.org/10.1002/jccs.201500488>
95. M.-L. Ho, J.-C. Wang, T.-Y. Wang, C.-Y. Lin, J. F. Zhu, Y.-A. Chen, & T.-C. Chen, The construction of glucose biosensor based on crystalline iridium(III)-containing coordination polymers with fiber-optic detection. *Sensors and Actuators B: Chemical*, **190** (2014) 479–485. <https://doi.org/10.1016/J.SNB.2013.08.100>
96. L.-L. Wu, Z. Wang, S.-N. Zhao, X. Meng, X.-Z. Song, J. Feng, S.-Y. Song, & H.-J. Zhang, A Metal-Organic Framework/DNA Hybrid System as a Novel Fluorescent Biosensor for Mercury(II) Ion Detection. *Chemistry - A European Journal*, **22** (2016) 477–480. <https://doi.org/10.1002/chem.201503335>
97. H.-H. Zeng, W.-B. Qiu, L. Zhang, R.-P. Liang, & J.-D. Qiu, Lanthanide Coordination Polymer Nanoparticles as an Excellent Artificial Peroxidase for Hydrogen Peroxide Detection. *Analytical Chemistry*, **88** (2016) 6342–6348. <https://doi.org/10.1021/acs.analchem.6b00630>

98. Y. Li, A. Guo, L. Chang, W.-J. Li, & W.-J. Ruan, Luminescent Metal-Organic-Framework-Based Label-Free Assay of Polyphenol Oxidase with Fluorescent Scan. *Chemistry - A European Journal*, **23** (2017) 6562–6569.
<https://doi.org/10.1002/chem.201605992>
99. H. Tan, Q. Li, Z. Zhou, C. Ma, Y. Song, F. Xu, & L. Wang, A sensitive fluorescent assay for thiamine based on metal-organic frameworks with intrinsic peroxidase-like activity. *Analytica Chimica Acta*, **856** (2015) 90–95.
<https://doi.org/10.1016/J.ACA.2014.11.026>
100. X. Lian, T. Miao, X. Xu, C. Zhang, & B. Yan, Eu³⁺ functionalized Sc-MOFs: Turn-on fluorescent switch for ppb-level biomarker of plastic pollutant polystyrene in serum and urine and on-site detection by smartphone. *Biosensors and Bioelectronics*, **97** (2017) 299–304. <https://doi.org/10.1016/J.BIOS.2017.06.018>
101. C. Xiong, W. Liang, Y. Zheng, Y. Zhuo, Y. Chai, & R. Yuan, Ultrasensitive Assay for Telomerase Activity via Self-Enhanced Electrochemiluminescent Ruthenium Complex Doped Metal–Organic Frameworks with High Emission Efficiency. *Analytical Chemistry*, **89** (2017) 3222–3227.
<https://doi.org/10.1021/acs.analchem.7b00259>
102. Y. Yin, C. Gao, Q. Xiao, G. Lin, Z. Lin, Z. Cai, & H. Yang, Protein-Metal Organic Framework Hybrid Composites with Intrinsic Peroxidase-like Activity as a Colorimetric Biosensing Platform. *ACS Applied Materials & Interfaces*, **8** (2016) 29052–29061. <https://doi.org/10.1021/acsami.6b09893>
103. G.-Y. Wang, C. Song, D.-M. Kong, W.-J. Ruan, Z. Chang, & Y. Li, Two luminescent metal–organic frameworks for the sensing of nitroaromatic explosives and DNA strands. *J. Mater. Chem. A*, **2** (2014) 2213–2220.
<https://doi.org/10.1039/C3TA14199C>
104. A. Foucault-Collet, K. A. Gogick, K. A. White, S. Villette, A. Pallier, G. Collet, C. Kieda, T. Li, S. J. Geib, N. L. Rosi, & S. Petoud, Lanthanide near infrared imaging in living cells with Yb³⁺ nano metal organic frameworks. *Proceedings of the National Academy of Sciences of the United States of America*, **110** (2013) 17199–204.
<https://doi.org/10.1073/pnas.1305910110>
105. F. R. S. Lucena, L. C. C. de Araújo, M. do D. Rodrigues, T. G. da Silva, V. R. A. Pereira, G. C. G. Militão, D. A. F. Fontes, P. J. Rolim-Neto, F. F. da Silva, & S. C. Nascimento, Induction of cancer cell death by apoptosis and slow release of 5-fluoracil from metal-organic frameworks Cu-BTC. *Biomedicine & Pharmacotherapy*, **67** (2013) 707–713. <https://doi.org/10.1016/J.BIOPHA.2013.06.003>

106. K. Lu, C. He, & W. Lin, Nanoscale Metal–Organic Framework for Highly Effective Photodynamic Therapy of Resistant Head and Neck Cancer. *Journal of the American Chemical Society*, **136** (2014) 16712–16715.
<https://doi.org/10.1021/ja508679h>
107. W. J. Rieter, K. M. L. Taylor, H. An, W. Lin, & W. Lin, Nanoscale Metal–Organic Frameworks as Potential Multimodal Contrast Enhancing Agents. *Journal of the American Chemical Society*, **128** (2006) 9024–9025.
<https://doi.org/10.1021/ja0627444>
108. K. M. L. Taylor-Pashow, J. Della Rocca, Z. Xie, S. Tran, & W. Lin, Postsynthetic Modifications of Iron-Carboxylate Nanoscale Metal–Organic Frameworks for Imaging and Drug Delivery. *Journal of the American Chemical Society*, **131** (2009) 14261–14263. <https://doi.org/10.1021/ja906198y>
109. V. Lykourinou, Y. Chen, X.-S. Wang, L. Meng, T. Hoang, L.-J. Ming, R. L. Musselman, & S. Ma, Immobilization of MP-11 into a Mesoporous Metal–Organic Framework, MP-11@mesoMOF: A New Platform for Enzymatic Catalysis. *Journal of the American Chemical Society*, **133** (2011) 10382–10385.
<https://doi.org/10.1021/ja2038003>
110. F. Lyu, Y. Zhang, R. N. Zare, J. Ge, & Z. Liu, One-Pot Synthesis of Protein-Embedded Metal–Organic Frameworks with Enhanced Biological Activities. *Nano Letters*, **14** (2014) 5761–5765. <https://doi.org/10.1021/nl5026419>
111. N. Yan, X. Zhou, Y. Li, F. Wang, H. Zhong, H. Wang, & Q. Chen, Fe₂O₃ Nanoparticles Wrapped in Multi-walled Carbon Nanotubes With Enhanced Lithium Storage Capability. *Scientific Reports*, **3** (2013) 3392.
<https://doi.org/10.1038/srep03392>
112. G. Gao, L. Yu, H. Bin Wu, & X. W. David Lou, Hierarchical Tubular Structures Constructed by Carbon-coated α -Fe₂O₃ Nanorods for Highly Reversible Lithium Storage. *Small*, **10** (2014) 1741–1745. <https://doi.org/10.1002/sml.201303818>
113. S. Sajjadi, H. Ghourchian, & H. Tavakoli, Choline oxidase as a selective recognition element for determination of paraoxon. *Biosensors and Bioelectronics*, **24** (2009) 2509–2514. <https://doi.org/10.1016/J.BIOS.2009.01.008>
114. L. Wang, Q. Zhang, S. Chen, F. Xu, S. Chen, J. Jia, H. Tan, H. Hou, & Y. Song, Electrochemical Sensing and Biosensing Platform Based on Biomass-Derived Macroporous Carbon Materials. *Analytical Chemistry*, **86** (2014) 1414–1421.
<https://doi.org/10.1021/ac401563m>
115. S. Dong, P. Zhang, H. Liu, N. Li, & T. Huang, Direct electrochemistry and electrocatalysis of hemoglobin in composite film based on ionic liquid and NiO

- microspheres with different morphologies. *Biosensors and Bioelectronics*, **26** (2011) 4082–4087. <https://doi.org/10.1016/J.BIOS.2011.03.039>
116. H. Dai, W. Lü, X. Zuo, Q. Zhu, C. Pan, X. Niu, J. Liu, H. Chen, & X. Chen, A novel biosensor based on boronic acid functionalized metal-organic frameworks for the determination of hydrogen peroxide released from living cells. *Biosensors and Bioelectronics*, **95** (2017) 131–137. <https://doi.org/10.1016/J.BIOS.2017.04.021>
117. L. Ruiyi, X. Qianfang, L. Zaijun, S. Xiulan, & L. Junkang, Electrochemical immunosensor for ultrasensitive detection of microcystin-LR based on graphene–gold nanocomposite/functional conducting polymer/gold nanoparticle/ionic liquid composite film with electrodeposition. *Biosensors and Bioelectronics*, **44** (2013) 235–240. <https://doi.org/10.1016/J.BIOS.2013.01.007>
118. R. Zhang & W. Chen, Recent advances in graphene-based nanomaterials for fabricating electrochemical hydrogen peroxide sensors. *Biosensors and Bioelectronics*, **89** (2017) 249–268. <https://doi.org/10.1016/J.BIOS.2016.01.080>
119. L. Peng, S. Dong, W. Wei, X. Yuan, & T. Huang, Synthesis of reticulated hollow spheres structure NiCo₂S₄ and its application in organophosphate pesticides biosensor. *Biosensors and Bioelectronics*, **92** (2017) 563–569. <https://doi.org/10.1016/J.BIOS.2016.10.059>
120. N. Chauhan, J. Narang, & C. S. Pundir, Immobilization of rat brain acetylcholinesterase on ZnS and poly(indole-5-carboxylic acid) modified Au electrode for detection of organophosphorus insecticides. *Biosensors and Bioelectronics*, **29** (2011) 82–88. <https://doi.org/10.1016/J.BIOS.2011.07.070>
121. H. Dzudzevic Cancar, S. Soylemez, Y. Akpınar, M. Kesik, S. Göker, G. Gunbas, M. Volkan, & L. Toppare, A Novel Acetylcholinesterase Biosensor: Core–Shell Magnetic Nanoparticles Incorporating a Conjugated Polymer for the Detection of Organophosphorus Pesticides. *ACS Applied Materials & Interfaces*, **8** (2016) 8058–8067. <https://doi.org/10.1021/acsami.5b12383>
122. G. Yu, W. Wu, Q. Zhao, X. Wei, & Q. Lu, Efficient immobilization of acetylcholinesterase onto amino functionalized carbon nanotubes for the fabrication of high sensitive organophosphorus pesticides biosensors. *Biosensors and Bioelectronics*, **68** (2015) 288–294. <https://doi.org/10.1016/J.BIOS.2015.01.005>
123. H. Zhao, X. Ji, B. Wang, N. Wang, X. Li, R. Ni, & J. Ren, An ultra-sensitive acetylcholinesterase biosensor based on reduced graphene oxide-Au nanoparticles- β -cyclodextrin/Prussian blue-chitosan nanocomposites for organophosphorus pesticides detection. *Biosensors and Bioelectronics*, **65** (2015) 23–30. <https://doi.org/10.1016/J.BIOS.2014.10.007>

124. Y. Qian, I. A. Khan, & D. Zhao, Electrocatalysts Derived from Metal-Organic Frameworks for Oxygen Reduction and Evolution Reactions in Aqueous Media. *Small*, **13** (2017) 1701143. <https://doi.org/10.1002/sml.201701143>
125. I. Hod, P. Deria, W. Bury, J. E. Mondloch, C.-W. Kung, M. So, M. D. Sampson, A. W. Peters, C. P. Kubiak, O. K. Farha, & J. T. Hupp, A porous proton-relaying metal-organic framework material that accelerates electrochemical hydrogen evolution. *Nature Communications*, **6** (2015) 8304. <https://doi.org/10.1038/ncomms9304>
126. W. P. Lustig, S. Mukherjee, N. D. Rudd, A. V. Desai, J. Li, & S. K. Ghosh, Metal-organic frameworks: functional luminescent and photonic materials for sensing applications. *Chemical Society Reviews*, **46** (2017) 3242–3285. <https://doi.org/10.1039/C6CS00930A>
127. M.-X. Wu & Y.-W. Yang, Metal-Organic Framework (MOF)-Based Drug/Cargo Delivery and Cancer Therapy. *Advanced Materials*, **29** (2017) 1606134. <https://doi.org/10.1002/adma.201606134>
128. M. Yabushita, P. Li, V. Bernales, H. Kobayashi, A. Fukuoka, L. Gagliardi, O. K. Farha, & A. Katz, Unprecedented selectivity in molecular recognition of carbohydrates by a metal-organic framework. *Chemical Communications*, **52** (2016) 7094–7097. <https://doi.org/10.1039/C6CC03266D>
129. F. Zheng, Z. Yin, H. Xia, G. Bai, & Y. Zhang, Porous MnO@C nanocomposite derived from metal-organic frameworks as anode materials for long-life lithium-ion batteries. *Chemical Engineering Journal*, **327** (2017) 474–480. <https://doi.org/10.1016/J.CEJ.2017.06.097>
130. G. K. H. Shimizu, J. M. Taylor, & S. Kim, Proton conduction with metal-organic frameworks. *Science*, **341** (2013) 354–355. <https://doi.org/10.1126/science.1239872>
131. N. S. Lopa, M. M. Rahman, F. Ahmed, S. Chandra Sutradhar, T. Ryu, & W. Kim, A base-stable metal-organic framework for sensitive and non-enzymatic electrochemical detection of hydrogen peroxide. *Electrochimica Acta*, **274** (2018) 49–56. <https://doi.org/10.1016/J.ELECTACTA.2018.03.148>
132. D. Zhang, J. Zhang, R. Zhang, H. Shi, Y. Guo, X. Guo, S. Li, & B. Yuan, 3D porous metal-organic framework as an efficient electrocatalyst for nonenzymatic sensing application. *Talanta*, **144** (2015) 1176–1181. <https://doi.org/10.1016/J.TALANTA.2015.07.091>
133. Y. Shu, Y. Yan, J. Chen, Q. Xu, H. Pang, & X. Hu, Ni and NiO Nanoparticles Decorated Metal-Organic Framework Nanosheets: Facile Synthesis and High-Performance Nonenzymatic Glucose Detection in Human Serum. *ACS Applied*

- Materials & Interfaces*, **9** (2017) 22342–22349.
<https://doi.org/10.1021/acsami.7b07501>
134. L. Yang, C. Xu, W. Ye, & W. Liu, An electrochemical sensor for H₂O₂ based on a new Co-metal-organic framework modified electrode. *Sensors and Actuators B: Chemical*, **215** (2015) 489–496. <https://doi.org/10.1016/J.SNB.2015.03.104>
135. C. Li, T. Zhang, J. Zhao, H. Liu, B. Zheng, Y. Gu, X. Yan, Y. Li, N. Lu, Z. Zhang, & G. Feng, Boosted Sensor Performance by Surface Modification of Bifunctional *rht* - Type Metal–Organic Framework with Nanosized Electrochemically Reduced Graphene Oxide. *ACS Applied Materials & Interfaces*, **9** (2017) 2984–2994.
<https://doi.org/10.1021/acsami.6b13788>
136. D. Zhang, J. Zhang, H. Shi, X. Guo, Y. Guo, R. Zhang, & B. Yuan, Redox-active micro-sized metal-organic framework for efficient nonenzymatic H₂O₂ sensing. *Sensors and Actuators B: Chemical*, **221** (2015) 224–229.
<https://doi.org/10.1016/J.SNB.2015.06.079>
137. J. Yang, F. Zhao, & B. Zeng, One-step synthesis of a copper-based metal–organic framework–graphene nanocomposite with enhanced electrocatalytic activity. *RSC Advances*, **5** (2015) 22060–22065. <https://doi.org/10.1039/C4RA16950F>
138. B. Yuan, R. Zhang, X. Jiao, J. Li, H. Shi, & D. Zhang, Amperometric determination of reduced glutathione with a new Co-based metal-organic coordination polymer modified electrode. *Electrochemistry Communications*, **40** (2014) 92–95.
<https://doi.org/10.1016/J.ELECOM.2014.01.006>
139. Z. Peng, Z. Jiang, X. Huang, & Y. Li, A novel electrochemical sensor of tryptophan based on silver nanoparticles/metal–organic framework composite modified glassy carbon electrode. *RSC Advances*, **6** (2016) 13742–13748.
<https://doi.org/10.1039/C5RA25251B>
140. H. Hosseini, H. Ahmar, A. Dehghani, A. Bagheri, A. Tadjarodi, & A. R. Fakhari, A novel electrochemical sensor based on metal-organic framework for electro-catalytic oxidation of L-cysteine. *Biosensors and Bioelectronics*, **42** (2013) 426–429.
<https://doi.org/10.1016/J.BIOS.2012.09.062>
141. M. M. Rahman, A. J. S. Ahammad, J.-H. Jin, S. J. Ahn, J.-J. Lee, M. M. Rahman, A. J. S. Ahammad, J.-H. Jin, S. J. Ahn, & J.-J. Lee, A Comprehensive Review of Glucose Biosensors Based on Nanostructured Metal-Oxides. *Sensors*, **10** (2010) 4855–4886. <https://doi.org/10.3390/s100504855>
142. T. D. Thanh, J. Balamurugan, S. H. Lee, N. H. Kim, & J. H. Lee, Effective seed-assisted synthesis of gold nanoparticles anchored nitrogen-doped graphene for

- electrochemical detection of glucose and dopamine. *Biosensors and Bioelectronics*, **81** (2016) 259–267. <https://doi.org/10.1016/J.BIOS.2016.02.070>
143. S. Park, H. Boo, & T. D. Chung, *Electrochemical non-enzymatic glucose sensors* (2006). <https://doi.org/10.1016/j.aca.2005.05.080>
144. J. Zhang, M. Liu, T. Yang, K. Yang, & H. Wang, A novel magnetic biochar from sewage sludge: synthesis and its application for the removal of malachite green from wastewater. *Water Science and Technology*, **74** (2016) 1971–1979. <https://doi.org/10.2166/wst.2016.386>
145. R. Yuan, H. Li, X. Yin, J. Lu, & L. Zhang, 3D CuO nanosheet wrapped nanofilm grown on Cu foil for high-performance non-enzymatic glucose biosensor electrode. *Talanta*, **174** (2017) 514–520. <https://doi.org/10.1016/J.TALANTA.2017.06.030>
146. B. Yuan, C. Xu, D. Deng, Y. Xing, L. Liu, H. Pang, & D. Zhang, Graphene oxide/nickel oxide modified glassy carbon electrode for supercapacitor and nonenzymatic glucose sensor. *Electrochimica Acta*, **88** (2013) 708–712. <https://doi.org/10.1016/J.ELECTACTA.2012.10.102>
147. D.-J. Lee, Q. Li, H. Kim, & K. Lee, Preparation of Ni-MOF-74 membrane for CO₂ separation by layer-by-layer seeding technique. *Microporous and Mesoporous Materials*, **163** (2012) 169–177. <https://doi.org/10.1016/J.MICROMESO.2012.07.008>
148. Y. Song, C. Zhu, H. Li, D. Du, & Y. Lin, A nonenzymatic electrochemical glucose sensor based on mesoporous Au/Pt nanodendrites. *RSC Advances*, **5** (2015) 82617–82622. <https://doi.org/10.1039/C5RA16953D>
149. B. Valeur & I. Leray, Design principles of fluorescent molecular sensors for cation recognition. *Coordination Chemistry Reviews*, **205** (2000) 3–40. [https://doi.org/10.1016/S0010-8545\(00\)00246-0](https://doi.org/10.1016/S0010-8545(00)00246-0)
150. A. P. de Silva, T. S. Moody, & G. D. Wright, Fluorescent PET (Photoinduced Electron Transfer) sensors as potent analytical tools. *The Analyst*, **134** (2009) 2385. <https://doi.org/10.1039/b912527m>
151. H. J. Carlson & R. E. Campbell, Genetically encoded FRET-based biosensors for multiparameter fluorescence imaging. *Current Opinion in Biotechnology*, **20** (2009) 19–27. <https://doi.org/10.1016/J.COPBIO.2009.01.003>
152. * and Jong Seung Kim† & D. T. Quang‡, Calixarene-Derived Fluorescent Probes. (2007). <https://doi.org/10.1021/CR068046J>
153. C. Lodeiro & F. Pina, Luminescent and chromogenic molecular probes based on polyamines and related compounds. *Coordination Chemistry Reviews*, **253** (2009) 1353–1383. <https://doi.org/10.1016/J.CCR.2008.09.008>

154. J. Wu, W. Liu, J. Ge, H. Zhang, & P. Wang, New sensing mechanisms for design of fluorescent chemosensors emerging in recent years. *Chemical Society Reviews*, **40** (2011) 3483. <https://doi.org/10.1039/c0cs00224k>
155. K. Kiyose, S. Aizawa, E. Sasaki, H. Kojima, K. Hanaoka, T. Terai, Y. Urano, & T. Nagano, Molecular Design Strategies for Near-Infrared Ratiometric Fluorescent Probes Based on the Unique Spectral Properties of Aminocyanines. *Chemistry - A European Journal*, **15** (2009) 9191–9200. <https://doi.org/10.1002/chem.200900035>
156. M. Kasha, Collisional Perturbation of Spin-Orbital Coupling and the Mechanism of Fluorescence Quenching. A Visual Demonstration of the Perturbation. *The Journal of Chemical Physics*, **20** (1952) 71–74. <https://doi.org/10.1063/1.1700199>
157. M. A. El-Sayed, Triplet state. Its radiative and nonradiative properties. *Accounts of Chemical Research*, **1** (1968) 8–16. <https://doi.org/10.1021/ar50001a002>
158. P. Svejda, R. R. Anderson, & A. H. Maki, Optical detection of magnetic resonance measurements of the effects of pH on the triplet states of benzimidazole and purine. *Journal of the American Chemical Society*, **100** (1978) 7131–7138. <https://doi.org/10.1021/ja00491a001>
159. H. Masuhara, H. Shioyama, T. Saito, K. Hamada, S. Yasoshima, & N. Mataga, Fluorescence quenching mechanism of aromatic hydrocarbons by closed-shell heavy metal ions in aqueous and organic solutions. *The Journal of Physical Chemistry*, **88** (1984) 5868–5873. <https://doi.org/10.1021/j150668a026>
160. † Charlotte N. Burress, † Martha I. Bodine, ‡ Oussama Elbjeirami, † Joseph H. Reibenspies, *, ‡ and Mohammad A. Omary, & † François P. Gabbaï*, Enhancement of External Spin–Orbit Coupling Effects Caused by Metal–Metal Cooperativity. (2007). <https://doi.org/10.1021/IC061998N>
161. H. N. Kim, W. X. Ren, J. S. Kim, & J. Yoon, Fluorescent and colorimetric sensors for detection of lead, cadmium, and mercury ions. *Chem. Soc. Rev.*, **41** (2012) 3210–3244. <https://doi.org/10.1039/C1CS15245A>
162. S. Lee, B. A. Rao, & Y.-A. Son, Colorimetric and “turn-on” fluorescent determination of Hg²⁺ ions based on a rhodamine–pyridine derivative. *Sensors and Actuators B: Chemical*, **196** (2014) 388–397. <https://doi.org/10.1016/j.snb.2014.02.025>
163. D.-H. Kim, J. Seong, H. Lee, & K.-H. Lee, Ratiometric fluorescence detection of Hg(II) in aqueous solutions at physiological pH and live cells with a chemosensor based on tyrosine. *Sensors and Actuators B: Chemical*, **196** (2014) 421–428. <https://doi.org/10.1016/j.snb.2014.02.029>

164. H. Zhu, Y. Lin, G. Wang, Y. Chen, X. Lin, & N. Fu, A coordination driven deaggregation approach toward Hg²⁺-specific chemosensors based on thioether linked squaraine-aniline dyads. *Sensors and Actuators B: Chemical*, **198** (2014) 201–209.
<https://doi.org/10.1016/j.snb.2014.03.021>
165. C. Wang, D. Zhang, X. Huang, P. Ding, Z. Wang, Y. Zhao, & Y. Ye, A ratiometric fluorescent chemosensor for Hg²⁺ based on FRET and its application in living cells. *Sensors and Actuators B: Chemical*, **198** (2014) 33–40.
<https://doi.org/10.1016/j.snb.2014.03.032>
166. A. Han, X. Liu, G. D. Prestwich, & L. Zang, Fluorescent sensor for Hg²⁺ detection in aqueous solution. *Sensors and Actuators B: Chemical*, **198** (2014) 274–277. <https://doi.org/10.1016/j.snb.2014.03.033>
167. L. Xu, S. Wang, Y. Lv, Y.-A. Son, & D. Cao, A highly selective and sensitive photoswitchable fluorescent probe for Hg²⁺ based on bisthienylethene–rhodamine 6G dyad and for live cells imaging. *Spectrochimica Acta Part A: Molecular and Biomolecular Spectroscopy*, **128** (2014) 567–574.
<https://doi.org/10.1016/j.saa.2014.03.001>
168. X. Li, C. Zheng, A. Yuan, L. Yang, H. Wang, & H. Wang, A highly selective ratiometric fluorescent sensor for Hg²⁺ based on 1,8-naphthalimide. *Coloration Technology*, **130** (2014) 236–242. <https://doi.org/10.1111/cote.12081>
169. R. Kavitha & T. Stalin, A highly selective chemosensor for colorimetric detection of Hg²⁺ and fluorescence detection of pH changes in aqueous solution. *Journal of Luminescence*, **149** (2014) 12–18. <https://doi.org/10.1016/j.jlumin.2013.11.044>
170. M. Wang, F.-Y. Yan, Y. Zou, N. Yang, L. Chen, & L.-G. Chen, A rhodamine derivative as selective fluorescent and colorimetric chemosensor for mercury (II) in buffer solution, test strips and living cells. *Spectrochimica Acta Part A: Molecular and Biomolecular Spectroscopy*, **123** (2014) 216–223.
<https://doi.org/10.1016/j.saa.2013.12.079>
171. S. Liu, Z. Shi, W. Xu, H. Yang, N. Xi, X. Liu, Q. Zhao, & W. Huang, A class of wavelength-tunable near-infrared aza-BODIPY dyes and their application for sensing mercury ion. *Dyes and Pigments*, **103** (2014) 145–153.
<https://doi.org/10.1016/j.dyepig.2013.12.004>
172. D. Udhayakumari & S. Velmathi, Colorimetric chemosensor for multi-signaling detection of metal ions using pyrrole based Schiff bases. *Spectrochimica Acta Part A: Molecular and Biomolecular Spectroscopy*, **122** (2014) 428–435.
<https://doi.org/10.1016/j.saa.2013.11.083>

173. N. Wanichacheva, O. Hanmeng, S. Kraithong, & K. Sukrat, Dual optical Hg²⁺-selective sensing through FRET system of fluorescein and rhodamine B fluorophores. *Journal of Photochemistry and Photobiology A: Chemistry*, **278** (2014) 75–81. <https://doi.org/10.1016/J.JPHOTOCHEM.2014.01.003>
174. N. Wanichacheva, P. Praikaew, T. Suwanich, & K. Sukrat, “Naked-eye” colorimetric and “turn-on” fluorometric chemosensors for reversible Hg²⁺ detection. *Spectrochimica Acta Part A: Molecular and Biomolecular Spectroscopy*, **118** (2014) 908–914. <https://doi.org/10.1016/j.saa.2013.09.140>
175. R. Puingam, A. Chindaduang, G. Tumcharern, D. S.-T. Phromyothin, & S. Pratontep, Theoretical Investigation of Rhodamine6G Derivative as Fluorescence Metal Ion Sensor. *Integrated Ferroelectrics*, **155** (2014) 126–133. <https://doi.org/10.1080/10584587.2014.905380>
176. X. Wang, J. Zhao, C. Guo, M. Pei, & G. Zhang, Simple hydrazide-based fluorescent sensors for highly sensitive and selective optical signaling of Cu²⁺ and Hg²⁺ in aqueous solution. *Sensors and Actuators B: Chemical*, **193** (2014) 157–165. <https://doi.org/10.1016/j.snb.2013.11.111>
177. Junhua Jia, Xiang Lin, Alexander J. Blake, * Neil R. Champness, * Peter Hubberstey, Limin Shao, Gavin Walker, and Claire Wilson, & M. Schröder*, Triggered Ligand Release Coupled to Framework Rearrangement: Generating Crystalline Porous Coordination Materials. (2006). <https://doi.org/10.1021/IC061095U>
178. L. Hao, H. Song, Y. Su, & Y. Lv, A cubic luminescent graphene oxide functionalized Zn-based metal-organic framework composite for fast and highly selective detection of Cu²⁺ ions in aqueous solution. *The Analyst*, **139** (2014) 764–770. <https://doi.org/10.1039/C3AN01943H>
179. J. Zhao, Y.-N. Wang, W.-W. Dong, Y.-P. Wu, D.-S. Li, & Q.-C. Zhang, A Robust Luminescent Tb(III)-MOF with Lewis Basic Pyridyl Sites for the Highly Sensitive Detection of Metal Ions and Small Molecules. *Inorganic Chemistry*, **55** (2016) 3265–3271. <https://doi.org/10.1021/acs.inorgchem.5b02294>
180. X. Lin, G. Gao, L. Zheng, Y. Chi, & G. Chen, Encapsulation of Strongly Fluorescent Carbon Quantum Dots in Metal–Organic Frameworks for Enhancing Chemical Sensing. *Analytical Chemistry*, **86** (2014) 1223–1228. <https://doi.org/10.1021/ac403536a>
181. P.-Y. Du, W. Gu, & X. Liu, Multifunctional Three-Dimensional Europium Metal–Organic Framework for Luminescence Sensing of Benzaldehyde and Cu²⁺ and Selective Capture of Dye Molecules. *Inorganic Chemistry*, **55** (2016) 7826–7828. <https://doi.org/10.1021/acs.inorgchem.6b01385>

182. J.-M. Zhou, W. Shi, H.-M. Li, H. Li, & P. Cheng, Experimental Studies and Mechanism Analysis of High-Sensitivity Luminescent Sensing of Pollutational Small Molecules and Ions in Ln_4O_4 Cluster Based Microporous Metal–Organic Frameworks. *The Journal of Physical Chemistry C*, **118** (2014) 416–426. <https://doi.org/10.1021/jp4097502>
183. Y. Xiao, Y. Cui, Q. Zheng, S. Xiang, G. Qian, & B. Chen, A microporous luminescent metal–organic framework for highly selective and sensitive sensing of Cu^{2+} in aqueous solution. *Chemical Communications*, **46** (2010) 5503. <https://doi.org/10.1039/c0cc00148a>
184. J. Wang, M. Jiang, L. Yan, R. Peng, M. Huangfu, X. Guo, Y. Li, & P. Wu, Multifunctional Luminescent Eu(III)-Based Metal–Organic Framework for Sensing Methanol and Detection and Adsorption of Fe(III) Ions in Aqueous Solution. *Inorganic Chemistry*, **55** (2016) 12660–12668. <https://doi.org/10.1021/acs.inorgchem.6b01815>
185. S.-S. Zhao, J. Yang, Y.-Y. Liu, & J.-F. Ma, Fluorescent Aromatic Tag-Functionalized MOFs for Highly Selective Sensing of Metal Ions and Small Organic Molecules. *Inorganic Chemistry*, **55** (2016) 2261–2273. <https://doi.org/10.1021/acs.inorgchem.5b02666>
186. J.-N. Hao & B. Yan, Amino-decorated lanthanide(iii) organic extended frameworks for multi-color luminescence and fluorescence sensing. *J. Mater. Chem. C*, **2** (2014) 6758–6764. <https://doi.org/10.1039/C4TC00962B>
187. P. Yi, H. Huang, Y. Peng, D. Liu, & C. Zhong, A series of europium-based metal organic frameworks with tuned intrinsic luminescence properties and detection capacities. *RSC Advances*, **6** (2016) 111934–111941. <https://doi.org/10.1039/C6RA23263A>
188. P. Kukkar, D. Kukkar, H. Sammi, K. Singh, M. Rawat, P. Singh, S. Basu, & K.-H. Kim, A facile means for the improvement of sensing properties of metal-organic frameworks through control on the key synthesis variables. *Sensors and Actuators B: Chemical*, **271** (2018) 157–163. <https://doi.org/10.1016/J.SNB.2018.05.118>
189. H. Xu, F. Liu, Y. Cui, B. Chen, & G. Qian, A luminescent nanoscale metal–organic framework for sensing of nitroaromatic explosives. *Chemical Communications*, **47** (2011) 3153. <https://doi.org/10.1039/c0cc05166g>
190. C. Zhang, L. Sun, Y. Yan, J. Li, X. Song, Y. Liu, & Z. Liang, A luminescent cadmium metal–organic framework for sensing of nitroaromatic explosives. *Dalton Transactions*, **44** (2015) 230–236. <https://doi.org/10.1039/C4DT02227K>

191. S. Khatua, S. Goswami, S. Biswas, K. Tomar, H. S. Jena, & S. Konar, Stable Multiresponsive Luminescent MOF for Colorimetric Detection of Small Molecules in Selective and Reversible Manner. *Chemistry of Materials*, **27** (2015) 5349–5360. <https://doi.org/10.1021/acs.chemmater.5b01773>
192. W. Xie, S.-R. Zhang, D.-Y. Du, J.-S. Qin, S.-J. Bao, J. Li, Z.-M. Su, W.-W. He, Q. Fu, & Y.-Q. Lan, Stable Luminescent Metal–Organic Frameworks as Dual-Functional Materials To Encapsulate Ln^{3+} Ions for White-Light Emission and To Detect Nitroaromatic Explosives. *Inorganic Chemistry*, **54** (2015) 3290–3296. <https://doi.org/10.1021/ic5029383>
193. R. Kaur, A. K. Paul, & A. Deep, Nanocomposite of europium organic framework and quantum dots for highly sensitive chemosensing of trinitrotoluene. *Forensic Science International*, **242** (2014) 88–93. <https://doi.org/10.1016/J.FORSCIINT.2014.06.028>
194. N. Campagnol, E. R. Souza, D. E. De Vos, K. Binnemans, & J. Fransaer, Luminescent terbium-containing metal–organic framework films: new approaches for the electrochemical synthesis and application as detectors for explosives. *Chem. Commun.*, **50** (2014) 12545–12547. <https://doi.org/10.1039/C4CC05742B>
195. K. Vellingiri, D. W. Boukhvalov, S. K. Pandey, A. Deep, & K.-H. Kim, Luminescent metal-organic frameworks for the detection of nitrobenzene in aqueous media. *Sensors and Actuators B: Chemical*, **245** (2017) 305–313. <https://doi.org/10.1016/J.SNB.2017.01.126>
196. P. Kumar, K.-H. Kim, V. Bansal, A. K. Paul, & A. Deep, Practical utilization of nanocrystal metal organic framework biosensor for parathion specific recognition. *Microchemical Journal*, **128** (2016) 102–107. <https://doi.org/10.1016/J.MICROC.2016.04.008>
197. L.-G. Qiu, Z.-Q. Li, Y. Wu, W. Wang, T. Xu, & X. Jiang, Facile synthesis of nanocrystals of a microporous metal–organic framework by an ultrasonic method and selective sensing of organoamines. *Chemical Communications*, **0** (2008) 3642. <https://doi.org/10.1039/b804126a>
198. J. Tao, X. Wang, T. Sun, H. Cai, Y. Wang, T. Lin, D. Fu, L. L. Y. Ting, Y. Gu, & D. Zhao, Hybrid Photonic Cavity with Metal-Organic Framework Coatings for the Ultra-Sensitive Detection of Volatile Organic Compounds with High Immunity to Humidity. *Scientific Reports*, **7** (2017) 41640. <https://doi.org/10.1038/srep41640>
199. K. Vellingiri, A. Deep, K.-H. Kim, D. W. Boukhvalov, P. Kumar, & Q. Yao, The sensitive detection of formaldehyde in aqueous media using zirconium-based metal

- organic frameworks. *Sensors and Actuators B: Chemical*, **241** (2017) 938–948.
<https://doi.org/10.1016/J.SNB.2016.11.017>
200. C. A. Kent, B. P. Mehl, L. Ma, J. M. Papanikolas, T. J. Meyer, & W. Lin, Energy Transfer Dynamics in Metal–Organic Frameworks. *Journal of the American Chemical Society*, **132** (2010) 12767–12769. <https://doi.org/10.1021/ja102804s>
201. Z. Guo, H. Xu, S. Su, J. Cai, S. Dang, S. Xiang, G. Qian, H. Zhang, M. O’Keeffe, & B. Chen, A robust near infrared luminescent ytterbium metal–organic framework for sensing of small molecules. *Chemical Communications*, **47** (2011) 5551.
<https://doi.org/10.1039/c1cc10897b>
202. C. Li, J. Huang, H. Zhu, L. Liu, Y. Feng, G. Hu, & X. Yu, Dual-emitting fluorescence of Eu/Zr-MOF for ratiometric sensing formaldehyde. *Sensors and Actuators B: Chemical*, **253** (2017) 275–282.
<https://doi.org/10.1016/J.SNB.2017.06.064>
203. L. Wang, G. Fan, X. Xu, D. Chen, L. Wang, W. Shi, & P. Cheng, Detection of polychlorinated benzenes (persistent organic pollutants) by a luminescent sensor based on a lanthanide metal–organic framework. *Journal of Materials Chemistry A*, **5** (2017) 5541–5549. <https://doi.org/10.1039/C7TA00256D>
204. F.-N. Shi, M. L. Pinto, D. Ananias, & J. Rocha, Structure, topology, gas adsorption and photoluminescence of multifunctional porous RE₃+-furan-2,5-dicarboxylate metal organic frameworks. *Microporous and Mesoporous Materials*, **188** (2014) 172–181. <https://doi.org/10.1016/J.MICROMESO.2014.01.012>
205. Z. Dou, J. Yu, H. Xu, Y. Cui, Y. Yang, & G. Qian, Preparation and thiols sensing of luminescent metal–organic framework films functionalized with lanthanide ions. *Microporous and Mesoporous Materials*, **179** (2013) 198–204.
<https://doi.org/10.1016/J.MICROMESO.2013.06.008>
206. N. B. Shustova, A. F. Cozzolino, S. Reineke, M. Baldo, & M. Dincă, Selective Turn-On Ammonia Sensing Enabled by High-Temperature Fluorescence in Metal–Organic Frameworks with Open Metal Sites. *Journal of the American Chemical Society*, **135** (2013) 13326–13329. <https://doi.org/10.1021/ja407778a>
207. P. Wu, J. Wang, C. He, X. Zhang, Y. Wang, T. Liu, & C. Duan, Luminescent Metal–Organic Frameworks for Selectively Sensing Nitric Oxide in an Aqueous Solution and in Living Cells. *Advanced Functional Materials*, **22** (2012) 1698–1703.
<https://doi.org/10.1002/adfm.201102157>
208. X.-Y. Xu & B. Yan, An efficient and sensitive fluorescent pH sensor based on amino functional metal–organic frameworks in aqueous environment. *Dalton Transactions*, **45** (2016) 7078–7084. <https://doi.org/10.1039/C6DT00361C>

209. Y.-J. Li, Y.-L. Wang, & Q.-Y. Liu, The Highly Connected MOFs Constructed from Nonanuclear and Trinuclear Lanthanide-Carboxylate Clusters: Selective Gas Adsorption and Luminescent pH Sensing. *Inorganic Chemistry*, **56** (2017) 2159–2164. <https://doi.org/10.1021/acs.inorgchem.6b02811>
210. X. Lian, D. Zhao, Y. Cui, Y. Yang, & G. Qian, A near infrared luminescent metal–organic framework for temperature sensing in the physiological range. *Chemical Communications*, **51** (2015) 17676–17679. <https://doi.org/10.1039/C5CC07532G>
211. R. H. Hashemi, William G. Bradley, & Christopher J. Lisanti, *MRI the basics*. Baltimore: Williams and Wilkins. (1997)
212. H. Bin Na, I. C. Song, & T. Hyeon, Inorganic Nanoparticles for MRI Contrast Agents. *Advanced Materials*, **21** (2009) 2133–2148. <https://doi.org/10.1002/adma.200802366>
213. R. Nishiyabu, N. Hashimoto, T. Cho, K. Watanabe, T. Yasunaga, A. Endo, K. Kaneko, T. Niidome, M. Murata, C. Adachi, Y. Katayama, M. Hashizume, & N. Kimizuka, Nanoparticles of Adaptive Supramolecular Networks Self-Assembled from Nucleotides and Lanthanide Ions. *Journal of the American Chemical Society*, **131** (2009) 2151–2158. <https://doi.org/10.1021/ja8058843>
214. M. D. Rowe, C.-C. Chang, D. H. Thamm, S. L. Kraft, J. F. Harmon, A. P. Vogt, B. S. Sumerlin, & S. G. Boyes, Tuning the Magnetic Resonance Imaging Properties of Positive Contrast Agent Nanoparticles by Surface Modification with RAFT Polymers. *Langmuir*, **25** (2009) 9487–9499. <https://doi.org/10.1021/la900730b>
215. † Young-wook Jun, ‡ Yong-Min Huh, † Jin-sil Choi, † Jae-Hyun Lee, ‡ Ho-Taek Song, ‡ Sungjun Kim, ‡ Sungjun Kim, § Sarah Yoon, § Kyung-Sup Kim, ⊥ Jeon-Soo Shin, *, ‡ and Jin-Suck Suh, & † Jinwoo Cheon*, Nanoscale Size Effect of Magnetic Nanocrystals and Their Utilization for Cancer Diagnosis via Magnetic Resonance Imaging. (2005). <https://doi.org/10.1021/JA0422155>
216. J.-H. Lee, Y.-M. Huh, Y. Jun, J. Seo, J. Jang, H.-T. Song, S. Kim, E.-J. Cho, H.-G. Yoon, J.-S. Suh, & J. Cheon, Artificially engineered magnetic nanoparticles for ultra-sensitive molecular imaging. *Nature Medicine*, **13** (2007) 95–99. <https://doi.org/10.1038/nm1467>
217. J. Lee & A. Koretsky, Manganese Enhanced Magnetic Resonance Imaging. *Current Pharmaceutical Biotechnology*, **5** (2004) 529–537. <https://doi.org/10.2174/1389201043376607>
218. K. Brindle, New approaches for imaging tumour responses to treatment. *Nature Reviews Cancer*, **8** (2008) 94–107. <https://doi.org/10.1038/nrc2289>

219. D. P. Cormode, E. Roessl, A. Thran, T. Skajaa, R. E. Gordon, J.-P. Schlomka, V. Fuster, E. A. Fisher, W. J. M. Mulder, R. Proksa, & Z. A. Fayad, Atherosclerotic Plaque Composition: Analysis with Multicolor CT and Targeted Gold Nanoparticles. *Radiology*, **256** (2010) 774–782. <https://doi.org/10.1148/radiol.10092473>
220. D. Pan, E. Roessl, J.-P. Schlomka, S. D. Caruthers, A. Senpan, M. J. Scott, J. S. Allen, H. Zhang, G. Hu, P. J. Gaffney, E. T. Choi, V. Rasche, S. A. Wickline, R. Proksa, & G. M. Lanza, Computed Tomography in Color: NanoK-Enhanced Spectral CT Molecular Imaging. *Angewandte Chemie International Edition*, **49** (2010) 9635–9639. <https://doi.org/10.1002/anie.201005657>
221. J. P. Schlomka, E. Roessl, R. Dorscheid, S. Dill, G. Martens, T. Istel, C. Bäumer, C. Herrmann, R. Steadman, G. Zeitler, A. Livne, & R. Proksa, Experimental feasibility of multi-energy photon-counting K-edge imaging in pre-clinical computed tomography. *Physics in Medicine and Biology*, **53** (2008) 4031–4047. <https://doi.org/10.1088/0031-9155/53/15/002>
222. E. Roessl, B. Brendel, K.-J. Engel, J.-P. Schlomka, A. Thran, & R. Proksa, Sensitivity of Photon-Counting Based K -Edge Imaging in X-ray Computed Tomography. *IEEE Transactions on Medical Imaging*, **30** (2011) 1678–1690. <https://doi.org/10.1109/TMI.2011.2142188>
223. W. J. Song, Intracellular DNA and microRNA sensing based on metal-organic framework nanosheets with enzyme-free signal amplification. *Talanta*, **170** (2017) 74–80. <https://doi.org/10.1016/j.talanta.2017.02.040>
224. J.-C. Tan, P. J. Saines, E. G. Bithell, & A. K. Cheetham, Hybrid Nanosheets of an Inorganic–Organic Framework Material: Facile Synthesis, Structure, and Elastic Properties. *ACS Nano*, **6** (2012) 615–621. <https://doi.org/10.1021/nn204054k>
225. H. Furukawa, F. Gándara, Y.-B. Zhang, J. Jiang, W. L. Queen, M. R. Hudson, & O. M. Yaghi, Water Adsorption in Porous Metal–Organic Frameworks and Related Materials. *Journal of the American Chemical Society*, **136** (2014) 4369–4381. <https://doi.org/10.1021/ja500330a>
226. Y. Wu, J. Han, P. Xue, R. Xu, & Y. Kang, Nano metal–organic framework (NMOF)-based strategies for multiplexed microRNA detection in solution and living cancer cells. *Nanoscale*, **7** (2015) 1753–1759. <https://doi.org/10.1039/C4NR05447D>
227. C. Tian, L. Zhu, F. Lin, & S. G. Boyes, Poly(acrylic acid) Bridged Gadolinium Metal–Organic Framework–Gold Nanoparticle Composites as Contrast Agents for Computed Tomography and Magnetic Resonance Bimodal Imaging. *ACS Applied Materials & Interfaces*, **7** (2015) 17765–17775. <https://doi.org/10.1021/acsami.5b03998>

228. Y.-M. Wang, W. Liu, & X.-B. Yin, Self-Limiting Growth Nanoscale Coordination Polymers for Fluorescence and Magnetic Resonance Dual-Modality Imaging. *Advanced Functional Materials*, **26** (2016) 8463–8470. <https://doi.org/10.1002/adfm.201602925>
229. V. M. Suresh, S. Chatterjee, R. Modak, V. Tiwari, A. B. Patel, T. K. Kundu, & T. K. Maji, Oligo(*p* -phenyleneethynylene)-Derived Porous Luminescent Nanoscale Coordination Polymer of Gd^{III}: Bimodal Imaging and Nitroaromatic Sensing. *The Journal of Physical Chemistry C*, **118** (2014) 12241–12249. <https://doi.org/10.1021/jp501030h>
230. D. Liu, C. He, C. Poon, & W. Lin, Theranostic nanoscale coordination polymers for magnetic resonance imaging and bisphosphonate delivery. *J. Mater. Chem. B*, **2** (2014) 8249–8255. <https://doi.org/10.1039/C4TB00751D>
231. J. Fang, Y. Yang, W. Xiao, B. Zheng, Y.-B. Lv, X.-L. Liu, & J. Ding, Extremely low frequency alternating magnetic field-triggered and MRI-traced drug delivery by optimized magnetic zeolitic imidazolate framework-90 nanoparticles. *Nanoscale*, **8** (2016) 3259–3263. <https://doi.org/10.1039/C5NR08086J>
232. W. Morris, C. J. Doonan, H. Furukawa, R. Banerjee, & O. M. Yaghi, Crystals as Molecules: Postsynthesis Covalent Functionalization of Zeolitic Imidazolate Frameworks. *Journal of the American Chemical Society*, **130** (2008) 12626–12627. <https://doi.org/10.1021/ja805222x>
233. T. Isobe, Y. Arai, S. Yanagida, S. Matsushita, & A. Nakajima, Solvothermal preparation and gas permeability of an IRMOF-3 membrane. *Microporous and Mesoporous Materials*, **241** (2017) 218–225. <https://doi.org/10.1016/J.MICROMESO.2016.12.031>
234. A. R. Chowdhuri, T. Singh, S. K. Ghosh, & S. K. Sahu, Carbon Dots Embedded Magnetic Nanoparticles @Chitosan @Metal Organic Framework as a Nanoprobe for pH Sensitive Targeted Anticancer Drug Delivery. *ACS Applied Materials & Interfaces*, **8** (2016) 16573–16583. <https://doi.org/10.1021/acsami.6b03988>
235. K. E. deKrafft, W. S. Boyle, L. M. Burk, O. Z. Zhou, & W. Lin, Zr- and Hf-based nanoscale metal-organic frameworks as contrast agents for computed tomography. *Journal of Materials Chemistry*, **22** (2012) 18139. <https://doi.org/10.1039/c2jm32299d>
236. C. Wang, O. Volotskova, K. Lu, M. Ahmad, C. Sun, L. Xing, & W. Lin, Synergistic Assembly of Heavy Metal Clusters and Luminescent Organic Bridging Ligands in Metal-Organic Frameworks for Highly Efficient X-ray Scintillation. *Journal of the American Chemical Society*, **136** (2014) 6171–6174. <https://doi.org/10.1021/ja500671h>

Chapter 12

Nanoscale Metal Organic Framework for Phototherapy of Cancer

Fulya Gülbağça¹, Fatima Elmusa¹, Kemal Cellat¹, Anish Khan^{2,3}, Fatih Şen^{1,*}

¹Sen Research Group, Department of Biochemistry, Faculty of Arts and Science, Dumlupınar University, Evliya Çelebi Campus, 43100 Kütahya, Turkey

²Chemistry Department, Faculty of Science, King Abdulaziz University, Jeddah-21589, P.O. Box 80203, Saudi Arabia

³Center of Excellence for Advanced Materials Research, King Abdulaziz University, Jeddah 21589, P.O. Box 80203, Saudi Arabia

*fatih.sen@dpu.edu.tr

Abstract

Phototherapy is generally used to describe Ultraviolet B (UVB) therapy, but it is a general term and concept using the non-ionizing electromagnetic radiation and its therapeutic effects. Photodynamic therapy (PDT) and Photothermal therapy (PTT) are the basis of phototherapy. In PDT, there is usually a need for Photosensitizers (PSs). In this way, the selectivity, safety and efficiency of phototherapy can be increased via increased singlet oxygen production and photothermal responses in PTT. Effective and selective administration of PSs to diseased tissues is of great importance in both cases. Nano-scale metal-organic frameworks (nMOFs), made of metal anchor points and bridge ligands for high biocompatibility, compositional and structural adjustment, were investigated as nano-carriers for drug delivery as a new class of hybrid materials. This review summarizes the growing and evolving areas of nMOFs as nanoparticle photosensitizers for PDT and PTT.

Keywords

Nano-Scale Metal-Organic Frameworks, n(MOFs), Cancer, Photodynamic Therapy (PDT), Photothermal Therapy (PTT), Photosensitizers (PSs).

Contents

1. Introduction.....	363
-----------------------------	------------

2.	Nanoscience and nanotechnology.....	365
2.1	Tumor ablation and nanotechnology in cancer treatment	366
3.	Metal organic frameworks (MOFs)	366
4.	Photothermal therapy (PTT).....	367
5.	Photodynamic therapy (PDT).....	367
6.	Historical development of phototherapy	368
7.	Mechanism of phototherapy	370
7.1	Basic elements of photodynamic therapy	372
7.1.1	Singlet oxygen	372
7.1.2	Light sources.....	373
8.	Photosensitizers (PSs).....	374
8.1	First generation photosensitizers	374
8.2	Second generation photosensitizers.....	374
8.3	Third generation photosensitizers.....	375
8.4	Introduction of tumor cells and intracellular localization of photosensitizer	376
9.	Cell death in phototherapy	376
10.	nMOFs for PDT	377
11.	nMOFs for PTT	383
11.1	Surface plasmon resonance (SPR) mechanism and plasmonic photothermal treatment (PPTT) method	385
11.1.1	Mie theory.....	385
11.1.2	Gold nanostructures	385
11.1.3	Photothermal properties of different gold nanostructures	386
11.1.4	Gold nanospheres used in photothermal therapy.....	387
11.1.5	Gold nanocages and nanorods used in photothermal therapy	387
11.1.6	Bioconjugation of gold nanostructures used in photothermal therapy	388
11.1.7	Determination of temperature changes in gold surface.....	389
12.	Results and Perspectives	396

References397

1. Introduction

Abnormal cell divisions are the most important defining feature of cancer, which prevents the tissue or organs from suppressing the function, growing out of the control, proliferating in various parts of the body and spreading to other organs. Scientists maintain their work to find a cure for cancer. Although the cancer diagnosis rate has increased, cancer-based deaths are almost constant. This is motivating scientists for cancer treatment [1].

Drugs used in cancer treatment can be removed from the body without reaching the tumor. However, high doses may cause side effects, and these drugs may occasionally damage healthy cells.

Surgery, chemotherapy and radiotherapy are the three basic methods used to treat cancer at the present time. General anesthesia is a method of treatment in which the cancerous tissue is partially or completely removed. The recovery of patients during surgery can take a long time, which is likely to be persistent.

If necessary, chemotherapy and/or radiotherapy treatment can also be performed after the operation. Chemotherapy is the method of drug therapy that kills cancer cells with the possibility of damaging the healthy cells. This treatment method usually lasts several months as several hour sessions at two- or three-week intervals. Many side effects such as weakness, hair loss and nausea occur as a result of chemotherapy. Radiotherapy is the treatment method using the beam (x-ray). This treatment method can be performed as one or several sessions depending on the state of the tumor tissue. Some side effects can be observed such as fatigue, skin redness, burning sensation, frustration, and diarrhea.

Due to the disadvantages of the previous treatment methods, new methods have been developing for cancer treatment. One of these methods is phototherapy. It is a treatment of radiation that origins date back to ancient times [2-3]. Niels Ryberg Finsen healed lupus vulgaris disease using shortwave light, and in 1903 received the Nobel Prize. Phototherapy (light therapy) or heliotherapy is the method that treats some diseases with sunlight and certain wavelengths using light or multi-colored polarized lights, lasers, light-emitting diodes, fluorescent lamps, dichroic very bright lamps, full-spectrum light types. The light can be applied at certain times of the day. Pure phototherapy can only be used for the treatment of superficial diseases as a result of the poor tissue penetration of light.

Mainly used for effective treatment;

- **Photosensitizers (PSs),**
- **Photodynamic therapy (PDT),**
- **Photothermal therapy (PTT) is used.**

PSs are localized to tumor sites with a combination of light and tissue oxygen and can target only tumor cells by preserving healthy tissues. In the application of PDT, the photosensitizing agent, not show toxic effects alone, exposed to light. As a result, free radicals and singlet oxygen (the triplet molecules in the environment turn into singlet oxygen) kill cancer cells through necrosis or apoptosis (programmed cell death) by interacting biological molecules. The positive effects of various types of cancers in PDT therapy has been reported in the literature [4–8].

The singlet oxygen ($^1\text{O}_2$), which is very short-lived and local, occurs as a result of the reactions that are caused by the absorption of light by the photosensitizer and causes only necrosis (cell death) in the region where the tumor is located and does not harm the surrounding tissue. PDT is more advantageous than conventional oncotherapy methods because of the fact that the light can only be applied to the tumor area by selective accumulation of photosensitizer, by this way healthy tissue damage can be prevent without causing systematic toxicity and the reproducibility until the desired result is achieved [9].

Phthalocyanine compounds are one of the most common compound groups used as a photosensitizer in PDT applications. High triplet state quantum yields and long life (triplet), able to produce singlet oxygen, absorbing high wavelength light (about 700 nm) nontoxic effects when the light is not used reasons such as phthalocyanine compounds effective in photodynamic therapy increases its usability. Phthalocyanine compounds have an important role in the treatment of cancer by photodynamic therapy as a second generation of photosensitizers. Therefore, a phthalocyanine compound named Photosens is used for the treatment of cancer patients. A similar example is the use of a phthalocyanine compound called pc4 as a photosensitizer in clinical trials [10].

When used as a photosensitizer, phthalocyanine compounds become more functional as a result of their binding to the phthalocyanine ring via the alkyne linkage. Since the onset of acetylene chemistry, electron delocalization is achieved through conjugation of the alkyne bond. Nowadays, phthalocyanine compounds containing alkyne bonds have also begun to take their place in PDT applications.

Porphyrin and its Derivatives, near infrared adsorbing porphyrins for biomedicine applications has been an attractive field of application. In biological applications, there is

an increasing interest in photodynamic cancer treatment for the diagnosis and treatment of some of the materials discussed so far [10–11]. Porphyrins are used as donors to improve oxygen-sensitive phosphorus in other important medical applications. Foscan, Photofrin, Verteporfin, Photoclor and Talaporfin are the most frequently used medical and technical applications approved for clinical use. Further research is required on effective delivery of PSs to tumors for improving the therapeutic effects of PDT[6,12–14].

2. Nanoscience and nanotechnology

The one atom is about 1 Angstrom (A), 0.1 nm or 10^{-10} meters in size, a nanometer (nm) size structure is formed by a combination of several atoms or by atom clusters. One nanometer is about 1/80,000 the diameter of human hair. As a new field of science, nanotechnology requires the study of materials with nanostructured materials and nanoscale devices. The chemical and physical properties of a substance at the molecular level are governed by nanotechnology. It is a result of scientific research that the properties of the materials on the nanometer scale depend on their size and shape. Most proteins are approximately 10 nm in size. Nanotechnology has a big importance on the fields of physics, chemistry and medical sciences. Biotechnology and nanotechnology are two of the most promising technologies of the 21st century, and they come together as nanobiotechnology. This hybrid discipline aims at combining atomic-scale machines or biological systems at the molecular level [15]. It is expected that this technology will create innovations and play an important role in various biomedical applications. Drug release and gene therapy, molecular imaging, biological and biosensors are counted among these applications [16–25]. Nanoparticles can be considered as the pioneers of cancer treatment with the use of nanotechnology in the biomedical field with target-specific drug treatment and early diagnosis methods of pathologies [26].

Some of the biomedical applications of nanotechnology are as follows;

- ✓ Tissue engineering,
- ✓ Drug and gene release systems,
- ✓ Diagnosis,
- ✓ Biomolecules and separation and purification of cells
- ✓ Tumor destruction with temperature rise (Hyperthermia),
- ✓ Biosensors,
- ✓ Nanobiomotors,
- ✓ Fluorescent biomarkers.

2.1 Tumor ablation and nanotechnology in cancer treatment

Surgical resection and tumor ablation are widely used methods in the treatment of solid tumors. Thermal treatments, photodynamic therapies and reactive oxygen species producing agents are among the tumor ablation methods (ROS). In thermal therapy; radiofrequency, microwave and high intensity focused ultrasound waves are used as the energy source, and the tumor cells are eliminated with thermal energy. Other methods cause apoptosis and cell death by creating a high level of oxidative molecules in tumor cells. PDT and ROS producing agents can be safely applied on surgical resection or in cases when the resection is not possible. The intensity of ablation with the previously indicated energy types can be increased by using nanoparticles [27].

Generally nanomaterials can be examined under three main topics:

- (1) Fully organic nanomaterials such as dendrimers [28], liposomes [29], micelles [30] and polymeric hydrogel nanoparticles [31];
- (2) Completely inorganic nanomaterials such as quantum dots [32], metal NPs [33], zeolite nanoparticles [34], metal oxide NPs [35], silica NPs [36] and carbon [37][38];
- (3) Hybrid nanomaterials constructed through coordination bonds between organic and inorganic components such as nCPs (nanoscale coordination polymers) and nMOFs (nanoscale metal-organic frameworks) [39–41].

3. Metal organic frameworks (MOFs)

Metal Organic Frameworks (MOF), one of the most important nanomaterials, emerged in the 1990s as a result of the search for materials with larger surface area and pore volume. MOFs consist of metal compounds and organic binders which bind these metal compounds.

MOF, which has been studied as an alternative adsorbent in various industrial environmental applications, is the developing porous nanomaterials. Metal organic lattice structures are formed by bonding metal ions (M^+) and poly-functional organic molecules with one, two or three dimensions.

MOFs often have hybrid matrix membranes and sometimes individual use. Surface area and pore sizes are the most important elements to determine the properties of MOFs in gas adsorption. Research on MOFs has accelerated in recent years due to their large surface areas, interchangeable pore diameters, variable geometrical structures and easy processability. These characteristics of MOFs are used in many areas due to their large surface area and pore volume such as flexible cage structure and magnetic properties, gas storage, gas separation, controlled drug release, radiation, catalyst, magnetism, separation

of pollutants and medical applications. Various combinations of MOFs, metals and ligands in different structures can be obtained by varying the substances used in the synthesis or changing the synthesis method [42–47].

As a method of synthesis of MOFs, it is the most cheap and preferable method in laboratory applications. However, due to the reaction time is long; the synthesis of MOF is negatively affected. The last step is the analysis of the synthesis results. The devices used in these results are; BET (surface characterization), XRD with X-ray diffraction method, FTIR, TGA and SEM [48–50].

4. Photothermal therapy (PTT)

PTT, photothermal interaction is one of the targeted treatment methods of light energy transforming mechanism in tissues. Photothermal damage of this mechanism, which appears as a temperature increase in the hyperthermia treatment method, is defined by mitochondrial swelling, denaturation of proteins, edema, whitening and tissue necrosis. Water, hemoglobin, oxyhemoglobin and melanins are considered as absorbents of the waves in the primary tissue. Absorption of these components of the beam selectively damages the tumor tissue and leads to photothermal local tissue damage. Near infra red waves of 700-900 nm are counted as light waves with minimum absorption [51].

PTT treatment may be used in the treatment of hypoxic cancers that typically do not respond to PDT treatment because they are not based on local oxygen. Many potent PSs, such as plasmonic gold nanorods [33] and phthalocyanine [52] have been developed to further increase PTT activity.

5. Photodynamic therapy (PDT)

Photodynamic therapy (PDT) is an interdisciplinary cancer treatment that is the common denominator of physics, chemistry and pharmacology (Fig. 1) [1]. PDT is a method of cancer treatment that is less harmful and effective than other treatment modalities currently used in the presence of photosensitive substance (photosensitizer), light and oxygen molecules. This method is based on the principle of eliminating the tumor by introducing the photosensitizer to the patient and then by stimulating the photosensitizer with the wavelength of the absorbing light, by giving the energy to the oxygen present in the environment, by activating the oxygen molecule. When these light-sensitive substances are targeted at the design stage, their tendency to accumulate and maintain in the tumor tissue compared to normal tissue can be achieved [53].

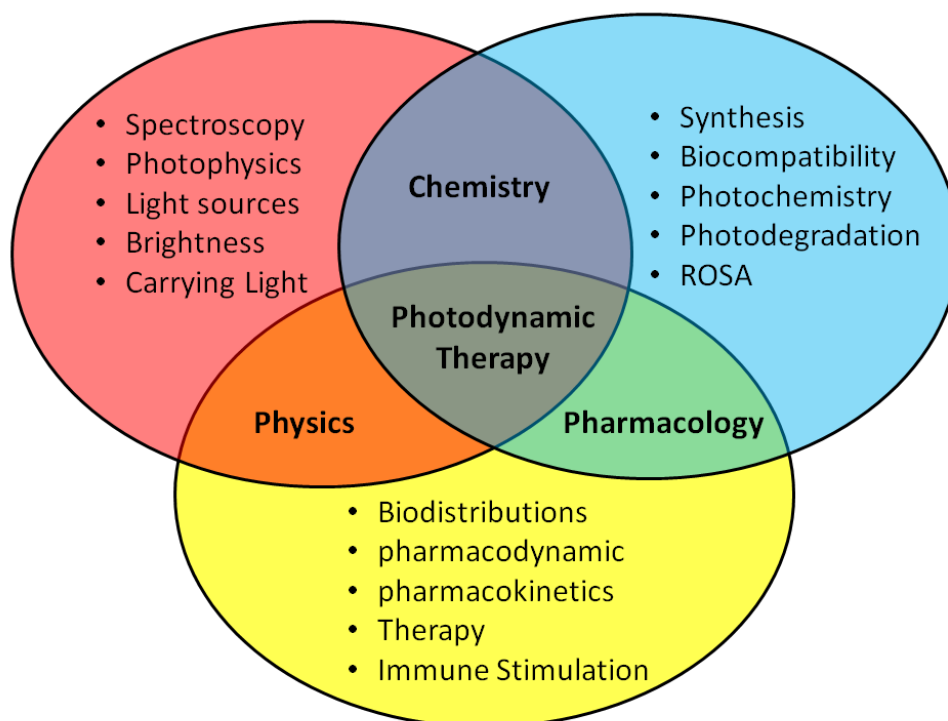


Fig. 1 Interdisciplinary schematic of photodynamic therapy.

The photosensitizer that will be used in the body, which is threatened and damaged by the cancer cells, depends on the application of the light and photosensitizing agent. In some applications, the agent is applied directly to the skin and in another method; it can be injected into the blood. The effectiveness of treatment is depending on the method, type of photosensitizer agent, light source, and the treatment modalities. After the managing of the photosensitive agent used in the treatment of cancer cells, the light at certain wavelength absorbed by the agent is applied only to the area of the cancer cells. PDT is an important treatment method for the destruction of blood vessels that feed cancer cells, and stimulation of the immune system against cancer cells. Depending on the photosensitizing agent used, the time period between the administration of the photosensitive agent and the light may vary [54].

6. Historical development of phototherapy

A limited number of sources such as fire, light-emitting organisms (such as fireflies) and the sun, could be counted as sources of light in ancient times. In the 3000 BC, people believed that there was a strong connection between sunlight and health, because people

in ancient Egypt worshiped the sun. In 1666, Sir Isaac Newton discovered that sunlight was divided into different colors with the prism. In 1678, Christian Huygens realized that there was the wave feature of light in his work. Further studies towards the end of the 1800s, scientists discovered that sunlight has parts that are not visible to the naked eye, which are ultraviolet and infra-red. It was found that violet light had fatal effects on bacteria and some microorganisms. Hence, clues about the first connection between sunlight and human disturbances was exhibited [55].

The first example of treatment with photodynamic therapy was the observation of a toxic effect by the reaction of Raab's acridine orange in 1900. It was observed that paramecium (a single-celled animal) died using acridine dye and light combination. Since the same experiment could not reproduced in a light-free environment, it was concluded that the paint interacted with light [56]. The literature was obtained by Tappeiner and Jesionek in 1905 on 6 patients with malignant tumors of the basal cells. Long-term sunlight and arc lamps were used using 1% eosin solution; the studies resulted in improvement in the tumors of 4 patients. In 1908, Hausmann showed active photosensitizers for hematoporphyrin, paramecium and erythrocytes. It has been observed that they react differently according to photosensitizer and light dose. Another importance of this study is that Hausmann proposed the hypothesis that the effect of PDT is related to the damage of basal vessels. In order to observe the effects of hematoporphyrin, F. Meyer-Betz injected 200 mg hematoporphyrin intravenously and was exposed to sunlight until it showed photosensitivity. As a result, the sun rays caused edema and staining [57]. These studies showed that hematoporphyrin is an active photosensitizer for various tissues, including skin.

Albert Policard observed experimentally the fluorescence emission from malignant tumors in 1924 in sarcomas of laboratory mice. In another study conducted in 1955, hematoporphyrin at doses of 300-1000 mg was injected into the blood of the patients 12-72 hours before the operation, and the tumor was exposed to UV-A light with a wavelength in the range 315 to 400 nm, as a result, fluorescence emission was observed. This is a study showing that hematoporphyrin can be used for monitoring the tumor during surgery and determining size [56]. Modern photodynamic therapy has begun with the studies of Lipson and colleagues in 1961. They focused on the hematoporphyrin derivative (HPD) [58]. The main development of photodynamic therapy was in the 1970s, the successful results were obtained experimentally by using of intravenous hematoporphyrin in animal tumors.

In 1987, Dougherty et al. investigated 113 skin and subcutaneous malignant tumors; results indicated that 111 tumors and partially or fully recovered [59]. Pigmented tumor cells spread over a large surface and showed a higher dose of HPD. To prevent healthy

skin damage, the light reduced the dose or increased the time between the administration of photosensitizer and the application of light [60].

A large number of clinical studies were performed, which included the treatment of tumors in different regions of various systems. In many studies, successful results are obtained in the treatment of superficial and small tumors by photodynamic therapy, while the amount of drug or intensity of light should be increased for the treatment of larger and deeper tumors. This has led to complications. In 1984, Parker and his colleagues achieved a regression in experimental iris neovascularization using the hematoporphyrin derivative (HPD) [61]. Later in 1993, Kliman et al. were successful in the experimental choroidal neovascularization of monkeys using chloro aluminum sulfonate phthalocyanine [62]. Miller et al. have achieved successful results using rose Bengal [63]. All these studies have not been applied to clinical practice, the main advances in photodynamic therapy have been the introduction of new and more effective drugs [64–65].

7. Mechanism of phototherapy

Photodynamic therapy is the treatment of negative changes that may occur in the tissue as a result of the conversion of light energy into chemical energy through a non-toxic light-sensitive substance and transfer of this chemical energy to the target tissue. In photodynamic therapy, the introduction of photosensitive substance to the body and the photochemical effect in the target region should be composed of two basic steps. There are basically two selective properties: one is the collection of the light-sensitive substance given to the body, especially in the target area, and the other is the application of the light to the desired region.

The mechanism of action of the photodynamic therapy, as shown in the (Fig. 2), is that the photosensitive substance, which is in the basic state, becomes a high-energy triplet by stimulating it with the wavelength of light which can be absorbed. The triplet state with longer half-life allows the activated photosensitizer to interact with the surrounding molecules. The photosensitizers, which are tripletized by light stimulation, follow two different ways to interact with biomolecules, type I and type II reactions [66–67].

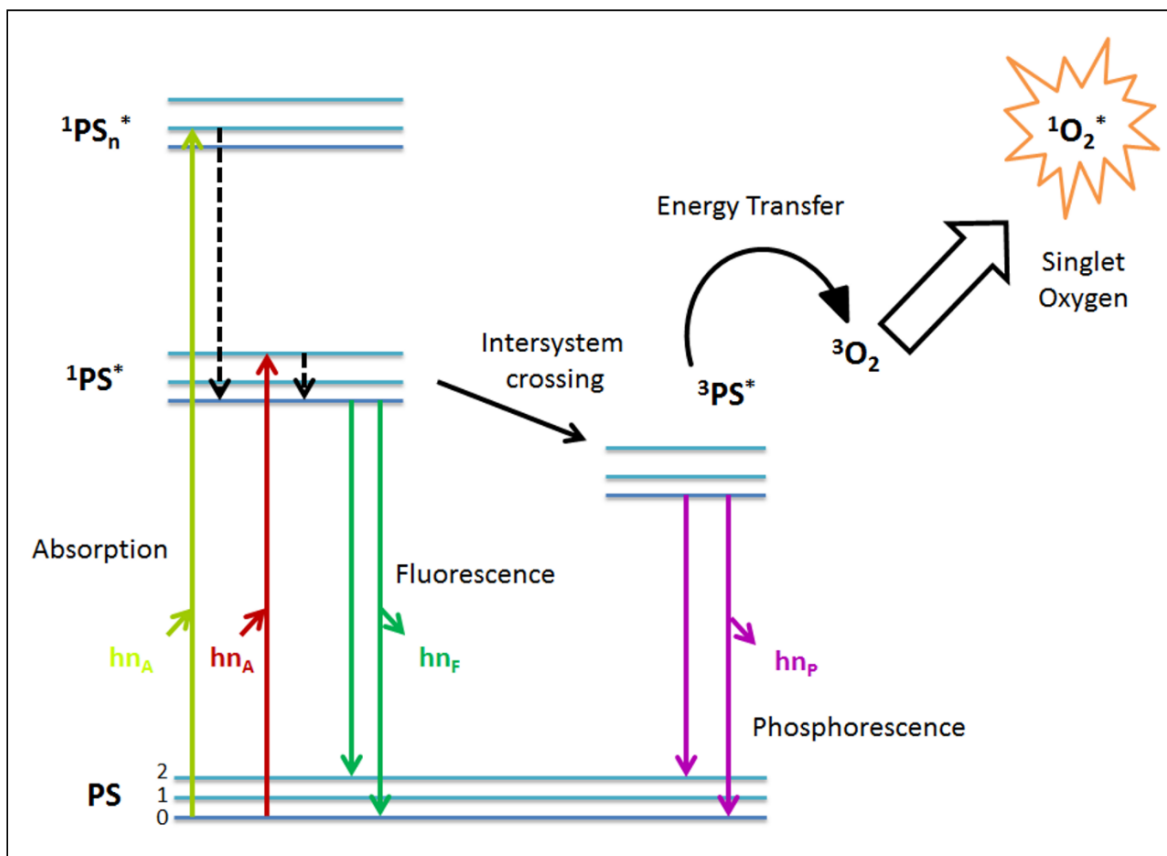


Fig 2 Singlet oxygen formation.

In the mechanism defined as type I reactions, electron transfer reactions that cause ROS (Reactive Oxygen Species) formation occur. Another mechanism, Type II reactions, is singlet oxygen ($^1\text{O}_2$), which causes energy transfer reactions (Fig. 3) [68]. In Type I reactions, highly reactive property radicals, particularly hydroxy and hydrogen peroxide radicals, which are generated by transferring the hydrogen atom of the photosensitizer in the excited state to a molecule present in the cell, react with molecular oxygen to produce oxygenated products. The effects of many photosensitive substances used in photodynamic therapy are shown by Type II reaction mechanisms, mostly through a ROS of $^1\text{O}_2$. In the case of Type II reactions, the stimulated photosensitizer gives energy directly to molecular oxygen (O_2) and causes singlet oxygen ($^1\text{O}_2$) formation. Singlet oxygen ($^1\text{O}_2$), the electronically stimulated form of molecular oxygen, oxidizes the biomolecules and causes cellular damage [69].

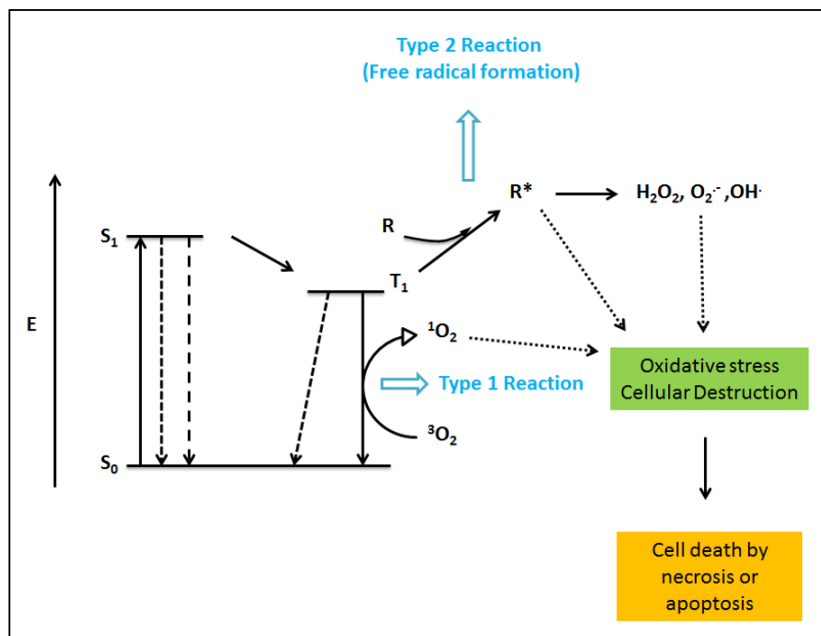


Fig. 3 Type I and type II reaction mechanisms.

7.1 Basic elements of photodynamic therapy

7.1.1 Singlet oxygen

The importance of oxygen, one of the three essential elements in photodynamic therapy, is due to the transition to singlet oxygen form. In many previous studies in the literature, singlet oxygen has been investigated and its importance has been emphasized [70]. While oxygen is in its basic state, there are two electrons which are not matched separately in the outer anti-bond orbitals. Singlet oxygen formed by changing the direction of rotation of one of these external electrons is highly reactive. Singlet oxygen interacts with other molecules due to its high reactivity and transfers its energy [71]. Although singlet oxygen is mostly described as diradical, the findings of the fact that it is actually polarized zwitter ion are found in the literature [72–73].

On the other hand, studies on the importance of oxygen in the success of photodynamic therapy in pre-clinical photodynamic therapy revealed the importance of light power. Compared to experimental applications, high power light is used in clinical applications, while decreasing the light power, on the other hand, does not correspond to practical applications since it increases the application time [74–75]. Singlet oxygen produced in the tumor is a parameter that demonstrates the efficacy of photodynamic therapy. This parameter indicating that PDT activity depends on the amount of molecular oxygen present in the tissue medium.

7.1.2 Light sources

The wavelength of light used in photodynamic therapy is very important from the point of view of the penetration of light. Along with the wavelength of the light used here, the diffraction of this light by cells and other microstructures and the absorption by some molecules such as hemoglobin, melanin and water also affect penetration. The hemoglobin molecule present in the blood shows a clear absorption of light at wavelengths of 425, 544, 577 nm, resulting in a decrease in tissue penetration. On the other hand, since there is an inverse relationship between the wavelength and energy of the light used, it is more preferable to use light with the high wavelength in order to minimize the side effects of the applied therapy. However, wavelengths greater than 1200 nm are observed in the absorption of water molecules. Therefore, the optimal wavelength range for clinical PDT applications was found to be between 650 and 850 nm and this interval was called the 'Phototherapeutic window' [76].

Conventional arc lamps, which are cheap and easy to use, can be used to stimulate the photosensitizer. This type of lamps have broad spectrum, UV and IR filters can be used to prevent heating. On the other hand, it is not efficient to use such lamps in clinical applications because of the loss of power during the connection of the light conduction fibers [77].

Filament lamps are also inexpensive and have been applied in photodynamic therapy. Kennedy and Pettier used a projector lamp as a light source for the treatment of basal cell carcinoma using aminolevulinic acid as a prodrug [78].

With the development of semiconductor technology, LEDs with a wide wavelength range have the opportunity to be applied in many areas as the light source. The light power is poor, but they are inexpensive, on the other hand, LEDs can be produced in desired wavelength. Depending on the type of semiconductor material, the LED will be emitted in the desired color. LEDs are used in photodynamic therapy by utilizing these features [79–80].

Another important source of light is the laser light, which can be emitted in a single color and in form of synchronized light waves, with a slight deviation that makes it easier to focus the light rays. Linear light-emitting lasers with an approximately constant wavelength provide an advantage for fiber-based applications due to the focused light. Lasers have some characteristic features for use in photodynamic therapy. These include the study of optical fibers in photodynamic therapy, the treatment of endoscopic internal tumors and the placement of the light source in the tumor tissue. The high power of laser light is used for the activation of the photosensitizer, especially in photodynamic therapy [81].

8. Photosensitizers (PSs)

Photosensitizers are chemical compounds that absorb the energy of light in a suitable wavelength range for their structures and transfer them to biomolecules which they absorb from the basic state. Photodynamic therapy involves cytotoxic production of energy transfer and reactive oxygen formation. The photosensitizer to be used in the application is expected to accumulate in tumor tissues consisting of cancer cells with proliferative activity [82]. Moreover, transferring in a short time to the desired area, while not accumulating in healthy tissues, non-toxic effect in the absence of light providing stimulation, and the tendency to create singlet oxygen with high efficiency are the other features expected from an ideal photosensitizer [80–83].

8.1 First generation photosensitizers

After the Rabb realized the photodynamic effect in 1900, the chemical structure of Schwartz obtained hematoporphyrin derivative (HPD), when given to the body, it was noticed that it had accumulated in tumor tissues [84]. HPD, the one of the first generation of photosensitizer drugs, was used in the early studies with photodynamic therapy. Lipson et al. used HPD for human tumor tissue identification and treatment [58]. In the following years, porfimer sodium, a water-soluble derivative of hematoporphyrin, which is marketed as ‘photofrin’, has been used by Dougherty et al. for photodynamic therapy. Photofrin, which has a stronger effect than HPD, has been detected that cause fewer skin reactions [85].

Porfimer sodium, a first generation light sensitive drug, provides limited tissue penetration at a wavelength of 630 nm. At present, porfimer sodium, still continue to be used for the treatment of cancer in many centers in North America and in Europe, has been the initiator of photodynamic therapy and pioneered the development of second generation light-sensitive drugs [67].

8.2 Second generation photosensitizers

The limited characteristics of the first generation of photosensitizers have led scientists working in this field to focus on second-generation light-sensitive drugs. For obtaining a safer and more effective photodynamic therapy, photosensitizers that have lower half-life are needed. Thus, they have fewer side effects, can absorb light at higher wavelengths, and achieve potential oxygen-induced reactions. An important part of the drugs in this group is composed of molecules containing tetrapyrrole ring. Examples of drugs most commonly used in clinical or experimental use include chlorines, bacteriochlorins, benzoporphyrin derivatives, purpurines, phthalocyanines, and naphthalocyanines. Due to the differences in the chemical structure, it is possible to divide the second generation of

photosensitizers into three classes as lipophilic, hydrophilic and amphiphilic according to their polar or apolar behaviors. The class that the molecule possesses plays the most fundamental role in determining the route in which the drug is taken into the cell and where it will go inside the cell. The process of incorporation into the cell takes three different forms. Firstly, hydrophilic molecules are taken into the cell via pinocytosis or endocytosis and accumulate in the lysosomes, in particular within the cell. The latter is to be taken through diffusion. The third is that molecules with hydrophobic properties are taken into the cell by receptor-dependent endocytosis via transporting them through the lipoproteins in the blood. Here, the photosensitizer accumulates primarily in the mitochondria and then diffuse to the cytoplasm.

Although the second generation of photosensitive drugs such as rose bengal, chloro-aluminum sulfonate phthalocyanine and bacteriochlorin-A were successful in regressing experimental ocular neovascularization, it was not possible to use them for clinical purposes because of the neurological side effects they caused in animal experiments. However, benzoporphyrin monoacid, aluminum phthalocyanine tetrasulfanate, tin ethyl ethopurpurine, lutetium teksafirin, mono-L-aspartyl chlorine e6 and the second generation of drugs with low side effects such as ATX-S10 were found to be more widely used [69], [86].

8.3 Third generation photosensitizers

The major disadvantage of the cancer treatment methods currently in use is the damage to healthy cells as well as cancer cells. Therefore, directing the administered drug to the target provides more effective treatment as well as less or no harm to healthy cells.

During photodynamic therapy, the destruction of healthy cells, besides cancer cells, has led to the development of third generation photosensitizers, which are already at the beginner level. Here, the photosensitizer is designed to improve the properties of transfer to tumor tissue [87]. In addition, recent studies have shown that selective targeting to subcellular structures such as mitochondria can be performed [46].

The targeting in photodynamic therapy is very important due to the nanoseconds lifetime of singlet oxygen formed as a result of light stimulation, causing damage to the tissue as close to the target tissue. Functional groups that provide the transport of the photosensitizer by taking advantage of the known properties of tissue harboring the tumor cells are the basic principle that ensures the efficacy of targeted therapy and third-generation photosensitive substances [88].

8.4 Introduction of tumor cells and intracellular localization of photosensitizer

The target points of photodynamic therapy are mitochondria, plasma membranes, lysosomes and endoplasmic reticulum found in tumor cells. The main factors that determine the accumulation and positioning of photosensitizer in the tumor cell include the degree of lipophilic properties and accumulation of the sensitizer [80,89]. Hydrophobic photosensitizers are selective in tumor tissue due to intravenous circulation, and they have ability to bind strongly with high and low-density lipoproteins. The lipophilic photosensitizer accumulates because of the high number of low-density fat membrane receptors of cancer cells. By the introduction of these photosensitizers into the cell via endocytosis, the lipophilic character of tumor cells accumulates in the plasma, mitochondria, endoplasmic reticulum, nuclei and lysosomal membranes. The hydrophilic photosensitizers that are taken intravenously into the cell show a tendency to accumulate in the interstitial space and vascular stroma in the tumor tissue after being transported by albumin and other serum proteins [80].

The hydrophobic characterizing sensitizers exhibit the ability to act directly on tumor cells, but the hydrophilic photosensitizers have indirect effects. Oxygen and other nutrients required by the cell can cause photodynamic effects by damaging the blood vessels [80].

9. Cell death in phototherapy

The basic principle of cell death in photodynamic therapy is based on damaging the vascular structure in the tumor region and activating the immune system. Knowing the characteristics of the tissue in the tumor region is the basis of the destruction to be created in this region. These properties also determine how the destruction of cancerous tissue will occur. The number of veins in the tumor region and the number of immune system cells it has is one of the mentioned features. Cellular response in photodynamic therapy depends on many parameters such as type, density, amount of light used, wavelength, incubation conditions, cell metabolic properties, oxygen level in tissue, genetic characteristics of cell [90]. As noted before, the positive result that can be obtained in photodynamic therapy depends on the intracellular positioning of the photosensitizer [91]. The singlet oxygen has a life span of fewer than 0.05 μ s and can only diffuse up to 0.02 μ m, because of that intracellular localization is so important. This determines which organelle will be damaged initially. In addition, the short life span of singlet oxygen and most of the photosensitizers are localized outside the nucleus; the mutagenic effect of photodynamic therapy is very low. After administration of photodynamic therapy, cell death occurs as apoptosis, necrosis or both apoptosis and necrosis.

10. nMOFs for PDT

Porous materials with the high surface area have always been of great importance for chemical process technologies. Nowadays, porous materials used in sanitary are generally based on inorganic or solid carbon. While researchers were working on different materials in the 1990s, Omar Yaghi introduced metal organic frames using metal oxides and organic groups together as molecular building blocks.

Metal organic lattice structures are composed of metal ions (M^+) and poly-functional organic molecules connected to each other in one, two or three dimensions. Research on MOFs has gained momentum in recent years due to their large surface areas, interchangeable pore diameters, variable geometrical structures and easy processability. These properties are used in many areas such as gas storage, gas separation, radiation, catalyst, magnetism, drug release. Various combinations of metals and ligands, the variation of the substances used in the synthesis or alteration of the synthesis method can be resulted in different constructs of MOFs [92].

The structural properties of MOFs vary with the angular properties and bonding length, as well as the effect of different anions, temperature, and solubility. The figure 4 shows the general structure of MOF.

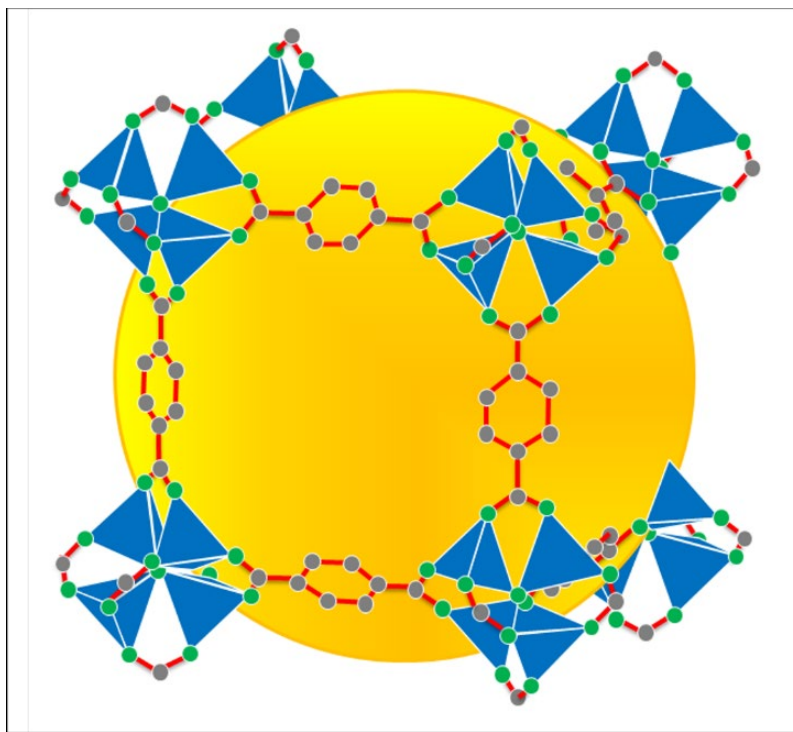


Fig. 4 The structure of MOF.

In recent years, metal organic lattice structures have attracted considerable attention in scientific studies. The source of this great interest is the variety of interesting molecular structures, as well as the properties and promising applications. Metal-organic frames are new class of porous materials having the highest internal surface area, high pore volumes, flexible lattice structures, high adsorption capacity, chirality and magnetism. It is expected that metal-organic frameworks will have revolutionary effects on the chemical process technologies with the combination of the listed properties. In the structure of MOF; Metal ion and organic binders are shown in figure 5. Large surface area, high pore volume, flexible cage structure, and high capacity of gas adsorption are make MOFs are preferable [92].

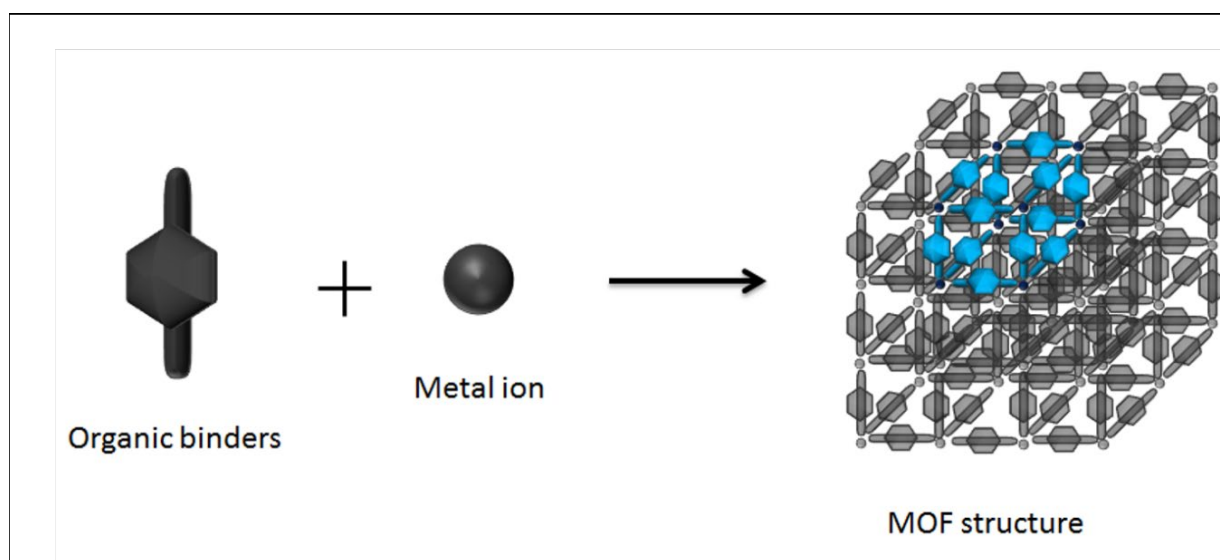


Fig. 5 General structure and formation of MOF.

To explain the structure of a MOF nanoparticle, we need to understand the secondary building units (SBU). Organic binders are important SBUs and their structure may change as the MOF is formed. The organic linker, in the structure of MOFs, affects the usable pore volume and the adsorption area in the metal part. Connecting organic binders and metal clusters to each other in different geometries. The controllable polarity of MOFs gives various physical and chemical properties [93]. These features are extract, pore volume, BET specific area and adsorption ability. The length of the organic binder may alter the adsorption properties or increase the length of the binder and increase the pore volume and density. There may also be isotherms of MOFs affecting the pore size. The metal ion affects the lattice flexibility of MOF.

Synthesis of nano-scale MOF (nMOF) by synthetic methods such as surfactant-doping, solvothermal and reverse microemulsion has been shown to be effective as a result of trials and errors [39]. It is essential to successfully synthesize these nMOFs with the desired structures, compositions, morphologies and particle sizes for the rational design.

A series of nMOFs including magnetic resonance imaging (MRI), biomedical imaging [94–95], computed tomography (CT) [96–97], and optical imaging have been designed and investigated with the correct selection of functional SBUs and/or bridge ligands [98,99,100].

Drug delivery is detected by nMOFs, including chemotherapeutic agents [101–103], PTT and PDT agents [104–131], nucleic acid [95,132] and gas molecules such as nitric oxide [133,134,135]. nMOFs have several advantages over purely organic and inorganic nano-carriers;

- (1) The higher charge carrying capacity than the various diagnostic and therapeutic agents, due to the higher porosity of the nMOFs.
- (2) As a result of the compound and structural diversity of the synthesized nMOFs; various chemical properties, different morphologies and dimensions, and multiple functionalities have emerged.
- (3) Prolonged toxicity decreases due to the biodegradability of nMOFs.

As a result, high PS loads can be achieved without self-extinguishing nMOFs. Long-term toxicity has been reduced due to the biodegradability of nMOFs; For PDT applications, the optimization of nMOF, nPSs is carried out by means of adjustable compositions and structures. Since the first report on PDT with nMOF in 2014 [104], at least 13 more articles on the PDT of nMOFs have been published, highlighting the intense interest in the use of nMOFs for PDT [104–136]. All nMOFs examined for PDT to date are summarized in table 1.

Table 1. Effectiveness of PDT and PDT-based combination therapies.

Cell lines & PSs/nMOFs concentration	nMOFs	PSs: type; position; loading	Anticancer efficacy	Irradiation: wavelength; power; time	Ref.
CT26 & HT29 cells In vitro: 20 μ M DBC In vivo: 1 mg DBC-Hf/kg	DBC-Hf Nanoplate $\sim 150 \times 5 \text{ nm}^2$	Cholrin (DBC); Ligands; 64 wt%	In vitro: $\sim 20\%$ cell viability In vivo: Tumor decreased from ~ 150 to $\sim 10 \text{ mm}^3$	650 nm 100 mW/cm^2 In vitro: 15 min In vivo: 15 min	[105]
SQ20B cells In vitro: 20 μ M DBP In vivo: 3.5 mg DBP/kg	DBP-Hf Nanoplate $\sim 100 \times 10 \text{ nm}^2$	Porphyrin (DBP); Ligands; 77 wt%	In vitro: $\sim 20\%$ cell viability In vivo: Tumor decreased from ~ 150 to $\sim 3 \text{ mm}^3$	640 nm 100 mW/cm^2 In vitro: 15 min In vivo: 30 min	[104]

CT26 & MC38 cells In vitro: 20 IM TBC In vivo: 20 Imol TBC/kg 1.5 mg IDOi/kg	IDOi@TBC-Hf Nanorice ~75 × 45 nm	Cholrin (TBC); Ligands; TBC: 62 wt% IDOi: 4.7%	In vitro: ~15% cell viability, immunogenic cell death In vivo: Abscopal effect, both treated and untreated tumors shrank	650 nm100 mW/cm ² In vitro: 15 min In vivo: 15 min	[116]
CT26 & MC38 cells In vitro: 20 IM TBC In vivo: 20 Imol TBC/kg 1.5 mg IDOi/kg	IDOi@TBC-Hf Nanorice ~75 × 45 nm	Cholrin (TBC); Ligands; TBC: 62 wt% IDOi: 4.7%	In vitro: ~15% cell viability, immunogenic cell death In vivo: Abscopal effect, both treated and untreated tumor regressed	650 nm100 mW/cm ² In vitro: 15 min In vivo: 15 min	[116]
4T1 cells In vitro: 80 mg TBC/L In vivo: 0.5 mg TCPP/mouse	Hf-TCPP-PEG ~130 nm	Porphyrin (TCPP); Ligands; 55 wt%	In vitro: ~20% cell viability, In vivo: Tumor grew slowly	661 nm5 mW/cm ² In vitro: 15 min In vivo: 60 min X-ray: 6 Gy	[126]

B16 melanoma cells In vitro:20 IM TCPP	TCPP/BCDTE@ UiO-66 ~70 nm	Porphyrin (TCPP); Attached to SBUs;	In vitro: ~30% cell viability	420 nm100 mW/cm ² In vitro: 30 min	[128]
HeLa cells In vitro:3.5 IM TMPyP	TMPyP@HKUS T-1 ~100 nm	Porphyrin (TMPyP); Encapsulated in HKUST-1; 32.8 wt%	In vitro: ~30% cell viability	660 nm100 mW/cm ² In vitro: 15 min	[127]
B16F10, CT26, and C26 Cells	UiO-PDT ~70 nm	BODIPY (I2-BDP);	In vitro: <20% cell viability for	420 or 80 mW/cm ² In vitro: 10 min	[130]
HeLa cells In vitro:20 IM TCPP	PCN-224 ~90 nm	Porphyrin (TCPP); Ligands;	In vitro: ~20% cell viability	630 nm100 mW/cm ² In vitro: 30 min	[129]
MDA-MB-468 cells In vitro:100 lg/mL	UCNPs@PCN-224 ~52 nm	Porphyrin (TCPP); Ligands;	In vitro: ~20% cell viability	980 nm 15.9 W/cm ² In vitro: 20 min	[108]
PL 45 Cells In vitro:8 lg MB/mL	UCNPs/MB@ZI F-8@catalase ~500 nm	Methylene blue (MB); Encapsulated in ZIF-8; 1.97 wt%	In vitro: 40% cell viability	980 nm1 W/cm ² In vitro: 5 min	[131]

HeLa cells In vitro:4 IM TCPP	PCN-222 Nanorice 50–70 nm	Porphyrin (TCPP); Ligands;	In vitro: <5% cell viability	>600 nm 50 mW/cm ² In vitro: 15 min	[111]
HeLa cells In vitro:1.6 IM Ce6 equiv	Ce6-Peptide @MIL-101 ~95 nm	Chlorin (Ce6); Encapsulated in MIL- 101;3.2 wt% 3.3	In vitro: <10% cell viability	660 nm 200 mW/cm ² In vitro: 5 min	[110]
HepG2 and HeLa cells In vitro:25 lg/mL	UiO-AM@POP ~176 nm	Porphyrin (H2P); In POP; ~8%	In vitro: ~15% cell viability	450 nm45 mW/cm ² In vitro: 15 min	[109]

11. nMOFs for PTT

The human body maintains its temperature at 37 °C. Healthy cells can survive at temperatures above 42 °C. According to the National Cancer Institute, the cancer treatment methods of hypertension mentioned in the cancer region, the temperature of 42–45 °C, if the cancer cells begin to die [137]. In this method of treatment, the temperature of the tumor region is maintained at 41–43 °C over a long period and the death of cancer cells is targeted [138–140]. PTT, which attracts attention in recent years, is a thermal therapeutic treatment caused by near infrared light energy. Unlike PDT, PTT is an ROS-mediated process that is independent of the oxygen mediated by photothermal agents.

According to literature, magnetic nanoparticles below a certain size can pass through vascular systems and reach all parts of the body. When the nanoparticles are applied to the magnetic field, they can be concentrated to a certain point in the body. Magnetic nanoparticles are of great interest in transporting drugs and antibodies to patient tissues and organs in the body [141]. As shown in figure 6, the position of the magnetic nanoparticles used in drug delivery systems is determined by the gravitational factor of the magnetic field by nanoparticles. When the power of the applied magnetic field exceeds the linear flow rate (10 cms⁻¹) of the arteries or the capillaries(0.05 cms⁻¹), the nanoparticles begin to be retained by the endothelial cells of the target tissue [142].

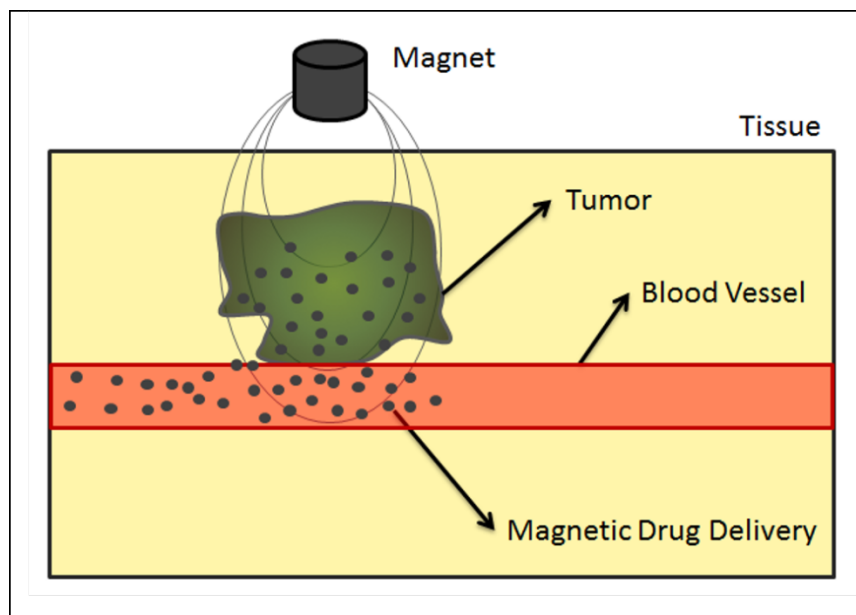


Fig. 6 Mechanism of magnetic nanoparticles.

In PTT, the light is normally emitted at a wavelength, close to the infrared range. Then, the activated PS falls back into the soil and releases the vibration energy to generate heat. As a result of such non-radiative relaxation process, the light is rapidly converted to local heat and can increase the temperature in the tumor area by sufficiently increasing the tumors [51]. PTT therapy not based on local oxygen, it can be used in the treatment of hypoxic cancers that typically do not respond to PDT treatment. Many powerful PS, such as plasmonic gold nanorods [33] and phthalocyanine [52], have been developed to enhance activity of PTT.

Photothermal treatment of the light energy in tissues; hyperthermia appears as an increase in temperature in the treatment method. Photothermal damage occurs when the tissue reaches 55-90 °C in minutes; mitochondrial swelling, protein denaturation, edema, whitening and tissue necrosis [143–144]. NIR waves between 700-900 nm are counted from light waves with minimum absorption [145].

In recent years, using of laser beam has been shown to be a very promising method for the treatment of cancer. Photothermal methods used in cancer treatment cause the energy waves to focus on the surface of the nanoparticles and consequently damage and destruction of the tumor. However, in the new nanoscience studies, the use of nano structures of the original metals, their unique photophysical properties, and the photothermal applications used in the treatment of cancer seem extremely appropriate. In this method, when the waves are used at low frequencies, another absorptive agent causes

PTT with gold. PTT is considered to be one of the types of use of the waves in high frequencies or in the mechanism of focusing them on the specific tumor without using the absorption agent. When the photothermal method uses gold nanoparticles and laser together, this method is called Plasmonic Photothermal Treatment (PPTT). The basis of PPTT is due to the Surface Plasmon Resonance (SPR) mechanism. The SPR will be described in detail below. The photoabsorption method is considered to be a highly developed treatment technique in combination with gold nanoparticles and it is more selective and effective strategy for conjugated gold nanoparticles [146].

11.1 Surface plasmon resonance (SPR) mechanism and plasmonic photothermal treatment (PPTT) method

11.1.1 Mie theory

Scattering of electromagnetic waves from spherical parts is called Mie theory [147]. Mie theory is actually the answer to a Maxwell equation. This theory explains the relationship between gold nanoparticles. In the presence of electromagnetic channels, free electrons resonate and their vibrations may cause SPR phenomenon. However, the SPR occurs when the wavelength is smaller than the diameter of the nanoparticle [148].

The SPR mechanism used in this method vibrates the valence electrons on the surface when the light interacts with the surface of a solid material. The resonance frequency of the surface electrons must be equal to the frequency of the photons to form the resonance. The SPR mechanism is formed if the frequency of the incoming wave is equal to the resonance frequency of the nanoparticle. The gold nanoparticles can be resonated by UV waves around 532 nm [149–150]. PPTT method, which is one of the methods used in cancer treatment, is considered an efficient and novel technique. In this method, the use of targeted gold nanoparticles can reduce the energy of the laser by absorbing the energy to destroy selective tumor cells. In this type of cancer treatment, a certain amount of energy is sent directly into the tumor mass to increase the heat. The PPTT method used in tumor ablation has been successfully used in liver lesions with minimal harmful properties to normal cells [151]. However, all of the aforementioned treatment methods fall into the cancer treatment category because they can perform thermal ablation.

11.1.2 Gold nanostructures

Gold nanoparticles absorb the energy very well or allow them to be scattered due to the plasmon resonances in the visible area of the light. By this way, it can be possible to use them optically. Changing the size of the particles, and scattering of light allows working in various colors. When gold nanoparticles absorb light, the free electrons are stimulated. This excitation at the plasmon resonance frequency causes the free electrons to vibrate in

bulk. This interaction between the crystal network and the electrons of the particle leads to the transfer of thermal energy from the particle to its environment. Gold nanoparticles are frequently used in the treatment of cancer cells based on these properties. Cells that are highly sensitive to heat changes; over a few degrees of body temperature, it is damaged by hyperthermia at temperatures above 42 °C. As in the drug transport systems, it is planned to cause localized cell death by stimulating the particles from outside, after the diseased cells are attached to the surface of the particles, which are conjugated to the cancerous cells [152].

11.1.3 Photothermal properties of different gold nanostructures

In recent years, due to the unique optical and structural properties of metal nanostructures, their use in biomedical and medical fields has increased significantly [140–149][157]. Gold nanoparticles are the most commonly used metal nanoparticles in the biomedical field. Large surface areas, local surface plasmon resonance properties and superior biocompatibility characteristics can be listed [158–160]. Gold nanoparticles, which do not show toxic properties and have plasmonic properties, are frequently used in the detection of cancerous cells and in the destruction of malignant cells without damaging healthy cells [161–162].

Thanks to the LSPR feature, gold nanoparticles absorb the light energy at a particular wavelength, causing the free electrons on the metal surface to vibrate at a certain frequency. As a result, the absorbed light energy is transformed into heat energy and the environment of the gold nanostructures starts to warm up (Fig. 7). This phenomenon is defined as the photothermal effect of gold. The gold nanoparticles absorb very strongly the light energy in the visible-infrared wavelength range depending on their shape and size.

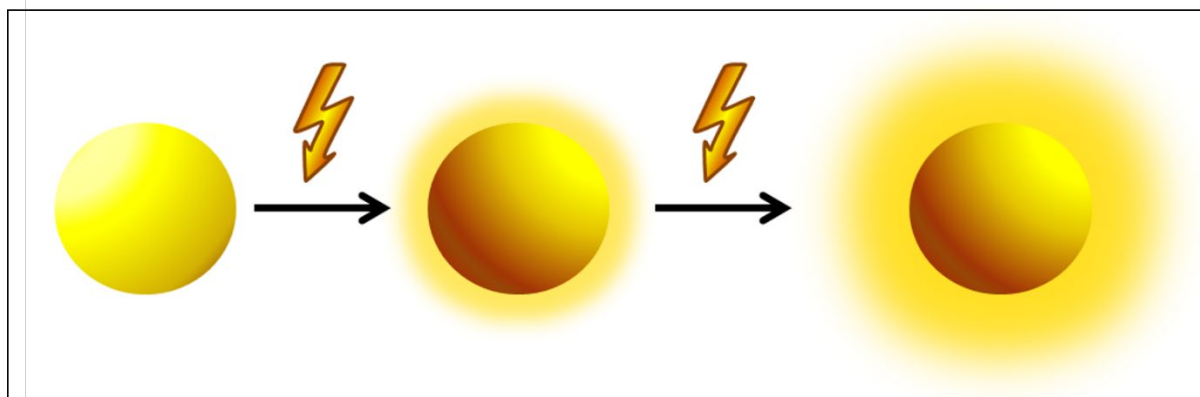


Fig. 7 Schematic representation of gold nanostructures.

11.1.4 Gold nanospheres used in photothermal therapy

In 1999, Lin et al. [163] performed selective photothermal therapy using light-absorbing microparticles in the visible region, for the first time. Gold nanospheres are nanoparticles that can absorb light in the visible region. In 2003, it was exposed to the laser beam in the visible region by using lymphocyte cells, which were added to the gold nanospheres of 10-30 nm. This transformation resulted in increased permeability of the plasma membrane of the lymphocyte cells and thus observed by selective photothermal therapy in where the cell death occurred [164].

By carrying out parameters such as the number, size and laser energy of gold nanoparticles, researchers were able to make changes in cellular functions without causing any cell destruction. In the same year, Zharov et al. carried out detailed studies using photothermal contrast techniques about heat dynamics and threshold values around nanoparticles combined with cancer cells [165]. In another study, gold nanoparticles of 40 nm in size were placed in the environment of the malignant cells by covering the epidermal growth factor receptor (EGFR) antibodies. Then, cells exposed to argon laser beams in the visible region. The gold nanoparticles were heated and the cancer cells were killed. No cell death was observed when the same laser beam was applied to cancer cells without the addition of gold nanoparticles [166–167]. This indicate that how effective studies can be performed by using photothermal properties of gold nanoparticles. However, the use of nanoparticles that can absorb visible light is limited to the types of cancer seen in areas close to skin cancer or the skin surface [146]. This is mainly due to the inadequacy of light in the visible region to penetrate the skin and tissue. The depth of penetration is a measure of how deep the light can penetrate into a material [168].

When an electromagnetic wave rises over the surface of the material, a part of the light is reflected while the other part transmitted the energy to the material. This electromagnetic field interacts with electrons and atoms in the material. Depending on the structure of the material, the distance of the electromagnetic field varies. The penetration depth of light in living tissues depends on the intensity of the light source and the wavelength.

11.1.5 Gold nanocages and nanorods used in photothermal therapy

In recent years, in the treatment of cancer, gold nanostructures that absorb the laser rays around the infrared wavelength are more preferred instead of photothermal studies using visible light. The reason for this is that because the near infrared rays are low-energy, the cells do not absorb these rays in any way and thus the rays can penetrate into the cell without affecting the cells [169]. Gold nanocages and nanorods that can absorb infrared rays are the most widely used nanostructures in photothermal cancer therapy studies [170].

The use of gold nanorods in selective photothermal therapy was first performed using lasers with infrared wavelength [145,171,167]. In another study, the rod-shaped gold nanostructures were coated with primary antibodies and placed on gram-negative bacteria. These bacteria were destroyed when subjected to infra-red rays for ten minutes [160]. In the hyperthermic therapy of KB oral cancer cells, gold nanorods were conjugated with folic acid ligands and used with continuous wave Ti:Sapphire lasers [159]. As a result of laser irradiation, very large protrusions have occurred on the cell membrane surface.

In a study to prove the photothermal effect of gold nanocapsules, gold nanocapsules were stored in the carbon coated TEM grid and exposed to camera light. After imaging, it was observed that gold nanocapsules melted into spherical droplets [172]. The heat generated due to poor thermal conductivity has been shown to be airborne from the gold surface. In another study, gold nanocapsules synthesized by the galvanic displacement method and subsequently modified with monoclonal antibodies were mixed with breast cancer cells and subjected to near-infrared rays for five minutes, thereby killing cancer cells [170].

Although these studies show that photothermal cancer therapies performed by infrared nanowires are visible and effective in photothermal cancer therapies, the most important problems of these methods are as follows;

- use of strong laser beams in cancer therapy,
- exposure to long-term laser beams for effective therapy
- using of high concentration gold particles.

11.1.6 Bioconjugation of gold nanostructures used in photothermal therapy

Most laser-based treatment methods are built on the use of endoscopes and fiber optic catheters, in particular for reaching the tumor area. Gold nanoparticles are promising structures for their integration with immune-targeting strategies, since they allow for easy bio-functionalization [146]. Many studies have been conducted for functionalization of gold nanoparticles with specific tumor-targeting molecules in photothermal cancer therapy [173–174].

Among these targeting strategies, the nanoparticles are inactivated by polyethylene glycol (PEG) or used in conjugated antibodies to biomarkers on diseased cells [146]. PEG is used to increase the biocompatibility and bioavailability of nanoparticles (Fig. 8). In this way, the biocompatibility of nanoparticles coated with PEG groups is greatly increased and their clustering is prevented. Furthermore, the surface properties of the nanoparticles are altered by coating with various agents to prevent the recognition of nanoparticles by

macrophages. In this way, the availability of nanoparticles to the target site is increased [175–176].

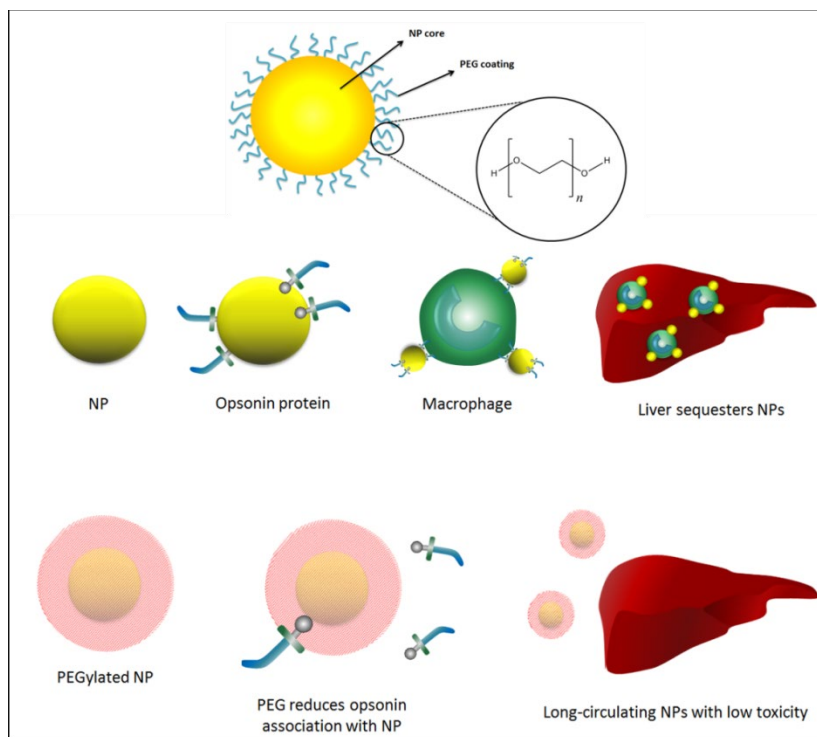


Fig. 8 PEG coated nanoparticles.

11.1.7 Determination of temperature changes in gold surface

Recently, the use of various types and sizes of gold nanoparticles in different forms and sizes of malignant cells used in photothermal therapy for cancer treatment is preferred by many researchers [158]. Although the harmful biological structures are detructed by photothermal therapy, the inability to detect controlled temperature, which increased on the gold surface, causes serious problems. Unfortunately, in such treatments, parameters, which optimum damage occurred, were determined by trial and error method and positive results were obtained with therapies using these parameters. A limited number of studies have been conducted to determine temperature changes on gold surfaces and only double-stranded oligonucleotides or DNA have been used in these studies (Fig. 9).

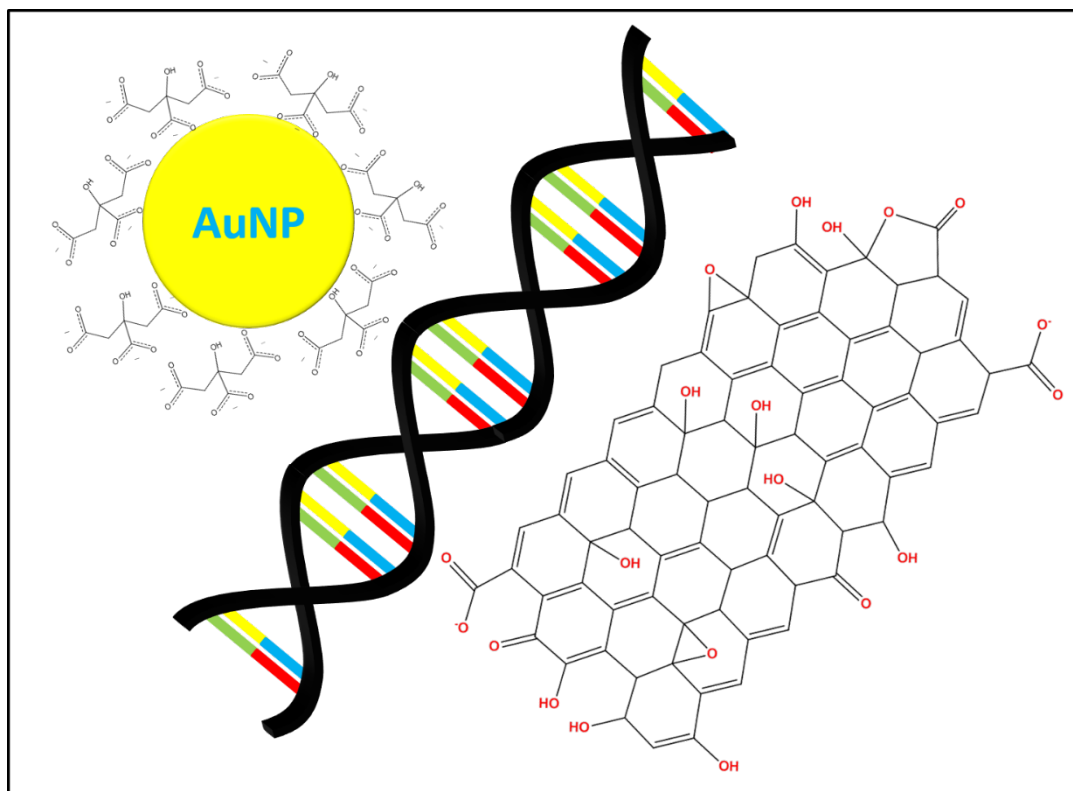


Fig. 9 Temperature change of gold nanoparticles with DNA.

In double-stranded nucleotides, the helical structure disintegrates at a given temperature and this decomposition temperature is called the melting point of the helical structure. In order to measure the temperature generated on the surfaces of gold nanostructures, one of the two helical structures must be conjugated to the gold surface by covalent bonds. The other spiral forms a double-helix structure in the form of DNA by adding to the coil on the gold surface. When the gold nanostructures are subjected to the laser beams they can absorb, the heat resulting from the double helix is reached by reaching the melting point. In this way, the nucleotide chain release, which is not bound to the gold surface by covalent bonds, is realized and the temperature rise on the gold surface has been tried to be determined by the detection of this oscillating spiral. The double strand of DNA containing 15 bases with a decomposition temperature of 54 °C was conjugated to the gold surface and it was determined that the double helix decomposed in a few seconds when subjected to a strong laser beam [177]. In another study, gold nanocrystals were coated with fluorescent dye-modified DNA double-stranded structures containing 50 bases and dissociation temperature of 70 °C. These gold nanostructures were mixed with living cells and subjected to a strong laser beam at near infrared. It was observed that the

binary helix decomposed in a short period of eight seconds without damaging the living cells. Fluorescent dyed helix was detected by fluorescence spectrometer and temperature increase was determined [178]. Although, it was said that oligonucleotide double helix structures give remarkable results, there is a considerable need for alternative methods due to difficulties and high costs of their synthesis.

Plasmonic gold nanostructures; Palladium (Pd) nanosheets [179], , polydopamine [180], nano-spheres [181], polyoxometal [182], nanoshells [183], nanodiamonds [184], nanorods [185], nanostars [186], nanocages [187], carbon (graphene) [188], iron oxide [189], carbon nanotubes [190], polyprol [191] and semiconductor polymer [192]; inorganic NPs was used as surface coatings to reduce the toxicity of PTT agents and to increase blood circulation time.

Compared to neighboring normal tissues, local temperature in the tumor region can be significantly increased by NP PTT agents with photothermal conversion yield and high light absorption. This leads to anticancer effects with low side effects. The potential biomedical application of nMOFs is considered a platform for PTT and PTT based combination therapies.

Finally, by encapsulating the functional components in nMOF cavities, it is possible to further increase the efficiency of PTT and PTT-based combination therapies. As shown in Table 2, nMOFs were used as PTT agents to combine PTT with diagnostic and therapeutic methods and hybrid nanomaterials for photothermal and combined photodynamic therapy.

Table 2. Effectiveness of PTT and PTT-based combination therapies.

Cell lines	Composites	Anticancer Efficacy	Functionality	Ref.
MCF-7	Fe ₃ O ₄ @C@ Porphyrin	In vitro: 35% cell viability after treated with 400 µg/mL particles, 180 J/cm ² laser for PDT and 600 J/cm ² laser for PTT; In vivo: tumors (200 mm ³) significantly regressed after treated with 10 mg/kg particles, 180 J/cm ² laser for PDT and 600 J/cm ² laser for PTT	Fluorescence, MRI, PTT, PDT	[107]

L929, HeLa	nMOFs for PDT + PTT Fe ₃ O ₄ /ZIF-8-Au ₂₅	In vitro: 15% cell viability after treated with 500 µg/mL particles and 300 J/cm ² laser; In vivo: Tumors (100 mm ³) were suppressed with 300 J/cm ² laser	MRI, PDT, PTT	[106]
MCF-7	Au nanorod@ZIF-8	In vitro: 18.7% cell viability after treated with 20 µg/mL particles and 600 J/cm ² laser	PTT	[113]
HepG2	Polypyrrole@MIL-100(Fe) with DOX-loaded	In vitro: 15% cell viability after treated with 500 µg/mL particles and 300 J/cm ² laser; In vivo: Tumors (100 mm ³) were suppressed with 300 J/cm ² laser	MRI, PAI, PTT, chemotherapy	[112]

HT-29	PB@Au	In vitro: less than 10% cell viability after treated with 100 µg/mL particles and 900 J/cm ² laser; In vivo: Tumors (100 mm ³) complete eradicated without recurrence treated with 500 mg/kg particles and 900 J/cm ² laser	PTT, CT, PAI	[115]
Hela	nMOF-enabled PTT Fe ^{III} ₄ [Fe ^{II} (CN) ₆] ₃ .nH ₂ O (PB)	In vitro: less than 10% cell viability after treated with 16 µg/mL particles and 1200 J/cm ² laser	PTT	[114]
4T1	nMOF-combined PTT ZIF-8@ graphene dots with DOX loaded	In vitro: 18% cell viability after treated with 100 µg/mL particles and 450 J/cm ² laser	PTT, NIR & pH-responsive chemotherapy	[118]

MCF-7	PB@mSiO ₂ -PEG with DOX loaded	In vitro: 25% cell viability after treated with 1000 µg/mL particles and 0.9 W/cm ² laser for 7 mins; In vivo: Tumors (100 mm ³) partially regressed treated with 25 mg/kg particles and 540 J/cm ² laser	PTT, MRI, NIR & pH-responsive chemotherapy,	[117]
Hela	PB@MIL-100(Fe) with artemisinin loaded	In vitro: 20% cell viability after treated with 100 µg/mL particles and 600 J/cm ² laser; In vivo: Tumors (200 mm ³) partially eradicated treated with 25 mg/kg particles and 600 J/cm ² laser	PTT, pH-responsive chemotherapy MRI, optical imaging,	[119]

SMMC-7721	Pd@Au@ZIF-8 with DOX loaded	In vitro: 11% cell viability after treated with 80 µg/mL particles and 1260 J/cm ² laser	PTT, NIR & pH-responsive chemotherapy	[123]
A549, HeLa, HepG2	Mn ₃ [Co(CN) ₆] ₂ @SiO ₂ @Ag with DOX loaded	In vitro: 16.92% cell viability after treated with 100 µg/mL particles and 1200 J/cm ² laser	Optical imaging, chemotherapy, PTT, MRI	[124]

12. Results and Perspectives

The investigation of nMOF structures began more than a decade ago in anticancer drug and biomedical imaging applications [94][193]. Potential applications of nMOF structures in phototherapy have been shown only 5 years ago. Numerous articles in phototherapy with nMOFs have emerged in the last 3 years, and this has highlighted the strong interest in the development of clinically related phototherapy regimens based on nMOFs.

nMOFs have been a promising nPS platform for PDT since its first release in 2014. For PDT the nMOFs offer several advantages over other nPSs:

- (1) nMOFs include PSs are organic binders and reach very high PS loads. Furthermore, the crystal structures of the nMOFs, which prevent their accumulation, prevent the self-extinguishing of PSs;
- (2) Although facilitating diffusion of ROS and oxygen, the loading of various therapeutic and diagnostic agents for synergistic and therapeutic therapy is also due to the highly porous nature of nMOFs;
- (3) Monocarboxylic modulators coated on nMOFs with other carboxyl modified functional molecules such as PEG and targeting ligands can be readily altered to contribute to biocompatibility and increase tumor accumulation.

nMOFs have the potential to be the next generation PS due to these features. Further efforts will be given to the design of new nMOFs for PDT, taking into account the synthetic adjustability of NMOFs. Research showing that PDT is a good treatment method explains that future efforts should focus on the in vivo studies of nMOF PSs. Assessing the clinical relevance of nMOFs in PDT is in early stage with very few in vivo data obtained. Combining PDT with immunotherapy for the treatment of metastatic cancers provides a powerful approach.

Localized PDT treatment results in a strong inflammatory response by inducing immunogenic cell death. Data and results of combining nMOF-active IDO and PDT inhibition for cancer treatment will inspire the search for this strategy using other nMOFs and control point inhibitors. In the near future, a significant amount of research work is expected in combining nMOF-mediated PDT and control point blockage immunotherapy. PTT monotherapy with nMOFs was not investigated in depth compared to PDT. Instead, the researchers have investigated the combination therapies with other imaging and treatment modalities of PTT (fluorescence, MRI, PAI, chemotherapy, radiotherapy and immune control point blockage treatment) by adding multiple functionalities to the nMOF mechanisms and using nMOFs. Typically, nMOF compared with the clinical dose of an acceptable 180 J/cm^2 is several times greater than the mild dose in PTT studies [1]. Different attempts have been made to incorporate the imaging and diagnostics functions into PTT-enabled nMOFs. However, it is difficult to predict utilization method of such nMOF therapeutics in the clinic. Regulatory barriers for multi-component nMOF installations can be significantly higher. Fine tuning of nMOFs for enhanced PTT and PDT activity will be possible thanks to the synthetic adjustability of nMOFs. It is possible to use nMOF phototherapy together with other therapeutic modalities in order to benefit from the unique properties of nMOFs and lead to superior antitumor activity. All studies and researches have shown that NMOF based phototherapy is very promising for the future. Finding future applications in phototherapy or related treatment modalities nMOFs are likely to be available for the treatment of cancer in the clinic.

References

1. J. R. Heath & M. E. Davis, Nanotechnology and Cancer. *Annual Review of Medicine*, **59** (2008) 251–265. <https://doi.org/10.1146/annurev.med.59.061506.185523>.
2. R. Ackroyd, C. Kelty, N. Brown, & M. Reed, The history of photodetection and photodynamic therapy. *Photochemistry and photobiology*, **74** (2001) 656–69.
3. S. K. Pushpan, S. Venkatraman, V. G. Anand, J. Sankar, D. Parmeswaran, S. Ganesan, & T. K. Chandrashekar, Porphyrins in photodynamic therapy - a search for ideal photosensitizers. *Current medicinal chemistry. Anti-cancer agents*, **2** (2002) 187–207.

4. P. Agostinis, K. Berg, K. A. Cengel, T. H. Foster, A. W. Girotti, S. O. Gollnick, S. M. Hahn, M. R. Hamblin, A. Juzeniene, D. Kessel, M. Korbelik, J. Moan, P. Mroz, D. Nowis, J. Piette, B. C. Wilson, & J. Golab, Photodynamic therapy of cancer: An update. *CA: A Cancer Journal for Clinicians*, **61** (2011) 250–281.
<https://doi.org/10.3322/caac.20114>.
5. A. Master, M. Livingston, & A. Sen Gupta, Photodynamic nanomedicine in the treatment of solid tumors: Perspectives and challenges. *Journal of Controlled Release*, **168** (2013) 88–102. <https://doi.org/10.1016/j.jconrel.2013.02.020>.
6. D. E. J. G. J. Dolmans, D. Fukumura, & R. K. Jain, Photodynamic therapy for cancer. *Nature Reviews Cancer*, **3** (2003) 380–387. <https://doi.org/10.1038/nrc1071>.
7. P.-J. Lou, L. Jones, & C. Hopper, Clinical Outcomes of Photodynamic Therapy for Head-and-Neck Cancer. *Technology in Cancer Research & Treatment*, **2** (2003) 311–317. <https://doi.org/10.1177/153303460300200405>.
8. M. G. Bredell, E. Besic, C. Maake, & H. Walt, The application and challenges of clinical PD–PDT in the head and neck region: A short review. *Journal of Photochemistry and Photobiology B: Biology*, **101** (2010) 185–190.
<https://doi.org/10.1016/J.JPHOTOBIO.2010.07.002>.
9. D. Nowis, M. Makowski, T. Stokłosa, M. Legat, T. Issat, & J. Gołab, Direct tumor damage mechanisms of photodynamic therapy. *Acta biochimica Polonica*, **52** (2005) 339–52.
10. H. Abrahamse & M. R. Hamblin, New photosensitizers for photodynamic therapy. *Biochemical Journal*, **473** (2016) 347–364. <https://doi.org/10.1042/BJ20150942>.
11. J. A. González-Delgado, P. J. Kennedy, M. Ferreira, J. P. C. Tomé, & B. Sarmiento, Use of Photosensitizers in Semisolid Formulations for Microbial Photodynamic Inactivation. *Journal of Medicinal Chemistry*, **59** (2016) 4428–4442.
<https://doi.org/10.1021/acs.jmedchem.5b01129>.
12. J. Bhaumik, A. K. Mittal, A. Banerjee, Y. Chisti, & U. C. Banerjee, Applications of phototheranostic nanoagents in photodynamic therapy. *Nano Research*, **8** (2015) 1373–1394. <https://doi.org/10.1007/s12274-014-0628-3>.
13. S. Kwiatkowski, B. Knap, D. Przystupski, J. Saczko, E. Kędzierska, K. Knap-Czop, J. Kotlińska, O. Michel, K. Kotowski, & J. Kulbacka, Photodynamic therapy – mechanisms, photosensitizers and combinations. *Biomedicine & Pharmacotherapy*, **106** (2018) 1098–1107. <https://doi.org/10.1016/j.biopha.2018.07.049>.
14. R. Chouikrat, A. Seve, R. Vanderesse, H. Benachour, M. Barberi-Heyob, S. Richeter, L. Raehm, J.-O. Durand, M. Verelst, & C. Frochot, Non Polymeric Nanoparticles for Photodynamic Therapy Applications: Recent Developments.

Current Medicinal Chemistry, **19** (2012) 781–792.

<https://doi.org/10.2174/092986712799034897>.

15. E. Corredor, P. S. Testillano, M. J. Coronado, P. González-Melendi, R. Fernández-Pacheco, C. Marquina, M. R. Ibarra, J. M. De La Fuente, D. Rubiales, A. Pérez-De-Luque, & M. C. Risuño, Nanoparticle penetration and transport in living pumpkin plants: In situ subcellular identification. *BMC Plant Biology*, **9** (2009) 1–11. <https://doi.org/10.1186/1471-2229-9-45>.
16. R. Ayranci, G. Baskaya, M. Guzel, S. Bozkurt, M. Ak, A. Savk, & F. Sen, Enhanced optical and electrical properties of PEDOT via nanostructured carbon materials: A comparative investigation. *Nano-Structures and Nano-Objects*, **11** (2017) 13–19. <https://doi.org/10.1016/j.nanoso.2017.05.008>.
17. S. Bozkurt, B. Tosun, B. Sen, S. Akocak, A. Savk, M. F. Ebeoğlu, & F. Sen, A Hydrogen Peroxide Sensor Based on TNM Functionalized Reduced Graphene Oxide Grafted with Highly Monodisperse Pd Nanoparticles. *Analytica Chimica Acta*, **989** (2017) 88–94. <https://doi.org/10.1016/j.aca.2017.07.051>.
18. R. Ayranci, G. Başkaya, M. Güzel, S. Bozkurt, F. Şen, & M. Ak, Carbon Based Nanomaterials for High Performance Optoelectrochemical Systems. *ChemistrySelect*, **2** (2017) 1548–1555. <https://doi.org/10.1002/slct.201601632>.
19. F. Şen & G. Gökağaç, Improving Catalytic Efficiency in The Methanol Oxidation Reaction by Inserting Ru in Face-Centered Cubic Pt Nanoparticles Prepared by A New Surfactant, Tert-octanethiol. *Energy and Fuels*, **22** (2008) 1858–1864. <https://doi.org/10.1021/ef700575t>.
20. B. Şen, A. Aygün, A. Şavk, S. Akocak, & F. Şen, Bimetallic Palladium–iridium Alloy Nanoparticles as Highly Efficient and Stable Catalyst for The Hydrogen Evolution Reaction. *International Journal of Hydrogen Energy*, **43** (2018) 20183–20191. <https://doi.org/10.1016/j.ijhydene.2018.07.081>.
21. B. Şen, S. Kuzu, E. Demir, & F. Akocak, Süleyman Şen, Highly Monodisperse RuCo Nanoparticles Decorated on Functionalized Multiwalled Carbon Nanotube with The Highest Observed Catalytic Activity in The Dehydrogenation of Dimethylamine–borane. *International Journal of Hydrogen Energy*, **42** (2017) 23292–23298. <https://doi.org/10.1016/j.ijhydene.2017.06.032>.
22. B. Sen, E. Kuyuldar, B. Demirkan, T. Onal Okyay, A. Şavk, & F. Sen, Highly Efficient Polymer Supported Monodisperse Ruthenium-nickel Nanocomposites for Dehydrocoupling of Dimethylamine Borane. *Journal of Colloid and Interface Science*, **526** (2018) 480–486. <https://doi.org/10.1016/j.jcis.2018.05.021>.

23. Y. Yıldız, S. Kuzu, B. Sen, A. Savk, S. Akocak, & F. Şen, Different Ligand Based Monodispersed Pt Nanoparticles Decorated with rGO As Highly Active and Reusable Catalysts for The Methanol Oxidation. *International Journal of Hydrogen Energy*, **42** (2017) 13061–13069. <https://doi.org/10.1016/j.ijhydene.2017.03.230>.
24. B. Sen, B. Demirkan, B. Şimşek, A. Savk, & F. Sen, Monodisperse Palladium Nanocatalysts for Dehydrocoupling of Dimethylamineborane. *Nano-Structures & Nano-Objects*, **16** (2018) 209–214. <https://doi.org/10.1016/j.nanoso.2018.07.008>.
25. B. Şahin, E. Demir, A. Aygün, H. Gündüz, & F. Şen, Investigation of The Effect Of Pomegranate Extract And Monodisperse Silver Nanoparticle Combination on MCF-7 Cell Line. *Journal of Biotechnology*, **260** (2017) 79–83. <https://doi.org/10.1016/j.jbiotec.2017.09.012>.
26. A. Minchom, C. Aversa, & J. Lopez, Dancing with the DNA damage response: next-generation anti-cancer therapeutic strategies. *Therapeutic advances in medical oncology*, **10** (2018) 1758835918786658. <https://doi.org/10.1177/1758835918786658>.
27. R. L. Manthe, S. P. Foy, N. Krishnamurthy, B. Sharma, & V. Labhasetwar, Tumor Ablation and Nanotechnology. (n.d.). <https://doi.org/10.1021/mp1001944>.
28. C. C. Lee, J. A. MacKay, J. M. J. Fréchet, & F. C. Szoka, Designing dendrimers for biological applications. *Nature Biotechnology*, **23** (2005) 1517–1526. <https://doi.org/10.1038/nbt1171>.
29. V. P. Torchilin, Recent advances with liposomes as pharmaceutical carriers. *Nature Reviews Drug Discovery*, **4** (2005) 145–160. <https://doi.org/10.1038/nrd1632>.
30. K. Kataoka, A. Harada, & Y. Nagasaki, Block copolymer micelles for drug delivery: design, characterization and biological significance. *Advanced Drug Delivery Reviews*, **47** (2001) 113–131. [https://doi.org/10.1016/S0169-409X\(00\)00124-1](https://doi.org/10.1016/S0169-409X(00)00124-1).
31. M. Hamidi, K. Rostamizadeh, & M. A. Shahbazi, Hydrogel Nanoparticles in Drug Delivery. *Intelligent Nanomaterials: Processes, Properties, and Applications*, **60** (2012) 583–624. <https://doi.org/10.1002/9781118311974.ch15>.
32. X. Gao, Y. Cui, R. M. Levenson, L. W. K. Chung, & S. Nie, In vivo cancer targeting and imaging with semiconductor quantum dots. *Nature Biotechnology*, **22** (2004) 969–976. <https://doi.org/10.1038/nbt994>.
33. X. Huang, I. H. El-Sayed, W. Qian, & M. A. El-Sayed, Cancer Cell Imaging and Photothermal Therapy in the Near-Infrared Region by Using Gold Nanorods. *Journal of the American Chemical Society*, **128** (2006) 2115–2120. <https://doi.org/10.1021/ja057254a>.
34. Z. Li, J. Hüve, C. Krampe, G. Luppi, M. Tsotsalas, J. Klingauf, L. De Cola, & K. Riehemann, Internalization Pathways of Anisotropic Disc-Shaped Zeolite L

- Nanocrystals with Different Surface Properties in HeLa Cancer Cells. *Small*, **9** (2013) 1809–1820. <https://doi.org/10.1002/sml.201201702>.
35. A. K. Gupta & M. Gupta, Synthesis and surface engineering of iron oxide nanoparticles for biomedical applications. *Biomaterials*, **26** (2005) 3995–4021. <https://doi.org/10.1016/j.biomaterials.2004.10.012>.
36. Z. Li, J. C. Barnes, A. Bosoy, J. F. Stoddart, & J. I. Zink, Mesoporous silica nanoparticles in biomedical applications. *Chemical Society Reviews*, **41** (2012) 2590. <https://doi.org/10.1039/c1cs15246g>.
37. A. Bianco, K. Kostarelos, C. D. Partidos, & M. Prato, Biomedical applications of functionalised carbon nanotubes. *Chemical Communications*, (2005) 571–577. <https://doi.org/10.1039/b410943k>.
38. J. Shen, L. Zhao, & G. Han, Lanthanide-doped upconverting luminescent nanoparticle platforms for optical imaging-guided drug delivery and therapy. *Advanced Drug Delivery Reviews*, **65** (2013) 744–755. <https://doi.org/10.1016/j.addr.2012.05.007>.
39. C. He, D. Liu, & W. Lin, Nanomedicine Applications of Hybrid Nanomaterials Built from Metal–Ligand Coordination Bonds: Nanoscale Metal–Organic Frameworks and Nanoscale Coordination Polymers. *Chemical Reviews*, **115** (2015) 11079–11108. <https://doi.org/10.1021/acs.chemrev.5b00125>.
40. M. Giménez-Marqués, T. Hidalgo, C. Serre, & P. Horcajada, Nanostructured metal–organic frameworks and their bio-related applications. *Coordination Chemistry Reviews*, **307** (2016) 342–360. <https://doi.org/10.1016/j.ccr.2015.08.008>.
41. M. Lismont, L. Dreesen, & S. Wuttke, Metal-Organic Framework Nanoparticles in Photodynamic Therapy: Current Status and Perspectives. *Advanced Functional Materials*, **27** (2017) 1606314. <https://doi.org/10.1002/adfm.201606314>.
42. H. Göksu, B. Çelik, Y. Yıldız, F. Şen, & B. Kılbaş, Superior Monodisperse CNT-Supported CoPd (CoPd@CNT) Nanoparticles for Selective Reduction of Nitro Compounds to Primary Amines with NaBH₄ in Aqueous Medium. *ChemistrySelect*, **1** (2016) 2366–2372. <https://doi.org/10.1002/slct.201600509>.
43. S. Günbatar, A. Aygun, Y. Karataş, M. Gülcan, & F. Şen, Carbon-nanotube-based Rhodium Nanoparticles as Highly-Active Catalyst for Hydrolytic Dehydrogenation of Dimethylamineborane at Room Temperature. *Journal of Colloid and Interface Science*, **530** (2018) 321–327. <https://doi.org/10.1016/j.jcis.2018.06.100>.
44. N. M. Iverson, P. W. Barone, M. Shandell, L. J. Trudel, S. Sen, F. Sen, V. Ivanov, E. Atolia, E. Farias, T. P. McNicholas, N. Reuel, N. M. A. Parry, G. N. Wogan, & M. S. Strano, In vivo Biosensing via Tissue-localizable Near-infrared-fluorescent Single-

- walled Carbon Nanotubes. *Nature Nanotechnology*, **8** (2013) 873–880.
<https://doi.org/10.1038/nnano.2013.222>.
45. S. Sen, F. Sen, A. A. Boghossian, J. Zhang, & M. S. Strano, Effect of Reductive Dithiothreitol and Trolox on Nitric Oxide Quenching of Single-walled Carbon Nanotubes. *The Journal of Physical Chemistry C*, **117** (2013) 593–602.
<https://doi.org/10.1021/jp307175f>.
46. Z. W. Ulissi, F. Sen, X. Gong, S. Sen, N. Iverson, A. A. Boghossian, L. C. Godoy, G. N. Wogan, D. Mukhopadhyay, & M. S. Strano, Spatiotemporal Intracellular Nitric Oxide Signaling Captured Using Internalized, Near-infrared Fluorescent Carbon Nanotube Nanosensors. *Nano Letters*, **14** (2014) 4887–4894.
<https://doi.org/10.1021/nl502338y>.
47. M. P. Landry, H. Ando, A. Y. Chen, J. Cao, V. I. Kottadiel, L. Chio, D. Yang, J. Dong, T. K. Lu, & M. S. Strano, Single-molecule detection of protein efflux from microorganisms using fluorescent single-walled carbon nanotube sensor arrays. *Nature Nanotechnology*, **12** (2017) 368–377. <https://doi.org/10.1038/nnano.2016.284>.
48. J. D. Evans, B. Garai, H. Reinsch, W. Li, S. Dissegna, V. Bon, I. Senkovska, R. A. Fischer, S. Kaskel, C. Janiak, N. Stock, & D. Volkmer, Metal–organic frameworks in Germany: From synthesis to function. *Coordination Chemistry Reviews*, **380** (2019) 378–418. <https://doi.org/10.1016/j.ccr.2018.10.002>.
49. Y.-R. Lee, J. Kim, & W.-S. Ahn, Synthesis of metal-organic frameworks: A mini review. *Korean Journal of Chemical Engineering*, **30** (2013) 1667–1680.
<https://doi.org/10.1007/s11814-013-0140-6>.
50. C. Vaitsis, G. Sourkouni, & C. Argiris, Metal Organic Frameworks (MOFs) and ultrasound: A review. *Ultrasonics Sonochemistry*, (2018) 0–1.
<https://doi.org/10.1016/j.ultsonch.2018.11.004>.
51. T. L. Doane & C. Burda, The unique role of nanoparticles in nanomedicine: imaging, drug delivery and therapy. *Chemical Society Reviews*, **41** (2012) 2885.
<https://doi.org/10.1039/c2cs15260f>.
52. J. Peng, L. Zhao, X. Zhu, Y. Sun, W. Feng, Y. Gao, L. Wang, & F. Li, Hollow silica nanoparticles loaded with hydrophobic phthalocyanine for near-infrared photodynamic and photothermal combination therapy. *Biomaterials*, **34** (2013) 7905–7912. <https://doi.org/10.1016/j.biomaterials.2013.07.027>.
53. J. Wang, T. T. Wang, P. F. Gao, & C. Z. Huang, Biomolecules-conjugated nanomaterials for targeted cancer therapy. *J. Mater. Chem. B*, **2** (2014) 8452–8465.
<https://doi.org/10.1039/C4TB01263A>.

54. R. R. Allison, H. C. Mota, V. S. Bagnato, & C. H. Sibata, Bio-nanotechnology and photodynamic therapy—State of the art review. *Photodiagnosis and Photodynamic Therapy*, **5** (2008) 19–28. <https://doi.org/10.1016/j.pdpdt.2008.02.001>.
55. A. F. McDonagh, Phototherapy: From Ancient Egypt to the New Millennium. *Journal of Perinatology*, **21** (2001) S7–S12. <https://doi.org/10.1038/sj.jp.7210625>.
56. D. S. Rassmussen-Taxdal, G. E. Ward, & F. H. J. Figge, Fluorescence of human lymphatic and cancer tissues following high doses of intravenous hematoporphyrin. *Cancer*, **8** (1955) 78–81. [https://doi.org/10.1002/1097-0142\(1955\)8:1<78::AID-CNCR2820080109>3.0.CO;2-L](https://doi.org/10.1002/1097-0142(1955)8:1<78::AID-CNCR2820080109>3.0.CO;2-L).
57. H. v. Tappeiner, Die photodynamische Erscheinung (Sensibilisierung durch fluoreszierende Stoffe). *Ergebnisse der Physiologie*, **8** (1909) 698–741. <https://doi.org/10.1007/BF02321096>.
58. R. L. LIPSON, E. J. BALDES, & A. M. OLSEN, Hematoporphyrin derivative: a new aid for endoscopic detection of malignant disease. *The Journal of thoracic and cardiovascular surgery*, **42** (1961) 623–9.
59. T. J. Dougherty, STUDIES ON THE STRUCTURE OF PORPHYRINS CONTAINED IN PHOTOFRIN® II. *Photochemistry and Photobiology*, **46** (1987) 569–573. <https://doi.org/10.1111/j.1751-1097.1987.tb04815.x>.
60. T. J. Dougherty, Photodynamic therapy—new approaches. *Seminars in Surgical Oncology*, **5** (1989) 6–16. <https://doi.org/10.1002/ssu.2980050104>.
61. J. G. PARKER, The Importance of Singlet Delta Oxygen in Cancer Photoradiation Therapy. *Johns Hopkins APL Technical Digest*, **5** (1984) 48–50.
62. G. H. Kliman, C. A. Puliafito, G. A. Grossman, & W. A. Gregory, Retinal and choroidal vessel closure using phthalocyanine photodynamic therapy. *Lasers in Surgery and Medicine*, **15** (1994) 11–18. <https://doi.org/10.1002/lsm.1900150104>.
63. H. Miller & B. Miller, Photodynamic Therapy of Subretinal Neovascularization in the Monkey Eye. *Archives of Ophthalmology*, **111** (1993) 855–860. <https://doi.org/10.1001/archoph.1993.01090060145039>.
64. A. J. Packer, D. T. Tse, X. Q. Gu, & S. S. Hayreh, Hematoporphyrin photoradiation therapy for iris neovascularization. A preliminary report. *Archives of ophthalmology (Chicago, Ill. : 1960)*, **102** (1984) 1193–7.
65. S. K. Nanda, D. L. Hatchell, J. S. Tiedeman, J. J. Dutton, M. C. Hatchell, & T. McAdoo, A new method for vascular occlusion. Photochemical initiation of thrombosis. *Archives of ophthalmology (Chicago, Ill. : 1960)*, **105** (1987) 1121–4.
66. C. S. Foote, Definition of type I and type II photosensitized oxidation. *Photochemistry and photobiology*, **54** (1991) 659.

67. Sharman, Allen, & van Lier JE, Photodynamic therapeutics: basic principles and clinical applications. *Drug discovery today*, **4** (1999) 507–517.
68. T. Dai, B. B. Fuchs, J. J. Coleman, R. A. Prates, C. Astrakas, T. G. St Denis, M. S. Ribeiro, E. Mylonakis, M. R. Hamblin, & G. P. Tegos, Concepts and principles of photodynamic therapy as an alternative antifungal discovery platform. *Frontiers in microbiology*, **3** (2012) 120. <https://doi.org/10.3389/fmicb.2012.00120>.
69. L. B. Josefsen & R. W. Boyle, Photodynamic therapy: novel third-generation photosensitizers one step closer? **154** (2008) 1–3. <https://doi.org/10.1038/bjp.2008.98>.
70. A. Ormond, H. Freeman, A. B. Ormond, & H. S. Freeman, Dye Sensitizers for Photodynamic Therapy. *Materials*, **6** (2013) 817–840. <https://doi.org/10.3390/ma6030817>.
71. J. Saczko, J. Kulbacka, A. Chwiłkowska, M. Lugowski, & T. Banaś, Levels of lipid peroxidation in A549 cells after PDT in vitro. *Roczniki Akademii Medycznej w Białymstoku* (1995), **49 Suppl 1** (2004) 82–4.
72. B. W. Henderson & T. J. Dougherty, HOW DOES PHOTODYNAMIC THERAPY WORK? *Photochemistry and Photobiology*, **55** (1992) 145–157. <https://doi.org/10.1111/j.1751-1097.1992.tb04222.x>.
73. B. J. Tromberg, A. Orenstein, S. Kimel, S. J. Barker, J. Hyatt, J. S. Nelson, & M. W. Berns, In vivo tumor oxygen tension measurements for the evaluation of the efficiency of photodynamic therapy. *Photochemistry and photobiology*, **52** (1990) 375–85.
74. A. Manuscript & S. R. Ablation, NIH Public Access. **4** (2008) 208–214. <https://doi.org/10.1021/mp1001944.Tumor>.
75. J. M. Ang, I. Bin Riaz, M. U. Kamal, G. Paragh, & N. C. Zeitouni, Photodynamic therapy and pain: A systematic review. *Photodiagnosis and Photodynamic Therapy*, **19** (2017) 308–344. <https://doi.org/10.1016/j.pdpdt.2017.07.002>.
76. C. H. Sibata, V. C. Colussi, N. L. Oleinick, & T. J. Kinsella, Photodynamic therapy: a new concept in medical treatment. *Brazilian journal of medical and biological research = Revista brasileira de pesquisas medicas e biologicas*, **33** (2000) 869–80.
77. A. M. van den Besselaar & A. C. Moor, Photodynamic treatment of pooled coumarin plasma for external quality assessment of the prothrombin time. *Journal of clinical pathology*, **53** (2000) 470–5.
78. J. C. Kennedy & R. H. Pottier, New trends in photobiology. *Journal of Photochemistry and Photobiology B: Biology*, **14** (1992) 275–292. [https://doi.org/10.1016/1011-1344\(92\)85108-7](https://doi.org/10.1016/1011-1344(92)85108-7).

79. C. H. Yang, J. C. Lee, C. H. Chen, C. Y. Hui, H. S. Hong, & H. W. Kuo, Photodynamic therapy for bowenoid papulosis using a novel incoherent light-emitting diode device. *The British journal of dermatology*, **149** (2003) 1297–9.
80. Z. Luksiene, Photodynamic therapy: mechanism of action and ways to improve the efficiency of treatment. *Medicina (Kaunas, Lithuania)*, **39** (2003) 1137–50.
81. S. Karrer, R.-M. Szeimies, U. Hohenleutner, & M. Landthaler, Role of Lasers and Photodynamic Therapy in the Treatment of Cutaneous Malignancy. *American Journal of Clinical Dermatology*, **2** (2001) 229–237. <https://doi.org/10.2165/00128071-200102040-00004>.
82. T. S. Mang, Lasers and light sources for PDT: past, present and future. *Photodiagnosis and photodynamic therapy*, **1** (2004) 43–8. [https://doi.org/10.1016/S1572-1000\(04\)00012-2](https://doi.org/10.1016/S1572-1000(04)00012-2).
83. S. Tuncel, A. Trivella, D. Atilla, K. Bennis, H. Savoie, F. Albrieux, L. Delort, H. Billard, V. Dubois, V. Ahsen, F. Caldefie-Chézet, C. Richard, R. W. Boyle, S. Ducki, & F. Dumoulin, Assessing the Dual Activity of a Chalcone–Phthalocyanine Conjugate: Design, Synthesis, and Antivascular and Photodynamic Properties. *Molecular Pharmaceutics*, **10** (2013) 3706–3716. <https://doi.org/10.1021/mp400207v>.
84. L. Cohen & S. Schwartz, Modification of radiosensitivity by porphyrins. II. Transplanted rhabdomyosarcoma in mice. *Cancer research*, **26** (1966) 1769–73.
85. T. J. Dougherty, A brief history of clinical photodynamic therapy development at Roswell Park Cancer Institute. *Journal of clinical laser medicine & surgery*, **14** (1996) 219–21. <https://doi.org/10.1089/clm.1996.14.219>.
86. R. R. Allison & C. H. Sibata, Oncologic photodynamic therapy photosensitizers: A clinical review. *Photodiagnosis and Photodynamic Therapy*, **7** (2010) 61–75. <https://doi.org/10.1016/j.pdpdt.2010.02.001>.
87. R. Hudson, M. Carcenac, K. Smith, L. Madden, O. J. Clarke, A. Pèleguin, J. Greenman, & R. W. Boyle, The development and characterisation of porphyrin isothiocyanate-monoclonal antibody conjugates for photoimmunotherapy. *British journal of cancer*, **92** (2005) 1442–9. <https://doi.org/10.1038/sj.bjc.6602517>.
88. H. Dummin, T. Cernay, & H. W. Zimmermann, Selective photosensitization of mitochondria in HeLa cells by cationic Zn (II) phthalocyanines with lipophilic side-chains. *Journal of photochemistry and photobiology. B, Biology*, **37** (1997) 219–29.
89. R. Sidbury, D. M. Davis, D. E. Cohen, K. M. Cordoro, T. G. Berger, J. N. Bergman, S. L. Chamlin, K. D. Cooper, S. R. Feldman, J. M. Hanifin, A. Krol, D. J. Margolis, A. S. Paller, K. Schwarzenberger, R. A. Silverman, E. L. Simpson, W. L. Tom, H. C. Williams, C. A. Elmets, J. Block, C. G. Harrod, W. S. Begolka, L. F.

- Eichenfield, & American Academy of Dermatology, Guidelines of care for the management of atopic dermatitis. *Journal of the American Academy of Dermatology*, **71** (2014) 327–349. <https://doi.org/10.1016/j.jaad.2014.03.030>.
90. A. C. Moor, Signaling pathways in cell death and survival after photodynamic therapy. *Journal of Photochemistry and Photobiology B: Biology*, **57** (2000) 1–13. [https://doi.org/10.1016/S1011-1344\(00\)00065-8](https://doi.org/10.1016/S1011-1344(00)00065-8).
91. S. L. Manoto, N. Houreld, N. Hodgkinson, & H. Abrahamse, Modes of Cell Death Induced by Photodynamic Therapy Using Zinc Phthalocyanine in Lung Cancer Cells Grown as a Monolayer and Three-Dimensional Multicellular Spheroids. *Molecules*, **22** (2017) 791. <https://doi.org/10.3390/molecules22050791>.
92. N. Gargiulo, F. Pepe, & D. Caputo, CO₂ adsorption by functionalized nanoporous materials: a review. *Journal of nanoscience and nanotechnology*, **14** (2014) 1811–22.
93. J. Kim, B. Chen, T. M. Reineke, H. Li, M. Eddaoudi, D. B. Moler, M. O’Keeffe, & O. M. Yaghi, Assembly of metal-organic frameworks from large organic and inorganic secondary building units: New examples and simplifying principles for complex structures. *Journal of the American Chemical Society*, **123** (2001) 8239–8247. <https://doi.org/10.1021/ja010825o>.
94. W. J. Rieter, K. M. L. Taylor, H. An, W. Lin, & W. Lin, Nanoscale Metal–Organic Frameworks as Potential Multimodal Contrast Enhancing Agents. *Journal of the American Chemical Society*, **128** (2006) 9024–9025. <https://doi.org/10.1021/ja0627444>.
95. K. M. L. Taylor, W. J. Rieter, & W. Lin, Manganese-Based Nanoscale Metal–Organic Frameworks for Magnetic Resonance Imaging. *Journal of the American Chemical Society*, **130** (2008) 14358–14359. <https://doi.org/10.1021/ja803777x>.
96. K. E. deKrafft, Z. Xie, G. Cao, S. Tran, L. Ma, O. Z. Zhou, & W. Lin, Iodinated Nanoscale Coordination Polymers as Potential Contrast Agents for Computed Tomography. *Angewandte Chemie*, **121** (2009) 10085–10088. <https://doi.org/10.1002/ange.200904958>.
97. K. E. deKrafft, W. S. Boyle, L. M. Burk, O. Z. Zhou, & W. Lin, Zr- and Hf-based nanoscale metal–organic frameworks as contrast agents for computed tomography. *Journal of Materials Chemistry*, **22** (2012) 18139. <https://doi.org/10.1039/c2jm32299d>.
98. A. Foucault-Collet, K. A. Gogick, K. A. White, S. Villette, A. Pallier, G. Collet, C. Kieda, T. Li, S. J. Geib, N. L. Rosi, & S. Petoud, Lanthanide near infrared imaging in living cells with Yb³⁺ nano metal organic frameworks. *Proceedings of the National*

- Academy of Sciences of the United States of America*, **110** (2013) 17199–204.
<https://doi.org/10.1073/pnas.1305910110>.
99. C. He, K. Lu, & W. Lin, Nanoscale Metal–Organic Frameworks for Real-Time Intracellular pH Sensing in Live Cells. *Journal of the American Chemical Society*, **136** (2014) 12253–12256. <https://doi.org/10.1021/ja507333c>.
100. R. Xu, Y. Wang, X. Duan, K. Lu, D. Micheroni, A. Hu, & W. Lin, Nanoscale Metal–Organic Frameworks for Ratiometric Oxygen Sensing in Live Cells. *Journal of the American Chemical Society*, **138** (2016) 2158–2161.
<https://doi.org/10.1021/jacs.5b13458>.
101. C. He, K. Lu, D. Liu, & W. Lin, Nanoscale Metal–Organic Frameworks for the Co-Delivery of Cisplatin and Pooled siRNAs to Enhance Therapeutic Efficacy in Drug-Resistant Ovarian Cancer Cells. *Journal of the American Chemical Society*, **136** (2014) 5181–5184. <https://doi.org/10.1021/ja4098862>.
102. R. C. Huxford, K. E. deKrafft, W. S. Boyle, D. Liu, & W. Lin, Lipid-coated nanoscale coordination polymers for targeted delivery of antifolates to cancer cells. *Chem. Sci.*, **3** (2012) 198–204. <https://doi.org/10.1039/C1SC00499A>.
103. K. M. L. Taylor, A. Jin, & W. Lin, Surfactant-Assisted Synthesis of Nanoscale Gadolinium Metal–Organic Frameworks for Potential Multimodal Imaging. *Angewandte Chemie*, **120** (2008) 7836–7839. <https://doi.org/10.1002/ange.200802911>.
104. K. Lu, C. He, & W. Lin, Nanoscale Metal–Organic Framework for Highly Effective Photodynamic Therapy of Resistant Head and Neck Cancer. *Journal of the American Chemical Society*, **136** (2014) 16712–16715. <https://doi.org/10.1021/ja508679h>.
105. K. Lu, C. He, & W. Lin, A Chlorin-Based Nanoscale Metal–Organic Framework for Photodynamic Therapy of Colon Cancers. *Journal of the American Chemical Society*, **137** (2015) 7600–7603. <https://doi.org/10.1021/jacs.5b04069>.
106. D. Yang, G. Yang, S. Gai, F. He, G. An, Y. Dai, R. Lv, & P. Yang, Au 25 cluster functionalized metal–organic nanostructures for magnetically targeted photodynamic/photothermal therapy triggered by single wavelength 808 nm near-infrared light. *Nanoscale*, **7** (2015) 19568–19578.
<https://doi.org/10.1039/C5NR06192J>.
107. H. Zhang, Y.-H. Li, Y. Chen, M.-M. Wang, X.-S. Wang, & X.-B. Yin, Fluorescence and Magnetic Resonance Dual-Modality Imaging-Guided Photothermal and Photodynamic Dual-Therapy with Magnetic Porphyrin-Metal Organic Framework Nanocomposites. *Scientific Reports*, **7** (2017) 44153.
<https://doi.org/10.1038/srep44153>.

108. L. He, M. Brasino, C. Mao, S. Cho, W. Park, A. P. Goodwin, & J. N. Cha, DNA-Assembled Core-Satellite Upconverting-Metal-Organic Framework Nanoparticle Superstructures for Efficient Photodynamic Therapy. *Small*, **13** (2017) 1700504. <https://doi.org/10.1002/sml.201700504>.
109. X. Zheng, L. Wang, Q. Pei, S. He, S. Liu, & Z. Xie, Metal–Organic Framework@Porous Organic Polymer Nanocomposite for Photodynamic Therapy. *Chemistry of Materials*, **29** (2017) 2374–2381. <https://doi.org/10.1021/acs.chemmater.7b00228>.
110. J. Liu, L. Zhang, J. Lei, H. Shen, & H. Ju, Multifunctional Metal–Organic Framework Nanoprobe for Cathepsin B-Activated Cancer Cell Imaging and Chemo-Photodynamic Therapy. *ACS Applied Materials & Interfaces*, **9** (2017) 2150–2158. <https://doi.org/10.1021/acsami.6b14446>.
111. D. Bůžek, J. Zelenka, P. Ulbrich, T. Ruml, I. Křížová, J. Lang, P. Kubát, J. Demel, K. Kirakci, & K. Lang, Nanoscaled porphyrinic metal–organic frameworks: photosensitizer delivery systems for photodynamic therapy. *Journal of Materials Chemistry B*, **5** (2017) 1815–1821. <https://doi.org/10.1039/C6TB03230C>.
112. X. Chen, M. Zhang, S. Li, L. Li, L. Zhang, T. Wang, M. Yu, Z. Mou, & C. Wang, Facile synthesis of polypyrrole@metal–organic framework core–shell nanocomposites for dual-mode imaging and synergistic chemo-photothermal therapy of cancer cells. *Journal of Materials Chemistry B*, **5** (2017) 1772–1778. <https://doi.org/10.1039/C6TB03218D>.
113. L. Fang, W. Wang, Y. Liu, Z. Xie, & L. Chen, Zeolitic imidazole framework coated Au nanorods for enhanced photothermal therapy and stability. *Dalton Transactions*, **46** (2017) 8933–8937. <https://doi.org/10.1039/C7DT00613F>.
114. G. Fu, W. Liu, S. Feng, & X. Yue, Prussian blue nanoparticles operate as a new generation of photothermal ablation agents for cancer therapy. *Chemical Communications*, **48** (2012) 11567. <https://doi.org/10.1039/c2cc36456e>.
115. L. Jing, X. Liang, Z. Deng, S. Feng, X. Li, M. Huang, C. Li, & Z. Dai, Prussian blue coated gold nanoparticles for simultaneous photoacoustic/CT bimodal imaging and photothermal ablation of cancer. *Biomaterials*, **35** (2014) 5814–5821. <https://doi.org/10.1016/J.BIOMATERIALS.2014.04.005>.
116. K. Lu, C. He, N. Guo, C. Chan, K. Ni, R. R. Weichselbaum, & W. Lin, Chlorin-Based Nanoscale Metal–Organic Framework Systemically Rejects Colorectal Cancers via Synergistic Photodynamic Therapy and Checkpoint Blockade Immunotherapy. *Journal of the American Chemical Society*, **138** (2016) 12502–12510. <https://doi.org/10.1021/jacs.6b06663>.

117. Y. Y. Su, Z. Teng, H. Yao, S. J. Wang, Y. Tian, Y. L. Zhang, W. F. Liu, W. Tian, L. J. Zheng, N. Lu, Q. Q. Ni, X. D. Su, Y. X. Tang, J. Sun, Y. Liu, J. Wu, G. F. Yang, G. M. Lu, & L. J. Zhang, A Multifunctional PB@mSiO₂-PEG/DOX Nanoplatfom for Combined Photothermal-Chemotherapy of Tumor. *ACS Applied Materials & Interfaces*, **8** (2016) 17038–17046. <https://doi.org/10.1021/acsami.6b01147>.
118. Z. Tian, X. Yao, K. Ma, X. Niu, J. Grothe, Q. Xu, L. Liu, S. Kaskel, & Y. Zhu, Metal–Organic Framework/Graphene Quantum Dot Nanoparticles Used for Synergistic Chemo- and Photothermal Therapy. *ACS Omega*, **2** (2017) 1249–1258. <https://doi.org/10.1021/acsomega.6b00385>.
119. D. Wang, J. Zhou, R. Chen, R. Shi, G. Zhao, G. Xia, R. Li, Z. Liu, J. Tian, H. Wang, Z. Guo, H. Wang, & Q. Chen, Controllable synthesis of dual-MOFs nanostructures for pH-responsive artemisinin delivery, magnetic resonance and optical dual-modal imaging-guided chemo/photothermal combinational cancer therapy. *Biomaterials*, **100** (2016) 27–40. <https://doi.org/10.1016/J.BIOMATERIALS.2016.05.027>.
120. S. Wang, L. Shang, L. Li, Y. Yu, C. Chi, K. Wang, J. Zhang, R. Shi, H. Shen, G. I. N. Waterhouse, S. Liu, J. Tian, T. Zhang, & H. Liu, Metal-Organic-Framework-Derived Mesoporous Carbon Nanospheres Containing Porphyrin-Like Metal Centers for Conformal Phototherapy. *Advanced Materials*, **28** (2016) 8379–8387. <https://doi.org/10.1002/adma.201602197>.
121. Y. Yang, Y. Chao, J. Liu, Z. Dong, W. He, R. Zhang, K. Yang, M. Chen, & Z. Liu, Core-shell and co-doped nanoscale metal-organic particles (NMOPs) obtained via post-synthesis cation exchange for multimodal imaging and synergistic thermo-radiotherapy. *NPG Asia Materials*, **9** (2017) e344–e344. <https://doi.org/10.1038/am.2016.205>.
122. Y. Yang, J. Liu, C. Liang, L. Feng, T. Fu, Z. Dong, Y. Chao, Y. Li, G. Lu, M. Chen, & Z. Liu, Nanoscale Metal–Organic Particles with Rapid Clearance for Magnetic Resonance Imaging-Guided Photothermal Therapy. *ACS Nano*, **10** (2016) 2774–2781. <https://doi.org/10.1021/acsnano.5b07882>.
123. W.-K. Tsai, C.-I. Wang, C.-H. Liao, C.-N. Yao, T.-J. Kuo, M.-H. Liu, C.-P. Hsu, S.-Y. Lin, C.-Y. Wu, J. R. Pyle, J. Chen, & Y.-H. Chan, Molecular design of near-infrared fluorescent Pdots for tumor targeting: aggregation-induced emission *versus* anti-aggregation-caused quenching. *Chemical Science*, **10** (2019) 198–207. <https://doi.org/10.1039/C8SC03510E>.
124. D. Wang, Z. Guo, J. Zhou, J. Chen, G. Zhao, R. Chen, M. He, Z. Liu, H. Wang, & Q. Chen, Novel Mn₃[Co(CN)₆]₂@SiO₂@Ag Core-Shell Nanocube: Enhanced Two-Photon Fluorescence and Magnetic Resonance Dual-Modal Imaging-Guided

- Photothermal and Chemo-therapy. *Small*, **11** (2015) 5956–5967.
<https://doi.org/10.1002/sml.201502102>.
125. J. Park, D. Feng, S. Yuan, & H.-C. Zhou, Photochromic Metal-Organic Frameworks: Reversible Control of Singlet Oxygen Generation. *Angewandte Chemie*, **127** (2015) 440–445. <https://doi.org/10.1002/ange.201408862>.
126. J. F. Liu, Y. B. Guo, T. M. Butler, & M. L. Weaver, Crystallography, compositions, and properties of white layer by wire electrical discharge machining of nitinol shape memory alloy. *Materials & Design*, **109** (2016) 1–9.
<https://doi.org/10.1016/J.MATDES.2016.07.063>.
127. L. Zhang, J. Lei, F. Ma, P. Ling, J. Liu, & H. Ju, A porphyrin photosensitized metal–organic framework for cancer cell apoptosis and caspase responsive theranostics. *Chemical Communications*, **51** (2015) 10831–10834.
<https://doi.org/10.1039/C5CC03028E>.
128. J. Park, Q. Jiang, D. Feng, & H.-C. Zhou, Controlled Generation of Singlet Oxygen in Living Cells with Tunable Ratios of the Photochromic Switch in Metal-Organic Frameworks. *Angewandte Chemie International Edition*, **55** (2016) 7188–7193. <https://doi.org/10.1002/anie.201602417>.
129. J. Park, Q. Jiang, D. Feng, L. Mao, & H.-C. Zhou, Size-Controlled Synthesis of Porphyrinic Metal–Organic Framework and Functionalization for Targeted Photodynamic Therapy. *Journal of the American Chemical Society*, **138** (2016) 3518–3525. <https://doi.org/10.1021/jacs.6b00007>.
130. W. Wang, L. Wang, Z. Li, & Z. Xie, BODIPY-containing nanoscale metal–organic frameworks for photodynamic therapy. *Chemical Communications*, **52** (2016) 5402–5405. <https://doi.org/10.1039/C6CC01048B>.
131. H.-J. Cai, T.-T. Shen, J. Zhang, C.-F. Shan, J.-G. Jia, X. Li, W.-S. Liu, & Y. Tang, A core–shell metal–organic-framework (MOF)-based smart nanocomposite for efficient NIR/H₂O₂-responsive photodynamic therapy against hypoxic tumor cells. *Journal of Materials Chemistry B*, **5** (2017) 2390–2394.
<https://doi.org/10.1039/C7TB00314E>.
132. W. Morris, W. E. Briley, E. Auyeung, M. D. Cabezas, & C. A. Mirkin, Nucleic Acid–Metal Organic Framework (MOF) Nanoparticle Conjugates. *Journal of the American Chemical Society*, **136** (2014) 7261–7264.
<https://doi.org/10.1021/ja503215w>.
133. B. Xiao, P. S. Wheatley, X. Zhao, A. J. Fletcher, S. Fox, A. G. Rossi, I. L. Megson, S. Bordiga, L. Regli, K. Mark Thomas, & R. E. Morris, High-Capacity

- Hydrogen and Nitric Oxide Adsorption and Storage in a Metal–Organic Framework. (2007). <https://doi.org/10.1021/JA066098K>.
134. A. C. McKinlay, B. Xiao, D. S. Wragg, P. S. Wheatley, I. L. Megson, & R. E. Morris, Exceptional Behavior over the Whole Adsorption–Storage–Delivery Cycle for NO in Porous Metal Organic Frameworks. *Journal of the American Chemical Society*, **130** (2008) 10440–10444. <https://doi.org/10.1021/ja801997r>.
135. A. C. McKinlay, J. F. Eubank, S. Wuttke, B. Xiao, P. S. Wheatley, P. Bazin, J.-C. Lavalley, M. Daturi, A. Vimont, G. De Weireld, P. Horcajada, C. Serre, & R. E. Morris, Nitric Oxide Adsorption and Delivery in Flexible MIL-88(Fe) Metal–Organic Frameworks. *Chemistry of Materials*, **25** (2013) 1592–1599. <https://doi.org/10.1021/cm304037x>.
136. G. Lan, K. Ni, R. Xu, K. Lu, Z. Lin, C. Chan, & W. Lin, Nanoscale Metal-Organic Layers for Deeply Penetrating X-ray-Induced Photodynamic Therapy. *Angewandte Chemie International Edition*, **56** (2017) 12102–12106. <https://doi.org/10.1002/anie.201704828>.
137. J. L. Phillips & J. L. Phillips, A Topical Review of Magnetic Fluid Hyperthermia. (n.d.).
138. A. Jordan, R. Scholz, P. Wust, H. Fähling, & Roland Felix, Magnetic fluid hyperthermia (MFH): Cancer treatment with AC magnetic field induced excitation of biocompatible superparamagnetic nanoparticles. *Journal of Magnetism and Magnetic Materials*, **201** (1999) 413–419. [https://doi.org/10.1016/S0304-8853\(99\)00088-8](https://doi.org/10.1016/S0304-8853(99)00088-8).
139. A. DIEING, O. Ahlers, T. Kerner, P. Wust, R. Felix, J. Löffel, H. Riess, & B. Hildebrandt, Whole body hyperthermia induces apoptosis in subpopulations of blood lymphocytes. *Immunobiology*, **207** (2003) 265–273. <https://doi.org/10.1078/0171-2985-00236>.
140. R. Hergt, R. Hiergeist, I. Hilger, W. . Kaiser, Y. Lapatnikov, S. Margel, & U. Richter, Maghemite nanoparticles with very high AC-losses for application in RF-magnetic hyperthermia. *Journal of Magnetism and Magnetic Materials*, **270** (2004) 345–357. <https://doi.org/10.1016/J.JMMM.2003.09.001>.
141. S. Goodwin, C. Peterson, C. Hoh, & C. Bittner, Targeting and retention of magnetic targeted carriers (MTCs) enhancing intra-arterial chemotherapy. *Journal of Magnetism and Magnetic Materials*, **194** (1999) 132–139. [https://doi.org/10.1016/S0304-8853\(98\)00584-8](https://doi.org/10.1016/S0304-8853(98)00584-8).
142. I. Coroiu, Relaxivities of different superparamagnetic particles for application in NMR tomography. *Journal of Magnetism and Magnetic Materials*, **201** (1999) 449–452. [https://doi.org/10.1016/S0304-8853\(99\)00025-6](https://doi.org/10.1016/S0304-8853(99)00025-6).

143. S. Thomsen, Pathologic analysis of photothermal and photomechanical effects of laser-tissue interactions. *Photochemistry and photobiology*, **53** (1991) 825–35.
144. A. J. Welch & M. J. C. van Gemert, Overview of Optical and Thermal Laser-Tissue Interaction and Nomenclature. *Opt. Response Laser-Irradiated Tissue* (Dordrecht: Springer Netherlands, 2010), pp. 3–11. https://doi.org/10.1007/978-90-481-8831-4_1.
145. M. J. van Gemert, A. J. Welch, J. W. Pickering, O. T. Tan, & G. H. Gijsbers, Wavelengths for laser treatment of port wine stains and telangiectasia. *Lasers in surgery and medicine*, **16** (1995) 147–55.
146. X. Huang, P. K. Jain, I. H. El-Sayed, & M. A. El-Sayed, Plasmonic photothermal therapy (PPTT) using gold nanoparticles. *Lasers in Medical Science*, **23** (2008) 217–228. <https://doi.org/10.1007/s10103-007-0470-x>.
147. G. Mie & G., Contributions to the optics of turbid media, particularly of colloidal metal solutions. Contributions to the optics of turbid media, particularly of colloidal metal solutions Transl. into ENGLISH from Ann. Phys. (Leipzig), v. 25, no. 3, 1908 p 377-445, (1976).
148. E. Boisselier & D. Astruc, Gold nanoparticles in nanomedicine: preparations, imaging, diagnostics, therapies and toxicity. *Chemical Society Reviews*, **38** (2009) 1759. <https://doi.org/10.1039/b806051g>.
149. L. R. Hirsch, R. J. Stafford, J. A. Bankson, S. R. Sershen, B. Rivera, R. E. Price, J. D. Hazle, N. J. Halas, & J. L. West, Nanoshell-mediated near-infrared thermal therapy of tumors under magnetic resonance guidance. *Proceedings of the National Academy of Sciences*, **100** (2003) 13549–13554. <https://doi.org/10.1073/pnas.2232479100>.
150. C. Loo, A. Lin, L. Hirsch, M.-H. Lee, J. Barton, N. Halas, J. West, & R. Drezek, Nanoshell-Enabled Photonics-Based Imaging and Therapy of Cancer. *Technology in Cancer Research & Treatment*, **3** (2004) 33–40. <https://doi.org/10.1177/153303460400300104>.
151. A. Vogel & V. Venugopalan, Mechanisms of Pulsed Laser Ablation of Biological Tissues. (2003). <https://doi.org/10.1021/CR010379N>.
152. P. Ghosh, G. Han, M. De, & C. K. Kim, Gold nanoparticles in delivery applications. *Advanced Drug Delivery Reviews*, **60** (2008) 1307–1315. <https://doi.org/10.1016/J.ADDR.2008.03.016>.
153. T. M. Allen & P. R. Cullis, Drug Delivery Systems: Entering the Mainstream. *Science*, **303** (2004) 1818–1822. <https://doi.org/10.1126/science.1095833>.

154. G. Mayer & A. Heckel, Biologically Active Molecules with a “Light Switch.” *Angewandte Chemie International Edition*, **45** (2006) 4900–4921. <https://doi.org/10.1002/anie.200600387>.
155. H. W. Lei, B. Wu, C. S. Cha, & H. Kita, Electro-oxidation of glucose on platinum in alkaline solution and selective oxidation in the presence of additives. *Journal of Electroanalytical Chemistry*, (1995). [https://doi.org/10.1016/0022-0728\(94\)03673-Q](https://doi.org/10.1016/0022-0728(94)03673-Q).
156. Y. M. Lvov, D. G. Shchukin, H. Möhwald, & R. R. Price, Halloysite Clay Nanotubes for Controlled Release of Protective Agents. *ACS Nano*, **2** (2008) 814–820. <https://doi.org/10.1021/nn800259q>.
157. L. Zhang, J. M. Chan, F. X. Gu, J.-W. Rhee, A. Z. Wang, A. F. Radovic-Moreno, F. Alexis, R. Langer, & O. C. Farokhzad, Self-Assembled Lipid–Polymer Hybrid Nanoparticles: A Robust Drug Delivery Platform. *ACS Nano*, **2** (2008) 1696–1702. <https://doi.org/10.1021/nn800275r>.
158. X. Huang, P. K. Jain, I. H. El-Sayed, & M. A. El-Sayed, Gold nanoparticles: interesting optical properties and recent applications in cancer diagnostics and therapy. *Nanomedicine*, **2** (2007) 681–693. <https://doi.org/10.2217/17435889.2.5.681>.
159. L. Tong, Y. Zhao, T. B. Huff, M. N. Hansen, A. Wei, & J.-X. Cheng, Gold Nanorods Mediate Tumor Cell Death by Compromising Membrane Integrity. *Advanced Materials*, **19** (2007) 3136–3141. <https://doi.org/10.1002/adma.200701974>.
160. R. S. Norman, J. W. Stone, A. Gole, C. J. Murphy, Tara L., & Sabo-Attwood, Targeted Photothermal Lysis of the Pathogenic Bacteria, *Pseudomonas aeruginosa*, with Gold Nanorods. (2007). <https://doi.org/10.1021/NL0727056>.
161. K. Bhattacharyya, B. S. Goldschmidt, M. Hannink, S. Alexander, A. Jurkevic, & J. A. Viator, Gold Nanoparticle–Mediated Detection of Circulating Cancer Cells. *Clinics in Laboratory Medicine*, **32** (2012) 89–101. <https://doi.org/10.1016/j.cll.2012.01.001>.
162. S. K. Maji, A. K. Mandal, K. T. Nguyen, P. Borah, & Y. Zhao, Cancer Cell Detection and Therapeutics Using Peroxidase-Active Nanohybrid of Gold Nanoparticle-Loaded Mesoporous Silica-Coated Graphene. *ACS Applied Materials & Interfaces*, **7** (2015) 9807–9816. <https://doi.org/10.1021/acsami.5b01758>.
163. C. P. Lin, M. W. Kelly, S. A. B. Sibayan, M. A. Latina, & R. R. Anderson, Selective cell killing by microparticle absorption of pulsed laser radiation. *IEEE Journal of Selected Topics in Quantum Electronics*, **5** (1999) 963–968. <https://doi.org/10.1109/2944.796318>.
164. C. M. Pitsillides, E. K. Joe, X. Wei, R. R. Anderson, & C. P. Lin, Selective cell targeting with light-absorbing microparticles and nanoparticles. *Biophysical journal*, **84** (2003) 4023–32. [https://doi.org/10.1016/S0006-3495\(03\)75128-5](https://doi.org/10.1016/S0006-3495(03)75128-5).

165. V. P. Zharov, V. Galitovsky, & M. Viegas, Photothermal detection of local thermal effects during selective nanophotothermolysis. *Applied Physics Letters*, **83** (2003) 4897–4899. <https://doi.org/10.1063/1.1632546>.
166. I. ELSAYED, X. HUANG, & M. ELSAYED, Selective laser photo-thermal therapy of epithelial carcinoma using anti-EGFR antibody conjugated gold nanoparticles. *Cancer Letters*, **239** (2006) 129–135. <https://doi.org/10.1016/j.canlet.2005.07.035>.
167. X. Huang, P. K. Jain, I. H. El-Sayed, & M. A. El-Sayed, Determination of the Minimum Temperature Required for Selective Photothermal Destruction of Cancer Cells with the Use of Immunotargeted Gold Nanoparticles. *Photochemistry and Photobiology*, **82** (2006) 412. <https://doi.org/10.1562/2005-12-14-RA-754>.
168. R. P. (Richard P. Feynman, R. B. Leighton, & M. L. (Matthew L. Sands, *The Feynman lectures on physics. Volume 1* (Addison-Wesley, 2011).
169. G. Wu, A. Mikhailovsky, H. A. Khant, C. Fu, W. Chiu, & J. A. Zasadzinski, Remotely Triggered Liposome Release by Near-Infrared Light Absorption via Hollow Gold Nanoshells. *Journal of the American Chemical Society*, **130** (2008) 8175–8177. <https://doi.org/10.1021/ja802656d>.
170. J. Chen, D. Wang, J. Xi, L. Au, A. Siekkinen, A. Warsen, Z.-Y. Li, H. Zhang, Y. Xia, & X. Li, Immuno Gold Nanocages with Tailored Optical Properties for Targeted Photothermal Destruction of Cancer Cells. *Nano Letters*, **7** (2007) 1318–1322. <https://doi.org/10.1021/nl070345g>.
171. C. Loo, A. Lowery, N. Halas, J. West, & R. Drezek, Immunotargeted Nanoshells for Integrated Cancer Imaging and Therapy. *Nano Letters*, **5** (2005) 709–711. <https://doi.org/10.1021/nl050127s>.
172. J. Chen, B. Wiley, Z.-Y. Li, D. Campbell, F. Saeki, H. Cang, L. Au, J. Lee, X. Li, & Y. Xia, Gold Nanocages: Engineering Their Structure for Biomedical Applications. *Advanced Materials*, **17** (2005) 2255–2261. <https://doi.org/10.1002/adma.200500833>.
173. H. L. and & J. H. Hafner*, Gold Nanorod Bioconjugates. (2005). <https://doi.org/10.1021/CM050935K>.
174. T. Niidome, M. Yamagata, Y. Okamoto, Y. Akiyama, H. Takahashi, T. Kawano, Y. Katayama, & Y. Niidome, PEG-modified gold nanorods with a stealth character for in vivo applications. *Journal of Controlled Release*, **114** (2006) 343–347. <https://doi.org/10.1016/J.JCONREL.2006.06.017>.
175. J. Kreuter, Application of nanoparticles for the delivery of drugs to the brain. *International Congress Series*, **1277** (2005) 85–94. <https://doi.org/10.1016/J.ICS.2005.02.014>.

176. G. Liu, M. R. Garrett, P. Men, X. Zhu, G. Perry, & M. A. Smith, Nanoparticle and other metal chelation therapeutics in Alzheimer disease. *Biochimica et Biophysica Acta (BBA) - Molecular Basis of Disease*, **1741** (2005) 246–252.
<https://doi.org/10.1016/j.bbadis.2005.06.006>.
177. J. Stehr, C. Hrelescu, R. A. Sperling, G. Raschke, Michael Wunderlich, § Alfons Nichtl, § Dieter Heindl, W. J. P. Konrad Kürzinger, & J. Thomas A. Klar, Feldmann, Gold NanoStoves for Microsecond DNA Melting Analysis. (2008).
<https://doi.org/10.1021/NL073028I>.
178. S. E. Lee, G. L. Liu, F. Kim, & L. P. Lee, Remote Optical Switch for Localized and Selective Control of Gene Interference. *Nano Letters*, **9** (2009) 562–570.
<https://doi.org/10.1021/nl802689k>.
179. S. Tang, M. Chen, & N. Zheng, Sub-10-nm Pd Nanosheets with Renal Clearance for Efficient Near-Infrared Photothermal Cancer Therapy. *Small*, **10** (2014) 3139–3144. <https://doi.org/10.1002/sml.201303631>.
180. X. Song, H. Gong, S. Yin, L. Cheng, C. Wang, Z. Li, Y. Li, X. Wang, G. Liu, & Z. Liu, Ultra-Small Iron Oxide Doped Polypyrrole Nanoparticles for In Vivo Multimodal Imaging Guided Photothermal Therapy. *Advanced Functional Materials*, **24** (2014) 1194–1201. <https://doi.org/10.1002/adfm.201302463>.
181. M. Aioub & M. A. El-Sayed, A Real-Time Surface Enhanced Raman Spectroscopy Study of Plasmonic Photothermal Cell Death Using Targeted Gold Nanoparticles. *Journal of the American Chemical Society*, **138** (2016) 1258–1264.
<https://doi.org/10.1021/jacs.5b10997>.
182. C. Zhang, W. Bu, D. Ni, C. Zuo, C. Cheng, Q. Li, L. Zhang, Z. Wang, & J. Shi, A Polyoxometalate Cluster Paradigm with Self-Adaptive Electronic Structure for Acidity/Reducibility-Specific Photothermal Conversion. *Journal of the American Chemical Society*, **138** (2016) 8156–8164. <https://doi.org/10.1021/jacs.6b03375>.
183. R. Bardhan, W. Chen, C. Perez-Torres, M. Bartels, R. M. Hushka, L. L. Zhao, E. Morosan, R. G. Pautler, A. Joshi, & N. J. Halas, Nanoshells with Targeted Simultaneous Enhancement of Magnetic and Optical Imaging and Photothermal Therapeutic Response. *Advanced Functional Materials*, **19** (2009) 3901–3909.
<https://doi.org/10.1002/adfm.200901235>.
184. T.-K. Ryu, S. W. Baek, R. H. Kang, & S.-W. Choi, Selective Photothermal Tumor Therapy Using Nanodiamond-Based Nanoclusters with Folic Acid. *Advanced Functional Materials*, **26** (2016) 6428–6436. <https://doi.org/10.1002/adfm.201601207>.
185. Z. Zhang, L. Wang, J. Wang, X. Jiang, X. Li, Z. Hu, Y. Ji, X. Wu, & C. Chen, Mesoporous Silica-Coated Gold Nanorods as a Light-Mediated Multifunctional

- Theranostic Platform for Cancer Treatment. *Advanced Materials*, **24** (2012) 1418–1423. <https://doi.org/10.1002/adma.201104714>.
186. S. Wang, P. Huang, L. Nie, R. Xing, D. Liu, Z. Wang, J. Lin, S. Chen, G. Niu, G. Lu, & X. Chen, Single Continuous Wave Laser Induced Photodynamic/Plasmonic Photothermal Therapy Using Photosensitizer-Functionalized Gold Nanostars. *Advanced Materials*, **25** (2013) 3055–3061. <https://doi.org/10.1002/adma.201204623>.
187. Y. Xia, W. Li, C. M. Cobley, J. Chen, X. Xia, Q. Zhang, M. Yang, E. C. Cho, & P. K. Brown, Gold Nanocages: From Synthesis to Theranostic Applications. *Accounts of Chemical Research*, **44** (2011) 914–924. <https://doi.org/10.1021/ar200061q>.
188. Y.-W. Chen, Y.-L. Su, S.-H. Hu, & S.-Y. Chen, Functionalized graphene nanocomposites for enhancing photothermal therapy in tumor treatment. *Advanced Drug Delivery Reviews*, **105** (2016) 190–204. <https://doi.org/10.1016/J.ADDR.2016.05.022>.
189. S. Shen, S. Wang, R. Zheng, X. Zhu, X. Jiang, D. Fu, & W. Yang, Magnetic nanoparticle clusters for photothermal therapy with near-infrared irradiation. *Biomaterials*, **39** (2015) 67–74. <https://doi.org/10.1016/J.BIOMATERIALS.2014.10.064>.
190. J. Song, F. Wang, X. Yang, B. Ning, M. G. Harp, S. H. Culp, S. Hu, P. Huang, L. Nie, J. Chen, & X. Chen, Gold Nanoparticle Coated Carbon Nanotube Ring with Enhanced Raman Scattering and Photothermal Conversion Property for Theranostic Applications. *Journal of the American Chemical Society*, **138** (2016) 7005–7015. <https://doi.org/10.1021/jacs.5b13475>.
191. Z. Zha, X. Yue, Q. Ren, & Z. Dai, Uniform Polypyrrole Nanoparticles with High Photothermal Conversion Efficiency for Photothermal Ablation of Cancer Cells. *Advanced Materials*, **25** (2013) 777–782. <https://doi.org/10.1002/adma.201202211>.
192. Y. Lyu, Y. Fang, Q. Miao, X. Zhen, D. Ding, & K. Pu, Intraparticle Molecular Orbital Engineering of Semiconducting Polymer Nanoparticles as Amplified Theranostics for *in Vivo* Photoacoustic Imaging and Photothermal Therapy. *ACS Nano*, **10** (2016) 4472–4481. <https://doi.org/10.1021/acsnano.6b00168>.
193. K. M. L. Taylor-Pashow, J. Della Rocca, Z. Xie, S. Tran, & W. Lin, Postsynthetic Modifications of Iron-Carboxylate Nanoscale Metal–Organic Frameworks for Imaging and Drug Delivery. *Journal of the American Chemical Society*, **131** (2009) 14261–14263. <https://doi.org/10.1021/ja906198y>.

Keyword Index

Activated Carbon.....	290
Antibacterial	239
Applications.....	49
Biogas	19
Biosensing and Bioimaging.....	308
Biosensors.....	239
Cancer	361
Carbon Dioxide Capture.....	85
Catalysis.....	107
Cathode.....	177
Clean Energy	85
Composite.....	177
Computed Tomography.....	308
Drug Delivery	239, 290
Enzymatic-MOF.....	308
Fluorescence	308
Fuel Cells.....	85
Functionalization	107
Gas Separation.....	107, 290
Harmful Gas Removal.....	85
Hybrid Capacitor	177
Hybrid Co ₃ O ₄ C Nanowire MOF.....	140
Hydrogen Storage.....	1, 19, 85
Lithium-Ion Batteries	32
Lithium-Sulphur Batteries	32
Magnetic Resonance Imaging	308
Modification Strategies.....	49
n(MOFs)	361
Nanomedicine.....	239

Nano-Scale Metal-Organic Frameworks.....	361
Ni ₃ (HITP) ₂ MOF.....	140
OER Process	140
Organic Linkers	290
Photo Catalysis.....	85
Photodynamic Therapy (PDT).....	361
Photosensitizers (PSs).....	361
Photothermal Therapy (PTT).....	361
Porosity	107
Porous Materials	290
Production Methodologies	49
Quantum Dot Composites.....	49
Renewable Energy	19, 140
Stability	107
Storage	19
Super Capacitance.....	140
Supercapacitors	85, 177
Therapeutic Applications.....	239
Zeolites.....	290

About the Editors

Dr. Anish Khan is currently working as Assistant Professor, at Chemistry Department, Centre of Excellence for Advanced Materials Research (CEAMR), Faculty of Science, King Abdulaziz University, Jeddah, Saudi Arabia. Ph.D. Completed from Aligarh Muslim University, India in 2010. He has 13 years research experience of working in the field of organic-inorganic electrically conducting nano-composites and its applications in making chemical sensor. He completed Postdoctoral from School of Chemical Sciences, University Sains Malaysia (USM) on electroanalytical chemistry for one year. More than 115 research articles have been published in refereed international journals. More than 10 international conferences/ workshop and 7 books published and 15 Book chapters. Around 20 research project completed. Member of American Nano Society, Field of specialization is polymer nanocomposite/cation-exchanger/chemical sensor/micro biosensor/nanotechnology, application of nanomaterials in electroanalytical chemistry, material chemistry, ion-exchange chromatography and electro-analytical chemistry, dealing with the synthesis, characterization (using different analytical techniques) and derivatization of inorganic ion-exchanger by the incorporation of electrically conducting polymers. Preparation and characterization of hybrid nano composite materials and their applications, Polymeric inorganic cation –exchange materials, Electrically conducting polymeric, materials, Composite material use as Sensors, Green chemistry by remediation of pollution, Heavy metal ion-selective membrane electrode, Biosensor on neurotransmitter.

Prof. Francis Verpoort received his DPhil from Ghent University in 1996. In 1998, he became a professor at the same university. In 2004, he founded a spin-off company based on olefin metathesis catalysts. In 2008, he became an editor of Applied Organometallic Chemistry. Currently, he is a professor at Wuhan University of Technology, Khalifa University of Science and Technology and at Ghent University (Global Campus). He received the title of Honorary professor from Liaoning University and Shenyang University of chemical Technology next to other awards and honors of which the most important ones are: In 2012, he has been appointed as ‘National Distinguished Expert, P. R. China. In 2015 he was appointed as High-level Expert of the Russian Federation. In 2016 he was selected as Distinguished Fellow of the International Engineering and Technology Institute (IETI, Hong Kong) and also nominated as Director-General of IETI. He has been guest professor at several universities He published more then 270 articles and is owner of 20 patents. His main research interests concern the structure and mechanisms of organometallic material chemistry, homogeneous and heterogeneous

catalysis, MOFs and MOPs, water splitting, olefin metathesis and carbon dioxide conversion.

Prof. Mohammed Muzibur Rahman received his B.Sc. and M.Sc. from Shahjalal University of Science & Technology, Sylhet, Bangladesh on 1999 and 2001 respectively. He received his Ph.D. from the Chonbuk National University, South Korea, in 2007. After his Ph.D., he worked as postdoctoral fellowship and assistant professor in pioneer research centers and universities located in South Korea, Japan, and Saudi Arabia (2007 to 2011). Presently, he is working as associate professor in Center of Excellence for Advanced Materials Research (CEAMR) and Chemistry department at King Abdulaziz University, Saudi Arabia since 2011. He published more than 245 international and domestic conferences; and published several book chapters and ten-books as an editor. His research work has been largely in the area of Photocatalysis; Semiconductor; Nanoparticles; Carbon nanotubes; Nanotechnology; Electro-catalysis; Sensors; Ionic liquid; Surface Chemistry; Electrochemistry; Nanomaterials; etc.

Dr. Illyas Md Isa, Ph.D (USM), M.Sc. (USM), B.Appl.Sc. (USM), Expertise : Analytical Chemistry, Chemical and Biosensor; Email : illyas@fsmt.upsi.edu.my; Tel. (O) : 015-48797714; Scopus H. Index of 10 with more than 50 ISI articles were published. Reviewers for some ISI journals such as Analytical Chemistry (ACS), ACS Applied Materials & Interfaces (ACS), Analytical Letters (Taylor & Francis), Chemistry Central Journal (Springer), Electrochimica Acta (Elsevier), Electroanalysis (Wiley & Sons), Ionics (Springer), International Journal of Environmental Analytical Chemistry (Taylor & Francis), Journal of Alloys and Compounds (Elsevier), Journal of Applied Electrochemistry (Springer), Journal of Environmental Chemical Engineering (Elsevier), Journal of Hazardous Materials (Elsevier), Journal of Inorganic and Organometallic Polymers and Materials (Springer), Journal of Materials Science (Springer), Materials Science and Engineering C (Elsevier), Material Chemistry and Physics (Elsevier), Measurement (Elsevier), Microchemical Journal (Elsevier), Microchimica Acta (Springer), Procedia Chemistry (Elsevier), RSC Advances (Royal Society of Chemistry), Sensors and Actuators B (Elsevier), Sensor Letters (ASP), Talanta (Elsevier)

Editor of International Journals such as Global Journal of Control Engineering and Technology and Journal of Nanomedicine and Nanotechnology Research Grant Evaluator for National Science Centre, Poland and Committee of several International Conferences such as Conference on Sensor Device Technologies and Applications,

SENSORDeVICES (2016-until now) and International Conference on Sensors Engineering and Electronics Instrumental Advance (SEIA 2015) 2015, Dubai, UAE.

Prof. Abdullah Mohammed Ahmed Asiri is Professor in Chemistry Department – Faculty of Science -King Abdulaziz University. Ph.D. (1995) From University of Wales College of Cardiff, U.K. on Tribochromic compounds and their applications. More than 1000 Research articles and 20 books published. The chairman of the Chemistry Department, King Abdulaziz University currently and also the director of the center of Excellence for Advanced Materials Research. Director of Education Affair Unit–Deanship of Community services. Member of Advisory committee for advancing materials, (National Technology Plan, (King Abdul Aziz City of Science and Technology, Riyadh, Saudi Arabia). Color chemistry. Synthesis of novel photochromic and thermochromic systems, Synthesis of novel colorants and coloration of textiles and plastics, Molecular Modeling, Applications of organic materials into optics such as OEDS, High performance organic Dyes and pigments. New applications of organic photochromic compounds in new novelty. Organic synthesis of heterocyclic compounds as precursor for dyes. Synthesis of polymers functionalized with organic dyes. Preparation of some coating formulations for different applications. Photodynamic thereby using Organic Dyes and Pigments Virtual Labs and Experimental Simulations. He is member of Editorial board of Journal of Saudi Chemical Society, Journal of King Abdul Aziz University, Pigment and Resin Technology Journal, Organic Chemistry Insights, Libertas Academica, Recent Patents on Materials Science, Bentham Science Publishers Ltd. Beside that he has professional membership of International and National Society and Professional bodies.

Dr. Malik Abdul Rub received his M.Sc. and Ph.D. degrees from the Aligarh Muslim University. Now he has joined King Abdulaziz University as an Assistant Professor in the Center of Excellence for Advanced Materials Research. His current research interests are clouding phenomenon in amphiphilic systems and interaction of the amphiphilic drug with bile salts/triblock polymers/surfactants/proteins/ hydrotropes/lipids etc by using different techniques. He has published a more than 150 articles in the renowned and reviewed scientific journals at an international level.